



A National Center of Excellence in Advanced Technology Applications

ISSN 1520-295X

Analytical Investigation of the Structural Fuse Concept

by

Ramiro E. Vargas and Michel Bruneau
University at Buffalo, State University of New York
Department of Civil, Structural and Environmental Engineering
Ketter Hall
Buffalo, New York 14260

Technical Report MCEER-06-0004

March 16, 2006

This research was conducted at the University at Buffalo, State University of New York and was supported primarily by the Earthquake Engineering Research Centers Program of the National Science Foundation under award number EEC-9701471.

NOTICE

This report was prepared by the University at Buffalo, State University of New York as a result of research sponsored by the Multidisciplinary Center for Earthquake Engineering Research (MCEER) through a grant from the Earthquake Engineering Research Centers Program of the National Science Foundation under NSF award number EEC-9701471 and other sponsors. Neither MCEER, associates of MCEER, its sponsors, the University at Buffalo, State University of New York, nor any person acting on their behalf:

- a. makes any warranty, express or implied, with respect to the use of any information, apparatus, method, or process disclosed in this report or that such use may not infringe upon privately owned rights; or
- b. assumes any liabilities of whatsoever kind with respect to the use of, or the damage resulting from the use of, any information, apparatus, method, or process disclosed in this report.

Any opinions, findings, and conclusions or recommendations expressed in this publication are those of the author(s) and do not necessarily reflect the views of MCEER, the National Science Foundation, or other sponsors.



Analytical Investigation of the Structural Fuse Concept

by

Ramiro E. Vargas¹ and Michel Bruneau²

Publication Date: March 16, 2006

Submittal Date: April 13, 2005

Technical Report MCEER-06-0004

Task Number 8.2.2

NSF Master Contract Number EEC 9701471

- 1 Graduate Research Assistant, Department of Civil, Structural and Environmental Engineering, University at Buffalo, State University of New York
- 2 Professor, Department of Civil, Structural and Environmental Engineering, University at Buffalo, State University of New York

MULTIDISCIPLINARY CENTER FOR EARTHQUAKE ENGINEERING RESEARCH
University at Buffalo, State University of New York
Red Jacket Quadrangle, Buffalo, NY 14261

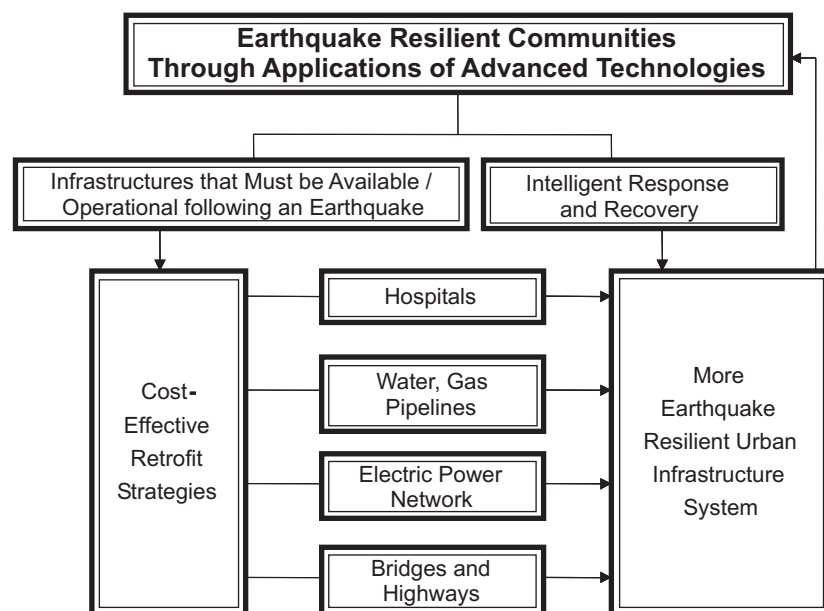
Preface

The Multidisciplinary Center for Earthquake Engineering Research (MCEER) is a national center of excellence in advanced technology applications that is dedicated to the reduction of earthquake losses nationwide. Headquartered at the University at Buffalo, State University of New York, the Center was originally established by the National Science Foundation in 1986, as the National Center for Earthquake Engineering Research (NCEER).

Comprising a consortium of researchers from numerous disciplines and institutions throughout the United States, the Center's mission is to reduce earthquake losses through research and the application of advanced technologies that improve engineering, pre-earthquake planning and post-earthquake recovery strategies. Toward this end, the Center coordinates a nationwide program of multidisciplinary team research, education and outreach activities.

MCEER's research is conducted under the sponsorship of two major federal agencies: the National Science Foundation (NSF) and the Federal Highway Administration (FHWA), and the State of New York. Significant support is derived from the Federal Emergency Management Agency (FEMA), other state governments, academic institutions, foreign governments and private industry.

MCEER's NSF-sponsored research objectives are twofold: to increase resilience by developing seismic evaluation and rehabilitation strategies for the post-disaster facilities and systems (hospitals, electrical and water lifelines, and bridges and highways) that society expects to be operational following an earthquake; and to further enhance resilience by developing improved emergency management capabilities to ensure an effective response and recovery following the earthquake (see the figure below).



A cross-program activity focuses on the establishment of an effective experimental and analytical network to facilitate the exchange of information between researchers located in various institutions across the country. These are complemented by, and integrated with, other MCEER activities in education, outreach, technology transfer, and industry partnerships.

This report presents an analytical study of the structural fuse concept, which is a system that is designed to concentrate seismic damage in easy-to-replace devices, in this case metallic dampers, to allow the primary structure to remain elastic. A comprehensive parametric study was conducted to investigate the range of validity of this concept, and identify combinations of key parameters essential to ensure adequate performance under seismic conditions. Nonlinear time history analyses were conducted to identify viable combinations of parameters. These were used to provide guidelines for several types of metallic dampers, including Buckling-restrained Braces (BRBs), Triangular Added Damping and Stiffness (TADAS), and Shear Panels (SP) for use in design and retrofit. As part of this research, floor demand velocities and accelerations were investigated to assess the applicability of the structural fuse concept to nonstructural components. A companion study provides the experimental validation of the analytical models developed in this report (see Technical report MCEER-06-0005).

ABSTRACT

Passive energy dissipation (PED) devices are useful to enhance structural performance by reducing seismically induced structural damage. Metallic dampers are one such PED. When they are designed such that all damage is concentrated on the PED devices, allowing the primary structure to remain elastic, they can be defined as structural fuses (SF). A comprehensive parametric study was conducted to investigate the SF concept, and to identify combinations of key parameters essential to ensure adequate seismic performance for SF systems. Non-linear time history analyses were conducted for several combinations of parameters, chosen to cover a range of feasible designs. Viable combinations of parameters are identified and used to provide guidelines to design and retrofit systems using Buckling-restrained Braces (BRBs), Triangular Added Damping and Stiffness (T-ADAS), and Shear Panels (SP) as examples of metallic dampers working as structural fuses. Studies focus on the application of the structural fuse concept to single-degree-of-freedom (SDOF) and multi-degree-of-freedom (MDOF) systems. As part of this research, floor demands velocities and accelerations are also investigated, with the objective of assessing the applicability of the structural fuse concept to protect nonstructural components.

ACKNOWLEDGEMENTS

This research is conducted at the State University of New York at Buffalo under the supervision of Dr. Michel Bruneau, and is supported by the Earthquake Engineering Research Centers Program of the National Sciences Foundation under Award Number EEC-9701471 to the Multidisciplinary Center for Earthquake Engineering Research. This support is greatly appreciated.

TABLE OF CONTENTS

SECTION	TITLE	PAGE
1	INTRODUCTION	1
2	LITERATURE REVIEW	5
2.1	Introduction	5
2.2	Structural Fuse Concept	5
2.3	Metallic Energy Dissipation Devices	12
2.3.1	Buckling-Restrained Brace (BRB)	13
2.3.2	Triangular Added Damping and Stiffness (T-ADAS)	15
2.3.3	Shear Panel (SP)	17
2.3.4	Friction Dampers (FD)	22
3	PARAMETRIC STUDY AND SEISMIC RESPONSE OF SINGLE DEGREE OF FREEDOM SYSTEMS WITH STRUCTURAL FUSES	31
3.1	Introduction	31
3.2	Analytical Model of a SDOF System with Structural Fuses	32
3.3	Parametric Formulation	40
3.4	Nonlinear Dynamic Response	41
3.4.1	Response plotted in tri-dimensional graphs	44
3.4.2	Response plotted in two-dimensional graphs	46
3.4.3	Allowable story drift	53
3.4.4	Earthquake duration and strain-hardening ratio effects	62
3.5	Generic Retrofit Case Study	74
3.6	Observations	79
4	DESIGN OF SINGLE DEGREE OF FREEDOM (SDOF) SYSTEMS WITH METALLIC STRUCTURAL FUSES	81
4.1	Introduction	81
4.2	Metallic Structural Fuses considered in the Analysis	81
4.2.1	Buckling-restrained Brace (BRB)	83
4.2.2	Triangular Added Damping and Stiffness (T-ADAS) System	86
4.2.3	Shear Panel (SP)	88
4.3	Design for a Specified set of Parameters	91
4.4	Sensitivity Analysis	100
4.5	Design Examples	108
4.5.1	Design Results	109
4.6	Retrofit Examples	119
4.6.1	Retrofit Results	120
4.7	Observations	122

TABLE OF CONTENTS (cont'd)

SECTION	TITLE	PAGE
5	FLOOR RESPONSE OF SINGLE DEGREE OF FREEDOM SYSTEMS WITH METALLIC STRUCTURAL FUSES	125
5.1	Introduction	125
5.2	Floor Response	126
5.3	Floor Spectra	142
5.4	Equivalent Sine-wave Floor Spectra	155
5.5	Observations	166
6	RESPONSE OF HYBRID SINGLE DEGREE OF FREEDOM SYSTEMS WITH METALLIC AND VISCOUS DAMPERS	167
6.1	Introduction	167
6.2	Equivalent Viscous Damping	168
6.3	Parametric Analysis of Hysteretic Damping	169
6.4	Parametric Analysis of Spectral Acceleration	182
6.5	Hysteretic Response	190
6.6	Analysis in the Frequency Domain	218
6.7	Observations	251
7	DESIGN OF MULTI DEGREE OF FREEDOM SYSTEMS WITH METALLIC STRUCTURAL FUSES	253
7.1	Introduction	253
7.2	Design for a Specified Set of Parameters	254
7.2.1	Elastic limit period for MDOF Systems	255
7.2.2	Story yield shear	257
7.2.3	Design Steps	257
7.3	New Buildings Design Examples	259
7.4	Retrofit Design Examples	287
7.5	Observations	297
8	CONCLUSIONS	299
9	REFERENCES	303
Appendix A:	EXAMPLES OF DESIGN AND RETROFIT OF SDOF SYSTEMS WITH BUCKLING-RESTRAINED BRACES	313
Appendix B:	MATHEMATICAL DERIVATION OF EQUATIONS 6.3 AND 6.4	325
Appendix C:	EXAMPLES OF DESIGN AND RETROFIT OF MDOF SYSTEMS WITH BUCKLING-RESTRAINED BRACES	331

LIST OF ILLUSTRATIONS

SECTION	TITLE	PAGE
2.1	Damage-Tolerant Structure	8
2.2	Repair Cost versus Earthquake Intensity (Connor et al., 1997)	8
2.3	Energy Response to the El Centro earthquake scaled to peak ground velocity of 50 cm/s) (Sugiyama, 1998)	11
2.4	Some Schematic Details used for Buckling Restrained Braces (Sabelli et al., 2003)	13
2.5	Details of Steel Welded T-ADAS Device (Tsai et al., 1993)	16
2.6	Prototype Building Including Shear Panels with Low-Yield Steel (Nakashima, 1995a)	18
2.7	Shear Panels Details and Dimensions of Test Specimens (Nakashima, 1995b)	18
2.8	Types of Seismic Control Members; (a) Pillar Type, (b) Bracing Type (Tanaka et al., 1998)	20
2.9	Conventional Design and Proposed Design (Shimizu et al., 1998)	21
2.10	Shear Panel Models	21
2.11	Limited Slip Bolt Joint (Pall et al., 1980)	22
2.12	Hysteresis Loops of Limited Slip Bolted Joints (Pall et al., 1980)	23
2.13	X-braced Friction Damper (Pall and Marsh, 1982)	23
2.14	Slotted Bolted Connection (FitzGerald et al., 1989)	24
2.15	Slotted Bolted Connection; (a) Free Body Diagrams, (b) Typical Load Deformation Diagrams (FitzGerald et al., 1989)	24
2.16	Friction Damping Device (Filiatrault and Cherry, 1989)	25
2.17	Hysteretic Behavior of Simple Friction-Damped Braced Frame during One Cycle of Loading (Filiatrault and Cherry, 1990)	26
2.18	External and Internal views of Energy Dissipating Restraint (Nims et al., 1993)	27
2.19	Energy Dissipating Restraint Complete Hysteresis Loop (Nims et al., 1993)	27
2.20	Analytical Double Flag-Shaped Hysteresis Loop (Nims et al., 1993)	28
2.21	Analytical Triangular-Shaped Hysteresis Loop (Nims et al., 1993)	28
3.1	Model of a SDOF system with structural fuse	33
3.2	General Pushover Curve	34
3.3a	Pushover Curves for the Studied Systems Normalized by V_{ys} , D_{ya}	36
3.3b	Pushover Curves for the Studied Systems, Normalized by V_{ps} , D_{ys}	37
3.4	Hysteresis Loops for the Studied Systems, Normalized by V_{ps} , D_{ys}	39
3.5a	Elastic Response Spectra for Synthetic Earthquakes ($\zeta = 5\%$)	42
3.5b	Average Elastic Response Spectrum for Synthetic Earthquakes ($\zeta = 5\%$)	43
3.6	Three-dimensional Representation of the Response as a function of V_{yd} / V_{ys} , K_a / K_p and ζ_{max}	45

LIST OF ILLUSTRATIONS (cont'd)

SECTION	TITLE	PAGE
3.7	Three-dimensional Representation of the Response as a function of T , T_f , and	46
3.8	Average Response in terms of Frame Ductility (ρ_f)	48
3.9	Average Response in terms of Global Ductility (ρ_g)	49
3.10	Pushover curves for two structures having the same ρ_{max} , ρ_g , and different periods (T)	50
3.11	Average Ductility Demand calculated using Equation 3.25	52
3.12	Elastic Demand Spectrum ($\rho = 5\%$) and different drift levels for $H = 3810\text{mm}$	54
3.13	Regions of Admissible Solutions in terms of Average Frame Ductility (ρ_f), and Story Drift of 2%	56
3.14	Regions of Admissible Solutions in terms of Average Global Ductility (ρ_g) and Story Drift of 2%	57
3.15	Regions of Admissible Solutions in terms of Average Frame Ductility (ρ_f) and Story Drift of 1%	60
3.16	Regions of Admissible Solutions in terms of Average Global Ductility (ρ_g) and Story Drift of 1%	61
3.17	Frame Ductility (ρ_f) as a function of a for $T = 0.1\text{s}$, $\rho_{max} = 5$, $\rho_g = 0.8$, and Earthquake of 15s	66
3.18	Frame Ductility (ρ_f) as a function of a for $T = 0.1\text{s}$, $\rho_{max} = 5$, $\rho_g = 0.8$, and Earthquake of 60s	67
3.19	Frame Ductility (ρ_f) as a function of a for $T = 1\text{s}$, $\rho_{max} = 5$, $\rho_g = 0.2$, and Earthquake of 15s	68
3.20	Frame Ductility (ρ_f) as a function of a for $T = 1\text{s}$, $\rho_{max} = 5$, $\rho_g = 0.2$, and Earthquake of 60s	69
3.21	Normalized Base Shear as a function of a for $T = 0.1\text{s}$, $\rho_{max} = 5$, $\rho_g = 0.8$, and Earthquake of 15s	70
3.22	Normalized Base Shear as a function of a for $T = 0.1\text{s}$, $\rho_{max} = 5$, $\rho_g = 0.8$, and Earthquake of 60s	71
3.23	Normalized Base Shear as a function of a for $T = 1\text{s}$, $\rho_{max} = 5$, $\rho_g = 0.2$, and Earthquake of 15s	72
3.24	Normalized Base Shear as a function of a for $T = 1\text{s}$, $\rho_{max} = 5$, $\rho_g = 0.2$, and Earthquake of 60s	73
3.25	Bare Frame (BF) Response and Story Drift Limit of 2% ($u_{max} = 76\text{mm}$)	75
3.26	Bare Frame (BF) and Structural Fuse (SF) Response	76
3.27	Bare Frame (BF) and Structural Fuse (SF) Time Histories	77
3.28	Energy Dissipated	78

LIST OF ILLUSTRATIONS (cont'd)

SECTION	TITLE	PAGE
4.1	Bare Frame Properties	82
4.2	Buckling-restrained Braces Components	83
4.3	Frame and BRB Properties	84
4.4	Frame and T-ADAS Properties	87
4.5	Frame and SP Properties	89
4.6	Overstrength Factor, W_o , as a function of β and β_{max}	92
4.7	Procedure to Design Systems satisfying the Structural Fuse Concept	93
4.7	Procedure to Design Systems satisfying the Structural Fuse Concept (cont'd)	94
4.8	Procedure for the Sensitivity Analysis	107
4.8	Procedure for the Sensitivity Analysis (cont'd)	108
4.9	Response Modification Factor R , Ductility Factor R_d , and Overstrength Factor, β_o	114
4.10	Response Modification Factor, R , as a function of β and T	117
4.11	Ductility Factor, R_d , as a function of β , β_{max} , β_o , and T	118
5.1	Floor Acceleration of SDOF Systems with Metallic Fuses	127
5.2	Floor Velocity of SDOF Systems with Metallic Fuses	128
5.3	Floor Acceleration of Structural Fuse Systems and Bare Frames for $\beta = 0.2$	130
5.4	Floor Acceleration of Structural Fuse Systems and Bare Frames for $\beta = 0.4$	131
5.5	Floor Acceleration of Structural Fuse Systems and Bare Frames for $\beta = 0.6$	132
5.6	Floor Acceleration of Structural Fuse Systems and Bare Frames for $\beta = 1.0$	133
5.7	Floor Velocity of Structural Fuse Systems and Bare Frames for $\beta = 0.2$	135
5.8	Floor Velocity of Structural Fuse Systems and Bare Frames for $\beta = 0.4$	136
5.9	Floor Velocity of Structural Fuse Systems and Bare Frames for $\beta = 0.6$	137
5.10	Floor Velocity of Structural Fuse Systems and Bare Frames for $\beta = 1.0$	138
5.11	Ratio of the Peak Floor Acceleration of Structural Fuse Systems with respect of the Peak Floor Acceleration of Bare Frames	140
5.12	Ratio of the Peak Floor Velocity of Structural Fuse Systems with respect of the Peak Floor Velocity of Bare Frames	141
5.13	Floor Acceleration Spectra of Structural Fuse Systems and Bare Frames for $T = 0.25$ s, and $\beta = 0.6$	144

LIST OF ILLUSTRATIONS (cont'd)

SECTION	TITLE	PAGE
5.14	Floor Acceleration Spectra of Structural Fuse Systems and Bare Frames for $T = 0.50$ s, and $\beta = 0.4$	145
5.15	Floor Acceleration Spectra of Structural Fuse Systems and Bare Frames for $T = 1.0$ s, and $\beta = 0.2$	146
5.16	Floor Velocity Spectra of Structural Fuse Systems and Bare Frames for $T = 0.25$ s, and $\beta = 0.6$	149
5.17	Floor Velocity Spectra of Structural Fuse Systems and Bare Frames for $T = 0.50$ s, and $\beta = 0.4$	150
5.18	Floor Velocity Spectra of Structural Fuse Systems and Bare Frames for $T = 1.0$ s, and $\beta = 0.2$	151
5.19	Example of Floor Acceleration Response History of a SDOF System with Metallic Fuses	157
5.20	Equivalent Sine-Wave Floor Acceleration Response History of a SDOF System with Metallic Fuses	157
5.21	Actual Acceleration Response Spectra vs Sine-wave Acceleration Response Spectra for $T = 0.25$ s, and $\beta = 0.6$	159
5.22	Actual Acceleration Response Spectra vs Sine-wave Acceleration Response Spectra for $T = 0.5$ s, and $\beta = 0.4$	160
5.23	Actual Acceleration Response Spectra vs Sine-wave Acceleration Response Spectra for $T = 1.0$ s, and $\beta = 0.2$	161
5.24	Actual Velocity Response Spectra vs Sine-wave Velocity Response Spectra for $T = 0.25$ s, and $\beta = 0.6$	162
5.25	Actual Velocity Response Spectra vs Sine-wave Velocity Response Spectra for $T = 0.5$ s, and $\beta = 0.4$	163
5.26	Actual Velocity Response Spectra vs Sine-wave Velocity Response Spectra for $T = 1.0$ s, and $\beta = 0.2$	164
6.1	Hysteretic Damping vs Increase in Viscous Damping for $T = 0.25$ s	171
6.2	Hysteretic Damping vs Increase in Viscous Damping for $T = 0.50$ s	172
6.3	Hysteretic Damping vs Increase in Viscous Damping for $T = 1.50$ s	173
6.4	Ratio of Hysteretic Damping with Respect to Original Hysteretic Damping vs Increase in Viscous Damping for $T = 0.25$ s	175
6.5	Ratio of Hysteretic Damping with Respect to Original Hysteretic Damping vs Increase in Viscous Damping for $T = 0.50$ s	176
6.6	Ratio of Hysteretic Damping with Respect to Original Hysteretic Damping vs Increase in Viscous Damping for $T = 1.50$ s	177
6.7	Ratio of Total Damping with Respect to Original Damping vs Increase in Viscous Damping for $T = 0.25$ s	179
6.8	Ratio of Total Damping with Respect to Original Damping vs Increase in Viscous Damping for $T = 0.50$ s	180

LIST OF ILLUSTRATIONS (cont'd)

SECTION	TITLE	PAGE
6.9	Ratio of Total Damping with Respect to Original Damping vs Increase in Viscous Damping for $T = 1.50$ s	181
6.10	Ratio of Floor Spectral Acceleration with Respect to Original Floor Spectral Acceleration vs Increase in Viscous Damping for $T = 0.25$ s	183
6.11	Ratio of Floor Spectral Acceleration with Respect to Original Floor Spectral Acceleration vs Increase in Viscous Damping for $T = 0.50$ s	184
6.12	Ratio of Floor Spectral Acceleration with Respect to Original Floor Spectral Acceleration vs Increase in Viscous Damping for $T = 1.50$ s	185
6.13	Ratio of Floor Spectral Acceleration with Respect to Original Floor Spectral Acceleration vs Global Ductility for $T = 0.25$ s	187
6.14	Ratio of Floor Spectral Acceleration with Respect to Original Floor Spectral Acceleration vs Global Ductility for $T = 0.50$ s	188
6.15	Ratio of Floor Spectral Acceleration with Respect to Original Floor Spectral Acceleration vs Global Ductility for $T = 1.50$ s	189
6.16	Normalized Inertial and Hysteretic Loops for $T = 0.25$ s, $\zeta = 0.2$, and 5% of Viscous Damping	194
6.17	Normalized Inertial and Hysteretic Loops for $T = 0.25$ s, $\zeta = 0.2$, and 10% of Viscous Damping	195
6.18	Normalized Inertial and Hysteretic Loops for $T = 0.25$ s, $\zeta = 0.2$, and 20% of Viscous Damping	196
6.19	Normalized Inertial and Hysteretic Loops for $T = 0.25$ s, $\zeta = 0.2$, and 30% of Viscous Damping	197
6.20	Normalized Inertial and Hysteretic Loops for $T = 0.25$ s, $\zeta = 1.0$, and 5% of Viscous Damping	198
6.21	Normalized Inertial and Hysteretic Loops for $T = 0.25$ s, $\zeta = 1.0$, and 10% of Viscous Damping	199
6.22	Normalized Inertial and Hysteretic Loops for $T = 0.25$ s, $\zeta = 1.0$, and 20% of Viscous Damping	200
6.23	Normalized Inertial and Hysteretic Loops for $T = 0.25$ s, $\zeta = 1.0$, and 30% of Viscous Damping	201
6.24	Normalized Inertial and Hysteretic Loops for $T = 0.50$ s, $\zeta = 0.2$, and 5% of Viscous Damping	202
6.25	Normalized Inertial and Hysteretic Loops for $T = 0.50$ s, $\zeta = 0.2$, and 10% of Viscous Damping	203
6.26	Normalized Inertial and Hysteretic Loops for $T = 0.50$ s, $\zeta = 0.2$, and 20% of Viscous Damping	204
6.27	Normalized Inertial and Hysteretic Loops for $T = 0.50$ s, $\zeta = 0.2$, and 30% of Viscous Damping	205
6.28	Normalized Inertial and Hysteretic Loops for $T = 0.50$ s, $\zeta = 1.0$, and 5% of Viscous Damping	206

LIST OF ILLUSTRATIONS (cont'd)

SECTION	TITLE	PAGE
6.29	Normalized Inertial and Hysteretic Loops for $T = 0.50$ s, $\zeta = 1.0$, and 10% of Viscous Damping	207
6.30	Normalized Inertial and Hysteretic Loops for $T = 0.50$ s, $\zeta = 1.0$, and 20% of Viscous Damping	208
6.31	Normalized Inertial and Hysteretic Loops for $T = 0.50$ s, $\zeta = 1.0$, and 30% of Viscous Damping	209
6.32	Normalized Inertial and Hysteretic Loops for $T = 1.50$ s, $\zeta = 0.2$, and 5% of Viscous Damping	210
6.33	Normalized Inertial and Hysteretic Loops for $T = 1.50$ s, $\zeta = 0.2$, and 10% of Viscous Damping	211
6.34	Normalized Inertial and Hysteretic Loops for $T = 1.50$ s, $\zeta = 0.2$, and 20% of Viscous Damping	212
6.35	Normalized Inertial and Hysteretic Loops for $T = 1.50$ s, $\zeta = 0.2$, and 30% of Viscous Damping	213
6.36	Normalized Inertial and Hysteretic Loops for $T = 1.50$ s, $\zeta = 1.0$, and 5% of Viscous Damping	214
6.37	Normalized Inertial and Hysteretic Loops for $T = 1.50$ s, $\zeta = 1.0$, and 10% of Viscous Damping	215
6.38	Normalized Inertial and Hysteretic Loops for $T = 1.50$ s, $\zeta = 1.0$, and 20% of Viscous Damping	216
6.39	Normalized Inertial and Hysteretic Loops for $T = 1.50$ s, $\zeta = 1.0$, and 30% of Viscous Damping	217
6.40	Schematic Representation of Inertial, Viscous Damper and Hysteretic Forces	219
6.41	Complex Plane Representation of Inertial Force, F_i , Viscous Damper Force, F_d , and Hysteretic Force, F_s , for $T = 0.25$ s, $\zeta = 0.2$, and 5% of Viscous Damping	221
6.42	Complex Plane Representation of Inertial Force, F_i , Viscous Damper Force, F_d , and Hysteretic Force, F_s , for $T = 0.25$ s, $\zeta = 0.2$, and 10% of Viscous Damping	222
6.43	Complex Plane Representation of Inertial Force, F_i , Viscous Damper Force, F_d , and Hysteretic Force, F_s , for $T = 0.25$ s, $\zeta = 0.2$, and 20% of Viscous Damping	223
6.44	Complex Plane Representation of Inertial Force, F_i , Viscous Damper Force, F_d , and Hysteretic Force, F_s , for $T = 0.25$ s, $\zeta = 0.2$, and 30% of Viscous Damping	224
6.45	Complex Plane Representation of Inertial Force, F_i , Viscous Damper Force, F_d , and Hysteretic Force, F_s , for $T = 0.25$ s, $\zeta = 1.0$, and 5% of Viscous Damping	225

LIST OF ILLUSTRATIONS (cont'd)

SECTION	TITLE	PAGE
6.46	Complex Plane Representation of Inertial Force, F_i , Viscous Damper Force, F_d , and Hysteretic Force, F_s , for $T = 0.25$ s, = 1.0, and 10% of Viscous Damping	226
6.47	Complex Plane Representation of Inertial Force, F_i , Viscous Damper Force, F_d , and Hysteretic Force, F_s , for $T = 0.25$ s, = 1.0, and 20% of Viscous Damping	227
6.48	Complex Plane Representation of Inertial Force, F_i , Viscous Damper Force, F_d , and Hysteretic Force, F_s , for $T = 0.25$ s, = 1.0, and 30% of Viscous Damping	228
6.49	Complex Plane Representation of Inertial Force, F_i , Viscous Damper Force, F_d , and Hysteretic Force, F_s , for $T = 0.50$ s, = 0.2, and 5% of Viscous Damping	229
6.50	Complex Plane Representation of Inertial Force, F_i , Viscous Damper Force, F_d , and Hysteretic Force, F_s , for $T = 0.50$ s, = 0.2, and 10% of Viscous Damping	230
6.51	Complex Plane Representation of Inertial Force, F_i , Viscous Damper Force, F_d , and Hysteretic Force, F_s , for $T = 0.50$ s, = 0.2, and 20% of Viscous Damping	231
6.52	Complex Plane Representation of Inertial Force, F_i , Viscous Damper Force, F_d , and Hysteretic Force, F_s , for $T = 0.50$ s, = 0.2, and 30% of Viscous Damping	232
6.53	Complex Plane Representation of Inertial Force, F_i , Viscous Damper Force, F_d , and Hysteretic Force, F_s , for $T = 0.50$ s, = 1.0, and 5% of Viscous Damping	233
6.54	Complex Plane Representation of Inertial Force, F_i , Viscous Damper Force, F_d , and Hysteretic Force, F_s , for $T = 0.50$ s, = 1.0, and 10% of Viscous Damping	234
6.55	Complex Plane Representation of Inertial Force, F_i , Viscous Damper Force, F_d , and Hysteretic Force, F_s , for $T = 0.50$ s, = 1.0, and 20% of Viscous Damping	235
6.56	Complex Plane Representation of Inertial Force, F_i , Viscous Damper Force, F_d , and Hysteretic Force, F_s , for $T = 0.50$ s, = 1.0, and 30% of Viscous Damping	236
6.57	Complex Plane Representation of Inertial Force, F_i , Viscous Damper Force, F_d , and Hysteretic Force, F_s , for $T = 1.50$ s, = 0.2, and 5% of Viscous Damping	237
6.58	Complex Plane Representation of Inertial Force, F_i , Viscous Damper Force, F_d , and Hysteretic Force, F_s , for $T = 1.50$ s, = 0.2, and 10% of Viscous Damping	238

LIST OF ILLUSTRATIONS (cont'd)

SECTION	TITLE	PAGE
6.59	Complex Plane Representation of Inertial Force, F_i , Viscous Damper Force, F_d , and Hysteretic Force, F_s , for $T = 1.50$ s, $\zeta = 0.2$, and 20% of Viscous Damping	239
6.60	Complex Plane Representation of Inertial Force, F_i , Viscous Damper Force, F_d , and Hysteretic Force, F_s , for $T = 1.50$ s, $\zeta = 0.2$, and 30% of Viscous Damping	240
6.61	Complex Plane Representation of Inertial Force, F_i , Viscous Damper Force, F_d , and Hysteretic Force, F_s , for $T = 1.50$ s, $\zeta = 1.0$, and 5% of Viscous Damping	241
6.62	Complex Plane Representation of Inertial Force, F_i , Viscous Damper Force, F_d , and Hysteretic Force, F_s , for $T = 1.50$ s, $\zeta = 1.0$, and 10% of Viscous Damping	242
6.63	Complex Plane Representation of Inertial Force, F_i , Viscous Damper Force, F_d , and Hysteretic Force, F_s , for $T = 1.50$ s, $\zeta = 1.0$, and 20% of Viscous Damping	243
6.64	Complex Plane Representation of Inertial Force, F_i , Viscous Damper Force, F_d , and Hysteretic Force, F_s , for $T = 1.50$ s, $\zeta = 1.0$, and 30% of Viscous Damping	244
6.65	Increase in the Inertial Force between a System with 5% and a System with 30% of Viscous Damping, for $T = 0.25$ s and $\zeta = 0.2$	245
6.66	Increase in the Inertial Force between a System with 5% and a System with 30% of Viscous Damping, for $T = 0.25$ s and $\zeta = 1.0$	246
6.67	Increase in the Inertial Force between a System with 5% and a System with 30% of Viscous Damping, for $T = 0.50$ s and $\zeta = 0.2$	247
6.68	Increase in the Inertial Force between a System with 5% and a System with 30% of Viscous Damping, for $T = 0.50$ s and $\zeta = 1.0$	248
6.69	Increase in the Inertial Force between a System with 5% and a System with 30% of Viscous Damping, for $T = 1.50$ s and $\zeta = 0.2$	249
6.70	Increase in the Inertial Force between a System with 5% and a System with 30% of Viscous Damping, for $T = 1.50$ s and $\zeta = 1.0$	250
7.1	Elevation of MCEER Demonstration Hospital Transverse Frame	254
7.2	Mode Shapes; (a) All Studied Cases, (b) Comparison of Mode Shapes determined from different Methods	256
7.3	Pushover Curves of MODF Systems Designed with BRB	265
7.4	Pushover Curves of MODF Systems Designed with T-ADAS	266
7.5	Pushover Curves of MODF Systems Designed with SP	267
7.6	First Story Shear vs Drift of MDOF Systems Designed with BRB	272
7.7	Second Story Shear vs Drift of MDOF Systems Designed with BRB	273
7.8	Third Story Shear vs Drift of MDOF Systems Designed with BRB	274

LIST OF ILLUSTRATIONS (cont'd)

SECTION	TITLE	PAGE
7.9	Fourth Story Shear vs Drift of MDOF Systems Designed with BRB	275
7.10	First Story Shear vs Drift of MDOF Systems Designed with T-ADAS	276
7.11	Second Story Shear vs Drift of MDOF Systems Designed with T-ADAS	277
7.12	Third Story Shear vs Drift of MDOF Systems Designed with T-ADAS	278
7.13	Fourth Story Shear vs Drift of MDOF Systems Designed with T-ADAS	279
7.14	First Story Shear vs Drift of MDOF Systems Designed with SP	280
7.15	Second Story Shear vs Drift of MDOF Systems Designed with SP	281
7.16	Third Story Shear vs Drift of MDOF Systems Designed with SP	282
7.17	Fourth Story Shear vs Drift of MDOF Systems Designed with SP	283
7.18	Energy of MDOF Systems Designed with BRB	284
7.19	Energy of MDOF Systems Designed with T-ADAS	285
7.20	Energy of MDOF Systems Designed with SP	286
7.21	Pushover Curves of MDOF Systems Retrofitted with Structural Fuses	291
7.22	First Story Shear vs Drift of MDOF Systems Retrofitted with Structural Fuses	292
7.23	Second Story Shear vs Drift of MDOF Systems Retrofitted with Structural Fuses	293
7.24	Third Story Shear vs Drift of MDOF Systems Retrofitted with Structural Fuses	294
7.25	Fourth Story Shear vs Drift of MDOF Systems Retrofitted with Structural Fuses	295
7.26	Energy of MDOF Systems Retrofitted with Structural Fuses	296
B.1	Behavior of Bilinear Hysteretic System with Yielding Damping Devices (Ramirez et al., 2000)	326

LIST OF TABLES

SECTION	TITLE	PAGE
3.1	Frame Ductility, μ_f and Hysteretic Energy	63
4.1	Recommended Values to Satisfy the Structural Fuse Concept	95
4.2	Influence of BRB Properties over Non-dimensional Variables	102
4.3	Influence of BRB Non-dimensional Variables over Target Parameters	102
4.4	Influence of T-ADAS Properties over Non-dimensional Variables	103
4.5	Influence of T-ADAS Non-dimensional Variables over Target Parameters	104
4.6	Influence of SP Properties over Non-dimensional Variables	105
4.7	Influence of SP Non-dimensional Variables over Target Parameters	106
4.8	Design of BRB Systems	110
4.9	Design of T-ADAS Systems	111
4.10	Design of SP Systems	112
4.11	Retrofit Examples using Metallic Fuse Systems for $\beta \leq 0.151$, $T \leq 0.53$ s (limits)	121
5.1	Approximately Critical Period, T_c , for Acceleration using the Average Equation	147
5.2	Approximately Critical Period, T_c , for Velocity using the Average Equation	148
5.3	Approximately Critical Period, T_c , for Acceleration using Regression Analysis	153
5.4	Approximately Critical Period, T_c , for Velocity using Regression Analysis	154
5.5	Ratio of Effective Peak Floor Acceleration with respect to Spectral Acceleration	156
7.1	Design of MDOF Systems with BRB	261
7.2	Design of MDOF Systems with T-ADAS	262
7.3	Design of MDOF Systems with SP	263
7.4	Design Parameters of MDOF Systems with BRB	268
7.5	Seismic Response of MDOF Systems with BRB	268
7.6	Design Parameters of MDOF Systems with T-ADAS	269
7.7	Seismic Response of MDOF Systems with T-ADAS	269
7.8	Design Parameters of MDOF Systems with SP	270
7.9	Seismic Response of MDOF Systems with SP	270
7.10	MDOF Systems Retrofitted with Structural Fuses	289
7.11	Design Parameters of MDOF Systems Retrofitted with Structural Fuses	290
7.12	Seismic Response of MDOF Systems Retrofitted with Structural Fuses	290

SECTION 1

INTRODUCTION

Passive energy dissipation (PED) devices have been implemented in recent years to enhance structural performance by reducing seismically induced structural damage (and, indirectly to some extent, non-structural damage). Soong and Spencer (2002) reported that, in the last 16 years, more than one hundred buildings in North America have been either retrofitted or built using PED devices. In the meantime, Japan has employed these structural protective systems in hundreds of buildings.

PED metallic dampers (a.k.a. hysteretic dampers) dissipate energy via inelastic deformations. Since their response is not sensitive to the frequency of loading, they are also called rate-independent dampers, or displacement-dependent dampers. The amount of damping they provide is somewhat proportional to the magnitude of their inelastic deformations. Although they also increase the stiffness of the primary structure to some degree, the possible increase in input energy due to the added stiffness is dissipated as part of the total hysteretic behavior of properly designed dampers, resulting in a net reduction on the response of the structural system in terms of lateral displacements, compared to response of the system without dampers. Accelerations and lateral forces are either increased or reduced depending on the ground motion and system features.

Metallic dampers are defined here to be structural fuses when they are designed such that all damage is concentrated on the PED devices, allowing the primary structure to remain elastic. Many benefices ensue from the structural fuse concept. For instance, following a damaging earthquake only the dampers would need to be replaced (hence the “fuse” analogy), making repair works easier and more expedient, without the need to shore the

building in the process. Furthermore, in that instance, self-recentering capabilities of the structure is possible in that, once the ductile fuse devices are removed, the elastic structure returns to its original position.

Many aspects regarding the structural fuse concept are considered in this study, which consists of seven sections briefly described as follows.

Section 2 presents a literature review of the state-of-the-art of the structural fuse concept. Some previous studies in this field are presented not only as structural fuses, but also as damage controlled or damage tolerant systems, and PED devices.

The structural fuse concept is described in Section 3 in a parametric formulation, considering the behavior of nonlinear single degree of freedom (SDOF) systems subjected to ground motions. Results are presented in dimensionless charts, that show as shaded areas the regions of admissible solutions that satisfy the structural fuse concept. Effects of earthquake duration and stiffness ratio are also investigated.

Section 4 uses the results from the dimensionless charts to analyze the response of actual systems either designed or retrofitted with various types of metallic dampers working as structural fuses. A general design procedure is provided, and some examples of application are presented for new construction designs, and for retrofitting of existing structures.

The floor demands of SDOF systems designed or retrofitted with metallic structural fuses are studied in Section 5. Floor velocity and acceleration are obtained and comparisons are made between the floor response of bare frames and the floor response of systems with metallic fuses. Furthermore, velocity and acceleration spectra are developed from the floor time history responses to assess how the behavior of nonstructural components may be influenced by the use of metallic fuses.

In Section 6 the use of viscous dampers acting in parallel with metallic dampers is analyzed as an alternative to reduce floor demands in terms of acceleration. Parametric analyses are conducted and hysteretic damping and spectral acceleration results are presented for short, intermediate, and long period structures. Furthermore, response is also investigated in the frequency domain, and resulting inertial force, viscous damper force, and hysteretic damper force are plotted on Argand diagrams to explain trends in behavior for these systems.

Results from Sections 3 and 4 are used in Section 7 to extend the structural fuse concept to multi degree of freedom systems. The design and retrofit procedures listed in Section 4 are modified to be applicable to multi story buildings. Examples are presented for new construction designs, and for retrofitting of existing multi story structures.

SECTION 2

LITERATURE REVIEW

2.1. Introduction

There have been important advances during the last decades in the knowledge and application of concepts that approach the structural fuse concept presented here, or that used the definition of structural fuse in a somewhat different manner. Some of the relevant research on this topic is presented in this section. Section 2.2 describes different criteria proposed by others to define structural fuse concepts and achieve damage-controlled or damage-tolerant structures. Descriptions of the metallic energy dissipation devices used in this study are then presented in Section 2.3, with emphasis on the seismic behavior of systems designed or retrofitted using Buckling-Restrained Brace (BRB), Triangular Added Damping and Stiffness (T-ADAS), Shear Panel (SP), and Friction Dampers (FD) working as elements engaged to protect the main structure.

2.2. Structural Fuse Concept

About seventy years ago seismic effects on buildings started to be modeled as static loads calculated as percentages of the structure weight and applied horizontally on the structure. Later, as a consequence of the better understanding of structural seismic response brought upon by the development of structural dynamic concepts and observations following earthquakes, the need to rely on ductile design to ensure satisfactory response was recognized, and expressed by the inelastic design approach. In this procedure the seismic loads are reduced by a response modification factor, R , which is related to the structure's

ability to undergo inelastic deformations and dissipate energy through hysteretic behavior. However, this methodology relies on the ability of the structural elements to accommodate inelastic deformations, without compromising the stability of the structure. Furthermore, inelastic behavior translates into some level of damage on these elements, and permanent system deformations following an earthquake, leading to high cost for repair works, in the cases when repairs are possible. In fact, it is frequently the case following earthquakes that damage is so large that repairs are not viable, even though the structure has not collapsed, and the building must be demolished.

To achieve stringent seismic performance objective for buildings, an alternative design approach is desirable. In that perspective, it would be attractive to concentrate damage on disposable and easy to repair structural elements (i.e., “structural fuse”), while the main structure would be designed to remain elastic (or sustain only minor inelastic deformations). The term “structural fuse” and “ductile fuse” have been used in the past, but often in slightly different contexts, as described below.

Roeder and Popov (1977) introduced the eccentrically braced frame concept to increase the hysteretic energy capacity, strength, and stiffness of steel frames. The segment of the beam yielding in shear due to action of the eccentrically connected braces was called a link as well as a “ductile fuse” by Roeder and Popov, because of its energy dissipation capability. While this system has a good seismic behavior, combining the stiffness of a braced structure with the energy dissipation of a moment-resistant frame, the link is a segment of the beam and cannot be considered a disposable element, because repairs required following an earthquake can be significant. Beyond issues related to link replacement, note that the large plastic deformations of the link can also damage the floor slab or other elements.

Fintel and Ghosh (1981) used the term “structural fuse” in a capacity design concept where beams were intentionally designed as weaker members that yield by plastic hinging, to protect columns and walls considered more crucial for the structure and

expected to remain elastic under seismic loads. The weaker elements were called “structural fuses.” However, as in the work done by Roeder and Popov (1977), these beams cannot be considered to be disposable elements.

Note that many other researchers have used the term “structural fuse” in the same perspective (e.g., Aristizabal-Ochoa, 1986, Basha and Goel, 1996, Carter and Iwankiw, 1998, Sugiyama, 1998, and Rezai et al. 2000, to name a few).

The concept of “damage-controlled” structures or “damage-tolerant” structures was proposed by Wada et al. (1992). This design approach has two separate components. One is the main structure (composed of beams and columns) designed to resist only gravity loads, and the other part consists of passive energy dissipation elements designed to resist the loads resulting from strong ground motions, as shown in Figure 2.1 (Wada et al. 1992). This concept has been continuously developed and further improved following the 1994 Northridge (USA) and 1995 Hyogoken-Nanbu (Japan) earthquakes (e.g., Connor et al. 1997, Shimizu et al. 1998, Wada and Huang, 1999, Huang et al. 2002). Because of the high cost encountered to repair conventionally designed structures damaged by these earthquakes, the idea of using disposable and easy to replace elements to dissipate energy became attractive. Figure 2.2, from Connor et al. (1997), schematically shows the relation between repair cost and earthquake intensity for conventional and damage-controlled structures. Damage-controlled structures were deemed more efficient (in terms of cost reduction) for larger earthquakes.

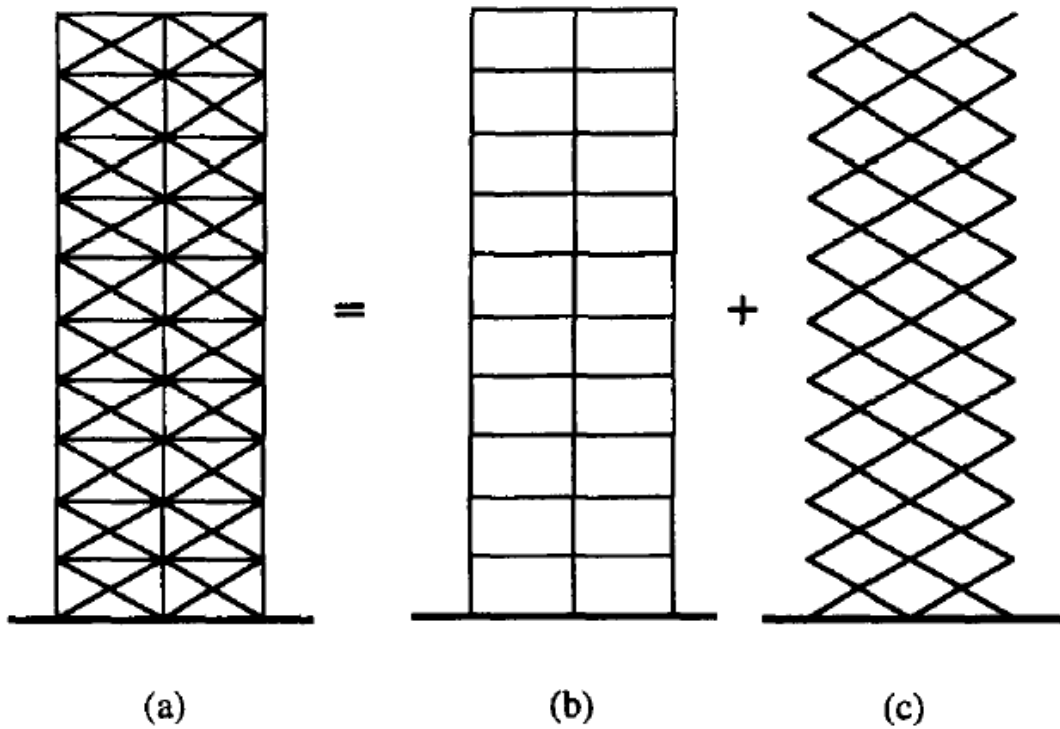


Figure 2.1. Damage-Tolerant Structure: (a) Total Structure; (b) Gravity Support Structure (to remain elastic); (c) Seismic-Resistant Structure (to behave elastic-plastic) (Wada et al., 1992)

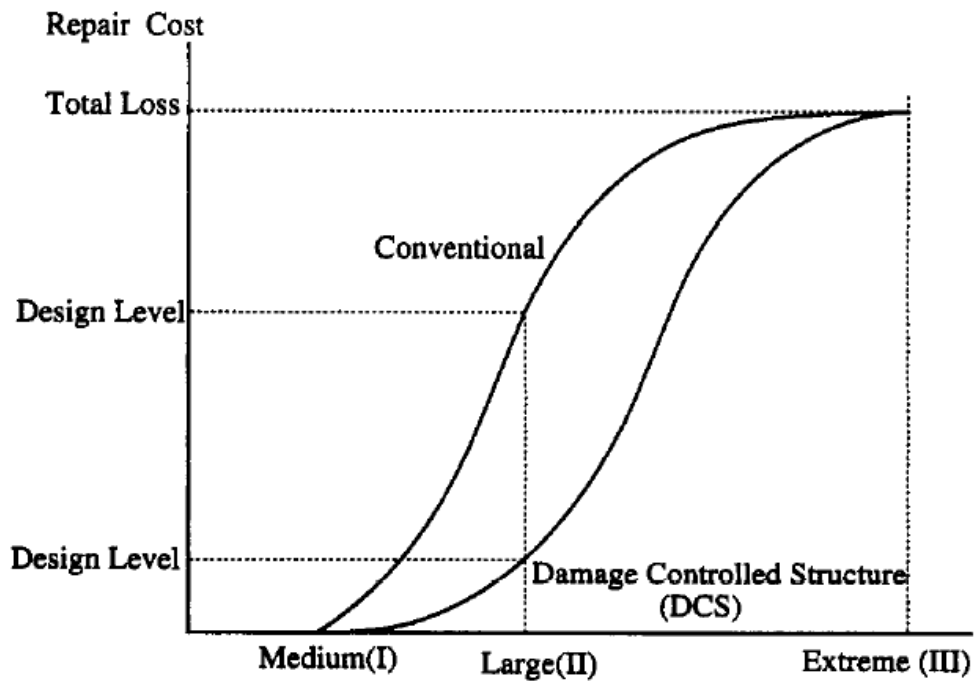


Figure 2.2. Repair Cost versus Earthquake Intensity (Connor et al., 1997)

Note that Wada et al. (1992) concluded that by using high strength steel for the main structure, and steel with low yield strength and high ductility for hysteretic dampers, a significant separation could be obtained between story drifts corresponding to the yield deformations of the devices and of the main structure. An example 40-story building designed using buckling-restrained braces as the damage-tolerant elements was presented. A sub frame model corresponding to a part of this building was experimentally studied, and corroborated the advantage of using the combination of high and low strength steels. It is worthwhile to mention that this building was designed intending that the main structure would remain elastic during earthquakes, and able to continue working once the damaged plastic dampers are replaced.

An approach based on balance of energy has been implemented by Wada and Huang (1995) to preliminarily design tall building structures, having either hysteretic dampers or viscous dampers. However, focus of the study was not to assess adequacy of the structural fuse concept, but rather to use such buildings as case studies to validate the energy balance approach, as well as a proposed flexural-shear beam model for the dynamic response analysis. It was observed in these tall buildings case studies that beams and columns remained elastic, and the whole seismic energy was dissipated by dampers.

A comprehensive study of damage-controlled structures in Japan was presented by Wada et al. (2000). This paper presents some research works done before on the development of the damage-controlled structure concept, and its potential to design new constructions and to retrofit existing structures. Some modifications to the flexural-shear beam model were also presented, as well as a dynamic analysis method for three-dimensional frames with elements used to achieve the damage-controlled structure concept. As part of this study, a series of moment resisting frames with and without buckling-restrained braces working as structural fuses were tested. These experiments contributed to validate the concept of damage-controlled structures, in the sense that the buckling-restrained braces served to absorb large amounts of energy through hysteretic behavior, and to protect beams and columns from yielding. Actual projects of application of the structural fuse

concept in tall buildings were also presented, along with the observation that the number of structures in Japan designed based on the damage-controlled concept was increasing.

In the above studies by Wada et al. (1992 and 1995), as well as in some other case studies (e.g., Shimizu et al. 1998), the main structure was designed to remain elastic, with damage concentrated in disposable elements. However, these design examples focused on tall buildings (i.e., structures with height greater than 100 m, and elastic period longer than 4 s). As a result, these flexible systems are subjected to smaller seismic loads than corresponding stiffer structures, and the structural fuses are used to reduce lateral displacements already subject to limited ductility demands in absence of the fuse. The amount of energy dissipated through inelastic behavior was reported to depend on the structural fuses relative contribution to resist lateral forces.

Structural fuse, damage-controlled, and damage tolerant concepts have been also implemented with the primary purpose of reducing the level of yielding in the main system. For example, Sugiyama (1998) presented a case study corresponding to a 26-story building (98m height) provided with Steel Slit Dampers (SSD). These metallic dampers were designed to reduce the fundamental period of the building from 2.46s to 1.85s in the weak direction, thus simultaneously reducing lateral displacements. As observed in Figure 2.3 (Sugiyama, 1998), the frame response (in terms of energy dissipated) was reduced, but not eliminated.

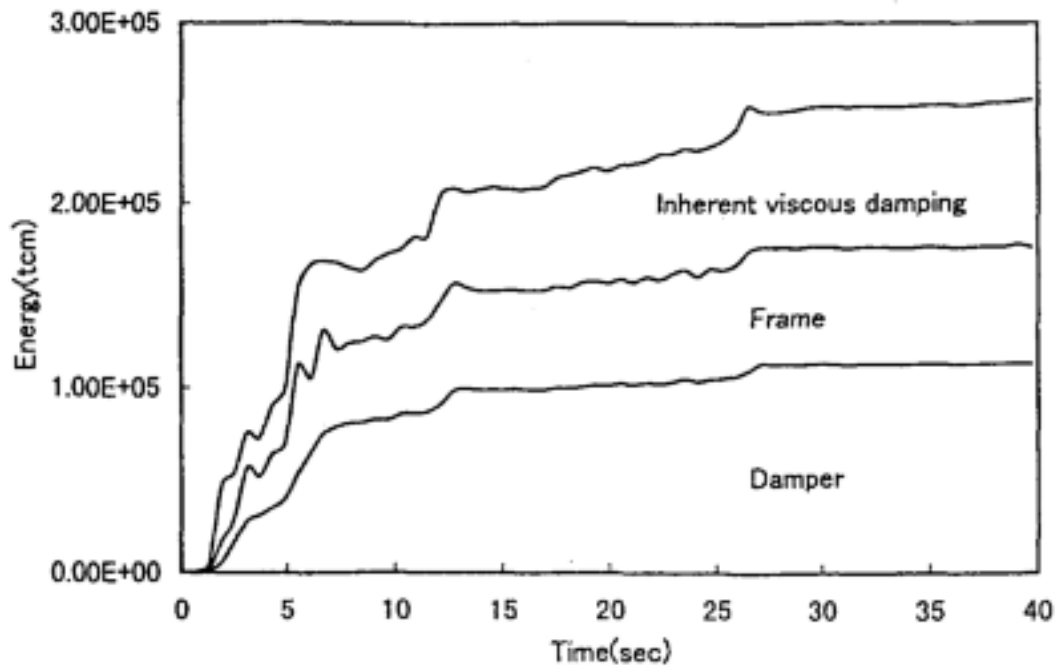


Figure 2.3. Energy Response to the El Centro earthquake scaled to peak ground velocity of 50 cm/s) (Sugiyama, 1998)

Friction dampers (Section 2.3.4) have also been proposed to serve as structural fuses, although never defined as such in the existing literature. Filiatrault and Cherry (1989) were the first to propose a design procedure for such systems. More recently, an equivalent linearization method was proposed by Fu and Cherry (2000) to design friction-damped structures. A trilinear pushover curve was used to model the seismic mechanism of SDOF friction-damped systems. Parametric analyses were performed, and the results led to the formulation of closed-form solutions to define the force modification factor for friction-damped structures. A six-story building was designed as an example of the proposed procedure, and the results were validated through nonlinear time history analyses. It was found that the seismic behavior of friction-damped systems depends basically on the damper slip force, the frame yield displacement, and the stiffness of the damping system. For design purposes, the authors recommended to have a damping system stiffness 4 to 10 times bigger than the frame stiffness, a response modification factor between 4 and 8, and a frame ductility between 1 to 1.5. However, in all cases,

nonlinear inelastic time history analyses are needed to verify that the resulting designs perform as intended.

In summary, the structural fuse concept has not been consistently defined in the past. In some cases, “fuses” have been defined as elements with well defined plastic yielding locations, but not truly replaceable as a fuse; in other cases, they were defined and used more in the context of reducing inelastic deformations of the existing frame (damage control). In a few cases, for high rise buildings having long structural periods (i.e., $T > 4$ s), fuses were used to achieve elastic response of frames that would otherwise develop limited inelastic deformations. Design procedures were also developed for systems with friction dampers intended to act as structural fuses, but these required design validation by nonlinear time history analyses. In that perspective, knowledge on how to achieve and implement a structural fuse concept that would limit damage to disposable structural elements for any general structure, and without the need for complex analyses is lacking. This would require identification of the key parameters that govern the behavior of systems having such structural fuses, and formulation of a general design approach that would make the concept broadly applicable, including for low rise buildings (e.g., single-degree-of-freedom systems). Furthermore, the research reported above did not investigate the impact of introducing structural fuses on resulting floor accelerations and velocities (which has an impact on seismic performance of non-structural components and building contents).

2.3. Metallic Energy Dissipation Devices

The subsequent sections describe previous works conducted to characterize the behavior of BRB, T-ADAS, SP, and FD systems working as metallic hysteretic dampers. A brief discussion of the most relevant studies that have served to support this current investigation is presented, focusing mainly on experimental investigations that have

corroborated the inherent capacity of these elements to protect structural systems from the action of strong ground motions.

2.3.1. Buckling-Restrained Brace (BRB)

This type of metallic device was initially developed in Japan by Nippon Steel Corporation in the mid-1980s with the name of unbonded braces (UBs). In North-America, UBs have also been called Buckling-Restrained Braces (BRBs), because they are essentially braces capable of yielding under compression loads, without braces buckling.

A BRB consists of a central core, usually of rectangular or cruciform cross sectional shape, surrounded by a tube having a global buckling strength greater than that required to axially yield the core. The space between the core and the tube is filled with mortar, and the core is covered with an unbonding material in order to keep it isolated and able to deform freely in the axial direction, i.e., to avoid transmission of loads between the core and mortar. The material used to de-bond the core from the mortar should be thin enough to avoid local buckling of the core, and yet thick enough to accommodate lateral expansion of the core due to Poisson's effects. Figure 2.4, from Sabelli et al. (2003), shows the components of a typical BRB and some detailed configurations.

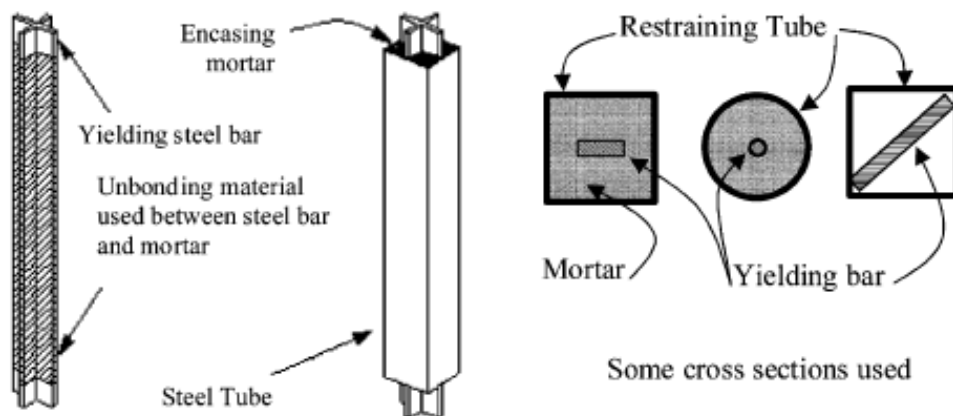


Figure 2.4. Some Schematic Details used for Buckling Restrained Braces (Sabelli et al., 2003)

Investigations on BRBs have been extensively conducted in Japan over the last 15 years. Watanabe et al. (1988) presented a summary of some of the early development of BRBs. The system has been well received by Japanese designers after the 1995 Kobe Earthquake. Other relevant developments in Japan have been presented by Saeki et al. (1996), which makes a comparison between analytical studies and experimental results. BRB behavior was modeled by finite elements considering material and geometric non-linearities (Saeki et al., 1996). Good agreement was found between the analytical and experimental results, although some minor discrepancies were noticed. Some of them were attributed to Bauschinger's effect, and local fracture of the mortar, which were not considered in the model.

An important experimental study (Iwata et al. 2000) evaluated the performance of BRBs used as hysteretic dampers. Four BRB specimens were designed having different buckling-restraining methods, and were tested to study the influence of these different restraining approaches on cyclic inelastic behavior. It was found that BRBs having the core completely restrained by grout and unbonding material had a more stable hysteretic behavior than those with cores not continuously restrained.

In North-America, BRBs have also been studied and implemented since the late 1990's. Aiken et al. (1999) presented a comprehensive study of BRBs in the United States context, and a design case-study for a multi-story steel structure having BRBs working as hysteretic dampers, although the proposed design method considered them as yielding braces. A series of test on large-scale models were also conducted using large inelastic cycles of loading, and to simulate near field loading history. Details on the first building application of BRBs in the United States (the University of California at Davis Plant and Environmental Sciences project) was also presented. It was found that BRBs are able to sustain stable cycles of hysteretic behavior even under large levels of displacements. Furthermore, experiments showed that these elements have high resistance to fracture, even after severe loads, while their force-displacement behavior is still stable.

Sabelli et al. (2003) analytically studied the seismic applications of BRB members. Implementation of BRBs was found to be an effective way to overcome the problems associated with concentrically braced special frames. Further research was recommended to thoroughly assess the characteristics and capacity of BRB, including experimental work to study bending and shear forces acting on actual BRBs and connections.

2.3.2. Triangular Added Damping and Stiffness (T-ADAS)

The T-ADAS damper is composed of triangular plates which when subjected to flexure achieve uniform yielding over their entire height to dissipate seismic energy (a variation, the ADAS damper, instead uses X-shape plate elements). The plates in T-ADAS dampers are bent in singular curvature because they are connected to a device support system through vertically slotted holes that prevent application of moments to the plates at that location (for comparison, double triangular plates in double curvature are used in the ADAS system). According to Tsai et al (1993), this pinned connection also avoids the transmission of vertical loads associated with gravity loads to the plates. Therefore, the plates are not susceptible to instabilities caused by P- effects. Furthermore, the device support system does not need to provide flexural resistance because it only resists the shear force applied at the tip of the cantilever plates. Figure 2.5, from Tsai et al. (1993), shows a detailed configuration of a T-ADAS system, and the details of the pinned connection.

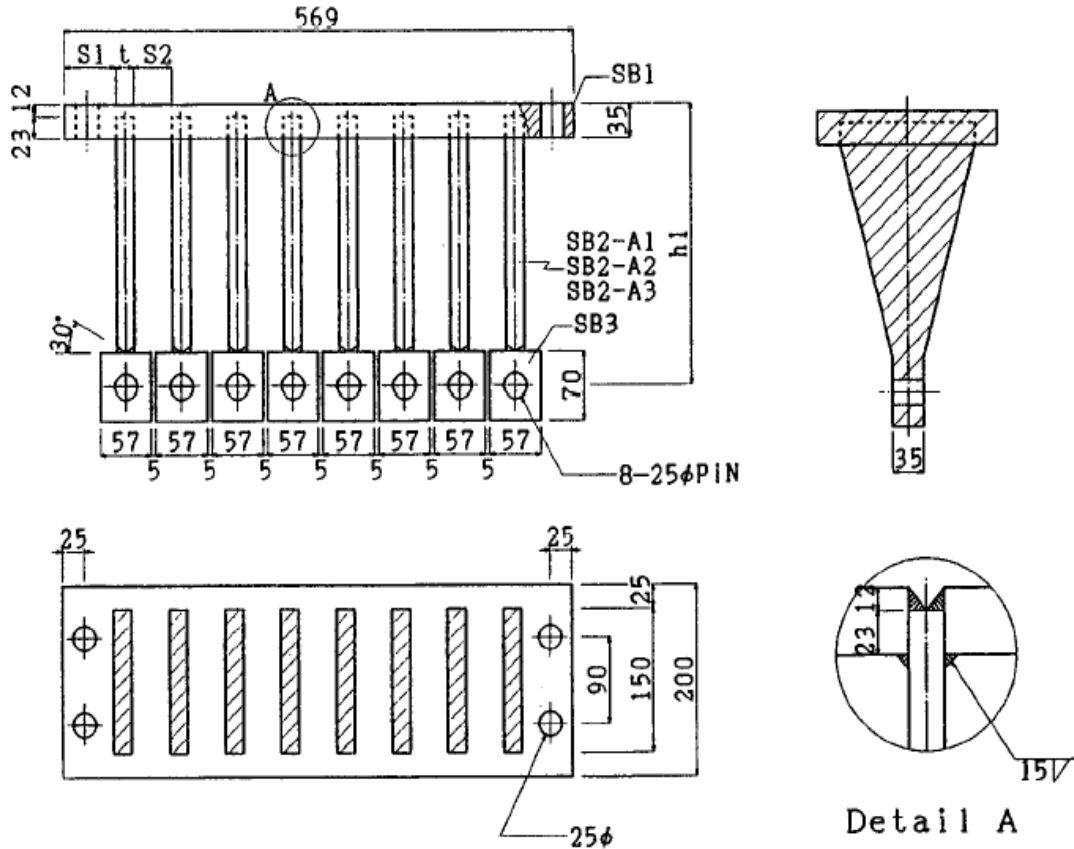


Figure 2.5. Details of Steel Welded T-ADAS Device (Tsai et al., 1993)

A design procedure for T-ADAS systems was proposed by Tsai et al. (1993). It was experimentally shown that T-ADAS systems can sustain a large number of yielding cycles without stiffness or strength degradation. Tsai et al. (1993) described the mechanical properties of the T-ADAS devices, and compared their analytical characteristics with experimental results obtained from pseudo-dynamic tests of two-story T-ADAS frame. In this study, the design procedure was based on the stiffness ratio (i.e., the ratio of the damping system and the bare frame stiffnesses), and the strength ratio of the dampers (i.e., the ratio of the total system strength corresponding to the frame yield deformation and the strength corresponding to the T-ADAS yield deformation). It was also found that the plastic rotational capacity of a T-ADAS system could exceed 0.25 radians. For a frame having a T-ADAS height equal to 10% of the story height ($h/H = 0.10$), this rotational capacity corresponds to a story drift of 2.5%, which is

sufficient to accommodate displacements less than the allowable story drift generally recommended by design codes (i.e., $\delta_a = 0.02 H$).

Dargush and Soong (1995) developed a nonlinear macroscopic model to describe the behavior of metallic plate dampers. These analytic formulations were compared with experimental results obtained previously by others. The proposed mathematical model is able to predict the experimentally observed stiffening of T-ADAS at large levels of displacements. Dargush and Soong also recommended more exhaustive experimental works, as well as development of three-dimensional finite element models to eliminate some of their assumptions and obtain more precise results.

Tena-Colunga (1997) also presented a mathematical model of the ADAS systems which accounts for the variation of cross-sectional area through flexibility methods. A comparison was made between the proposed model and the method used by Whittaker et al. (1989), which uses a simple procedure to define the load-deflection behavior considering the plates as rigidly connected at the ends, with perfect double curvature deformation. Analytical results were also compared with some experimental data. The proposed method was found useful to preliminary design and retrofit structures using ADAS systems, even though some small discrepancies were found between experimental and analytical results. These divergences in the results were attributed to the fact that, in actual systems, is almost impossible to obtain a perfectly fixed connection of the plates at the bottom flange of the beam. Additionally, the effects of axial forces (associated with gravity loads) on the general behavior were found to be difficult to account for in the proposed mathematical model.

2.3.3. Shear Panel (SP)

The shear panel, like the T-ADAS, is a yielding metallic device mounted on a device support system and connected to the bottom flange of a frame beam. The SP damper itself is a plate placed in a vertical plane oriented with the frame in such a way that plate

shear yielding is the mode of energy dissipation. Figures 2.6 and 2.7, from Nakashima (1995a) show a SP configuration used in a prototype building, and a detailed specimen tested as part of the investigation.

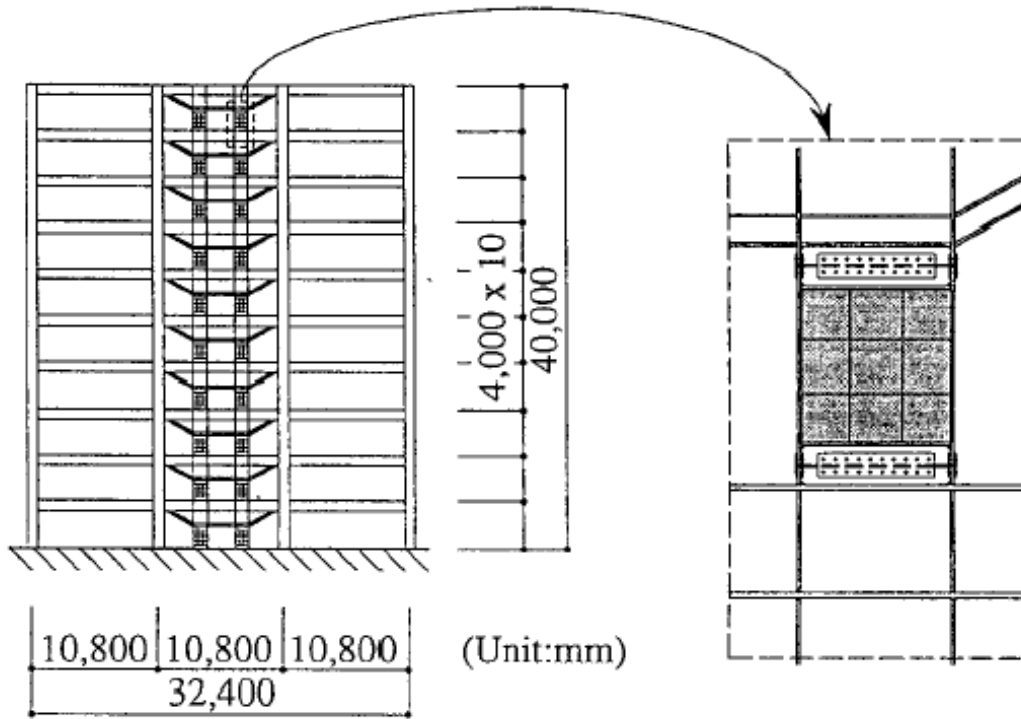


Figure 2.6. Prototype Building Including Shear Panels with Low-Yield Steel (Nakashima, 1995a)

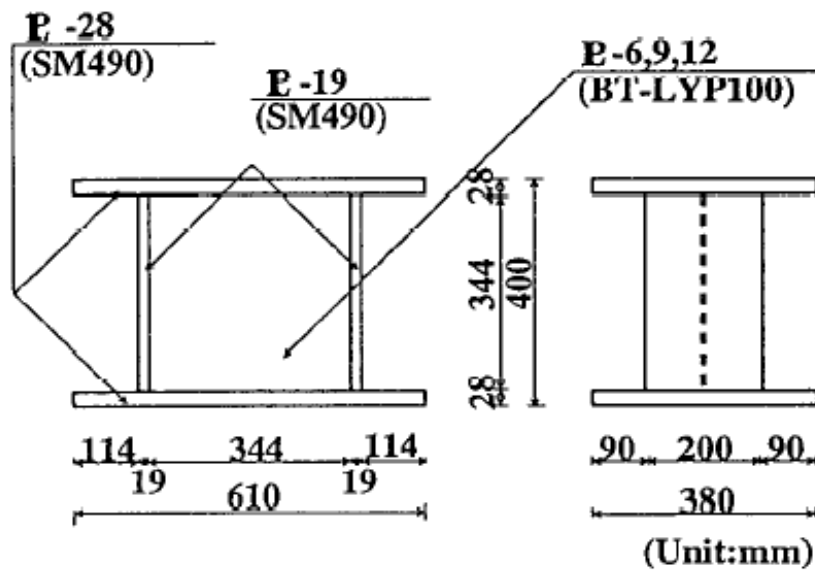


Figure 2.7. Shear Panels Details and Dimensions of Test Specimens (Nakashima, 1995b)

Many studies, conducted mainly in Japan, investigated the seismic performance of structures having SP dampers. Nakashima (1995b) investigated the hysteretic behavior of SPs made of low-yield steel. Two models were proposed in this study. One relies on a multi-surface model to simulate the hysteretic behavior, and the other consists of a simpler model based on bilinear behavior. Both analytical models were found to be in good agreement with experimental results of SP systems having variable loading conditions and width-to-thickness ratio. It was also found that the models were able to accurately predict strain-hardening behavior and stiffness degradation of the dampers.

Miyama et al. (1996) used SP plates made of low-yield point steel. Two parameters useful to design SP systems were introduced as part of this work. One is the stiffness ratio of the SP systems with respect to the frame, and the other is the yield strength ratio of the SP systems with respect to the design shear strength of the structure. The stiffness parameter is associated with the initial yield deformation, and the strength parameter is associated with the absorbed energy. This paper concluded that SP systems are able to dissipate a significant amount of hysteretic energy even after the panel buckles (i.e., post-buckling capacity).

Application of SP systems to a 21-story building was presented by Tanaka et al. (1998). Panels of 400mm x 700mm x 6mm of low-yield steel were implemented using two types of arrangements, called the pillar and the bracing type, respectively. In the pillar type, the support system is made of a tapered H-shaped section, while in the bracing type the damping support system is provided by braces. Capacity of both types of systems must be checked to avoid premature failures of the damping support members before yielding forces of the SP dampers are reached. Figure 2.8, from Tanaka et al. (1998) shows schematically these two configurations. It was found that savings of about 5% on the total amount of structural steel used resulted from implementation of SP dampers in the building considered. Systems designed with SP dampers were also alleged to be cheaper to repair following earthquakes when compared to similar structures without dampers.

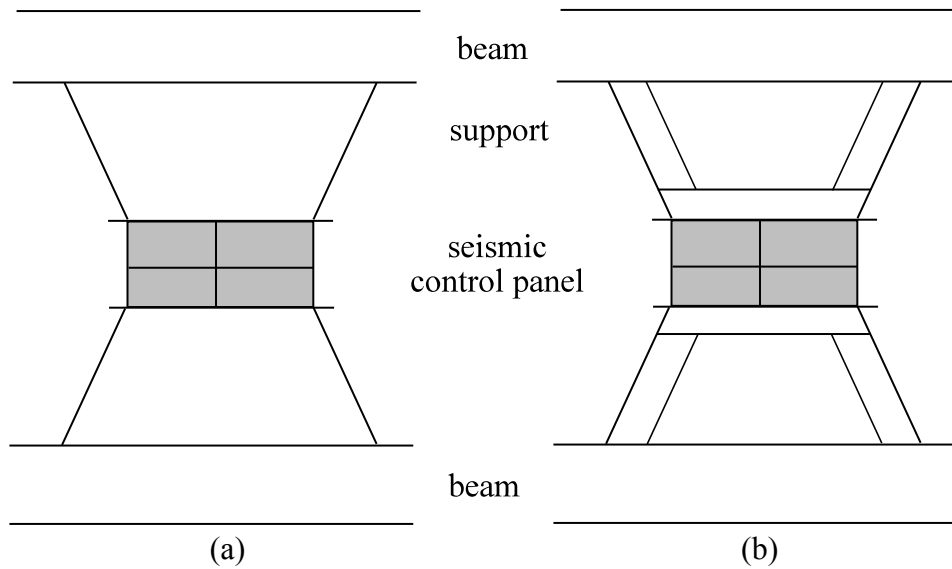


Figure 2.8. Types of Seismic Control Members: (a) Pillar Type; (b) Bracing Type (Tanaka et al., 1998)

Note that the terminology “shear panel” was used for an energy dissipation system in a tall building designed by Shimizu et al. (1998). However, it is not a shear panel of the same type as the SP system considered above. In this study, as shown in Figure 2.9 from Shimizu et al. (1998), a triangular shaped T-sectional member was proposed to be attached to column or beam ends, in order to use compact size and easy to replace structural elements. This damper configuration was found to be effective as an energy absorption system under several hazard earthquake levels. Figure 2.10, from Shimizu et al. (1998), shows the finite element model at two stages of deformation, and a simplified model built with beam, truss, and panel members.

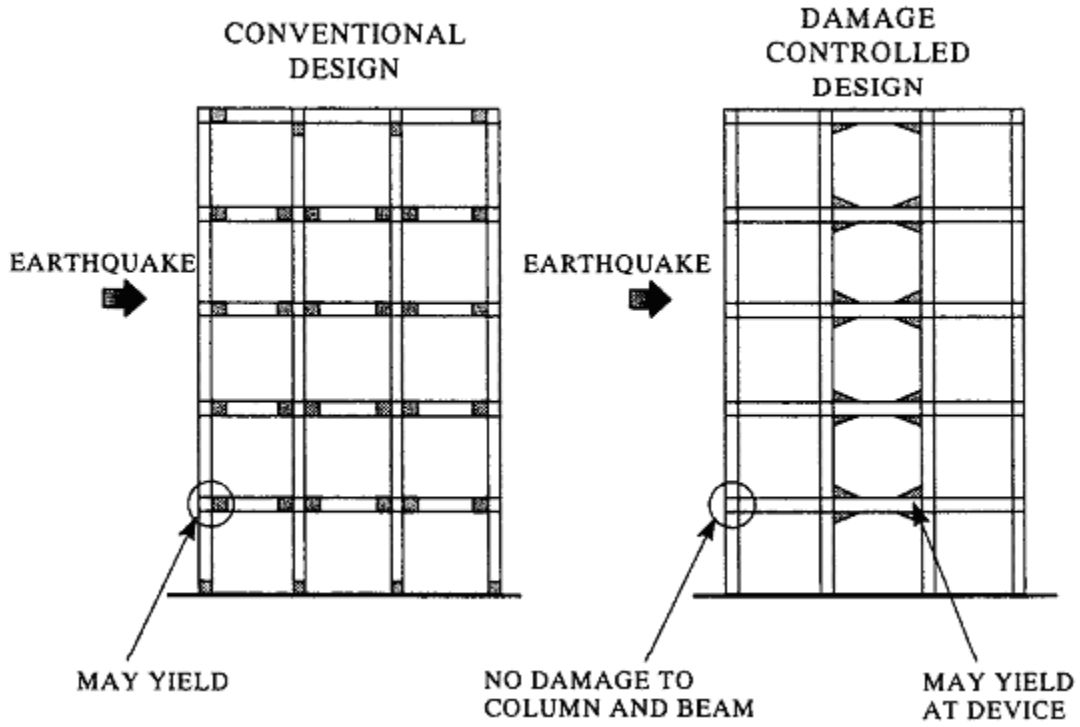


Figure 2.9. Conventional Design and Proposed Design (Shimizu et al., 1998)

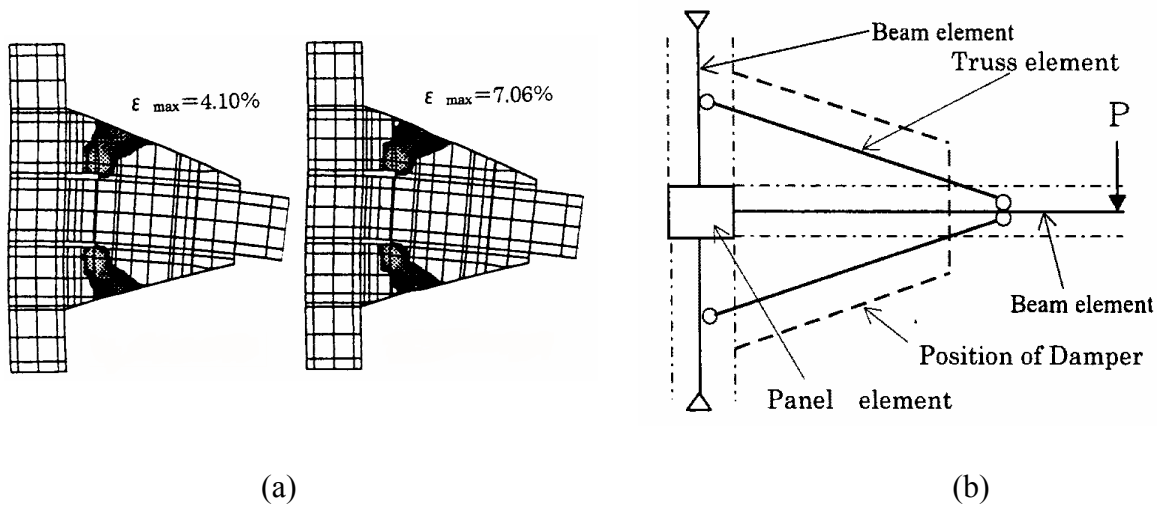


Figure 2.10. Shear Panel Models; (a) Equivalent Plastic Strain Distribution, (b) Simplified Model (Shimizu et al., 1998)

2.3.4. Friction Dampers (FD)

In the previous sections some devices that dissipate energy through inelastic deformation of metals have been examined. Hysteretic behavior can also be achieved without material yielding, by relying instead on friction mechanisms, recalling that friction is considered as a force that opposes the relative movement between sliding bodies. Work done by friction acting during the relative motion between the surfaces in contact is equal to the energy dissipated in the process. Soong and Dargush (1997) categorized this type of hysteretic behavior as solid friction.

Solid friction mechanism has been widely studied and applied to many engineering processes. However, the first implementation of friction devices in structural systems was conducted by Pall et al. (1980), who developed passive frictional dampers based on the principle of automotive brakes. Pall et al. (1980) proposed the use of brake lining pads between steel plates and developed the Limited Slip Bolted (LSB) joint to slow down the motion of large panel structures (Figure 2.11). The LSB joint designed from brake lining pads was found to have a stable and consistent hysteretic response (Figure 2.12). An alternative design was proposed by Pall and Marsh (1982) for implementation of this type of device on X-braced frames. Figure 2.13 shows the configuration of the proposed design.

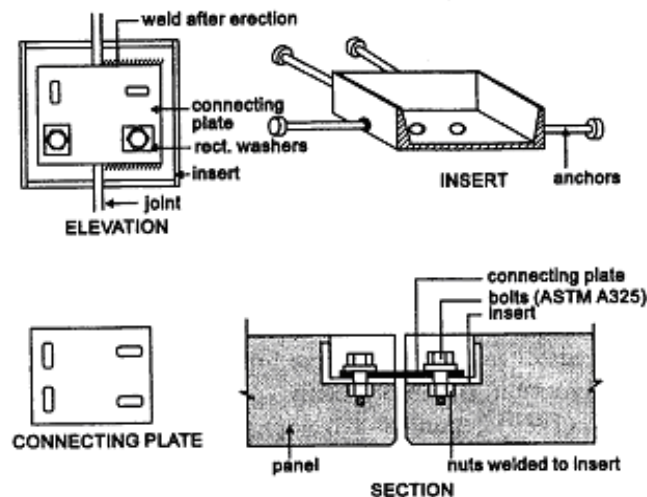


Figure 2.11. Limited Slip Bolt Joint (Pall et al., 1980)

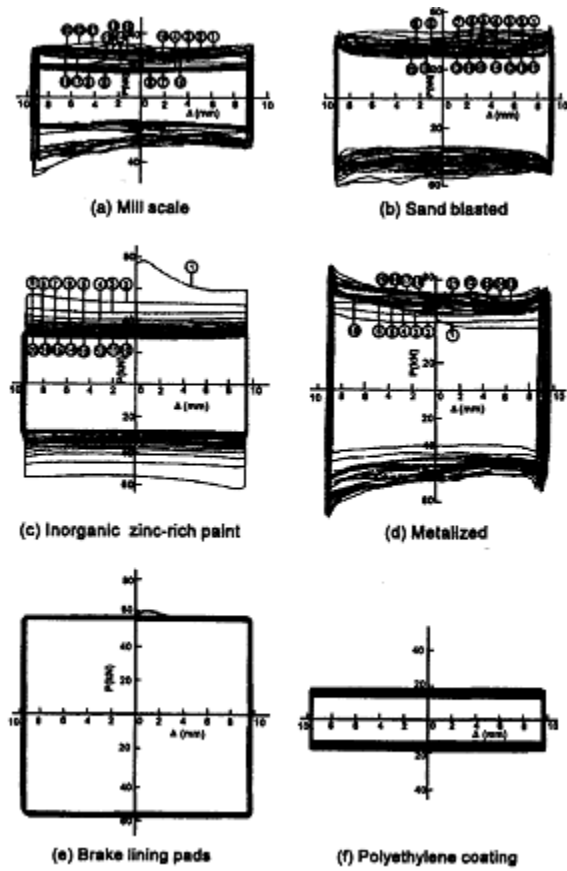


Figure 2.12. Hysteresis Loops of Limited Slip Bolted Joints (Pall et al., 1980)

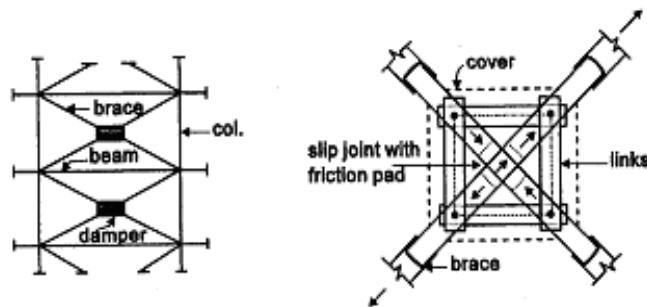


Figure 2.13. X-braced Friction Damper (Pall and Marsh, 1982)

Another configuration suited for concentrically braced frames is the Slotted Bolted Connection (SBC), developed by FitzGerald et al. (1989), and shown in Figure 2.14. According to this figure, the SBC consists of a gusset plate bolted to a pair of channels oriented back to back. It may be noted that two deformation states are possible, namely:

state 1, where the gusset plate slides between the channels; and state 2, where both channels slides between the gusset plate and the cover plates. Figure 2.15 shows the free body diagrams corresponding to both deformation states. Note that when the gap between the gusset plate and the bolts closes the friction force doubles its value, which is corroborated by the test shown in Figure 2.15. It was found that this sudden increase in the friction force acts as a stabilization mechanism against the accumulative lateral displacement in one direction.

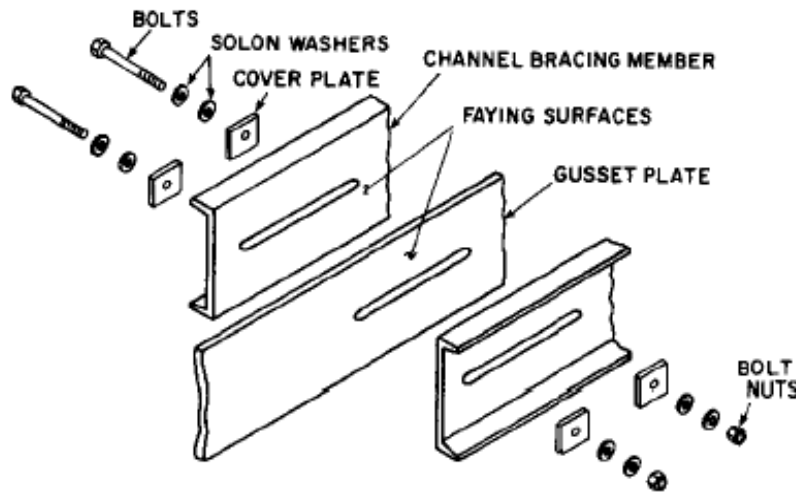


Figure 2.14. Slotted Bolted Connection (FitzGerald et al., 1989)

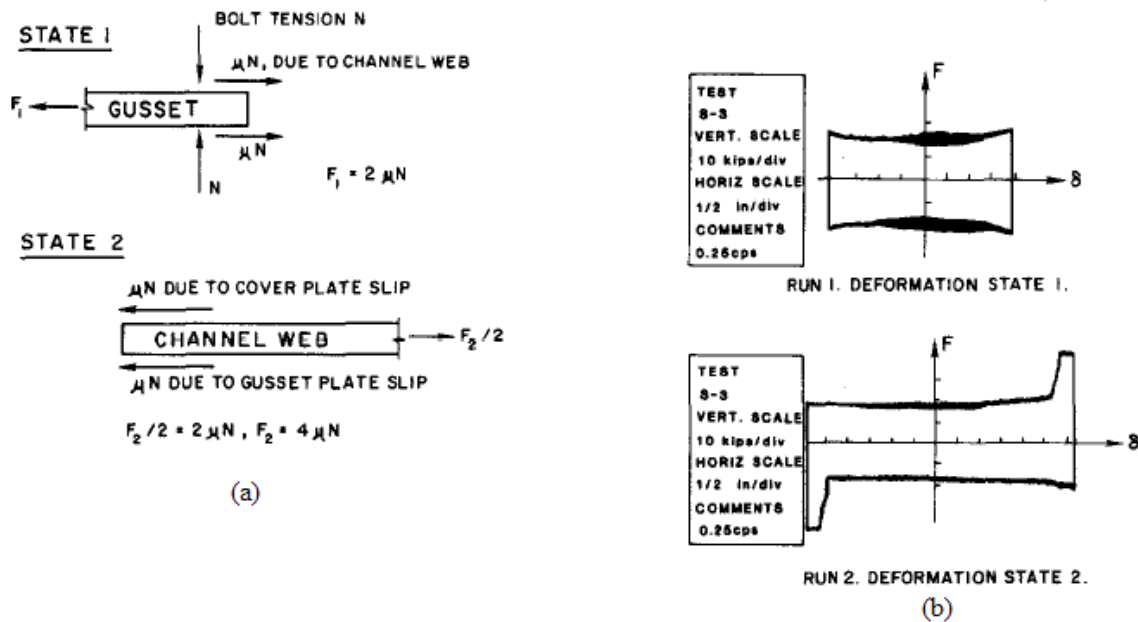


Figure 2.15. Slotted Bolted Connection; (a) Free Body Diagrams, (b) Typical Load Deformation Diagrams (FitzGerald et al., 1989)

However, braces in the SBC developed by FitzGerald et al. (1989) must be designed to resist the compressive forces transmitted by the sliding joints, which may not be economic. Filiatrault and Cherry (1989, 1990) proposed a SBC with slender members (i.e., tension only braces) and horizontal and vertical links, as shown in Figure 2.16. When slippage in tension occurs, the links rotate, forming a rhomboid shape and stretching the buckled brace, which activates this brace to immediately absorb tension loads when the cycle is reversed. Figure 2.17 shows one cycle of loading of a simple one-story friction damped frame. Filiatrault and Cherry (1989) also performed a parametric study of the optimum slip-load distribution for the FD, along with a sensitivity analysis to identify the parameters that exert more influence on the behavior. Results of analytical and experimental works led to the elaboration of design slip-load spectra, as part of a simplified procedure to evaluate the optimum slip-load distribution for single and multi-story buildings. This research represents the first known attempt to establish a simplified approach to optimally design friction-damped structures. Further research was recommended to assess the long-term reliability of the FD to determine whether periodic maintenance is required for the systems.

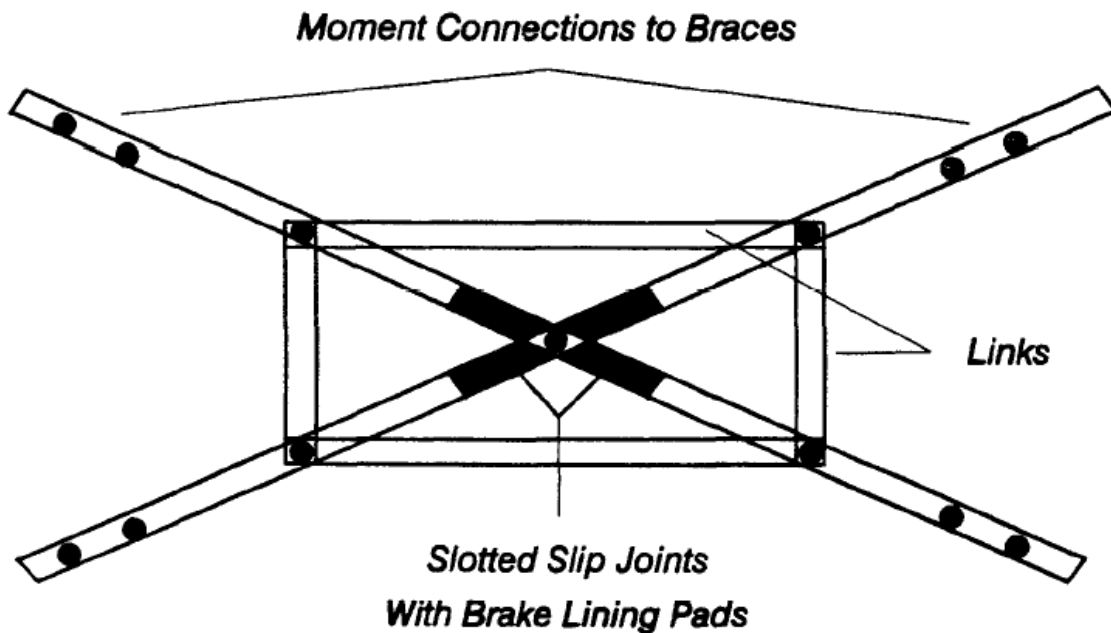


Figure 2.16. Friction Damping Device (Filiatrault and Cherry, 1989)

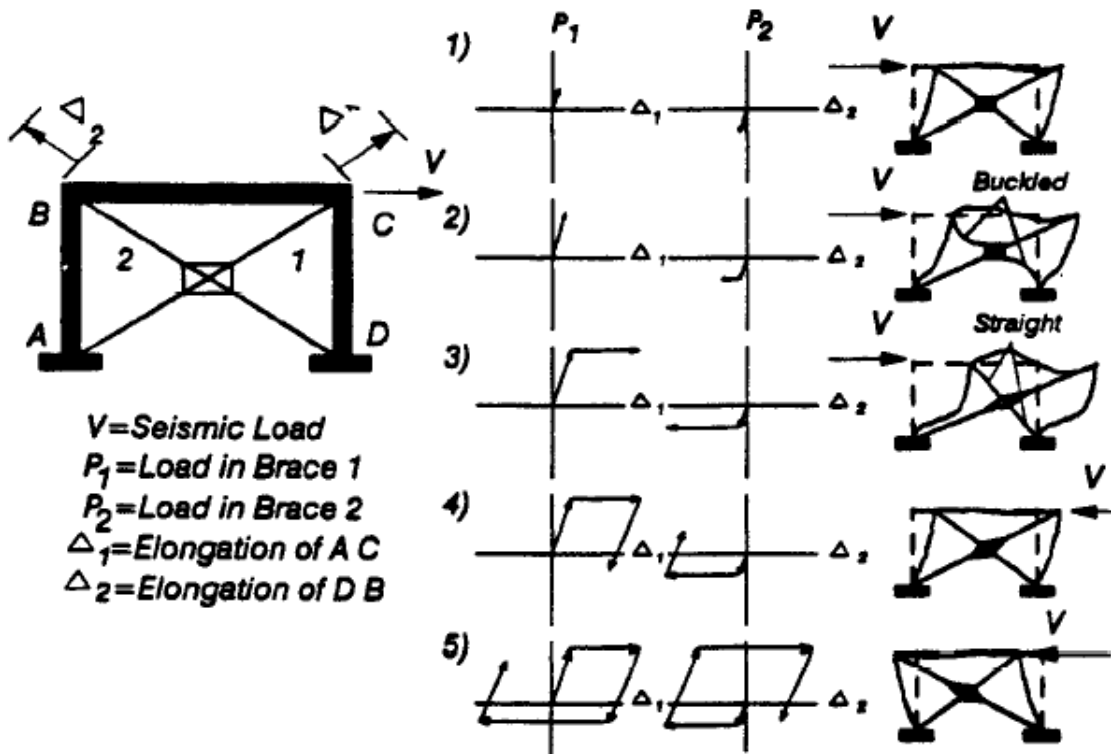


Figure 2.17. Hysteretic Behavior of Simple Friction-Damped Braced Frame during One Cycle of Loading (Filiatrault and Cherry, 1990)

The Energy Dissipating Restraint (EDR) manufactured by Flour Daniel, Inc. is another passive friction device used to enhance the seismic response of a structure. According to Nims et al. (1993), the EDR is a strongly self-centering passive FD having a wide range of hysteretic behaviors. General details of a typical EDR are depicted in Figure 2.18, where it may be noted that the internal spring, the compression wedges, friction wedges, stops, and gaps are the main components of the device. These elements define the hysteretic behavior of the EDR. Figure 2.19 shows the general hysteresis loop that can be developed by the EDR. Two particular cases were extensively studied by Nims et al. (1993), namely: the double flag-shaped hysteresis loop (Figure 2.20) which is obtained with zero gaps and the spring initially preloaded; and the triangular-shaped hysteresis loop (Figure 2.21) which is obtained with zero gaps and zero spring preloaded. Note that both systems have self-centering capabilities. It was found that the EDR may be

effectively used to reduce lateral displacements, without affecting significantly the acceleration levels.

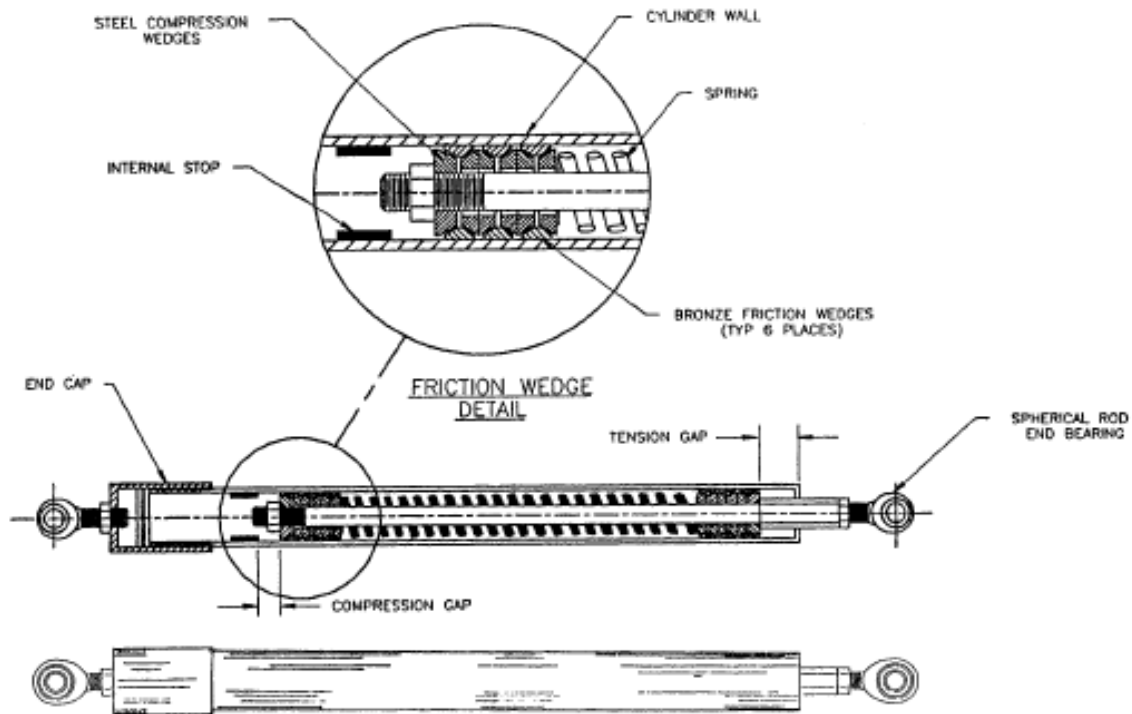


Figure 2.18. External and Internal views of Energy Dissipating Restraint (Nims et al., 1993)

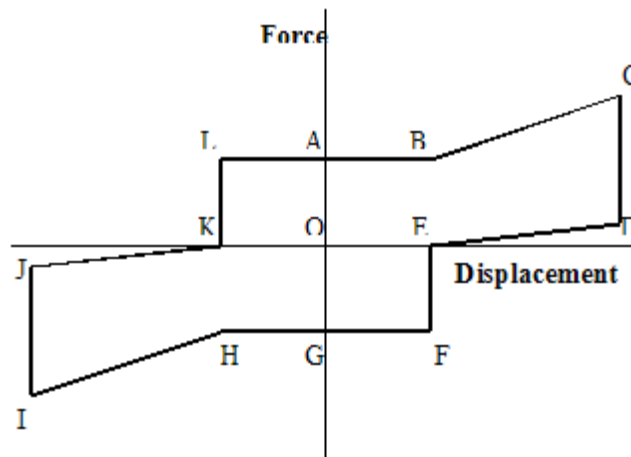


Figure 2.19. Energy Dissipating Restraint Complete Hysteresis Loop (Nims et al., 1993)

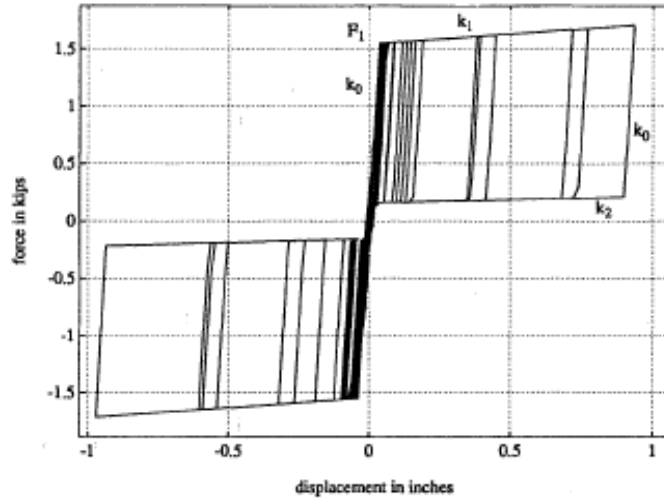


Figure 2.20. Analytical Double Flag-Shaped Hysteresis Loop (Nims et al., 1993)

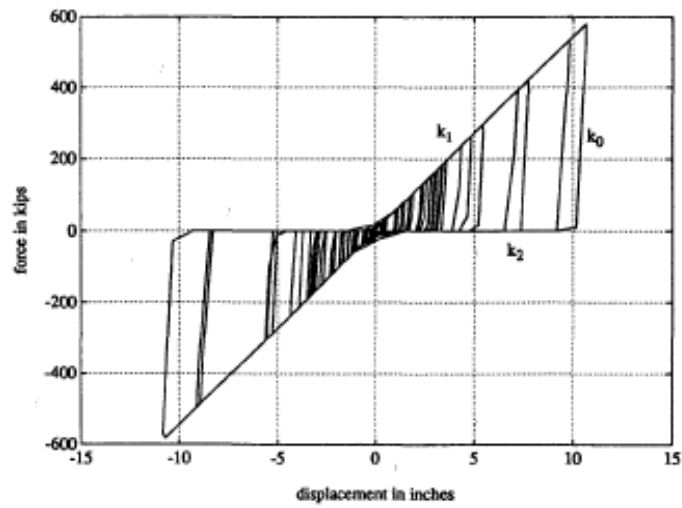


Figure 2.21. Analytical Triangular-Shaped Hysteresis Loop (Nims et al., 1993)

An experimental and analytical investigation of structures retrofitted with supplemental damping was conducted at University at Buffalo using viscoelastic, fluid viscous, friction, and fluid viscous walls devices (Reinhorn et al., 1995; Li and Reinhorn, 1995; and Reinhorn and Li, 1995). In the second part of the study, two types of friction devices (Tekton and Sumitomo friction dampers) were used to retrofit a 1:3 scale reinforced concrete structure, which was damaged by prior severe (simulated) earthquakes. In this study it was observed that a substantial reduction of the seismically induced damage on beams and columns can be achieved in properly retrofitted structures with friction dampers. Such reduction (between 80% and 90%) led to a significant decrease in the lateral deformations with minor increase in the acceleration response.

SECTION 3

PARAMETRIC STUDY AND SEISMIC RESPONSE OF SINGLE DEGREE OF FREEDOM SYSTEMS WITH STRUCTURAL FUSES

3.1. Introduction

The structural fuse concept is described in this section in a parametric formulation, considering the behavior of nonlinear single degree of freedom (SDOF) systems subjected to synthetic ground motions. Two and three dimensional graphs are examined as possible ways to present results. Finally, nonlinear dynamic response is presented in dimensionless charts normalized with respect to key parameters. Closed form solution are also developed through regression analyses, as an alternative to the charts.

Allowable story drift is introduced as an upper bound limit to the charts, which produces ranges of admissible solutions, shown as shaded areas in the graphs. Earthquake duration and stiffness ratio effects on short and long period structures are also discussed, in terms of ductility demand, and hysteretic energy dissipated.

Finally, a generic retrofit case study is presented to illustrate the benefits of adding metallic fuse elements to an existing frame. A comparative analysis is made between a bare frame (i.e., without metallic dampers), and the same frame retrofitted using metallic fuse elements, to improve the behavior of the existing structure.

3.2. Analytical Model of a SDOF System with Structural Fuses

Figure 3.1 depicts a single-story one-bay structure subjected to ground motion, whose frame, device support system, and metallic damper are modeled as a lumped mass connected to the ground by elasto-plastic springs, and the inherent system viscous damping action is represented by a linear dashpot (Figure 3.1b). The three-spring model can be simplified, as well, to an equivalent one-spring model (Figure 3.1c) with lateral stiffness, K_1 , equal to:

$$K_1 = K_f + K_a \quad (3.1)$$

where K_f and K_a are the lateral stiffness of the frame, and added damping system, respectively. The damping system consists of the device support system and damper itself, whose equivalent added stiffness, K_a , becomes:

$$K_a = \frac{K_s K_d}{K_s + K_d} \quad (3.2)$$

where K_s and K_d are the lateral stiffness of the device support system (which may be optional, depending on whether the device requires to be attached to a support system), and the damper, respectively. It is worthwhile to mention that for device support system much stiffer than dampers, the deformation of the device support system could be ignored, without significant loss of accuracy, and (3.1) simplifies to:

$$K_1 = K_f + K_d \quad (3.3)$$

Accordingly, the increased stiffness caused by the inclusion of metallic dampers reduces the period of the primary structure (bare frame), changing it from:

$$T_f = 2\pi \left(\frac{m}{K_f} \right)^{1/2} \quad (3.4)$$

to:

$$T = 2\pi \left(\frac{m}{K_f + K_a} \right)^{1/2} \quad (3.5)$$

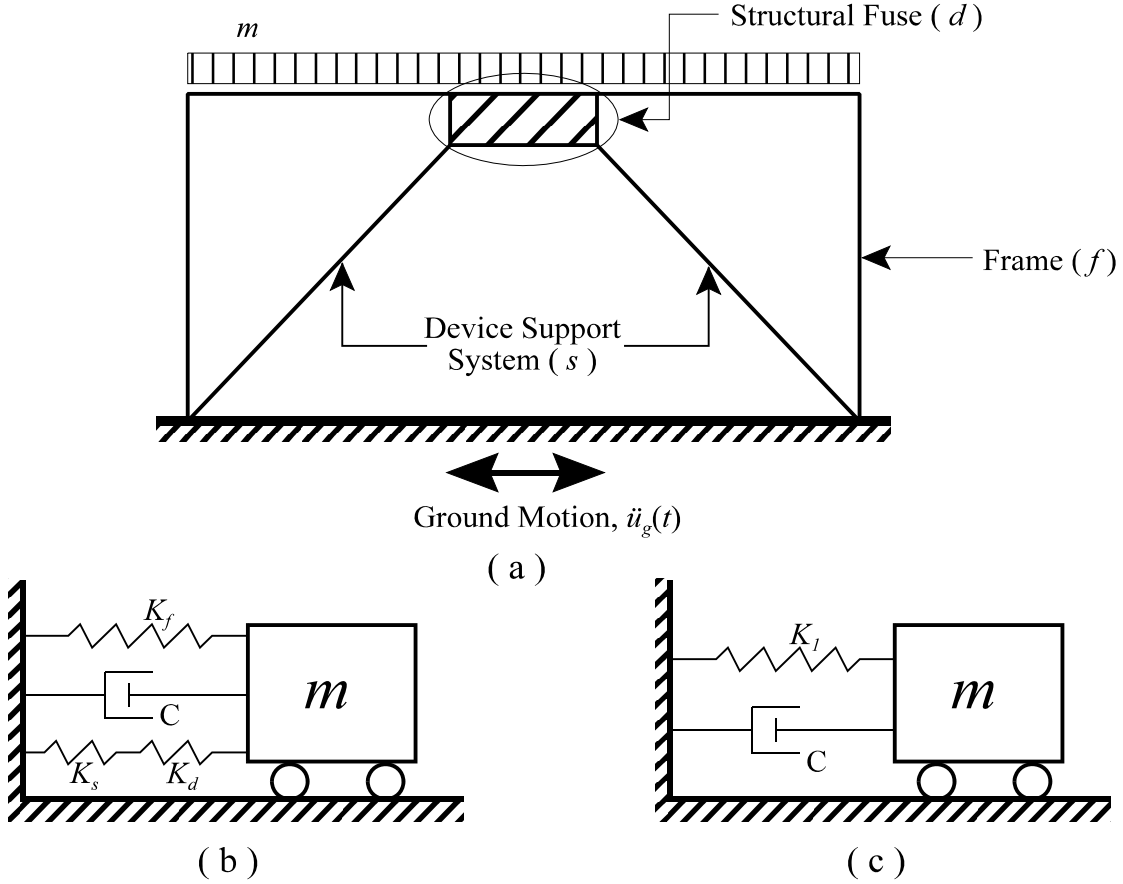


Figure 3.1. Model of a SDOF system with structural fuse; (a) One-bay single-story structure, (b) Equivalent three-spring system, (c) Equivalent one-spring system

The structural fuse concept requires that yield deformation of the damping system, Δ_{ya} , be less than the yield deformation corresponding to the bare frame, Δ_{yf} . Considering the deformation of the device support system, the yield deformation of the added damping system is equal to:

$$\Delta_{ya} = \Delta_{yd} \left(1 + \frac{K_d}{K_s} \right) \quad (3.6)$$

where Δ_{yd} is the damper yield deformation. Figure 3.2 shows a general pushover curve for a SDOF system with two elasto-plastic springs in parallel. The total curve is tri-linear

with the initial stiffness, K_1 , calculated using (3.1) and (3.2). Once the damping system reaches its yield deformation, Δ_{ya} , the increment on the lateral force is resisted only by the bare frame, being the second slope of the total curve equal to the frame stiffness, K_f . Two important parameters used in this study are obtained from Figure 3.2: the stiffness ratio, α , and the maximum displacement ductility, μ_{max} .

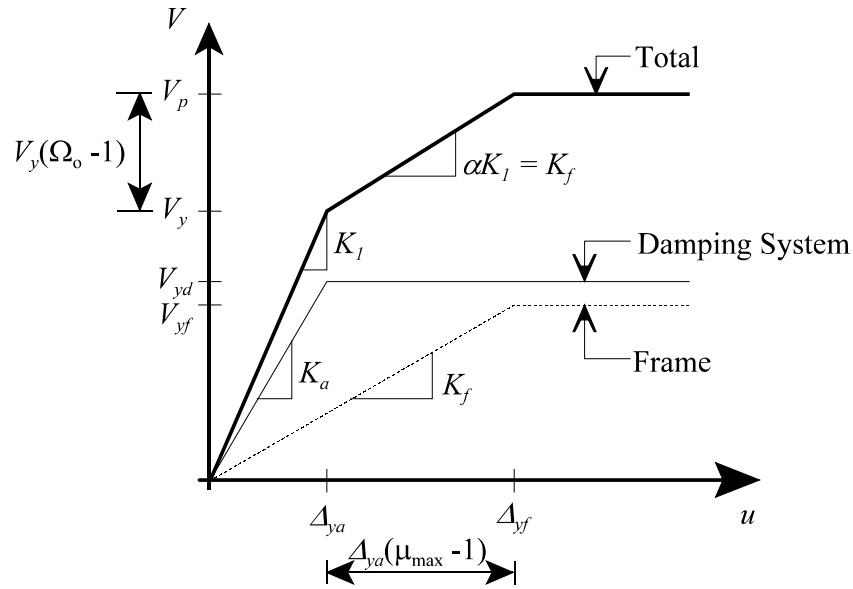


Figure 3.2. General Pushover Curve

The stiffness ratio, α , is the relation between the frame stiffness and the total initial stiffness, which can be calculated as:

$$\alpha = \frac{1}{1 + \frac{K_a}{K_f}} \quad (3.7)$$

with α being a dimensionless parameter less than one.

The maximum displacement ductility, μ_{max} , is the ratio of the frame yield displacement, Δ_{yf} , with respect to the yield displacement of the damping system, Δ_{ya} . In other words, μ_{max} is the maximum displacement ductility that the structure experiences before the frame undergoes inelastic deformations. This parameter can be written as:

$$\mu_{\max} = \frac{\Delta_{yf}}{\Delta_{ya}} = \frac{\Delta_{yf}}{\Delta_{yd} \left(1 + \frac{K_d}{K_s} \right)} \quad (3.8)$$

with μ_{\max} being greater than one.

In Figure 3.2, V_{yf} and V_{yd} are the base shear capacity of the bare frame and the damping system, respectively; and V_y and V_p are the total system yield strength and base shear capacity, respectively. Furthermore, note that in Figure 3.2, the calculation of the post-yielding stiffness, αK_1 , defines a relationship between α and μ_{\max} , equal to:

$$\alpha = \frac{\Omega_o - 1}{\mu_{\max} - 1} \quad (3.9)$$

where Ω_o is the overstrength factor, defined as:

$$\Omega_o = \frac{V_p}{V_y} \quad (3.10)$$

Pushover curves for different values of α and μ_{\max} are presented in Figures 3.3a and 3.3b. In Figure 3.3a, horizontal and vertical axes are respectively normalized with respect to the added device yield displacement, Δ_{ya} , and strength of the system at that corresponding displacement, V_y , as shown in Figure 3.2; while in Figure 3.3b the same axes are respectively normalized with respect to the yield displacement of the frame, Δ_{yf} , and the system total base shear capacity, V_p , as shown in Figure 3.2. Figure 3.3b is preferred because it shows the damping system and frame capacities as percentages of the total base shear capacity. This set of pushover curves is used in Section 3.4 for nonlinear dynamic analyses.

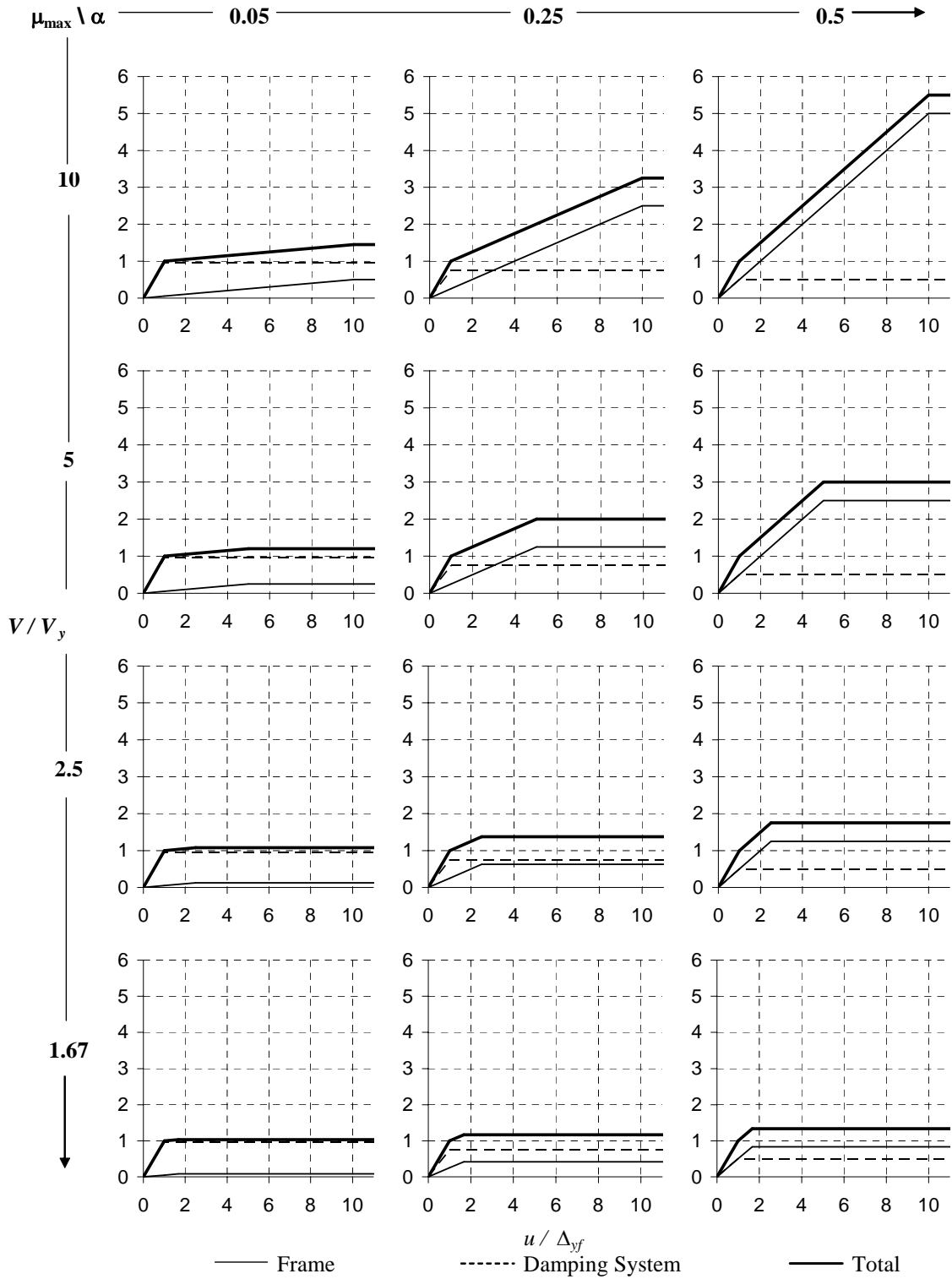


Figure 3.3a. Pushover Curves for the Studied Systems Normalized by V_y , and Δ_{ya}

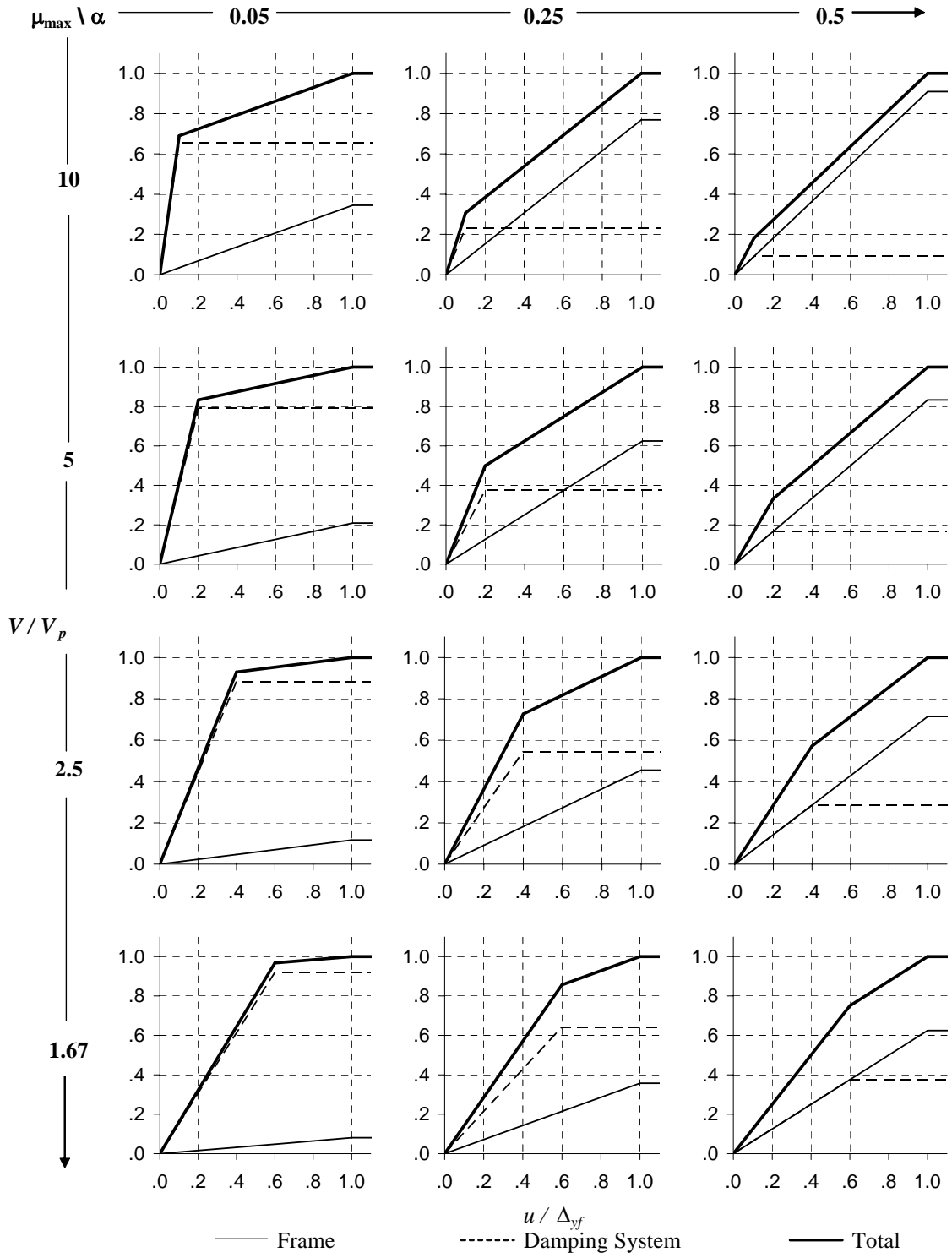


Figure 3.3b. Pushover Curves for the Studied Systems Normalized by V_y , and Δ_{ya}

Figures 3.3a and 3.3b also show the frame and damping system contributions to the total base shear capacity. The frame contribution increases with increases in both α and μ_{\max} , while the damping system contribution decreases with increases in α and μ_{\max} values. Note that the overstrength factor, Ω_o , is proportional to the frame contribution to the total base shear capacity.

Figure 3.4 shows the hysteresis loops corresponding to the total system capacity, with the axes normalized with respect to the base shear capacity point (Δ_{yf}, V_p) , as described before in Figure 3.3b (but over a slightly extended range of α and μ_{\max}). The area enclosed by these loops corresponds to the hysteretic energy dissipated per cycle when the system is subjected to an amplitude of motion equal to the frame yield displacement, Δ_{yf} . This dissipated energy decreases with increases in α , while the trend with respect to μ_{\max} is not consistent. For example, for $\alpha = 0.25$, systems having μ_{\max} of 2 and 5 would have the same enclosed area, with greater hysteretic energy values obtained for μ_{\max} between these values.

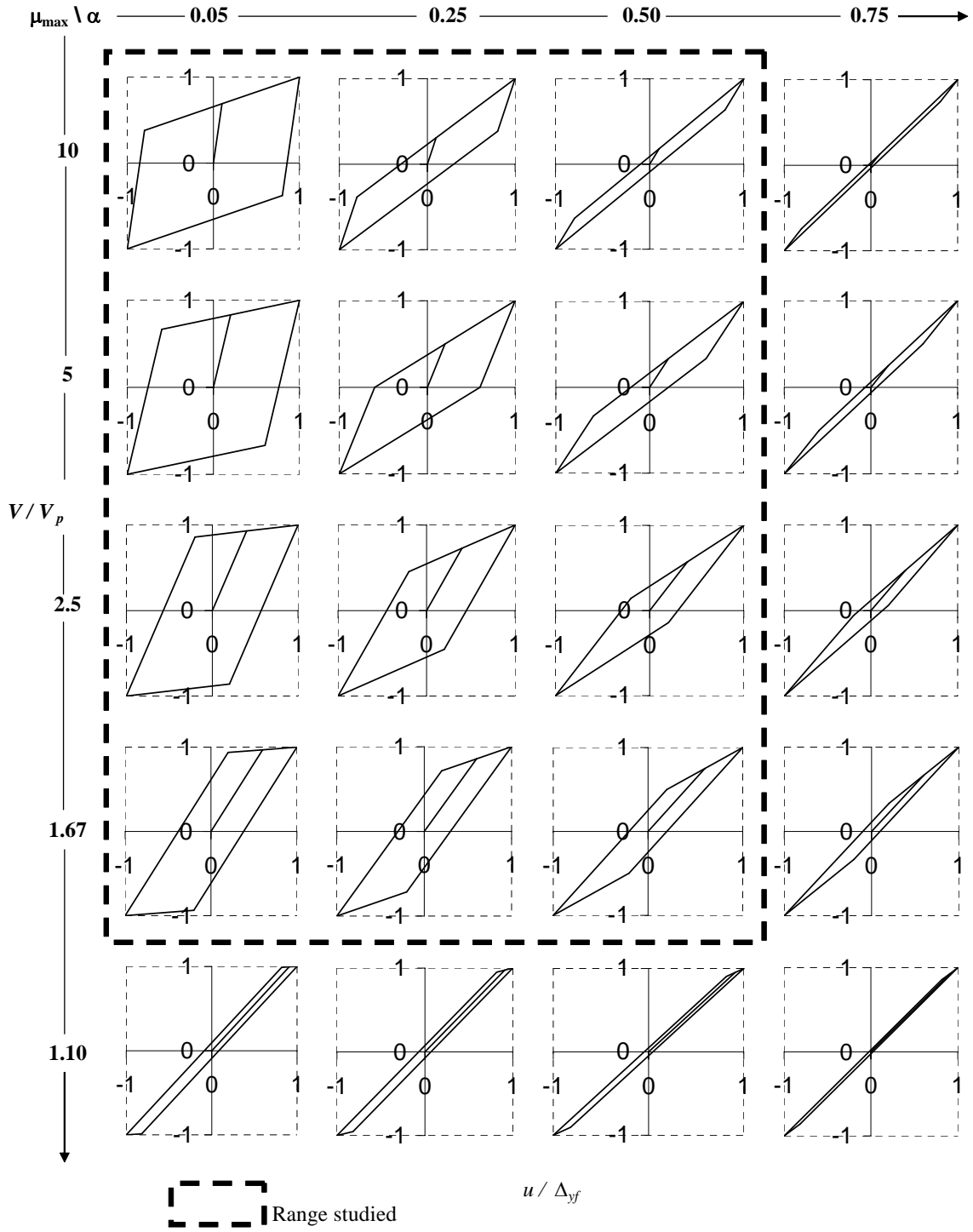


Figure 3.4. Hysteresis Loops for the Studied Systems, Normalized by V_p, Δ_{yf}

3.3. Parametric Formulation

In linear dynamic analysis of SDOF systems, the equation of motion is commonly written as:

$$m\ddot{u}(t) + c\dot{u}(t) + ku(t) = -m\ddot{u}_g(t) \quad (3.11)$$

where m , c , k , are the mass, damping coefficient, and linear spring stiffness of the system, respectively, and $\ddot{u}_g(t)$ is the ground acceleration. Solving (3.11) gives the system response, expressed in terms of the relative displacement, $u(t)$, relative velocity, $\dot{u}(t)$, and relative acceleration, $\ddot{u}(t)$.

For a nonlinear SDOF with hysteretic behavior, once the yield point is exceeded, the spring force is no longer proportional to the relative displacement. Mahin and Lin (1983) proposed a normalized version of the non-linear dynamic equation of motion adapted as shown below. Considering the force in the inelastic spring as time-dependent, $R(t)$, and substituting $R(t)$ for $ku(t)$ into (3.11), gives:

$$m\ddot{u}(t) + c\dot{u}(t) + R(t) = -m\ddot{u}_g(t) \quad (3.12)$$

Introducing the natural circular frequency, $\omega = \sqrt{k/m}$, and damping ratio, $\xi = c/(2m\omega)$, (3.12) can be written as:

$$\ddot{u}(t) + 2\xi\omega\dot{u}(t) + \frac{R(t)}{m} = -\ddot{u}_g(t) \quad (3.13)$$

Equation (3.13) can be transformed to express the system response in terms of displacement ductility, $\mu(t)$, of the added damping system, which is defined as:

$$\mu(t) = \frac{u(t)}{\Delta_{ya}} \quad (3.14)$$

where Δ_{ya} is the yield displacement of the damping system, calculated using (3.6).

Differentiating (3.14) with respect to time, yields:

$$\dot{\mu}(t) = \frac{\dot{u}(t)}{\Delta_{ya}} \quad (3.15)$$

and:

$$\ddot{\mu}(t) = \frac{\ddot{u}(t)}{\Delta_{ya}} \quad (3.16)$$

Substituting (3.14), (3.15), and (3.16) into (3.13) gives the normalized equation of motion used in this study:

$$\ddot{\mu}(t) + \frac{4\pi\xi}{T}\dot{\mu}(t) + \frac{4\pi^2}{T^2}\rho(t) = -\frac{4\pi^2}{T^2\eta} \left[\frac{\ddot{u}_g(t)}{\ddot{u}_{g\max}} \right] \quad (3.17)$$

where T is the elastic period of the structure, defined by (3.5), and $\rho(t)$ is the ratio between the force in the inelastic spring and the yield strength of the system, calculated as:

$$\rho(t) = \frac{R(t)}{V_y} \quad (3.18)$$

and η is the strength-ratio determined as the relation between the yield strength and the maximum ground force applied during the motion, defined as:

$$\eta = \frac{V_y}{m\ddot{u}_{g\max}} \quad (3.19)$$

where $\ddot{u}_{g\max}$ is the peak ground acceleration.

For a specific ground motion, $\ddot{u}_g(t)$, (3.17) can be solved in terms of the above parameters, assuming a damping ratio, ξ , of 0.05 in this study. Note that the impact of the stiffness ratio, α , (see (3.7)) on inelastic response is accounted for by the term defined in (3.18).

3.4. Nonlinear Dynamic Response

A design response spectrum was constructed based on the National Earthquake Hazard Reduction Program Recommended Provisions (NEHRP 2003) for Sherman Oaks, California, and site soil-type class B. This site was chosen because it corresponds to the

location of the Demonstration Hospital used by the Multidisciplinary Center for Earthquake Engineering Research (MCEER) in some of its projects. Accordingly, the design spectral accelerations for this site are $S_{DS} = 1.3$ g, and $S_{DI} = 0.58$ g. Using the Target Acceleration Spectra Compatible Time Histories (TARSCTHS) code, by Papageorgiou et al. (1999), spectra-compatible synthetic ground motions were generated to match the NEHRP 2003 target design spectrum.

Three artificial accelerograms were created using the TARSCTHS code, and their corresponding elastic response spectra for 5% of critical damping are shown in Figure 3.5a, superposed on the NEHRP 2003 target design spectrum. Furthermore, Figure 3.5b shows the average of the response spectra, for the three synthetic records which agrees well with the target design spectrum. All synthetic strong motion records generated were 15 seconds in duration. The effect of longer duration records is investigated in Section 3.4.4.

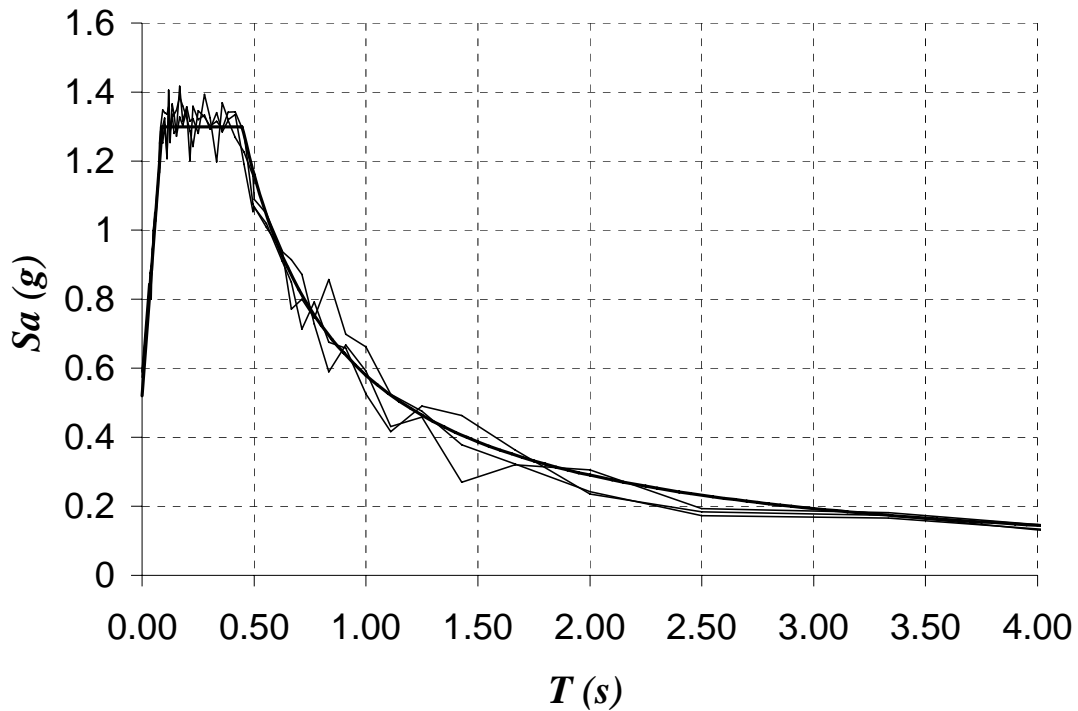


Figure 3.5a. Elastic Response Spectra for Synthetic Earthquakes ($\xi = 5\%$)

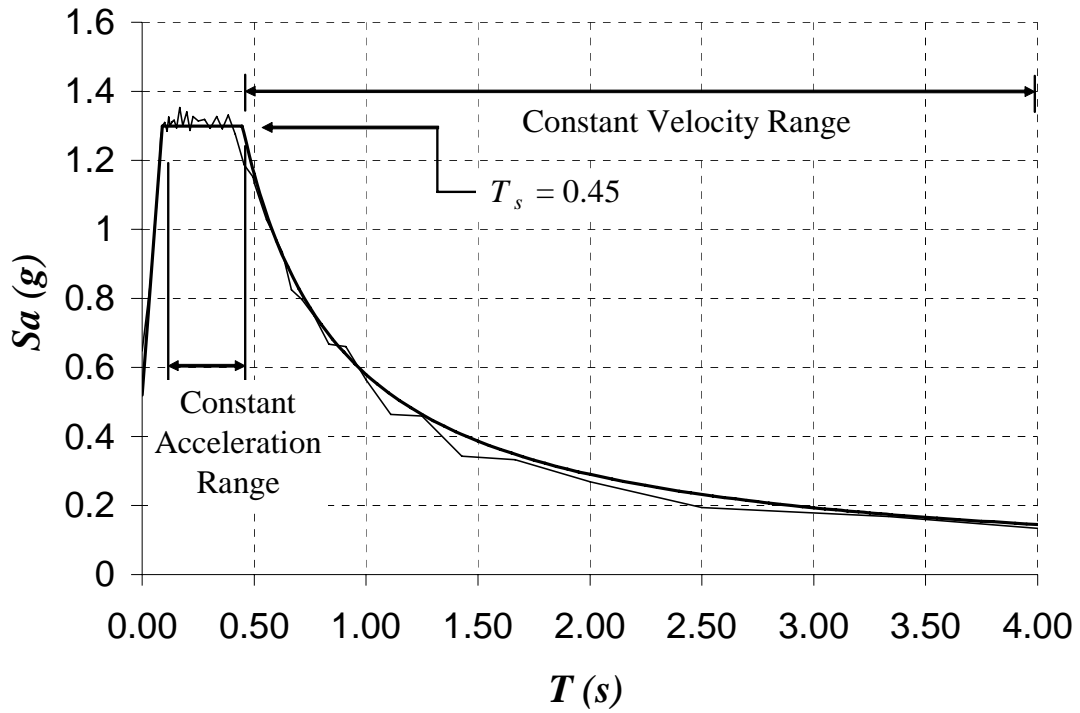


Figure 3.5b. Average Elastic Response Spectrum for Synthetic Earthquakes ($\xi = 5\%$)

Nonlinear time history analyses were conducted using the Structural Analysis Program, SAP 2000, (Computers and Structures, Inc. 2000). Analyses were performed for the range of systems described in Figure 3.3, using the following parameters: $\alpha = 0.05, 0.25, 0.50$; $\mu_{\max} = 10, 5, 2.5, 1.67$; $\eta = 0.2, 0.4, 0.6, 1.0$; and $T = 0.1 \text{ s}, 0.25 \text{ s}, 0.50 \text{ s}, 1.0 \text{ s}, 1.5 \text{ s}, 2.0 \text{ s}$. The combination of these parameters resulted in 288 analyses for each ground motion generated (i.e., a total of 864 nonlinear time history analyses).

The response of the system is expressed in terms of the frame ductility, μ_f , and the global ductility, μ , defined as follows:

$$\mu_f = \frac{u_{\max}}{\Delta_{yf}} \quad (3.20)$$

$$\mu = \frac{u_{\max}}{\Delta_{ya}} \quad (3.21)$$

where u_{\max} is the maximum absolute displacement of the system, taken as the average of the maximum absolute responses caused by each of the applied ground motion .

Response can be plotted in either two or tri-dimensional charts, depending on the parameters and the relationships employed. Some alternatives were considered, and two of them are discussed in Sections 3.4.1 and 3.4.2.

3.4.1. Response plotted in tri-dimensional graphs

Substituting $\Delta_{ya} = V_{yd} / K_a$, and $\Delta_{yf} = V_{yf} / K_f$ (Figure 3.2) into (3.8), gives:

$$\left(\frac{K_a}{K_f} \right) = \mu_{\max} \left(\frac{V_{yd}}{V_{yf}} \right) \quad (3.22)$$

which represents a straight line oriented by the given proportionality constant, μ_{\max} , in a nondimensional coordinates system with axes equal to V_{yd} / V_{yf} and K_a / K_f . Keeping μ_{\max} as a constant and varying the frame and damping system properties, K_f , V_{yf} , K_a and V_{yd} , different points along the same straight line can be obtained. Performing time history analysis the equation of motion can be solved to obtain the maximum displacement response, u_{\max} , corresponding to every point, which can be transformed into the frame ductility, μ_f , using (3.20). A representation of such results is possible in a 3-D space having V_{yd} / V_{yf} and K_a / K_f as the horizontal axes, and the ductility demand, μ_f , as the vertical axis. A schematic representation of this 3-D plot is shown in Figure 3.6 for specific values of η and μ_{\max} .

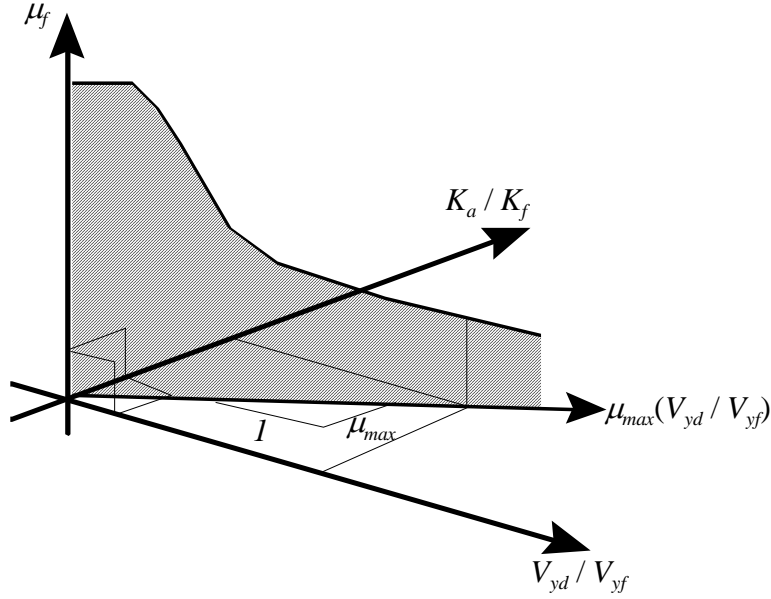


Figure 3.6. Three-dimensional Representation of the Response as a function of V_{yd} / V_{yf} , K_a / K_f , and μ_{max}

As an alternative to present the same data, tri-dimensional non-linear response spectra can be constructed recognizing that combining (3.4) and (3.5) gives:

$$T^2 = \alpha T_f^2 \quad (3.23)$$

which represents a straight line oriented by the given proportionality constant, α , in a coordinates system with axes equal to T_f^2 and T^2 . As for the previous case, keeping α as a constant and varying the frame and system initial periods, T_f and T , different points along the same straight line can be obtained. Once the equation of motion has been solved and the maximum displacement response, u_{max} , is transformed into the frame ductility, μ_f , for every point, a new 3-D plot can be made having T_f^2 and T^2 as the horizontal axes and μ_f as the vertical axis. Like Figure 3.6, Figure 3.7 depicts the ductility response for specific values of η and α .

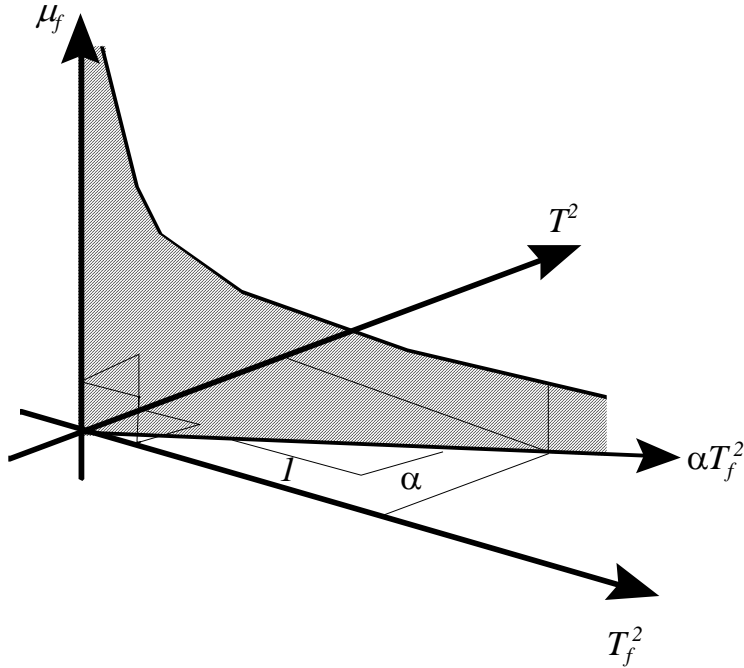


Figure 3.7. Three-dimensional Representation of the Response as a function of T , T_f , and α

While Figures 3.6 and 3.7 show the variation of the ductility response, μ_f , with respect to selected key parameters, a shortcoming is that they each are incomplete in some ways. Figure 3.6 does not account for the effect of α on the response, while the impact of μ_{\max} is not accounted for in Figure 3.7. In fact, both parameters are interdependent. This has been demonstrated in (3.9), which show the interdependence of α and μ_{\max} through Ω_o values. Consequently, in Figure 3.6, results shown along the curve for a given μ_{\max} correspond to cases with possibly different α values. Similarly, in Figure 3.7, results shown for a given α value do not necessarily have a constant value of μ_{\max} . Therefore, for the purpose of parametric analysis, a more appropriate presentation of results would benefit from keeping α and μ_{\max} fixed on the same plot, as done in next section.

3.4.2. Response plotted in two-dimensional graphs

Two-dimensional graphs were selected to overcome the limitations encountered in the above tri-dimensional plots. Figures 3.8 and 3.9 show results of the 864 non-linear

analyses conducted in terms of frame ductility, μ_f , and global ductility, μ , respectively, as a function of the elastic period, T . Every plot corresponds to a fixed set of α and μ_{\max} values, while each curve represents a constant strength-ratio, η . All the points having $\mu_f < 1$ in Figure 3.8 represent elastic behavior of the frame, while in Figure 3.9 these points appear below the horizontal line corresponding to μ_{\max} (i.e., $\mu < \mu_{\max}$). Note that in systems with elastic behavior of the frame (i.e., $\mu_f < 1$), the global ductility is entirely provided by yielding of the metallic dampers (i.e., global ductility is equal to the ductility of the metallic dampers).

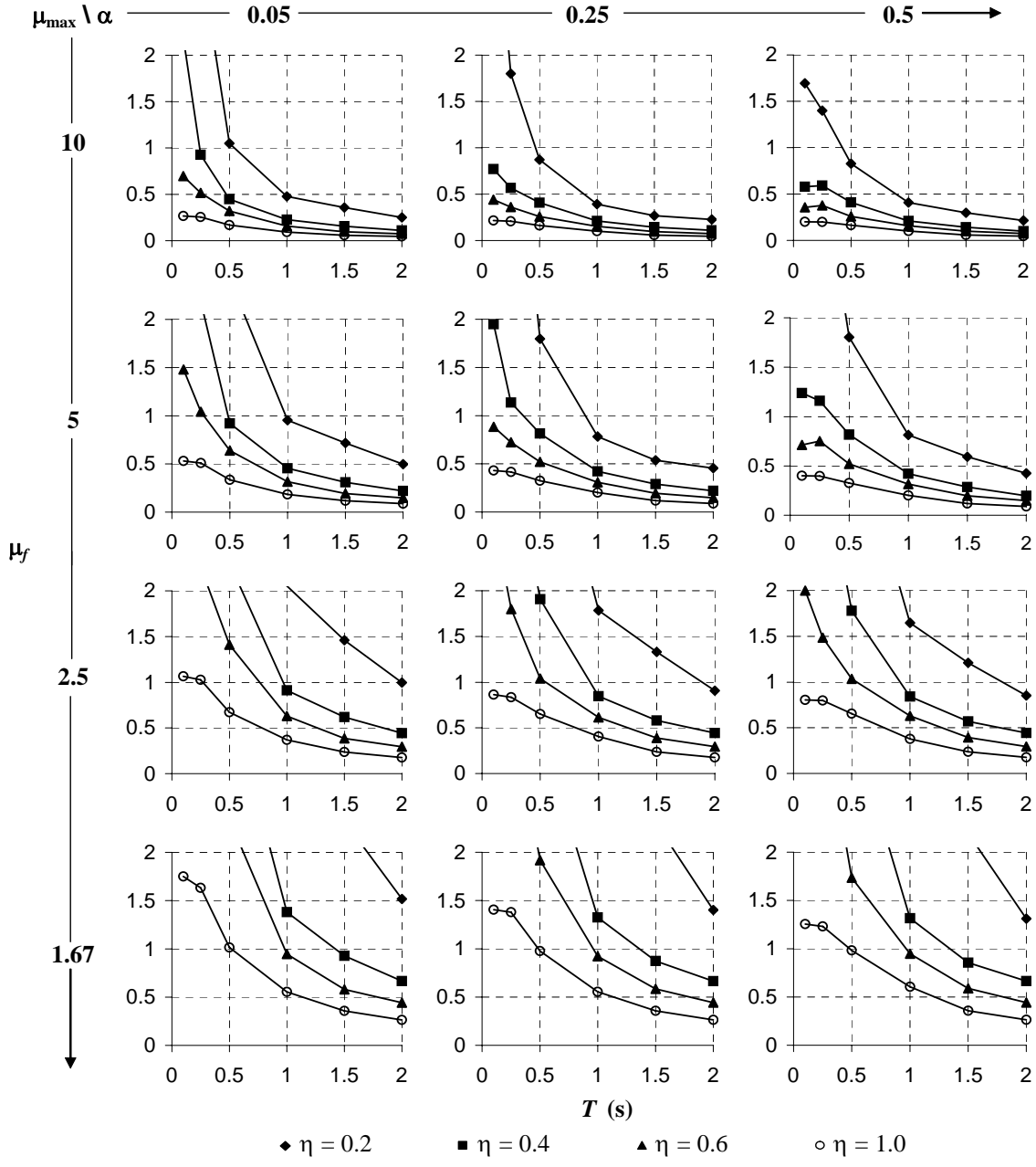


Figure 3.8. Average Response in terms of Frame Ductility (μ_f)

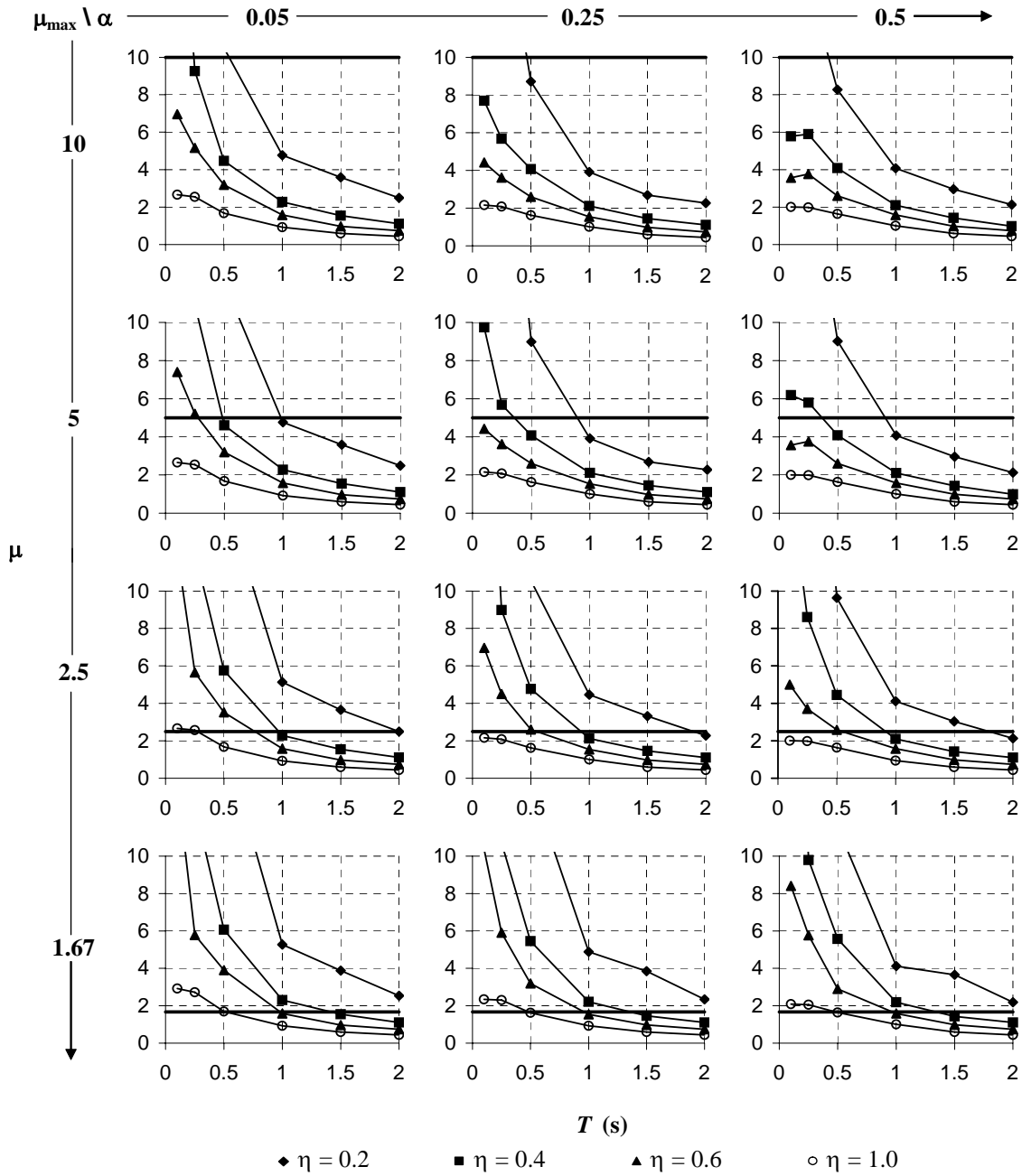


Figure 3.9. Average Response in terms of Global Ductility (μ)

As an example, two pushover curves having the same parameters (α , μ_{max} , and η) but different initial periods are presented in Figure 3.10. As shown in this figure, Structure 2 is twice more flexible than Structure 1, with a period increased by:

$$T_2 = \left(\frac{K_1}{K_2} \right)^{1/2} T_1 \quad (3.24)$$

which is $T_2 = 1.414T_1$ in this case. The damping system yield displacement, Δ_{ya} , and the frame yield displacement, Δ_{yf} for the two structures are also related by the same 2:1 ratio. Although seismic response does not increase proportionally, because of nonlinear behavior, a reduction of ductility demands (μ_f and μ) is expected for the structure having the longer period, as shown in Figures 3.8 and 3.9.

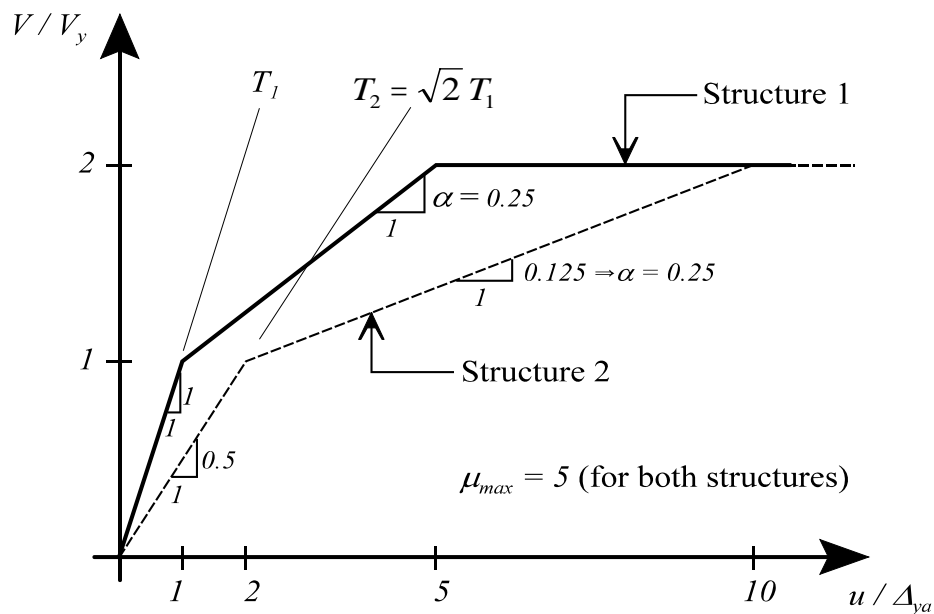


Figure 3.10. Pushover curves for two structures having the same α , μ_{max} , η , and different periods (T)

While the charts shown in Figures 3.8 and 3.9 can be used directly to read ductility demands as a function of other defined parameters, there may be instances where closed form solutions are desirable, as for use in computer programs or in the formulation of design algorithms. Such equations can be formulated from observation that the shape of the response curves shown in Figures 3.8 and 3.9 suggests a power decay of the ductility (μ_f and μ) with respect to the period. Based on this pattern, and the data presented in Figures 3.8 and 3.9 a regression analysis was performed to express the ductility as a function of α , μ_{\max} , η , and T . The following equations were obtained from the analysis:

$$\mu_f = \left(\frac{0.8239}{\mu_{\max}} \right) \eta^A T^B \eta^C \quad (3.25)$$

$$\mu = 0.8239 \eta^A T^B \eta^C \quad (3.26)$$

where

$$A = (0.25 \alpha - 1.3) \mu_{\max}^{\alpha(0.88 \alpha - 0.55)} \quad (3.27)$$

$$B = \alpha(0.38 - 0.68 \alpha) \mu_{\max} + 0.26 \alpha - 0.94 \quad (3.28)$$

$$C = (0.03 \alpha + 0.01) \mu_{\max} + 0.37 \alpha^2 - 0.3 \alpha - 0.34 \quad (3.29)$$

Equations (3.25) and (3.26) have an average error of 12%, and can be used as an alternative to the charts. Figure 3.11 shows a comparison between the ductility demand, μ_f , obtained by time history analyses and the same response obtained using (3.25). Note that the values calculated using (3.25) agree well with the actual ones, except when $T < 0.25$ s, in which the equation tends to overestimate the response. This overestimation is caused by the fact that μ_f does not increase significantly over short periods. However, for preliminary design purposes, for short period structures (having $T < 0.25$ s) the ductility demand corresponding to $T = 0.25$ s can be used without substantial loss of accuracy.

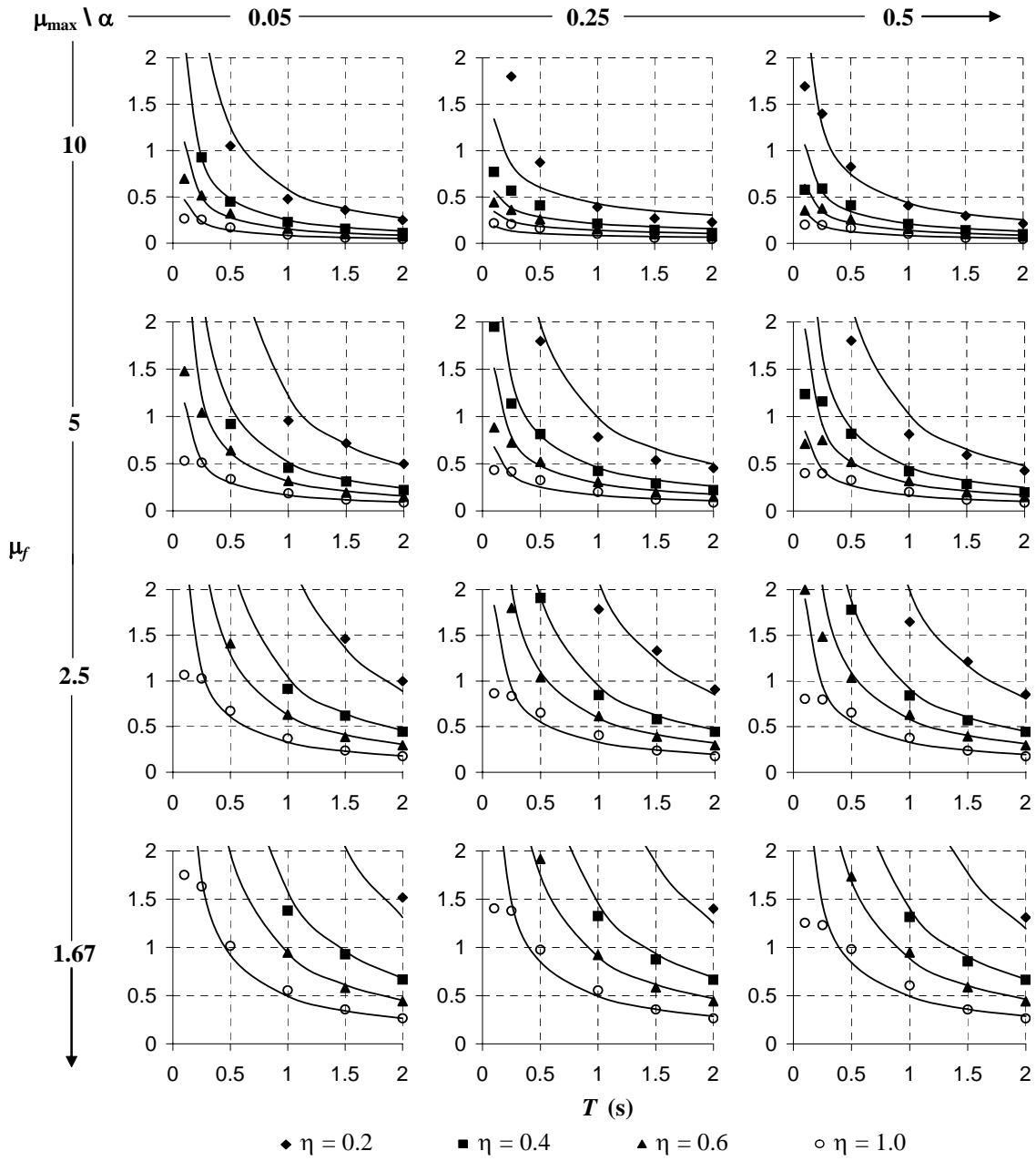


Figure 3.11. Average Ductility Demand calculated using Equation (3.25)

3.4.3. Allowable story drift

In some instances story drift (maximum relative displacement between consecutive floors) may need to be controlled. For example:

- Secondary effects (frequently called P- Δ effects) are directly related to story drift, where lateral deformation causes additional bending on vertical members, and instability problems may develop if the story drift exceeds tolerable levels (especially in structures with high gravity loads).
- Some nonstructural elements, such as partitions, ceilings, enclosures, windows and door frames are sensitive to lateral deformations. Limiting story drift indirectly allows to mitigate their damage. Given that the main purpose of introducing structural fuses in a structural system is to make easier and more expedient repair following an earthquake, the use of drift limits (albeit arbitrary ones) is justified if the purpose is to avoid or minimize damage on nonstructural components (unless the nonstructural elements are designed to accommodate lateral displacement limits larger than dictated by the other limit states).
- Metallic dampers typically undergo large deformations in the strain-hardening range to dissipate energy through hysteretic behavior. Maximum strain limits are usually imposed to prevent their failure by low cycle fatigue. For a given system geometry, these strain limits translate into lateral displacement limits.

For illustration purposes here, the NEHRP 2003 provisions recommended story drift limits can be used. Taking into account the selected story drift limit, the range of acceptable solutions that satisfy the structural fuse concept is defined on figures such as Figures 3.8 and 3.9 by the following boundaries:

- Maximum ductility (μ_f and μ): To keep the primary structure elastic, the frame ductility shall be less or equal to one (i.e., $\mu_f \leq 1.0$). Accordingly, the global ductility shall be less than the maximum displacement ductility (i.e., $\mu \leq \mu_{\max}$).
- Allowable drift limit (u_{\max} / H): To maintain the lateral displacement under a tolerable level, story drift shall be kept less than the selected limit, as a function of the story height, H .

Figure 3.12 shows the NEHRP 2003 elastic demand spectrum with different story drift levels for an arbitrary story height of 3810mm (hard conversion from 12.5 ft), which is used as a numerical value in Section 4 to study the behavior of actual systems. In Figure 3.12, two regions are defined and delimited by the transition period at $T_s = 0.45$ s (from Figure 3.5b), namely the constant velocity and constant acceleration regions of the spectrum.

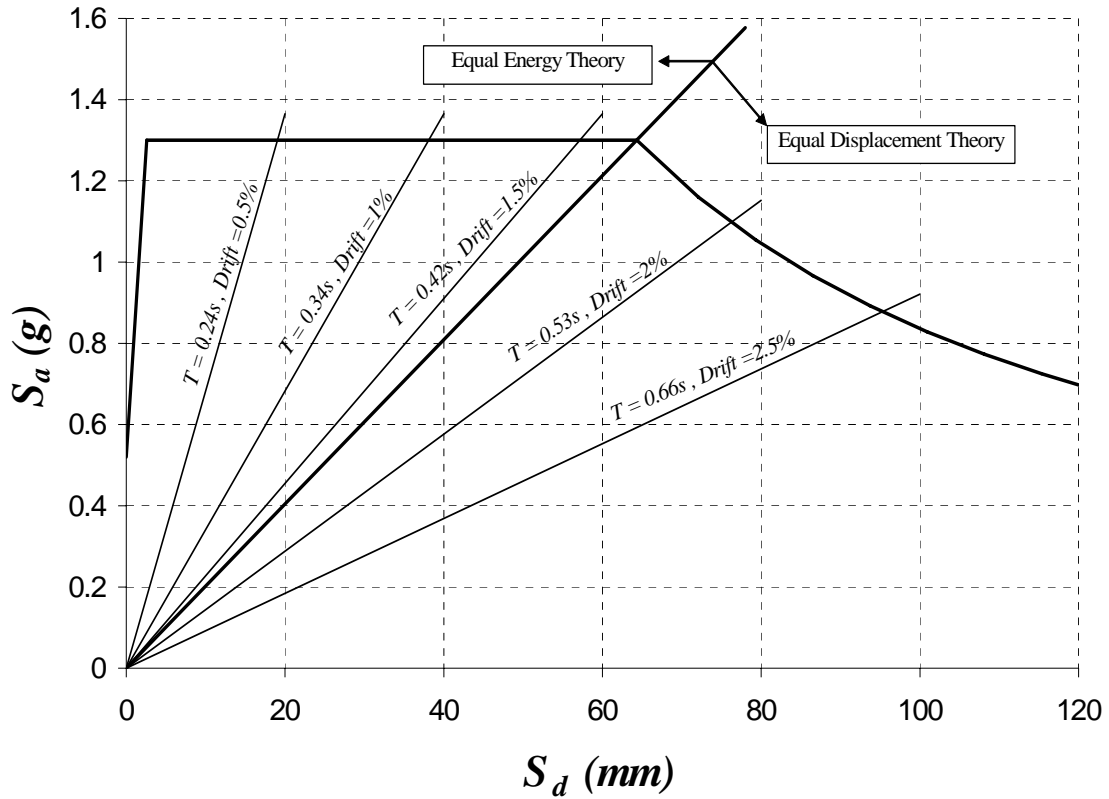


Figure 3.12. Elastic Demand Spectrum ($\xi = 5\%$) and different drift levels for $H = 3810\text{mm}$

In the constant velocity region ($T > T_s$), the equal displacement theory is considered. In other words, the maximum inelastic displacement for a given structure is assumed approximately equal to the maximum displacement that would be obtained if the structure behaved elastically. In that region, a drift limit can be converted into a corresponding period limit, T_L , by the following relationship:

$$T_L = \frac{4\pi^2}{S_{DI}} d \quad (3.30)$$

where d is the elastic displacement corresponding to the design drift limit. For example, for a drift limit of 2% and a story height of 3810 mm, the limit elastic displacement, d , is 76 mm, and (3.30) gives a period limit of 0.53 s. For most structures, the period limit corresponding to a 2% drift limit will be greater than the transition period, T_s . Figures 3.13 and 3.14 show by shaded areas the regions of admissible solutions for the structural fuse concept in terms of frame ductility, μ_f , and global ductility, μ , respectively. The solid line corresponds to the upper bound period limit obtained once time history analysis is performed to match the 2% drift limit. The dashed vertical line represents the period limit of 0.53 s, which can be used as a conservative value for practical purposes.

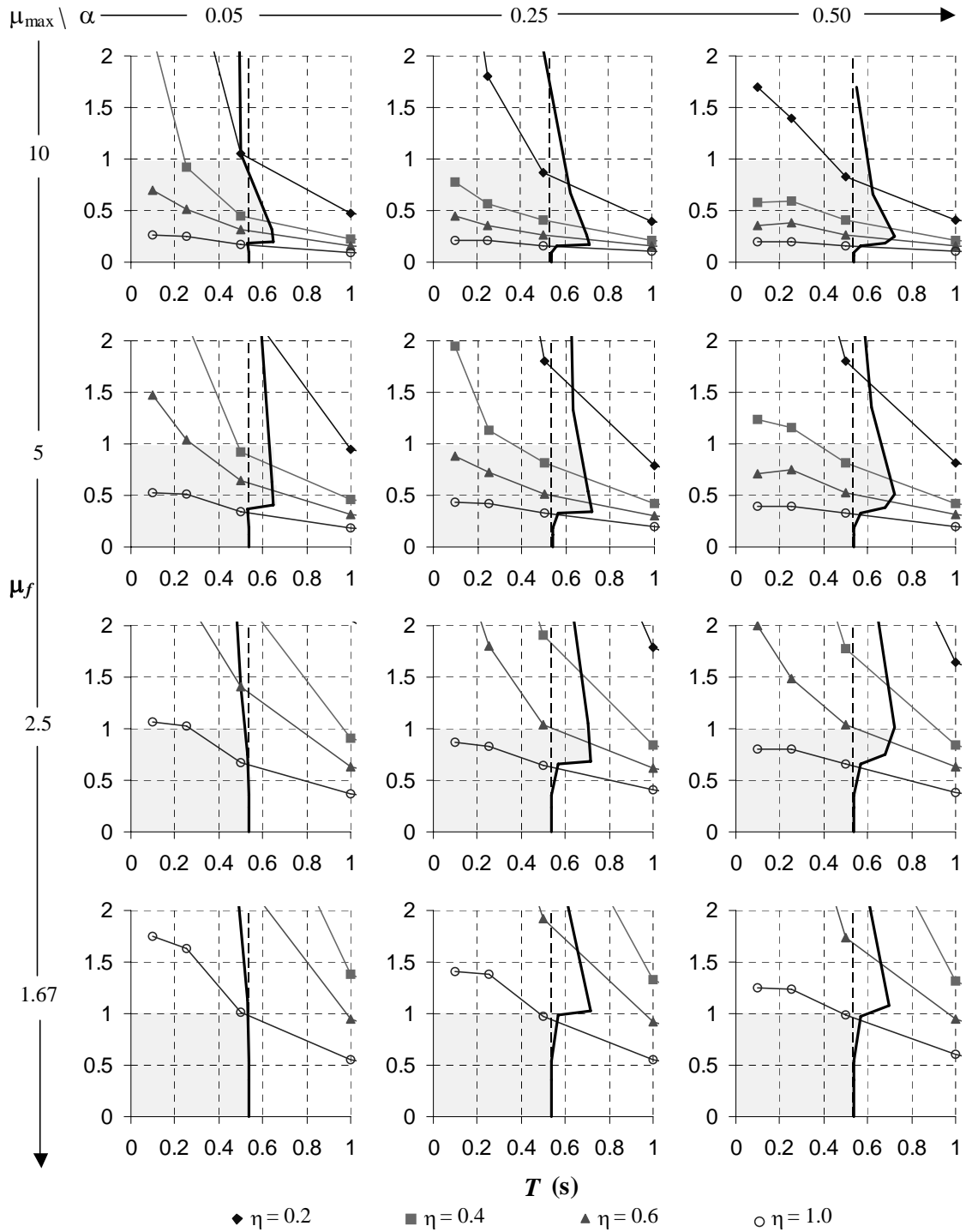


Figure 3.13. Regions of Admissible Solutions in terms of Average Frame Ductility (μ_f), and Story Drift of 2%

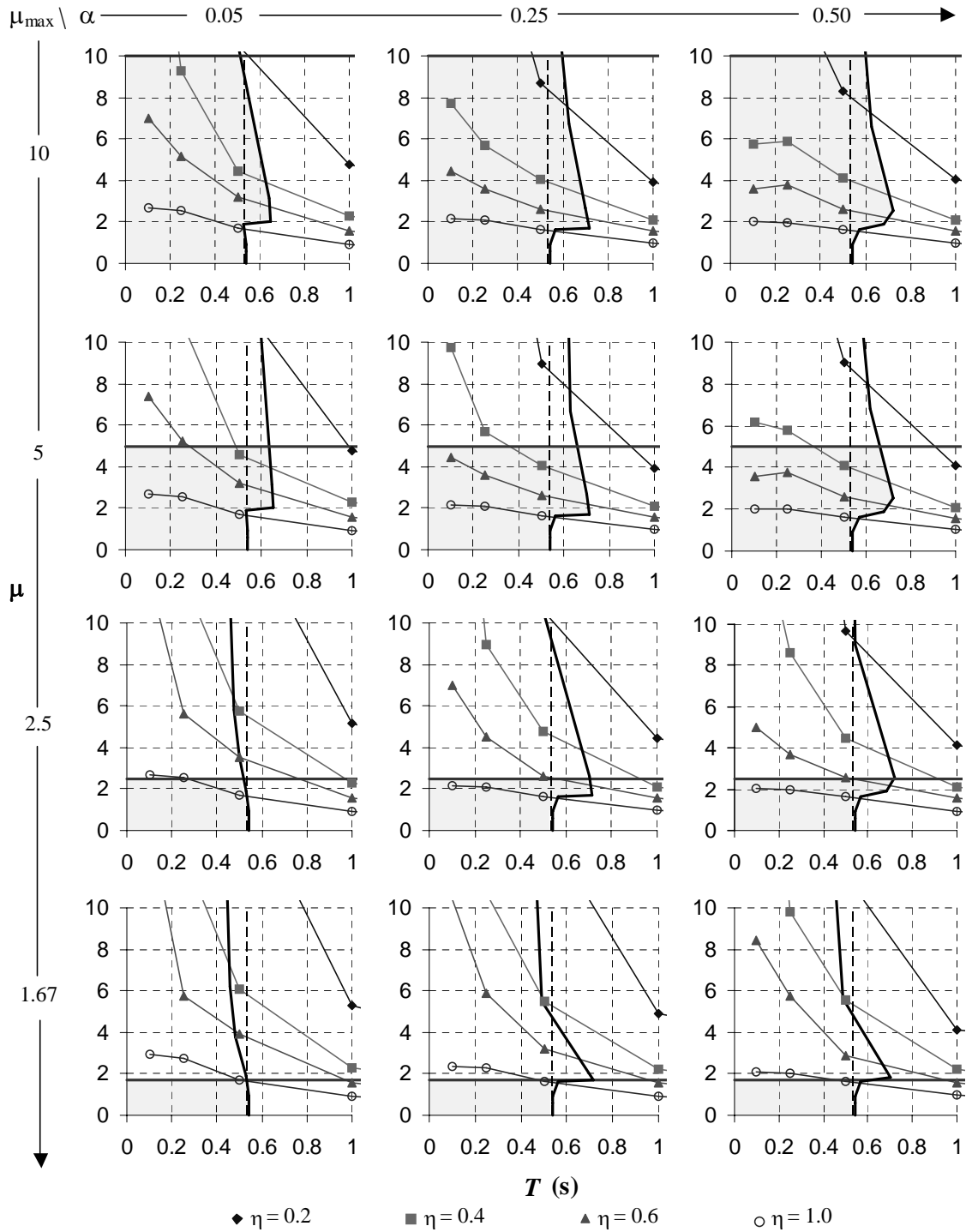


Figure 3.14. Regions of Admissible Solutions in terms of Average Global Ductility (μ), and Story Drift of 2%

The equal energy theory is considered in the constant acceleration region ($T < T_s$). Unlike the constant velocity region, in this range, the maximum inelastic displacement for a given structure is greater than its elastic one. According to the NEHRP Guidelines for the Seismic Rehabilitation of Buildings (FEMA 273 and FEMA 356), inelastic displacement can be calculated from the spectral elastic displacement corrected by a factor, as follows:

$$u_{\max} = d \left[1 + (R - 1) \frac{T_s}{T_L} \right] / R \quad (3.31)$$

where R is the response modification coefficient, given by:

$$R = \frac{S_a}{V_y/W} C_m \quad (3.32)$$

and where C_m is the effective mass factor taken as one for SDOF systems, and W is the structure weight. Using the parameters defined previously, (3.32) may be transformed to:

$$R = \frac{S_{DS}}{\eta \ddot{u}_{g\max}} \quad (3.33)$$

which can be simplified in the constant acceleration region to:

$$R = \frac{2.5}{\eta} \quad (3.34)$$

Substituting (3.34) into (3.31) gives:

$$u_{\max} = S_{DS} \frac{T_L^2}{10\pi^2} \left[1 + \left(\frac{2.5}{\eta} - 1 \right) \frac{T_s}{T_L} \right] \eta \quad (3.35)$$

which is a second order equation in terms of the elastic period limit, T_L . It may be noted

that for $\eta \geq 2.5$ (i.e., $R \leq 1$) the response is elastic, with $u_{max} = d$, and the corresponding period limit is:

$$T_L = 2\pi \sqrt{\frac{d}{S_{DS}}} \quad (3.36)$$

For example, for a drift limit of 1% and a story height of 3810 mm, the allowable displacement is $u_{max} = 38$ mm, and (3.36) gives a period limit of 0.34 s (and progressively less as η decreases, as given by (3.35)). Figures 3.15 and 3.16 show by shaded areas the regions of possible solutions for the structural fuse concept in terms of frame ductility, μ_f , and global ductility, μ , respectively. As shown in the previous example, the solid line corresponds to the upper bound period limit obtained once time history analysis is performed to match the 1% drift limit. The dashed line represents the period limit given by (3.35), which can be used conservatively for practical purposes. It may be noted that the vertical portion of the dashed line corresponds to the elastic period limit of 0.34 s calculated using (3.36).

Note that for large strength-ratio and period values (i.e., $\eta > 0.6$ and $T > 1.0$ s) the structure tends to behave elastically, which means that metallic dampers only provide additional stiffness with no energy dissipation. Elastic behavior of the metallic dampers contradicts the objective of using PED devices, other than the benefit of reducing the lateral displacements to below certain limits (something that could be done just as well with conventional structural elements).

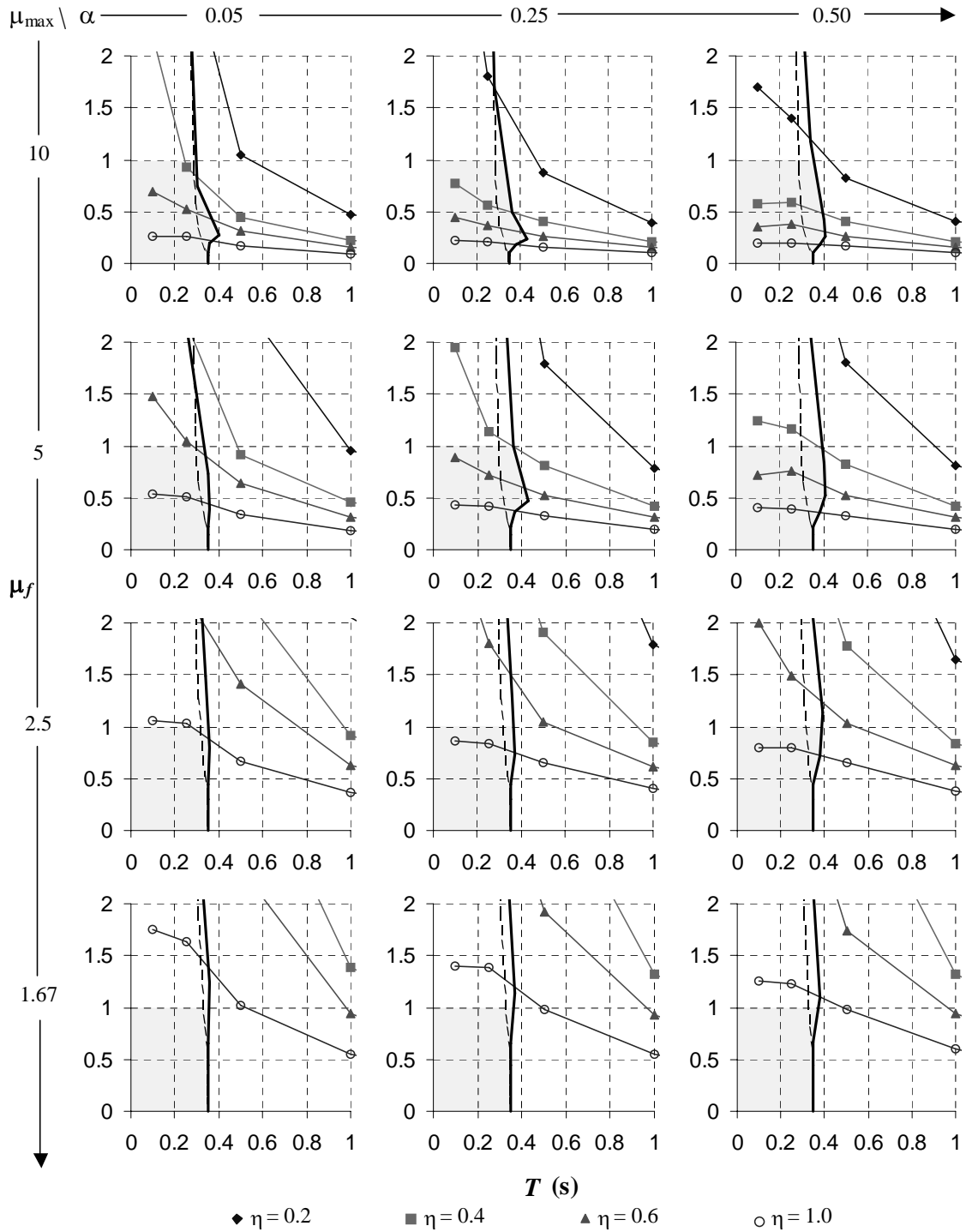


Figure 3.15. Regions of Admissible Solutions in terms of Frame Average Ductility (μ_f), and Story Drift of 1%

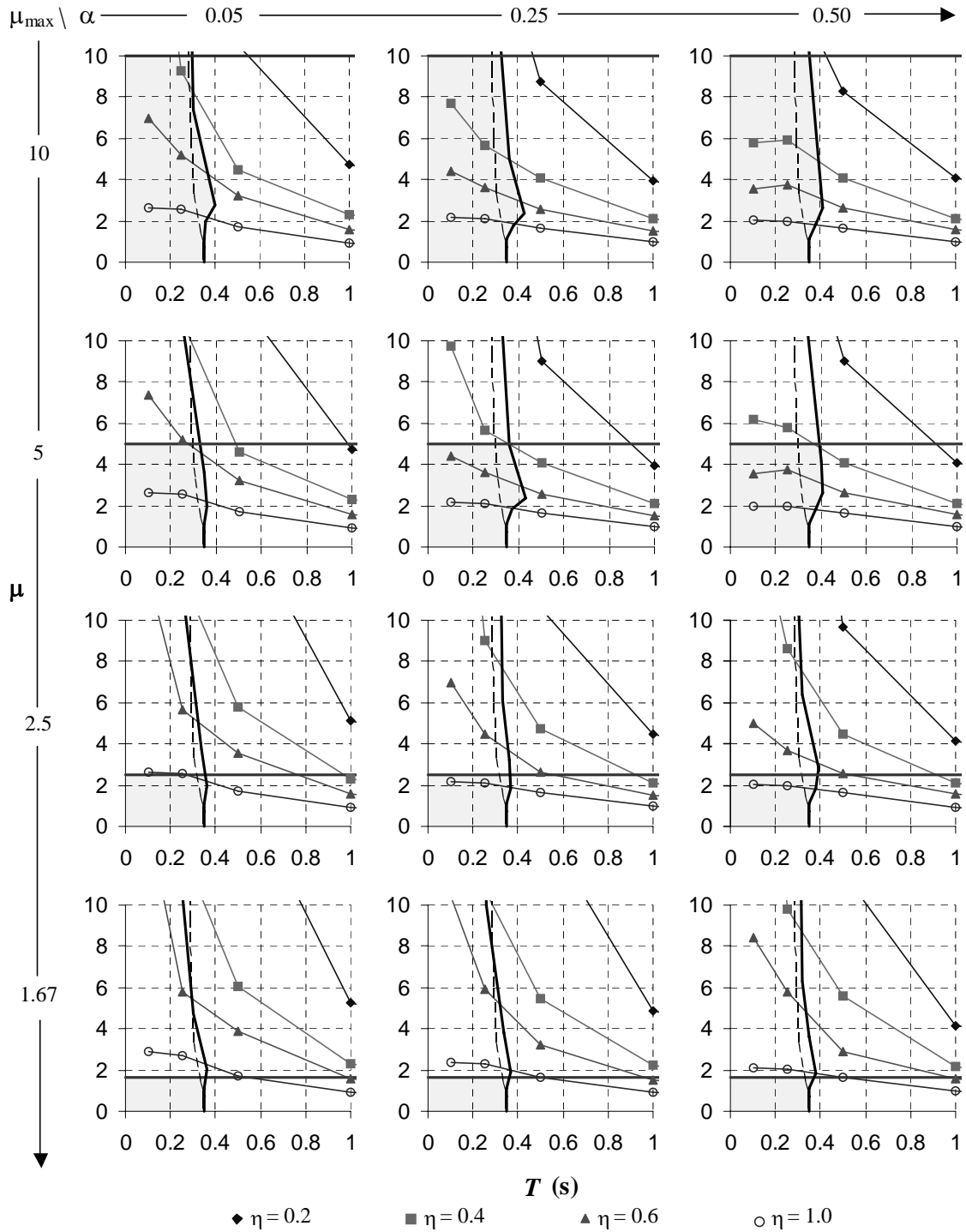


Figure 3.16. Regions of Admissible Solutions in terms of Average Global Ductility (μ), and Story Drift of 1%

3.4.4. Earthquake duration and stiffness ratio effects

To study the effects of earthquake duration on the above results for SDOF systems, 15 s and 60 s long synthetic accelerograms were generated using the TARSCETHS code. Simultaneously, to analyze the possible effects of stiffness ratio, α , on the differences in response obtained for different earthquake durations, time history analyses were performed for $\alpha = 0.05, 0.25, 0.50, \text{ and } 0.75$; for this limited study μ_{\max} was arbitrarily taken as 5. For comparison purposes, short ($T = 0.1$ s) and long ($T = 1.0$ s) period structures were studied. η values of 0.8 and 0.2 were selected to have a frame ductility close to one ($\mu_f \approx 1$) for short and long period systems, respectively.

Table 3.1 summarizes the frame ductility, μ_f , as well as total and normalized energy values obtained for earthquakes of 15 s and 60 s duration. In this table minimum, maximum and average frame ductility, μ_f , values are tabulated for short ($T = 0.1$ s) and long ($T = 1$ s) period structures. These tabulated results correspond to the set of three synthetic earthquakes generated for each duration case studied.

Table 3.1. Frame Ductility, μ_f , and Hysteretic Energy

α (1)	$T = 0.1s$			$\eta = 0.8$			$T = 1s$			$\eta = 0.2$		
	$t = 15s$			$t = 60s$			$t = 15s$			$t = 60s$		
	Min. (2)	Max. (3)	Avg. (4)	Min. (5)	Max. (6)	Avg. (7)	Min. (8)	Max. (9)	Avg. (10)	Min. (11)	Max. (12)	Avg. (13)
Frame Ductility, μ_f												
0.75	0.48	0.53	0.51	0.54	0.62	0.57	0.82	0.86	0.84	0.58	0.83	0.70
0.50	0.50	0.52	0.51	0.57	0.60	0.59	0.74	0.86	0.81	0.52	0.84	0.69
0.25	0.52	0.56	0.55	0.63	0.67	0.65	0.72	0.83	0.78	0.60	0.89	0.75
0.05	0.77	0.79	0.78	0.85	1.06	0.93	0.85	1.05	0.95	0.79	1.20	1.05
Absolute Hysteretic Energy (10^3 kN·mm)												
0.75	0.11	0.18	0.15	0.42	0.60	0.51	7.3	13.8	10.4	15.8	24.7	19.7
0.50	0.26	0.43	0.37	0.95	1.38	1.17	16.1	26.4	22.0	31.6	55.7	42.8
0.25	0.57	0.92	0.78	1.86	2.84	2.39	38.0	61.6	51.7	65.2	114.9	90.6
0.05	2.45	3.36	2.95	7.03	10.97	9.11	187.5	300.6	262.8	325.1	574.5	457.2
Hysteretic Energy Normalized with respect to $mg\Delta_{va}$												
0.75	3.3	5.5	4.7	13.0	18.6	15.8	0.7	1.3	1.0	1.5	2.4	1.9
0.50	5.4	8.9	7.7	19.5	28.4	24.2	1.0	1.7	1.4	2.1	3.6	2.8
0.25	7.4	12.0	10.1	24.2	36.8	30.9	1.2	2.0	1.7	2.1	3.7	2.9
0.05	9.3	12.8	11.3	26.8	41.8	34.7	1.2	2.0	1.7	2.1	3.7	3.0
Hysteretic Energy Normalized with respect to $V_{va}\Delta_{va}$												
0.75	7.1	11.9	10.1	27.7	39.8	33.8	6.1	11.5	8.6	13.2	20.6	16.4
0.50	11.5	19.0	16.4	41.7	60.8	51.7	8.9	14.7	12.2	17.6	30.9	23.8
0.25	15.9	25.6	21.6	51.6	78.7	66.1	10.6	17.1	14.3	18.1	31.9	25.2
0.05	20.0	27.4	24.1	57.3	89.4	74.2	10.4	16.7	14.6	18.1	31.9	25.4
Hysteretic Energy Normalized with respect to $V_{\eta}\Delta_{va}$												
0.75	1.8	3.0	2.5	6.9	10.0	8.5	1.5	2.9	2.2	3.3	5.2	4.1
0.50	3.8	6.3	5.5	13.9	20.3	17.2	3.0	4.9	4.1	5.9	10.3	7.9
0.25	7.9	12.8	10.8	25.8	39.4	33.1	5.3	8.5	7.2	9.0	16.0	12.6
0.05	16.6	22.8	20.1	47.7	74.5	61.8	8.7	13.9	12.2	15.0	26.6	21.2
Hysteretic Energy Normalized with respect to $V_{vd}\Delta_{va}$												
0.75	28.3	47.4	40.4	110.8	159.2	135.2	24.4	45.9	34.6	52.7	82.5	65.6
0.50	22.9	38.0	32.9	83.4	121.6	103.3	17.9	29.3	24.4	35.1	61.8	47.5
0.25	21.2	34.1	28.9	68.8	105.0	88.2	14.1	22.8	19.1	24.1	42.6	33.6
0.05	21.0	28.8	25.3	60.3	94.1	78.1	11.0	17.6	15.4	19.0	33.6	26.7
Hysteretic Energy Normalized with respect to one-cycle-area												
0.75	1.8	3.0	2.5	6.9	10.0	8.5	1.5	2.9	2.2	3.3	5.2	4.1
0.50	1.4	2.4	2.1	5.2	7.6	6.5	1.1	1.8	1.5	2.2	3.9	3.0
0.25	1.3	2.1	1.8	4.3	6.6	5.5	0.9	1.4	1.2	1.5	2.7	2.1
0.05	1.3	1.8	1.6	3.8	5.9	4.9	0.7	1.1	1.0	1.2	2.1	1.7

Comparing the effects of different earthquake durations for the case of $T = 0.1$ s, the average ductility values vary between 13% and 19% (comparing columns (4) and (7) in Table 3.1), while for the case of $T = 1$ s the variation is between 5% and 20% (comparing columns (10) and (13)). The maximum ductility demand differences ranges from 16% to 33% (comparing columns (3) and (6)), and from 2% to 14% (comparing columns (9) and (12)) for $T = 0.1$ s, and $T = 1$ s, respectively. Note that these variations are not significant considering the random characteristics of earthquake excitations.

The effects that the stiffness ratio, α , has on the response can be analyzed with respect to the frame ductility, μ_p , and with respect to the energy dissipated by inelastic deformations. For $0.25 \leq \alpha \leq 0.75$ the average ductility demand does not change substantially. However, substantially larger values are obtained for $\alpha = 0.05$. Therefore, systems with very low post-yielding stiffness are more likely to have large ductility demands values (although in the current structural fuse context these are all essentially intended to be less than one).

With respect to total hysteretic energy, the results shown in Table 3.1 corroborate the information presented in Figure 3.4, recognizing that the energy dissipated by inelastic deformation increases with decreases in α values.

Table 3.1 also shows the hysteretic energy normalized with respect to different criteria, namely, $mg\Delta_{ya}$, $V_y\Delta_{ya}$, and $V_p\Delta_{ya}$. The $mg\Delta_{ya}$ criterion was used by Christopoulos et al. (2002) to express the normalized hysteretic energy as a measure of potential structural damage, while $V_y\Delta_{ya}$ and $V_p\Delta_{ya}$ represent the area covered in the pushover curve (Figure 3.2) by the rectangles defined by the bounds V_y and Δ_{ya} , and V_p and Δ_{ya} , respectively. In this comparative study, mass, m , and yield strength, V_y , increase proportionally with decreases in α values, while Δ_{ya} is kept constant. Consequently, normalized hysteretic energy in Table 3.1 increase with decreases in α in the same proportion. However, the base shear capacity, V_p , increases proportionally but at a lower rate than the increase corresponding to m and V_y , which makes the normalized hysteretic

energy with respect to $V_p\Delta_{ya}$ increase proportionally larger than the ones obtained with respect to $mg\Delta_{ya}$ and $V_y\Delta_{ya}$, respectively.

Table 3.1 presents other normalization criteria for the hysteretic energy with respect to $V_{yd}\Delta_{ya}$ and the area covered by one full cycle hysteretic loop (Figure 3.4), respectively. In both cases, V_{yd} and the one full cycle area increase at the same rate with decreases in α values, and consequently the results corresponding to both normalization criteria vary in the same proportions. However, the increase in both V_{yd} and the area inside one hysteretic loop is larger than the increase corresponding to m and V_y . Consequently, the normalized hysteretic energy decrease proportionally with decreases in α values.

For illustration purposes, single earthquakes of 15 s and 60 s duration were selected to plot time history results. Figures 3.17 to 3.20 show the frame ductility, μ_f , time histories as a function of α for short ($T = 0.1$ s) and long ($T = 1$ s) period structures. In these figures the horizontal lines at $\mu_f = \pm 0.2$ correspond to the yield threshold for $\mu_{max} = 5$ specified in Figure 3.3b. Figures 3.21 to 3.24 show the hysteresis loops corresponding to the normalized base shear with respect to the system capacity, as a function of α for short ($T = 0.1$ s) and long ($T = 1$ s) period structures. Figures 3.21 to 3.24 also illustrate that even though earthquake duration does not appreciably affect the maximum ductility response, it does increase the number of hysteresis cycles developed during the motion, causing an important increase in the amount of energy dissipated. In some circumstances, this larger number of inelastic cycles could have an impact on the fatigue life of the structural fuses, but this is unlikely for well designed ductile devices, and consideration of this effect is beyond the scope of this study.

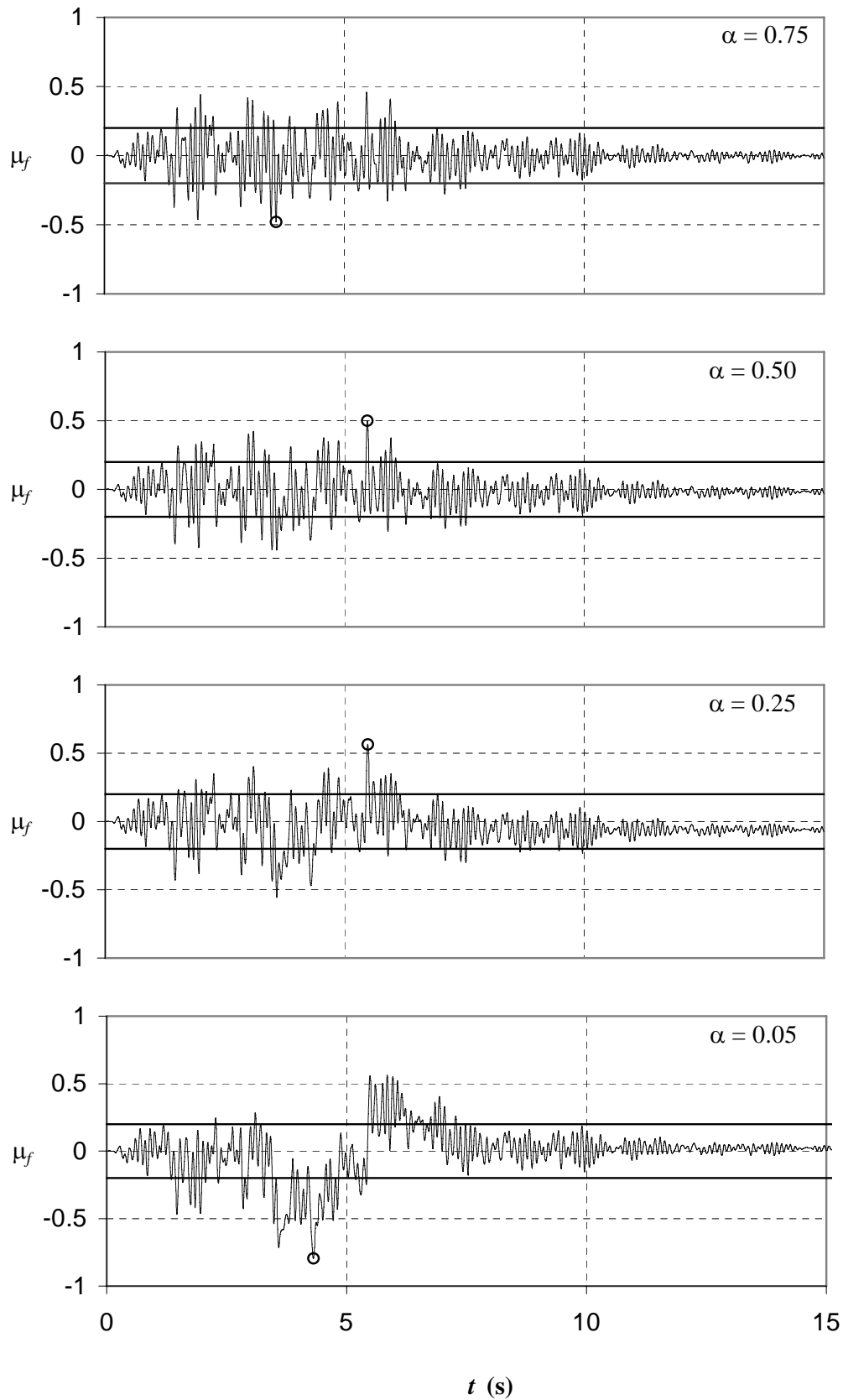


Figure 3.17. Frame Ductility (μ_f) as a function of α for $T = 0.1$ s, $\mu_{\max} = 5$, $\eta = 0.8$, and Earthquake of 15s

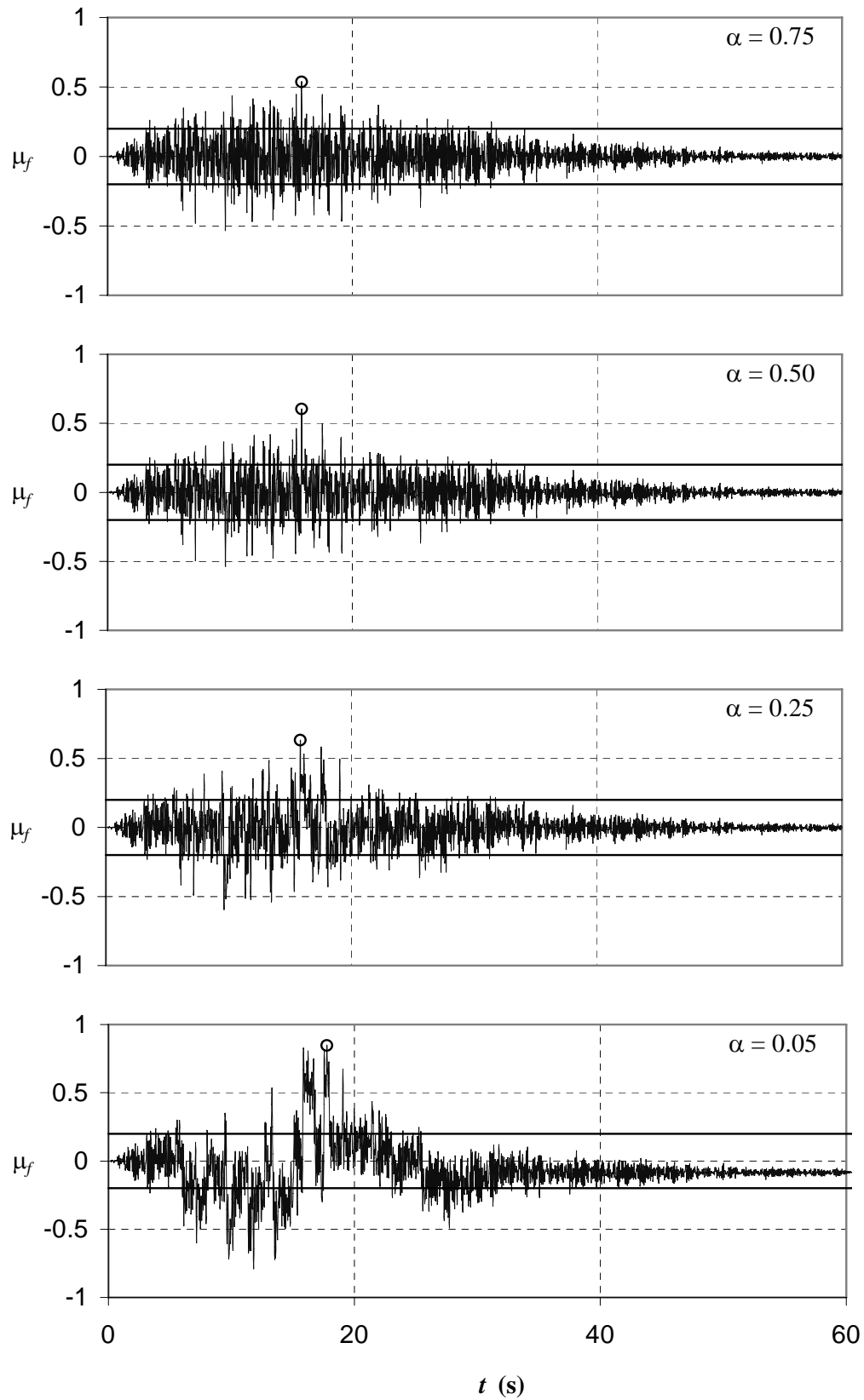


Figure 3.18. Frame Ductility (μ_f) as a function of α for $T = 0.1$ s, $\mu_{\max} = 5$, $\eta = 0.8$, and Earthquake of 60s

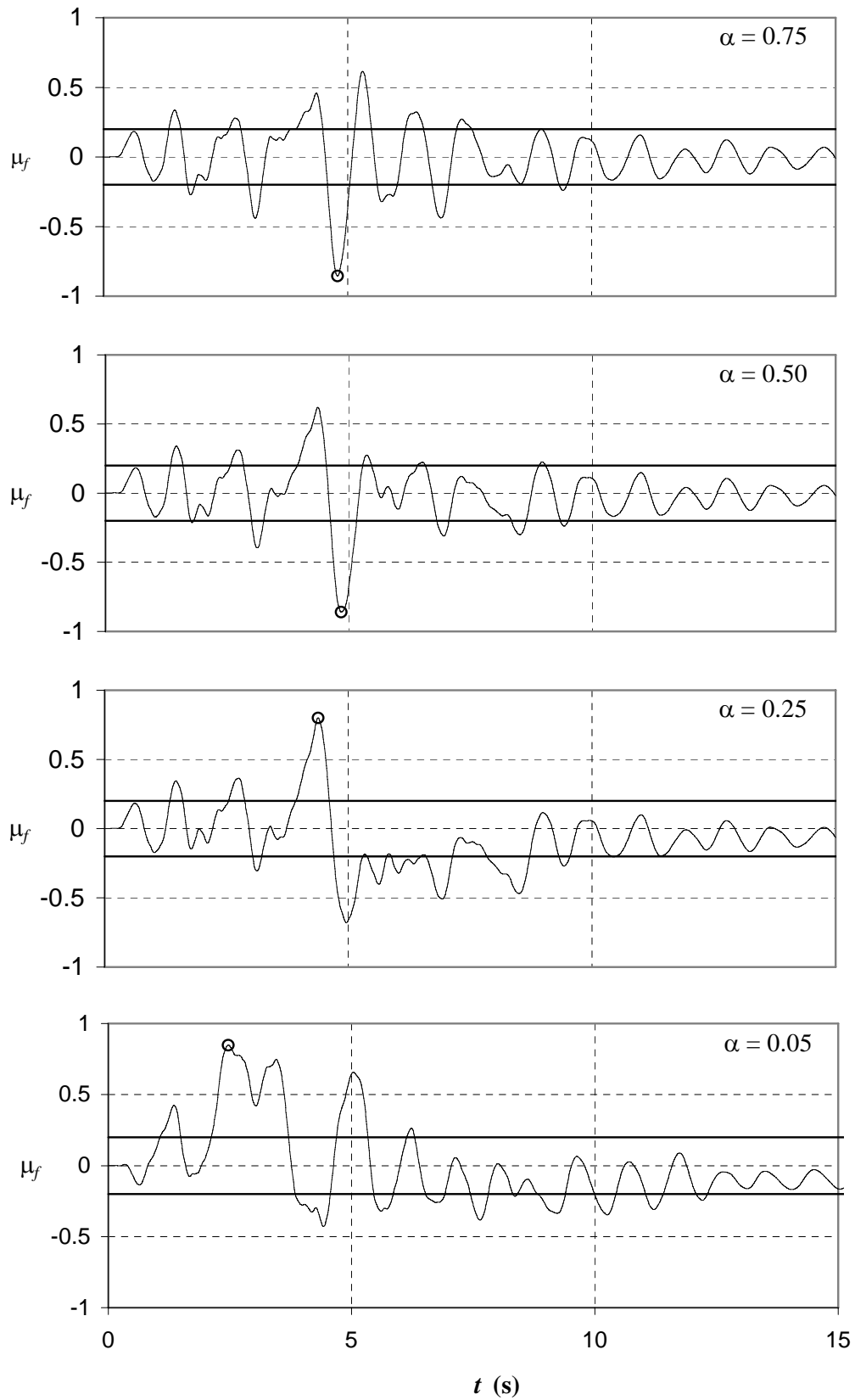


Figure 3.19. Frame Ductility (μ_f) as a function of α for $T = 1$ s, $\mu_{\max} = 5$, $\eta = 0.2$, and Earthquake of 15s

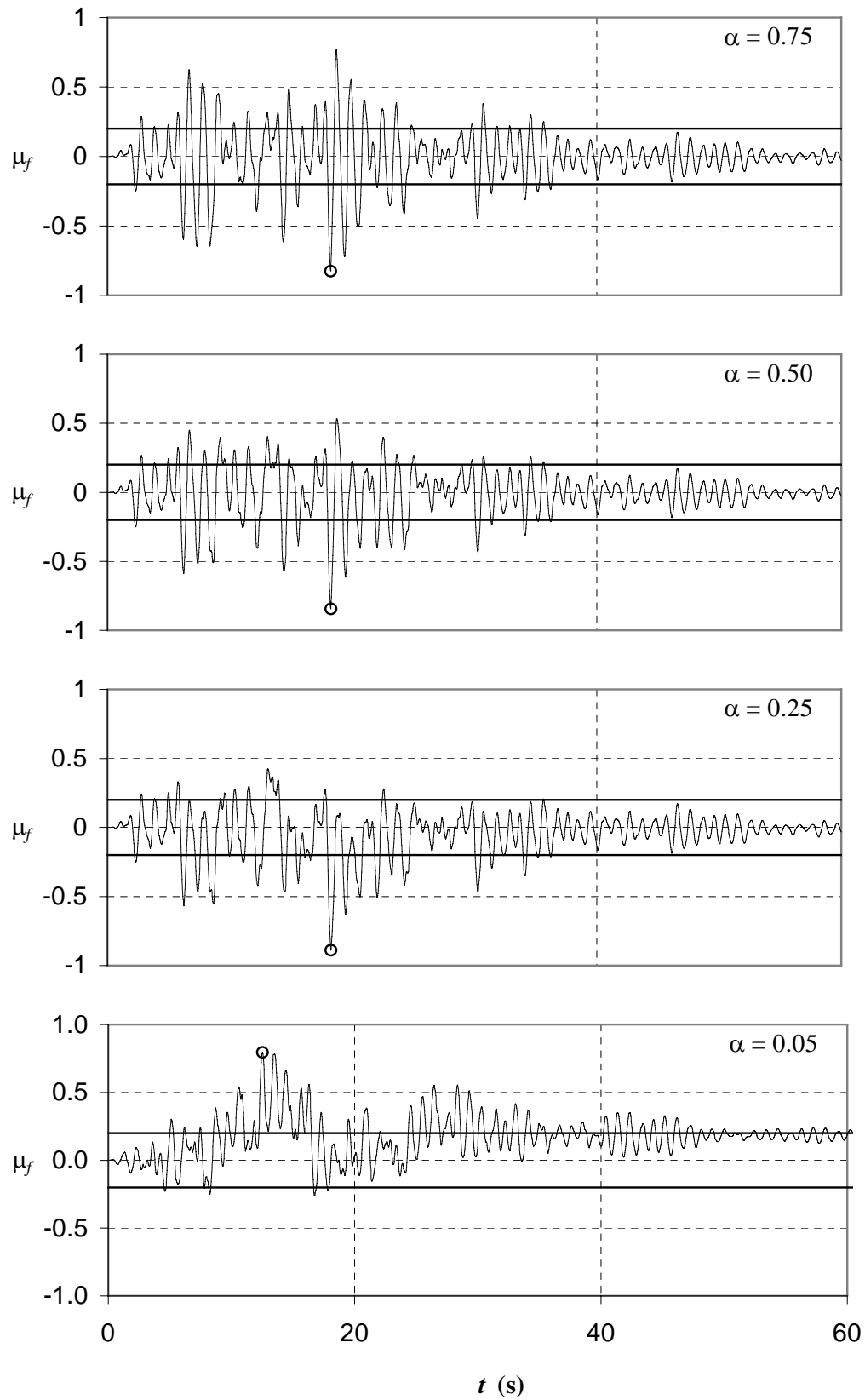


Figure 3.20. Frame Ductility (μ_f) as a function of α for $T = 1$ s, $\mu_{\max} = 5$, $\eta = 0.2$, and Earthquake of 60s

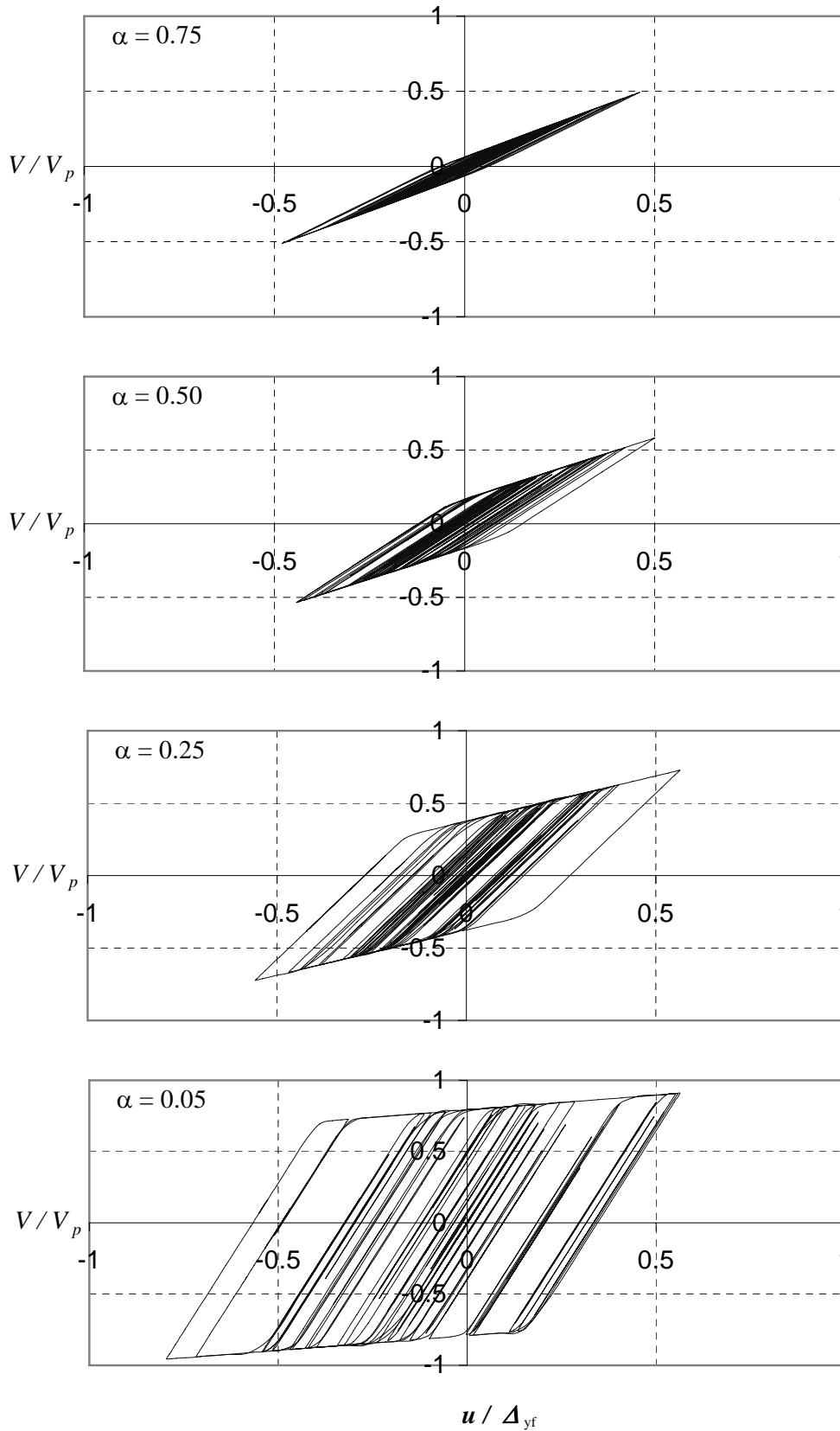


Figure 3.21. Normalized Base Shear as a function of α for $T = 0.1\text{s}$, $\mu_{\max} = 5$, $\eta = 0.8$, and Earthquake of 15s

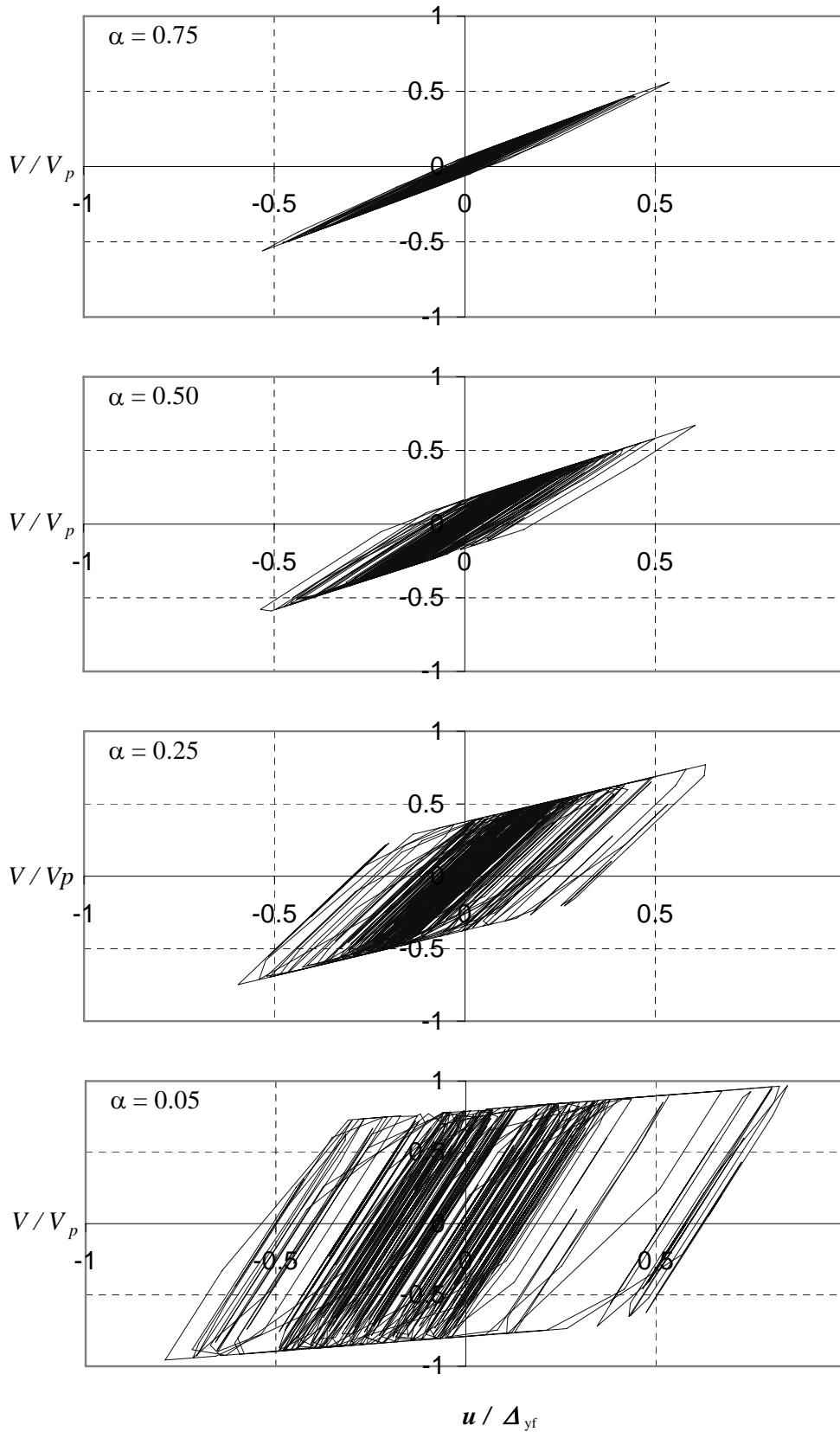


Figure 3.22. Normalized Base Shear as a function of α for $T = 0.1\text{s}$, $\mu_{\max} = 5$, $\eta = 0.8$, and Earthquake of 60s

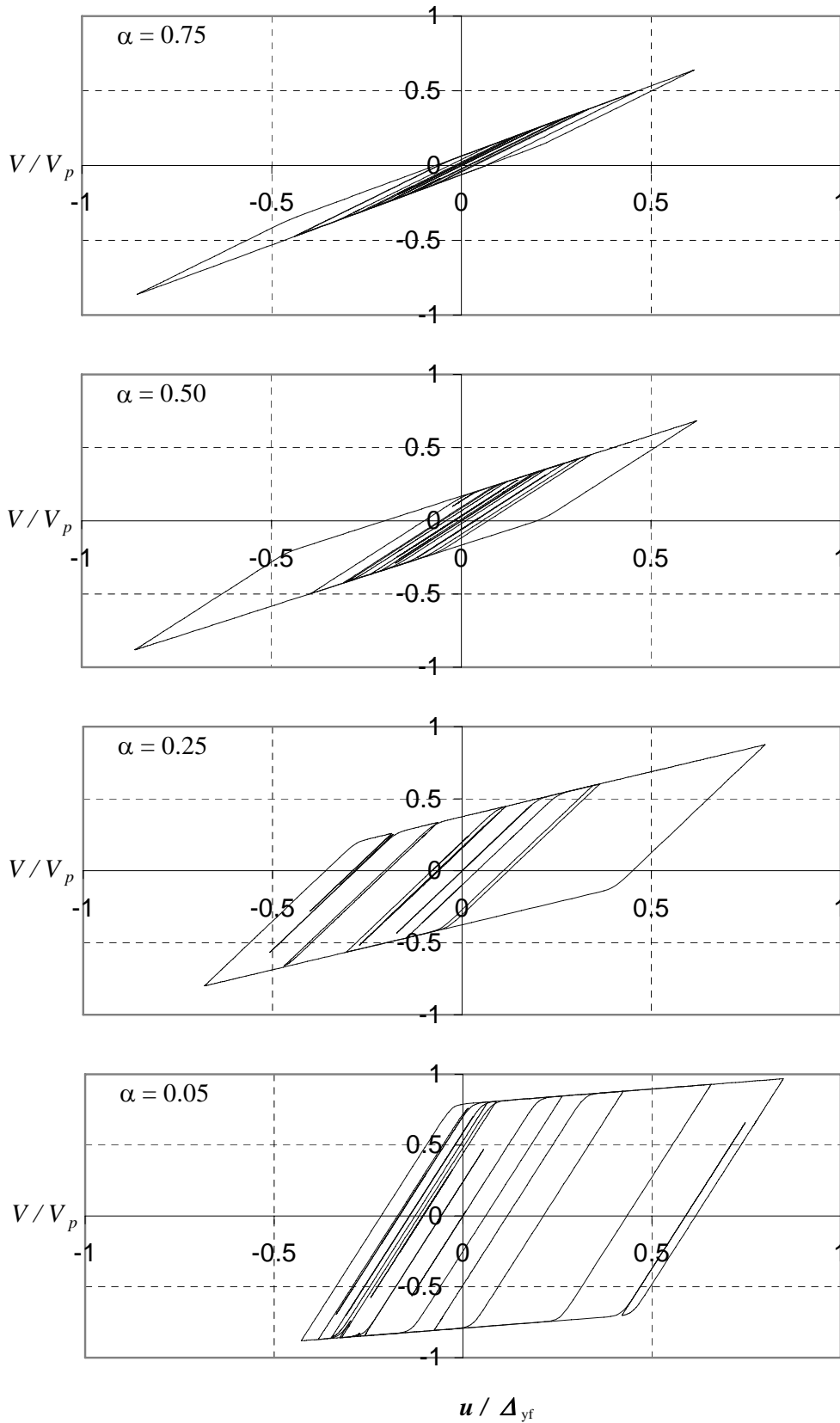


Figure 3.23. Normalized Base Shear as a function of α for $T = 1$ s, $\mu_{\max} = 5$, $\eta = 0.2$, and Earthquake of 15s

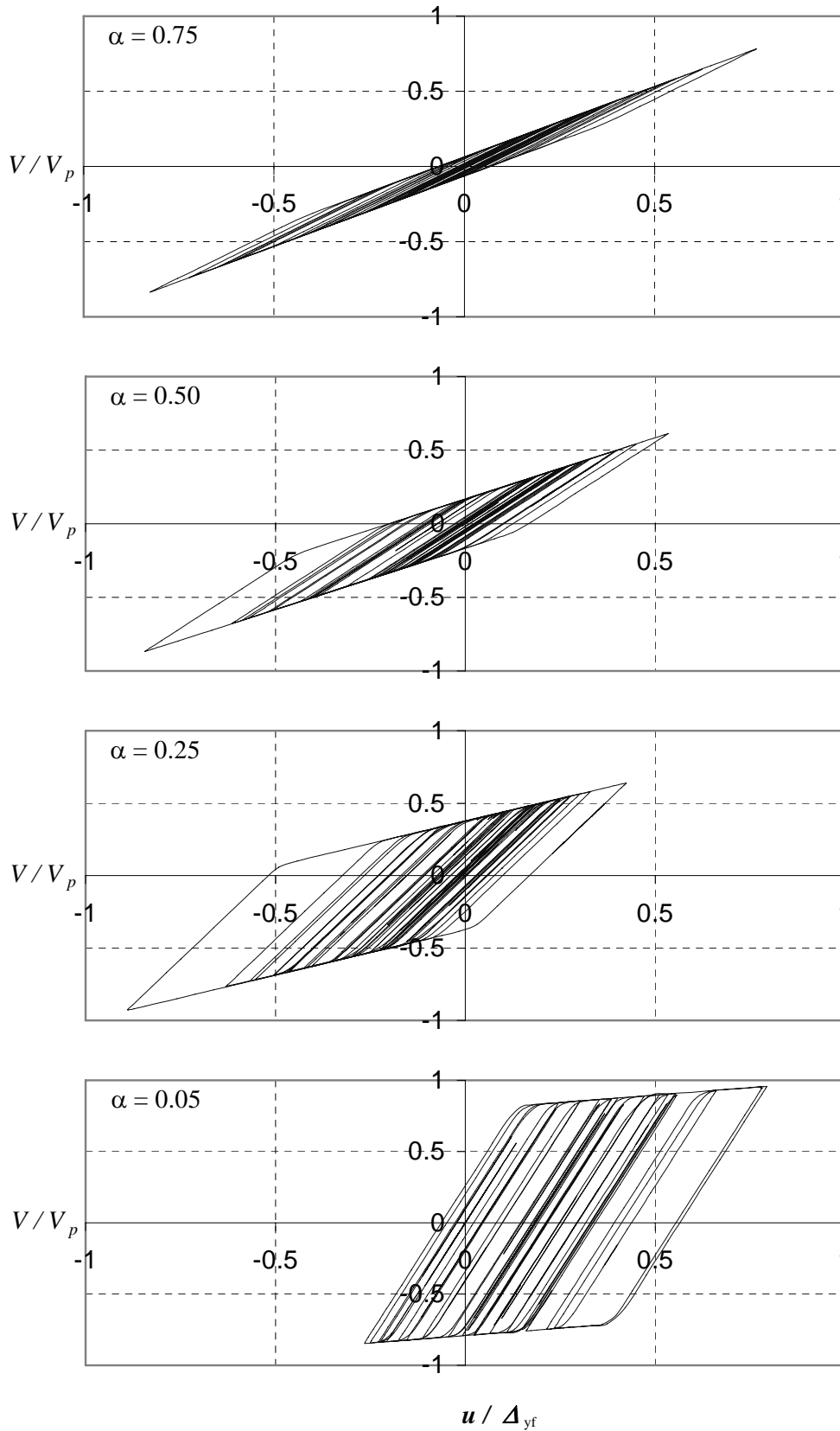


Figure 3.24. Normalized Base Shear as a function of α for $T = 1$ s, $\mu_{\max} = 5$, $\eta = 0.2$, and Earthquake of 60s

3.5. Generic Retrofit Case Study

In this section a case study comparison is made between seismic response of a SDOF without metallic dampers called the bare frame (BF) and the same SDOF system retrofitted with a structural fuse (SF). The same format used to present results for the SDOF system with structural fuses is used to show ductility demand of the BF system as a function of other characteristic parameters. The BF system is modeled as an elasto-plastic SDOF, i.e., with stiffness ratio and maximum displacement ductility taken as $\alpha = 1$, and $\mu_{\max} = \infty$, respectively. Response of the BF is completely defined by the elastic period (see (3.5)), and the frame strength-ratio, η_f , which in this case is equal to:

$$\eta_f = \frac{V_{yf}}{m \ddot{u}_{g\max}} \quad (3.37)$$

where V_{yf} is the yield strength of the frame shown in Figure 3.2.

The same drift limit of 2% for a story height of 3810 mm used in Section 3.4.3 ($u_{\max} = 76$ mm) is again shown in Figure 3.25, where the ductility response of the BF is plotted for a range of strength-ratio, η_f , values between 0.10 and 2.0. The allowable story drift imposes a maximum permissible period of approximately 0.5 s. For some of the BF systems considered, even at that drift limit, the frame must undergo large inelastic deformations. For example, a frame with $\eta_f = 0.4$ at the maximum drift limit has a displacement ductility close to 8, which implies large rotation demands on plastic hinges to dissipate energy via hysteretic behavior (i.e., damage to the primary structure). Elastic behavior would be achieved for systems having large strength-ratio (e.g., $\eta_f \geq 2.5$ as mentioned in Section 3.4.3). For the purpose of this case study, a BF with $m = 0.044$ kN·s²/mm, $K_f = 1.75$ kN/mm, and $V_{yf} = 127.4$ kN (i.e., $T = 1.0$ s and $\eta_f = 0.5$) is arbitrarily selected as a system that does not meet the drift requirements, and that would behave inelastically without seismic retrofit under an earthquake with peak ground acceleration of 0.58g. That existing frame is then retrofitted by the addition of a

structural fuse, with $K_a = 5.25$ kN/mm, and $V_{yd} = 76.4$ kN (i.e., $\alpha = 0.25$, $\mu_{max} = 5$, $T = 0.5$ s, and $\eta = 0.4$).

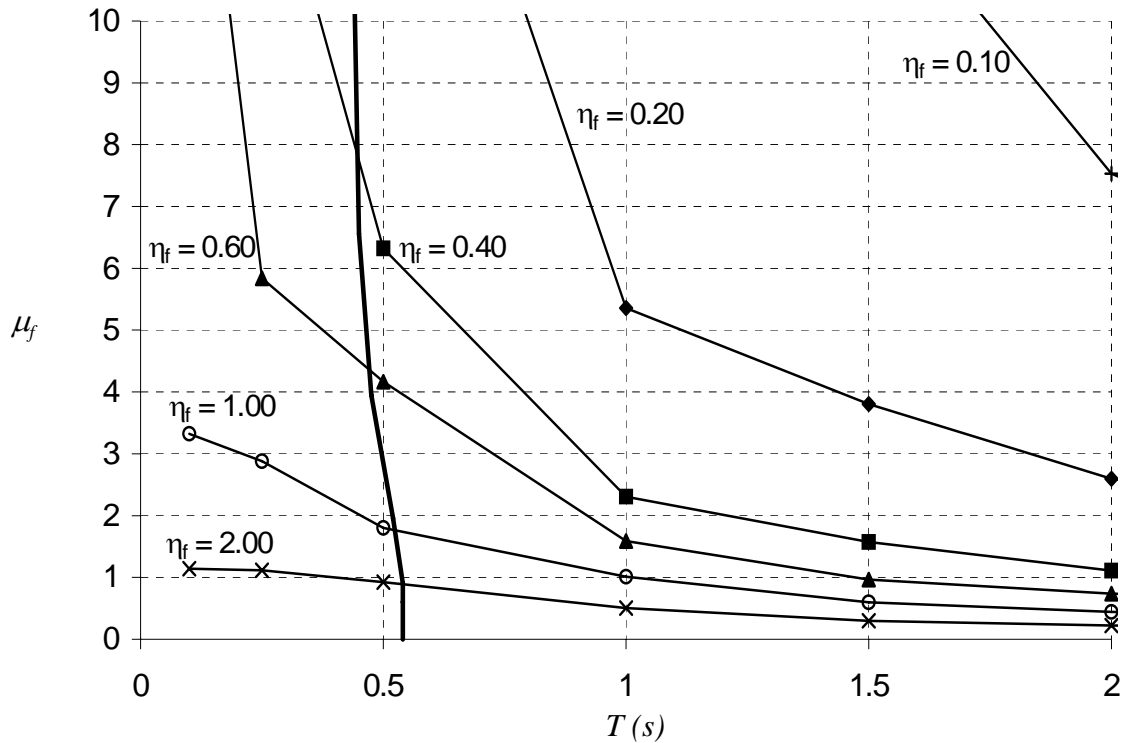


Figure 3.25. Bare Frame (BF) Response and Story Drift Limit of 2% ($u_{max} = 76$ mm)

Figure 3.26 shows the response of both systems. The arrow in Figure 3.26 shows how behavior of the retrofitted system has “moved” into the area of admissible solutions. The period is reduced to one half of the original value ($T = 0.5$ s), and the frame ductility reduces from 1.9 to 0.8, i.e., frame response remains elastic. Maximum ductility demand on the structural fuse is 4.0. Note the reduction of the strength-ratio of the systems (from 0.5 to 0.4). This is caused partly by the use of different definitions for η_f (see (3.37)) and η (see (3.19)), and partly by the fact that for the chosen parameters for the case study the SF has a yield strength lower than that of the corresponding BF (i.e., $V_y < V_{yf}$), as shown in Figure 3.3b.

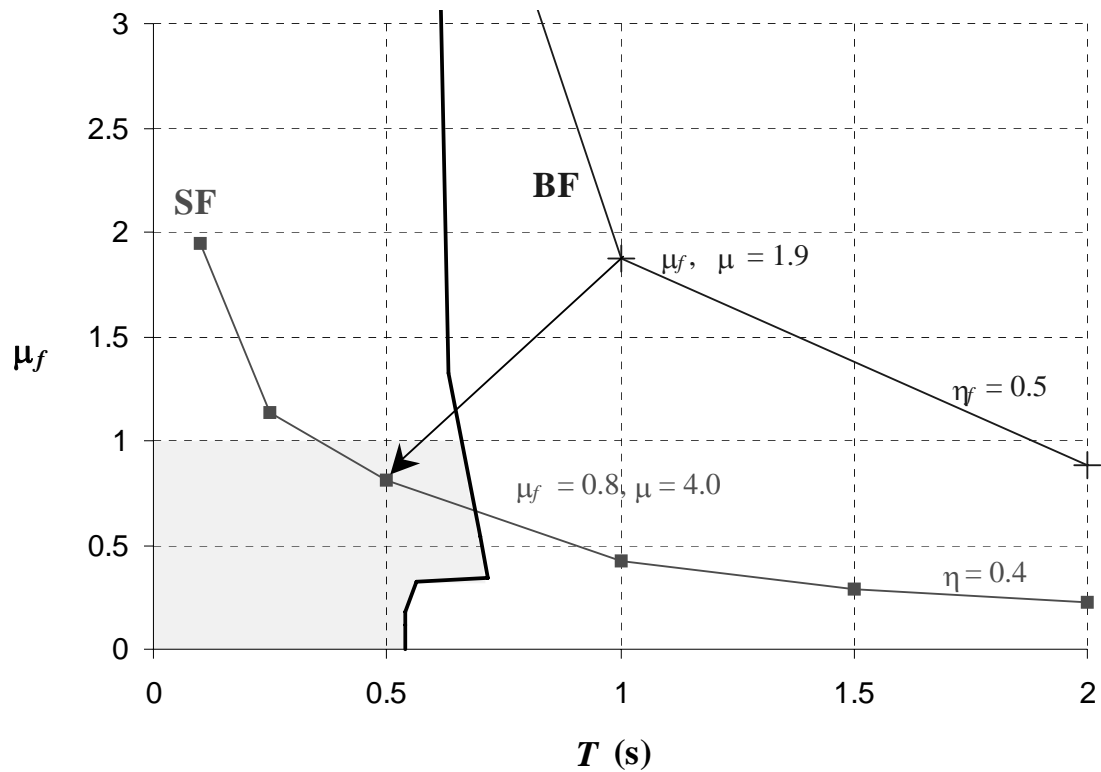


Figure 3.26. Bare Frame (BF) and Structural Fuse (SF) Response

The corresponding displacement, velocity, acceleration and energy dissipated time history results are shown in Figures 3.27 and 3.28. In Figure 3.27, a reduction of about 60% in both the maximum and the permanent deformations are observed when comparing the lateral displacements of the SF to that of the BF systems. A lesser but still important reduction of approximately 40% of the relative peak velocity is observed. However, in this particular case the maximum acceleration is slightly increased (about 14%), due to the additional stiffness provided by the inclusion of a metallic damper. Note that a period reduction of one half translates into an increase in the lateral stiffness of four times (see (3.24)), and the corresponding maximum base shear (related to peak acceleration) is also increased in this example (not shown here).

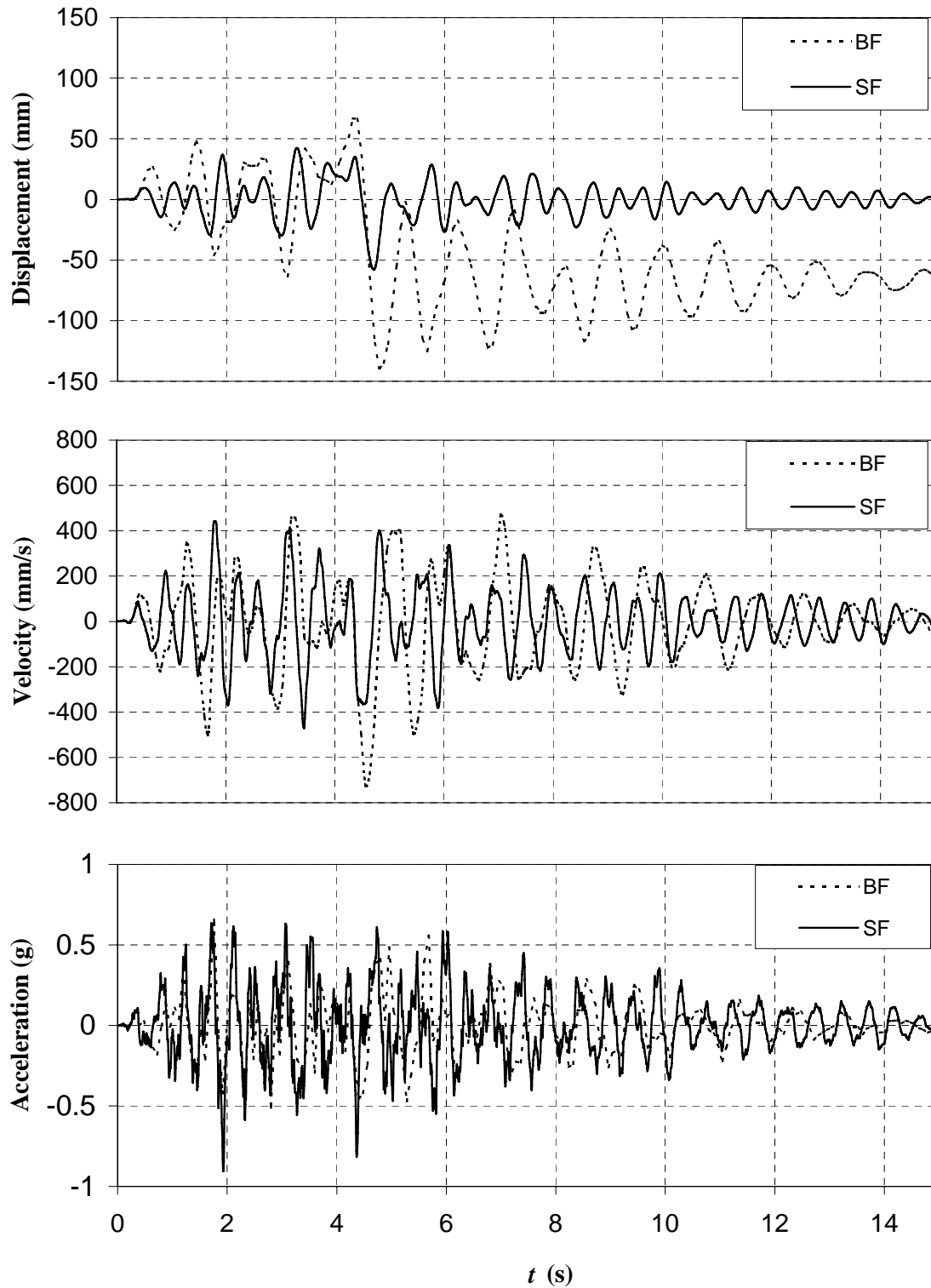


Figure 3.27. Bare Frame (BF) and Structural Fuse (SF) Time Histories

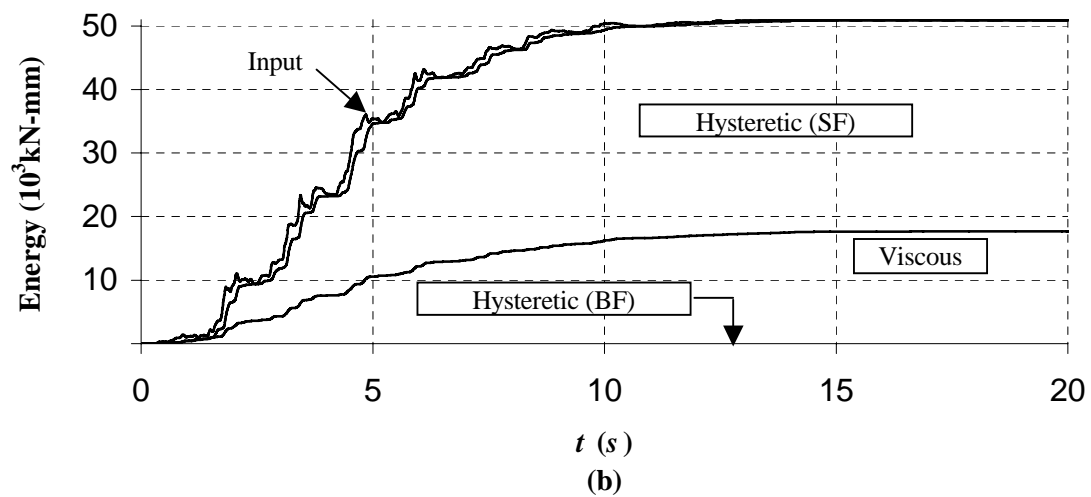
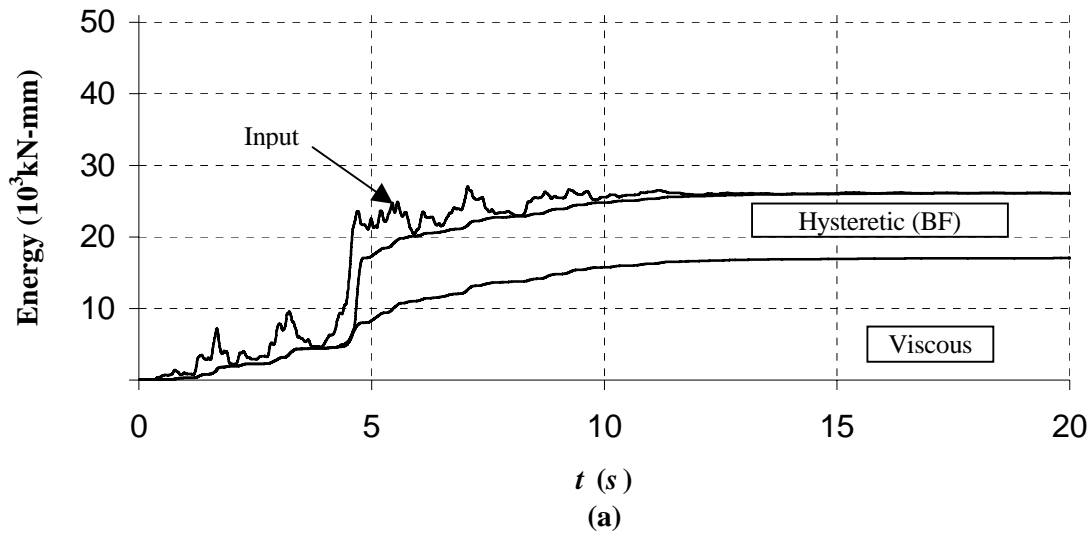


Figure 3.28. Energy Dissipated; (a) Bare Frame (BF), (b) Structural Fuses (SF)

Figure 3.28 shows the difference in energy dissipation between the BF and SF systems. Initially, in the BF, the energy is absorbed by viscous damping action while the frame is still elastic. Once the yield point is reached (at 4.7s) the increment in input energy is dissipated mainly by hysteretic behavior of the frame. The inclusion of a structural fuse eliminates any frame hysteretic energy in the SF case (i.e., BF remains elastic), by introducing hysteretic action exclusively in the fuses, while the energy absorbed by viscous damping is not significantly affected. While in this example, the inclusion of a

structural fuse causes an important increase in the input energy, this increase is totally absorbed by the fuse action, as shown in Figure 3.28.

3.6. Observations

The structural fuse concept has been introduced in this section and validated through a parametric study of the seismic response of SDOF systems. It has been found that the range of admissible solutions that satisfy the structural fuse concept can be parametrically defined, including (as an option) the story drift limit expressed as an elastic period limit (calculated by (3.30), or (3.35) and (3.36), for short and long period structures, respectively). As shown in Figures 3.13 to 3.16, as a design tool, this can be represented graphically with shaded areas delimiting the range of admissible solutions. Systems having $\mu_{\max} \geq 5$ offer a broader choice of acceptable designs over a greater range of η values.

Even though ductility demand, μ_f and μ , does not vary significantly with α (except for small values, i.e., $\alpha = 0.05$), the hysteretic energy substantially increases with decreases in α values. In other words, substantially different amount of hysteretic energy can be dissipated by system having identical ductility demands.

SECTION 4

DESIGN OF SINGLE DEGREE OF FREEDOM (SDOF) SYSTEMS WITH METALLIC STRUCTURAL FUSES

4.1. Introduction

The structural fuse concept can be implemented by adding to the primary structure metallic passive energy dissipating (PED) elements. These special structural elements serve no purpose other than to dissipate seismic energy by inelastic deformations.

Many types of metallic devices have been developed to serve as PED elements for implementation in new structures, and to improve seismic behavior of existing structures. Buckling-restrained Brace (BRB), Triangular Added Damping and Stiffness (T-ADAS) systems, and Shear Panel (SP) systems are three such devices; they have been chosen, for the purpose of this study, to illustrate how the structural fuse concept can be implemented for different types of PED devices working as metallic structural fuses. Furthermore, these PED systems have the advantage that they can be modeled as described in Figure 3.1, and their behavior can be studied using the parametric formulation developed in Section 3.

For each selected system, a general procedure is proposed for designing and retrofitting purposes, and some implementations on new and existing structures are presented as examples of how to operationalize the structural fuse concept. The influence of system-dependant properties is also discussed, in terms of constraints and sensitivity to parameters driving the design of actual systems.

4.2. Metallic Structural Fuses considered in the Analysis

BRB, TADAS, and SP devices are described in this section, and equations to calculate key parameters (i.e., α , μ_{\max} , η , and T) are also presented for the case of a SDOF system composed of a single-bay one-story frame. For a bare frame with pinned-base, as the one shown in Figure 4.1, lateral stiffness, K_f , shear capacity, V_{yf} , and yield deformation, Δ_{yf} , are equal to:

$$K_f = \frac{12EI_C}{H^3} \left[\frac{1}{2 + \frac{I_C L}{I_B H}} \right] \quad (4.1)$$

$$V_{yf} = \frac{2F_{yf} Z_B}{H} \quad (4.2)$$

$$\Delta_{yf} = \frac{F_{yf} Z_B H^2}{6EI_C} \left(2 + \frac{I_C L}{I_B H} \right) \quad (4.3)$$

where L and H are the frame length and height, respectively; I_B and Z_B are the moment of inertia and plastic modulus of the beam, respectively; I_C is the moment of inertia of the columns; F_{yf} and E are the specified yield stress and modulus of elasticity of the used material (i.e., steel in this case), respectively.

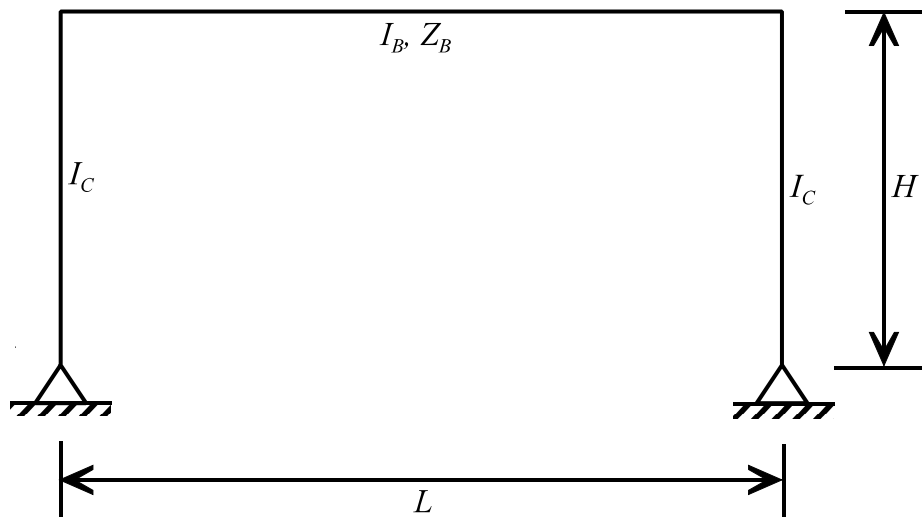


Figure 4.1. Bare Frame Properties

These equations define the pushover curve corresponding to the bare frame, as shown in Figure 3.2, and are used with the properties of the added device system in subsequent sections to calculate key parameters corresponding to each of the studied metallic fuse devices.

4.2.1. Buckling-restrained Brace (BRB)

BRBs have been implemented as an alternative to overcome some problems found in the design of concentric braced frames (CBF), for example: strength and stiffness degradation of the braces under cyclic loads, and significant difference between tension and compression capacity of the braces, which causes important out-of-balance loads on beams where braces connect. Figure 4.2, adapted from Nippon Steel Corporation, shows separately the components of an buckling-restrained brace.

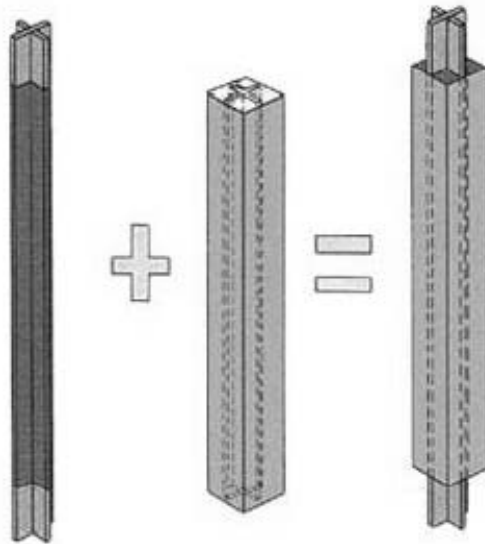


Figure 4.2. Buckling-restrained Braces Components (Nippon Steel Corporation, 1980's)

Figure 4.3 shows an buckling-restrained braced frame (BRBF), whose damper lateral stiffness, K_d , base shear capacity, V_{yd} , and yield deformation, Δ_{yd} , can be calculated as:

$$K_d = \frac{4A_b E}{L} \cos^3(\theta) \quad (4.4)$$

$$V_{yd} = 2F_{yd} A_b \cos(\theta) \quad (4.5)$$

$$\Delta_{yd} = \frac{F_{yd} L}{2E \cos^2(\theta)} \quad (4.6)$$

where A_b , F_{yd} , and θ are the cross-sectional area, the specified steel yield stress, and the inclination of the BRB from the horizontal, respectively. Other variables were previously defined. An BRBF does not require the use of device support system as defined in Section 3.2. Therefore, $K_a = K_d$ in (3.2), and $\Delta_{ya} = \Delta_{yd}$ in (3.6).

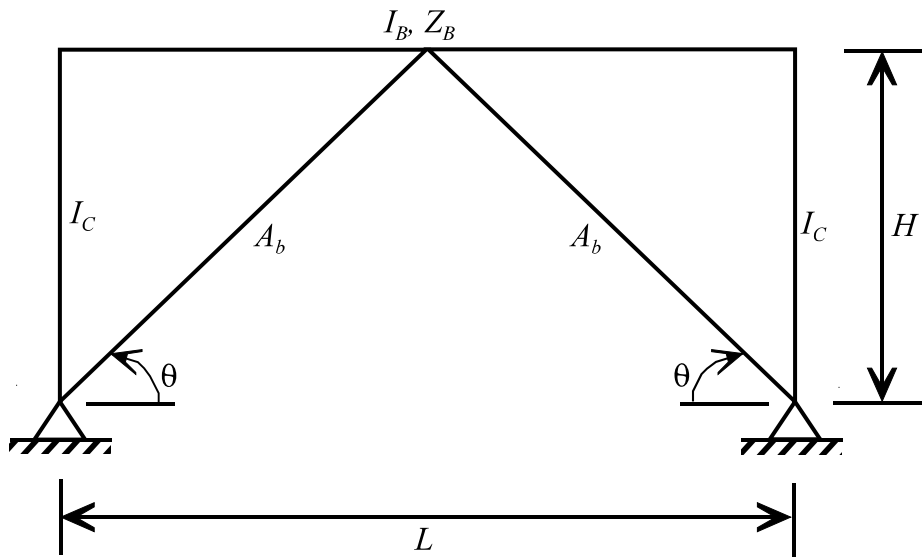


Figure 4.3. Frame and BRB Properties

These equations combined with (4.1), (4.2), and (4.3) provide the following set of equations to compute the key parameters for the BRB case:

$$\alpha = \frac{1}{1 + \frac{1}{3} \frac{ds}{g_{BRB}^{3/2}}} \quad (4.7)$$

$$\mu_{\max} = \frac{1}{3} \frac{e_{BRB} s}{g_{BRB}} \quad (4.8)$$

$$\eta = 2f_{BRB} \left(\frac{1}{g_{BRB}^{1/2}} + 3 \frac{g_{BRB}}{ds} \right) \quad (4.9)$$

$$T = \pi \left(\frac{l}{\frac{3}{s} + \frac{d}{g_{BRB}^{3/2}}} \right)^{1/2} \quad (4.10)$$

where

$$g_{BRB} = 1 + \left(2 \frac{H}{L} \right)^2 \quad (4.11)$$

$$s = 2 + \left(\frac{I_C}{I_B} \right) \left(\frac{L}{H} \right) \quad (4.12)$$

$$d = \frac{A_b H^3}{I_C L} \quad (4.13)$$

$$e_{BRB} = \frac{F_{yf} Z_B H^2}{F_{yd} I_C L} \quad (4.14)$$

$$f_{BRB} = \frac{F_{yd} A_b}{m \ddot{u}_{gmax}} \quad (4.15)$$

$$l = \frac{m H^3}{EI_C} \quad (4.16)$$

and m and \ddot{u}_{gmax} are the mass and the peak ground acceleration, respectively. The other variables have been defined previously.

This set of parameters is used in Sections 4.5 and 4.6 for new construction design, and retrofit of existing structures, respectively, using BRBs as metallic structural fuses.

4.2.2. Triangular Added Damping and Stiffness (T-ADAS) System

Figure 4.4 describes the components of a frame with T-ADAS dampers mounted on braces in chevron configuration. In Figure 4.4 the plate properties corresponding to the T-ADAS dampers are also shown. For this system, the damper lateral stiffness, K_d , base shear capacity, V_{yd} , and yield deformation, Δ_{yd} , are equal to:

$$K_d = \frac{NEbt^3}{6h^3} \quad (4.17)$$

$$V_{yd} = \frac{Nbt^2}{4h} F_{yd} \quad (4.18)$$

$$\Delta_{yd} = \frac{3}{2} \frac{F_{yd} h^2}{Et} \quad (4.19)$$

where N is the number of plates; b , h , and t are the base, height and thickness of the plates, respectively; and F_{yd} is the T-ADAS device specified steel yield stress. As shown in Figure 4.4, T-ADAS dampers must be mounted on a device support system, typically provided by concentric braces, whose lateral stiffness, K_s , can be calculated as:

$$K_s = \frac{4A_b E}{L} \cos^3(\theta) \quad (4.20)$$

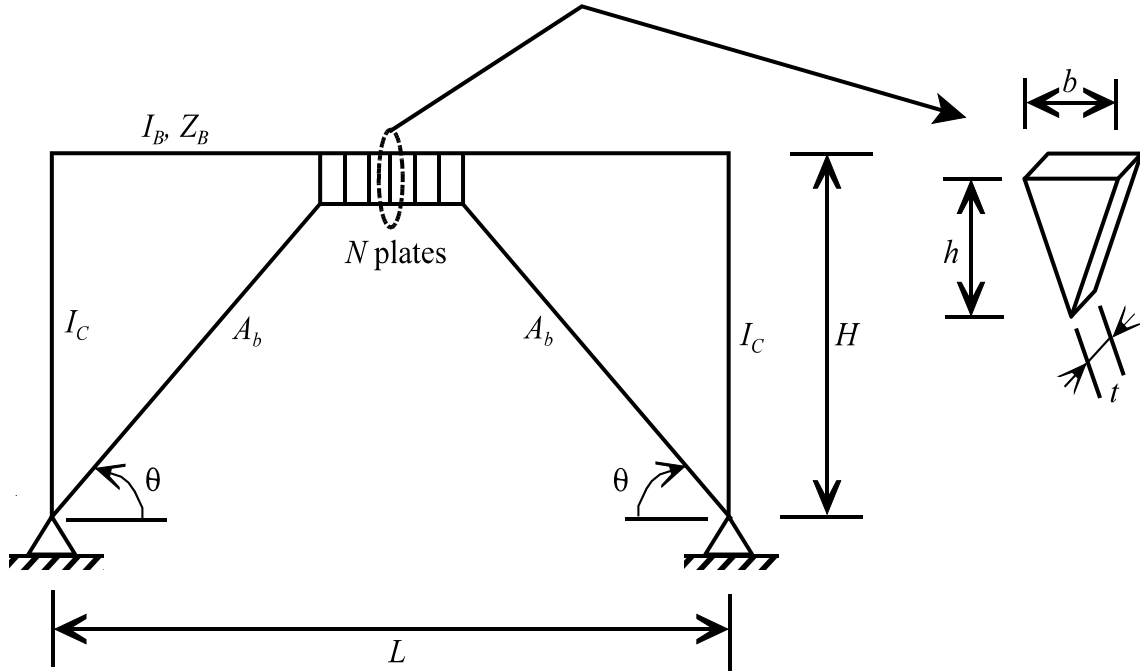


Figure 4.4. Frame and T-ADAS Properties

These equations combined with (4.1), (4.2), and (4.3) are used to compute the key parameters for the T-ADAS case:

$$\alpha = \frac{1}{1 + \frac{s}{\left[3 \left(\frac{g_{TADAS}^{3/2}}{d} \right) + \frac{72}{n_{TADAS}} \right]}} \quad (4.21)$$

$$\mu_{\max} = \frac{1}{9} \left[\frac{e_{TADAS} s}{\left(1 + \frac{1}{24} p_{TADAS} g_{TADAS}^{3/2} \right)} \right] \quad (4.22)$$

$$\eta = f_{TADAS} \left(1 + \frac{1}{24} p_{TADAS} g_{TADAS}^{3/2} \right) \left[\frac{1}{\left(\frac{1}{6} q g_{TADAS}^{3/2} + 4r \right)} + 18 \frac{v_{TADAS}}{s} \right] \quad (4.23)$$

$$T = \pi \left(\frac{l}{\frac{3}{s} + \frac{d}{g_{TADAS}^{3/2} + 24/p_{TADAS}}} \right)^{1/2} \quad (4.24)$$

where

$$g_{TADAS} = 1 + \left(\frac{2(H-h)}{L} \right)^2 \quad (4.25)$$

$$n_{TADAS} = \frac{NH^3 b t^3}{I_C h^3} \quad (4.26)$$

$$e_{TADAS} = \frac{F_{yf} Z_B H^2 t}{F_{yd} I_C h^2} \quad (4.27)$$

$$p_{TADAS} = \frac{NL b t^3}{A_b h^3} \quad (4.28)$$

$$f_{TADAS} = \frac{F_{yd} t^2}{m \ddot{u}_{gmax}} \quad (4.29)$$

$$q = \frac{L t^3}{A_b h^2} \quad (4.30)$$

$$r = \frac{h}{Nb} \quad (4.31)$$

$$v_{TADAS} = \frac{I_C h^2}{H^3 t^3} \quad (4.32)$$

This set of parameters is used in Sections 4.5 and 4.6 for new construction design, and retrofit of existing structures, respectively, using T-ADAS dampers as metallic structural fuses.

4.2.3. Shear Panel (SP)

Like the T-ADAS dampers case, the configuration used for the SP systems is the chevron arrangement (i.e., metallic panel mounted on a support system). For the frame with a SP

damper shown in Figure 4.5, the damper lateral stiffness, K_d , base shear capacity, V_{yd} , and yield deformation, Δ_{yd} , are equal to:

$$K_d = \frac{5}{6} \frac{Gwt}{h} \quad (4.33)$$

$$V_{yd} = \frac{\sqrt{3}}{3} F_{yd} wt \quad (4.34)$$

$$\Delta_{yd} = \frac{2\sqrt{3}}{5} \frac{F_{yd} h}{G} \quad (4.35)$$

where w , t and h are the width, thickness, and height of the SP, respectively; and G is the steel shear modulus. Like in the T-ADAS case, the lateral stiffness of the device support system, K_s , can be calculated using (4.20).

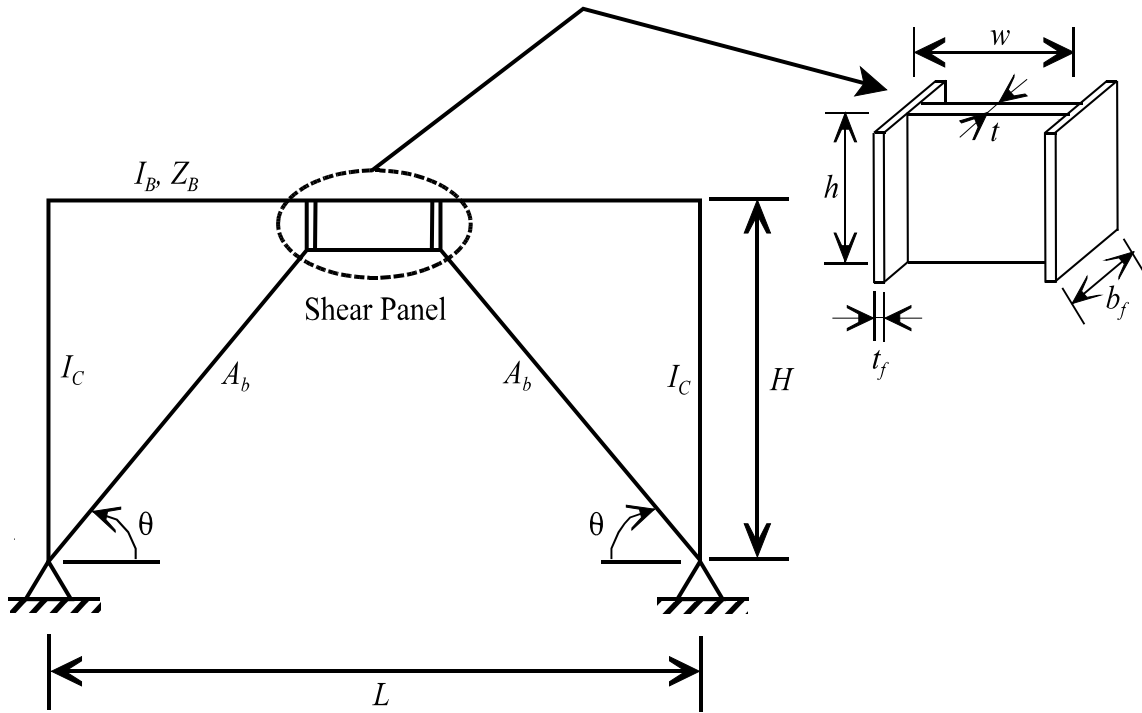


Figure 4.5. Frame and SP Properties

These equations combined with (4.1), (4.2), and (4.3) are used to calculate the key parameters for the SP dampers case:

$$\alpha = \frac{1}{1 + \frac{s}{\left[3 \left(\frac{g_{SP}^{3/2}}{d_{SP}} \right) + \left(\frac{72}{5} \frac{1}{n_{SP}} \right) \right]}} \quad (4.36)$$

$$\mu_{\max} = \frac{5\sqrt{3}}{36} \left[\frac{e_{SP} s}{1 + \left(\frac{5}{24} p_{SP} g_{SP}^{3/2} \right)} \right] \quad (4.37)$$

$$\eta = \sqrt{3} f_{SP} \left(1 + \frac{5}{24} p_{SP} g_{SP}^{3/2} \right) \left[\frac{1}{\left(3 + \frac{5}{8} p_{SP} g_{SP}^{3/2} \right)} + \frac{24}{5} \frac{v_{SP}}{s} \right] \quad (4.38)$$

$$T = \pi \left(\frac{l}{\left(\frac{3}{s} + \frac{d_{SP}}{g_{SP}^{3/2} + \left(\frac{24}{5} p_{SP} \right)} \right)} \right)^{1/2} \quad (4.39)$$

where

$$g_{SP} = 1 + \left(\frac{2(H-h)}{L-w} \right)^2 \quad (4.40)$$

$$d_{SP} = \frac{A_b H^3}{I_C (L-w)} \quad (4.41)$$

$$n_{SP} = \frac{GH^3 bt}{EI_C h} \quad (4.42)$$

$$e_{SP} = \frac{F_{yf}}{F_{yd}} \frac{GZ_B H^2}{EI_C h} \quad (4.43)$$

$$p_{SP} = \frac{Gwt(L-w)}{EA_b h} \quad (4.44)$$

$$f_{SP} = \frac{F_{yd} w t}{m \ddot{u}_{gmax}} \quad (4.45)$$

$$v_{SP} = \frac{EI_C h}{GH^3 w t} \quad (4.46)$$

This set of parameters is used in Sections 4.5 and 4.6 for new construction design and retrofit of existing structures, respectively, using SPs as metallic structural fuses.

4.3. Design for a Specified set of Parameters

The results presented in Figures 3.13 to 3.16 show that the structural fuse concept can be satisfied by many combinations of parameters that define the structural system and its seismic response. However, some of these combinations may not be efficient (or even correspond to physical systems of realistic or practical sizes and dimensions). One possible measure of structural efficiency can be defined by the selection of the lightest possible steel structure that behaves in a desired way. To have an efficient (and realistic) design, it is useful to have some guidance on how (and in which order) to select the values for the key parameters that define satisfactory fuse systems. Such guidance is provided in the following.

Section 3 showed that α and μ_{max} define the characteristics of the system pushover curve. These parameters are interrelated through the system overstrength factor, Ω_o , in (3.9), which can be rewritten as:

$$\Omega_o = \alpha(\mu_{max} - 1) + 1 \quad (4.47)$$

In other words, given α and μ_{max} , the overstrength factor, Ω_o , can be calculated using (4.47). This equation is plotted in Figure 4.6 as a set of straight lines for different values of α , with μ_{max} values on the horizontal axis. It may be noted that Ω_o values are between

one and the maximum ductility (i.e., $1 < \Omega_o < \mu_{\max}$), depending on α values (since $0 < \alpha < 1.0$).

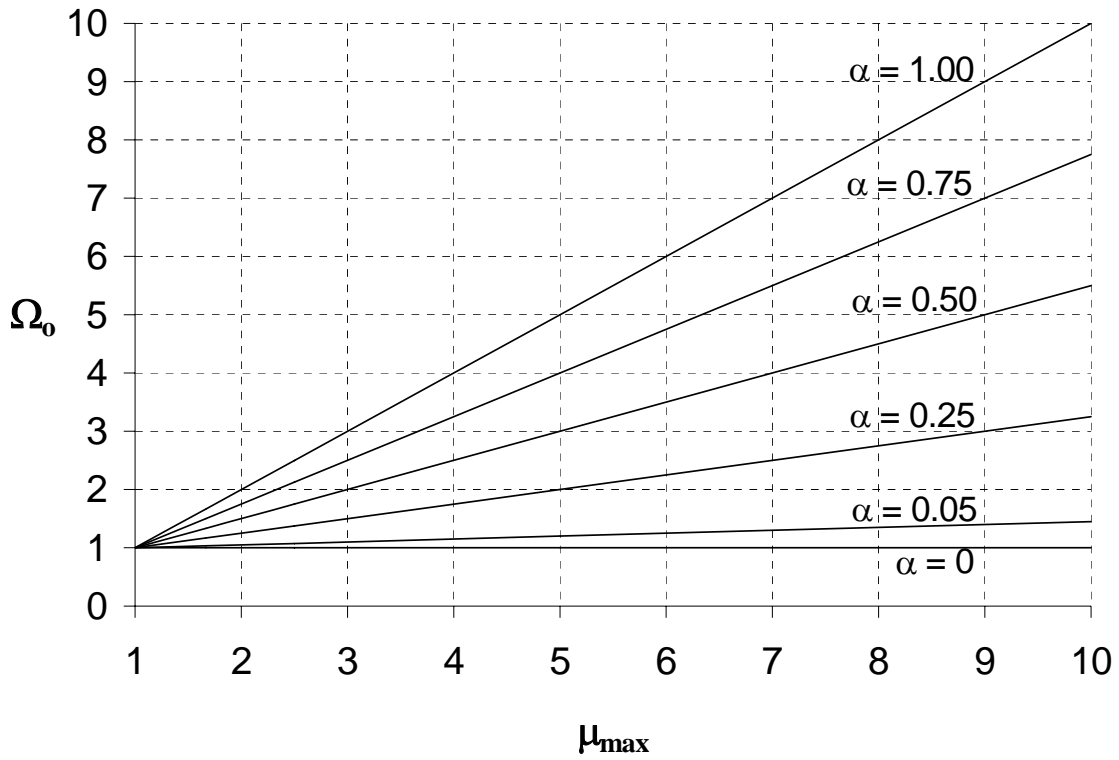


Figure 4.6. Overstrength Factor, Ω_o , as a function of α and μ_{\max}

For a target set of α , μ_{\max} , and η values chosen to provide a satisfactory system response with the structural fuse concept, the procedure listed below shows how satisfactory designs can be obtained for a frame with given geometry, for given structural mass and yield strength of beams and columns, and for given seismic conditions. Figure 4.7 shows the procedure in a flowchart.

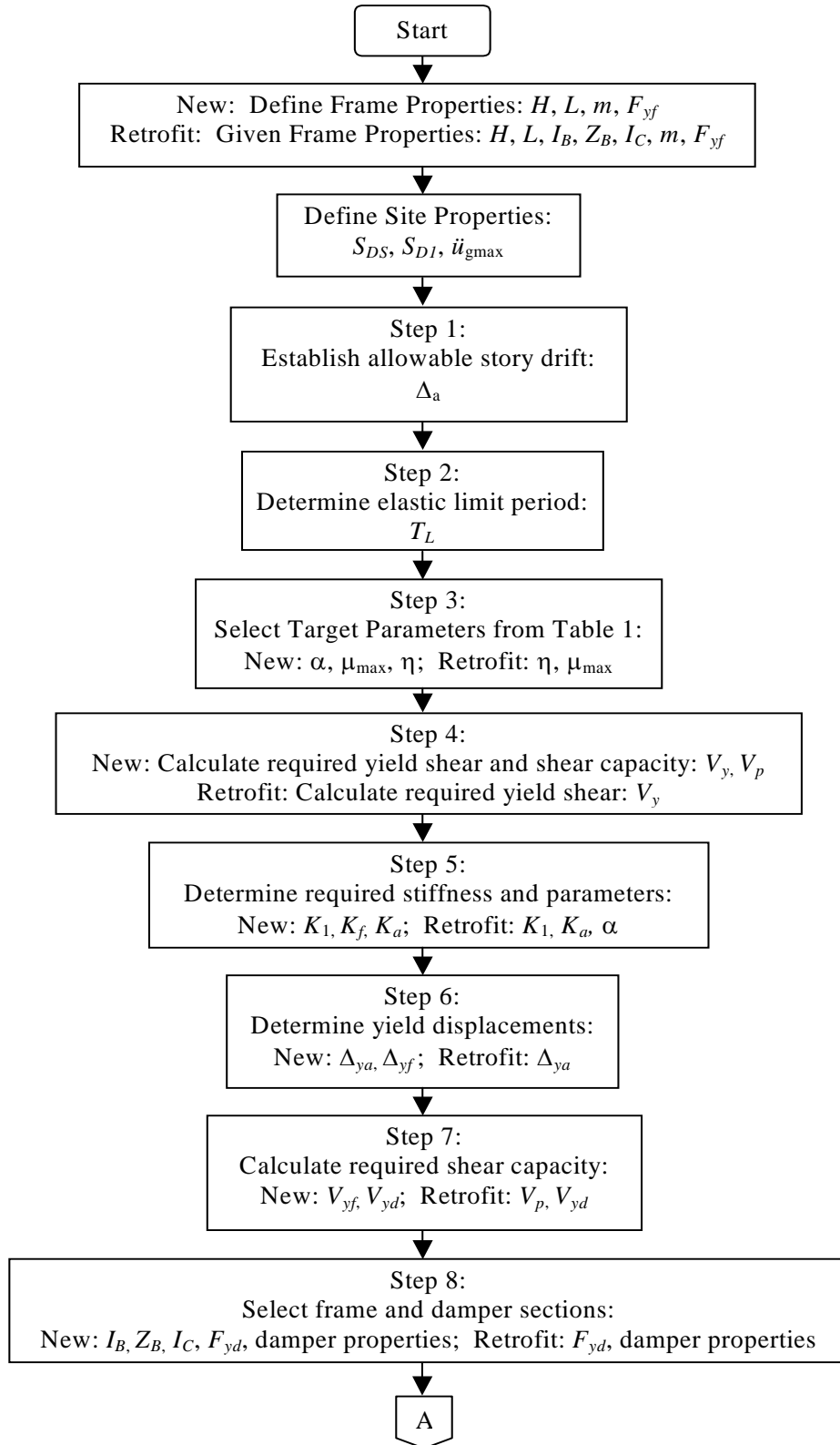


Figure 4.7. Procedure to Design Systems satisfying the Structural Fuse Concept

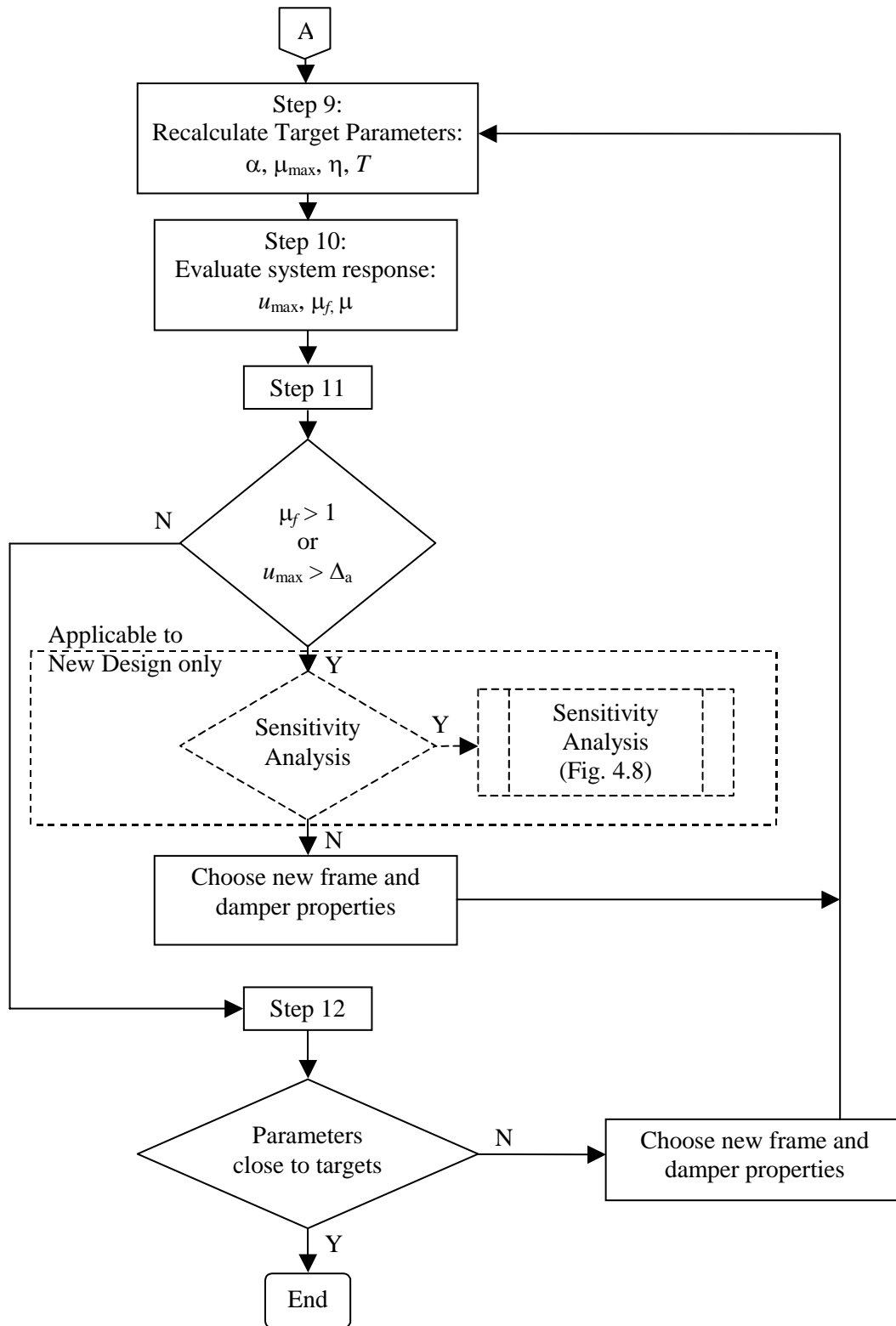


Figure 4.7. Procedure to Design Systems satisfying the Structural Fuse Concept (cont.)

- Step 1. Define the allowable drift limit as the upper bound lateral displacement (generally established as a percentage of the story height, H).
- Step 2. Determine the elastic period limit, T_L , corresponding to the drift limit from the target design spectrum, using (3.30) for flexible systems (i.e., $T_L > T_S$), or (3.35) for stiff systems (i.e., $T_L < T_S$), where T_S is the transition period that separates the constant velocity and constant acceleration regions of the target spectrum.
- Step 3. Given the elastic period limit, T_L , a set of target parameters (i.e., α , μ_{\max} , and η) may be selected from Table 4.1, which shows different combinations of parameters that satisfy the structural fuse concept (see Figure 3.8). Note that flexible and ductile systems (i.e., $T \geq 1.5$ s and $\mu_{\max} \geq 5$) require small strength-ratio values (i.e., $\eta < 0.15$ values). On the other hand, stiff and less ductile systems (i.e., $T < 0.5$ s and $\mu_{\max} < 5$) require large strength-ratio values (i.e., $\eta > 0.4$).

Table 4.1. Recommended η Values to Satisfy the Structural Fuse Concept

$\mu_{\max} \setminus T$ (s)	0.1	0.25	0.5	1	1.5	≥ 2
(1)	(2)	(3)	(4)	(5)	(6)	(7)
$\alpha = 0.05$						
1.67	N / A	N / A	1.00	0.60	0.40	0.35
2.5	N / A	1.00	0.80	0.40	0.30	0.20
5.0	0.80	0.60	0.40	0.20	0.15	0.10
10	0.50	0.40	0.20	0.10	0.08	0.05
$\alpha = 0.25$						
1.67	N / A	N / A	1.00	0.60	0.40	0.35
2.5	1.00	1.00	0.60	0.40	0.30	0.20
5.0	0.60	0.50	0.40	0.20	0.15	0.10
10	0.40	0.30	0.20	0.10	0.08	0.05
$\alpha = 0.50$						
1.67	N / A	N / A	1.00	0.60	0.40	0.35
2.5	1.00	1.00	0.60	0.40	0.30	0.20
5.0	0.50	0.50	0.40	0.20	0.15	0.10
10	0.30	0.30	0.20	0.10	0.08	0.05

Step 4. Given the mass, m , and the peak ground acceleration, \ddot{u}_{gmax} , calculate the required yield base shear, V_y , and base shear capacity, V_p , as:

$$V_y = \eta m \ddot{u}_{gmax} \quad (4.48)$$

$$V_p = \Omega_o V_y \quad (4.49)$$

Step 5. Calculate the target stiffness for the structure, K_1 , the frame, K_f , and the damping system, K_a , respectively, as:

$$K_1 = \frac{4 \pi^2}{T_L^2} m \quad (4.50)$$

$$K_f = \alpha K_1 \quad (4.51)$$

$$K_a = (1 - \alpha) K_1 \quad (4.52)$$

Step 6. Determine the yield displacements for the damping system, Δ_{ya} , and the frame, Δ_{yf} , respectively, as:

$$\Delta_{ya} = \frac{V_y}{K_1} \quad (4.53)$$

$$\Delta_{yf} = \mu_{max} \Delta_{ya} \quad (4.54)$$

Step 7. Calculate the base shear capacity for the frame, V_{yf} , and the damping system, V_{yd} , respectively, as:

$$V_{yf} = K_f \Delta_{yf} \quad (4.55)$$

$$V_{yd} = K_a \Delta_{ya} \quad (4.56)$$

Step 8. Design the bare frame and structural fuse elements to match as close as possible the stiffness and the base shear capacity requirements defined by (4.51), (4.52), (4.55), and (4.56). Required beam plastic modulus, Z_b , may be calculated from (4.2), given the story height, H , and the frame steel yield stress, F_{yf} , which allows to select a beam section with a plastic modulus as close as possible to this calculated value. Required moment of inertia for the columns may be determined from (4.1), given the story height, H , the bay span length, L , and the

beam moment of inertia, I_B , corresponding to the selected plastic modulus, Z_B . Selection of metallic fuses sizes and properties follows using equations in Sections 4.2.1 to 4.2.3 depending on the type of energy dissipation device selected. For example, area of buckling-restrained braces can be determined from (4.4), which allows to choose a plate with a cross sectional area as close as possible to this calculated value. The required steel yield strength for the braces may be determined from (4.5), given the selected brace area, A_b . For the T-ADAS and SP cases, many combinations of sizes and properties are possible, and judgement must be exercised in designing these elements.

- Step 9. Recalculate T , α , μ_{\max} , and η parameters from the actual properties obtained in Step 8.
- Step 10. Evaluate system response either by performing time history analysis, or indirectly by reading the charts (Figures 3.8 and 3.9), or using (3.25) and (3.26) (i.e., approximate closed form solutions).
- Step 11. Verify that the system response is still satisfactory. If the structural fuse concept is not satisfied (i.e., $\mu_f > 1$, or lateral displacements greater than allowable story drift are obtained), a sensitivity analysis can be performed (see Section 4.4), or new frame and damper properties may be chosen to improve the system seismic behavior, and the procedure is repeated from Step 9.
- Step 12. Verify that the new parameters calculated in Step 9 are sufficiently close to the target parameters selected at the beginning of the process. If not, new frame and damper properties should be selected to match as close as possible the target parameters, and the procedure is repeated from Step 9. Alternatively, in a worse case scenario, it may be necessary to change the frame geometry, and might even be possible to change the system mass, although project constraints may make this difficult.

This general procedure can be used to design SDOF systems using BRB, T-ADAS, or SP devices as metallic structural fuses. However, to retrofit an existing structure, the above procedure must be modified, because in addition to other constraints, the bare frame properties are generally fixed. Although the system original properties could be modified to some degree, for example by adding plates to reinforce beams and columns, by

reducing beams flexural capacity (i.e., creating reduced beam section [RBS]), or by incorporating additional mass, the cost involved in such works could makes these alternatives less desirable, and hence they are considered out of the scope of this study.

It may be noted from Table 4.1 that, in most cases, α has an insignificant influence on the set of η and μ_{\max} that can be chosen to satisfy the structural fuse concept. Therefore, in the retrofit case, η and μ_{\max} may be selected from Table 4.1 regardless of α value, because α can no longer be freely selected; it must be calculated as follows, provided that the frame stiffness, K_{yf} , and base shear capacity, V_{yf} are known:

$$\alpha = \frac{V_{yf}}{\eta \mu_{\max} m \ddot{u}_{gmax}} \quad (4.57)$$

where α shall not be greater than $(T_L^2 K_f) / (4\pi^2 m)$ to satisfy the drift limit defined in (3.30) and (3.36). Accordingly, the total stiffness, K_1 , and the elastic period, T , may be calculated, respectively, as:

$$K_1 = \frac{\eta \mu_{\max} m \ddot{u}_{gmax}}{\Delta_{yf}} \quad (4.58)$$

$$T = 2\pi \sqrt{\frac{\Delta_{yf}}{\eta \mu_{\max} \ddot{u}_{gmax}}} \quad (4.59)$$

where K_1 shall be greater than $(4\pi^2 m) / (T_L^2)$, and T shall not be greater than T_L to satisfy the drift limit defined in (3.30) and (3.36).

As a result of the above constraints, only the structural fuse properties can be modified to satisfy the retrofit design requirements. Figure 4.7 also shows the required modifications in the procedure to be followed when retrofitting existing structures. Note that η and μ_{\max} are the only parameters that can be arbitrarily specified, since α and T depend directly on the existing frame properties. Also, sensitivity analyses of the type described in Section 4.4 cannot be performed as part of the retrofit process, because they would require to modify not only the damper properties but also the frame properties.

It is important to note that the structural fuse concept objective can be achieved with this general design procedure for earthquakes that do not exceed the level of design specifications. High variability of earthquake records makes it possible that the target design objective may be violated for a given earthquake exceeding the design spectrum, but it should be recognized that in such cases, response of the system remains ductile and safe (i.e., safe failure). However, to minimize such probability of exceeding the design level, it is recommended to use target design spectra at maximum credible earthquake level (e.g., 2% of probability of being exceeded in 50 years).

Note that the procedure presented in this section has been specifically developed to design and retrofit systems with metallic dampers in order to satisfy the structural fuse concept according to the definition provided by this study. Therefore, this design guidance has been provided for the sizing of the fuse system as a function of the total system strength. However, it is considered worthwhile to acknowledge the general procedure also presented in the NEHRP Recommended Provisions (FEMA 450) to design structures with damping systems. Requirements presented in these provisions are generally applicable to systems designed with displacement-dependent or velocity-dependent damping devices.

Two specific step-by-step design examples are shown in Appendix A, illustrating the process to design an BRBF satisfying the structural fuse concept. The first has the following target design parameters: $\alpha = 0.25$, $\mu_{\max} = 5$, $\eta = 0.4$, and story drift limit of 2% of the story height (i.e., $u_{\max} = 76$ mm for $H = 3810$ mm, which translates into an elastic period limit of $T_L = 0.53$ s). The second example illustrates the iteration process required when target design parameters are not met in the first attempt. This example has the following target design parameters: $\alpha = 0.25$, $\mu_{\max} = 1.67$, $\eta = 1.0$, and story drift limit of 2% of the story height (i.e., $u_{\max} = 76$ mm like in the first example).

4.4. Sensitivity Analysis

Step 1 to 7 in the above procedure deal with ideal system properties independent of the type of structural fuse devices selected. Steps 8 to 11 involve the selection of actual physical properties for specific PED devices, which may result in the key parameters (i.e., α , μ_{\max} , η , and T) deviating from the original target values as available structural elements are selected. This deviation from the target parameters will be noted in the examples of Sections 4.5 and 4.6. Furthermore, in the design process (using Figures 3.13 to 3.16, and following the steps in Figure 4.7) it is often desirable to “move” along the same η curve to find a solution having a new period value, keeping constant α and μ_{\max} , in the search to improve system behavior (i.e., selecting a design that falls within the area of admissible solutions using the graphic representation of Figure 3.13). Another possibility in the design process would be to “move” vertically along the same period to find a solution with a new η value, keeping constant α and μ_{\max} .

As part of the design process, a difficulty arises because changing one design parameter often correspondingly change other key parameters that characterize response (e.g., variations in SP plates, thickness impact all of α , μ_{\max} , T , and η). Therefore, to manage this complex interdependency between physical properties and target parameters, it is helpful to identify all interdependencies and use this information to achieve a systematic design process.

The proposed approach starts by selecting physical properties that affect the largest number of parameters that are independent on the type of structural fuse selected, and then vary the other properties to complete the design, getting as close as possible to target parameters. For this purpose, tables of dependency have been prepared (Tables 4.2 to 4.7) to show the relationship between physical properties and target parameters. For each type of metallic fuse system, a set of two tables is used. The first table relates physical properties with non-dimensional variables used in each case to calculate target parameters. The second table shows the relationship between non-dimensional variables and target parameters. These tables could be merged together (eliminating the

intermediate step) to show directly the interdependency between physical properties and target parameters. However, a drawback of such a merged table is that more complex expressions to directly calculate target parameters from physical properties would be necessary and these are of a form that makes the design less manageable. Thus, non-dimensional variables that group many physical properties have been used to circumvent the difficulties found when attempting to design using a single merged table. Figure 4.8 shows in a flowcharts the procedure to “move” BRB, T-ADAS, and SP system responses to achieve an acceptable solution in the context of the sensitivity analysis. As shown in this figure, the procedure starts defining geometric, cross-sectional, and material properties of the members to match α , and μ_{\max} . Then T and η are matched changing the mass, m . As part of the procedure, the following properties have been kept constant: peak ground acceleration, $\ddot{u}_{g\max}$, which is function of the site; story height, H , which defines the allowable story drift; and the steel properties of the frame (i.e., modulus of elasticity, E , shear modulus, G , and yield stress, F_{yf}).

Table 4.2. Influence of BRB Properties over Non-dimensional Variables

	g_{BRB} (1)	s (2)	d (3)	e_{BRB} (4)	l (5)	f_{BRB} (6)
L	✓	✓	✓	✓		
H	✓	✓	✓	✓	✓	
I_B		✓				
Z_B				✓		
I_C		✓	✓	✓	✓	
A_b			✓			✓
E					✓	
F_{yf}				✓		
F_{yd}				✓		✓
m					✓	✓
\ddot{u}_{gmax}						✓

Table 4.3. Influence of BRB Non-dimensional Variables over Target Parameters

	α (1)	μ_{max} (2)	T (3)	η (4)
g_{BRB}	✓	✓	✓	✓
s	✓	✓	✓	✓
d	✓		✓	✓
e_{BRB}		✓		
l			✓	
f_{BRB}				✓

Table 4.4. Influence of T-ADAS Properties over Non-dimensional Variables

	g_{TADAS} (1)	s (2)	d (3)	n_{TADAS} (4)	p_{TADAS} (5)	q (6)	r (7)	v_{TADA} s (8)	e_{TADA} s (9)	l (10)	f_{TADAS} (11)
L	✓	✓	✓		✓	✓					
H	✓	✓	✓	✓				✓	✓	✓	
I_B		✓									
Z_B									✓		
I_C		✓	✓	✓				✓	✓	✓	
A_b			✓		✓	✓					
N				✓	✓		✓				
b				✓	✓		✓				
h	✓			✓	✓	✓	✓	✓	✓		
t				✓	✓	✓		✓	✓		✓
E										✓	
F_{yf}									✓		
F_{yd}									✓		✓
m										✓	✓
\ddot{u}_{gmax}											✓

Table 4.5. Influence of T-ADAS Non-dimensional Variables over Target Parameters

	α (1)	μ_{\max} (2)	T (3)	η (4)
g_{TADAS}	✓	✓	✓	✓
s	✓	✓	✓	✓
d	✓		✓	
n_{TADAS}	✓			
p_{TADAS}		✓	✓	✓
q				✓
r				✓
v_{TADAS}				✓
e_{TADAS}		✓		
l			✓	
f_{TADAS}				✓

Table 4.6. Influence of SP Properties over Non-dimensional Variables

	g_{SP} (1)	s (2)	d_{SP} (3)	n_{SP} (4)	p_{SP} (5)	v_{SP} (6)	e_{SP} (7)	l (8)	f_{SP} (9)
L	✓	✓	✓		✓				
H	✓	✓	✓	✓		✓	✓	✓	
I_B		✓							
Z_B							✓		
I_C		✓	✓	✓		✓	✓	✓	
A_b			✓		✓				
w	✓		✓	✓	✓	✓			✓
h	✓			✓	✓	✓	✓		
t				✓	✓	✓			✓
E				✓	✓	✓	✓	✓	
G				✓	✓	✓	✓		
F_{yf}							✓		
F_{yd}							✓		✓
m								✓	✓
\ddot{u}_{gmax}									✓

Table 4.7. Influence of SP Non-dimensional Variables over Target Parameters

	α (1)	μ_{\max} (2)	T (3)	η (4)
g_{SP}	✓	✓	✓	✓
s	✓	✓	✓	✓
d_{SP}	✓		✓	
n_{SP}	✓			
p_{SP}		✓	✓	✓
v_{SP}				✓
e_{SP}		✓		
l			✓	
f_{SP}				✓

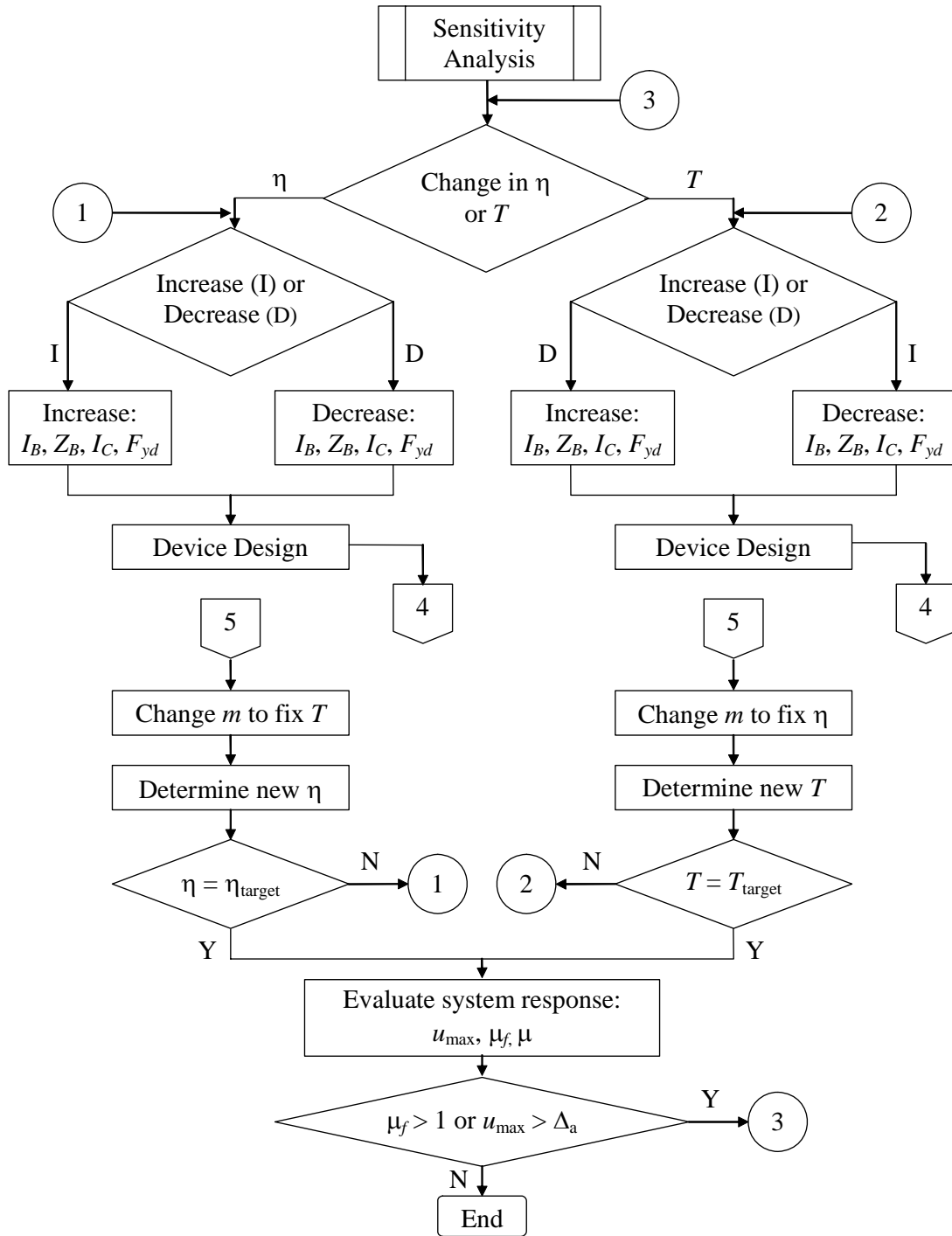


Figure 4.8. Procedure for the Sensitivity Analysis

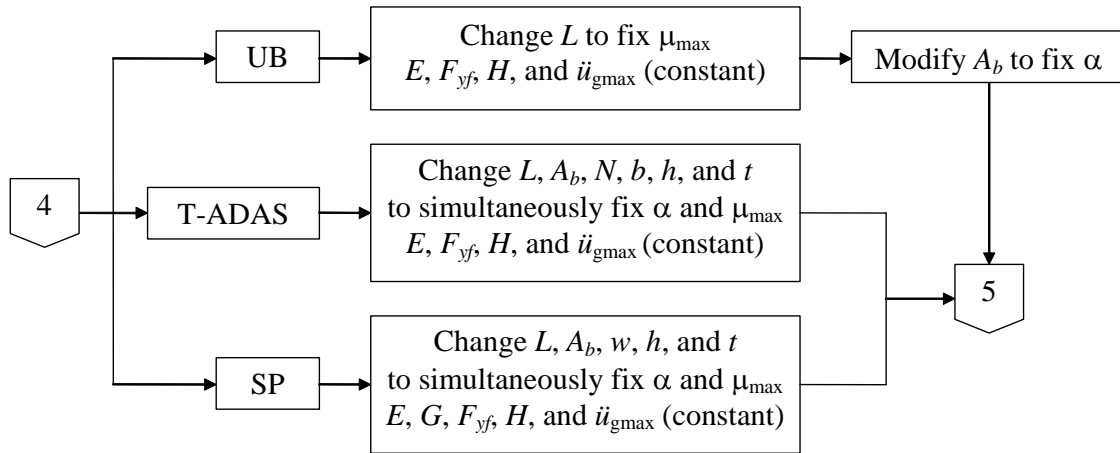


Figure 4.8. Procedure for the Sensitivity Analysis (cont.)

Note in these flowcharts that the procedure can only be implemented in new construction designs. In the case of retrofit of existing structures, where geometric and frame properties remain basically constant, variations made only in the structural fuse properties are not sufficient to modify the response in such a way that α and μ_{\max} are kept constants, while either η or T are changed.

4.5. Design Examples

Actual designs were conducted following the procedure listed in Section 4.3 for one-story one-bay SDOF structures with the following arbitrarily selected general properties: $L = 4877$ mm, $H = 3810$ mm, $m = 0.35$ kN·s²/mm, and $F_{yf} = 345$ MPa (hard conversion from 16 ft, 12.5 ft, 2 kip·s²/in, and 50 ksi, respectively).

A total of 12 different designs were developed for every metallic fuse system studied here to match as closely as possible the target pushover parameters, α and μ_{\max} , presented in Figure 3.13 (i.e., $\alpha = 0.05, 0.25, 0.50$; and $\mu_{\max} = 10, 5, 2.5, 1.67$). Target period was taken from Figure 3.13 as the upper bound limit of 0.53 s (dashed vertical line in the

figure), which corresponds to the elastic period limit, T_L , conservatively calculated using (3.30), with $S_d = 76$ mm as the allowable story drift of 2% for a story height of 3810 mm.

Many η values lie in the region of admissible solution in Figure 3.13 and are thus satisfactory. However, it was observed that the most efficient (lightest) systems that satisfy the structural fuse concept are those for which frame ductility is approaching one, and elastic period is close to the elastic period limit (i.e., $\mu_f \approx 1$ and $T \approx T_L = 0.53$ s, in this case). This is because systems having large μ_{\max} require small η values to satisfy the structural fuse concept, which translates into lighter structures because of the reduction in the yield base shear capacity, V_y , especially for systems having large device contributions (i.e., small α values). Therefore, in order to provide designs having the most favorable response, target η values were selected as the closest to $\mu_f = 1$ and T_L in Figure 3.13.

4.5.1. Design Results

Properties of the resulting designs conducted following the procedure in Section 4.3 (and illustrated in Appendix A) are presented in Tables 4.8, 4.9, and 4.10 for systems having BRB, T-ADAS, and SP devices, acting as metallic fuse elements, respectively. Results are tabulated as target values, design properties, design parameters, and response for every system. Target values include the parameters α , μ_{\max} , η , and T to be matched through the design process. Note that the target parameters can generally be matched fairly closely for the BRB and T-ADAS cases. In the SP dampers cases, it was found to be more difficult to match these parameters, especially for $\mu_{\max} \leq 5$.

Table 4.8. Design of BRB Systems

Target Values		Design Properties						Design Parameters							Response	
μ_{\max}	η	Beams	Columns	BRB (mm)	F_{yd} (MPa)	W_T (kN)	ρ (%)	α	η	μ_{\max}	T (s)	R	Ω_o	$R\mu$	μ_f	μ
(1)	(2)	(3)	(4)	(5)	(6)	(7)	(8)	(9)	(10)	(11)	(12)	(13)	(14)	(15)	(16)	(17)
Targets: $\alpha = 0.05$ $T = 0.53s$																
10	0.2	W14x53	W12x58	PL76x25	248	11.6	12	0.05	0.31	9.03	0.51	7.10	1.40	5.07	0.67	6.05
5	0.4	W14x53	W12x58	PL76x25	414	11.6	12	0.04	0.51	5.42	0.51	4.26	1.18	3.62	0.73	3.96
2.5	0.8	W14x30	W14x68	PL76x32	483	11.4	15	0.05	0.73	2.75	0.46	3.29	1.09	3.03	1.04	2.86
1.67	1.0	W14x22	W14x176	PL95x38	483	23.7	11	0.03	1.08	1.98	0.38	2.30	1.03	2.23	1.17	2.32
Targets: $\alpha = 0.25$ $T = 0.53s$																
10	0.2	W12x190	W14x176	PL57x25	248	13.3	8	0.23	0.28	7.90	0.53	7.39	2.59	2.86	0.79	6.24
5	0.4	W12x190	W14x211	PL57x25	345	38.0	3	0.25	0.40	5.04	0.53	5.24	2.02	2.59	0.86	4.34
2.5	0.6	W24x84	W14x176	PL57x25	483	26.6	4	0.25	0.56	2.68	0.53	3.76	1.42	2.65	1.17	3.14
1.67	1.0	W21x68	W12x279	PL95x25	483	37.5	4	0.16	0.84	1.96	0.43	2.97	1.15	2.57	1.00	1.96
Targets: $\alpha = 0.50$ $T = 0.53s$																
10	0.2	W12x336	W12x336	PL38x25	248	62.0	1	0.47	0.28	7.68	0.54	7.48	4.14	1.81	0.77	5.91
5	0.4	W14x342	W14x342	PL38x25	345	63.4	1	0.52	0.42	5.11	0.52	5.14	3.14	1.64	0.83	4.24
2.5	0.6	W33x130	W14x283	PL38x25	483	41.5	2	0.51	0.57	2.69	0.52	3.73	1.86	2.00	1.15	3.09
1.67	1.0	W30x99	W14x311	PL64x25	483	43.0	3	0.36	0.73	1.98	0.46	3.29	1.35	2.43	1.16	2.30

Table 4.9. Design of T-ADAS Systems

Targets Values		Design Properties (dimensions in mm)										Design Parameters						Response			
μ_{\max}	η	Beams	Columns	Braces (HSS)	N	b	h	t	F_{yd} (MPa)	W_T (kN)	ρ (%)	α	η	μ_{\max}	T (s)	R	Ω_o	$R\mu$	μ_f	μ	
(1)	(2)	(3)	(4)	(5)	(6)	(7)	(8)	(9)	(10)	(11)	(12)	(13)	(14)	(15)	(16)	(17)	(18)	(19)	(20)	(21)	
Targets: $\alpha = 0.05$ $T = 0.53s$																					
10	0.2	W14x53	W12x58	4x4x1/2	10	254	254	25	248	13.4	24	0.05	0.24	11.5	0.52	9.10	1.52	5.97	0.79	9.06	
5	0.4	W18x35	W12x58	6x6x3/8	8	254	318	32	414	12.9	31	0.05	0.40	5.14	0.53	5.34	1.21	4.42	0.85	4.37	
2.5	0.8	W16x36	W14x48	6x6x5/8	29	305	381	22	483	15.7	50	0.05	0.82	2.50	0.53	2.59	1.08	2.41	0.99	2.48	
1.67	1.0	W14x22	W14x211	6x6x5/8	35	356	254	16	483	32.0	22	0.03	0.86	1.83	0.44	2.89	1.02	2.82	1.08	1.98	
Targets: $\alpha = 0.25$ $T = 0.53s$																					
10	0.2	W12x190	W14x176	4x4x1/2	12	178	241	22	248	36.1	8	0.23	0.20	11.4	0.53	10.6	3.38	3.13	0.83	9.43	
5	0.4	W12x190	W14x211	6x6x1/2	23	305	381	22	248	43.3	15	0.25	0.42	4.87	0.52	5.04	1.97	2.56	0.86	4.19	
2.5	0.6	W24x84	W14x176	6x6x1/2	18	254	381	25	414	31.4	18	0.25	0.60	2.50	0.53	3.52	1.38	2.56	1.18	2.95	
1.67	1.0	W21x68	W12x279	6x6x5/8	30	254	381	25	483	43.6	18	0.17	1.05	1.46	0.45	2.37	1.08	2.20	1.15	1.68	
Targets: $\alpha = 0.50$ $T = 0.53s$																					
10	0.2	W27x194	W14x342	4x4x1/2	15	178	178	13	248	54.9	5	0.56	0.19	9.87	0.49	11.9	5.97	1.99	1.08	10.7	
5	0.4	W14x342	W14x342	4x4x1/2	13	254	381	25	248	66.4	6	0.51	0.40	5.50	0.51	5.49	3.30	1.67	0.83	4.57	
2.5	0.6	W33x130	W14x283	6x6x1/2	29	254	267	13	483	45.9	11	0.51	0.62	2.45	0.53	3.40	1.74	1.95	1.14	2.79	
1.67	1.0	W24x176	W12x336	6x6x5/8	37	356	318	13	483	34.6	20	0.50	0.91	1.87	0.52	2.35	1.44	1.64	1.07	2.00	

Table 4.10. Design of SP Systems

Targets Values		Design Properties (dimensions in mm)										Design Parameters							Response		
μ_{\max}	η	Beams	Columns	Braces (HSS)	w	h	t	b_f	t_f	F_{yd} (MPa)	W_T (kN)	ρ (%)	α	η	μ_{\max}	T (s)	R	Ω_o	$R\mu$	μ_f	μ
(1)	(2)	(3)	(4)	(5)	(6)	(7)	(8)	(9)	(10)	(11)	(12)	(13)	(14)	(15)	(16)	(17)	(18)	(19)	(20)	(21)	(22)
Targets: $\alpha = 0.05$ $T = 0.53s$																					
10	0.2	W10x49	W14x74	5x5x3/16	381	330	5	102	10	345	13.2	11	0.05	0.21	9.51	0.52	10.0	1.41	7.11	1.18	11.2
5	0.4	W14x34	W12x72	8x8x3/16	762	762	5	102	10	345	13.4	22	0.03	0.42	7.56	0.40	6.00	1.19	5.04	0.83	6.27
2.5	0.8	W14x30	W14x68	12x12x1/4	1651	254	5	102	10	345	15.1	36	0.03	0.90	3.39	0.38	2.78	1.06	2.62	0.90	3.05
1.67	1.0	W12x26	W12x210	12x12x5/16	1778	254	5	102	10	345	30.6	18	0.03	0.97	2.27	0.39	2.58	1.04	2.49	1.20	2.72
Targets: $\alpha = 0.25$ $T = 0.53s$																					
10	0.2	W30x99	W12x190	5x5x3/16	381	254	5	102	10	248	29.6	5	0.22	0.19	12.9	0.48	12.6	3.57	3.52	0.91	11.7
5	0.4	W14x149	W14x257	6x6x3/16	1524	254	5	102	10	248	42.8	8	0.27	0.79	4.69	0.38	3.15	1.98	1.59	0.50	2.35
2.5	0.6	W27x84	W14x176	10x10x1/4	2032	254	5	102	10	248	30.9	17	0.16	0.92	2.82	0.41	2.72	1.28	2.12	0.74	2.09
1.67	1.0	W21x101	W14x176	12x12x3/8	2667	254	5	102	10	248	34.8	23	0.18	1.24	1.90	0.45	2.01	1.16	1.73	0.80	1.52
Targets: $\alpha = 0.50$ $T = 0.53s$																					
10	0.2	W36x160	W14x342	5x5x3/16	432	432	5	102	10	248	51.1	3	0.41	0.25	10.2	0.41	10.1	4.79	2.12	0.97	9.93
5	0.4	W36x160	W14x257	6x6x3/16	1524	508	5	102	10	248	53.9	7	0.30	0.83	4.40	0.35	3.00	2.03	1.48	0.54	2.38
2.5	0.6	W33x130	W14x283	10x10x1/4	2667	254	5	102	10	248	53.9	15	0.30	1.44	2.07	0.41	1.73	1.32	1.31	0.69	1.43
1.67	1.0	W36x135	W12x305	10x10x1/2	2794	381	5	102	10	248	51.4	15	0.32	1.57	1.69	0.42	1.59	1.22	1.30	0.80	1.35

Frame and damper features are listed as design properties, as well as the total system weight, W_T , and weight ratio, ρ , defined as the ratio between fuse weight, W_F , with respect to the total system weight, calculated as:

$$\rho = \frac{W_F}{W_T} \quad (4.60)$$

The total system weight, W_T , includes the weight of beams, columns, and fuse system. The fuse weight, W_F , includes the following elements for each system: core plate, N triangular plates, and shear plate and flanges, for the BRB, T-ADAS, and SP systems, respectively.

Design parameters include the key parameters calculated using actual properties. Also under this category are the obtained response modification factor, R , the overstrength factor, Ω_o , and the ductility factor, R_μ , which are schematically depicted in Figure 4.9.

The overstrength factor, Ω_o , was previously defined, and the response modification factor, R , and the ductility factor, R_μ , can be determined, respectively as:

$$R = \frac{V_e}{V_y} \quad (4.61)$$

$$R_\mu = \frac{V_e}{V_p} \quad (4.62)$$

where V_e is the elastic base shear obtained from the elastic demand spectrum as:

$$V_e = m S_a \quad (4.63)$$

The system response is expressed in terms of frame ductility, μ_f , and global ductility, μ , obtained from inelastic time history analysis.

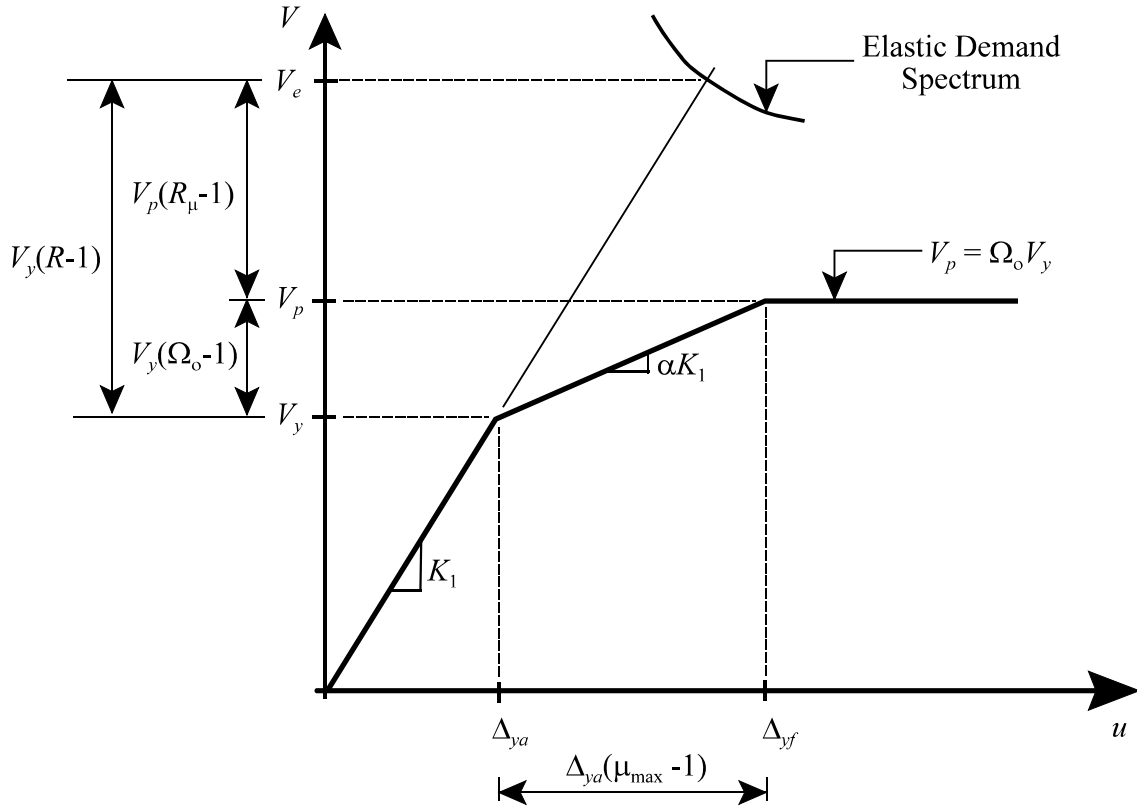


Figure 4.9. Response Modification Factor R , Ductility Factor R_{μ} , and Overstrength Factor, Ω_o

From the results presented in Tables 4.8, 4.9, and 4.10, it may be noted that frame and metallic fuses cross-sectional properties vary in such a way that frame base shear capacity increases while damping system base shear capacity decreases with both increases in α and μ_{\max} values, according to Figure 3.3b. However, according to Figure 3.4, systems with large frame stiffness and large frame base shear capacity (i.e., small contribution of devices to the total base shear strength) dissipate less energy than systems with large device stiffness and base shear capacity (i.e., small contribution of frame base shear). Therefore, systems having large devices base shear contribution (i.e., small α and μ_{\max} values) are the most desirable systems to design and retrofit as earthquake resisting structures using metallic fuses.

PED devices have been designed as plate elements assuming availability of six different structural steel grades, namely ASTM A36 Grade 36 ksi (248MPa), A572 Grades 50, 55, 60, and 65 ksi (345, 379, 414, and 448 MPa, respectively), and A852 Grade 70 ksi (483 MPa). In the case of BRB and T-ADAS systems, the selected yield stress, F_{yd} , increases with decreases in μ_{max} , which translates into systems less ductile than those designed using low yield strength steels. However, in the SP dampers case, F_{yd} does not vary significantly with the parameters α and μ_{max} . As shown in Figure 3.3, for a given value of α , the physical consequence of decreasing μ_{max} is that the damping system takes a bigger percentage of the total base shear, V_p . In other words, by increasing the strength of the damper system, only smaller values of μ_{max} can be developed (prior to yielding of the frame). From Table 4.10 it may be seen that in the SP dampers cases, this increase in percentage is obtained by increasing the plate dimensions, which is particularly noticeable for values of $\mu_{max} < 5$. Note that these large sizes for the required plates may not necessarily be practical. However, given that it is desirable that a structural fuse system with SP devices dissipates more hysteretic energy having large values of μ_{max} , this seems to suggest that application of the SP system with $\mu_{max} > 5$ is suitable.

On one hand, the total system weight, W_T , increases with α , as a result of larger resulting beams and columns. On the other hand, the weight ratio, ρ , decreases with α because of simultaneous reductions in damper cross-sectional properties, and increases in frame shape sizes.

As shown in columns (8), (12), and (13) of Tables 4.8, 4.9, and 4.10, respectively, the weight ratio, ρ , has the lowest values for the BRB systems. However, it is worthwhile to mention that for the BRB case, the fuse weight, W_F , has been calculated as the core plate weight excluding the exterior tube, the de-bonding material, and the mortar, which in precise cost assessments should be considered when comparing systems in terms of efficiency. It is possible that these omitted elements could increase the cost of the BRB system such that its total cost would be comparable to that for the T-ADAS system, which currently has the largest ρ values. Hence, in terms of cost efficiency alone,

preliminary results and rough estimates suggest that none of the studied systems appears to have significant advantages over the others.

Substituting V_e / R for V_y into (3.19), gives:

$$R = \frac{V_e}{\eta m \ddot{u}_{gmax}} \quad (4.64)$$

which may be rewritten by substituting $m S_a$ for V_e , giving:

$$R = \left(\frac{1}{\eta} \right) \left(\frac{S_a}{\ddot{u}_{gmax}} \right) \quad (4.65)$$

which is the elastic spectrum normalized with respect to the peak ground acceleration, \ddot{u}_{gmax} , scaled by the factor $1/\eta$. Figure 4.10 shows the response modification factor, R , obtained by (4.65) for the NEHRP 2003 target design spectrum used in Section 3 to generate the set of synthetic ground motions for time history analyses. It may be noted from Figure 4.10 and Tables 4.8 to 4.10 that for a given period and η value, R is uniquely defined. Tables 4.8 to 4.10 show that R values obtained from nonlinear time history analysis remain relatively constant for a given value of η , and T , irrespectively of the values of the stiffness ratio, α , and maximum ductility, μ_{max} . This is because the response modification factor, R (as shown in (4.61)) is defined by the ratio of two elastic properties, namely, the elastic base shear, V_e (which may be determined from the elastic period, T), and yield base shear, V_y (which defines the yield threshold determined from the strength ratio, η). In other words, systems having different inelastic properties (i.e., ductility and energy dissipation capabilities) can still have the same response modification factor, as long as they have the same initial period, and the same strength ratio values.

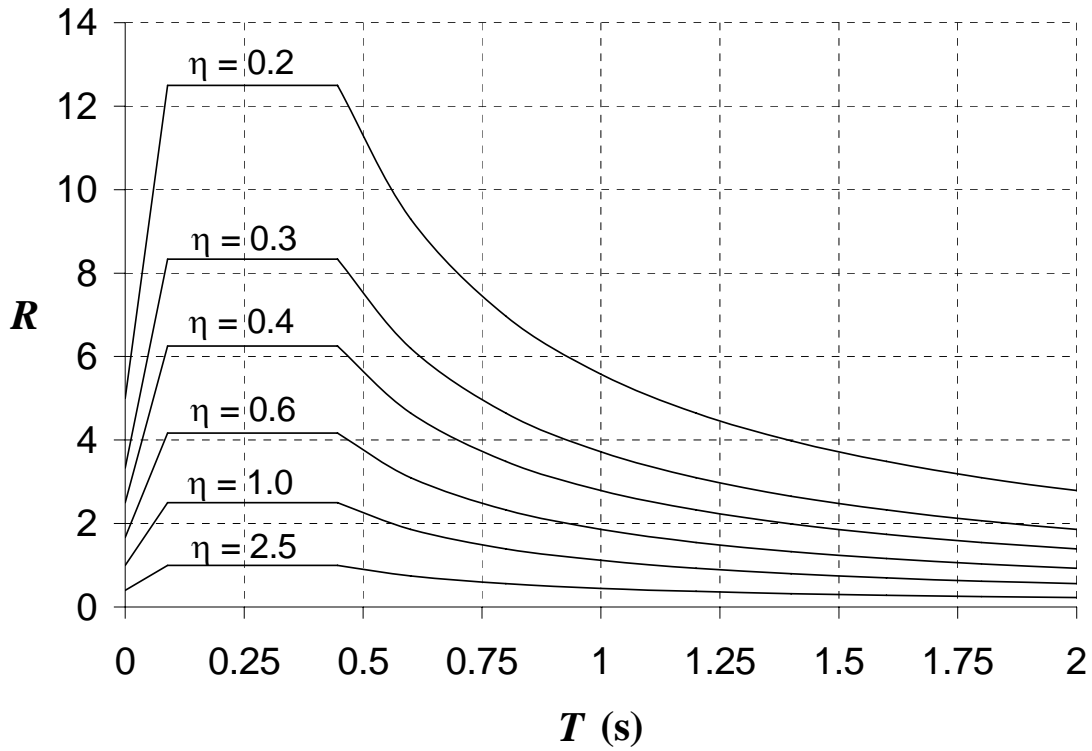


Figure 4.10. Response Modification Factor, R , as a function of η and T

Knowing that R is equal to $\Omega_o \cdot R_\mu$, (4.65) can be written as:

$$R_\mu = \left(\frac{1}{\Omega_o \eta} \right) \left(\frac{S_a}{\ddot{u}_{gmax}} \right) \quad (4.66)$$

which represents a set of normalized spectra corresponding to the response modification factor (from Figure 4.10) reduced by the overstrength factor, Ω_o . As mentioned before, the overstrength factor, Ω_o , is an inelastic parameter which is a function of the stiffness ratio, α , and the maximum ductility, μ_{max} (according to (4.47)). Consequently, the ductility factor, R_μ , can be represented as inelastic spectra varying with both parameters α and μ_{max} . Figure 4.11 shows such inelastic spectra corresponding to R_μ for the values of α and μ_{max} used in this study. It may be noted from Figure 4.11 and Tables 4.8 to 4.10 that systems with small values of α and μ_{max} (which also results in values of Ω_o close to one) have a seismic behavior close to elasto-perfectly plastic (see Figure 3.3a), which

translates into similar values for R and R_μ . However, according to the results shown in Figure 3.13, these systems require large values of strength ratio, η (i.e., small values of R) to satisfy the structural fuse concept. Seismic behavior of such systems is, therefore, almost elastic with insignificant hysteretic energy prior to yielding of the frame, which is not the desired objective when PED devices are implemented in the structural fuse concept.

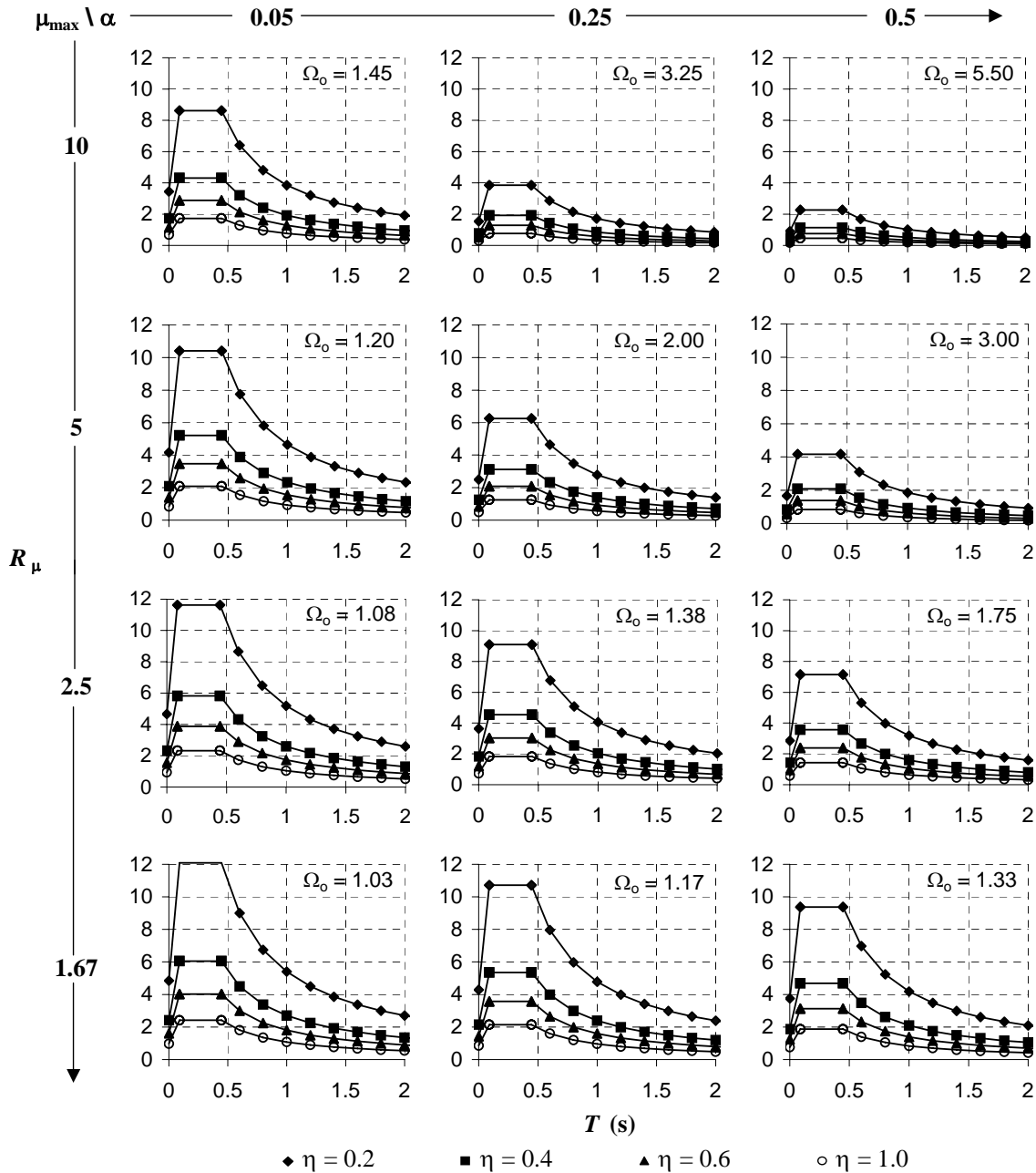


Figure 4.11. Ductility Factor as a function of α , μ_{\max} , η , and T

On the other hand, systems with large values of α and μ_{\max} (which also results in large values of Ω_o) require small values of η (i.e., large values of R) to satisfy the structural fuse concept, which implies that values of R_{μ} are also small, as shown in Figure 4.11. In other words, such systems have a small reduction in the elastic base shear, V_e , and low energy dissipation capability, because of their large stiffness ratio, which result in a non-efficient application of the structural fuse concept (it essentially corresponds to making the retrofitted system stronger, not necessarily taking advantage of ductile response of the PED).

Tables 4.8 to 4.10 show that system response in terms of frame ductility, μ_f , is generally close to the target value (i.e., $\mu_f \approx 1$) which validates the results presented in Figure 3.13. Also, for given μ_{\max} , and η values, the global ductility, μ , as well as the response modification factor, R , do not change significantly with respect to the strain hardening ratio, α . Note that systems having the same response in terms of ductility may have different energy dissipation capacity due to their different strain hardening ratios, as shown in Figure 3.4. In other words, systems with large ductility response can still have small energy dissipation capability.

4.6. Retrofit Examples

A bare frame has been arbitrarily selected to be retrofitted using BRB, T-ADAS, and SP devices in order to satisfy the structural fuse concept. The “existing” frame properties are: W27x84 beam, W14x145 columns, $L = 4877$ mm, $H = 3810$ mm, $m = 0.525$ kN·s²/mm, and $F_{yf} = 345$ MPa (hard conversion from 16 ft, 12.5 ft, 3 kip·s²/in, and 50 ksi, respectively). After time history analysis is performed, the system maximum average displacement is 250 mm, which is greater than the allowable story drift of 2% of the story height (i.e., 76 mm in this case). This lateral displacement translates into a frame ductility of 3.86 (i.e., $\mu_f = 3.86 > 1.0$), which implies inelastic rotations in plastic hinges and damage to the main structure during an earthquake compatible to the design

spectrum. Note that this frame would have been code-compliant and deemed satisfactory for designs done prior to the introduction of drift limits into codes of the 1970's. The objective of this example is to retrofit this frame and improve its seismic performance to satisfy the structural fuse concept using BRB, T-ADAS, and SP devices as metallic fuse systems.

Using (4.1), (4.2), and (4.3) the frame dynamic properties can be calculated as:

$K_f = 11.2$ kN/mm, $V_{yf} = 724$ kN, and $\Delta_{yf} = 65$ mm, respectively. These properties are considered constant for retrofitting purposes in this study. The previously determined elastic limit period of 0.53 s and story drift limit of 2% is again used in this section. Knowing that $T_L = 0.53$ s, from Table 4.1 many sets of η and μ_{\max} values can be selected to provide a response in the region of admissible solutions (see Figure 3.13). In the following examples, three sets of η and μ_{\max} values have been used: 0.2 with 10, 0.4 with 5, and 0.7 with 2.5. These groups of parameters serve to determine α and T from (4.57) and (4.58), respectively, as some of the target parameters used to design the damping systems for retrofitting the given frame.

4.6.1. Retrofit Results

Results of the retrofit examples are presented in Table 4.11, tabulated per type of metallic fuse, design properties, design parameters and system response. Note that as part of the design, it was found necessary to use different values of yield stress, F_{yd} , for different cases considered, even for a given device. As shown in column (6) of Table 4.11, the weight ratio, ρ , has the lowest values for the BRB system. However, for reasons described in Section 4.5.1, it should not be necessarily concluded that the BRB system is preferable over the other systems in terms of cost efficiency.

Table 4.11. Retrofit Examples using Metallic Fuse Systems for $\alpha \leq 0.151$, $T \leq 0.53s$ (limits)

Metallic Fuse	Design Properties (dimensions in mm)						Design Parameters						Response					
	(1)	(2)	(3)	(4)	(5)	(6)	α	η	μ_{max}	T (s)	R	Ω_o	$R\mu$	μ_f	(15)			
	Targets : $\mu_{max} = 10$						$\alpha = 0.135$						$T = 0.50s$					
BRB	Plate = 95 x 30						248	24.2	8	0.13	0.33	6.23	0.49	6.83	1.69	4.05	0.86	5.36
T-ADAS	$N=14, b=254, h=254, t=25$						248	27.2	19	0.13	0.24	8.38	0.50	9.28	1.99	4.67	0.84	7.06
SP	$w=762, h=381, t=5, b_f=102, t_f=13$						345	25.2	12	0.11	0.30	7.87	0.46	8.01	1.78	4.51	0.82	6.47
	Targets : $\mu_{max} = 5$						$\alpha = 0.135$						$T = 0.50s$					
BRB	Plate = 95 x 30						345	24.2	8	0.13	0.46	4.48	0.49	4.92	1.46	3.38	0.83	3.73
T-ADAS	$N=30, b=356, h=375, t=25$						248	30.2	26	0.14	0.49	4.06	0.50	4.52	1.41	3.20	0.84	3.42
SP	$w=1778, h=254, t=5, b_f=102, t_f=10$						248	27.2	18	0.12	0.52	4.30	0.48	4.55	1.40	3.24	0.82	3.53
	Targets : $\mu_{max} = 2.5$						$\alpha = 0.151$						$T = 0.53s$					
BRB	Plate = 102 x 32						483	24.4	9	0.12	0.71	3.20	0.47	3.34	1.26	2.65	0.88	2.81
T-ADAS	$N=11, b=254, h=381, t=38$						483	27.8	20	0.15	0.56	3.21	0.53	3.76	1.33	2.83	0.91	2.92
SP	$w=2159, h=254, t=5, b_f=102, t_f=10$						248	27.5	19	0.15	0.65	2.77	0.53	3.26	1.27	2.58	0.97	2.68

Note from Table 4.11, that all the observations made on the design examples developed before (see Section 4.6.1) apply once again to the retrofit cases. Since retrofitting is a particular case of the structural design, as shown in the flowchart in Figure 4.8, results with similar characteristics to the ones presented before, were expected in this Section.

4.7. Observations

Examples of new construction designs and retrofit of existing structures using BRB, T-ADAS, and SP systems have been presented, using the fundamental concepts and results from a parametric study in Section 3, and the design procedure in this section for given α , μ_{\max} , and η values.

From the results presented in Tables 4.8 to 4.11 it may be noted, on one hand, that systems having $\alpha \geq 0.50$ require a substantial frame (i.e., large beams and columns) to meet the objectives of the structural fuse concept. On the other hand, systems having $\mu_{\max} < 5$ require large fuse elements and high values of F_{yd} , which may be difficult to implement (not to mention that having $\mu_{\max} < 5$ implies less ductile behavior of the structural fuse, which is less desirable. Therefore, it is recommended for best seismic performance to use $0.25 \leq \alpha < 0.50$ and $\mu_{\max} \geq 5$ as target parameters. Furthermore, since the maximum value of η that satisfies the structural fuse concept depends mainly on the value of μ_{\max} , as shown in Figure 3.13, combining this result with the above observation, suggests that $\eta = 0.4$ is a good value for this target parameter when $\mu_{\max} \geq 5$.

Incidentally, using metallic fuse elements with low yield point steels (e.g., LYP steels with $F_{yd} = 100$ MPa) helps to increase substantially the μ_{\max} values, and hence, the system ductility.

Finally, it is noteworthy that the design procedure presented in this chapter was developed to satisfy the structural fuse concept for earthquakes that do not exceed the level of design specifications. However, due to the high variability of earthquake

records, it is recommended to use target design spectra at maximum credible earthquake level (e.g., 2% of probability of being exceeded in 50 years) in order to minimize the probability of exceeding the design level.

SECTION 5

FLOOR RESPONSE OF SINGLE DEGREE OF FREEDOM SYSTEMS WITH METALLIC STRUCTURAL FUSES

5.1. Introduction

In the 1964 Alaska and 1971 San Fernando earthquakes, extensive damage of nonstructural components was observed, which resulted in substantial economic losses with serious casualties and impediments to the buildings operation, although structural damage was found to be less significant (Lagorio, 1990). Consequently, since the 1970's, many research projects have focused on providing guidance to design, retrofit, and improve the seismic performance of nonstructural elements. An inventory and summary of past research, as well as comparisons of existing regulations to seismically design nonstructural components can be found in Filiatrault et al. (2002), where, as part of the study, recommendations are made for the development of rational research plans to investigate the seismic performance of nonstructural building components.

In previous sections, the structural fuse concept was investigated as a way to protect primary moment frame structures from experiencing inelastic behavior of beams and columns, by concentrating all damage on easily replaceable elements. Furthermore, limiting story drift indirectly allows to mitigate damage of nonstructural components that are sensitive to lateral deformations (i.e., elements that are generally attached to consecutive floors). However, many nonstructural elements are only attached to one floor, which makes them vulnerable to shifting or overturning. Damage to the internal components of sensitive equipment may also occur due to severe floor vibrations. In

order to protect these components, floor acceleration and, in some cases, floor velocity (e.g., in the case of toppling of furniture) should be kept under certain limits.

This section studies the floor velocity and acceleration response of SDOF systems designed with metallic dampers acting as structural fuses. Comparisons are made between the floor response of bare frames and the floor response of systems with metallic fuses. Furthermore, velocity and acceleration spectra are developed from floor time history responses to assess how the behavior of nonstructural components may be affected by the use of metallic fuses. Finally, an equivalent sine-wave floor acceleration response is proposed to generate acceleration and velocity spectra, that may be used to seismically design nonstructural components.

5.2. Floor Response

A parametric study was conducted to obtain floor accelerations and velocities for SDOF systems with metallic fuses, using the synthetic earthquakes generated in Section 3, for the same set of parameters previously considered (i.e., $\alpha = 0.05, 0.25, 0.50$; $\mu_{\max} = 10, 5, 2.5, 1.67$; $\eta = 0.2, 0.4, 0.6, 1.0$; and $T = 0.1 \text{ s}, 0.25 \text{ s}, 0.50 \text{ s}, 1.0 \text{ s}, 1.5 \text{ s}, 2.0 \text{ s}$).

Figures 5.1 and 5.2 show the results of the parametric study for floor acceleration, S_a , and floor velocity, S_v , respectively, as functions of the above parameters. The solid line in both figures corresponds to the NEHRP elastic design spectrum. It may be noted in Figure 5.1, that floor acceleration reduces with increases in η values. This is because the response modification factor, R , is inversely proportional to η , and has the largest values for short period systems (i.e., $T \leq 0.5 \text{ s}$), as shown in Figure 4.10. Note also, that as structures become more flexible (i.e., $T \geq 2.0 \text{ s}$) floor spectral accelerations progressively approach those obtained for elastic SDOF systems with little influence of parameters α , μ_{\max} , and η .

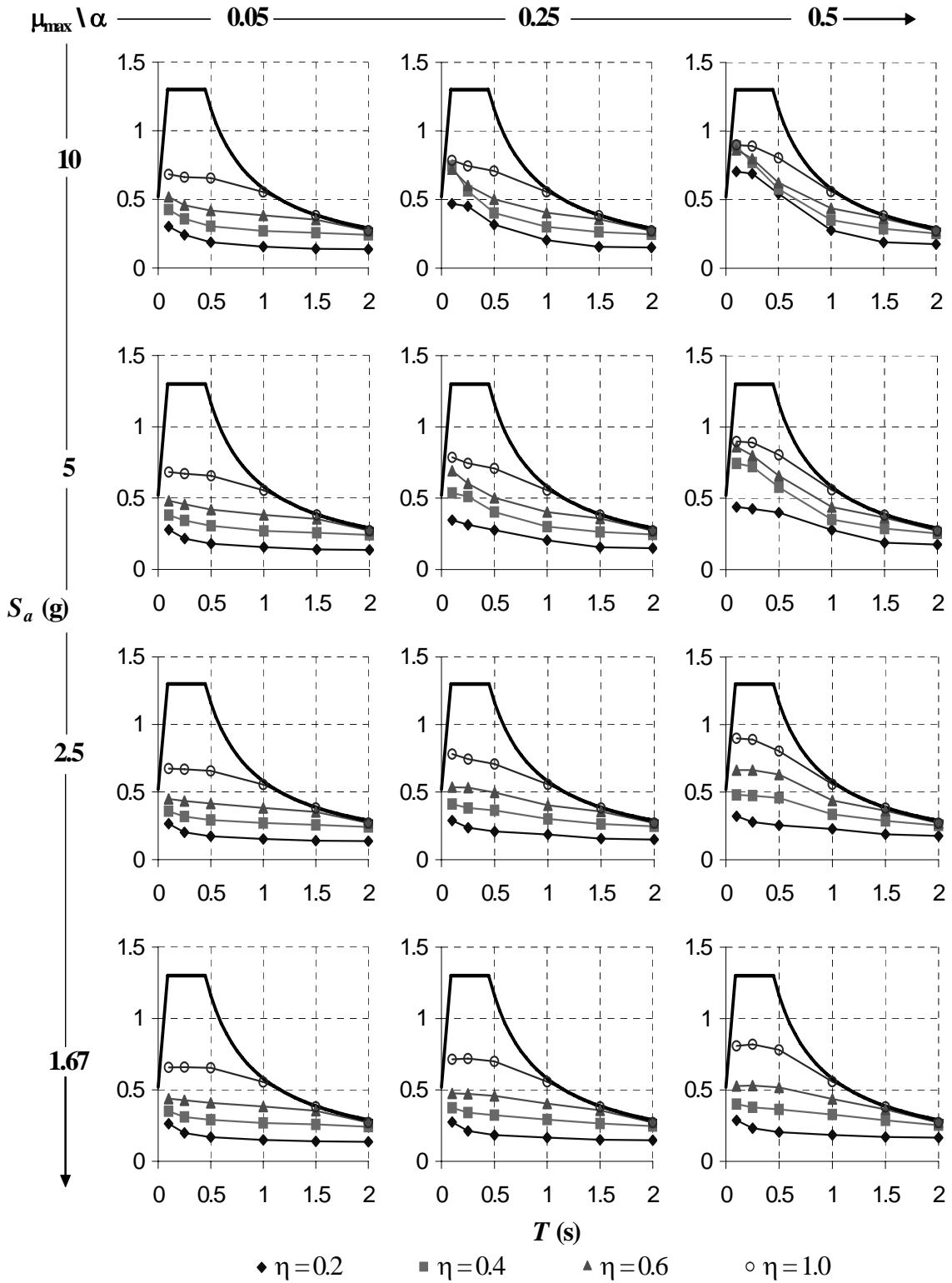


Figure 5.1. Floor Acceleration of SDOF Systems with Metallic Fuses

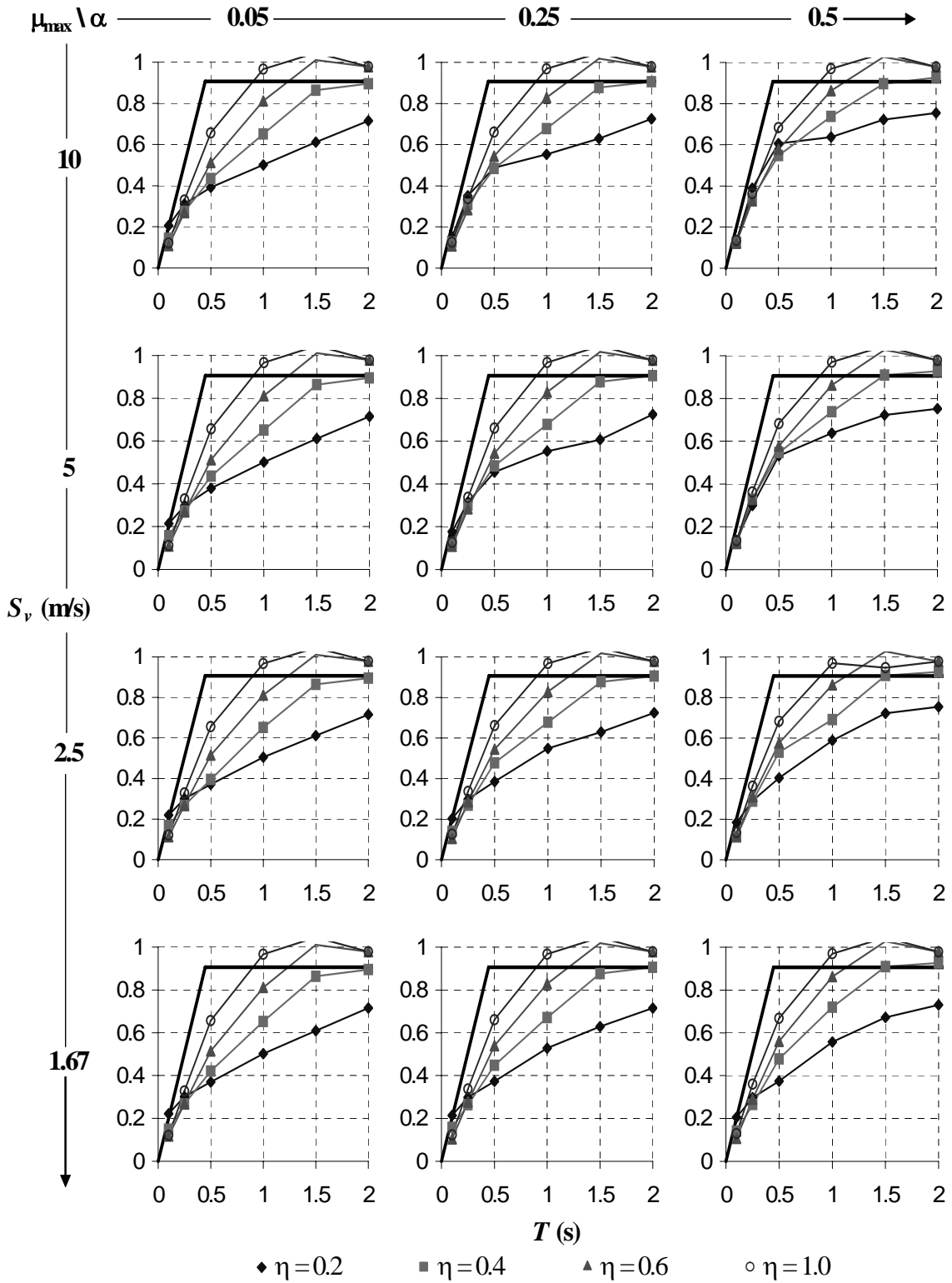


Figure 5.2. Floor Velocity of SDOF Systems with Metallic Fuses

Figure 5.2 shows, as expected, that the relative velocity is close to zero for short period systems. Like in the case of acceleration, floor velocity increases with η values, and for long period systems all the curves approach the NEHRP elastic design spectrum for $T \geq 2$ s. Furthermore, in Figures 5.1 and 5.2, it can be noted that both α and μ_{\max} have negligible influence on the acceleration and velocity demands.

To analyze how metallic fuses modify the floor response, comparisons between the response of bare frames and the response of structural fuse systems were made, in terms of acceleration and velocity. Figures 5.3 to 5.6 show the floor acceleration of structural fuse systems, along with the floor acceleration of the corresponding bare frame (i.e., without metallic dampers). Every figure corresponds to a different η value. Note that when metallic fuses are added to the system, the period of the system shortens. This is pointed out by (3.23), rewritten as:

$$T = \sqrt{\alpha} T_f \quad (5.1)$$

where T_f is the period of the corresponding bare frame system. As a result, the original six periods considered for the bare frame result in six new periods for each α considered. When comparing bare frame and retrofitted system response in Figures 5.3 to 5.6, one cannot directly read up from the horizontal axis, but should rather compare the results point-by-point for the six cases considered (alternatively, the figures could have been plotted as a function of the bare frame period on the horizontal axis, but it was felt worthwhile to also visually see the shift in period corresponding to each case).

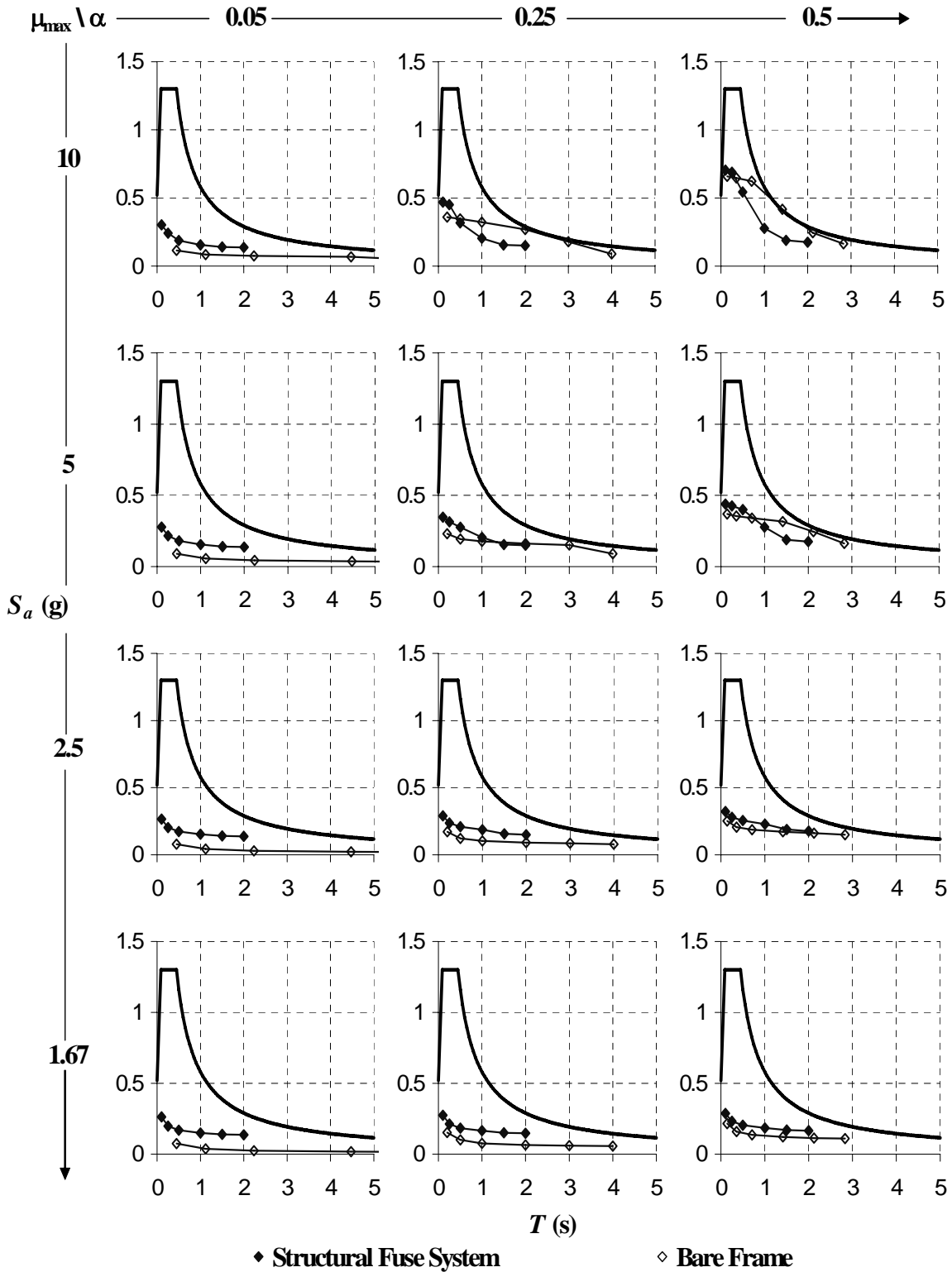


Figure 5.3. Floor Acceleration of Structural Fuse Systems and Bare Frames for $\eta = 0.2$

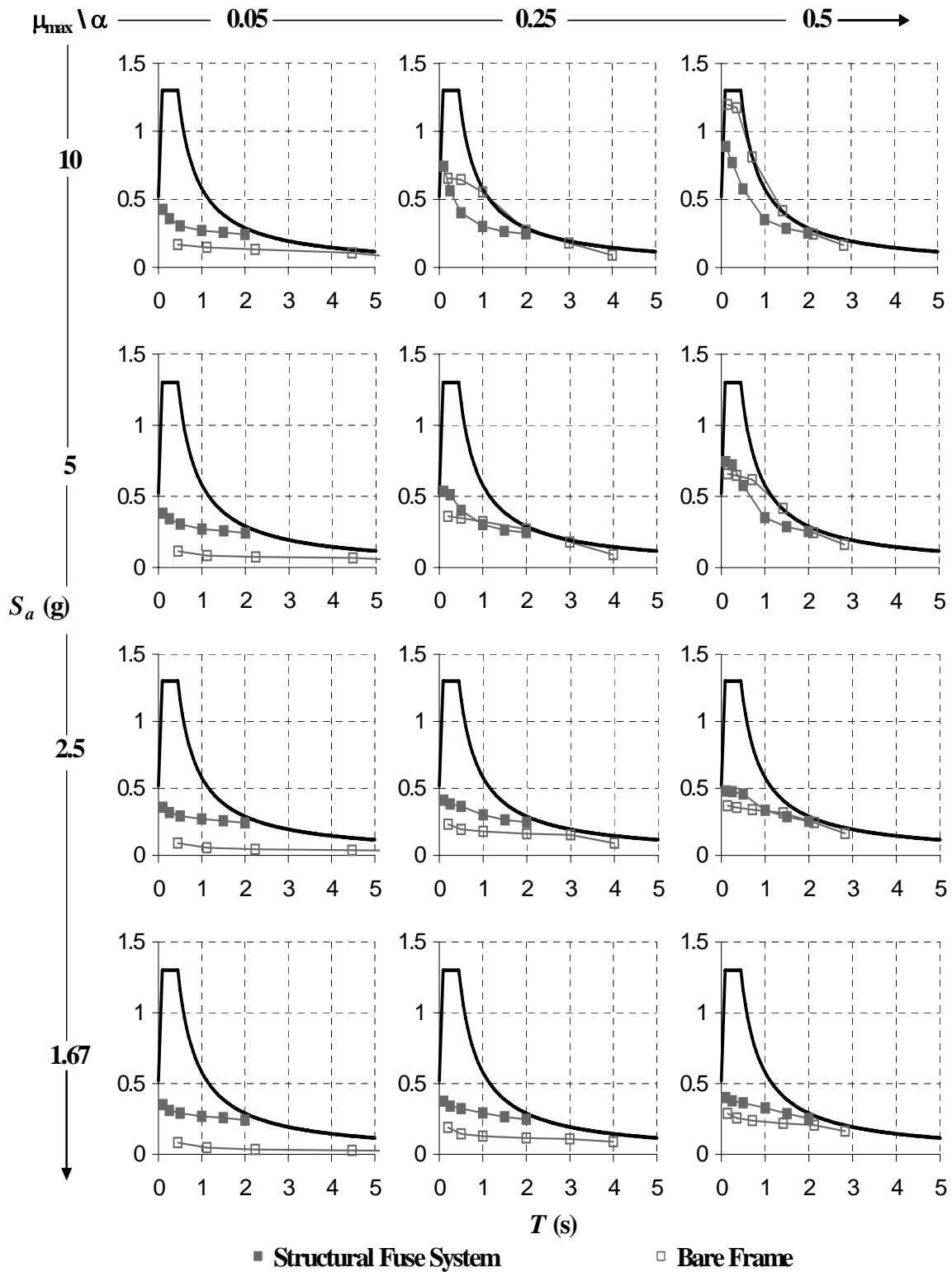


Figure 5.4. Floor Acceleration of Structural Fuse Systems and Bare Frames for $\eta = 0.4$

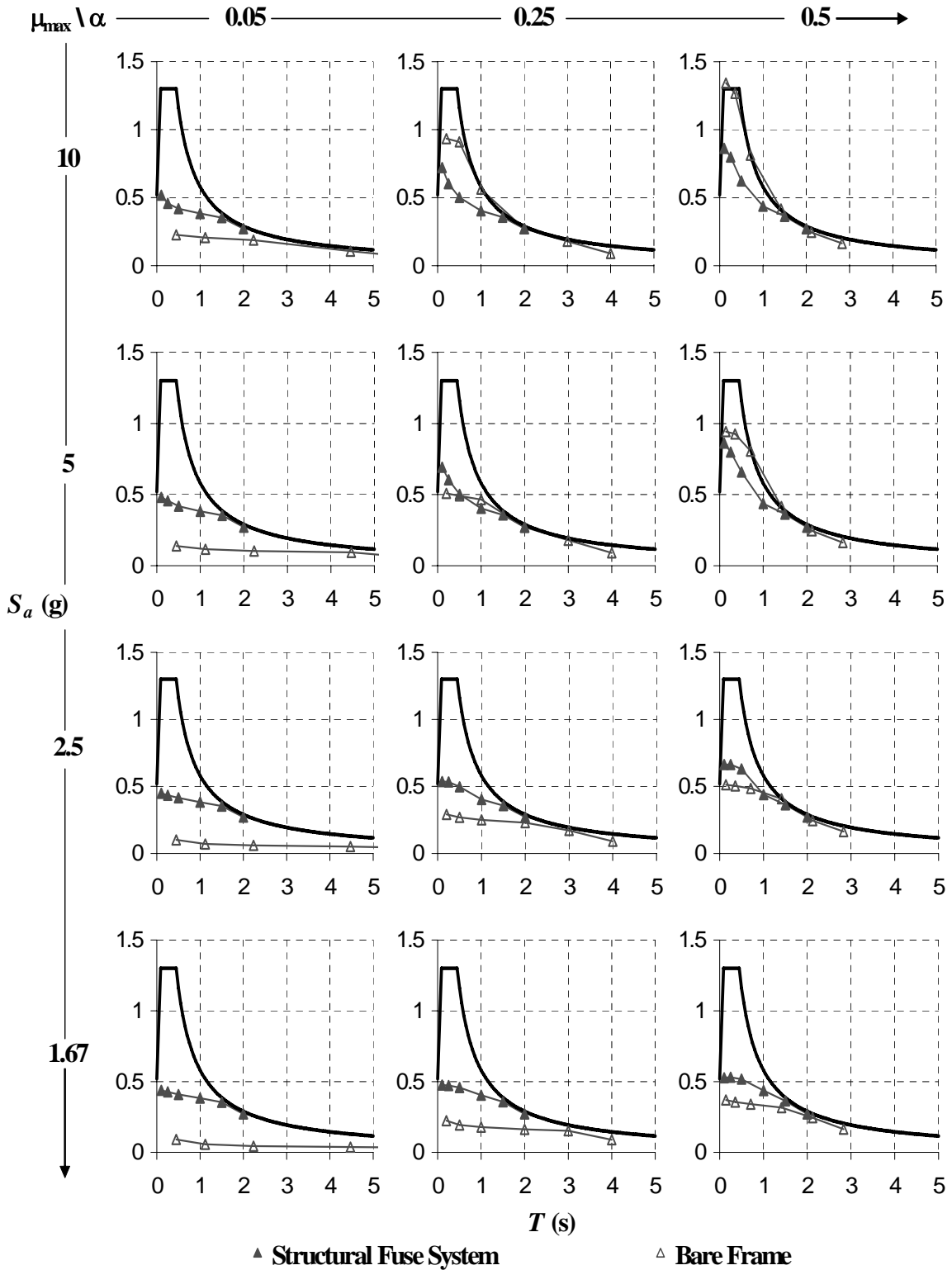


Figure 5.5. Floor Acceleration of Structural Fuse Systems and Bare Frames for $\eta = 0.6$

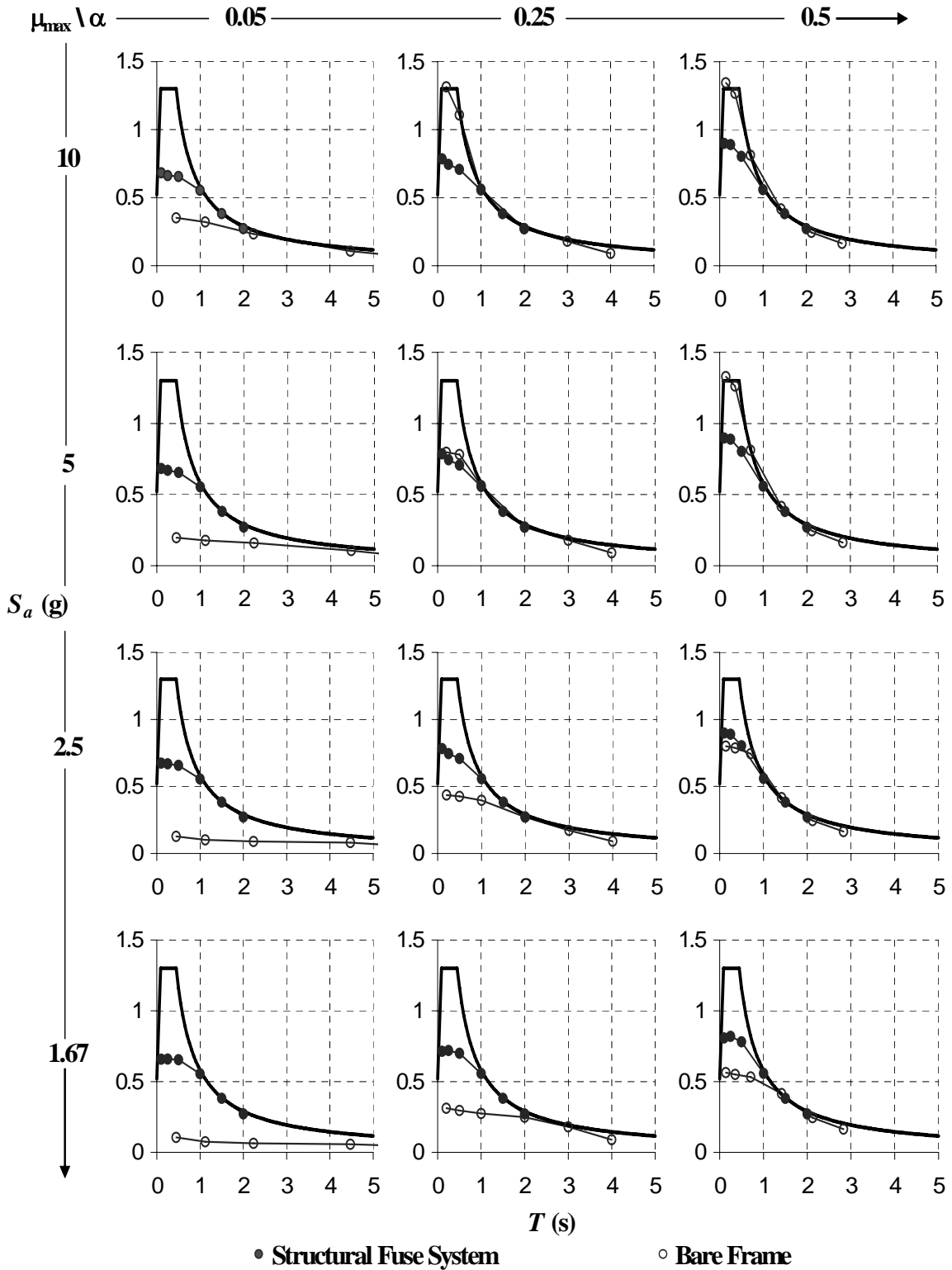


Figure 5.6. Floor Acceleration of Structural Fuse Systems and Bare Frames for $\eta = 1.0$

Figures 5.3 to 5.6 also show that, in most of the cases, floor acceleration is increased by adding metallic fuses to the system. However, a reduction in the floor acceleration may be seen for the case of systems with large stiffness ratio, and large maximum displacement ductility (i.e., $\alpha = 0.5$, and $\mu_{\max} = 10$), especially for short period structures (i.e., $T \leq 0.5$ s). This is consistent with results in Figures 3.3a and 3.3b, where for the case of $\alpha = 0.5$ and $\mu_{\max} = 10$, for example, adding metallic dampers decreased both the lateral displacement and the total base shear (i.e., less acceleration) compared to the response of the corresponding bare frame system.

Figures 5.7 to 5.10 show the floor response, in terms of velocity, for bare frames and structural fuse systems. In this case, the periods are also “shifted” according to the relationship given by (5.1). Unlike acceleration, velocity either decreases or remains equal in most of the cases, which implies that adding metallic fuses do not seem to change the velocity response of the systems.

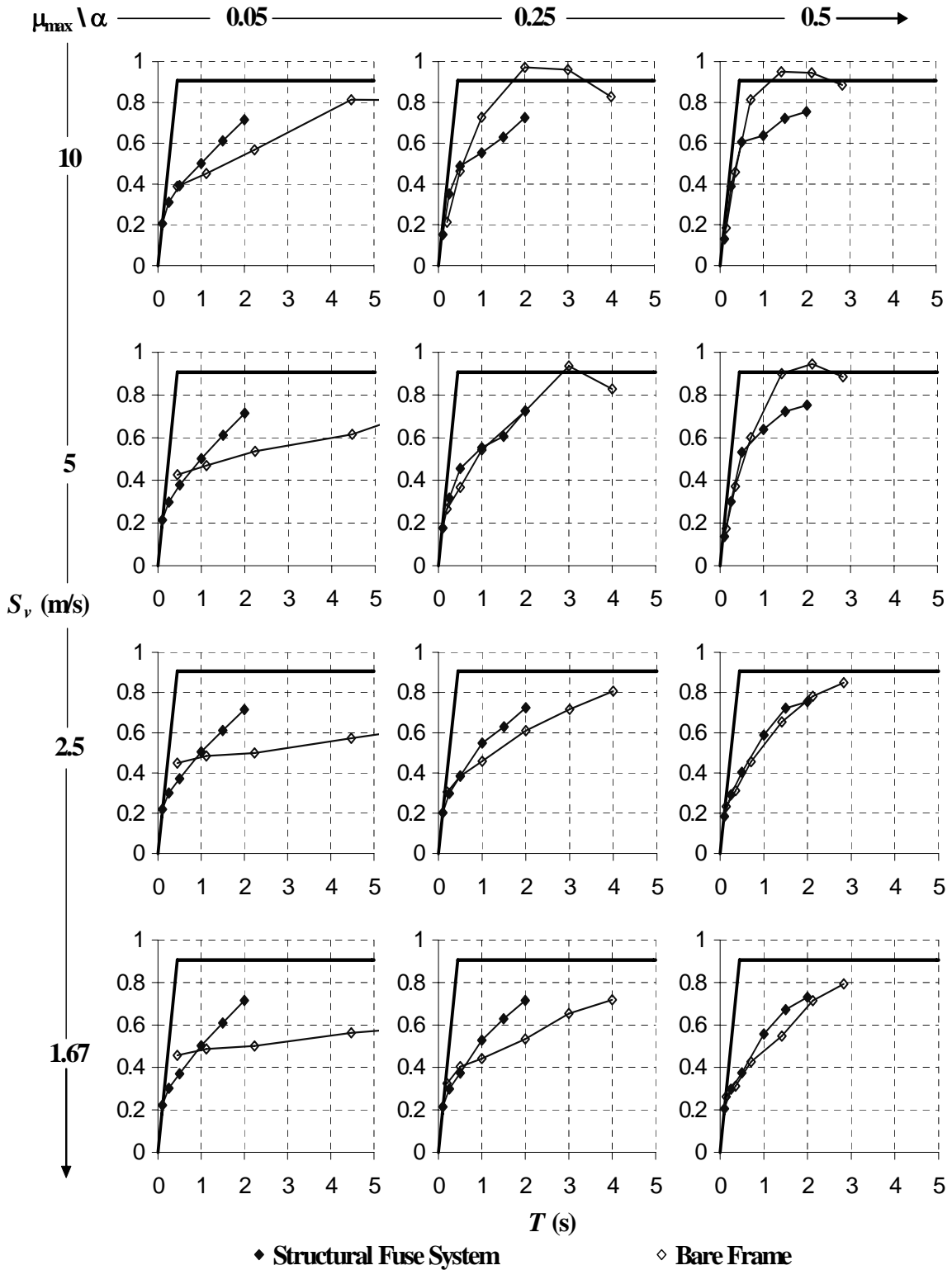


Figure 5.7. Floor Velocity of Structural Fuse Systems and Bare Frames for $\eta = 0.2$

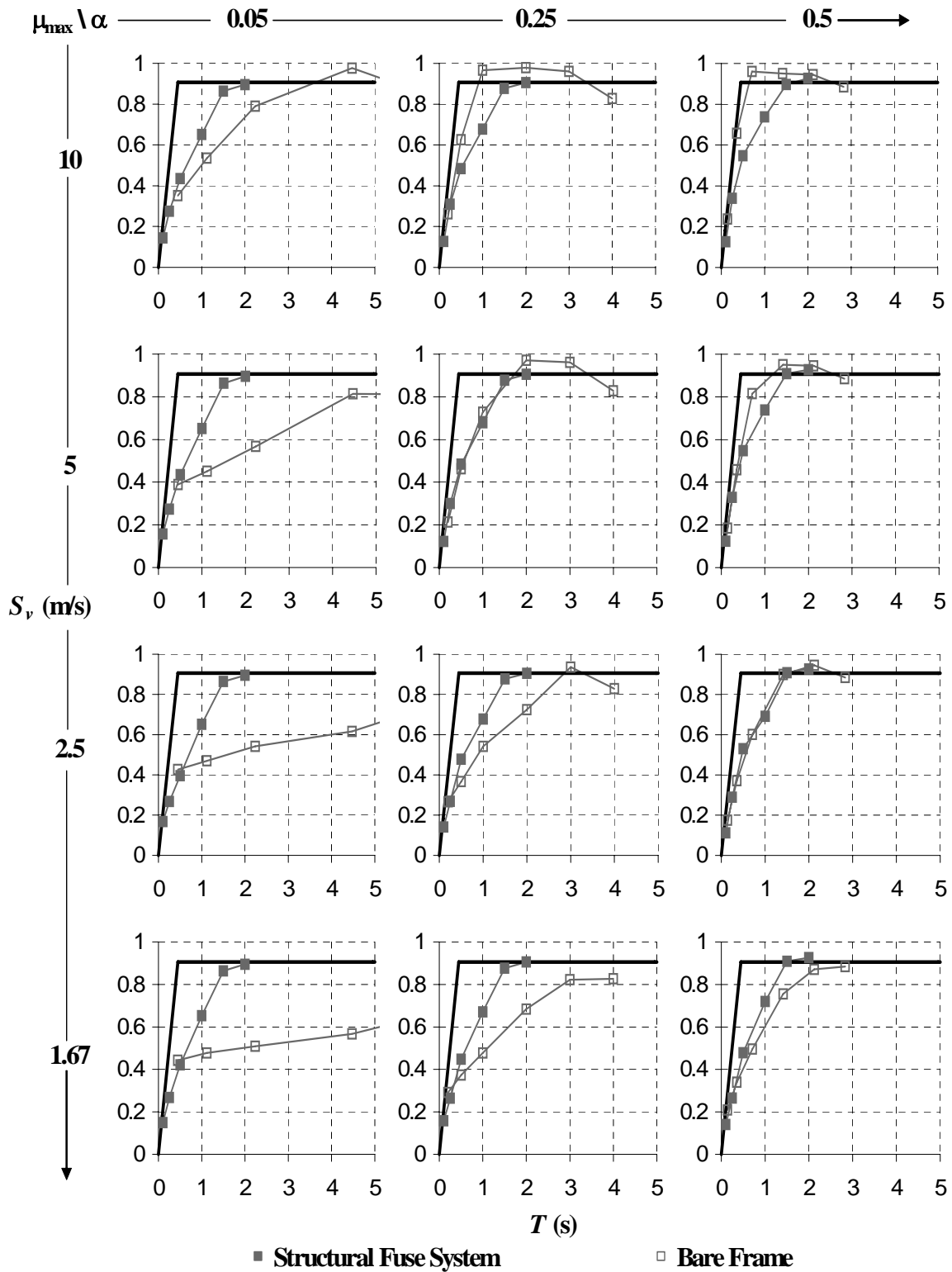


Figure 5.8. Floor Velocity of Structural Fuse Systems and Bare Frames for $\eta = 0.4$

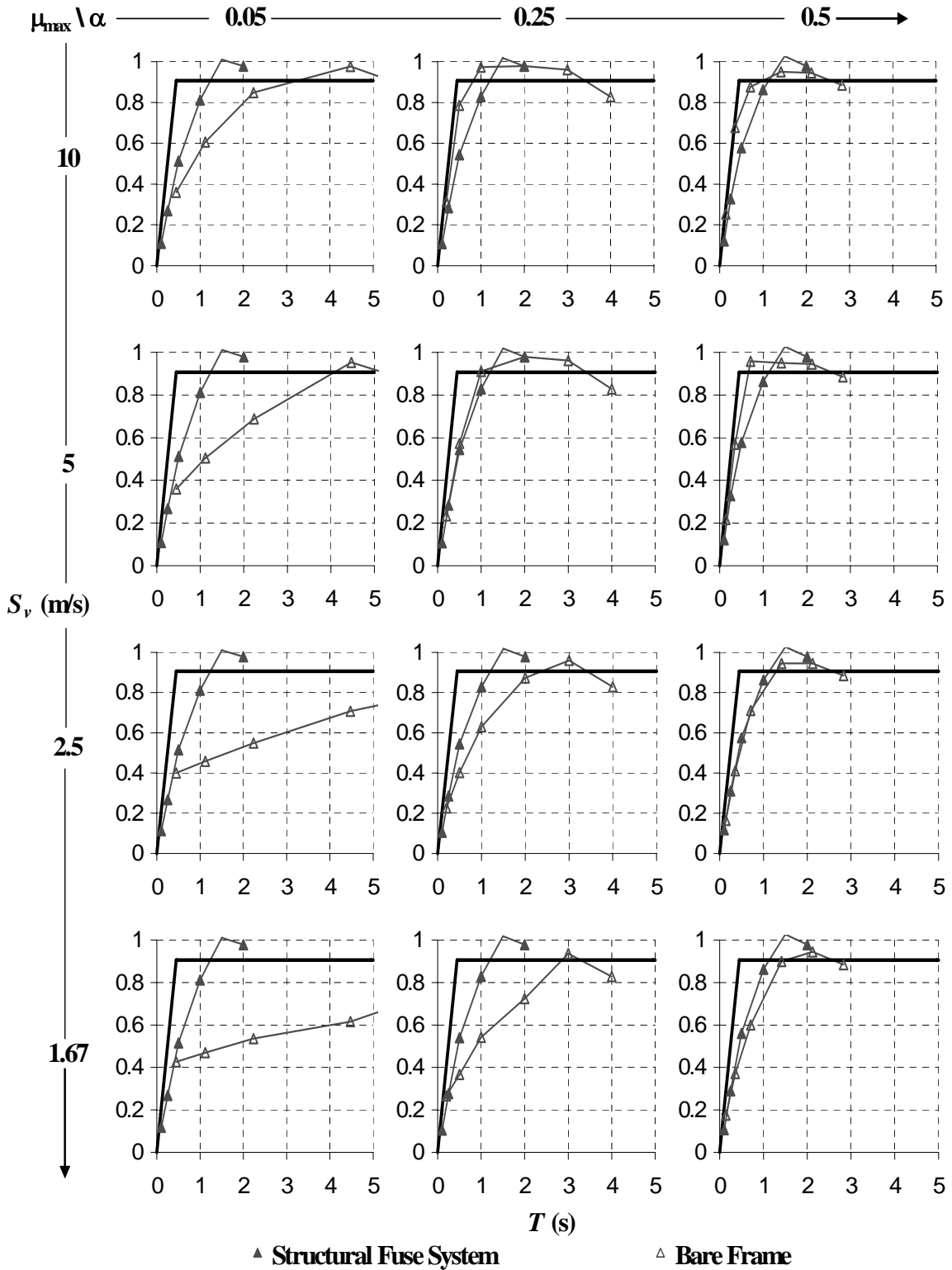


Figure 5.9. Floor Velocity of Structural Fuse Systems and Bare Frames for $\eta = 0.6$

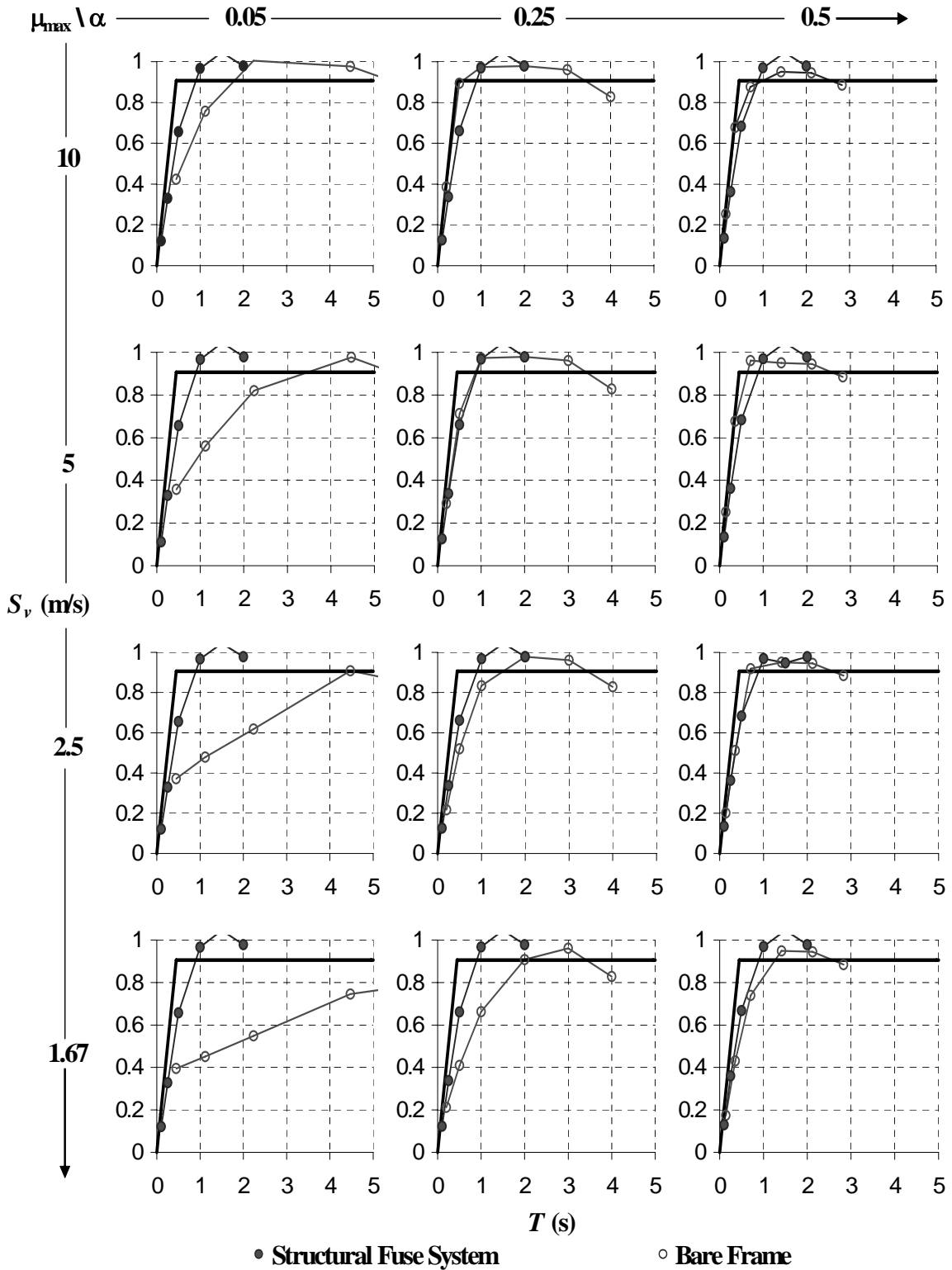


Figure 5.10. Floor Velocity of Structural Fuse Systems and Bare Frames for $\eta = 1.0$

A ratio of the peak floor acceleration of the structural fuse system, PFA_{SF} , with respect to the peak floor acceleration of the bare frame, PFA_{BF} , is plotted in Figure 5.11. Note that the amplification of the acceleration due to the addition of a structural fuse is sensitive to α values, especially for $\alpha = 0.05$ when $T \geq 1.0$ s, where it can be up to an order of magnitude larger in some cases. Recall from Figure 3.3b that in systems with small values of α , the frame contributes little to the total shear capacity of the system. Therefore, these systems are likely to have a significant amplification of the floor accelerations when metallic fuses are used. As an example of consequences from this observation, unsecured rigid nonstructural elements on the floor of these systems are more susceptible to start sliding as the friction force is exceeded, because of larger increases in the peak floor acceleration ratio (i.e., $PFA_{SF} / PFA_{BF} \gg 2$), however, it is recognized that sliding distance also depends on the impulsiveness of the excitation.

Finally, the ratio of the peak floor velocity of the structural fuse system with respect to the peak floor velocity of the bare frame, PFV_{SF} / PFV_{BF} , is also plotted in Figure 5.12. Again, it may be noted that the floor velocity either remains unchanged or decreases in most of the cases, except for $\alpha = 0.05$ and $T \geq 1.0$ s where an amplification up to 60% is observed.

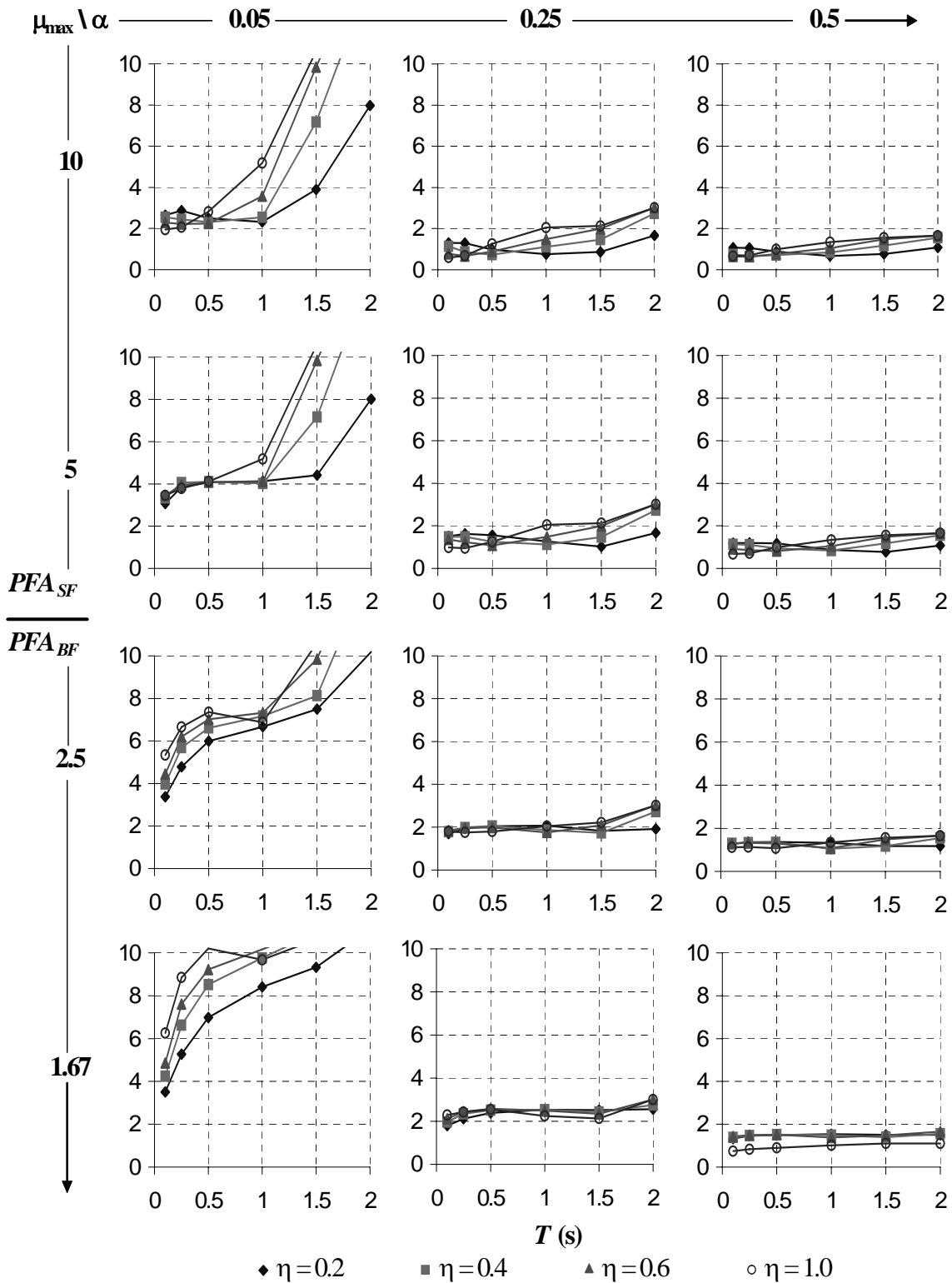


Figure 5.11. Ratio of the Peak Floor Acceleration of Structural Fuse Systems with respect of the Peak Floor Acceleration of Bare Frames

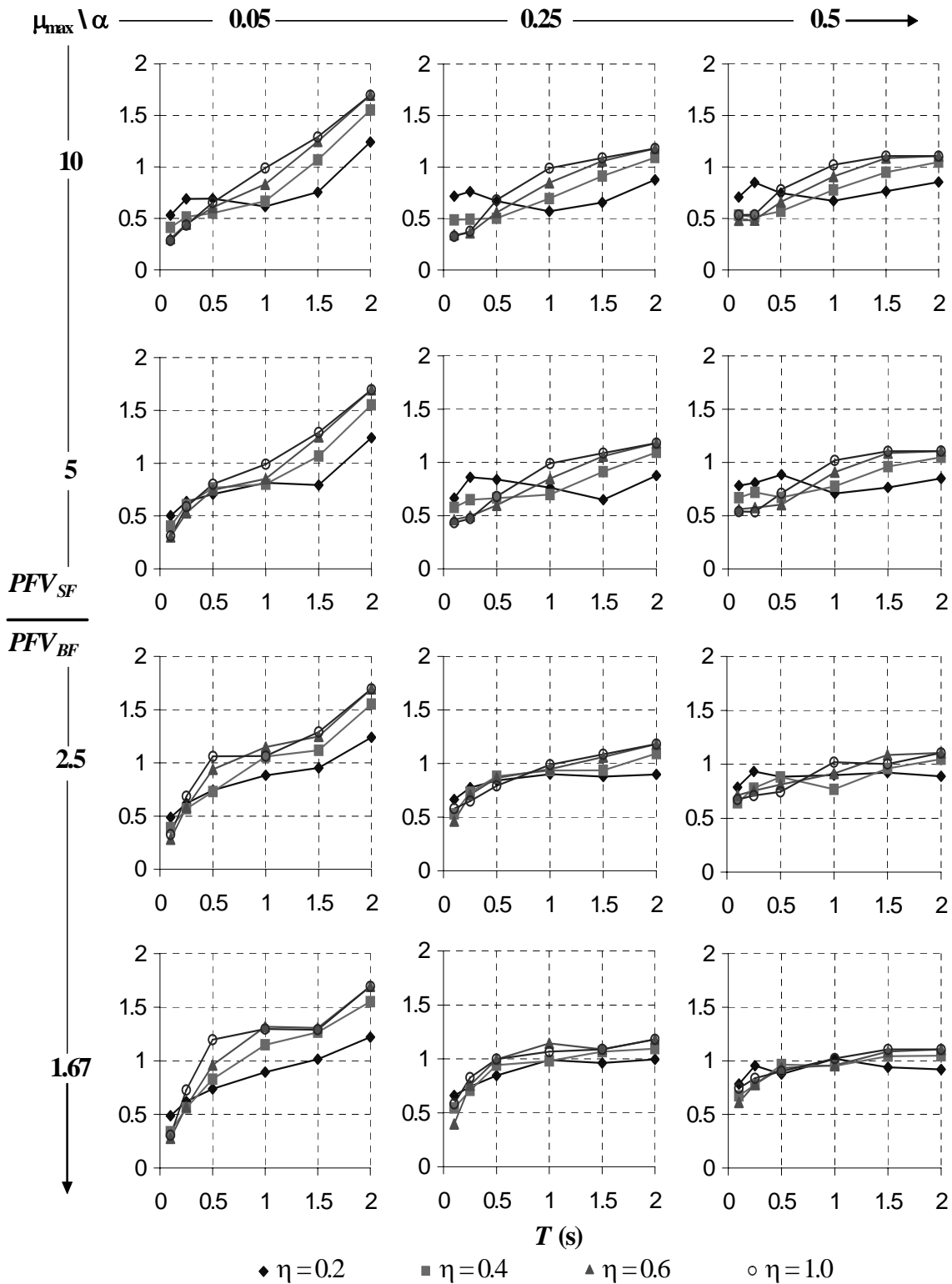


Figure 5.12. Ratio of the Peak Floor Velocity of Structural Fuse Systems with respect of the Peak Floor Velocity of Bare Frames

As a case study to illustrate in more details the above results, a SDOF system designed with buckling-restrained braces to satisfy the structural fuse concept was selected from the results presented in Table 4.8. The frame is a single-story one-bay structure composed of W14 x 211 columns and a W12 x 190 beam, with buckling-restrained braces made of rectangular plates (57 x 25 mm) in a chevron configuration. Design parameters for this example (obtained directly from Table 4.8) are: $\alpha = 0.25$, $\mu_{\max} = 5.04$, $\eta = 0.40$, and $T = 0.53$ s. In this case study, results obtained from time history analysis (or directly read from charts on Figures 5.1 to 5.12) indicate that floor spectral acceleration, S_a , and floor spectral velocity, S_v , are 0.40 g and 484 mm/s, respectively. Prior to adding the buckling-restrained braces, properties of the system were $\eta_f = 0.52$ and $T_f = 1.04$ s. Figures 5.4 and 5.8 show that S_a and S_v on the bare frame are respectively 0.32 g and 728 mm/s; the figures also show the aforementioned results for the buckling-restrained braced system. In this particular example, it may be noted that adding buckling-restrained braces to the system result in an increase of 25% in the floor acceleration, and a reduction of 33% in the floor velocity (i.e., $PFA_{SF} / PFA_{BF} = 1.25$, and $PFV_{SF} / PFV_{BF} = 0.67$).

5.3. Floor Spectra

Floor acceleration response histories of SDOF systems have been taken as the input signal to generate elastic floor acceleration and velocity spectra, to analyze the response of nonstructural components attached to the floor of bare frame systems, and structures designed with metallic fuses. A damping ratio of 5% was selected for this study.

Floor spectra were generated for systems with elastic periods arbitrarily selected as 0.25 s, 0.50 s, and 1.0 s. From Table 4.1, η values were selected to satisfy the structural fuse concept for systems with $\mu_{\max} \geq 5$, which is the range of target parameters recommended in Section 4 to have a satisfactory seismic performance. Accordingly, floor spectra were

generated for systems having $\eta = 0.6, 0.4,$ and $0.2,$ for the selected periods of 0.25 s, 0.50 s, and 1.0 s, respectively.

Figures 5.13 to 5.15 show the floor acceleration spectra, S_{anc} , for the selected structural fuse systems, and their corresponding bare frame systems, where the subscript “nc” denotes “nonstructural component.” In these plots, the horizontal axis corresponds to the elastic period of the nonstructural components, T_{nc} , since floor spectra were built to analyze the response of secondary elements attached to the floor of the primary structure. Note that, even though peak floor acceleration was found to increase in most of the cases, in floor acceleration spectra, two regions are defined by the critical period of the nonstructural component, T_c , where both spectra intersect. Nonstructural elements with a period shorter than this critical period are subjected to acceleration demands greater in structural fuse systems, than in the corresponding bare frame; whereas for components with a period longer than critical, the acceleration demand decreases for structural fuse systems. Approximately, the critical period, T_c , may be determined as the average between the period of the bare frame, T_p , and the period of the structural fuse system, T . Using (5.1), T_c may be calculated as:

$$T_c \approx \frac{1}{2} \left(1 + \frac{1}{\sqrt{\alpha}} \right) T \quad (5.2)$$

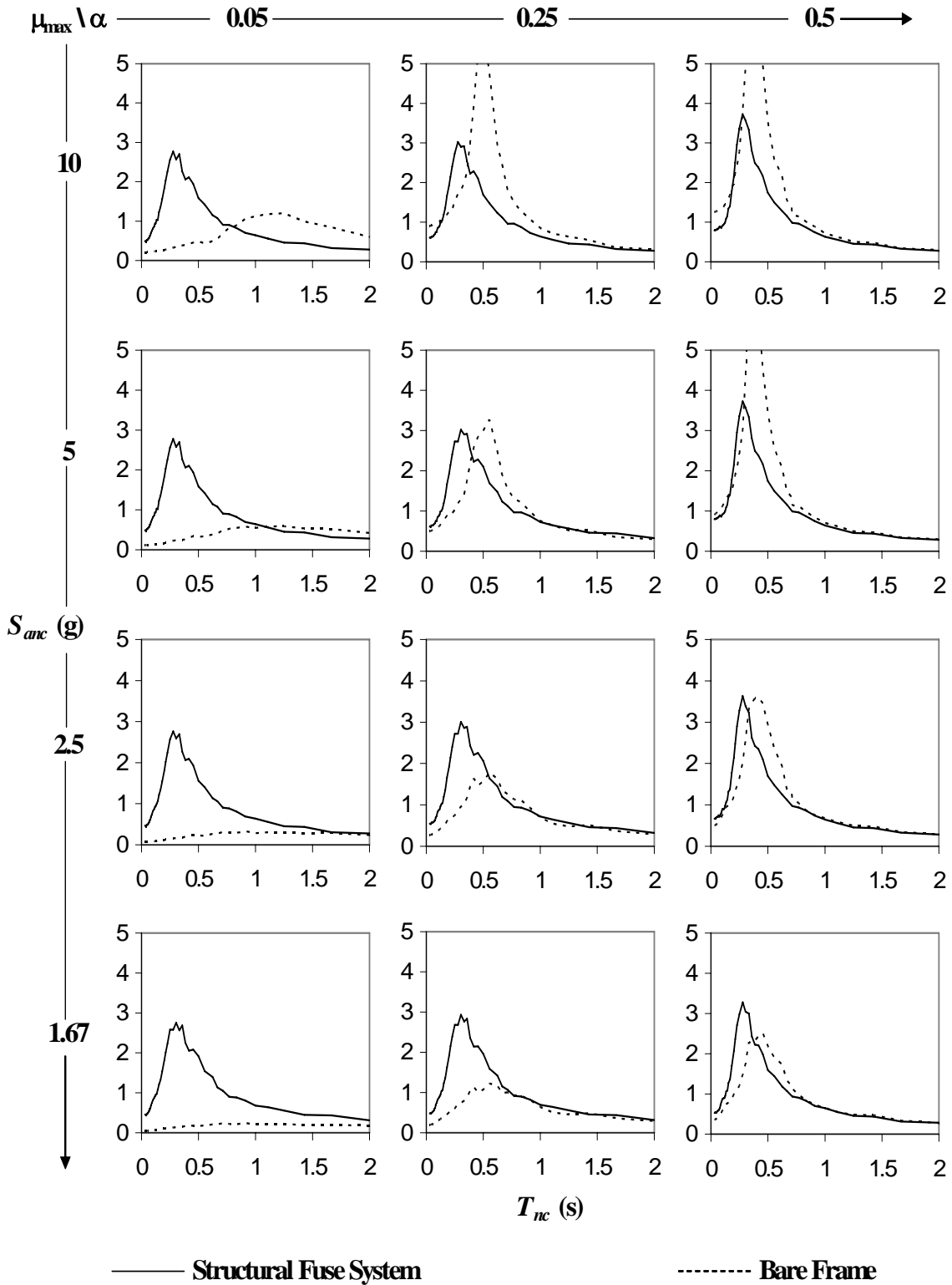


Figure 5.13. Floor Acceleration Spectra of Structural Fuse Systems and Bare Frames for $T = 0.25$ s, and $\eta = 0.6$

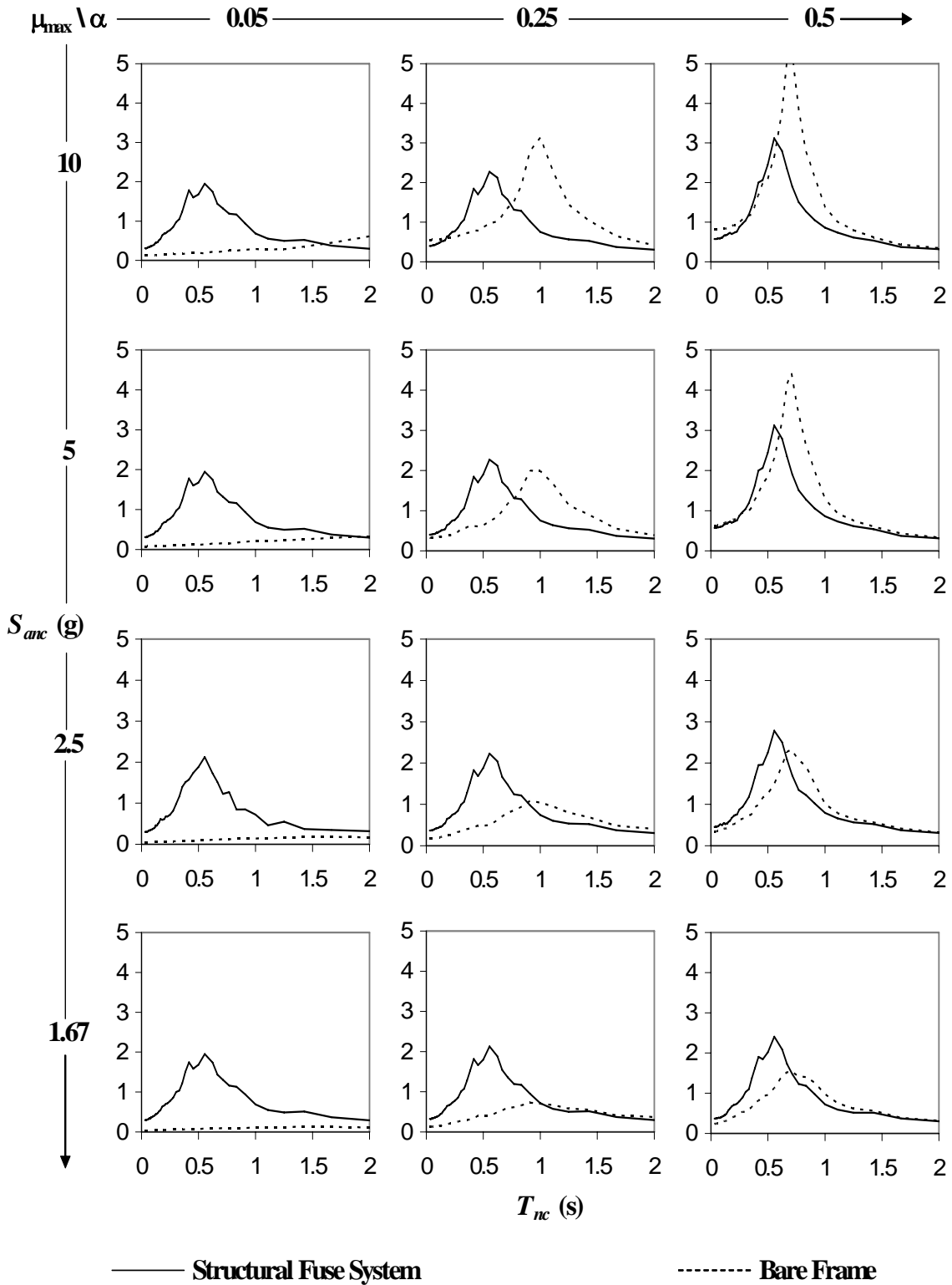


Figure 5.14. Floor Acceleration Spectra of Structural Fuse Systems and Bare Frames for $T = 0.50$ s, and $\eta = 0.4$

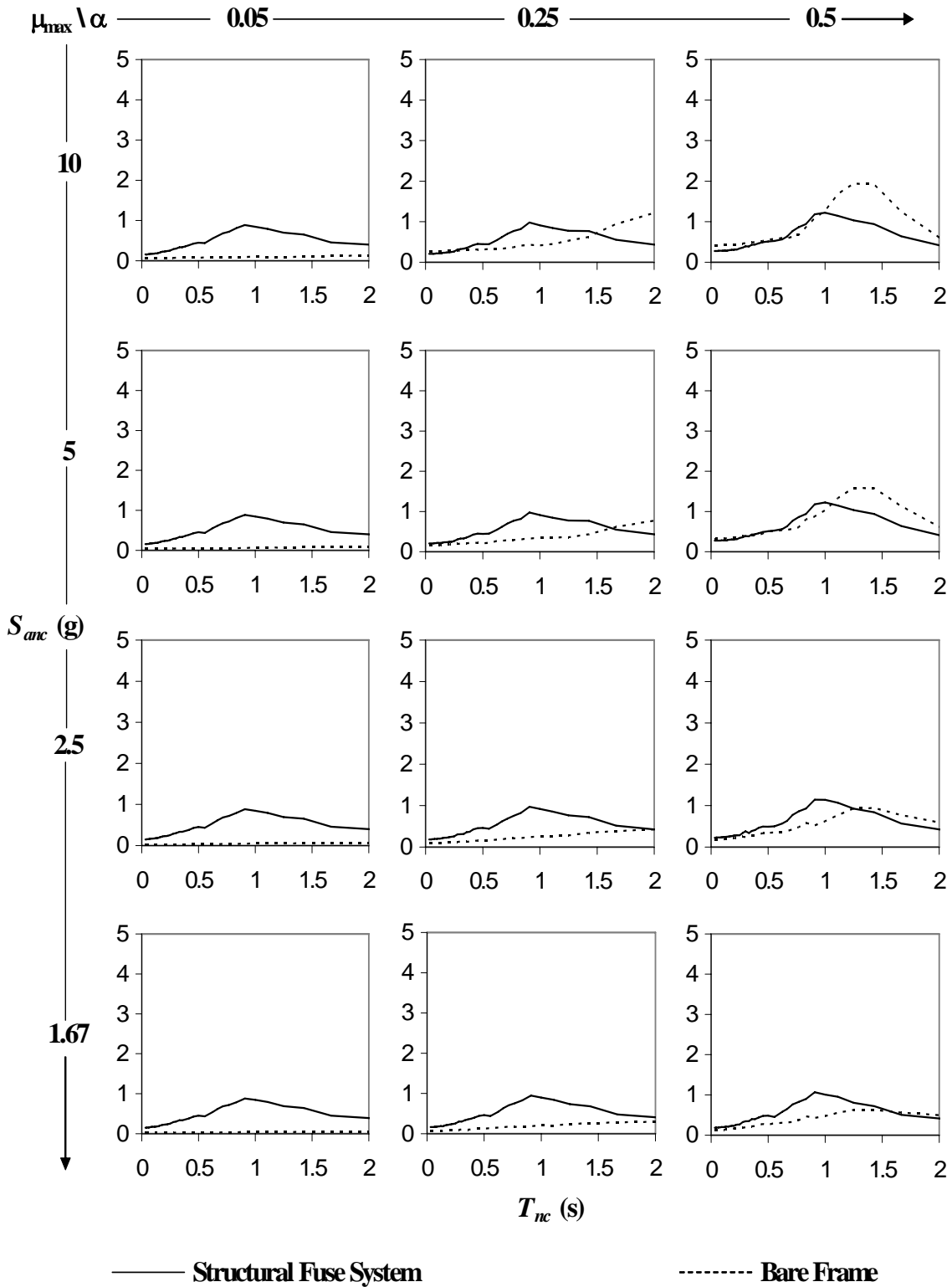


Figure 5.15. Floor Acceleration Spectra of Structural Fuse Systems and Bare Frames for $T = 1.0$ s, and $\eta = 0.2$

Table 5.1 shows the approximate values of T_c calculated using (5.2) for the set of α , and T values used in this study, as well as the actual values of T_c for the cases considered, and the percentage difference between these values. On average, the approximate equation gives results within 17% of the actual ones, with some results differing by as much as 51%.

Table 5.1. Approximately Critical Period, T_c , for Acceleration using the Average Equation

$\mu_{\max} \setminus \alpha$	0.05		0.25		0.50	
	T_c (s)	Diff.	T_c (s)	Diff.	T_c (s)	Diff.
(1)	Actual	%	Actual	%	Actual	%
(1)	(2)	(3)	(4)	(5)	(6)	(7)
$T = 0.25$ s, $\eta = 0.60$						
	T_c (s) = 0.68		T_c (s) = 0.38		T_c (s) = 0.30	
10	0.83	18%	0.36	6%	0.28	7%
5	1.11	39%	0.42	10%	0.28	7%
2.5	N/A	N/A	0.56	32%	0.33	9%
1.67	N/A	N/A	0.77	51%	0.38	21%
$T = 0.50$ s, $\eta = 0.40$						
	T_c (s) = 1.37		T_c (s) = 0.75		T_c (s) = 0.60	
10	1.55	12%	0.77	3%	0.56	7%
5	1.83	25%	0.77	3%	0.62	3%
2.5	N/A	N/A	0.91	18%	0.67	10%
1.67	N/A	N/A	1.00	25%	0.71	15%
$T = 1.00$ s, $\eta = 0.20$						
	T_c (s) = 2.74		T_c (s) = 1.50		T_c (s) = 1.21	
10	3.33	18%	1.50	0%	0.91	33%
5	3.33	18%	1.60	6%	1.11	9%
2.5	N/A	N/A	2.00	25%	1.25	3%
1.67	N/A	N/A	2.20	32%	1.67	28%

Floor velocity spectra, S_{vnc} , are shown in Figures 5.16 to 5.18 for the selected structural fuse systems, along with their corresponding bare frame systems. As was observed in floor acceleration spectra, in floor velocity spectra, regions of increases and decreases in the velocity demands are delimited by the critical period, T_c . Likewise, nonstructural elements with a period shorter than the critical period are subjected to velocity demands greater in structural fuse systems, than in the corresponding bare frame; whereas for components with a period longer than the critical, the velocity demand decreases for structural fuse systems. In Table 5.2 a comparison between actual values of T_c and approximate values calculated using (5.2) is shown for the spectral velocity case. On average, the approximate equation gives results within 19% of the actual ones, with some results differing by as much as 54%.

Table 5.2. Approximately Critical Period, T_c , for Velocity using the Average Equation

$\mu_{max} \setminus \alpha$	0.05		0.25		0.50	
	T_c (s)	Diff.	T_c (s)	Diff.	T_c (s)	Diff.
(1)	Actual	%	Actual	%	Actual	%
(2)	(3)	(4)	(5)	(6)	(7)	(7)
$T = 0.25$ s, $\eta = 0.60$						
	T_c (s) = 0.68		T_c (s) = 0.38		T_c (s) = 0.30	
10	0.91	25%	0.38	0%	0.30	0%
5	1.43	52%	0.42	10%	0.30	0%
2.5	N/A	N/A	0.56	32%	0.30	0%
1.67	N/A	N/A	0.83	54%	0.38	21%
$T = 0.50$ s, $\eta = 0.40$						
	T_c (s) = 1.37		T_c (s) = 0.75		T_c (s) = 0.60	
10	1.70	19%	0.77	3%	0.56	7%
5	2.10	35%	0.83	10%	0.62	3%
2.5	N/A	N/A	0.91	18%	0.67	10%
1.67	N/A	N/A	1.11	32%	0.71	15%
$T = 1.00$ s, $\eta = 0.20$						
	T_c (s) = 2.74		T_c (s) = 1.50		T_c (s) = 1.21	
10	2.60	5%	1.55	3%	1.00	21%
5	3.33	18%	1.67	10%	1.00	21%
2.5	N/A	N/A	2.10	29%	1.25	3%
1.67	N/A	N/A	2.50	40%	1.67	28%

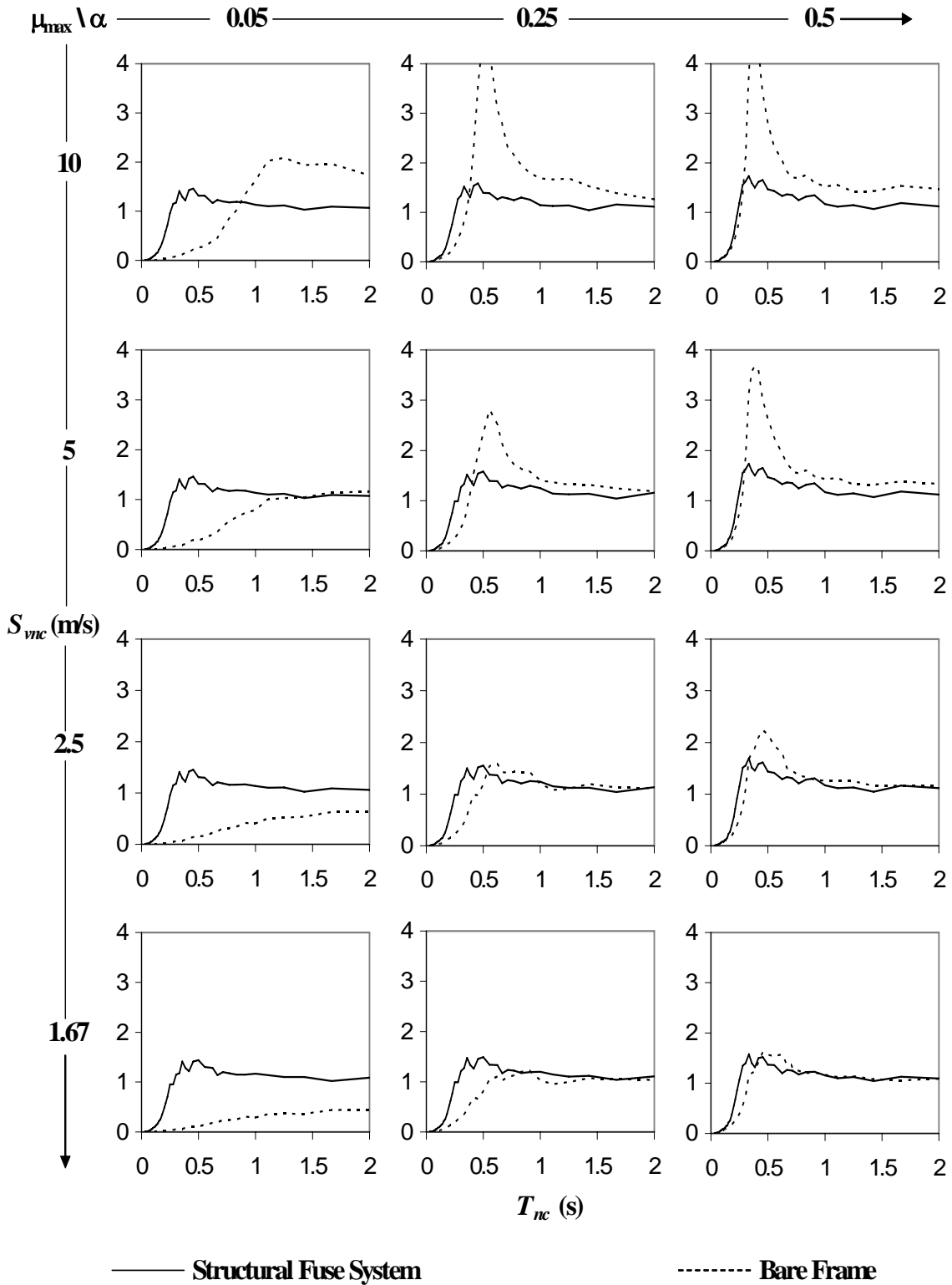


Figure 5.16. Floor Velocity Spectra of Structural Fuse Systems and Bare Frames for $T = 0.25$ s, and $\eta = 0.6$

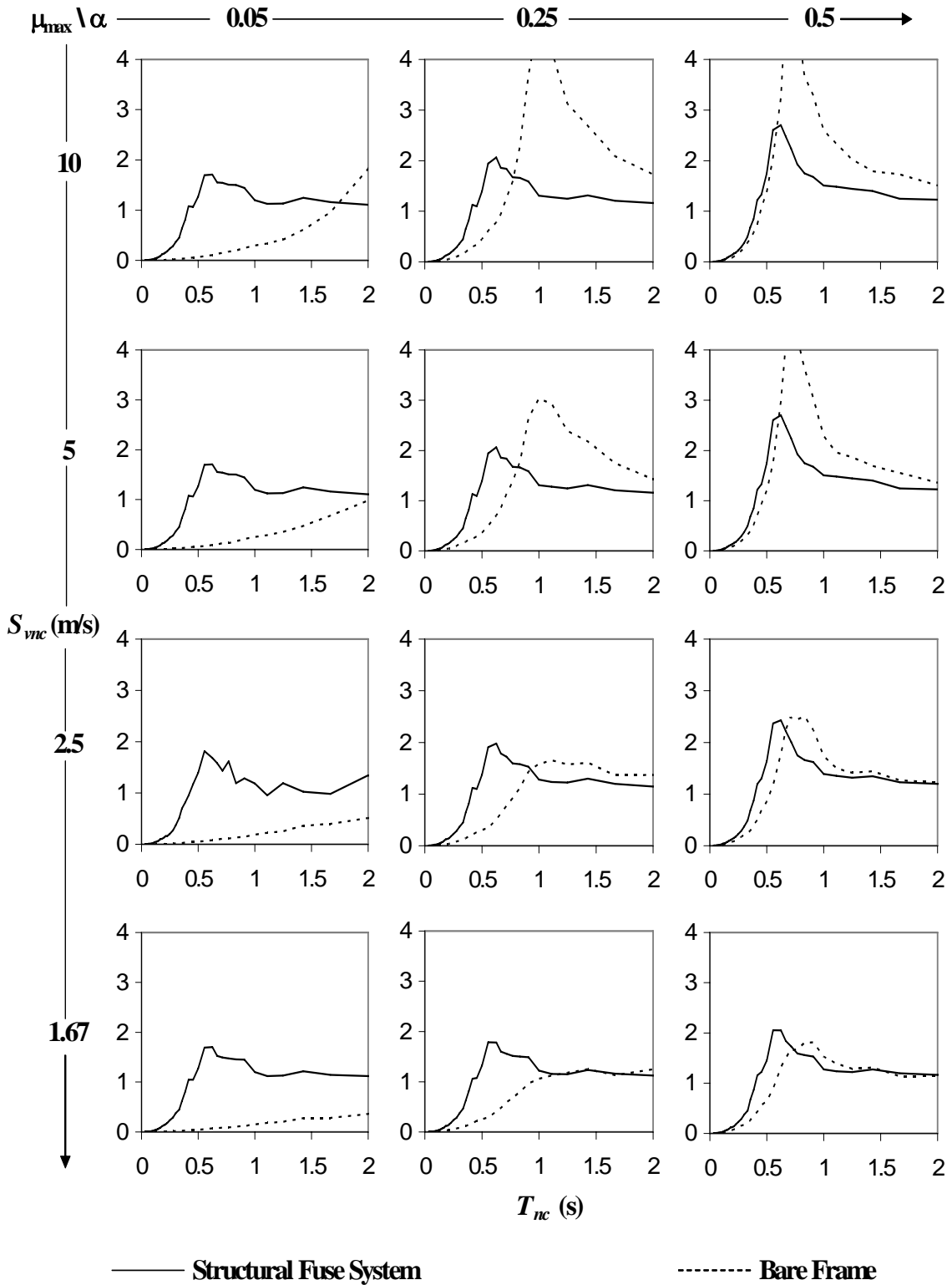


Figure 5.17. Floor Velocity Spectra of Structural Fuse Systems and Bare Frames for $T = 0.50$ s, and $\eta = 0.4$

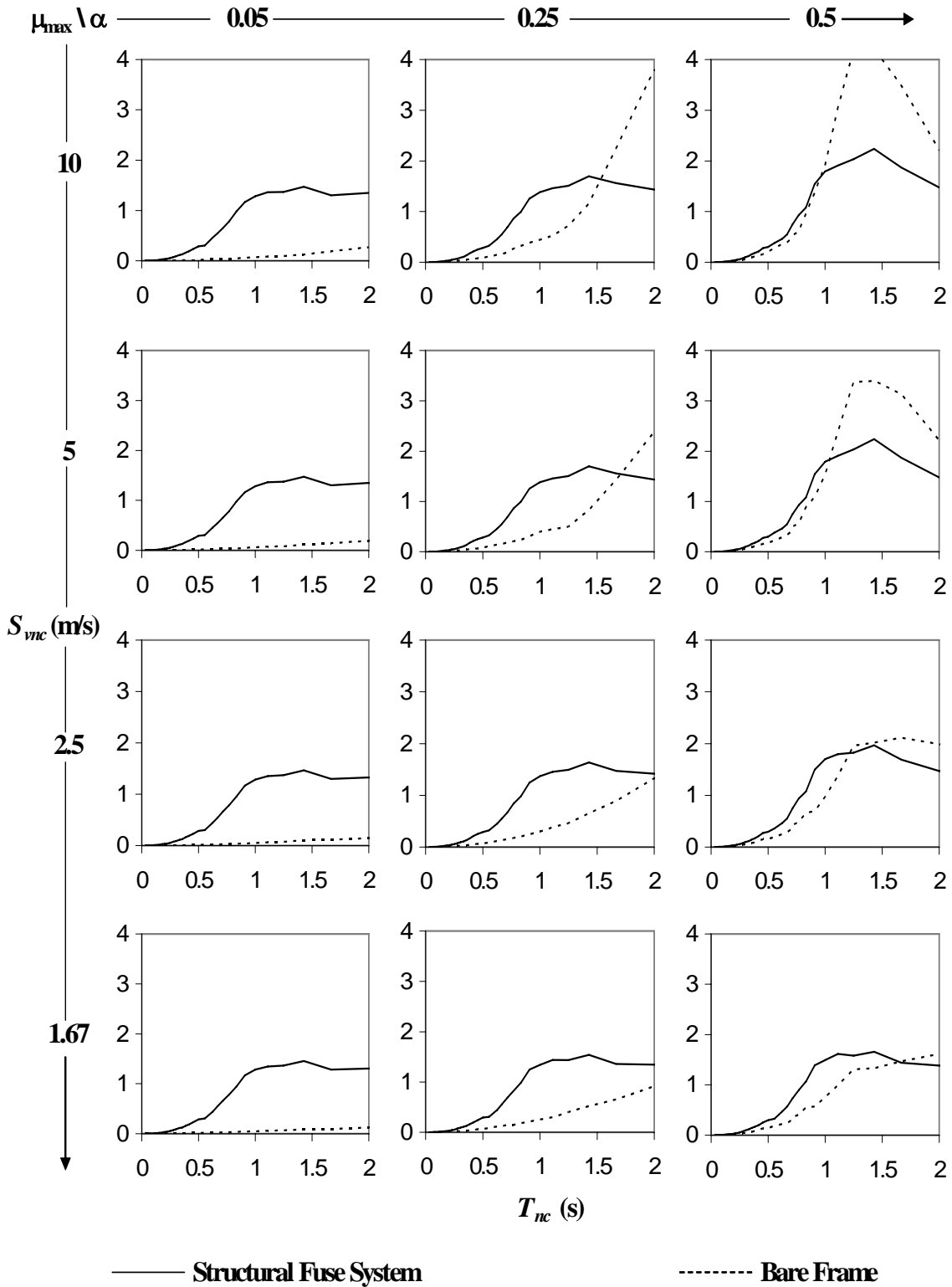


Figure 5.18. Floor Velocity Spectra of Structural Fuse Systems and Bare Frames for $T = 1.0$ s, and $\eta = 0.2$

From the results presented in Tables 5.1 and 5.2, a regression analysis was performed to obtain a more accurate closed form solution to determine the critical period, T_c . The following equations were obtained from the analysis:

$$T_c = A \cdot B \cdot \mu_{\max}^C \quad (5.3)$$

where

$$A = (1.31 \alpha^{-0.45}) T - 1.55 \alpha + 0.62 \quad (5.4)$$

$$B = (5.81 T^2 - 6.65 T + 6.06) \alpha^2 - (4.54 T^2 - 4.61 T + 3.14) \alpha + 2.86 T^2 - 3.53 T + 2.02 \quad (5.5)$$

$$C = (11.07 \alpha^2 - 4.82 \alpha - 1.06) T^2 - (19.56 \alpha^2 - 8.58 \alpha - 1.29) T + 6.25 \alpha^2 - 2.42 \alpha - 0.65 \quad (5.6)$$

Tables 5.3 and 5.4 show the results from the regression analysis, along with a comparison between approximate and actual values of T_c . It was found from the results that closed form solutions have an average error of 4% and 9% for spectral acceleration and velocity, respectively, with some results differing by as much as 14% and 22%, respectively. This more complex formulation provides substantial improvement over the results from (5.2), both in terms of average results and extreme values.

Table 5.3. Approximately Critical Period, T_c , for Acceleration using Regression Analysis

$\mu_{\max} \setminus \alpha$	0.05			0.25			0.50		
	T_c (s) Actual	T_c (s) Approx.	Diff. %	T_c (s) Actual	T_c (s) Approx.	Diff. %	T_c (s) Actual	T_c (s) Approx.	Diff. %
(1)	(2)	(3)	(4)	(5)	(6)	(7)	(8)	(9)	(10)
$T = 0.25$ s, $\eta = 0.60$									
10	0.83	0.83	0%	0.36	0.34	6%	0.28	0.27	5%
5	1.11	1.11	0%	0.42	0.45	8%	0.28	0.30	7%
2.5	N/A	N/A	N/A	0.56	0.60	8%	0.33	0.34	3%
1.67	N/A	N/A	N/A	0.77	0.71	8%	0.38	0.36	4%
$T = 0.50$ s, $\eta = 0.40$									
10	1.55	1.55	0%	0.77	0.75	2%	0.56	0.56	0%
5	1.83	1.83	0%	0.83	0.84	1%	0.62	0.62	0%
2.5	N/A	N/A	N/A	0.91	0.93	2%	0.67	0.67	0%
1.67	N/A	N/A	N/A	1.00	0.99	1%	0.71	0.71	0%
$T = 1.00$ s, $\eta = 0.20$									
10	3.33	2.96	11%	1.50	1.45	3%	0.91	0.89	2%
5	3.33	3.80	14%	1.60	1.70	6%	1.11	1.11	0%
2.5	N/A	N/A	N/A	2.00	1.98	1%	1.25	1.37	10%
1.67	N/A	N/A	N/A	2.20	2.17	1%	1.67	1.56	7%

Table 5.4. Approximately Critical Period, T_c , for Velocity using Regression Analysis

$\mu_{\max} \setminus \alpha$	0.05			0.25			0.50		
	T_c (s)	T_c (s)	Diff.	T_c (s)	T_c (s)	Diff.	T_c (s)	T_c (s)	Diff.
(1)	Actual	Approx.	%	Actual	Approx.	%	Actual	Approx.	%
(2)	(3)	(4)	(5)	(6)	(7)	(8)	(9)	(10)	
$T = 0.25$ s, $\eta = 0.60$									
10	0.91	0.83	9%	0.38	0.34	11%	0.30	0.27	11%
5	1.43	1.11	22%	0.42	0.45	8%	0.30	0.30	0%
2.5	N/A	N/A	N/A	0.56	0.60	8%	0.30	0.34	13%
1.67	N/A	N/A	N/A	0.83	0.71	14%	0.38	0.36	4%
$T = 0.50$ s, $\eta = 0.40$									
10	1.70	1.55	9%	0.77	0.75	2%	0.56	0.56	0%
5	2.10	1.83	13%	0.83	0.84	1%	0.62	0.62	1%
2.5	N/A	N/A	N/A	0.91	0.93	2%	0.67	0.67	0%
1.67	N/A	N/A	N/A	1.11	0.99	11%	0.71	0.71	0%
$T = 1.00$ s, $\eta = 0.20$									
10	2.60	2.96	14%	1.55	1.45	6%	1.00	0.89	11%
5	3.33	3.80	14%	1.67	1.70	2%	1.00	1.11	11%
2.5	N/A	N/A	N/A	2.10	1.98	6%	1.25	1.37	10%
1.67	N/A	N/A	N/A	2.50	2.17	13%	1.67	1.56	7%

Figures 5.13 to 5.18 demonstrate that, in a retrofit situation, the seismic behavior of the nonstructural components may (or may not) be improved with the addition of metallic dampers to the structural system. Positive or negative results may be obtained, depending on the dynamic characteristics of the nonstructural elements, relative to the properties of the retrofitted system.

For example, for the case study described in Section 5.2, the critical period is approximately equal to 0.83 s (see Figures 5.14 and 5.17). In this case, nonstructural components with an elastic period less than 0.83 s would experience an increase in acceleration and velocity by the addition of metallic dampers. On the other hand, components having a period greater than 0.83 s are more likely to be subjected to lower levels of acceleration and velocity when metallic dampers are added.

5.4. Equivalent Sine-wave Floor Spectra

Seismic performance of nonstructural components is an area of importance and increasing concern in earthquake engineering, and many studies have been devoted to estimate the seismic demand on these secondary systems (e.g., Manolis and Juhn, 1988; Cheng and Soong, 1989; Grigoriu et al., 1990; Lai and Soong, 1990; Singh et al., 1998; Grigoriu and Waisman, 1998, to name a few).

In Section 5.3, some floor response spectra for structures retrofitted using structural fuses were developed, and could be used to design nonstructural components and/or their anchorages. This section investigates whether an equivalent sine-wave floor acceleration response history could be used as a simplified way to generate acceleration and velocity spectra for that purpose. This method is based on a cascade analysis, in which only the effects of the primary system are considered, and the possible influences of the nonstructural components on the primary system are ignored (Ibrahim et al., 1989).

The dynamic response of a nonstructural component attached to the floor of a structural fuse system can be obtained through the following expression:

$$m_{nc} \ddot{u}_{nc} + c_{nc} \dot{u}_{nc} + k_{nc} u_{nc} = -m_{nc} \ddot{u}_F \quad (5.7)$$

where, again, the subscript “nc” denotes “nonstructural component”, and \ddot{u}_F is the floor acceleration (i.e., the input signal exciting the nonstructural component). Substituting an equivalent harmonic sine-wave motion for \ddot{u}_F gives, after arranging terms:

$$\ddot{u}_{nc} + \left(\frac{4\pi\xi_{nc}}{T_{nc}} \right) \dot{u}_{nc} + \left(\frac{4\pi^2}{T_{nc}^2} \right) u_{nc} = PFA_{eff} \sin\left(\frac{2\pi t}{T} \right) \quad (5.8)$$

where ξ_{nc} , T_{nc} , are the damping ratio and the period of the nonstructural component, respectively, and PFA_{eff} is the effective peak floor acceleration, defined here as the average of the absolute values of the peaks of the floor acceleration response history, between the first and last exceedances of a threshold acceleration (arbitrarily set at 25%

of the maximum floor acceleration in this study). Results for effective peak floor acceleration in Table 5.5 using this procedure, indicate that PFA_{eff} may be conservatively determined as 50% of the peak floor acceleration (i.e., $PFA_{eff} \approx 0.50 S_a$). Figures 5.19 and 5.20 show, respectively, the first 20 seconds of an actual floor acceleration response history, and its equivalent sine-wave floor acceleration response history generated per the above procedure.

Table 5.5. Ratio of Effective Peak Floor Acceleration with respect to Spectral Acceleration

$\mu_{max} \setminus \alpha$	0.05			0.25			0.50		
	S_a (g)	PFA_{eff} (g)	PFA_{eff}/S_a	S_a (g)	PFA_{eff} (g)	PFA_{eff}/S_a	S_a (g)	PFA_{eff} (g)	PFA_{eff}/S_a
(1)	(2)	(3)	(4)	(5)	(6)	(7)	(8)	(9)	(10)
$T = 0.25$ s, $\eta = 0.60$									
10	0.490	0.231	0.472	0.609	0.250	0.410	0.793	0.299	0.377
5	0.490	0.232	0.474	0.609	0.250	0.410	0.793	0.299	0.377
2.5	0.467	0.230	0.493	0.545	0.244	0.448	0.665	0.275	0.413
1.67	0.457	0.227	0.497	0.481	0.243	0.505	0.528	0.256	0.484
$T = 0.50$ s, $\eta = 0.40$									
10	0.308	0.166	0.538	0.403	0.181	0.448	0.575	0.221	0.385
5	0.308	0.166	0.538	0.403	0.181	0.448	0.575	0.221	0.385
2.5	0.301	0.165	0.546	0.367	0.179	0.489	0.454	0.198	0.437
1.67	0.299	0.166	0.555	0.327	0.172	0.525	0.365	0.190	0.520
$T = 1.00$ s, $\eta = 0.20$									
10	0.158	0.092	0.583	0.204	0.097	0.474	0.277	0.125	0.453
5	0.157	0.092	0.584	0.204	0.096	0.470	0.277	0.125	0.453
2.5	0.153	0.092	0.599	0.185	0.096	0.518	0.227	0.111	0.491
1.67	0.151	0.091	0.602	0.165	0.094	0.570	0.185	0.100	0.542

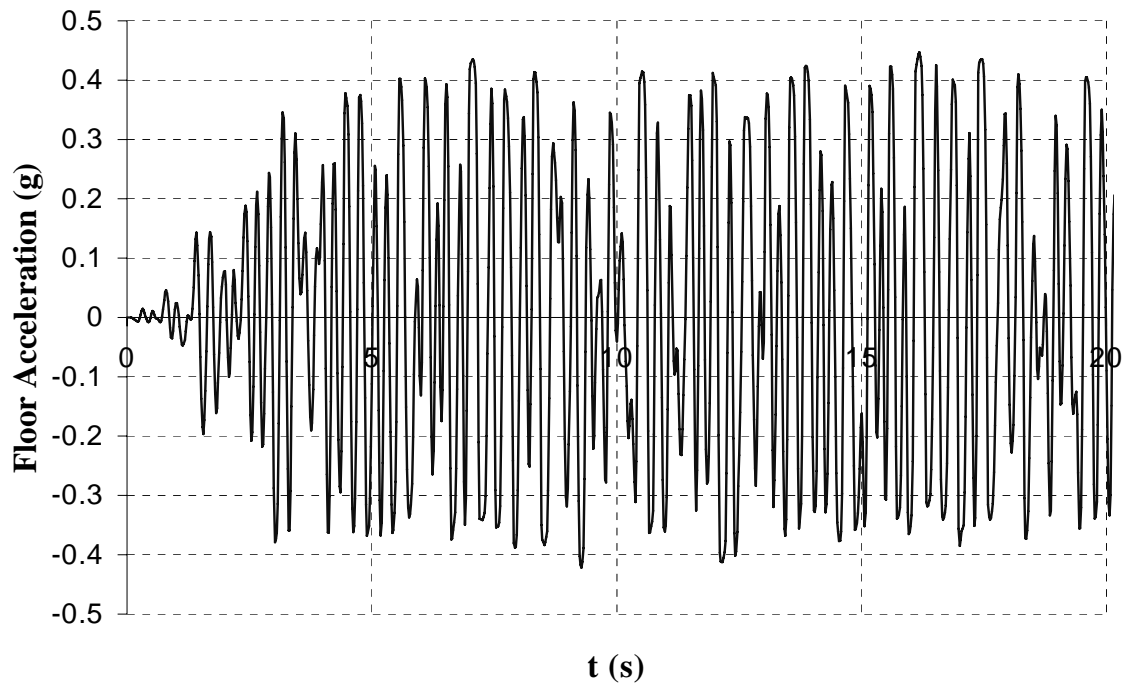


Figure 5.19. Example of Floor Acceleration Response History of a SDOF System with Metallic Fuses

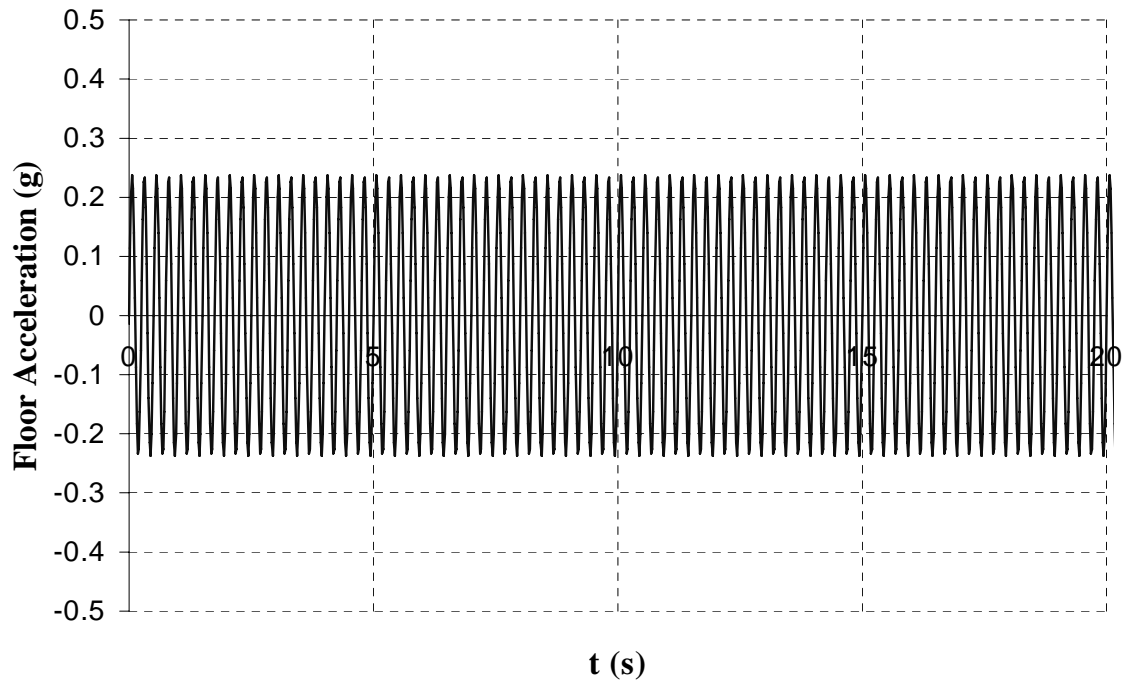


Figure 5.20. Equivalent Sine-Wave Floor Acceleration Response History of a SDOF System with Metallic Fuses

Closed form solutions for the spectral acceleration, S_{anc} , and velocity, S_{vnc} , of nonstructural components for the equivalent sine-wave floor acceleration may be obtained from (5.8) through the following equations:

$$S_{anc} = PFA_{eff} \left[\left(\frac{T_{nc}}{T} \right)^2 \frac{1}{\sqrt{[1 - (T_{nc}/T)^2]^2 + [2\xi_{nc}(T_{nc}/T)]^2}} + 1 \right] \quad (5.9)$$

$$S_{vnc} = PFA_{eff} \left[\left(\frac{T_{nc}^2}{2\pi T} \right) \frac{1}{\sqrt{[1 - (T_{nc}/T)^2]^2 + [2\xi_{nc}(T_{nc}/T)]^2}} \right] \quad (5.10)$$

Figures 5.21 to 5.26 show actual acceleration and velocity spectra for the studied cases, along with the sine-wave response obtained from (5.9) and (5.10), assuming a damping ratio of 5% for the nonstructural components (i.e., $\xi_{nc} = 5\%$).

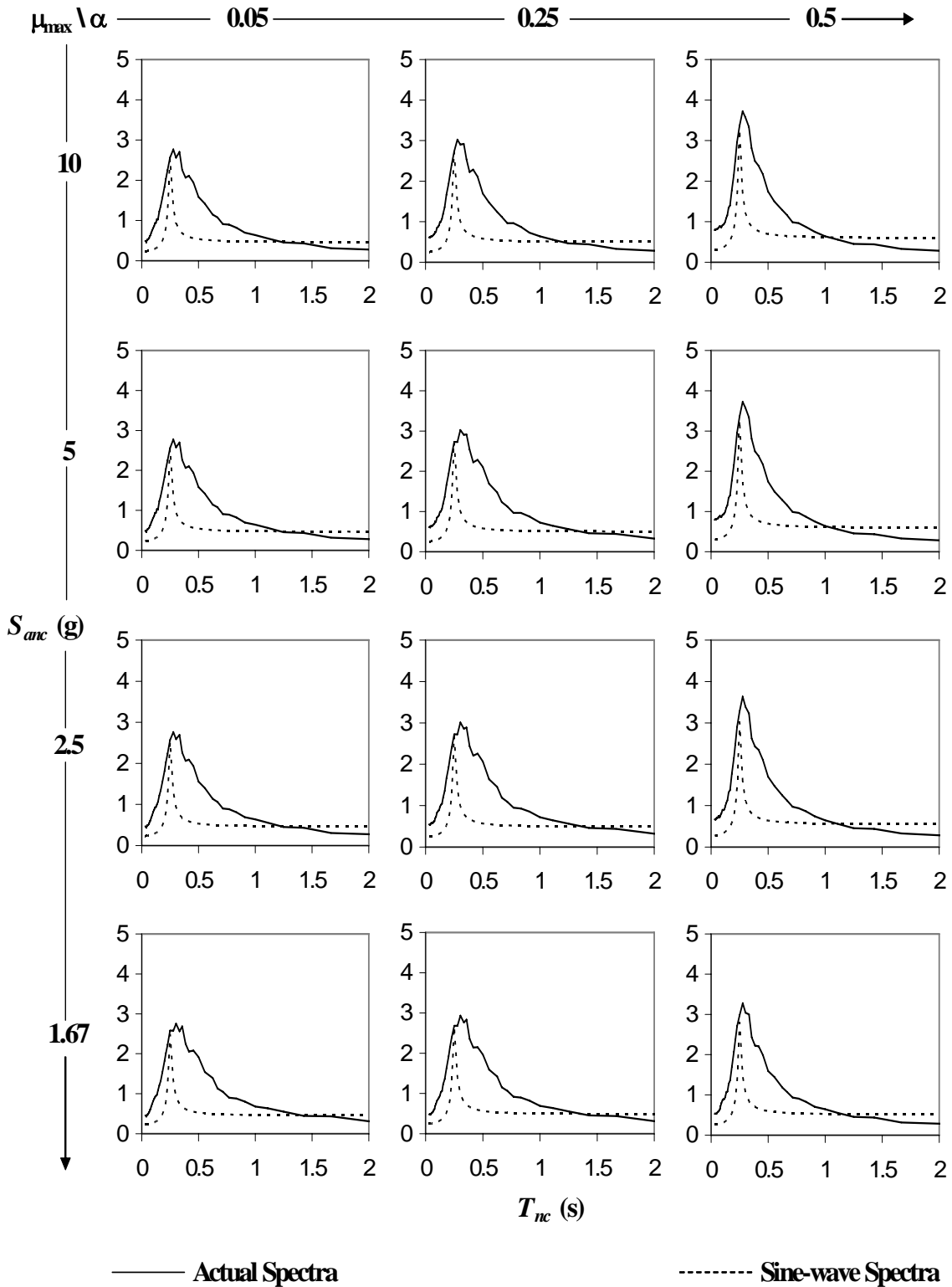


Figure 5.21. Actual Acceleration Response Spectra vs Sine-wave Acceleration Response Spectra for $T = 0.25$ s, and $\eta = 0.6$

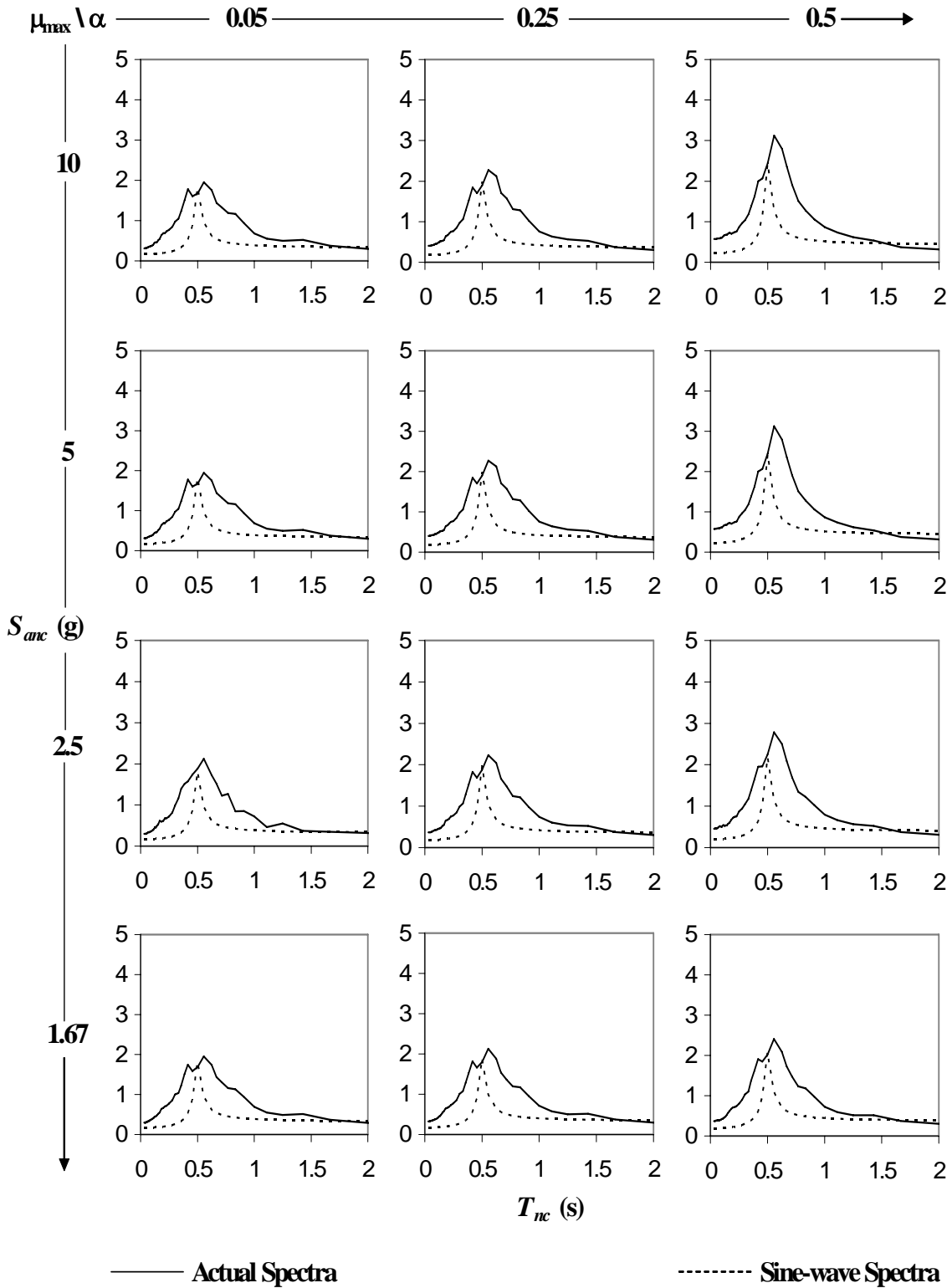


Figure 5.22. Actual Acceleration Response Spectra vs Sine-wave Acceleration Response Spectra for $T = 0.5$ s, and $\eta = 0.4$

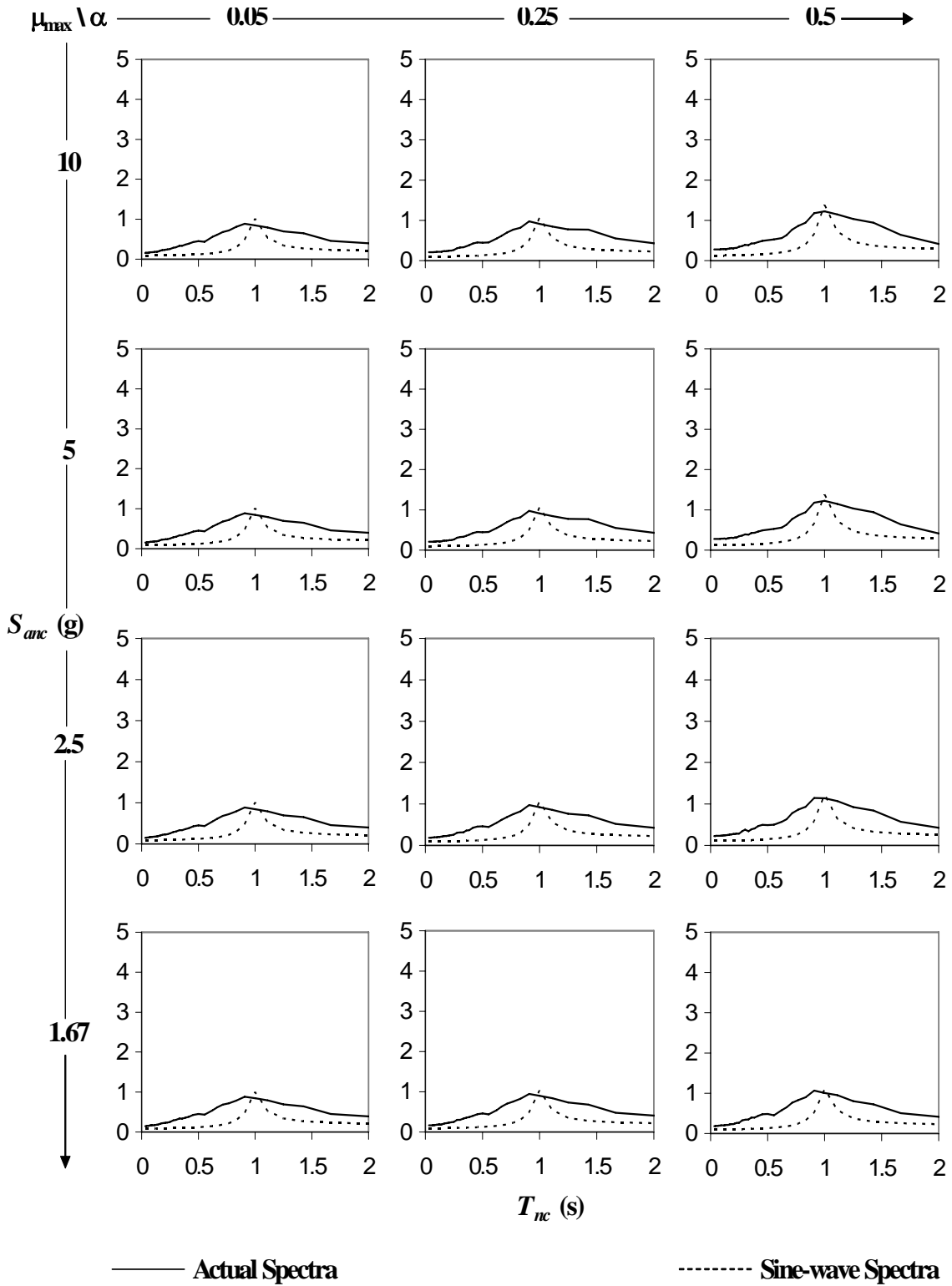


Figure 5.23. Actual Acceleration Response Spectra vs Sine-wave Acceleration Response Spectra for $T = 1.0$ s, and $\eta = 0.2$

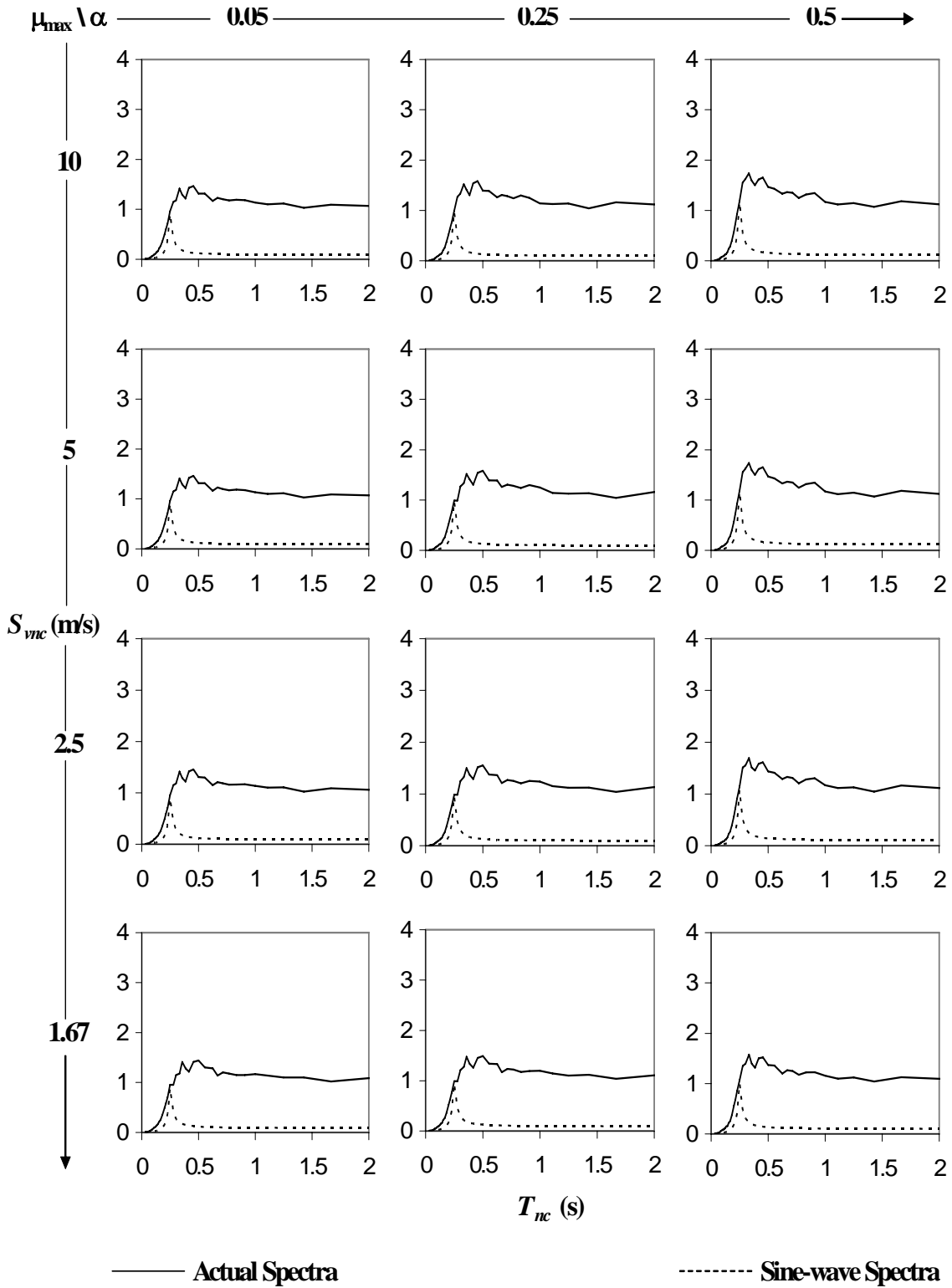


Figure 5.24. Actual Velocity Response Spectra vs Sine-wave Velocity Response Spectra for $T = 0.25$ s, and $\eta = 0.6$

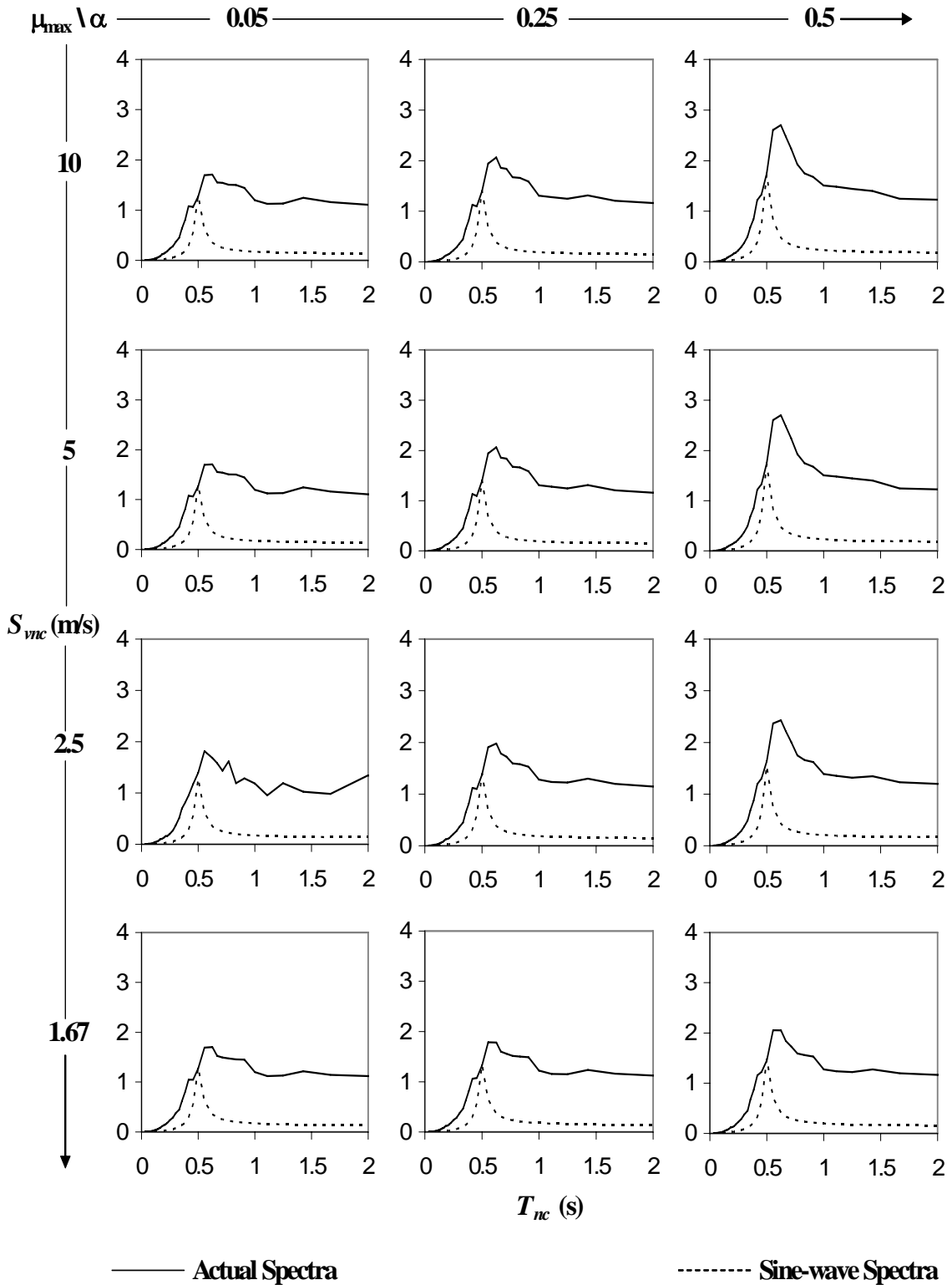


Figure 5.25. Actual Velocity Response Spectra vs Sine-wave Velocity Response Spectra for $T = 0.5$ s, and $\eta = 0.4$

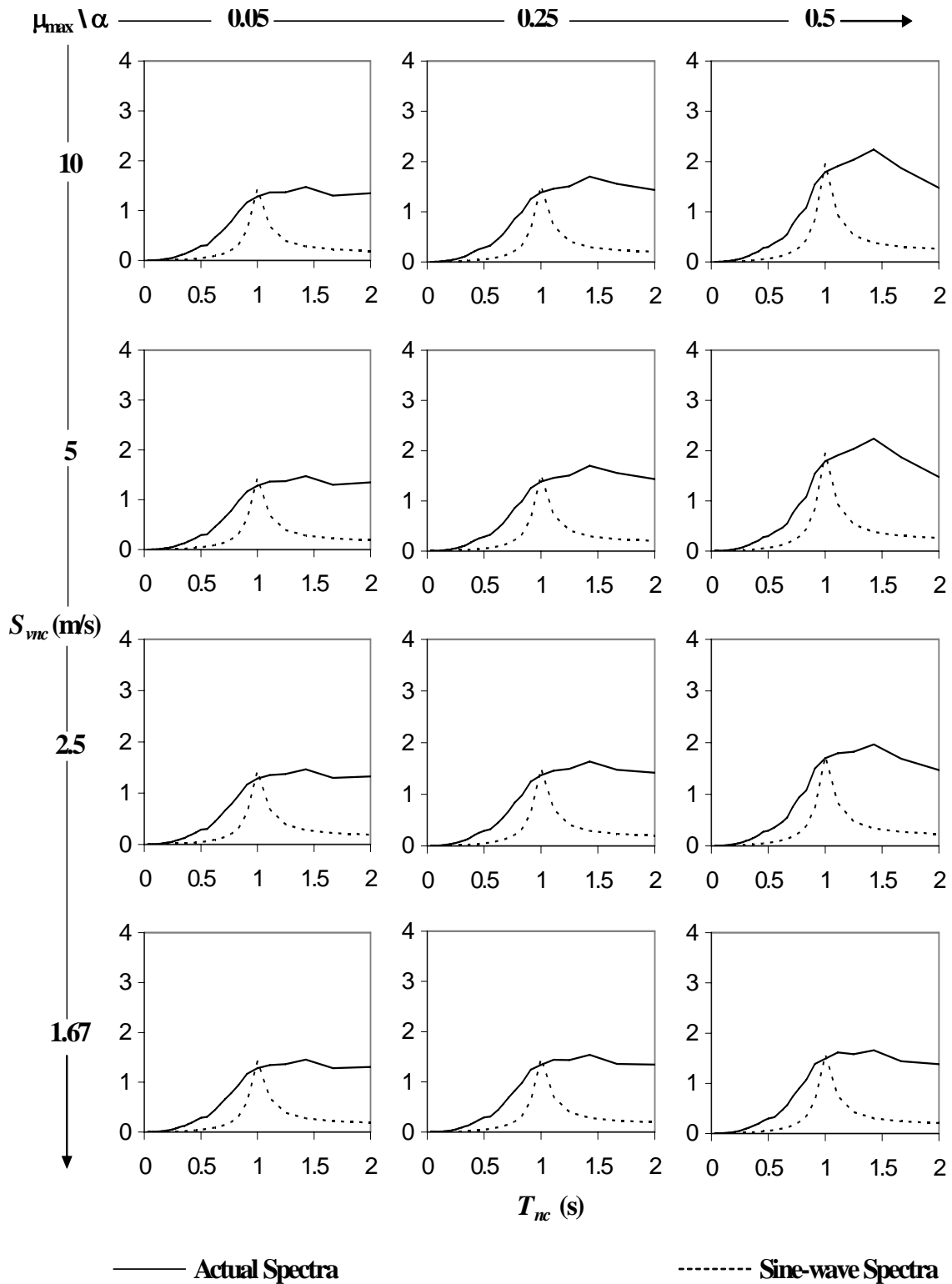


Figure 5.26. Actual Velocity Response Spectra vs Sine-wave Velocity Response Spectra for $T = 1.0$ s, and $\eta = 0.2$

Usually, dynamic properties of nonstructural components are unknown or difficult to obtain. Conservatively, in those cases it is recommended to design the nonstructural components and/or their anchorages for the maximum S_{anc} , and S_{vnc} (i.e., when $T_{nc} = T$) calculated from the following equations:

$$S_{anc} = PFA_{eff} \left(\frac{1}{2\xi_{nc}} + 1 \right) \quad (5.11)$$

$$S_{vnc} = PFA_{eff} \left(\frac{T}{4\pi\xi_{nc}} \right) \quad (5.12)$$

where ξ_{nc} shall be estimated from experimental data (if available) and engineering judgement. In multi-degree of freedom systems, a modal distribution may be used to determine acceleration and velocity demands for nonstructural components located at a specific degree of freedom, i , and (5.11) and (5.12) become:

$$S_{anc_i} = PFA_{eff} \left(\frac{1}{2\xi_{nc}} + 1 \right) \Gamma_1 \phi_{1i} \quad (5.13)$$

$$S_{vnc_i} = PFA_{eff} \left(\frac{T}{4\pi\xi_{nc}} \right) \Gamma_1 \phi_{1i} \quad (5.14)$$

As an example, the case study from Section 5.2 will be subjected to a peak floor acceleration of 0.40 g at the roof level (Figure 5.1). Conservatively, taking an effective peak floor acceleration of 0.50 S_a , and assuming a damping ratio of 5% (i.e., $PFA_{eff} = 0.20$ g, and $\xi_{nc} = 5\%$), a nonstructural component located at mid-height of the building (i.e., assuming $\Gamma_1 \phi_{1i} = 0.5$), may be conservatively designed to resist an acceleration, $S_{anc_i} = 1.1$ g, and a velocity, $S_{vnc_i} = 0.78$ m/s. These results are corroborated by Figures 5.22 and 5.25.

5.5. Observations

Floor accelerations and velocities for SDOF systems with metallic fuses have been studied in this section through a parametric analysis. It was found that, in most of the cases, floor acceleration increases when using metallic fuses, although there are a few cases where acceleration demands were found to marginally decrease (i.e., $\alpha = 0.5$ and $\mu_{\max} = 10$).

It was also found that the critical period, T_c , is an useful indicator to identify when using metallic fuses can increase or decrease the dynamic acceleration and velocity response of nonstructural components. It was observed that nonstructural elements having a period shorter than T_c may be susceptible to greater acceleration (which would increase their likelihood of sliding on their support if unrestrained, for example), and greater velocity (which would for example increase their probability of overturning) when metallic fuses are added. On the other hand, it was found that retrofit works may improve the seismic behavior of flexible nonstructural components that have a period longer than T_c ; however, adequate judgement must be exercised in retrofitting these elements.

Furthermore, using the equivalent sine-wave criterion, it is also possible to determine spectral acceleration and velocity to conservatively design nonstructural components and/or their anchorages. This criterion may be applied to multi-degree of freedom systems assuming a linear variation of floor acceleration over the building height.

SECTION 6

RESPONSE OF HYBRID SINGLE DEGREE OF FREEDOM SYSTEMS WITH METALLIC AND VISCOUS DAMPERS

6.1. Introduction

In Section 5 it was found that, in most of the cases, the use of metallic damper causes increases in floor accelerations, which may negatively affect the seismic behavior of nonstructural components. Based on these results, Section 6 investigates the seismic performance of SDOF systems with metallic and viscous dampers installed in parallel. The purpose of this section is, therefore, to analyze the alternative of using hysteretic dampers to mitigate lateral displacements, along with viscous dampers to reduce acceleration demands.

Fluid dampers have been widely studied, and recently, significant efforts have been directed to implement these devices in structural systems (Soong and Dargush, 1997). Fluid dampers generally work on the principle of energy dissipation of incompressible fluids forced to flow through orifices (Constantinou and Symans, 1992). In viscous (linear) dampers, the damping force, F_d , is proportional to the velocity of motion, \dot{u} , according to the following expression:

$$F_d = c\dot{u} \quad (6.1)$$

which is used in applications of structural engineering to design systems against wind or earthquake loads, and is the expression used in this study. In some special applications, nonlinear dampers have been implemented according to:

$$F_d = c |\dot{u}|^a \text{sgn}(\dot{u}) \quad (6.2)$$

where a takes values between 0.3 and 2.0. According to Hanson and Soong (2001), small values of a (i.e., $a \leq 0.5$) are effective to mitigate high-velocity shocks, such as isolation of military hardware.

Parametric analyses of hysteretic damping and spectral acceleration are presented for short, intermediate, and long period structures. Furthermore, response in the frequency domain is also shown as graphics of inertial, viscous damper, and hysteretic forces represented in the complex plane. These results are used to provide a preliminary assessment of the effectiveness of using metallic and viscous dampers in parallel to reduce floor accelerations.

6.2. Equivalent Viscous Damping (Hysteretic Damping)

In many structural analyses such as the Nonlinear Static Procedure (FEMA 356), the dynamic characteristics of a structure having hysteretic dampers are transformed to an effective period, T_{eff} , which is obtained from the secant or effective stiffness, K_{eff} , of the combined system (i.e., bare frame plus dampers) to the point of maximum displacement, and an equivalent viscous damping (a.k.a hysteretic damping), ξ_h , both determined from specific hysteresis loops as obtained per the time history analyses described in Section 3.4 for the parametric study considered here. Generally, the hysteretic damping for a metallic damper is obtained by setting the area within a hysteresis loop equal to the area within a viscous damper cycle, provided that the area contained within one cycle of motion is the energy dissipated per cycle (Hanson and Soong, 2001).

Consequently, the hysteretic damping, ξ_h , may be determined from the following expression, from Ramirez et al. (2000):

$$\xi_h = \frac{2q_h(1 - 1/\mu_f) + 2(V_{yd}/V_{yf})(1 - 1/\mu)}{\pi(1 + V_{yd}/V_{yf})} \geq 0 \quad (6.3)$$

where q_h is the quality factor, taken as 1.0 for bilinear systems, and V_{yf} , V_{yd} , μ , and μ_f , have been defined previously in Sections 3.2 and 3.4. Substituting $q_h = 1.0$, $V_{yd} = V_y(1 - \alpha)$, and $V_{yf} = V_y \alpha \mu_{\max}$ into (6.3), gives:

$$\xi_h = \left(\frac{2}{\pi} \right) \left[\frac{(1 - 1/\mu_f) + \frac{(1 - \alpha)(1 - 1/\mu)}{\alpha \mu_{\max}}}{1 + \frac{(1 - \alpha)}{\alpha \mu_{\max}}} \right] \geq 0 \quad (6.4)$$

which is the expression used in this study. Derivation of these two equations are in Appendix B. Note that for $\mu < 0$ (and therefore, $\mu_f < 0$), the system remains elastic, which translates into no dissipation of energy through hysteretic behavior and, therefore, no hysteretic damping is developed (i.e., $\xi_h = 0$).

6.3. Parametric Analysis of Hysteretic Damping

A parametric study was conducted to analyze how the hysteretic damping, ξ_h , is affected by increasing the viscous damping, $\Delta\xi_v$, in SDOF systems with structural fuses. Short, intermediate, and long period structures ($T = 0.25$ s, 0.50 s, and 1.50s, respectively) were then analyzed for increases in viscous damping of 0%, 5%, 15%, and 25% from a base value of 5%. Hysteretic damping was determined using (6.4), for a given set of parameters, and the values of global ductility, μ , and frame ductility, μ_f , obtained from the system response.

Figures 6.1 to 6.3 show how the hysteretic damping, ξ_h , decreases with increases in viscous damping, $\Delta\xi_v$, for system periods of 0.25 s, 0.50 s, and 1.50 s, respectively. This is because the hysteretic damping is proportional to the ductility demand, which decreases with increases in viscous damping. Since hysteretic damping is directly

proportional to ductility demand, all the observed relationships between demand and key parameters (i.e., α , μ_{\max} , η , and T) can explain how hysteretic damping relates to the same key parameters. For instance, in Section 3, it was found that increases in both α and μ_{\max} result in decreases in the ductility demand for systems without viscous dampers, which lead to a significant reduction in the hysteretic damping.

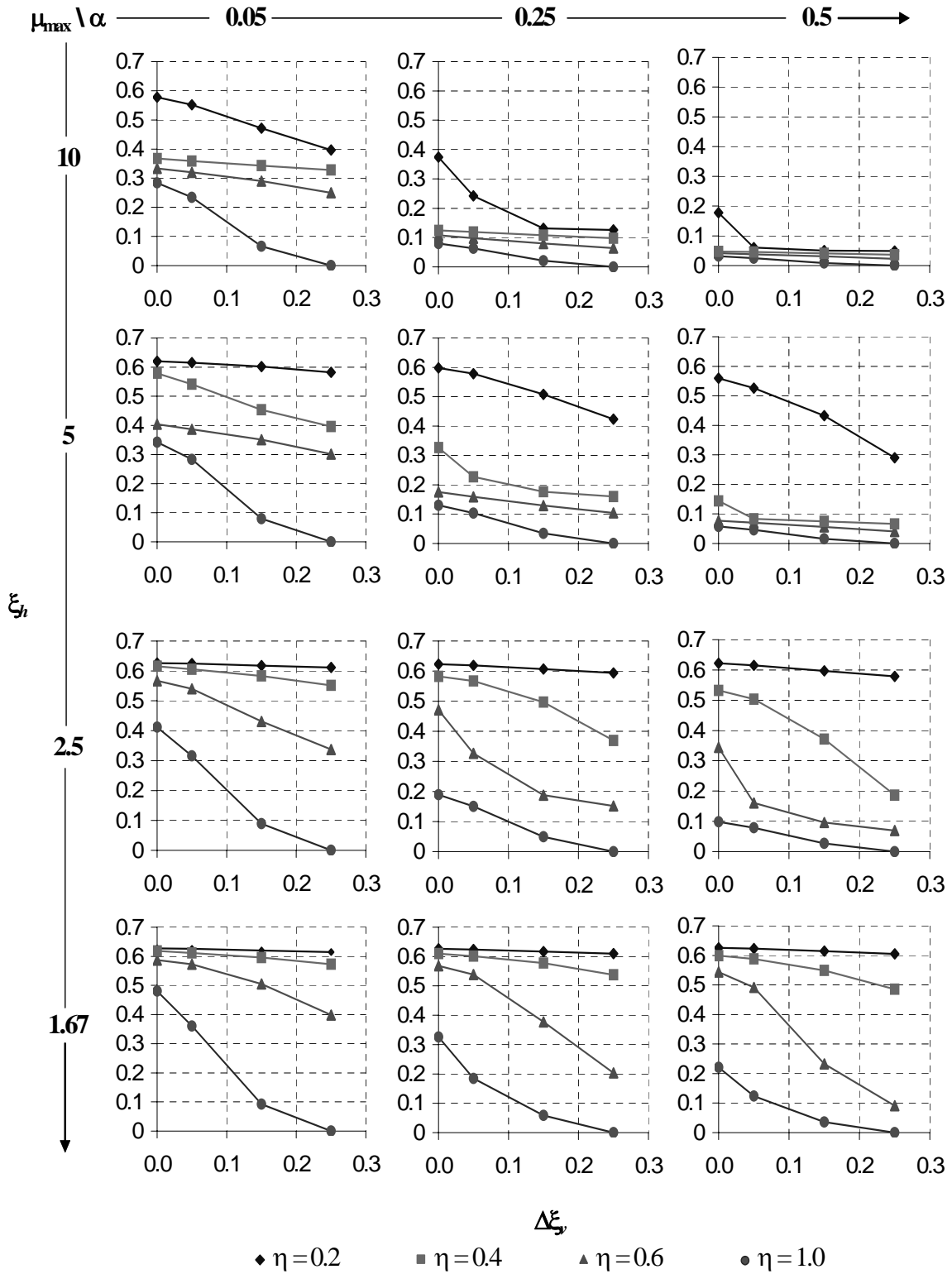


Figure 6.1. Hysteretic Damping vs Increase in Viscous Damping for $T = 0.25$ s

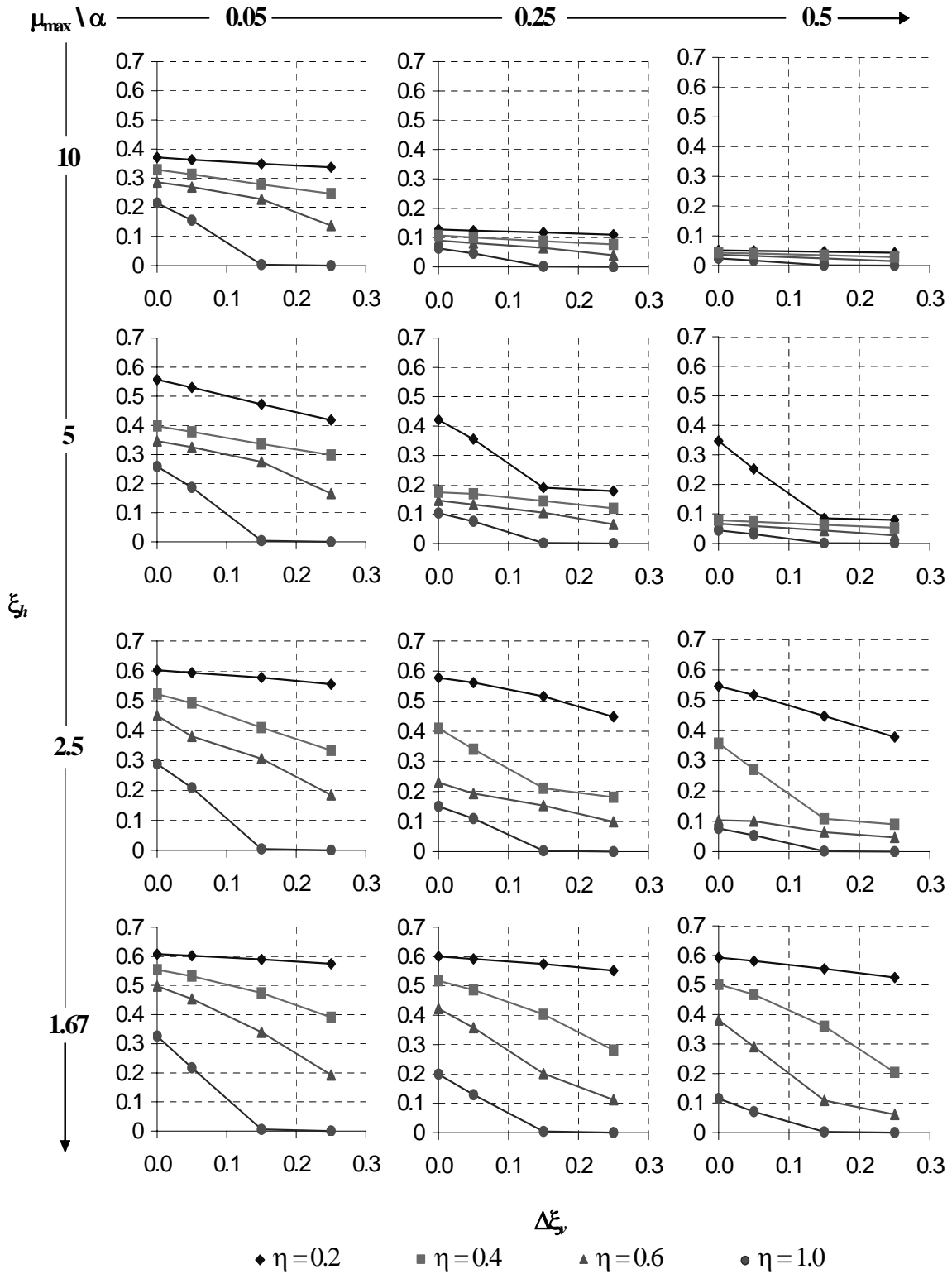


Figure 6.2. Hysteretic Damping vs Increase in Viscous Damping for $T = 0.50$ s

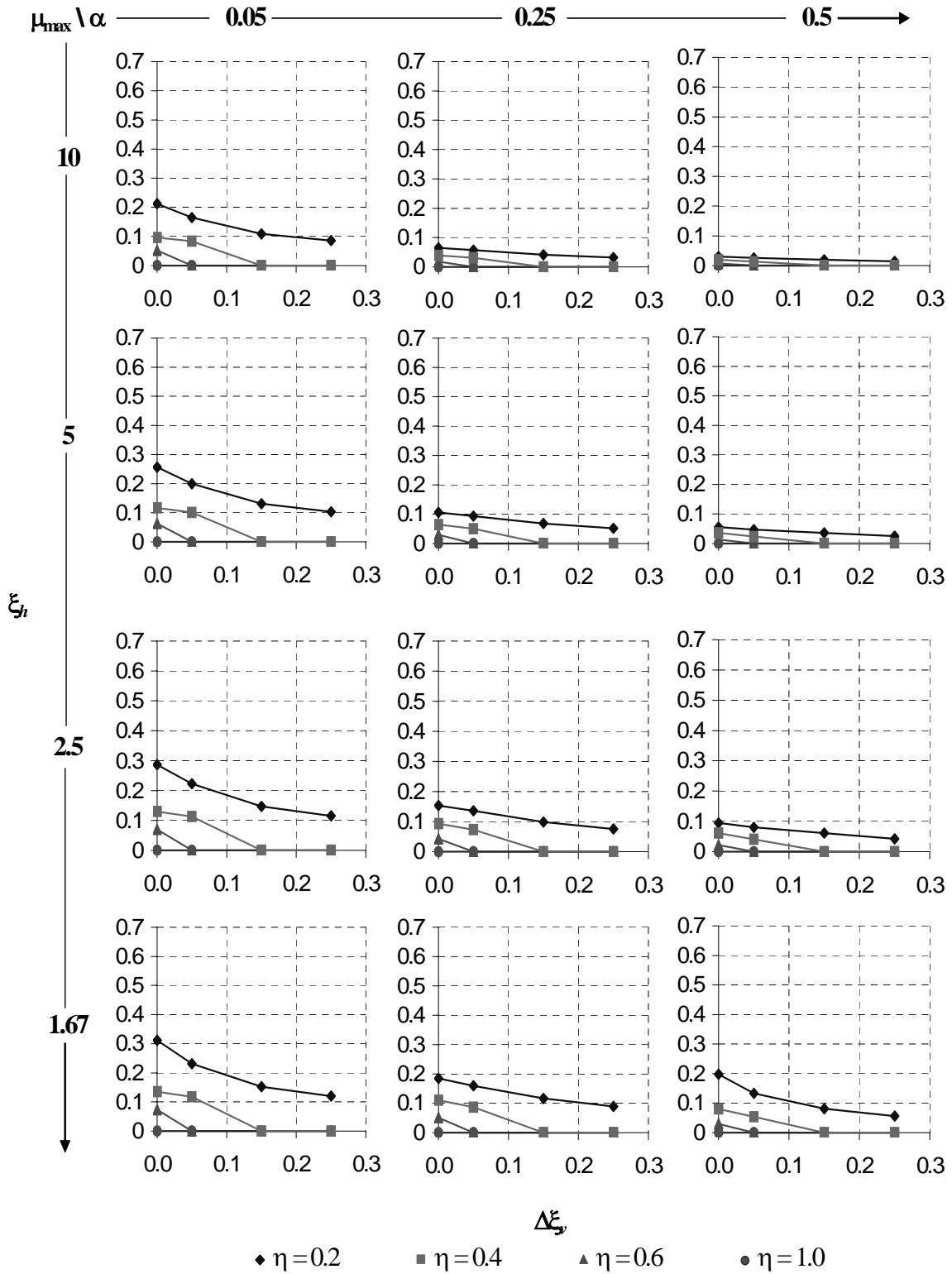


Figure 6.3. Hysteretic Damping vs Increase in Viscous Damping for $T = 1.50$ s

It was also observed in Section 3, that the ductility demand reduces with increases in η and T , which again, result in decreases in the hysteretic damping (see Figures 3.8 and 3.9). Note that the largest values of hysteretic damping were obtained for systems having small values of α , μ_{\max} , η , and T ; whereas the smallest values of hysteretic damping were obtained for large values of these parameters. For example, in a short period system ($T = 0.25$ s) with $\alpha = 0.05$, $\mu_{\max} = 2.5$, and $\eta = 0.4$, the hysteretic damping reduces from 62% to 55% when viscous damping is increased by 25% (Figure 6.1). On the other hand, in a long period system ($T = 1.50$ s) with $\alpha = 0.50$, $\mu_{\max} = 5$, and $\eta = 0.6$, the hysteretic damping reduces from 1% to 0% when viscous damping is increased by 5% (Figure 6.3), as the system becomes elastic and remains elastic even if viscous damping is further increased.

In Figures 6.4 to 6.6, the ratio of the hysteretic damping with respect to the hysteretic damping of the original system, ξ_h / ξ_{ho} , is plotted versus the increase in viscous damping, $\Delta\xi_v$. In this section, the system that was studied in previous sections for a viscous damping of 5%, along with its corresponding hysteretic damping, ξ_{ho} , is called the “original system.” Figures 6.4 to 6.6 show how “fast” the hysteretic damping is reduced by increases in the viscous damping due to decreases in the ductility demand (see (6.4)). Note that in long period systems the hysteretic damping reduces “faster” to the level of elastic response (i.e., $\xi_h = 0$), than in short period structures. This is because the ductility demand has smaller values for long period original systems, and therefore, small increases in viscous damping can make the structure respond elastically (see Figure 6.6).

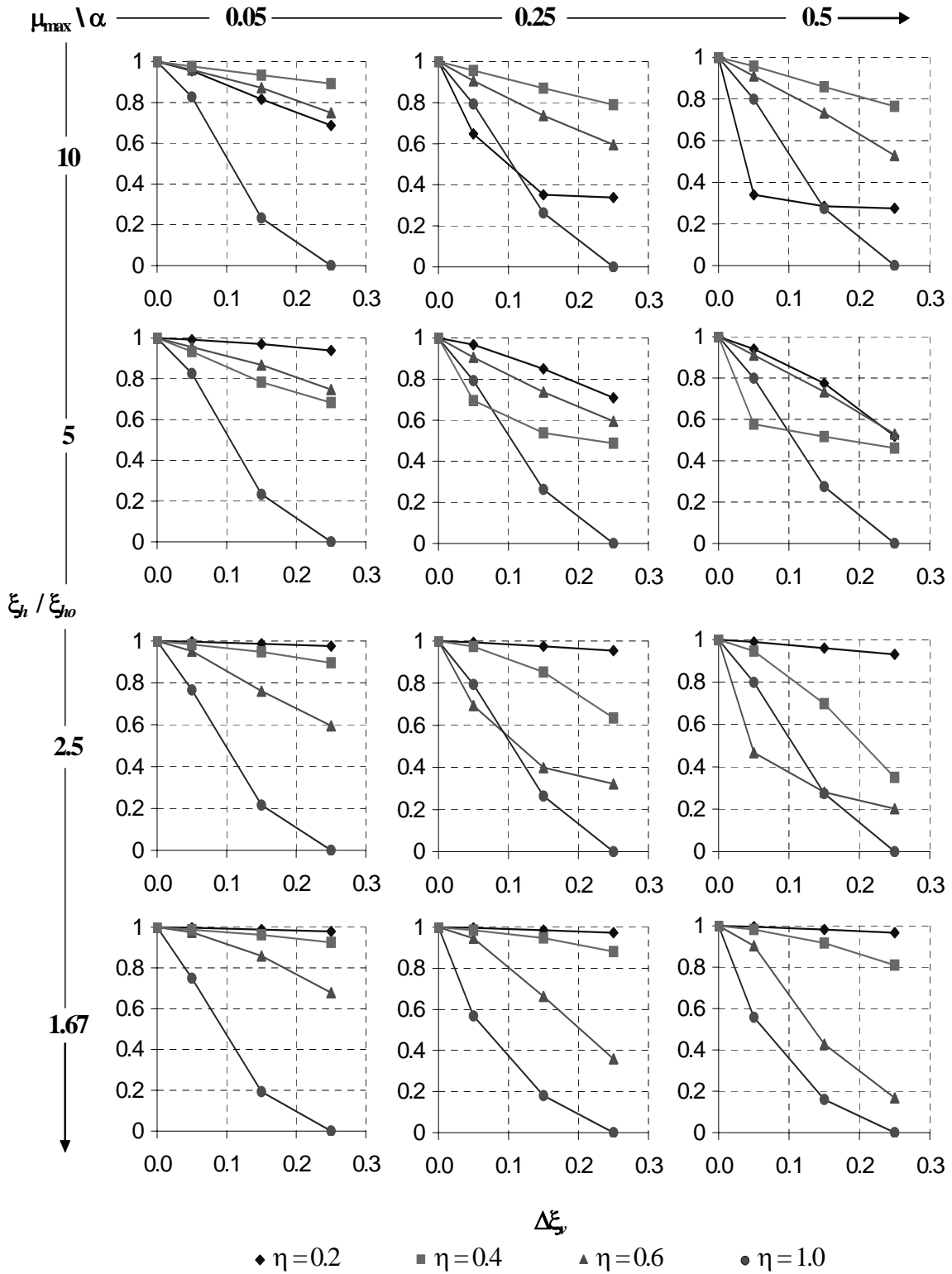


Figure 6.4. Ratio of Hysteretic Damping with Respect to Original Hysteretic Damping vs Increase in Viscous Damping for $T = 0.25$ s

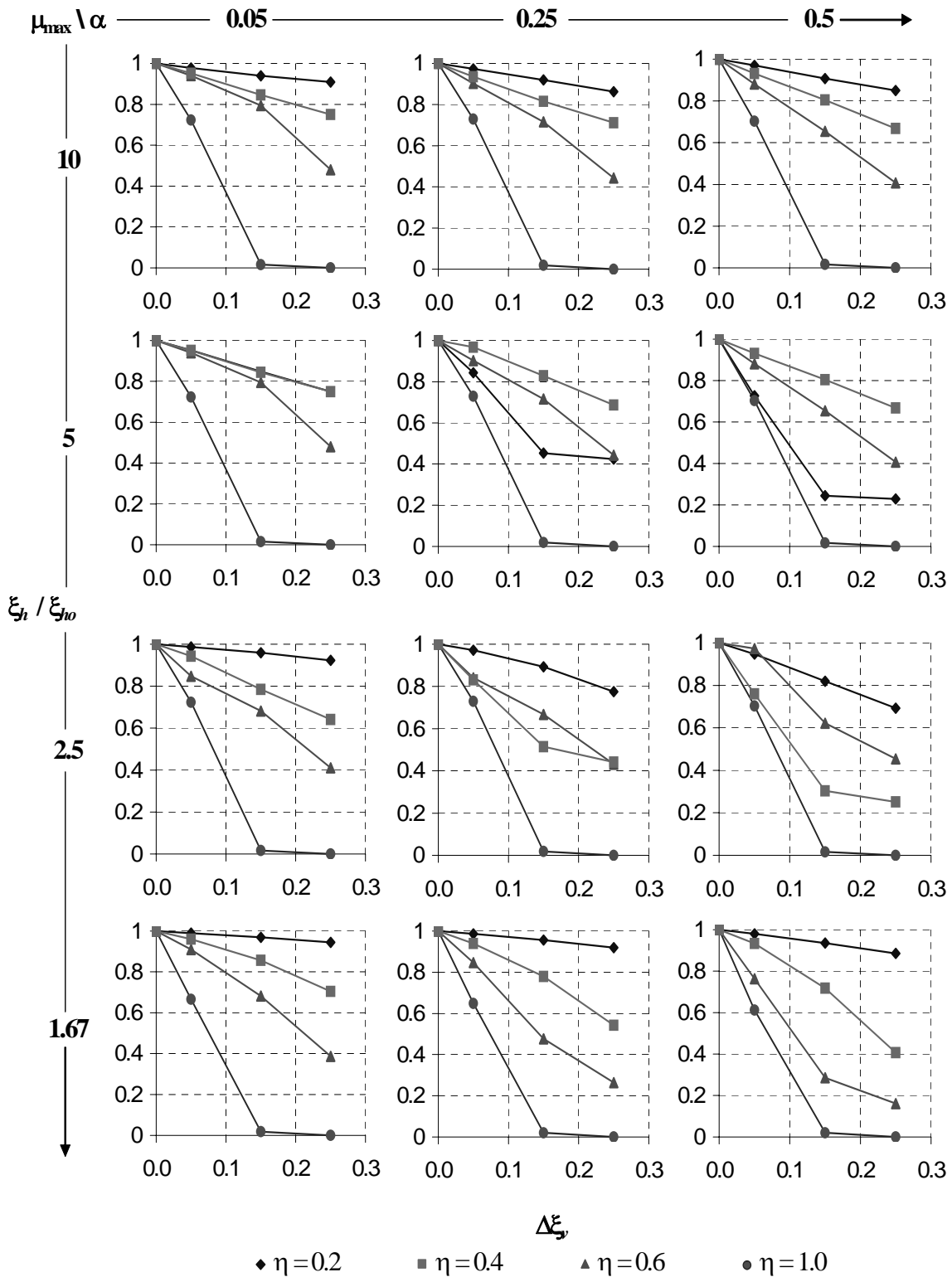


Figure 6.5. Ratio of Hysteretic Damping with Respect to Original Hysteretic Damping vs Increase in Viscous Damping for $T = 0.50$ s

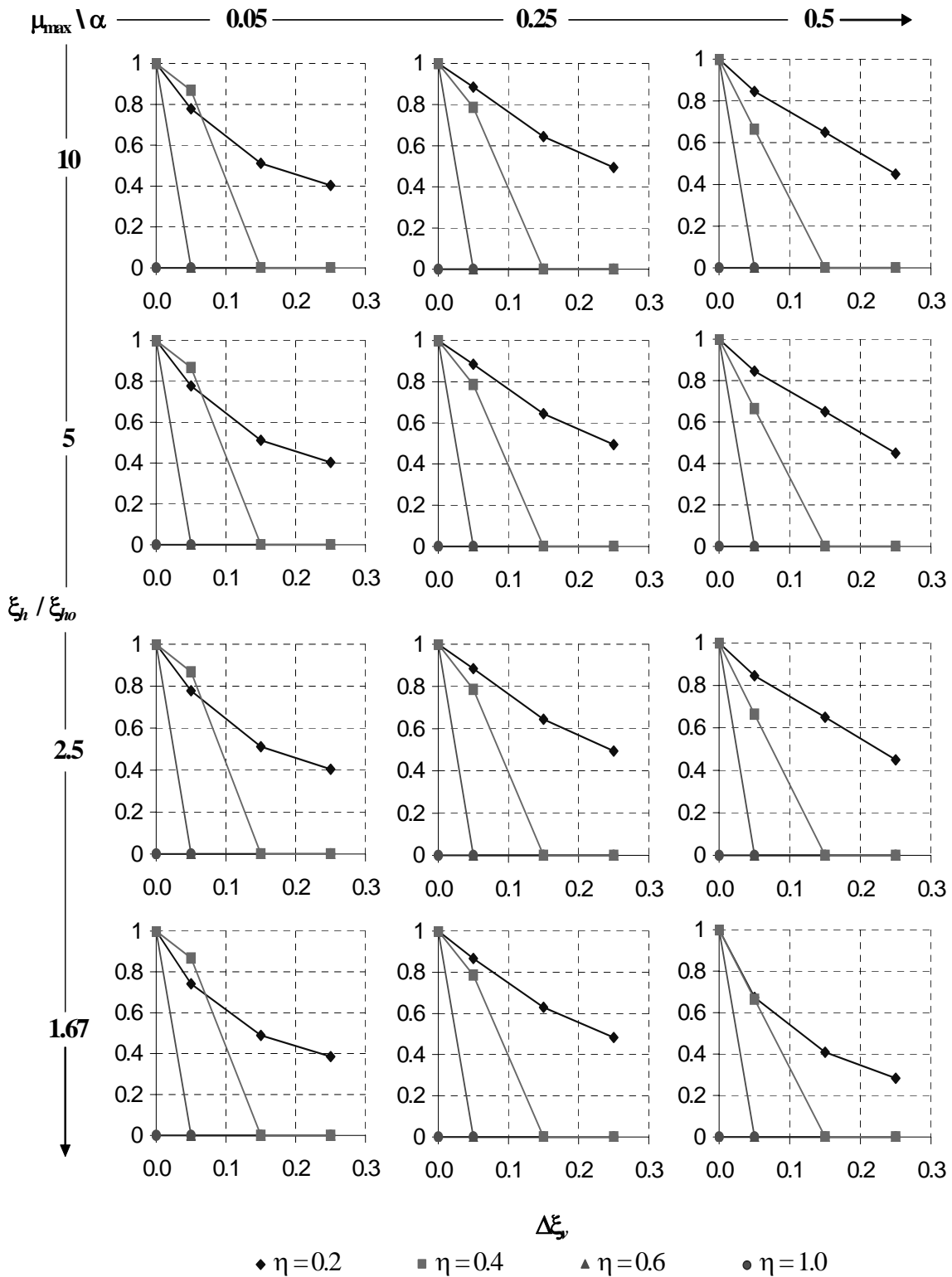


Figure 6.6. Ratio of Hysteretic Damping with Respect to Original Hysteretic Damping vs Increase in Viscous Damping for $T = 1.50$ s

Furthermore, in Figures 6.7 to 6.9, the ratio of total damping, ξ_t , with respect the total damping of the original system, ξ_{to} , is plotted vs the increase in viscous damping, $\Delta\xi_v$. Total damping is determined summing the contributions from viscous and hysteretic damping, using the following expressions:

$$\xi_{to} = \xi_{vo} + \xi_{ho} = 0.05 + \xi_{ho} \quad (6.5)$$

$$\xi_t = \xi_v + \xi_h = 0.05 + \Delta\xi_v + \xi_h \quad (6.6)$$

Because hysteretic damping decreases non-linearly with increases in viscous damping, the total damping, ξ_t , calculated using (6.6), may result in a gain or loss of equivalent damping, depending on the relative values of $\Delta\xi_h$ and $\Delta\xi_v$. In Figures 6.7 to 6.9, a value of $\xi_t / \xi_{to} > 1.0$ corresponds to a gain of total damping (i.e., $\Delta\xi_v > |\Delta\xi_h|$). Unlike the hysteretic damping, the total damping increases with the values of α , μ_{max} , and T . Note also that for short and intermediate period systems having $\alpha \leq 0.25$ and $\mu_{max} \geq 5$, increases in viscous damping tend to be compensated by decreases in hysteretic damping (i.e., $\Delta\xi_v \approx |\Delta\xi_h|$), and therefore, no gain of total damping is appreciated. On the other hand, in long period structures, significant gains of total damping are consistently observed (i.e., $\Delta\xi_v \gg |\Delta\xi_h|$), since elastic behavior of the system is “quickly” achieved by increases in viscous damping (i.e., $\xi_h = 0$). For example, in a short period system ($T = 0.25$ s) with $\alpha = 0.05$, $\mu_{max} = 2.5$, and $\eta = 0.4$, the total damping increases by a factor of 1.28 when viscous damping is increased by 25% (Figure 6.7). On the other hand, in a long period system ($T = 1.50$ s) with $\alpha = 0.50$, $\mu_{max} = 5$, and $\eta = 0.6$, the total damping increases by a factor of 4.76 when viscous damping is increased by 25% (Figure 6.9).

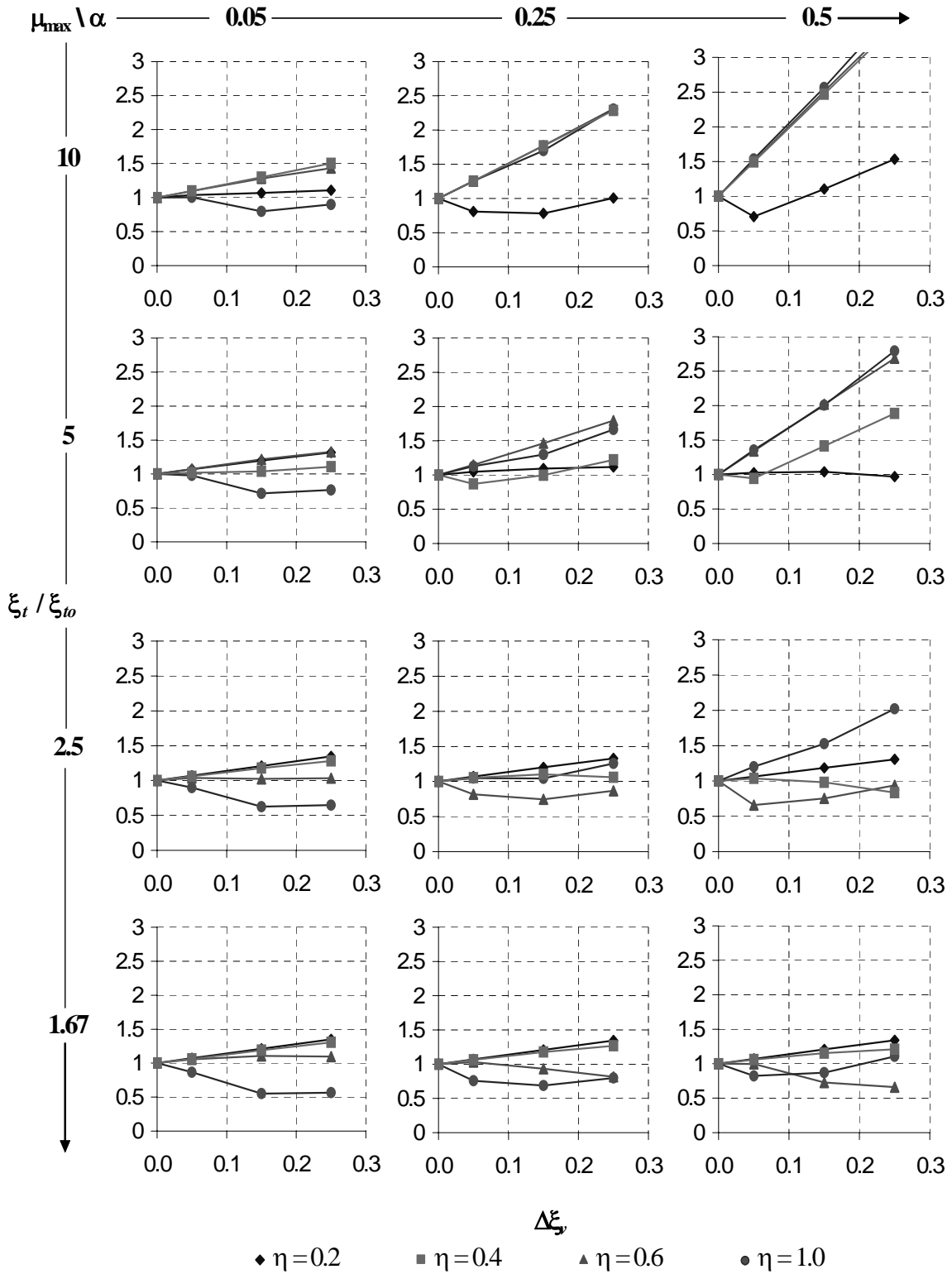


Figure 6.7. Ratio of Total Damping with Respect to Original Damping vs Increase in Viscous Damping for $T = 0.25$ s

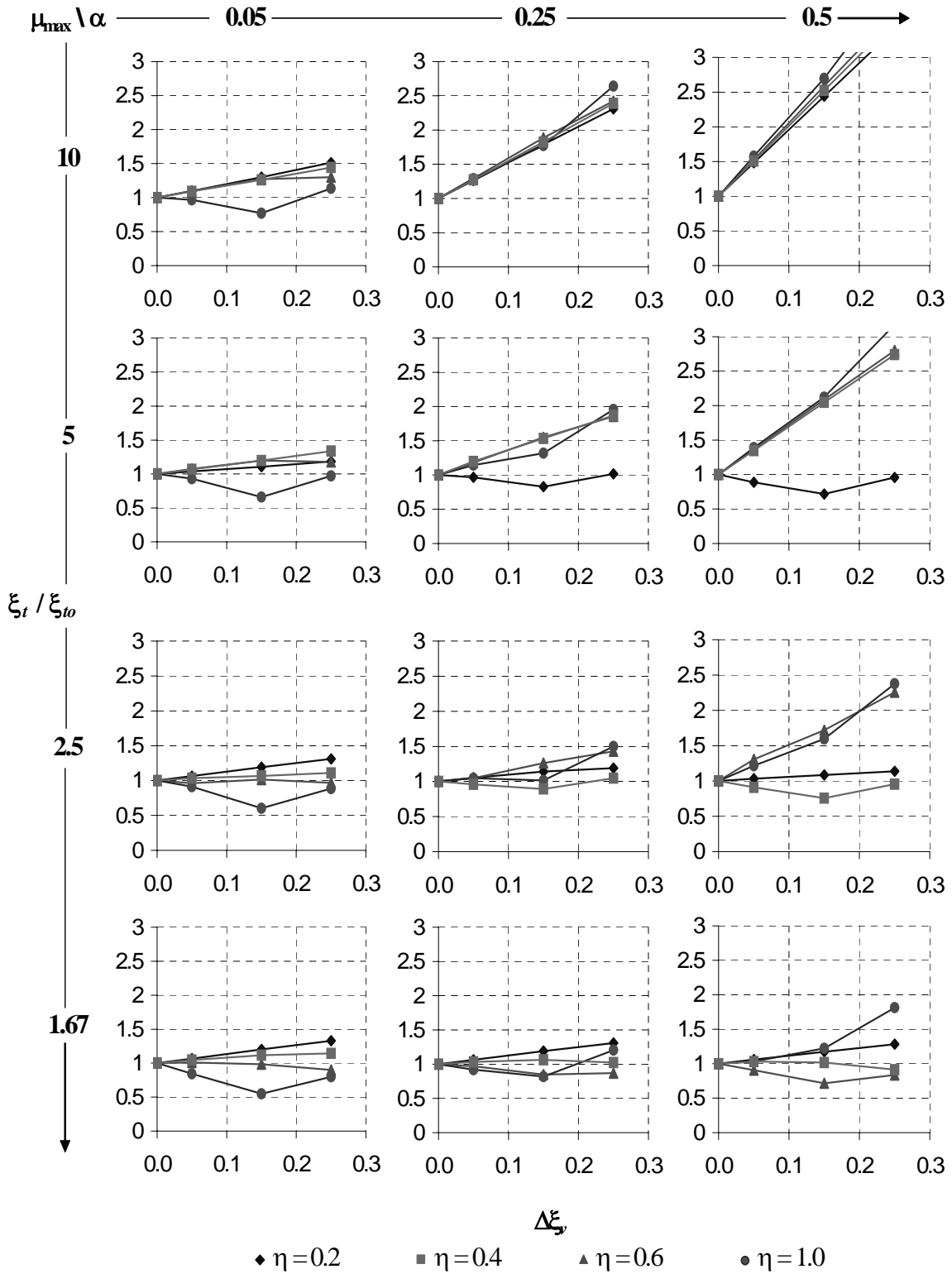


Figure 6.8. Ratio of Total Damping with Respect to Original Damping vs Increase in Viscous Damping for $T = 0.50$ s

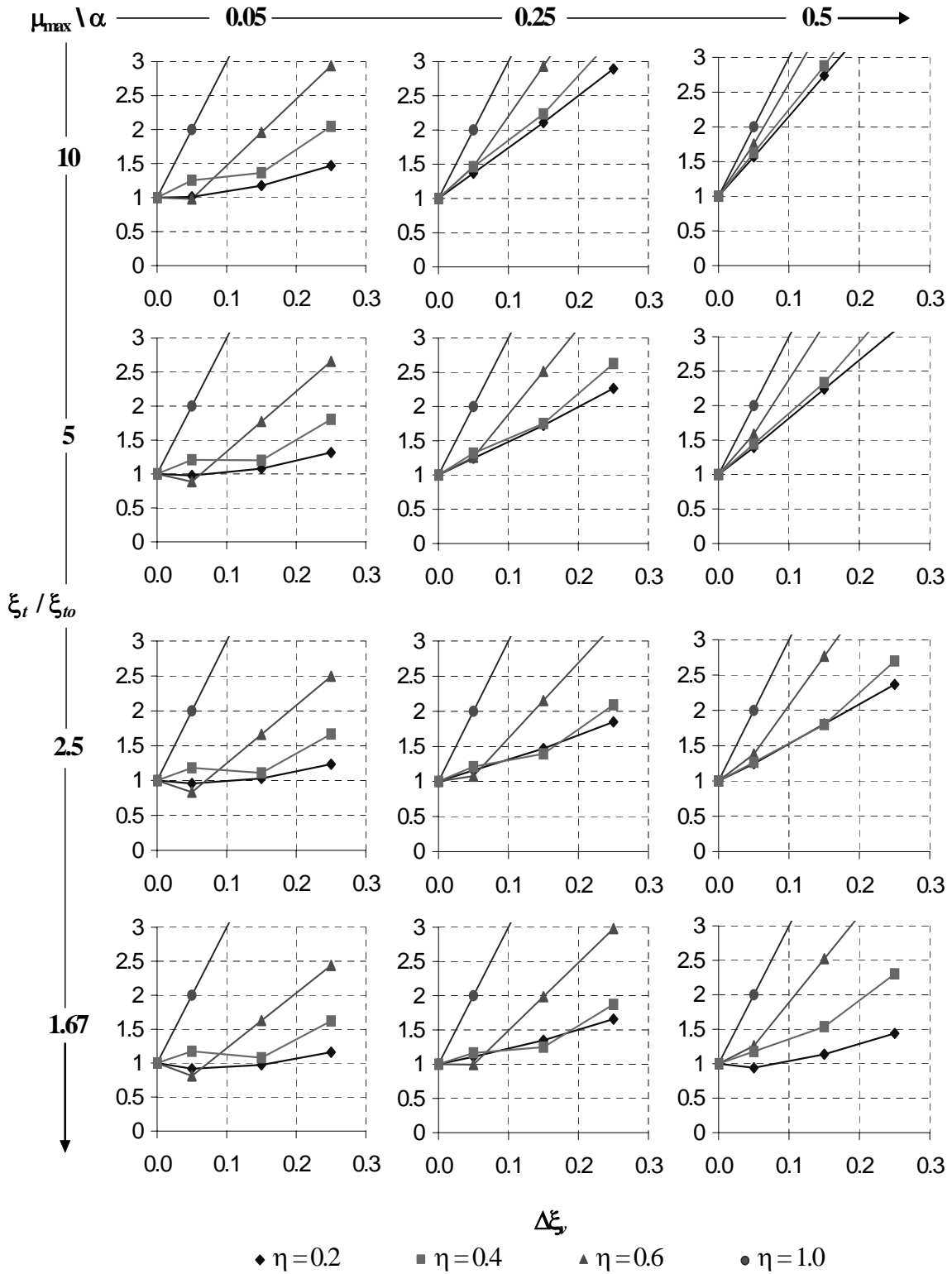


Figure 6.9. Ratio of Total Damping with Respect to Original Damping vs Increase in Viscous Damping for $T = 1.50$ s

6.4. Parametric Analysis of Spectral Acceleration

A parametric study was conducted to analyze how floor accelerations are affected by increases in viscous damping in SDOF systems with metallic fuses, using the set of synthetic earthquakes and parameters established in previous sections.

In Figures 6.10 to 6.12, response was plotted as a ratio of floor spectral acceleration, S_a , with respect to the floor spectral acceleration of the original system, S_{a0} , for systems with periods of 0.25 s, 0.50 s, and 1.50 s, respectively. It may be noted that for short and intermediate period systems, the spectral acceleration increases with viscous damping, except for large values of α and μ_{\max} (i.e., $\alpha = 0.5$ and $\mu_{\max} = 5$), where a reduction in spectral acceleration may be seen for values of $\eta \geq 0.4$. For example, in a short period system ($T = 0.25$ s) with $\alpha = 0.05$, $\mu_{\max} = 2.5$, and $\eta = 0.4$, the spectral acceleration increases by a factor of 1.51 when viscous damping is increased by 25%. However, in a short period system ($T = 0.25$ s) with $\alpha = 0.50$, $\mu_{\max} = 5$, and $\eta = 0.6$, the spectral acceleration is reduced by 28% when viscous damping is increased by 25% (see Figure 6.10).

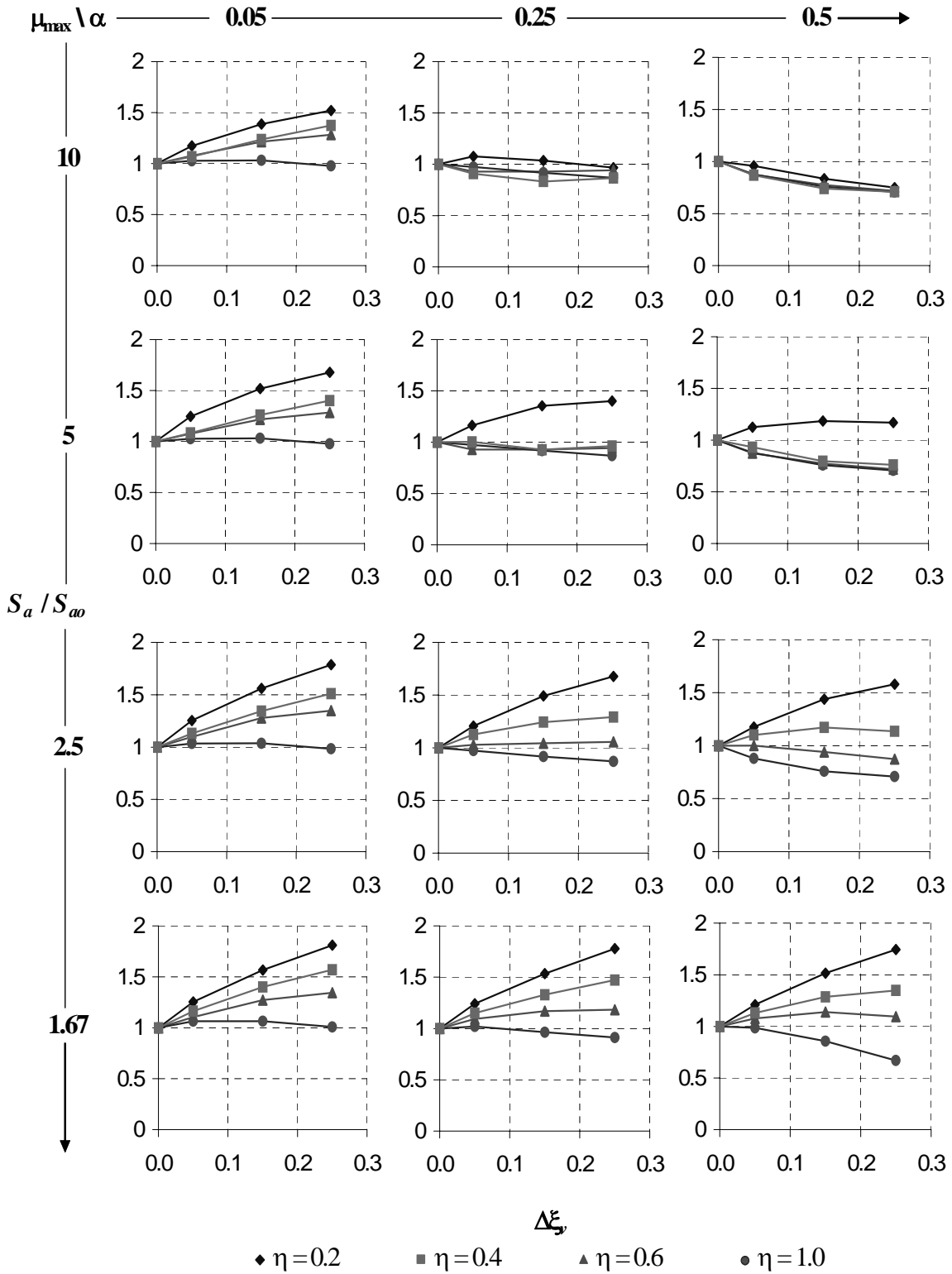


Figure 6.10. Ratio of Floor Spectral Acceleration with Respect to Original Floor Spectral Acceleration vs Increase in Viscous Damping for $T = 0.25$ s

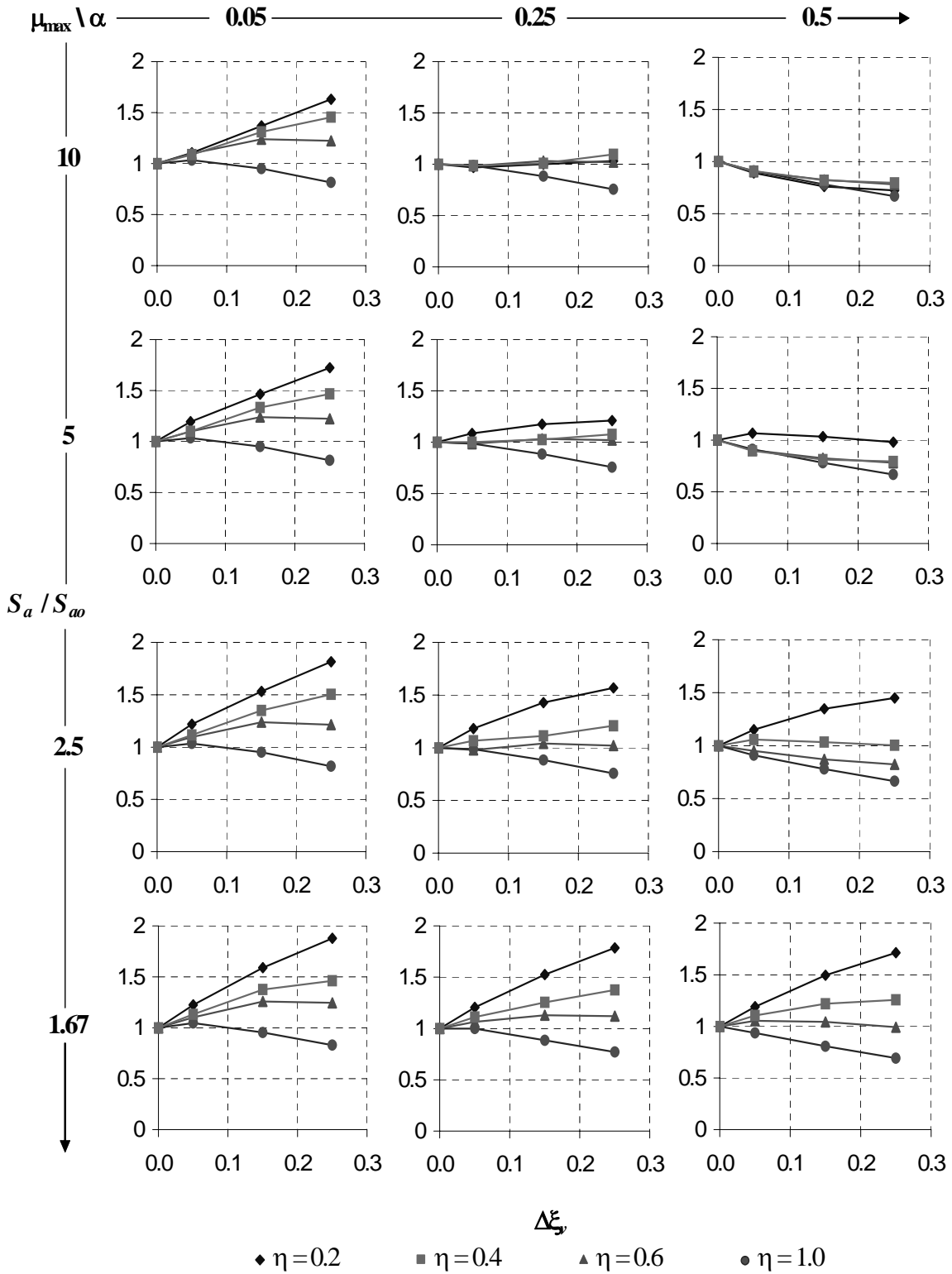


Figure 6.11. Ratio of Floor Spectral Acceleration with Respect to Original Floor Spectral Acceleration vs Increase in Viscous Damping for $T = 0.50$ s

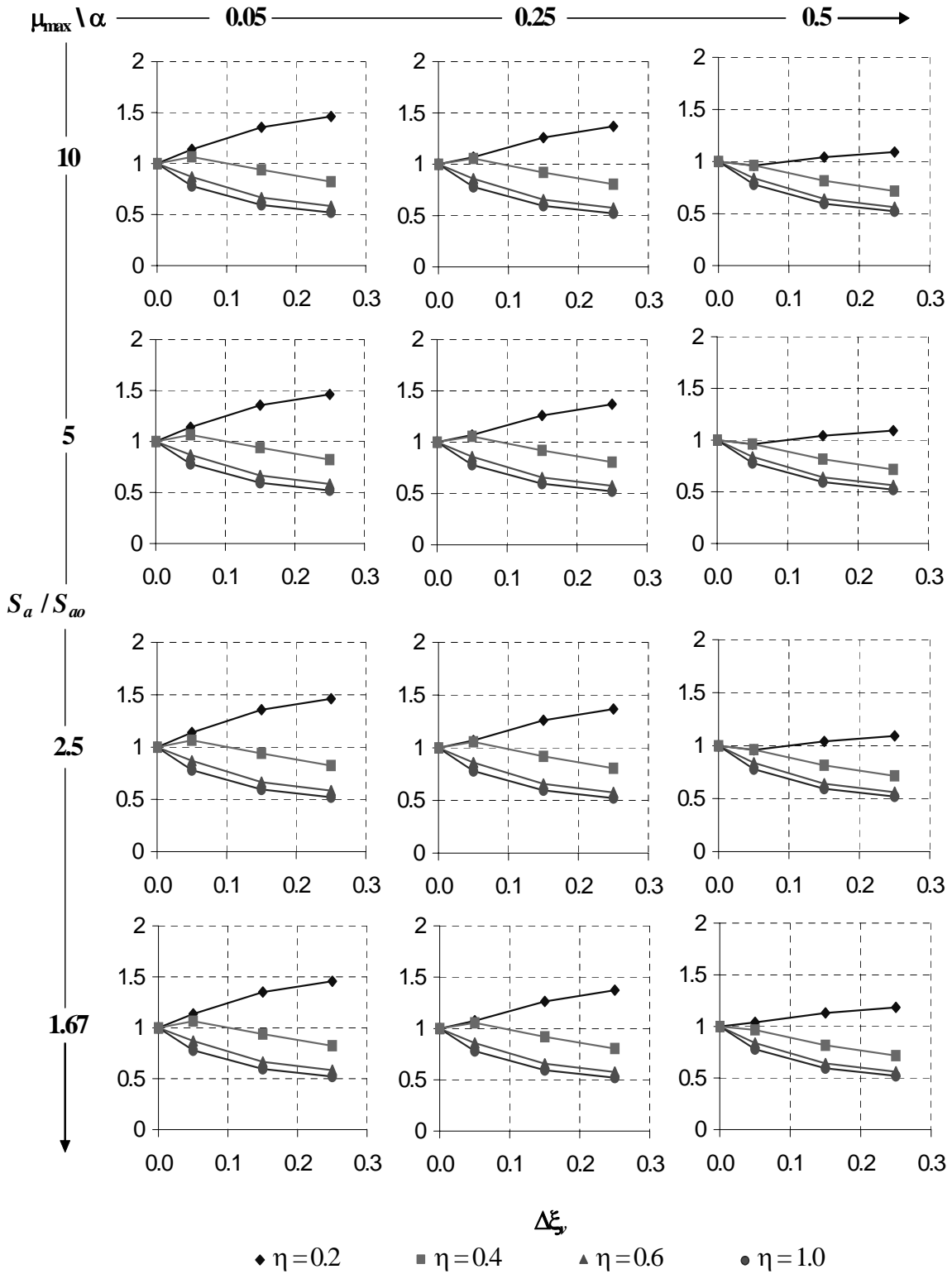


Figure 6.12. Ratio of Floor Spectral Acceleration with Respect to Original Floor Spectral Acceleration vs Increase in Viscous Damping for $T = 1.50$ s

On the other hand, for long period structures (Figure 6.12), the spectral acceleration generally decreases with increases in the viscous damping, except for small η values (i.e., $\eta = 0.2$). These results agree with the fact that, for long period systems, the total damping substantially increases with viscous damping, since the reduction in hysteretic damping is insignificant (i.e., $\Delta\xi_h \approx 0$, and $\Delta\xi_v \gg |\Delta\xi_h|$). For example, in a long period system ($T = 1.50$ s) with $\alpha = 0.05$, $\mu_{\max} = 2.5$, and $\eta = 0.4$, the spectral acceleration reduces by 18% when viscous damping is increased by 25%. However, in a long period system ($T = 1.50$ s) with $\alpha = 0.50$, $\mu_{\max} = 5$, and $\eta = 0.2$, the spectral acceleration slightly increases by 9% when viscous damping is increased by 25% (see Figure 6.12).

Figures 6.13 to 6.15 show the relationship between S_a / S_{ao} and global ductility, μ , recalling that both are affected by increases in viscous damping (i.e., the highest value of μ in every curve corresponds to $\Delta\xi_v = 0$, and the lowest one corresponds to $\Delta\xi_v = 25\%$). Note that original systems that respond with a ductility approximately equal to two (i.e., $\mu \approx 2$ for $\Delta\xi_v = 0$), are more likely to have a reduction in acceleration demands by increases in viscous damping. This is because systems that have small ductility demands can be changed into systems that behave elastically by adding more viscous damping. In other words, adding viscous damping is effective in reducing accelerations and displacements response of systems that behave elastically, or that can be modified such as to behave elastically (Chopra, 2001). For example, in a long period system ($T = 1.50$ s) with $\alpha = 0.50$, $\mu_{\max} = 5$, and $\eta = 0.4$, the global ductility, μ , reduces from 1.51 to 0.68, and the spectral acceleration is reduced by 29% when viscous damping is increased by 25% (see Figure 6.15). Subsequent sections are devoted to further investigate the relationship between viscous damping and acceleration response of elastic an inelastic systems.

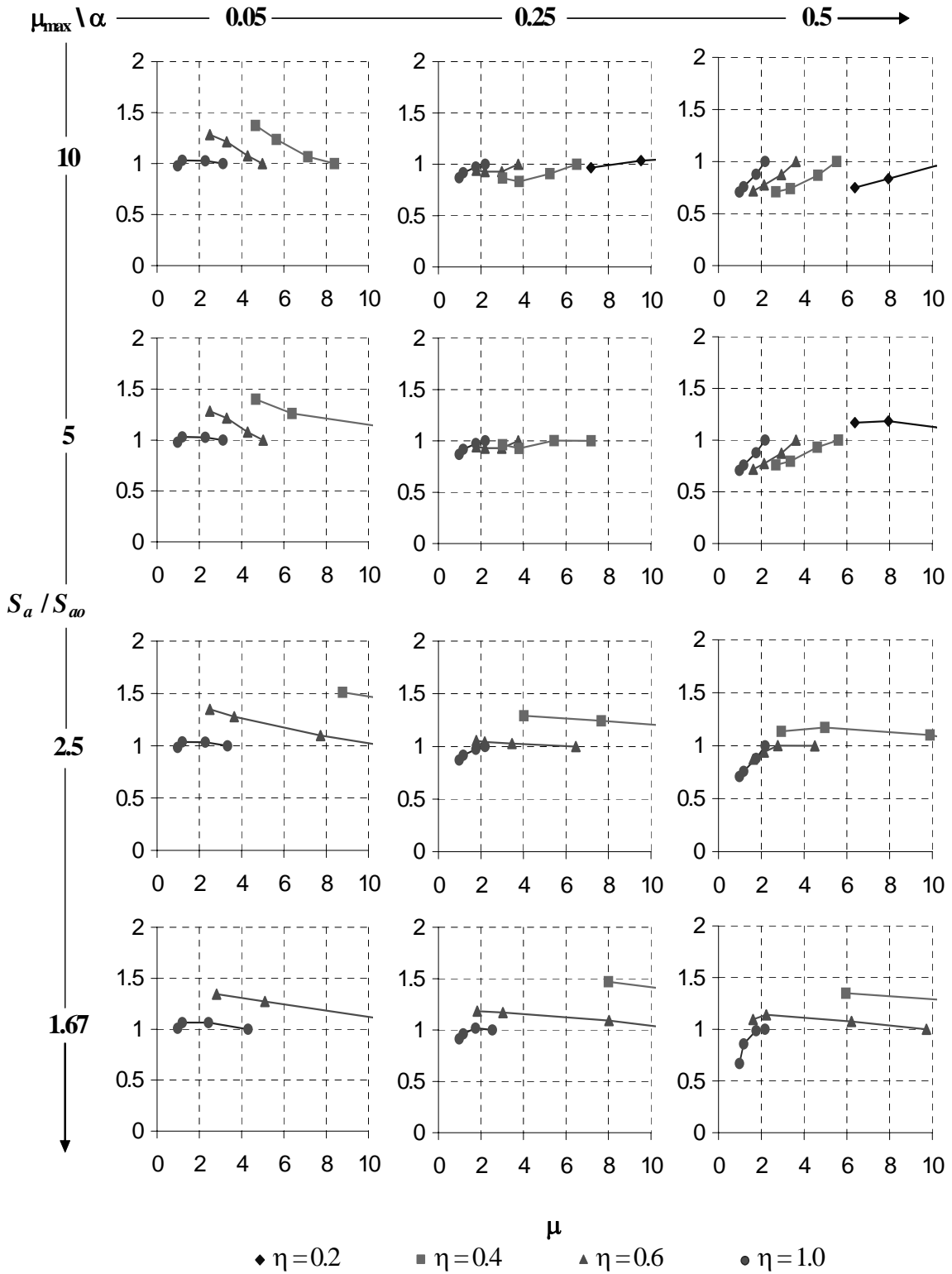


Figure 6.13. Ratio of Floor Spectral Acceleration with Respect to Original Floor Spectral Acceleration vs Global Ductility for $T = 0.25$ s

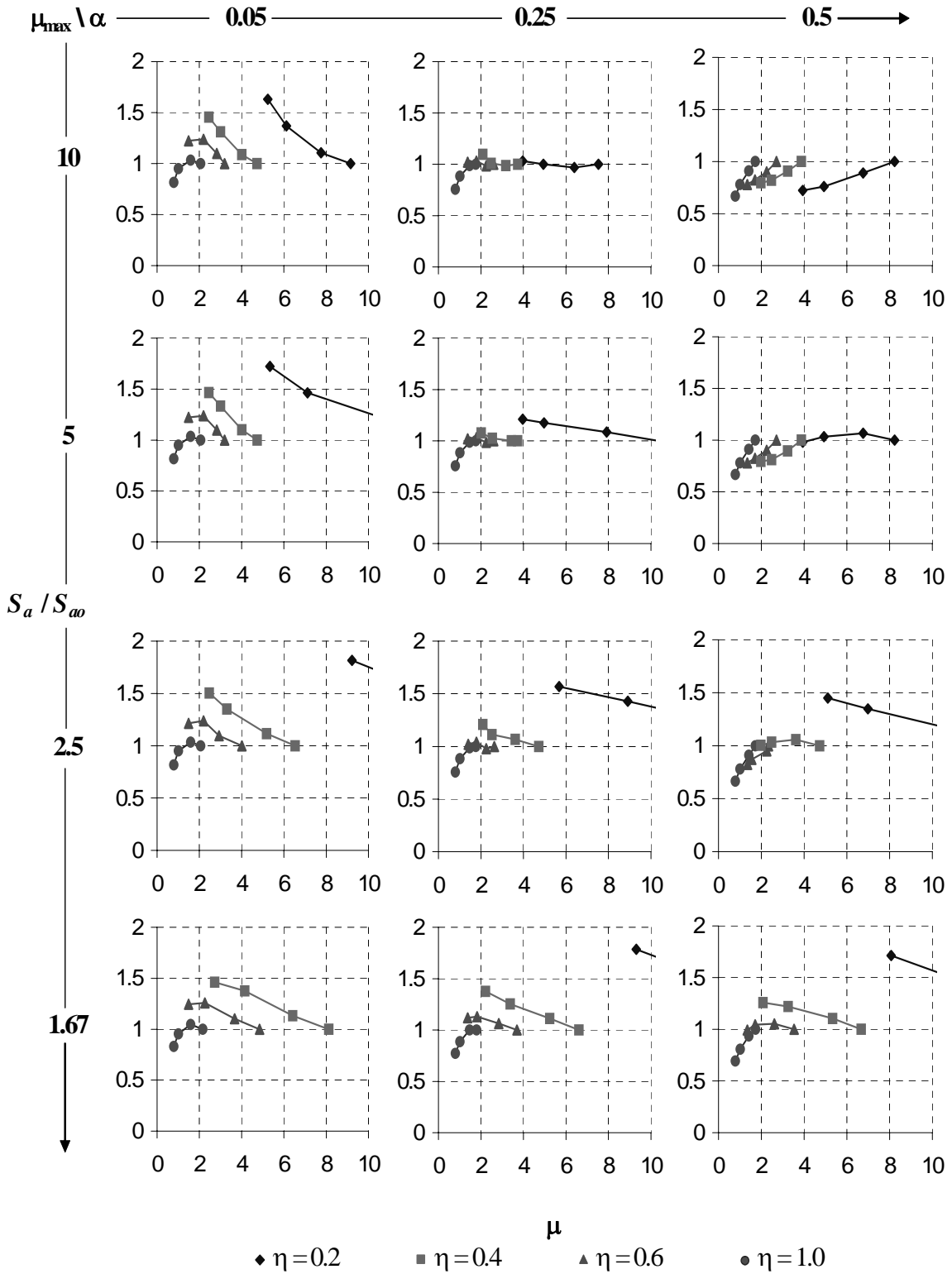


Figure 6.14. Ratio of Floor Spectral Acceleration with Respect to Original Floor Spectral Acceleration vs Global Ductility for $T = 0.50$ s

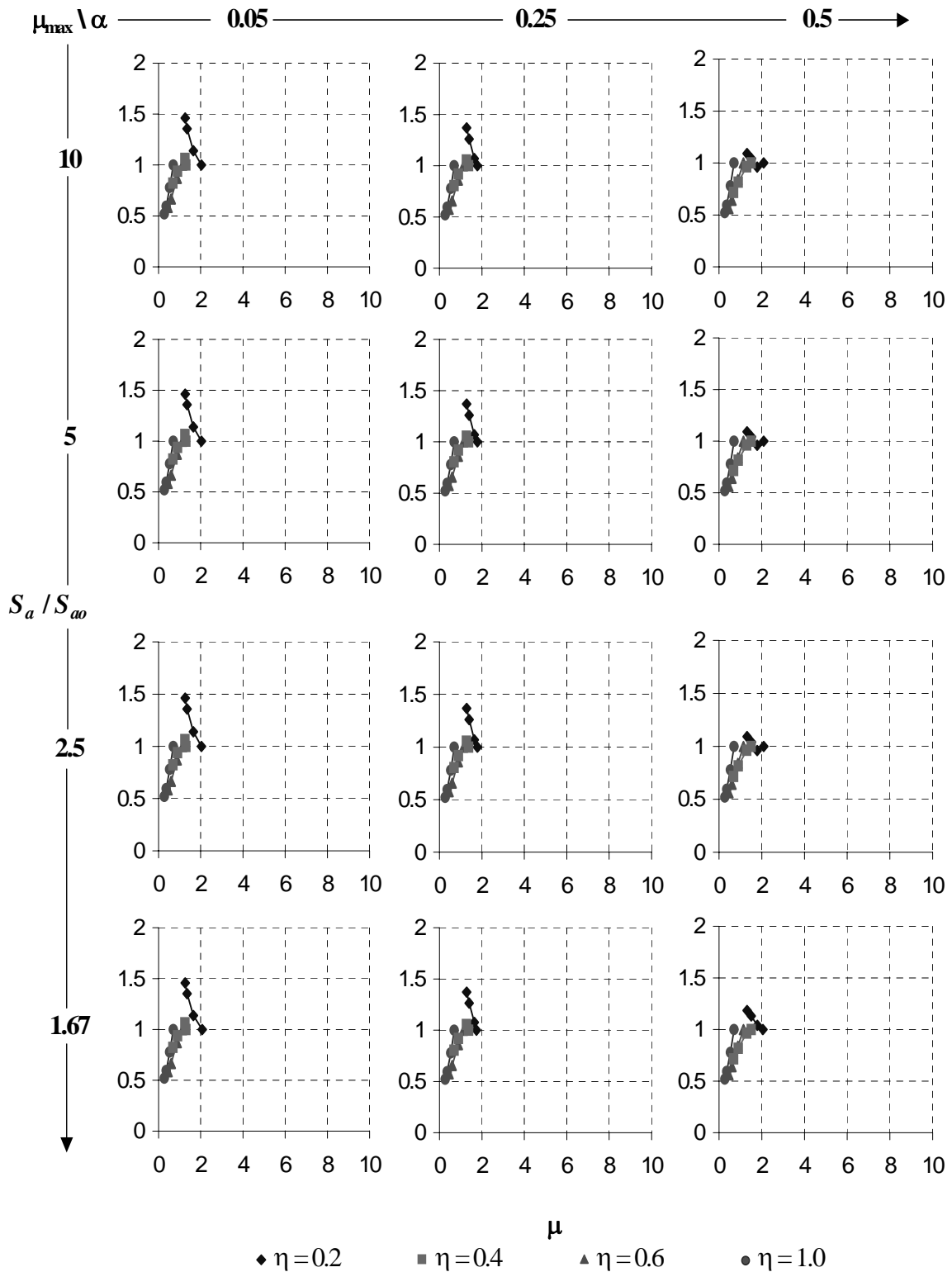


Figure 6.15. Ratio of Floor Spectral Acceleration with Respect to Original Floor Spectral Acceleration vs Global Ductility for $T = 1.50$ s

6.5. Hysteretic Response

As previously mentioned, the main purpose of this section is to investigate whether using viscous fluid dampers in parallel with metallic dampers can simultaneously reduce lateral displacements and floor accelerations. Although lateral displacement always decreases when using metallic, viscous, or both kind of dampers acting together, it was found (in previous section) that floor acceleration increases in most of the considered cases, even for systems designed with large viscous damping (except for cases where $\alpha \geq 0.5$ and $\mu_{\max} \geq 10$). This section focuses on studying the hysteretic response of short, intermediate, and long period systems, using the lowest and highest values of η from previous analyses (i.e., $\eta = 0.2$ and $\eta = 1.0$), along with several levels of viscous damping (i.e., 5%, 10%, 20%, and 30%), to understand the reason for these observed increases in acceleration.

Using d'Alembert's principle, it is possible to express the equation of motion of a SDOF system as an equation of dynamic equilibrium (Clough and Penzien, 1993). Therefore, for a SDOF subjected to ground excitation, the equation of motion may be written as:

$$F_i + F_d + F_s = 0 \quad (6.7)$$

where F_i is the inertial force, calculated as:

$$F_i = m(\ddot{u}_g + \ddot{u}) \quad (6.8)$$

F_d is the viscous damper force calculated using (6.2), and F_s is the sum of the metallic damper force and the structural frame force, called here the hysteretic force, determined according to the following expression:

$$F_s = \begin{cases} K_1 u, & u < \Delta_{ya} \\ V_y + \alpha K_1 (u - \Delta_{ya}), & \Delta_{ya} \leq u < \Delta_{yf} \\ V_p, & \Delta_{yf} \leq u \end{cases} \quad (6.9)$$

where all variables are defined in Figure 3.2. Note that for undamped systems (i.e., $F_d = 0$), the inertial and hysteretic forces must be equal and opposite to satisfy the

dynamic equilibrium of (6.7). In damped systems, increases in viscous damping result in decreases in the lateral displacement, u , and therefore, decreases in the hysteretic force, F_s , according to (6.9) (assuming that the system is designed such that $u < \Delta_{yf}$, which is required to satisfy the structural fuse concept). Consequently, acceleration demand, \ddot{u} , may increase (or decrease) to satisfy the dynamic equilibrium. The resultant increase or decrease in the inertial force depends on the increase in F_d value relative to the decrease in the value of F_s . For instance, if $\Delta F_d > |\Delta F_s|$ then $\Delta \ddot{u} > 0$ (i.e., acceleration increases), and if $\Delta F_d < |\Delta F_s|$ then $\Delta \ddot{u} < 0$ (i.e., acceleration decreases).

Figures 6.16 to 6.39 show the superposed hysteresis loops for the inertial force and hysteretic force normalized with respect to the yield point (V_y, Δ_y) , for systems with $T = 0.25$ s, 0.50 s, and 1.50 s; $\eta = 0.2$, and 1.0; and viscous damping of 5%, 10%, 20%, and 30%. The difference between the curves is equal to the viscous damper force, F_d . Note that when the maximum displacement is reached (i.e., $\dot{u} = 0$) the values of both curves coincide (i.e., $|F_i| = |F_s|$). Maximum difference between the curves is obtained when $u = 0$ (i.e., maximum velocity), since the hysteretic force has its minimum value at this point. For elastic systems (i.e., $u < \Delta_{ya}$), when $u = 0$, $F_s = 0$, the inertial force and the damping force are equal (i.e., $|F_i| = |F_d|$).

Note that for systems that behave inelastically and for which the frame remains elastic (i.e., $\Delta_{ya} \leq u < \Delta_{yf}$), the stiffness ratio, α , has a significant influence on the acceleration demand, since $F_s = V_y + \alpha K_1 (u - \Delta_{ya})$ in this region. Since $F_s \approx V_y$ in systems with small values of α , a reduction in the hysteretic force when viscous damping is added is not significant. On the other hand, F_s may be significantly reduced in systems with large values of α , when maximum displacement decreases by the addition of viscous damping. For example, in a system with $T = 0.5$ s, $\eta = 0.2$, $\alpha = 0.05$, $\mu_{\max} = 10$ (Figs. 6.24 to 6.27), the hysteretic force remains almost constant (i.e., $\Delta F_s \approx 0$), and the acceleration demand consequently increases by about 60%, when 25% of extra viscous damping is added. For the same system, but with $\alpha = 0.50$ instead, F_s is reduced by 40% when 25% of viscous

damping is added (i.e., $\Delta F_d < |\Delta F_s|$), and accordingly, the acceleration demand decreases by about 30%.

Also, it may be noted that for elastic systems (i.e., $F_s = K_1 u$), the displacement and acceleration demands both decrease by increasing the viscous damping, since the decrease in the hysteretic force is always larger than the increase in the viscous damper force (i.e., $\Delta F_d < |\Delta F_s|$). For example, in a system with $T = 1.50$ s, $\eta = 1.0$, $\alpha = 0.25$, $\mu_{\max} = 2.5$ (Figures 6.36 to 6.39), the hysteretic force reduces by 40% when 25% of viscous damping is added (i.e., $\Delta F_d < |\Delta F_s|$), and the acceleration demand accordingly decreases by about 50%.

These results corroborate the fact that the addition of viscous damping is effective in reducing the displacements and acceleration demands of elastic or near-elastic (e.g., $\alpha = 0.5$) systems, but is ineffective (and in fact detrimental) for nonlinear systems. However, metallic dampers with elastic behavior are not effective, since they only provide additional stiffness to reduce lateral displacements, which is something that could be done just as well with conventional structural elements, as mentioned in Section 3.

Ramirez et al. (2000) proposed the following expression to approximate the maximum acceleration, A_{\max} , in inelastic systems with viscous damping devices:

$$A_{\max} = A \left(CF_1 + \frac{2\pi\beta_{\text{veff}}}{\lambda} CF_2 \right) \quad (6.10)$$

where A is the acceleration at the point of maximum displacement, CF_1 and CF_2 are the load combination factors to calculate the response at the time of maximum acceleration, β_{veff} is the effective viscous damping, and λ is a parameter calculated as:

$$\lambda = 4 \cdot 2^a \frac{\Gamma^2(1+a/2)}{\Gamma(2+a)} \quad (6.11)$$

where Γ is the gamma function. For inelastic systems with linear viscous damping (i.e.,

$a = 1$), $\lambda = \pi$, $CF_1 = 1.0$, $CF_2 = \sin \delta$, and $\delta = 2\beta_{veff}$, and Eq. 6.10 becomes:

$$A_{\max} = A \left[1.0 + 2\beta_{veff} \sin(2\beta_{veff}) \right] \quad (6.12)$$

For instance, in an inelastic system with 30% of effective viscous damping, the maximum acceleration increases in about 33% with respect to the acceleration at the point of maximum displacement. Comparing the values predicted by Eq. 6.12 with the results obtained in this study (Figs. 6.16 to 6.39) it is observed that Eq. 6.12 can be accurate to estimate the increase in the maximum acceleration for intermediate to large values of the stiffness ratio (i.e., $0.25 < \alpha < 0.50$). However, some discrepancies were observed for systems with low stiffness ratio (i.e., $\alpha < 0.25$).

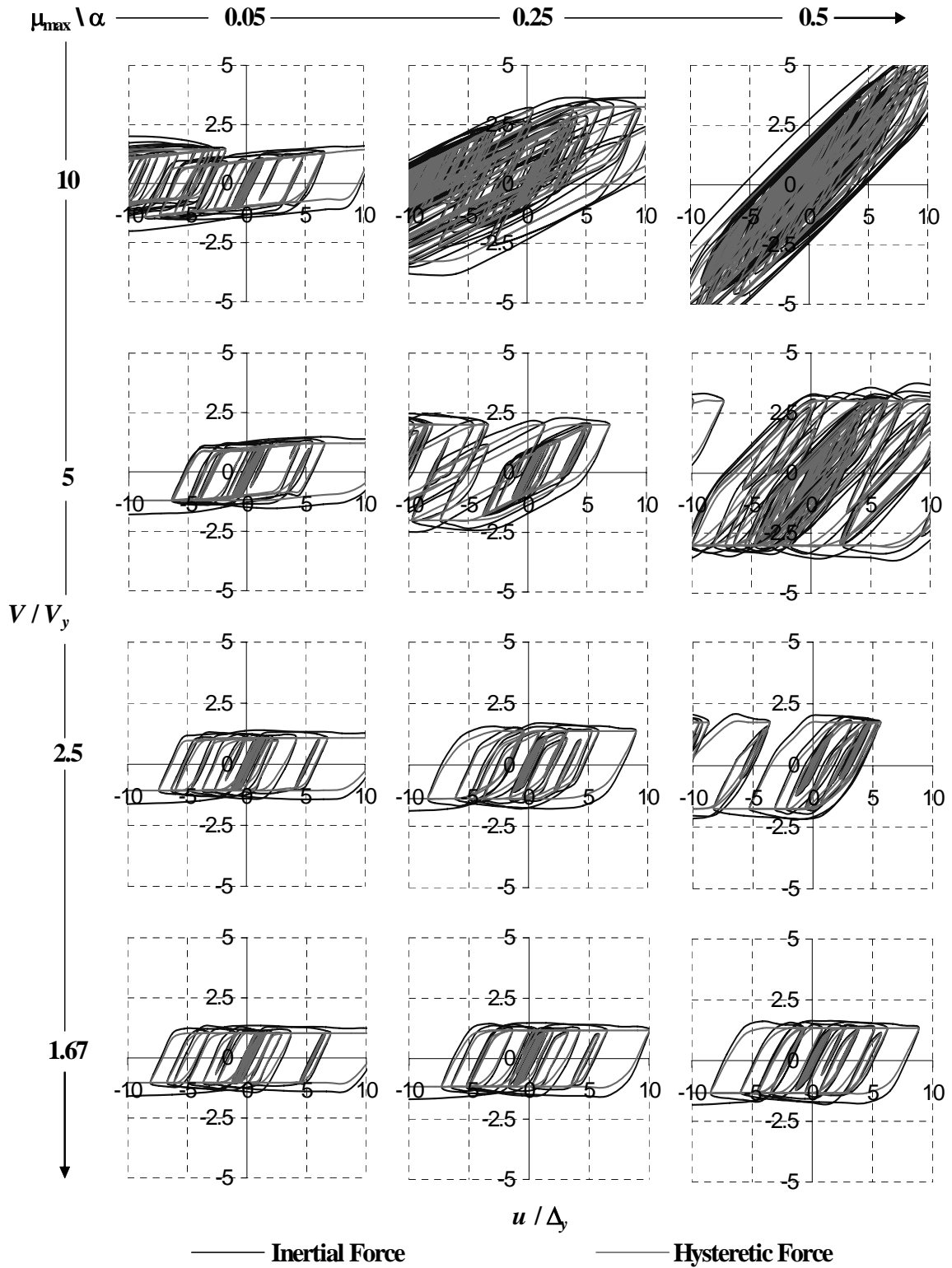


Figure 6.16. Normalized Inertial and Hysteretic Loops for $T = 0.25$ s, $\eta = 0.2$, and 5% of Viscous Damping

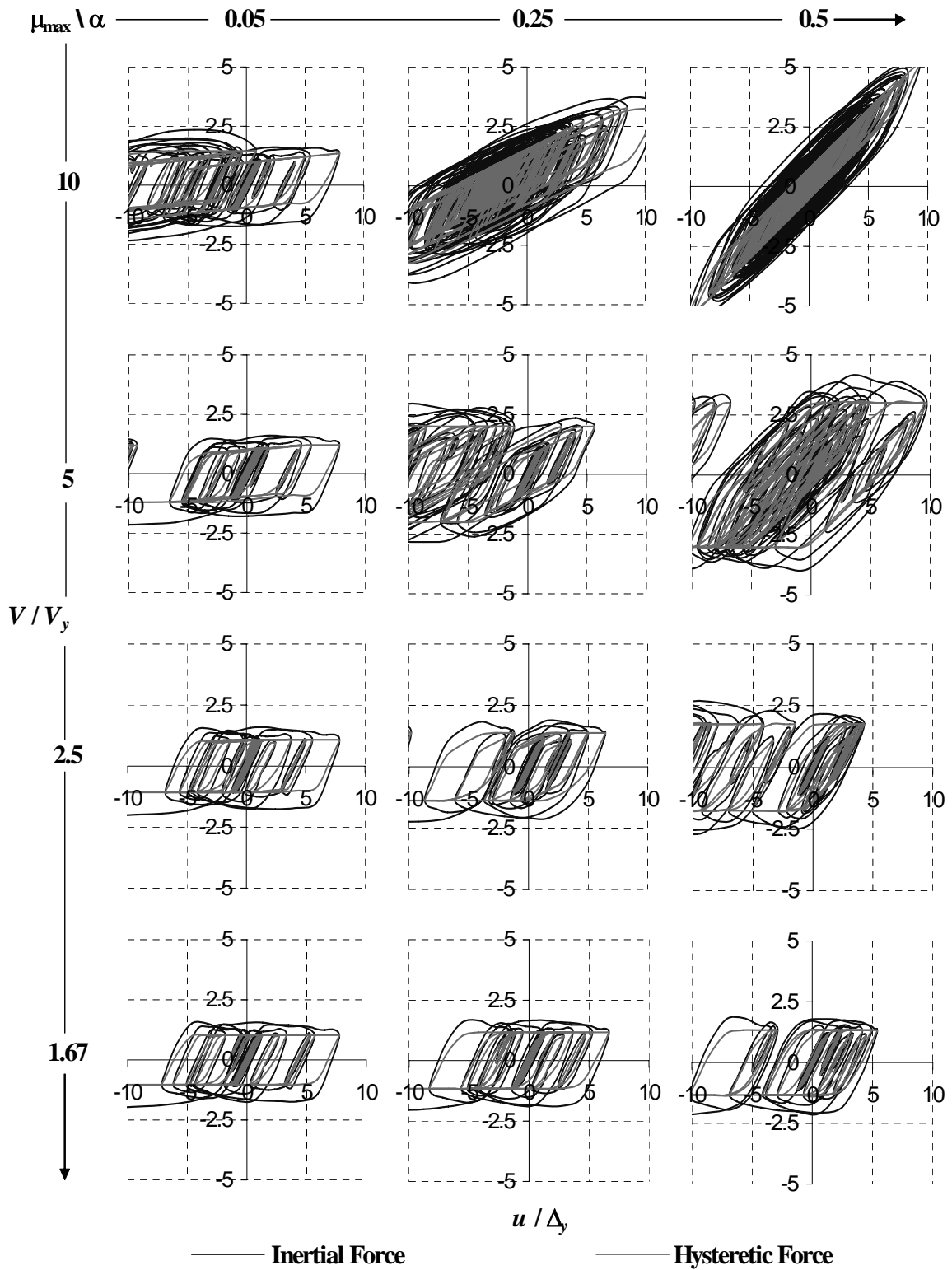


Figure 6.17. Normalized Inertial and Hysteretic Loops for $T = 0.25$ s, $\eta = 0.2$, and 10% of Viscous Damping

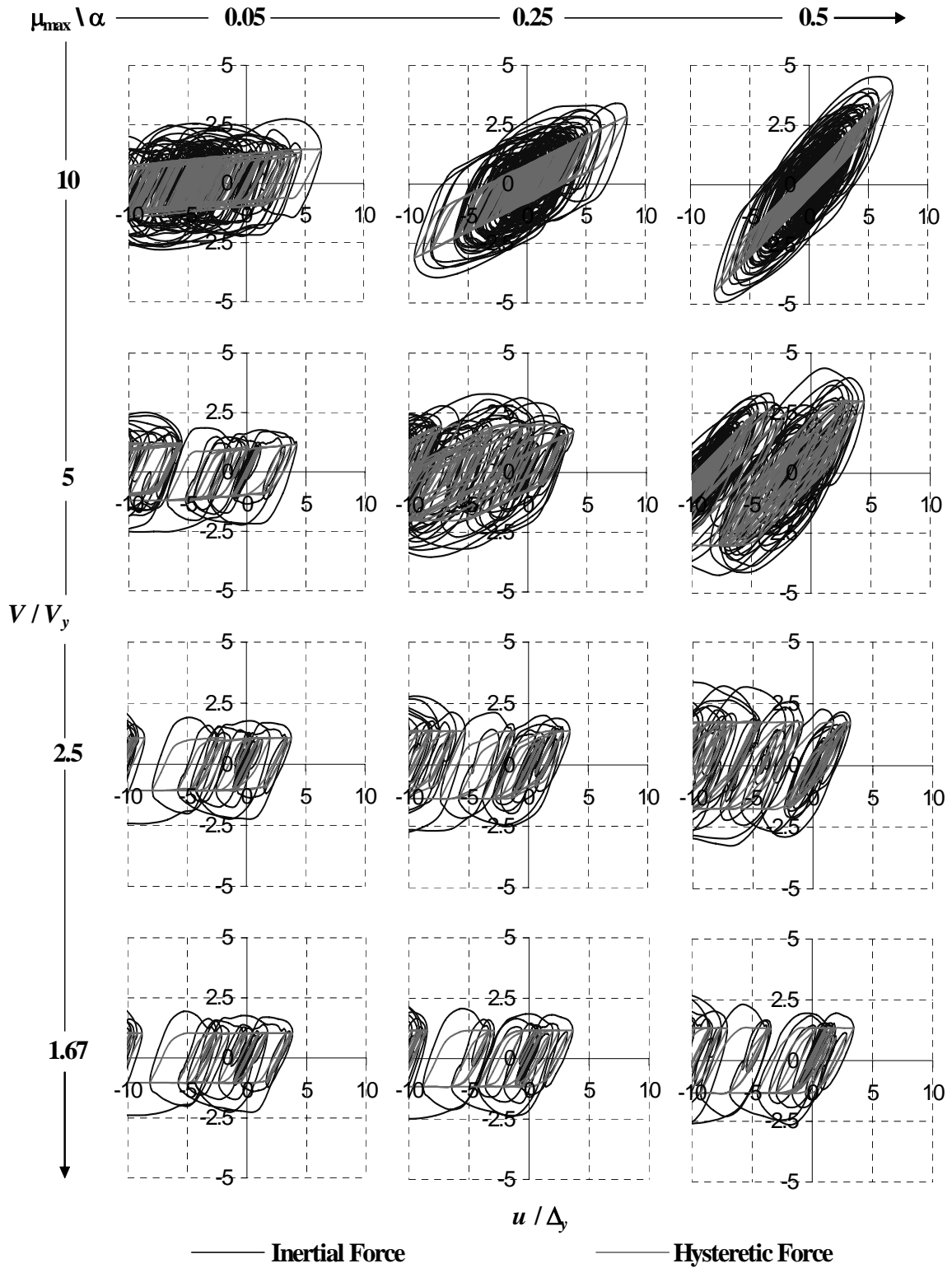


Figure 6.18. Normalized Inertial and Hysteretic Loops for $T = 0.25$ s, $\eta = 0.2$, and 20% of Viscous Damping

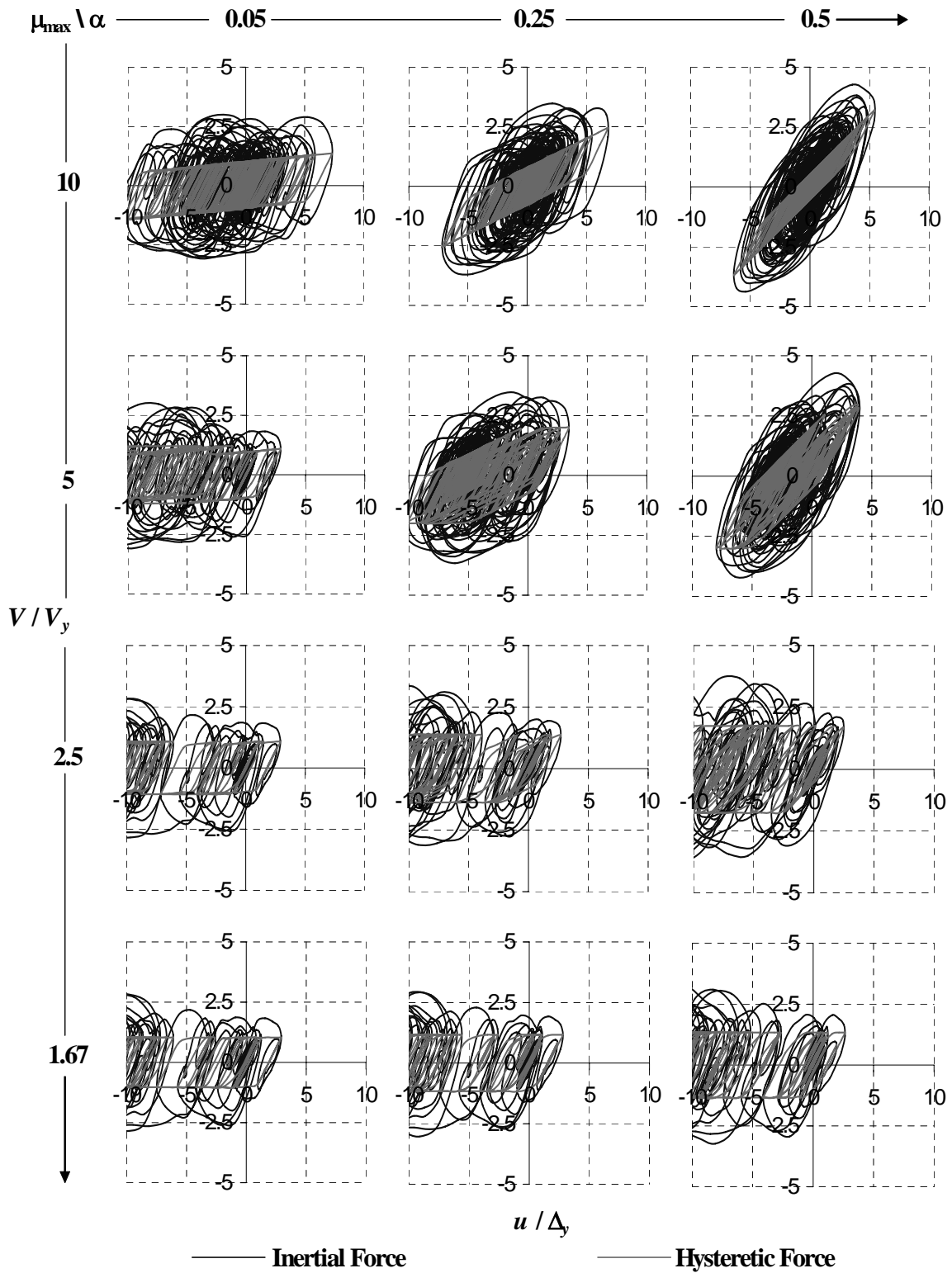


Figure 6.19. Normalized Inertial and Hysteretic Loops for $T = 0.25$ s, $\eta = 0.2$, and 30% of Viscous Damping

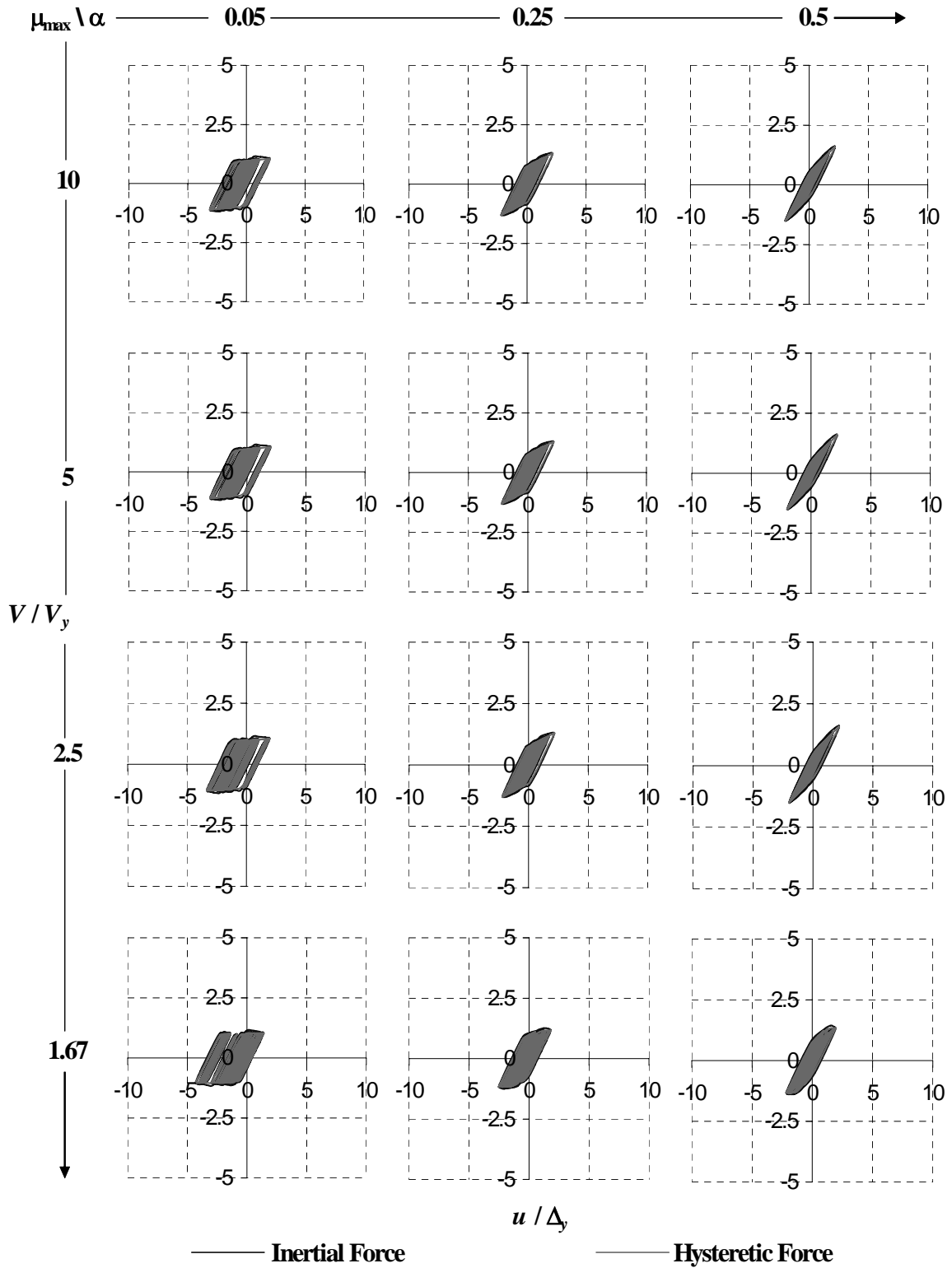


Figure 6.20. Normalized Inertial and Hysteretic Loops for $T = 0.25$ s, $\eta = 1.0$, and 5% of Viscous Damping

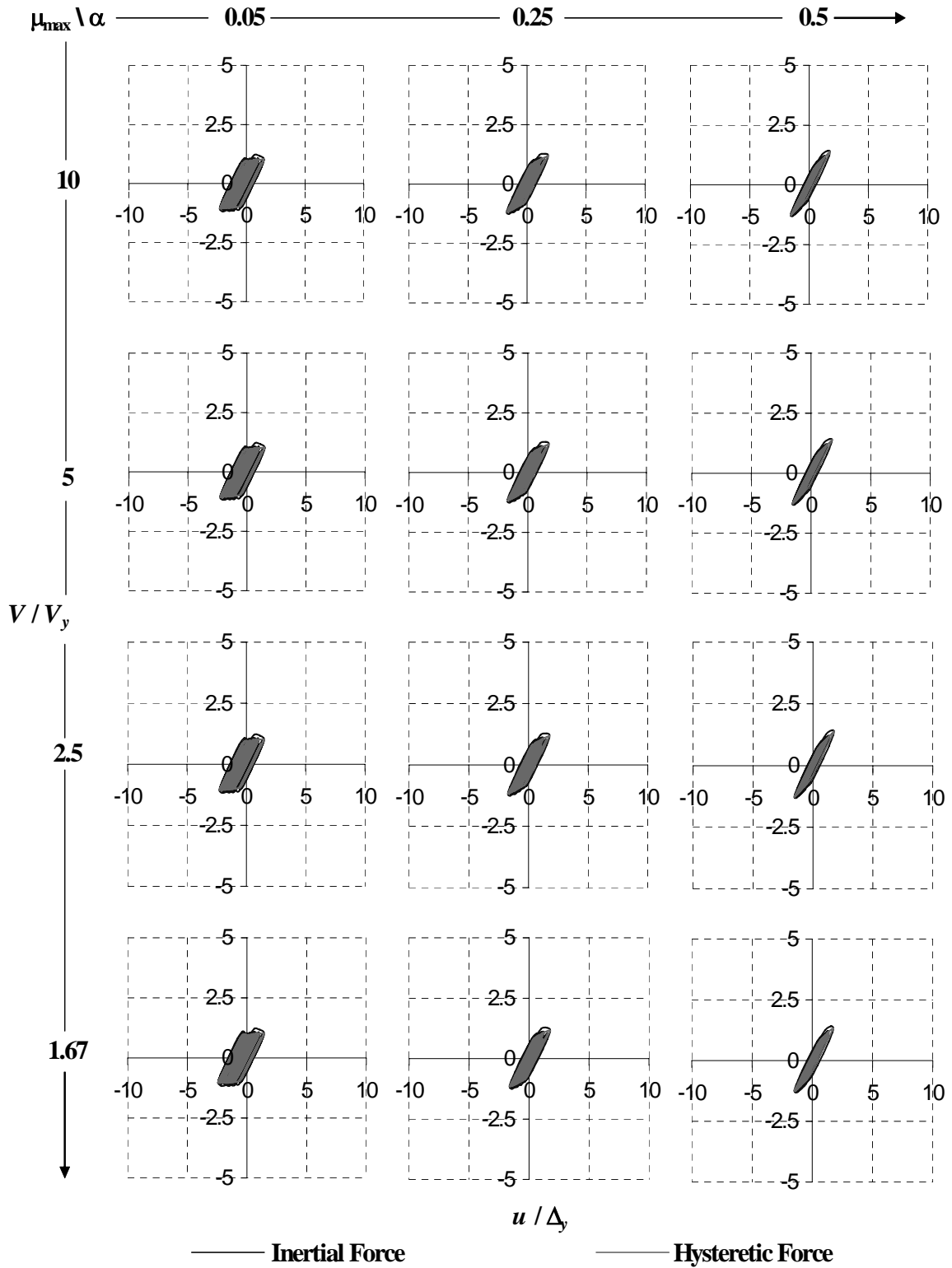


Figure 6.21. Normalized Inertial and Hysteretic Loops for $T = 0.25$ s, $\eta = 1.0$, and 10% of Viscous Damping

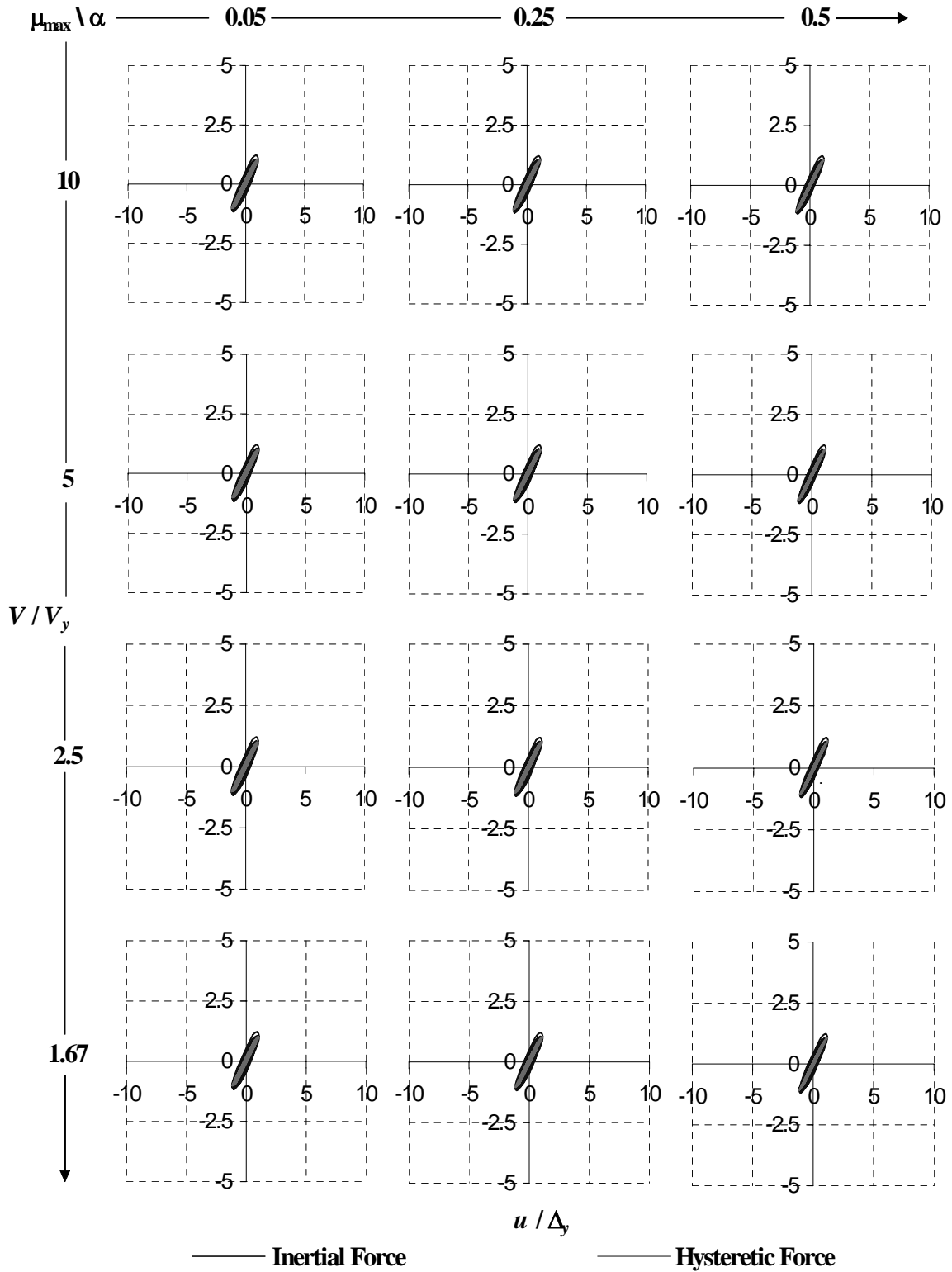


Figure 6.22. Normalized Inertial and Hysteretic Loops for $T = 0.25$ s, $\eta = 1.0$, and 20% of Viscous Damping

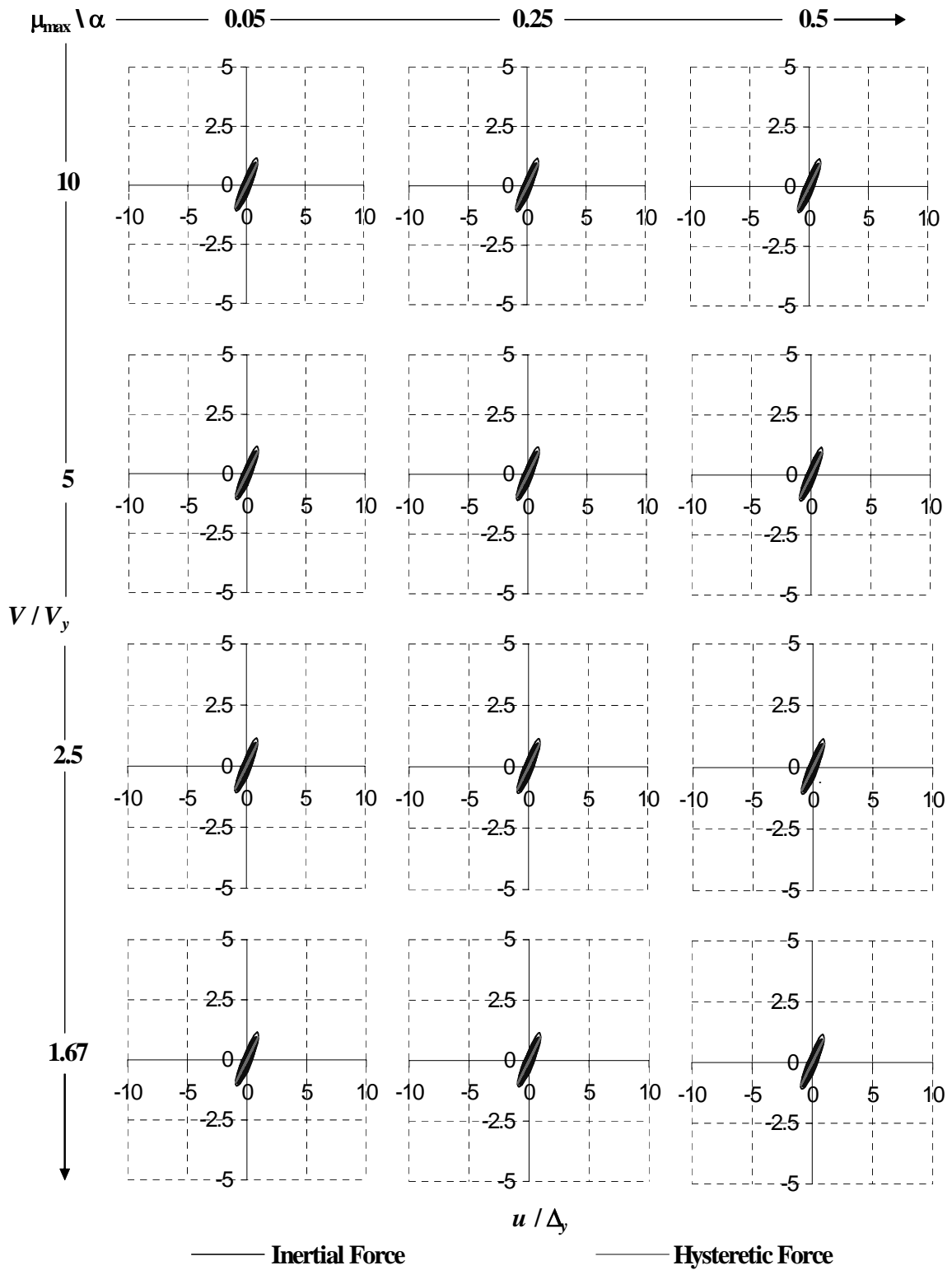


Figure 6.23. Normalized Inertial and Hysteretic Loops for $T = 0.25$ s, $\eta = 1.0$, and 30% of Viscous Damping

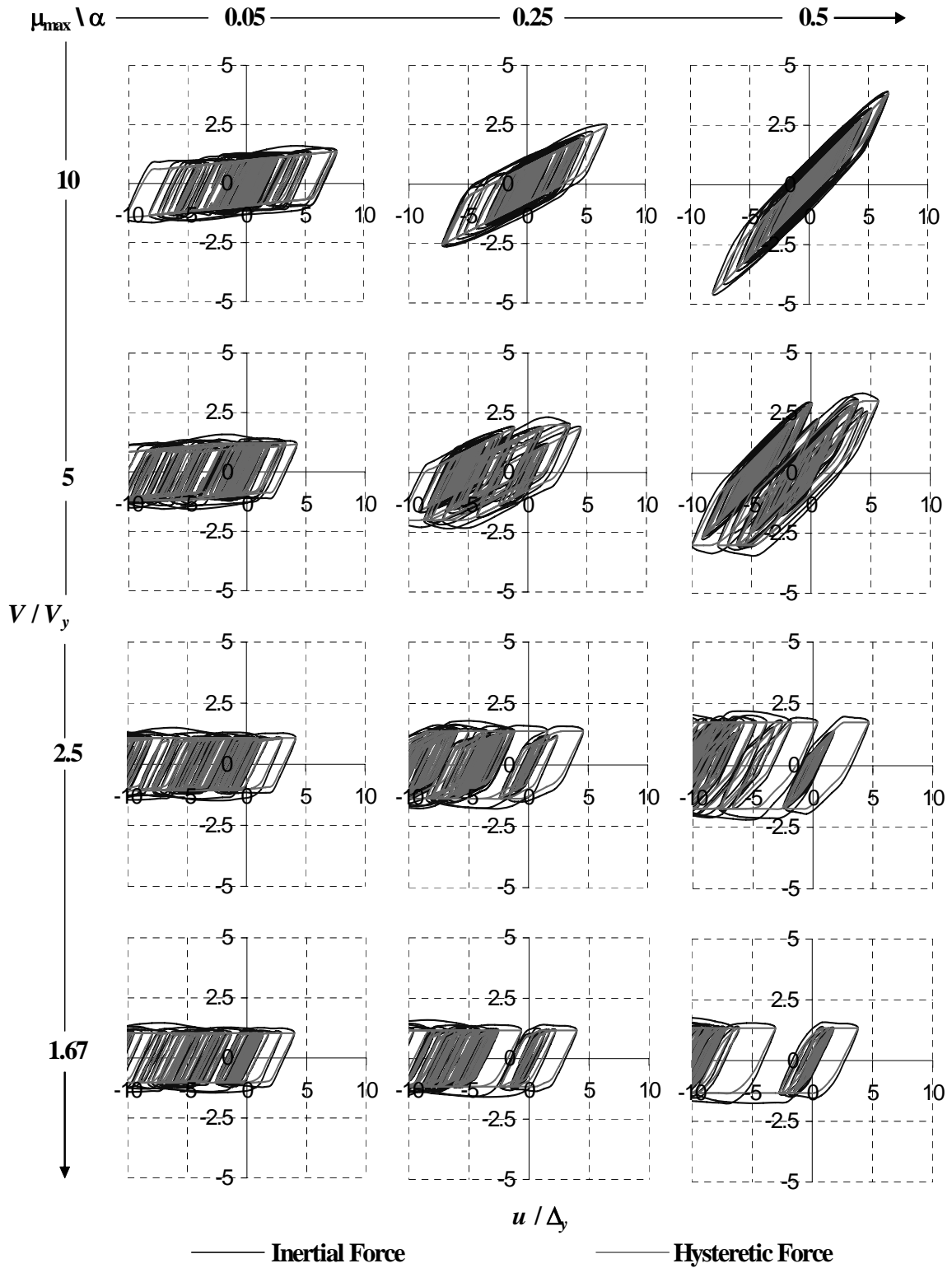


Figure 6.24. Normalized Inertial and Hysteretic Loops for $T = 0.50$ s, $\eta = 0.2$, and 5% of Viscous Damping

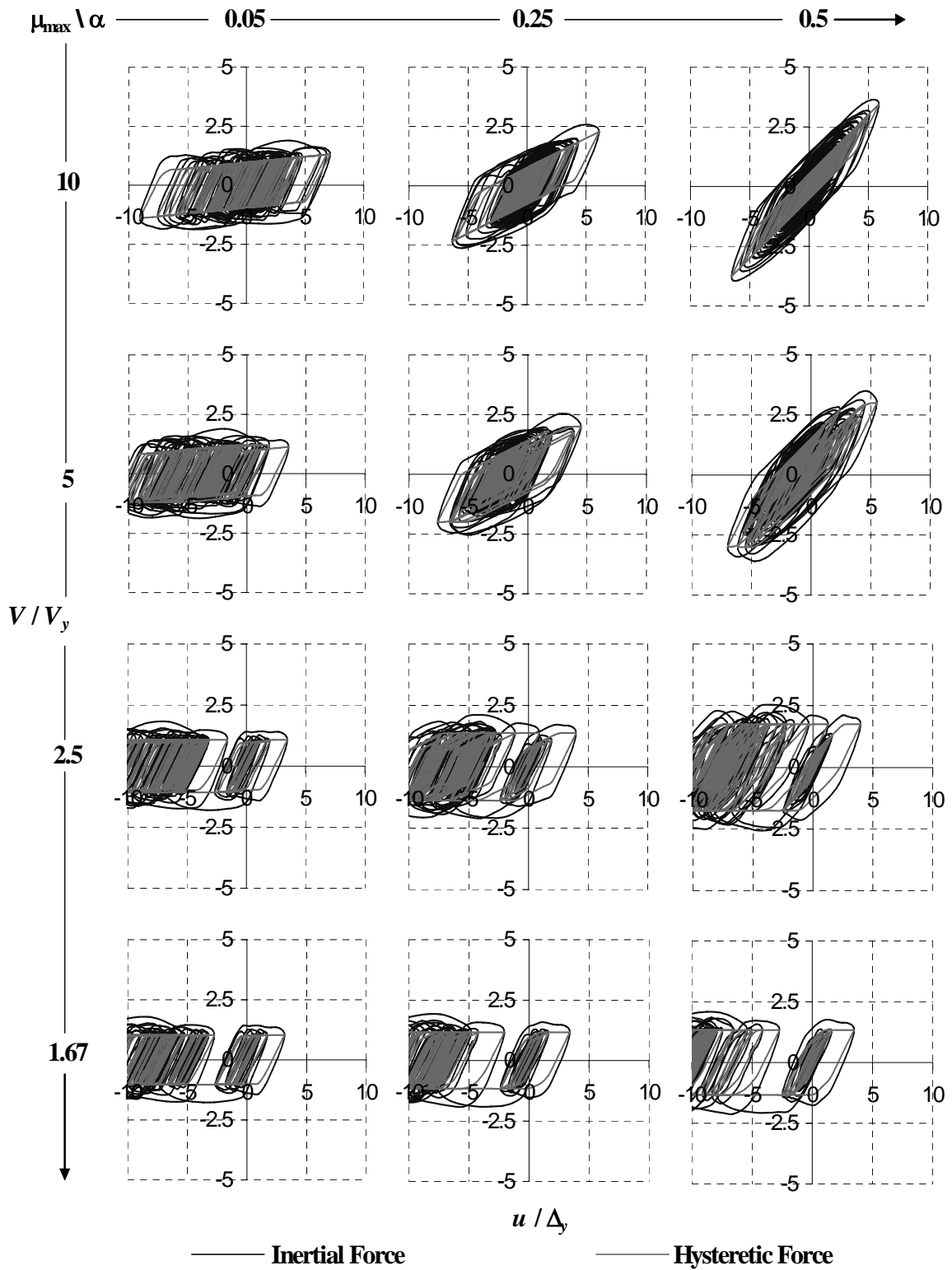


Figure 6.25. Normalized Inertial and Hysteretic Loops for $T = 0.50$ s, $\eta = 0.2$, and 10% of Viscous Damping

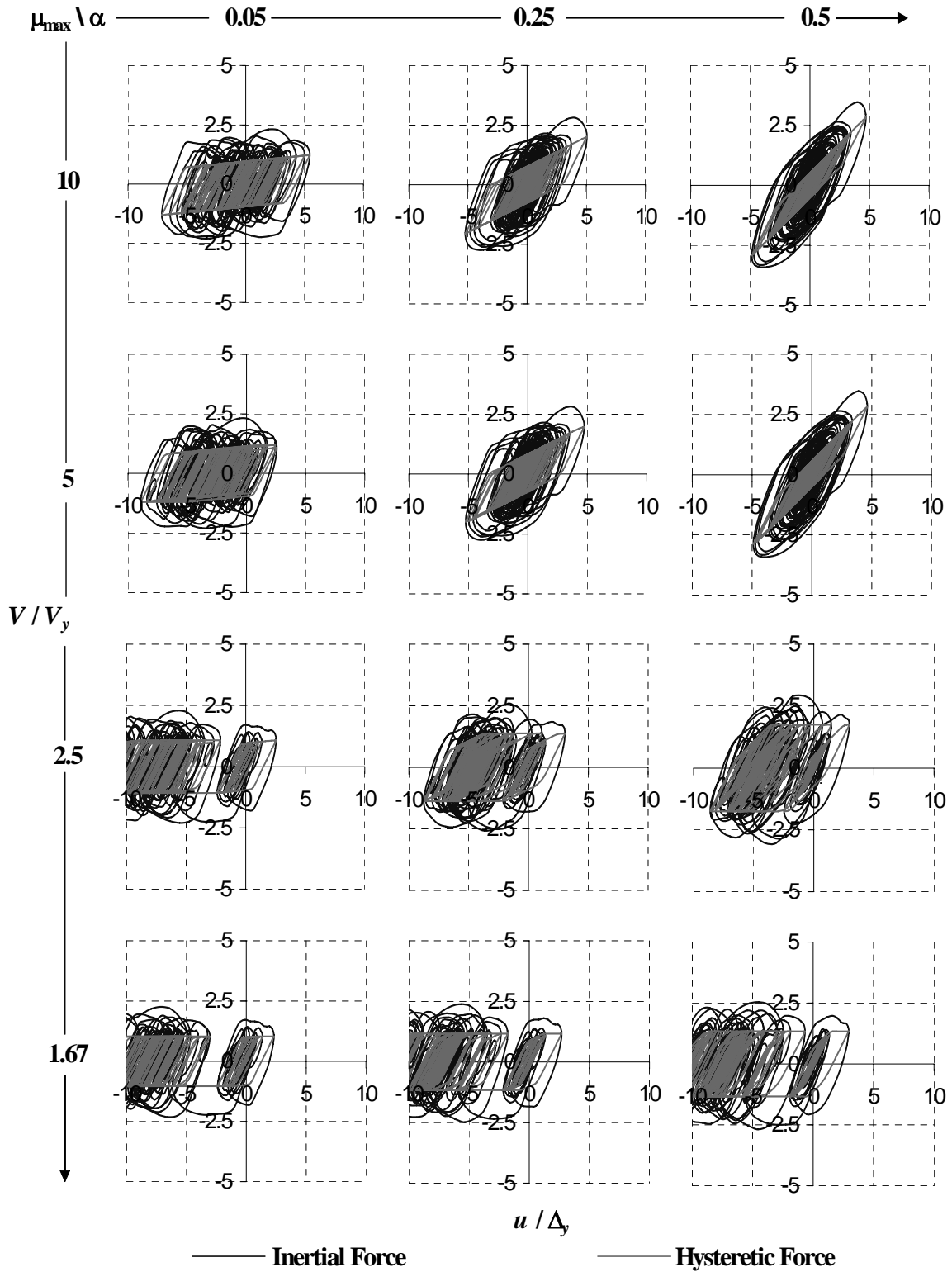


Figure 6.26. Normalized Inertial and Hysteretic Loops for $T = 0.50$ s, $\eta = 0.2$, and 20% of Viscous Damping

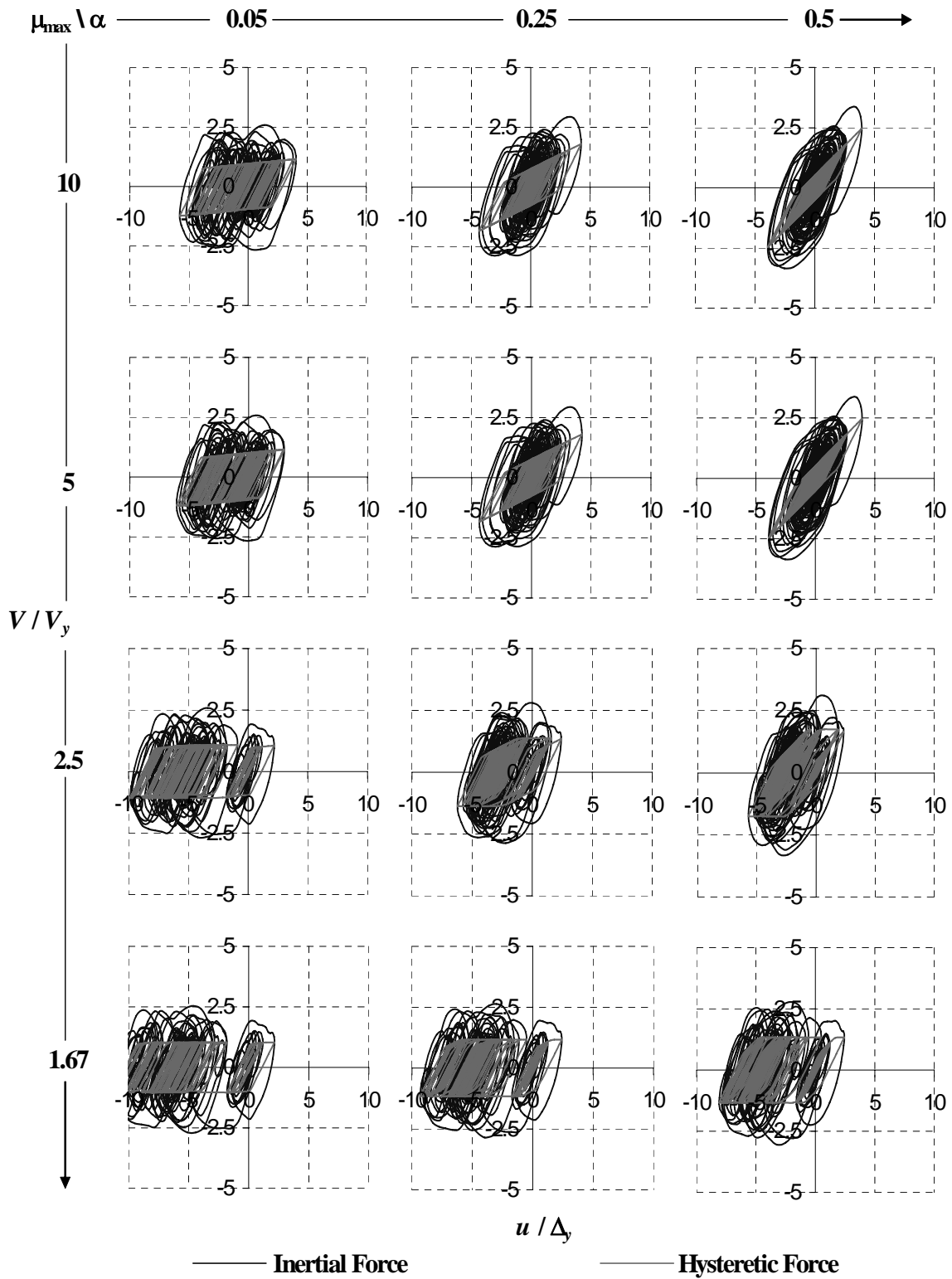


Figure 6.27. Normalized Inertial and Hysteretic Loops for $T = 0.50$ s, $\eta = 0.2$, and 30% of Viscous Damping

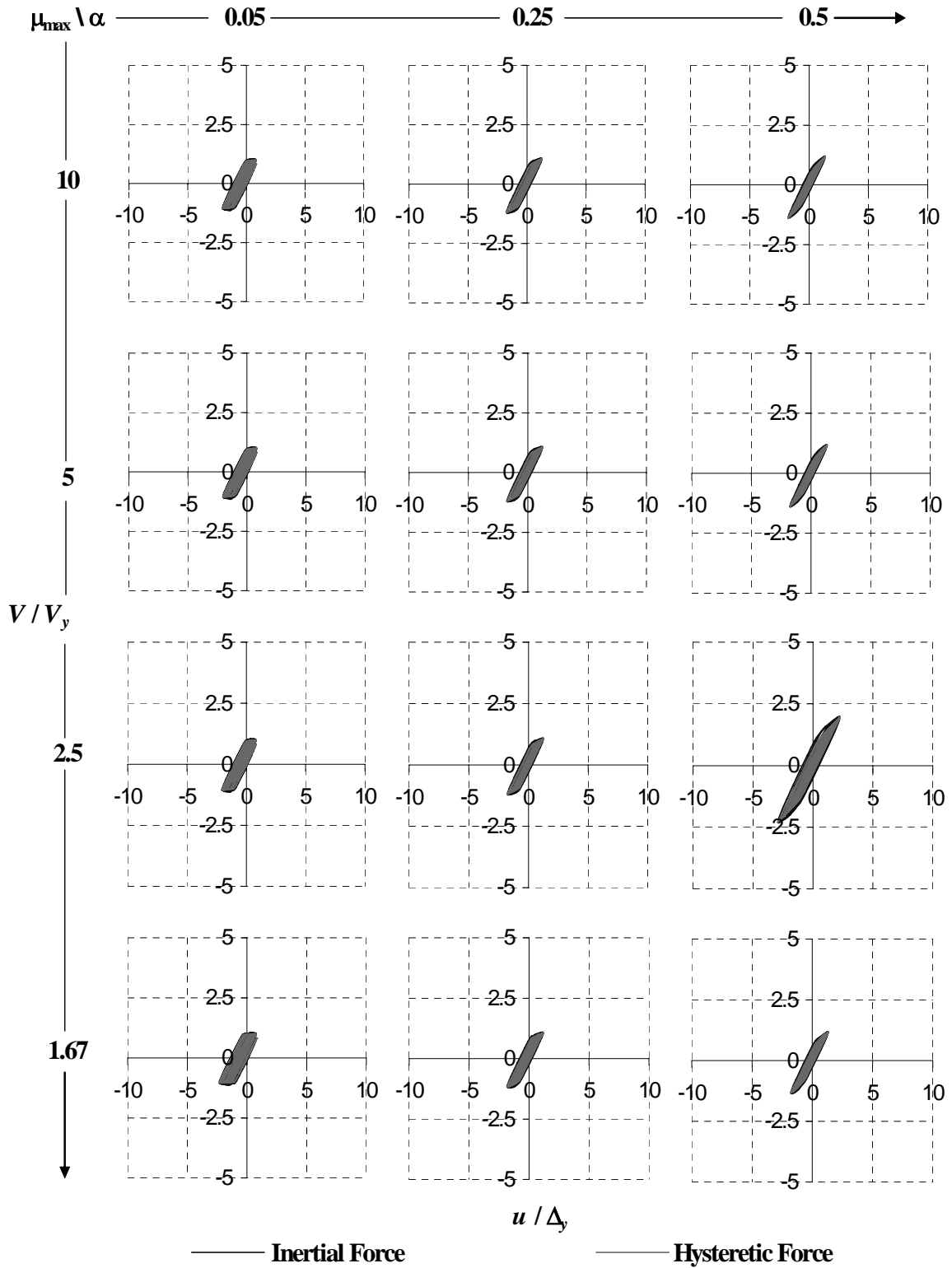


Figure 6.28. Normalized Inertial and Hysteretic Loops for $T = 0.50$ s, $\eta = 1.0$, and 5% of Viscous Damping

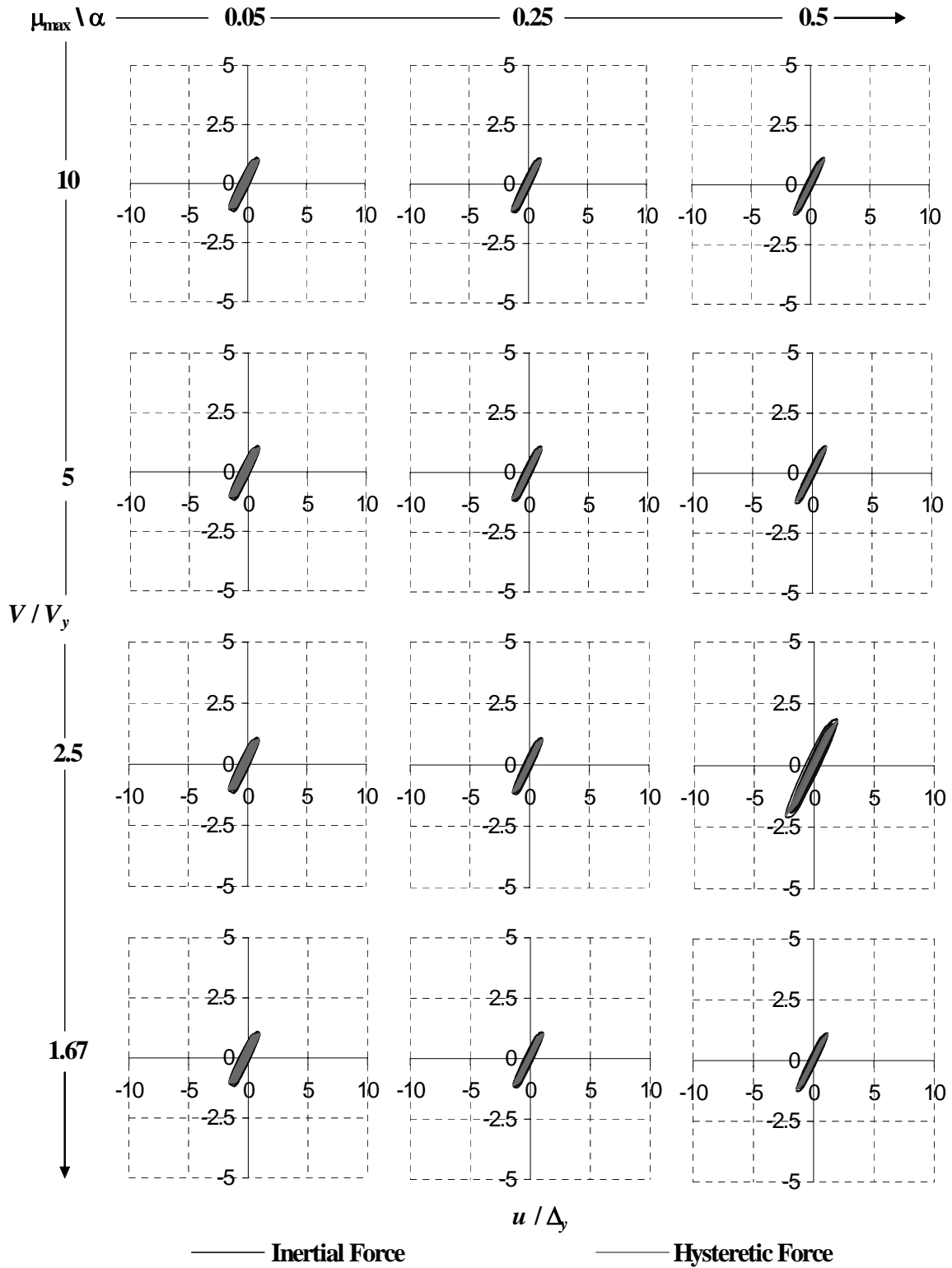


Figure 6.29. Normalized Inertial and Hysteretic Loops for $T = 0.50$ s, $\eta = 1.0$, and 10% of Viscous Damping

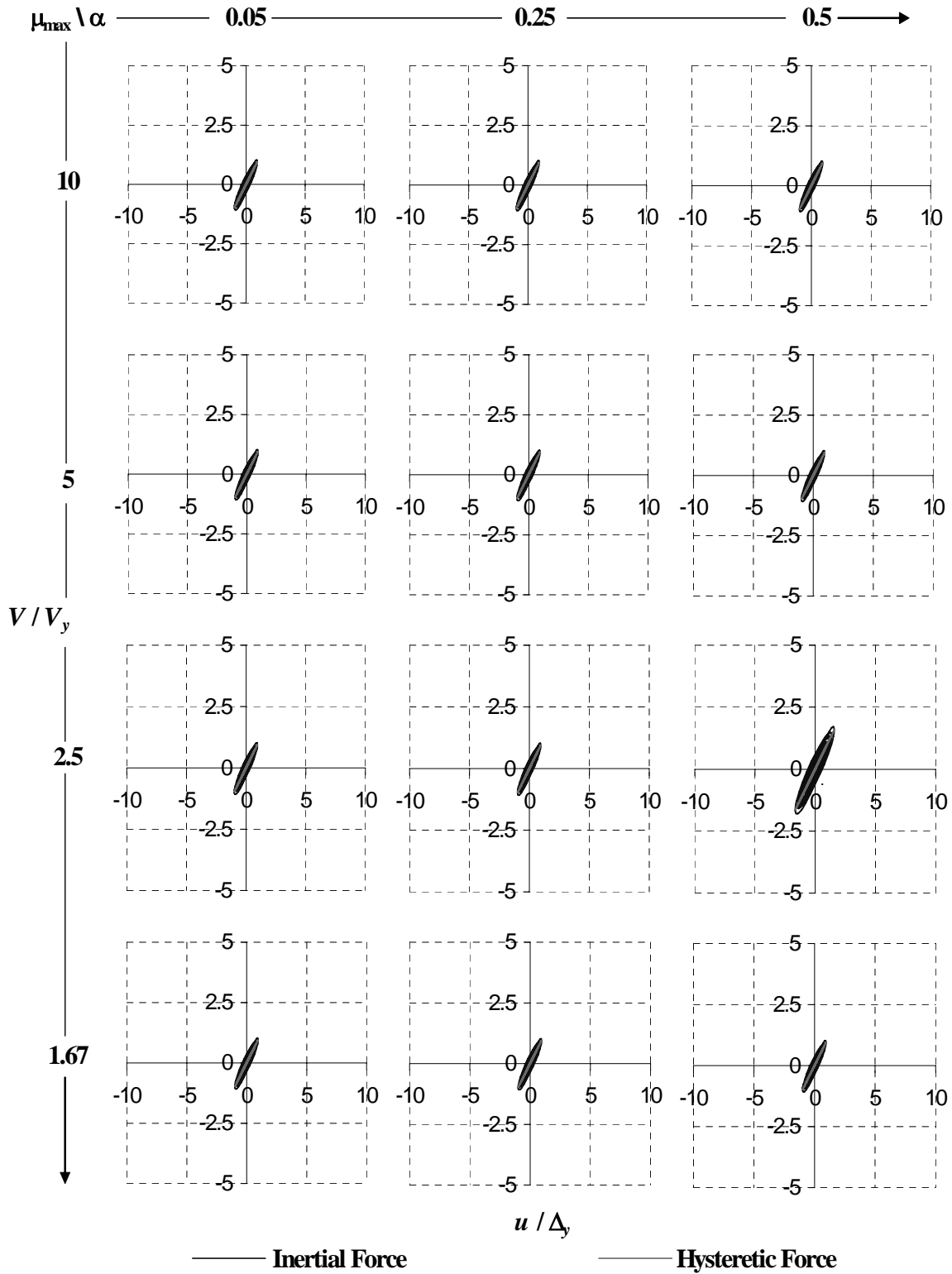


Figure 6.30. Normalized Inertial and Hysteretic Loops for $T = 0.50$ s, $\eta = 1.0$, and 20% of Viscous Damping

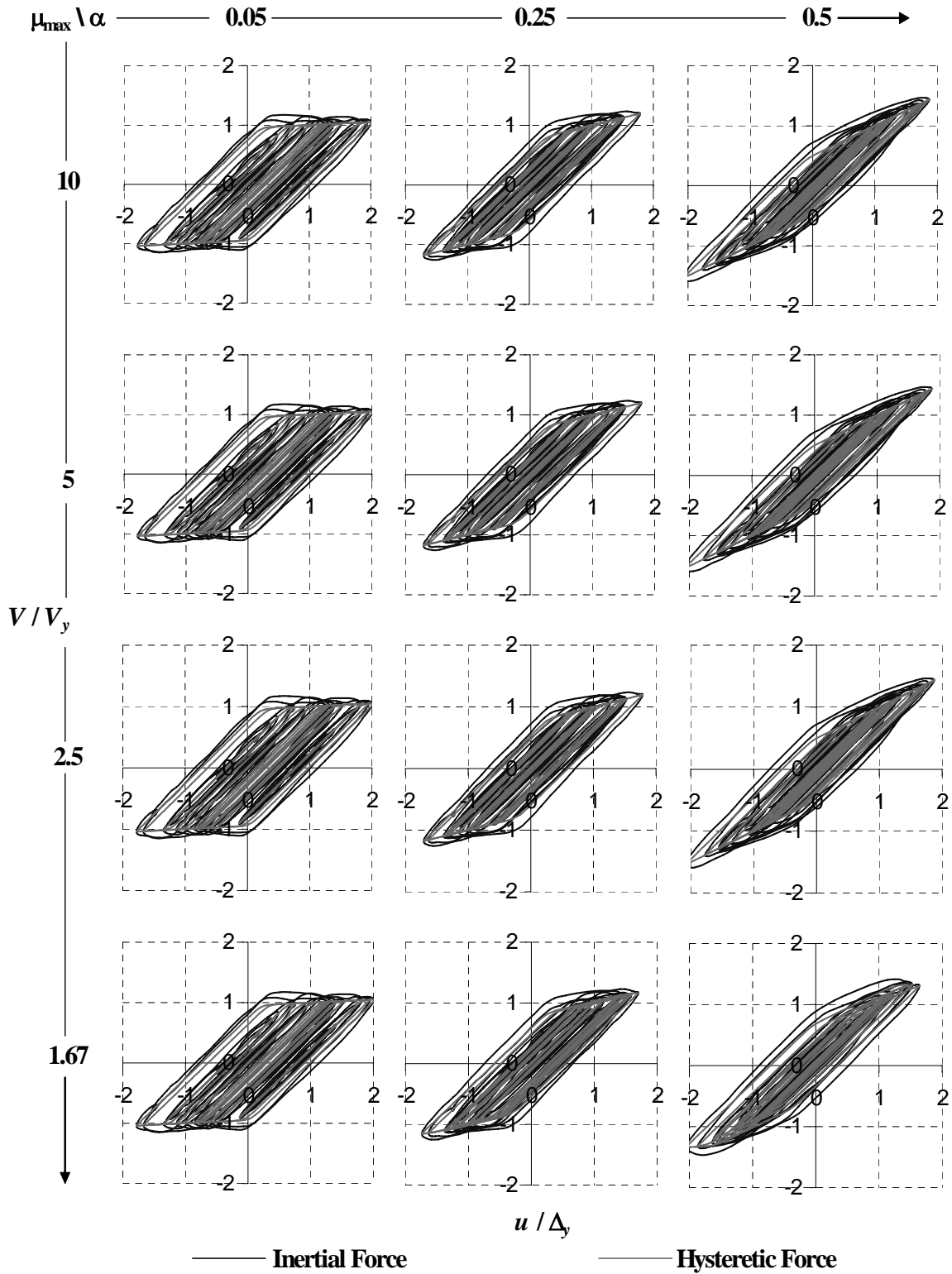


Figure 6.32. Normalized Inertial and Hysteretic Loops for $T = 1.50$ s, $\eta = 0.2$, and 5% of Viscous Damping

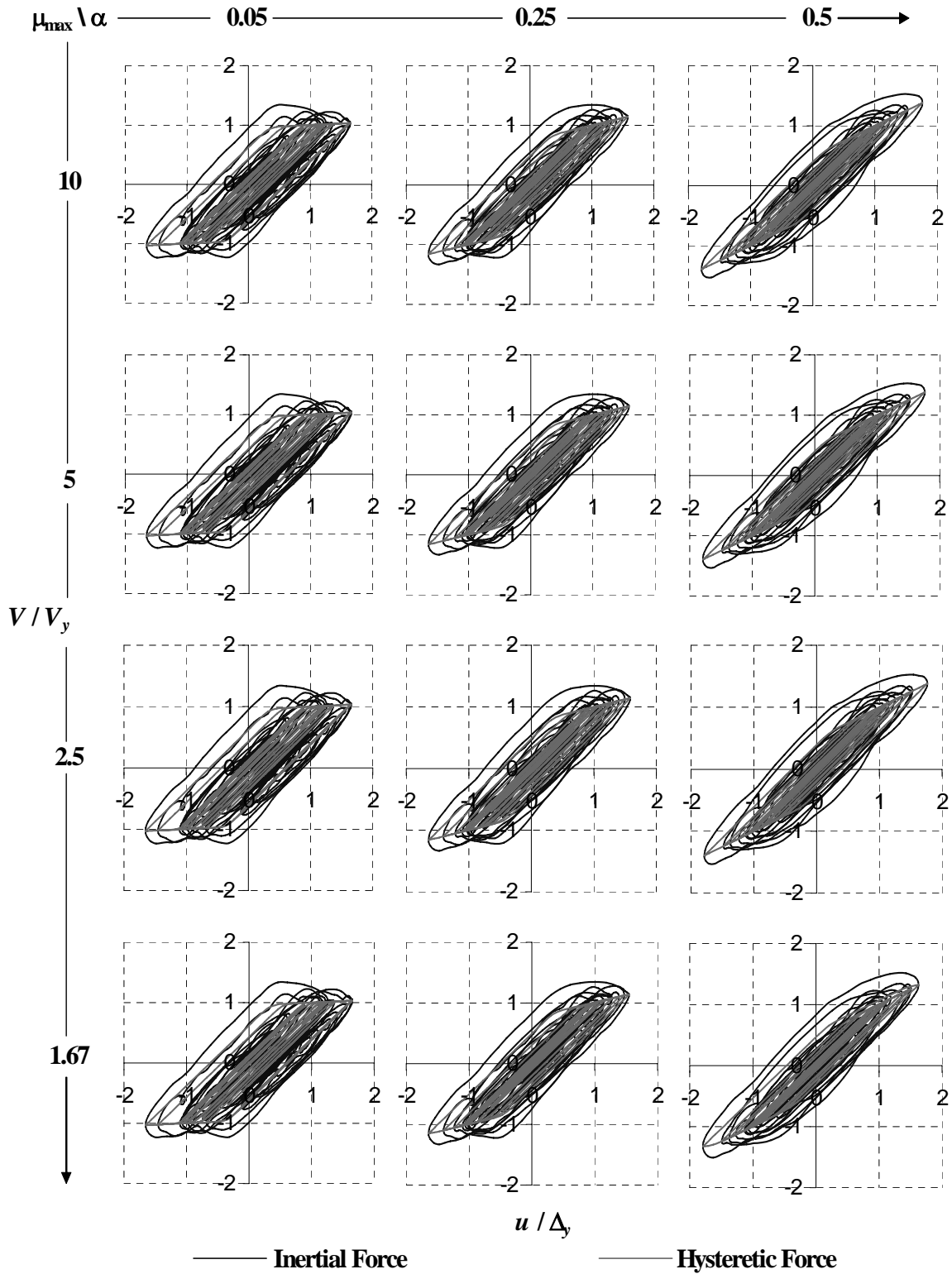


Figure 6.33. Normalized Inertial and Hysteretic Loops for $T = 1.50$ s, $\eta = 0.2$, and 10% of Viscous Damping

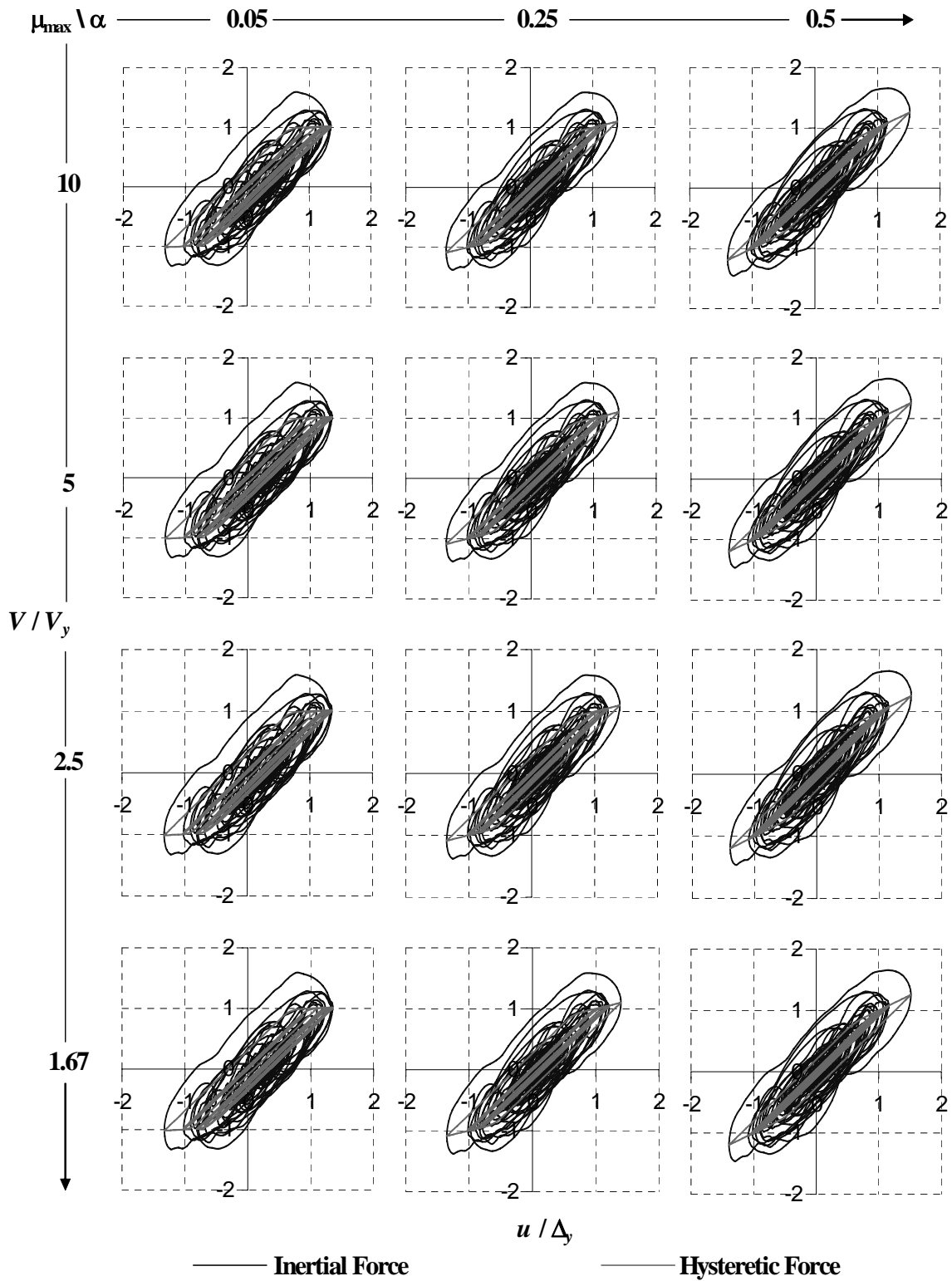


Figure 6.34. Normalized Inertial and Hysteretic Loops for $T = 1.50$ s, $\eta = 0.2$, and 20% of Viscous Damping

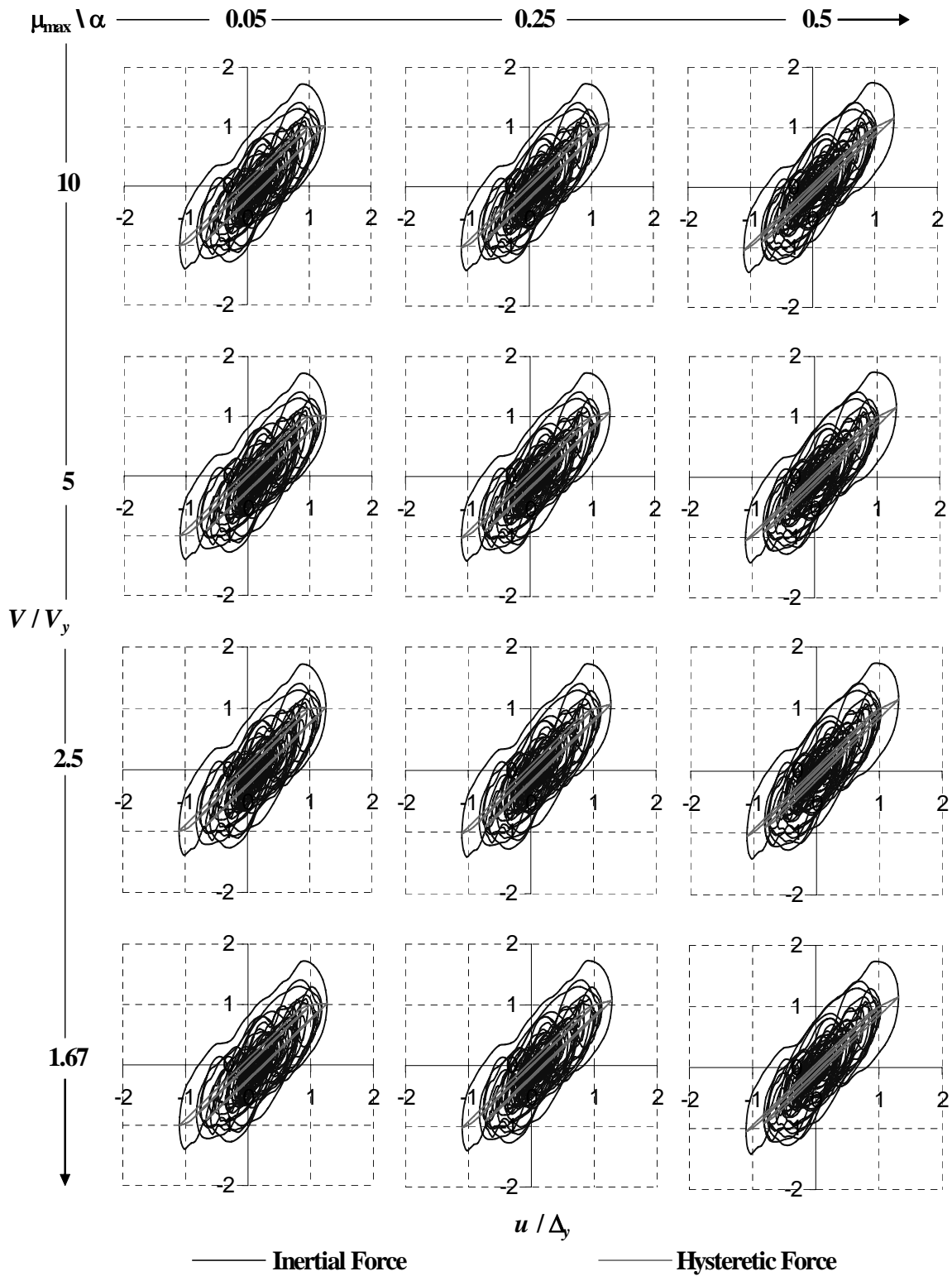


Figure 6.35. Normalized Inertial and Hysteretic Loops for $T = 1.50$ s, $\eta = 0.2$, and 30% of Viscous Damping

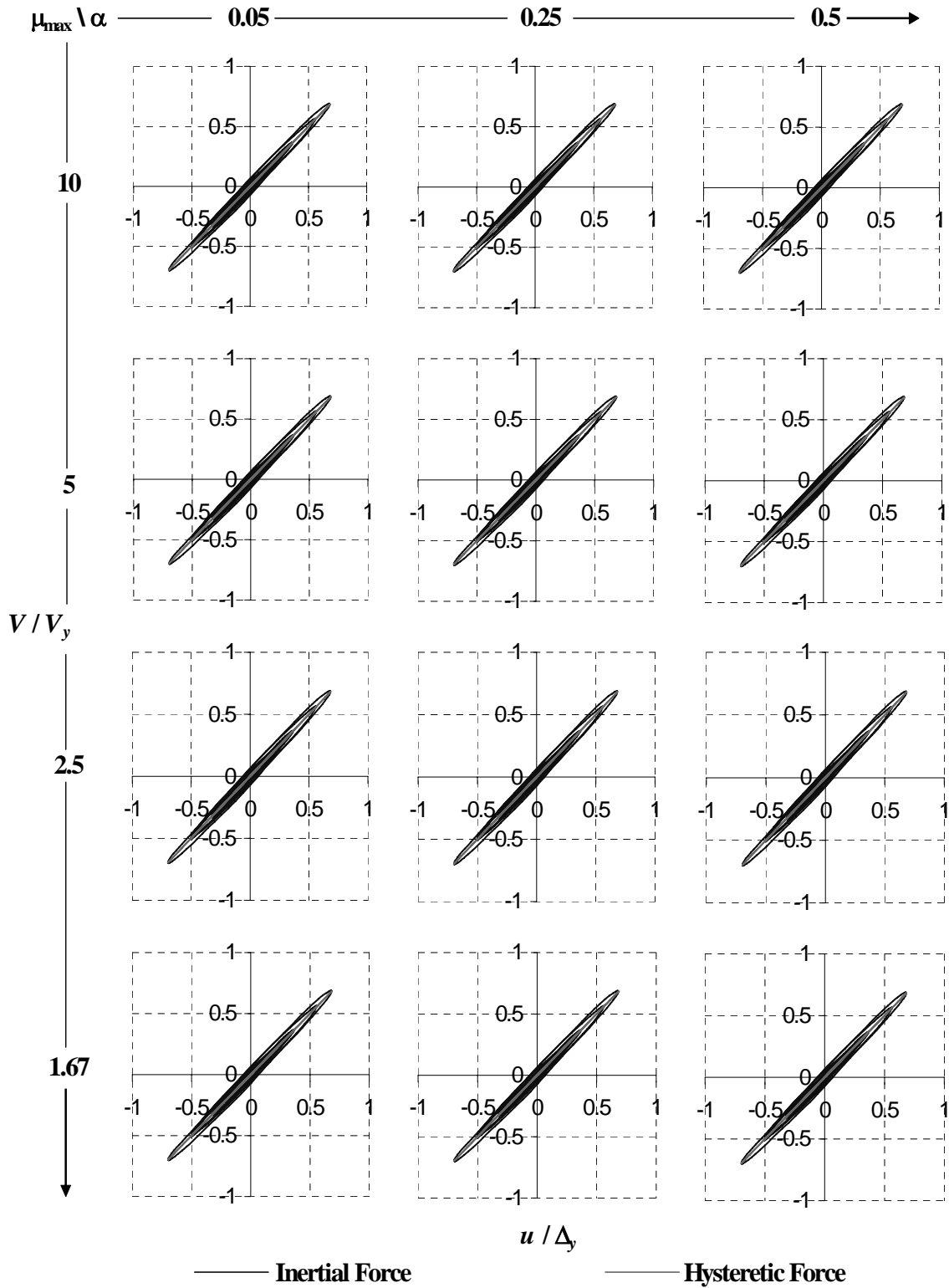


Figure 6.36. Normalized Inertial and Hysteretic Loops for $T = 1.50$ s, $\eta = 1.0$, and 5% of Viscous Damping

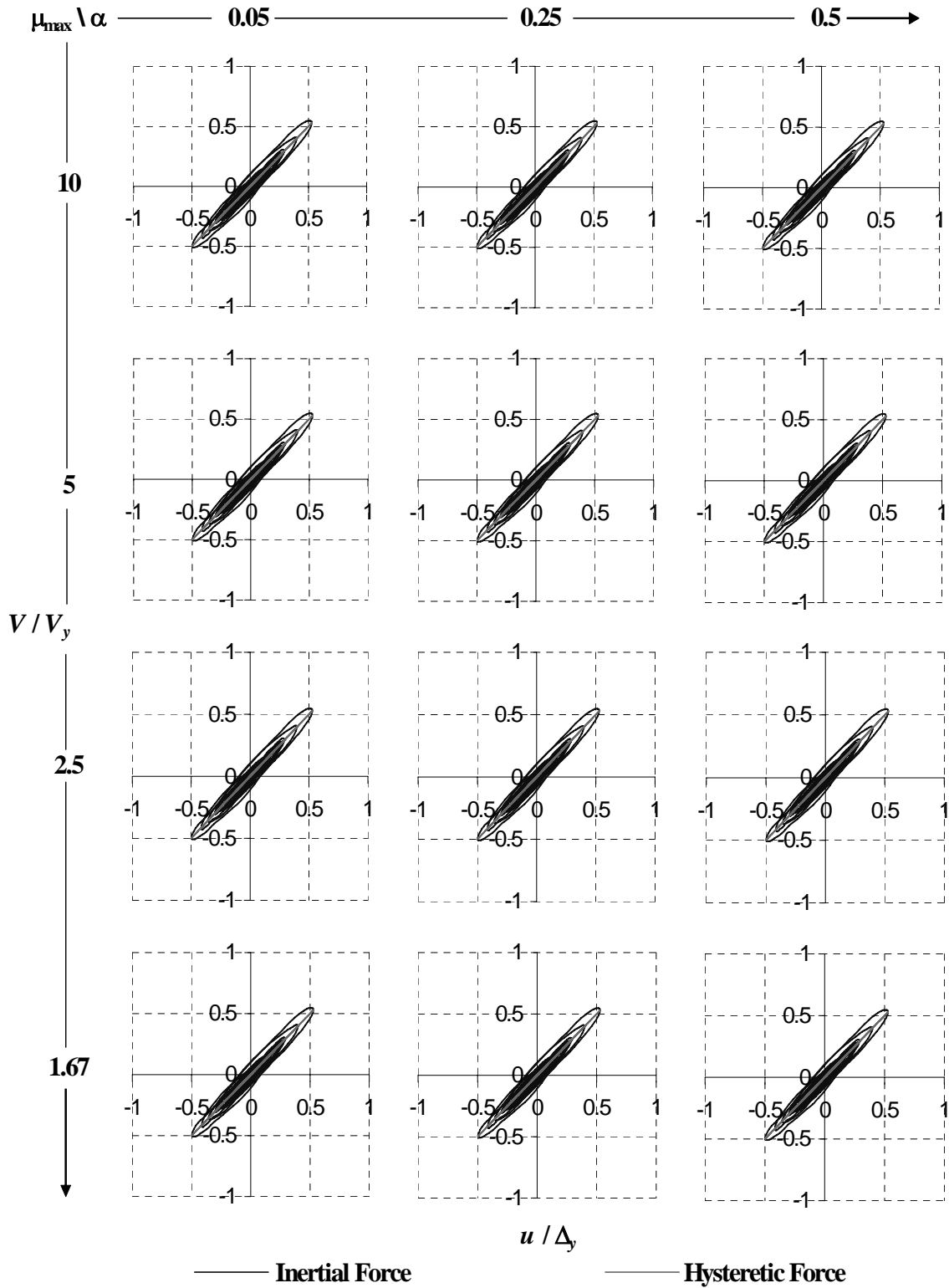


Figure 6.37. Normalized Inertial and Hysteretic Loops for $T = 1.50$ s, $\eta = 1.0$, and 10% of Viscous Damping

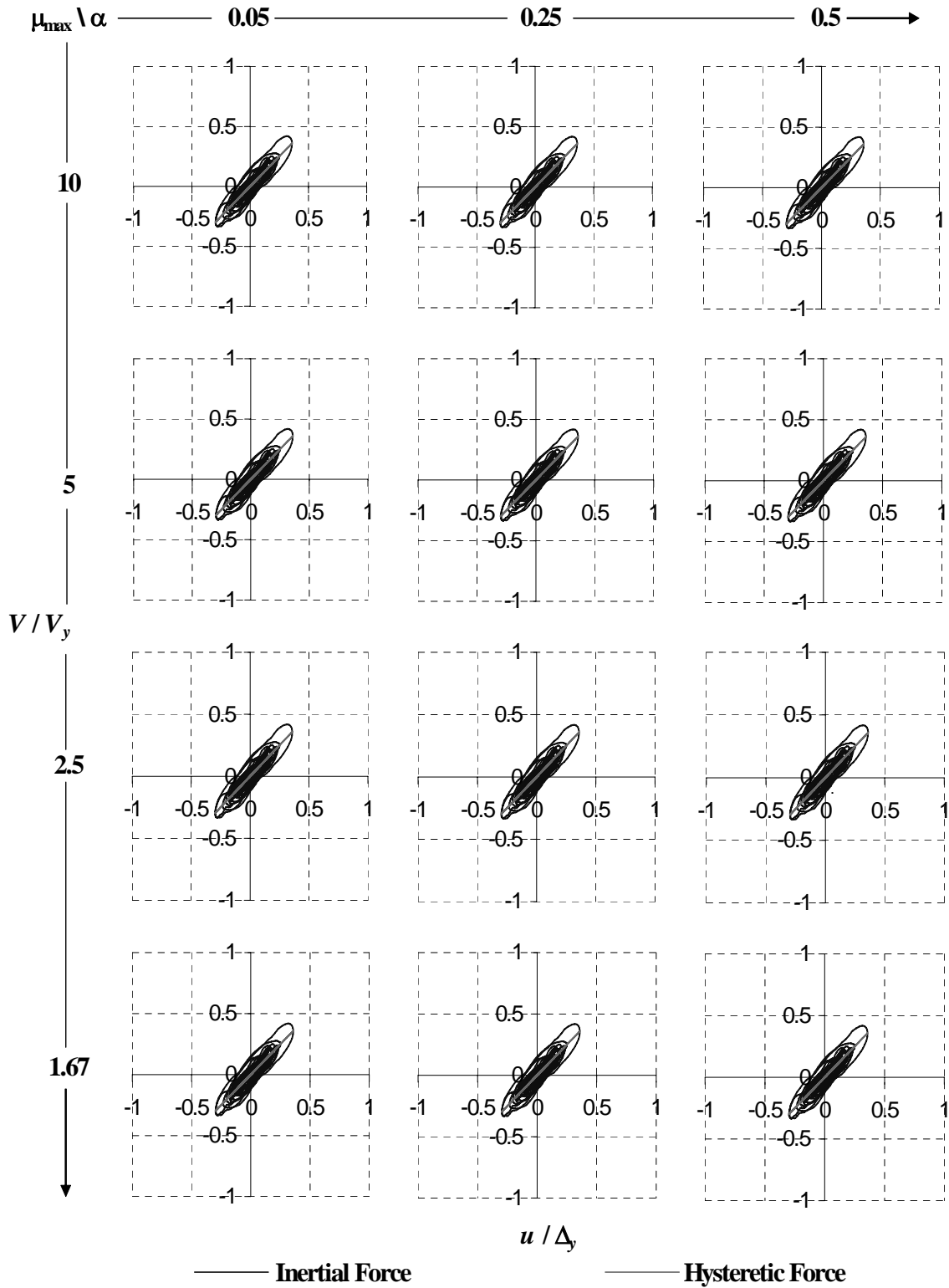


Figure 6.38. Normalized Inertial and Hysteretic Loops for $T = 1.50$ s, $\eta = 1.0$, and 20% of Viscous Damping

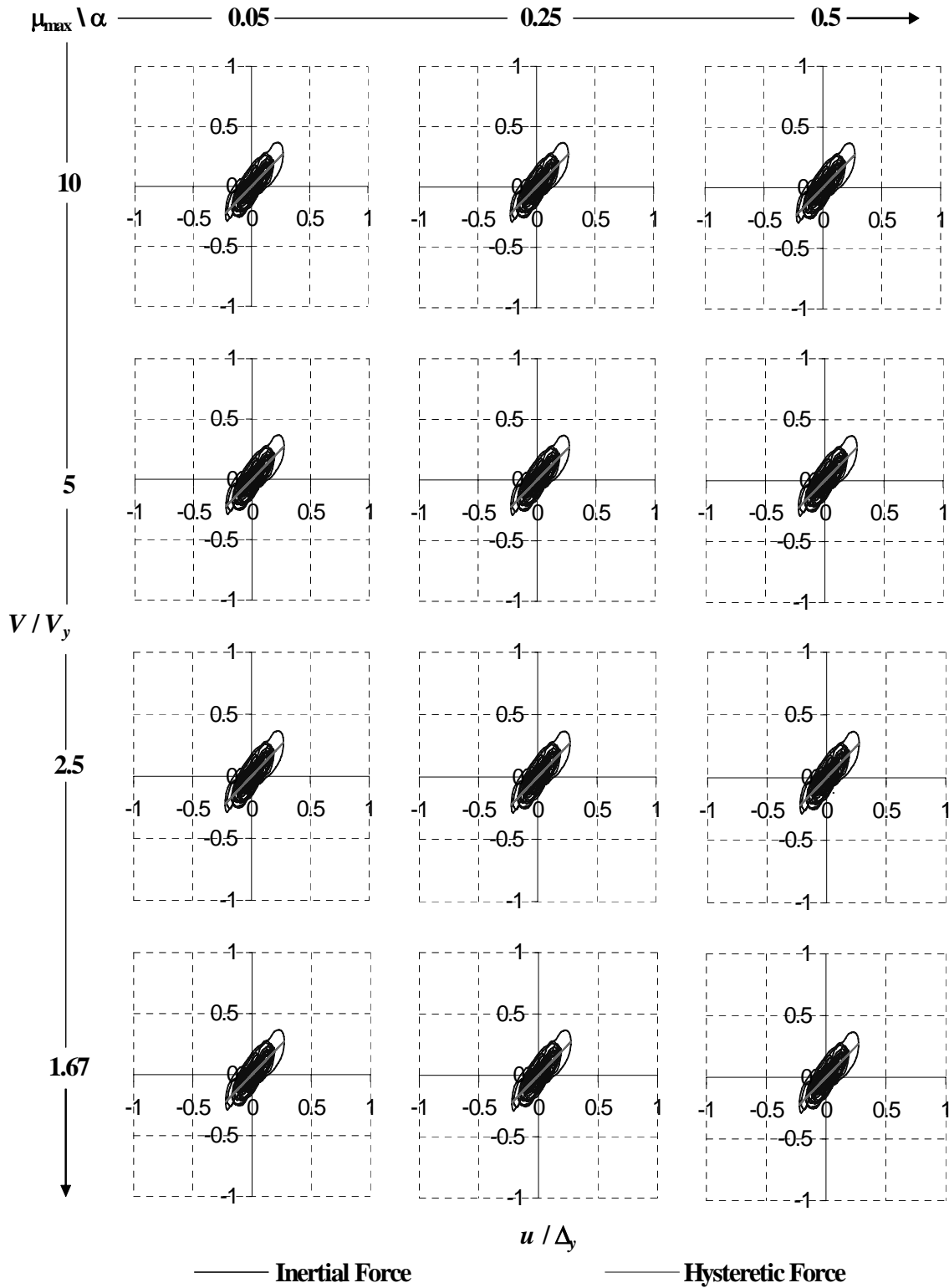


Figure 6.39. Normalized Inertial and Hysteretic Loops for $T = 1.50$ s, $\eta = 1.0$, and 30% of Viscous Damping

6.6. Analysis in the Frequency Domain

An alternative approach is proposed here to explain the observed accelerations on inelastic systems with viscous damping devices. Results from the systems studied in Section 6.4 are analyzed in this section in the frequency domain. Using the Fast Fourier Transform (FFT) algorithm (Cooley and Tukey, 1965), response of the systems studied parametrically here were transformed from the time domain to the frequency domain, in which inertial, viscous damper, and hysteretic forces can be represented as rotational vectors in the complex plane, as schematically shown in Figure 6.40 (a.k.a. Argand diagrams (Clough and Penzien, 1993)). Figure 6.40a shows a representation of the equation of motion (see (6.10)) at a particular time during the earthquake time history. Note that the inertial force is the resultant from the ground motion component, $m\ddot{u}_g$, and the component associated with the system response, $m\ddot{u}$. Figure 6.40b shows that the inertial force is equal to the resultant of the viscous damper and the hysteretic forces. In Figure 6.40c, it may be seen that the forces from the equation of motion form a closed polygon of vectors, in which dynamic equilibrium must be satisfied at every particular time. It is important to note that the frequency domain analysis is an exact method for linear systems subjected to harmonic loads (Clough and Penzien, 1993). However, in this particular study, the frequency domain analysis was used as an approximation to the response because of the inelastic behavior of the system and the random characteristics of the excitation. Despite this, it was observed that the method produced reasonable estimations of the response in the frequency domain.

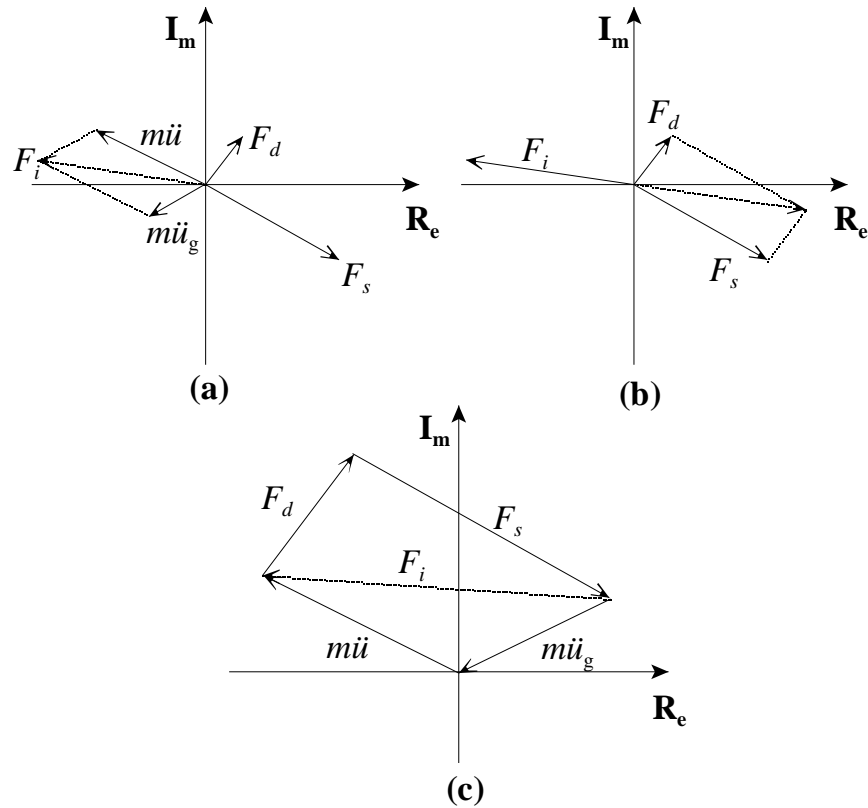


Figure 6.40. Schematic Representation of Inertial, Viscous Damper, and Hysteretic Forces: (a) Inertial Force Components; (b) Dynamic Equilibrium; (c) Polygon of Forces

Based on the schematic representation depicted in Figure 6.40b, results on Argand Diagrams are shown in Figures 6.41 to 6.64, for systems with $T = 0.25$ s, 0.50 s, and 1.50 s; $\eta = 0.2$, and 1.0; and viscous damping of 5%, 10%, 20%, and 30%. Every plot corresponds to the maximum value of inertial force obtained during the time history of response, along with the corresponding viscous and hysteretic forces at that particular time. All the forces are normalized with respect to the inertial force (i.e., inertial force is plotted as an unitary vector, and viscous and hysteretic forces are represented as fractions of the inertial force), and the results from the frequency domain analysis were used to determine the orientation of the vectors in the complex plane.

Note that for small viscous damping (i.e., 5%), the inertial force and the hysteretic force are almost equal. On the other hand, for systems with large viscous damping (i.e., 30%),

the inertial force is considerably greater than the hysteretic force. This vectorial addition shows how a greater damping force can lead to the acceleration increases described in the previous section. Incidentally, this observation has been reported by some practitioners that have considered using viscous dampers to retrofit buildings in selective case studies, and have noticed increases in the floor accelerations if the structure remains inelastic after the retrofit, but could not explain why (e.g., personal communication, Dr. Chris Tokas, Manager, California Hospital Seismic Retrofit Program, State of California Office of Statewide Health Planning and Development).

Finally, in Figures 6.65 to 6.70 a comparison is made between the response of a system with 5% of viscous damping (shown as solid lines with the subscript “o” for the forces), and a system with 30% of viscous damping (shown as dashed lines). These results further corroborate and explain the results presented in Section 6.3.

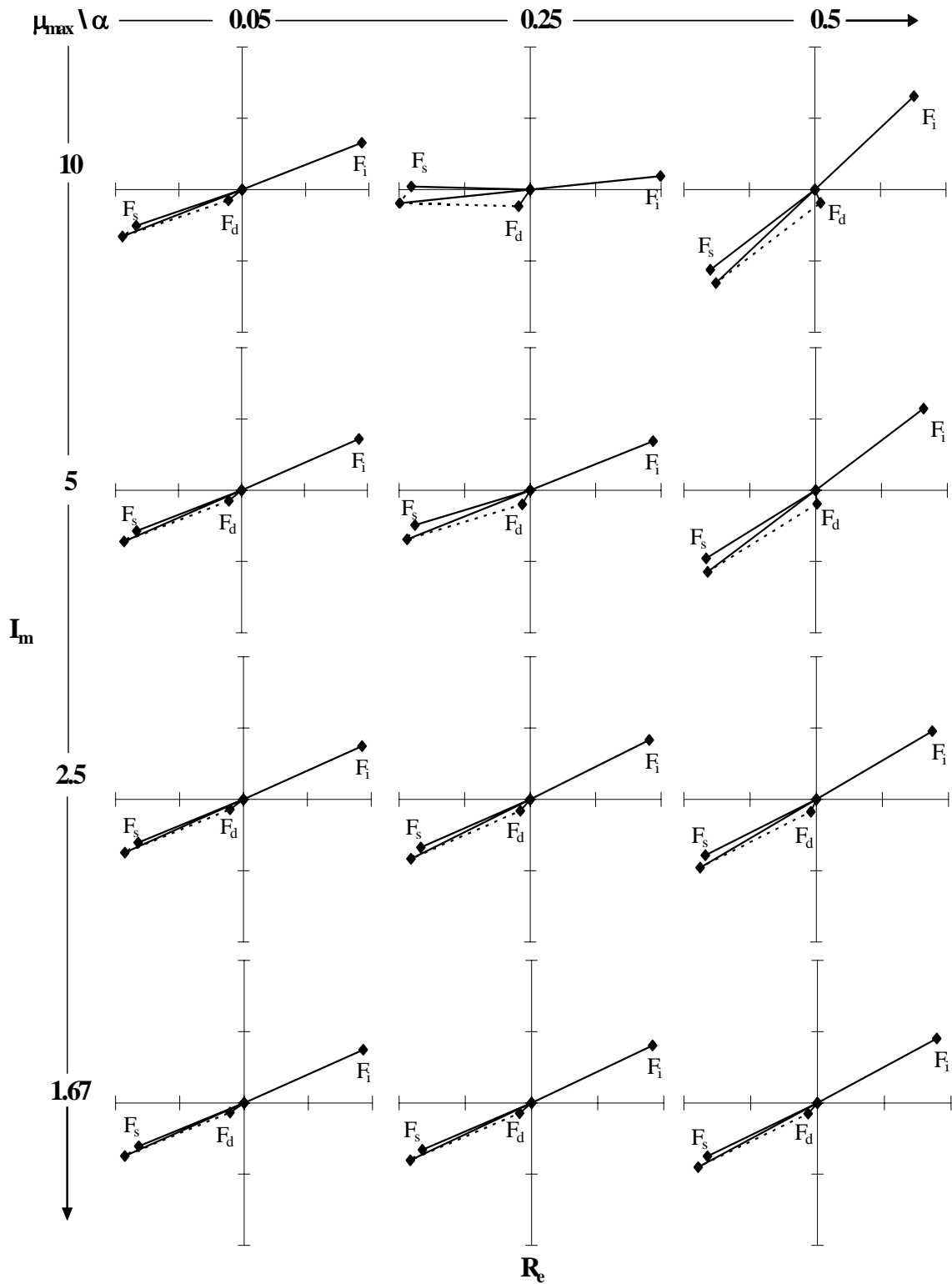


Figure 6.41. Complex Plane Representation of Inertial Force, F_i , Viscous Damper Force, F_d , and Hysteretic Force, F_s , for $T = 0.25$ s, $\eta = 0.2$, and 5% of Viscous Damping

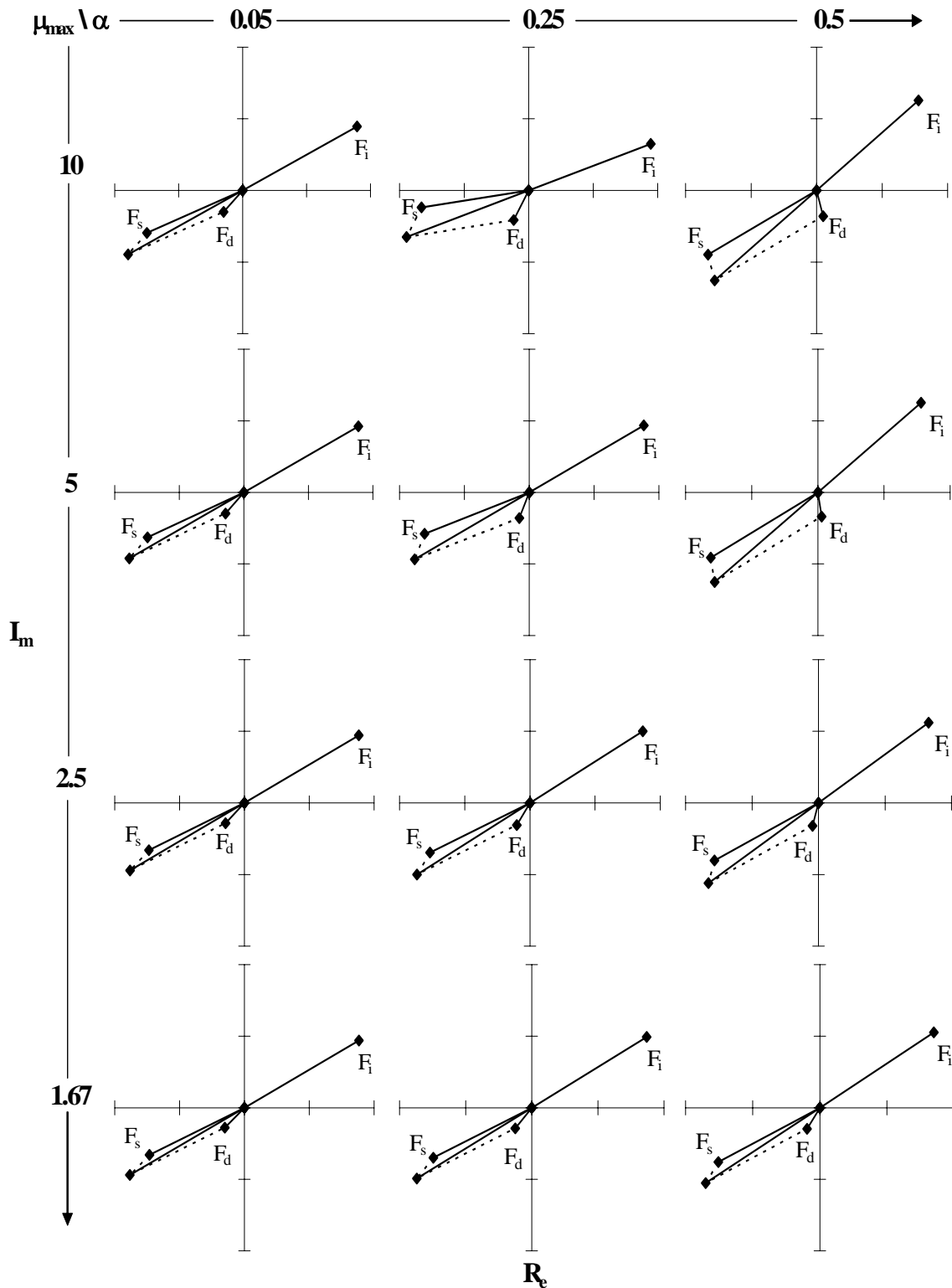


Figure 6.42. Complex Plane Representation of Inertial Force, F_i , Viscous Damper Force, F_d , and Hysteretic Force, F_s , for $T = 0.25$ s, $\eta = 0.2$, and 10% of Viscous Damping

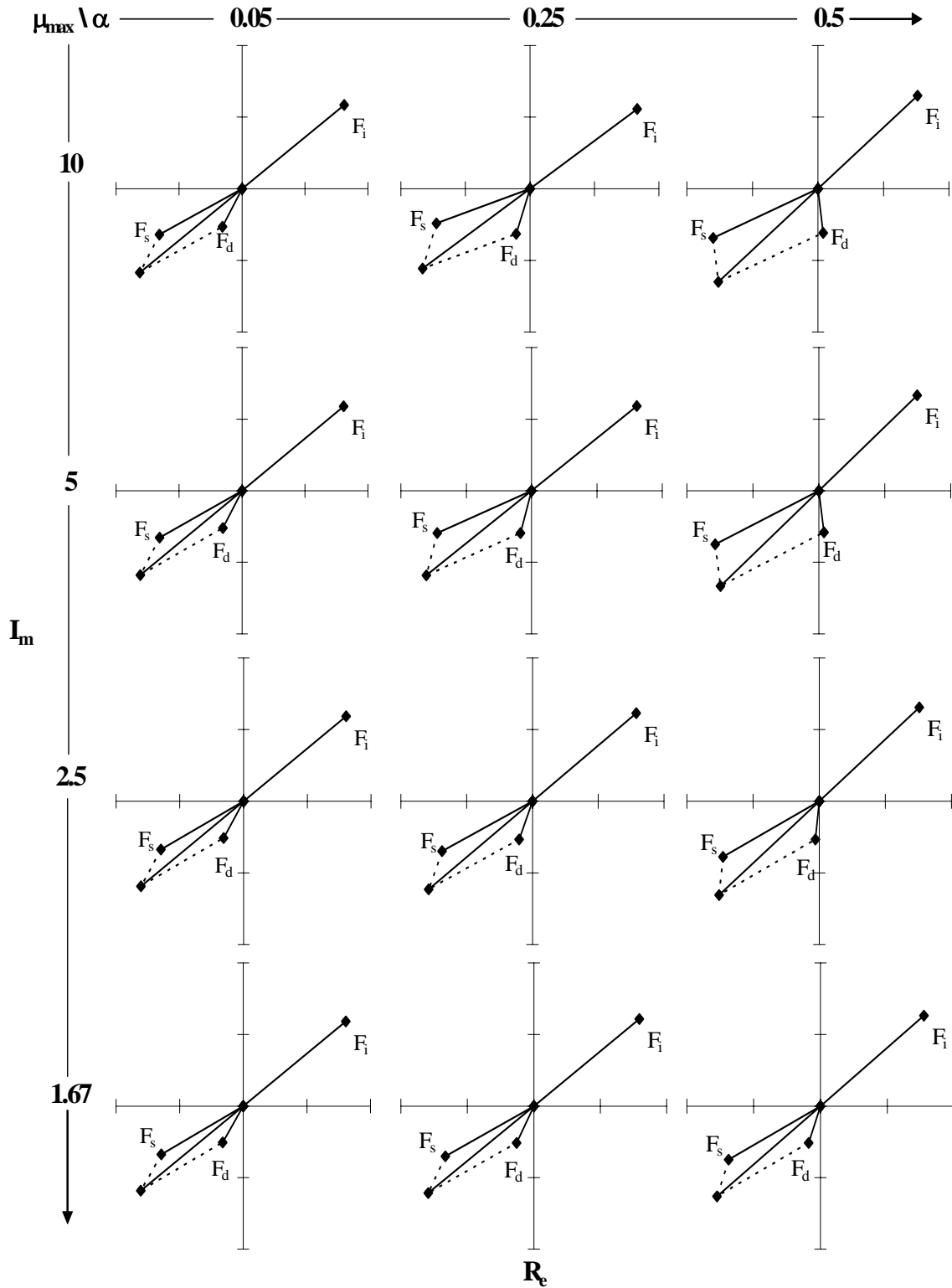


Figure 6.43. Complex Plane Representation of Inertial Force, F_i , Viscous Damper Force, F_d , and Hysteretic Force, F_s , for $T = 0.25$ s, $\eta = 0.2$, and 20% of Viscous Damping

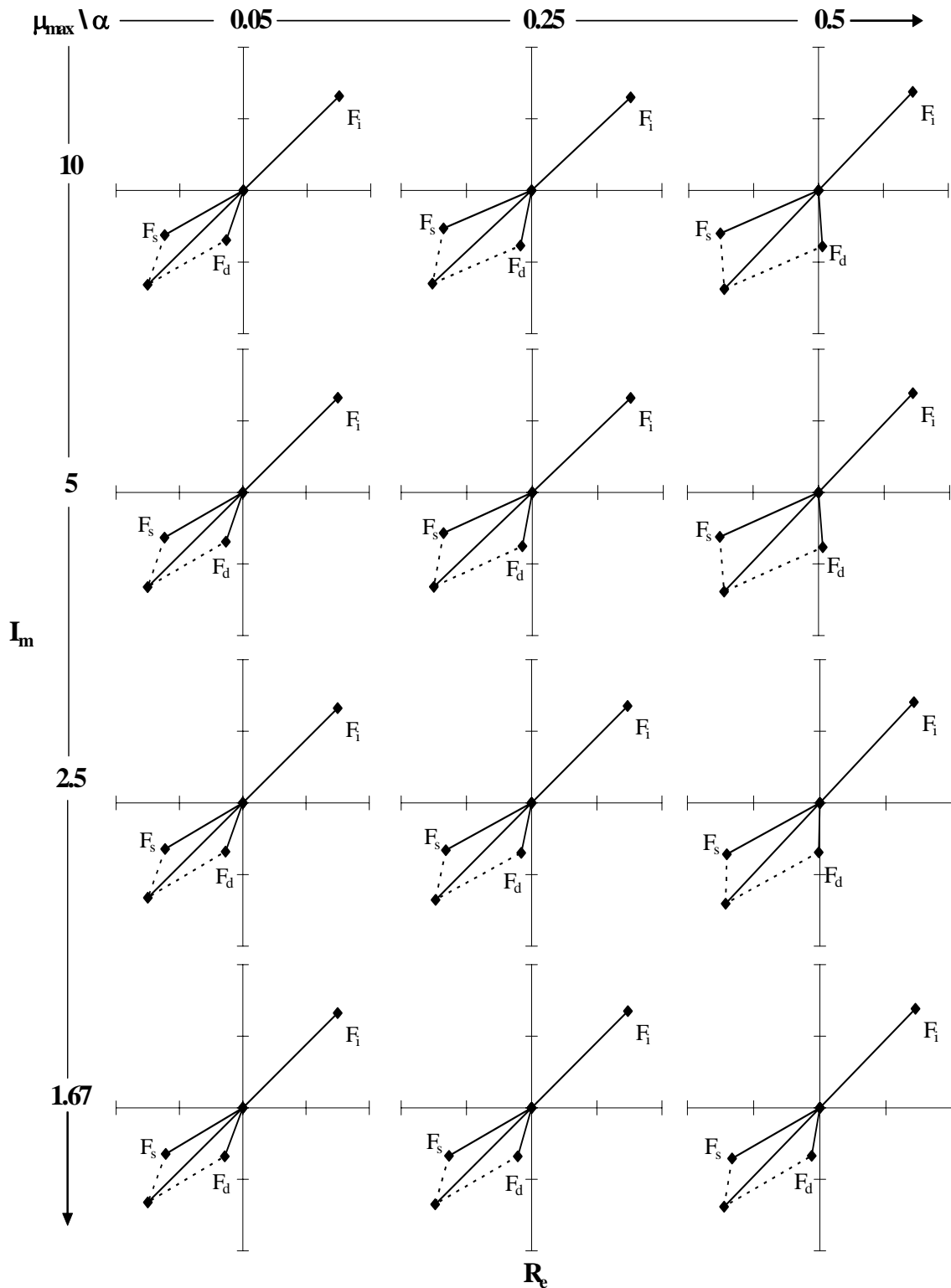


Figure 6.44. Complex Plane Representation of Inertial Force, F_i , Viscous Damper Force, F_d , and Hysteretic Force, F_s , for $T = 0.25$ s, $\eta = 0.2$, and 30% of Viscous Damping

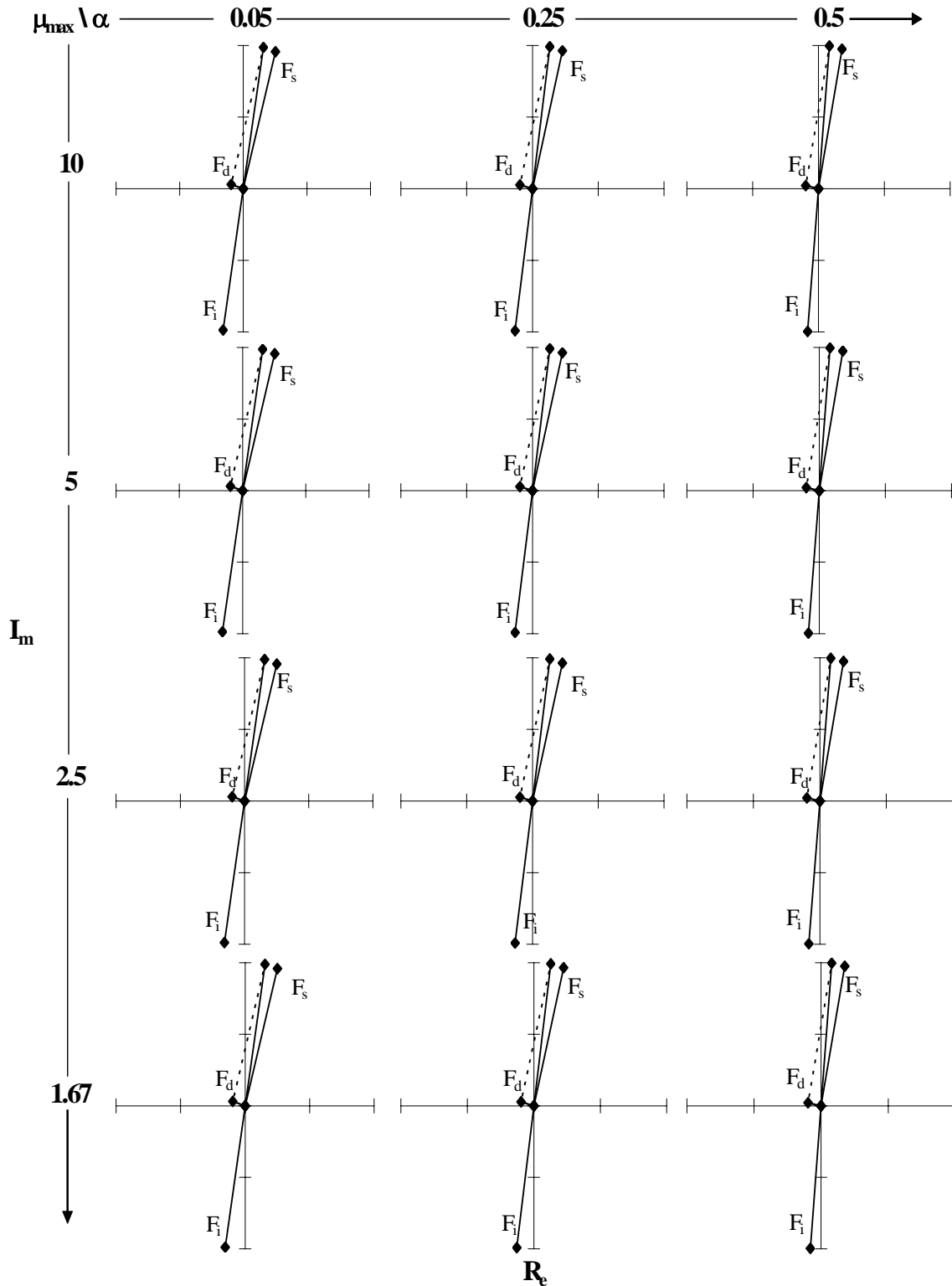


Figure 6.45. Complex Plane Representation of Inertial Force, F_i , Viscous Damper Force, F_d , and Hysteretic Force, F_s , for $T = 0.25$ s, $\eta = 1.0$, and 5% of Viscous Damping

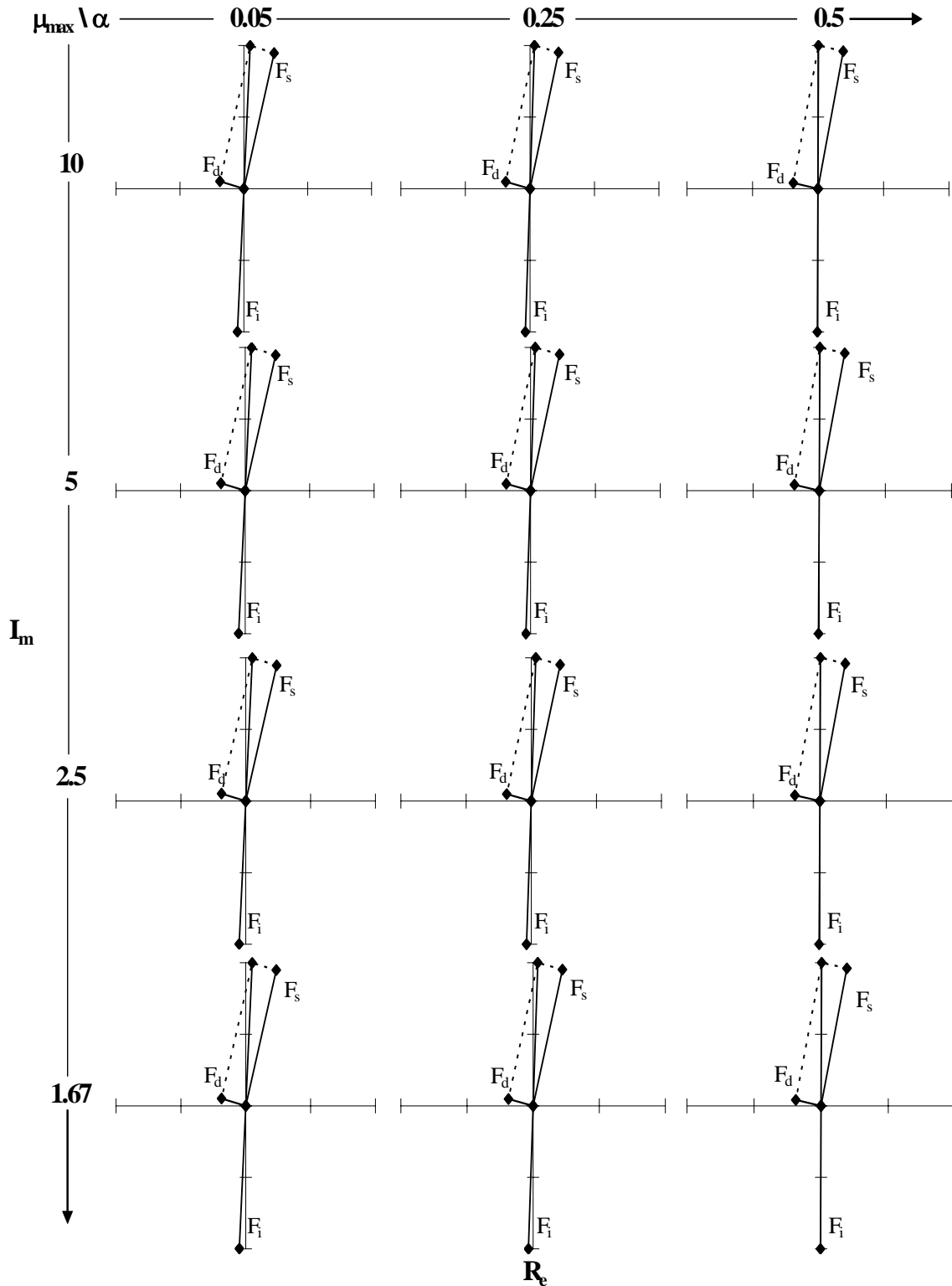


Figure 6.46. Complex Plane Representation of Inertial Force, F_i , Viscous Damper Force, F_d , and Hysteretic Force, F_s , for $T = 0.25$ s, $\eta = 1.0$, and 10% of Viscous Damping

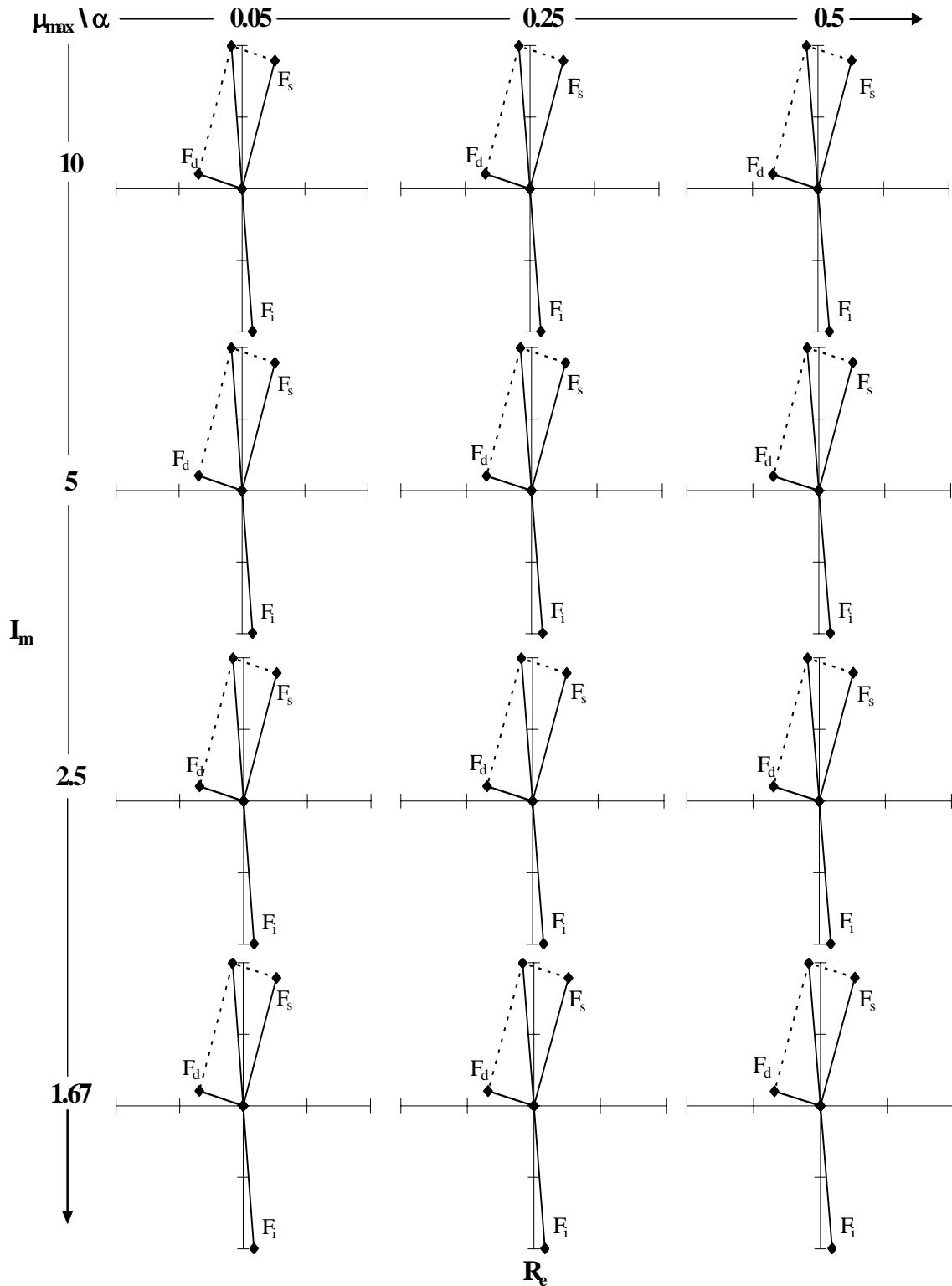


Figure 6.47. Complex Plane Representation of Inertial Force, F_i , Viscous Damper Force, F_d , and Hysteretic Force, F_s , for $T = 0.25$ s, $\eta = 1.0$, and 20% of Viscous Damping

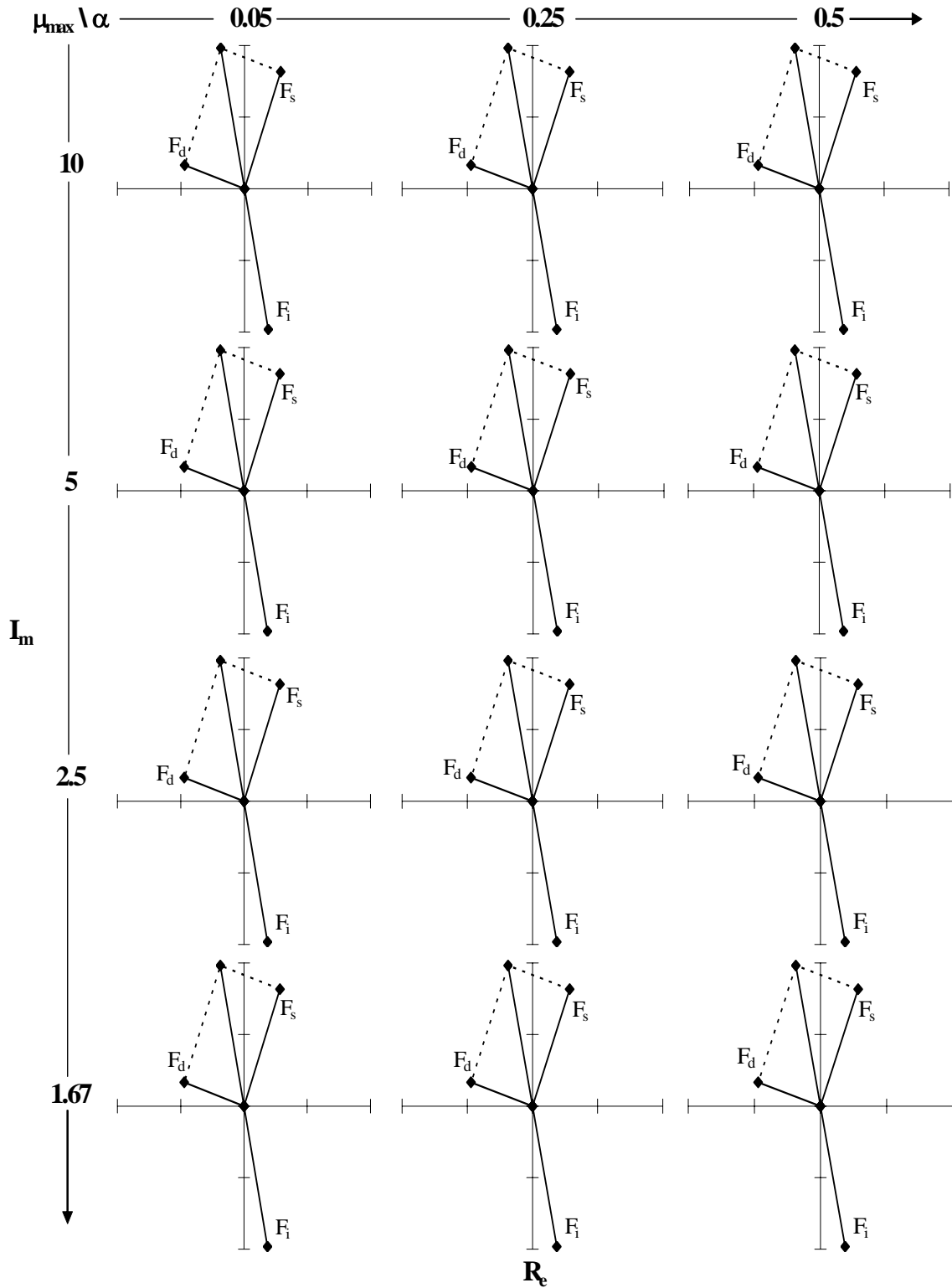


Figure 6.48. Complex Plane Representation of Inertial Force, F_i , Viscous Damper Force, F_d , and Hysteretic Force, F_s , for $T = 0.25$ s, $\eta = 1.0$, and 30% of Viscous Damping

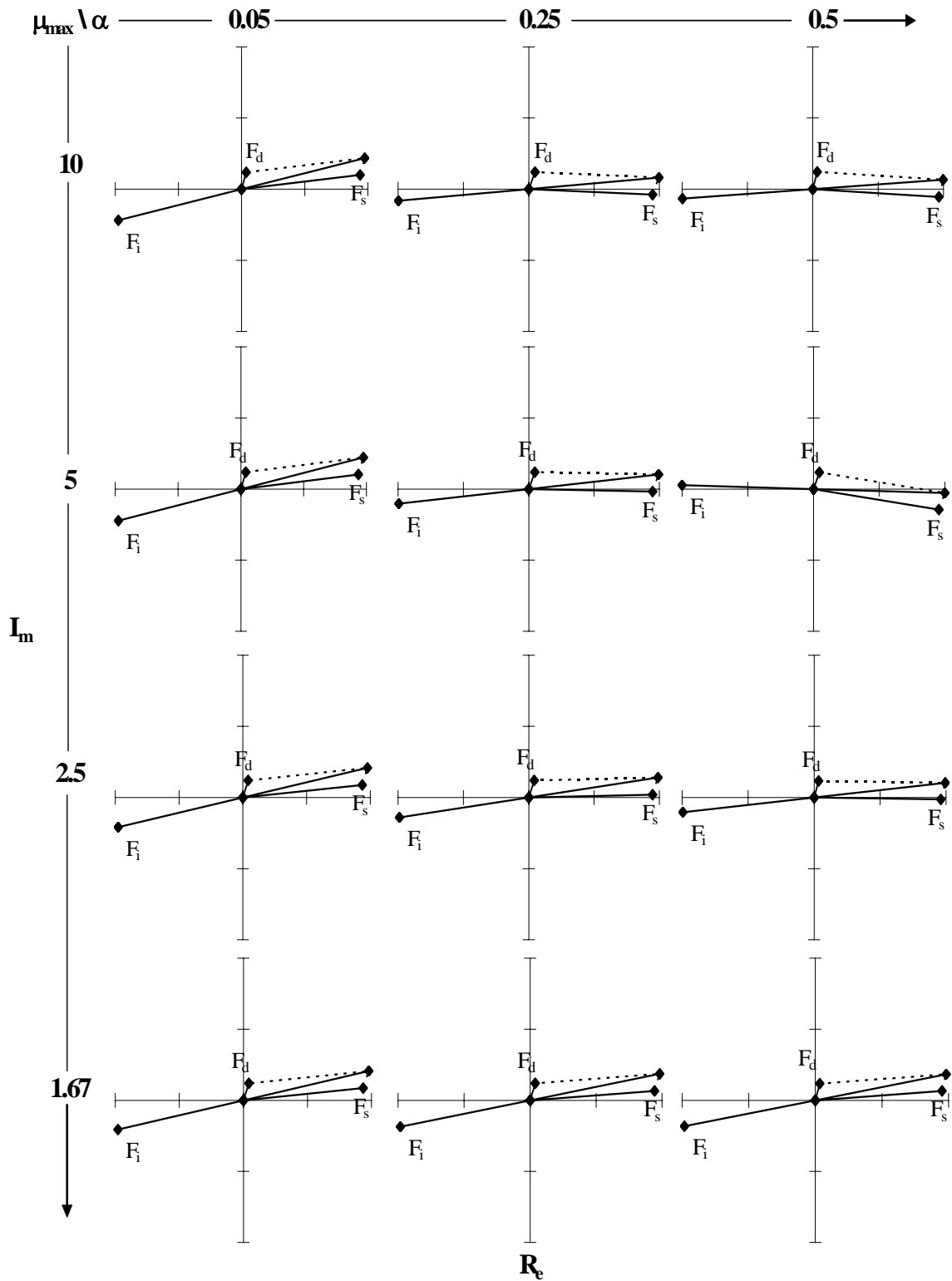


Figure 6.49. Complex Plane Representation of Inertial Force, F_i , Viscous Damper Force, F_d , and Hysteretic Force, F_s , for $T = 0.50$ s, $\eta = 0.2$, and 5% of Viscous Damping

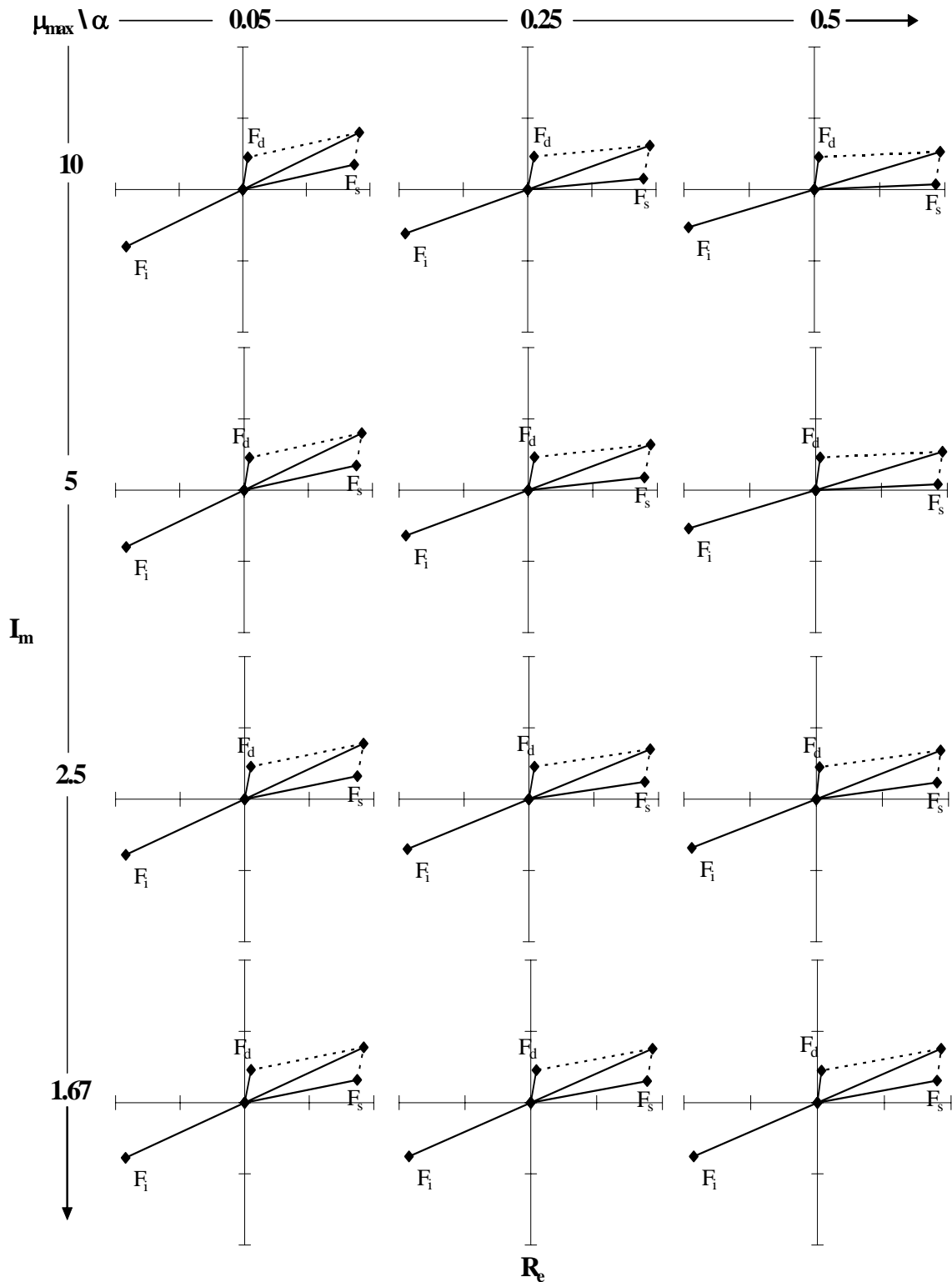


Figure 6.50. Complex Plane Representation of Inertial Force, F_i , Viscous Damper Force, F_d , and Hysteretic Force, F_s , for $T = 0.50$ s, $\eta = 0.2$, and 10% of Viscous Damping

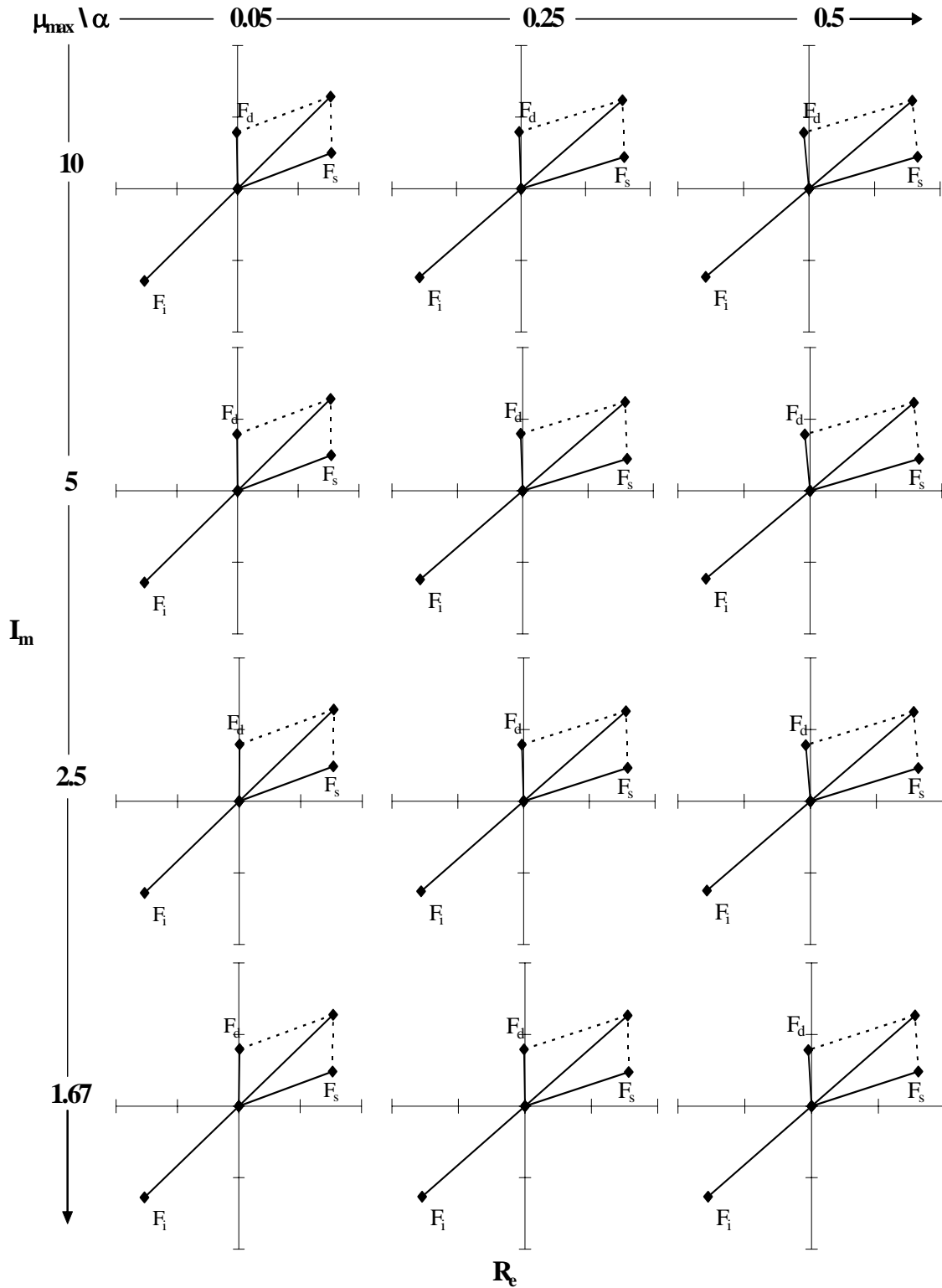


Figure 6.51. Complex Plane Representation of Inertial Force, F_i , Viscous Damper Force, F_d , and Hysteretic Force, F_s , for $T = 0.50$ s, $\eta = 0.2$, and 20% of Viscous Damping

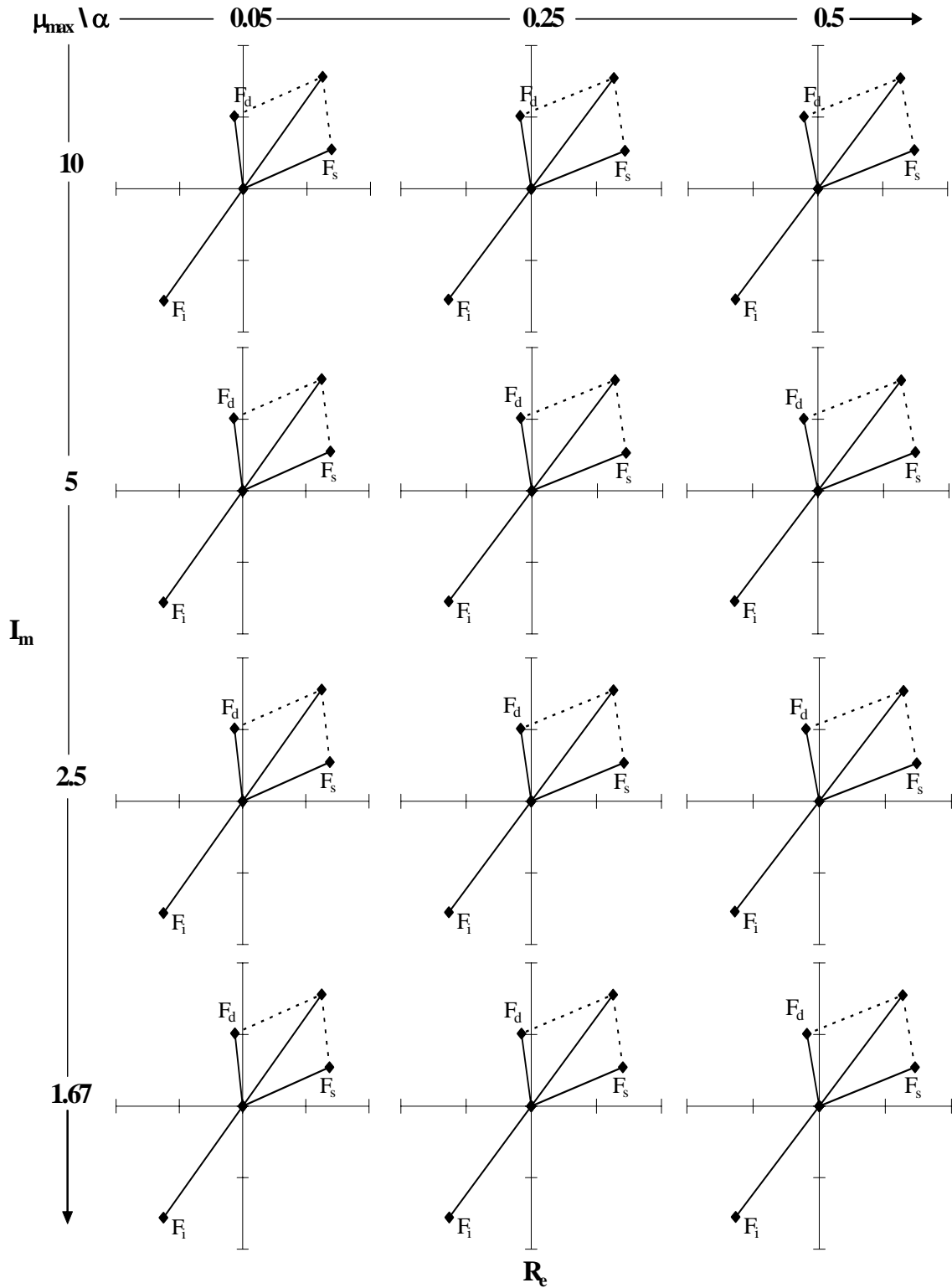


Figure 6.52. Complex Plane Representation of Inertial Force, F_i , Viscous Damper Force, F_d , and Hysteretic Force, F_s , for $T = 0.50$ s, $\eta = 0.2$, and 30% of Viscous Damping

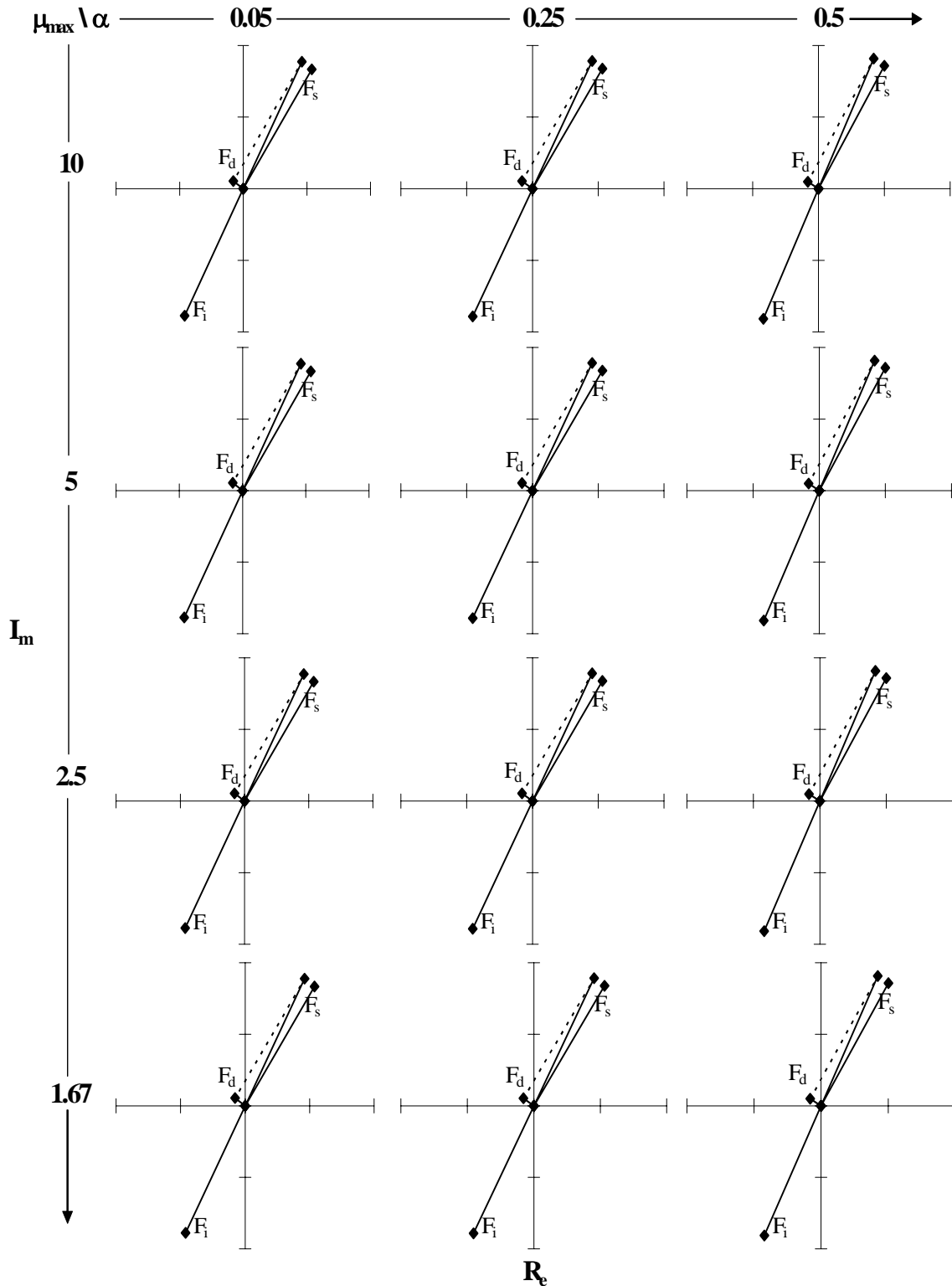


Figure 6.53. Complex Plane Representation of Inertial Force, F_i , Viscous Damper Force, F_d , and Hysteretic Force, F_s , for $T = 0.50$ s, $\eta = 1.0$, and 5% of Viscous Damping

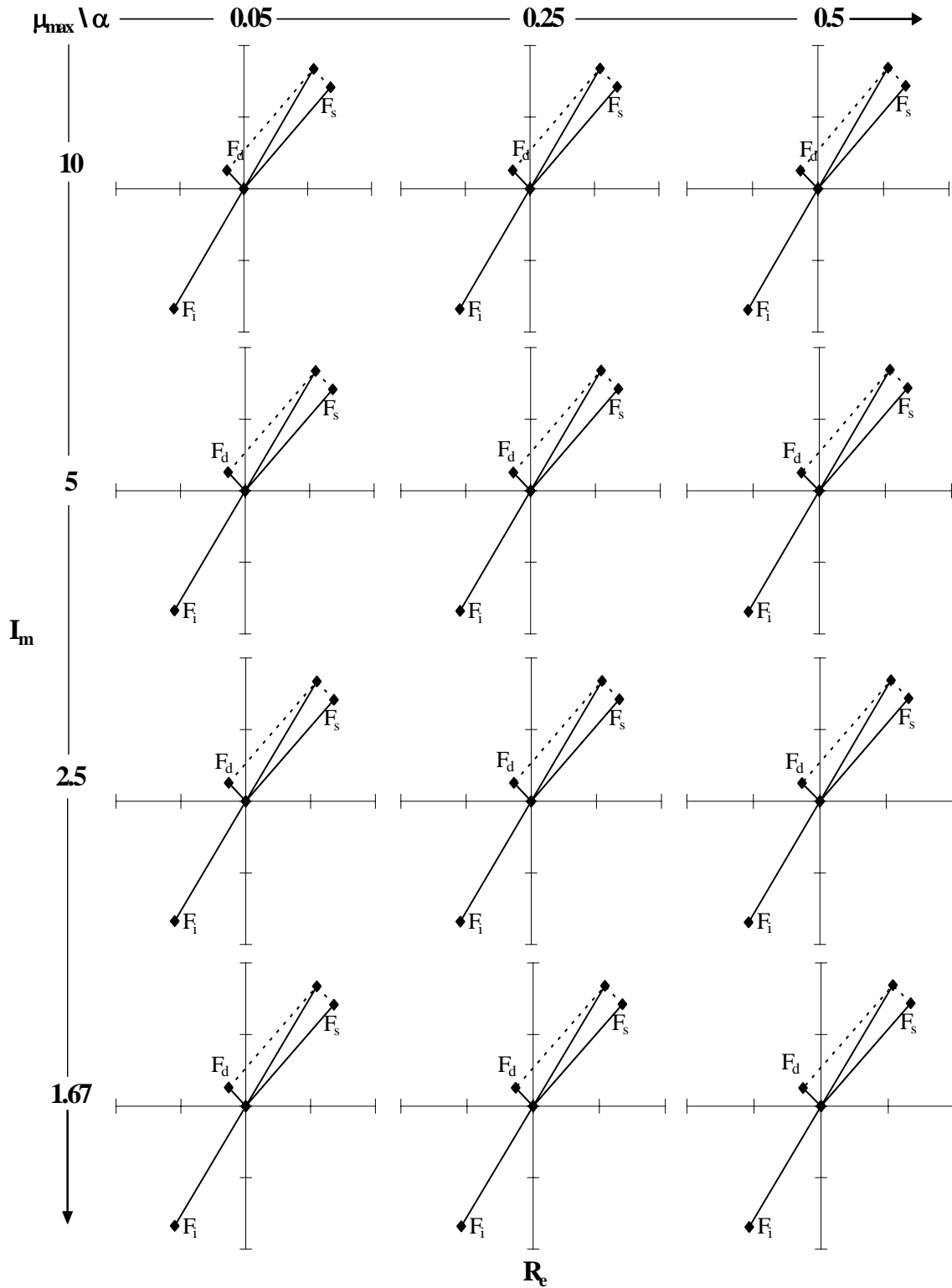


Figure 6.54. Complex Plane Representation of Inertial Force, F_i , Viscous Damper Force, F_d , and Hysteretic Force, F_s , for $T = 0.50$ s, $\eta = 1.0$, and 10% of Viscous Damping

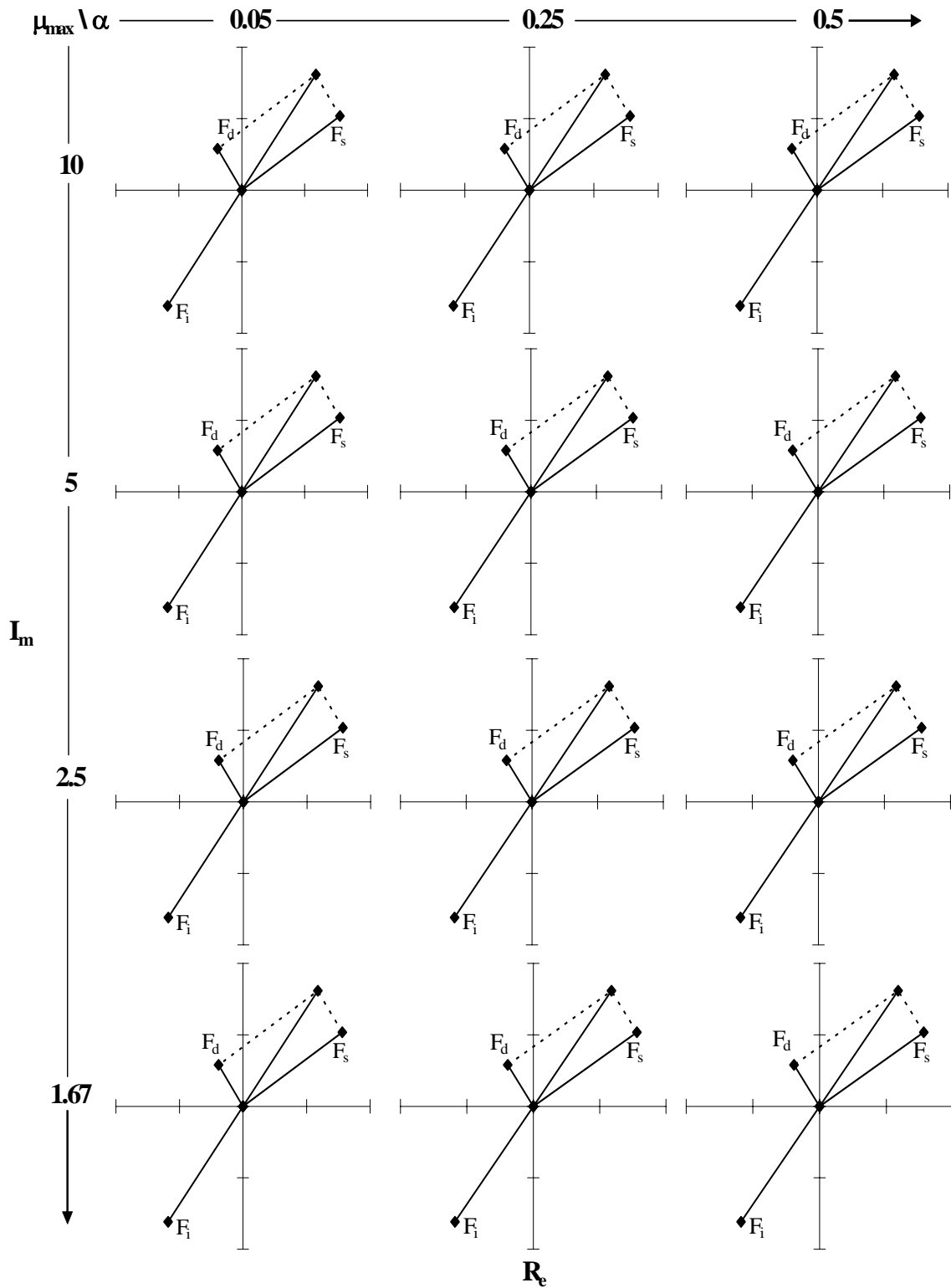


Figure 6.55. Complex Plane Representation of Inertial Force, F_i , Viscous Damper Force, F_d , and Hysteretic Force, F_s , for $T = 0.50$ s, $\eta = 1.0$, and 20% of Viscous Damping

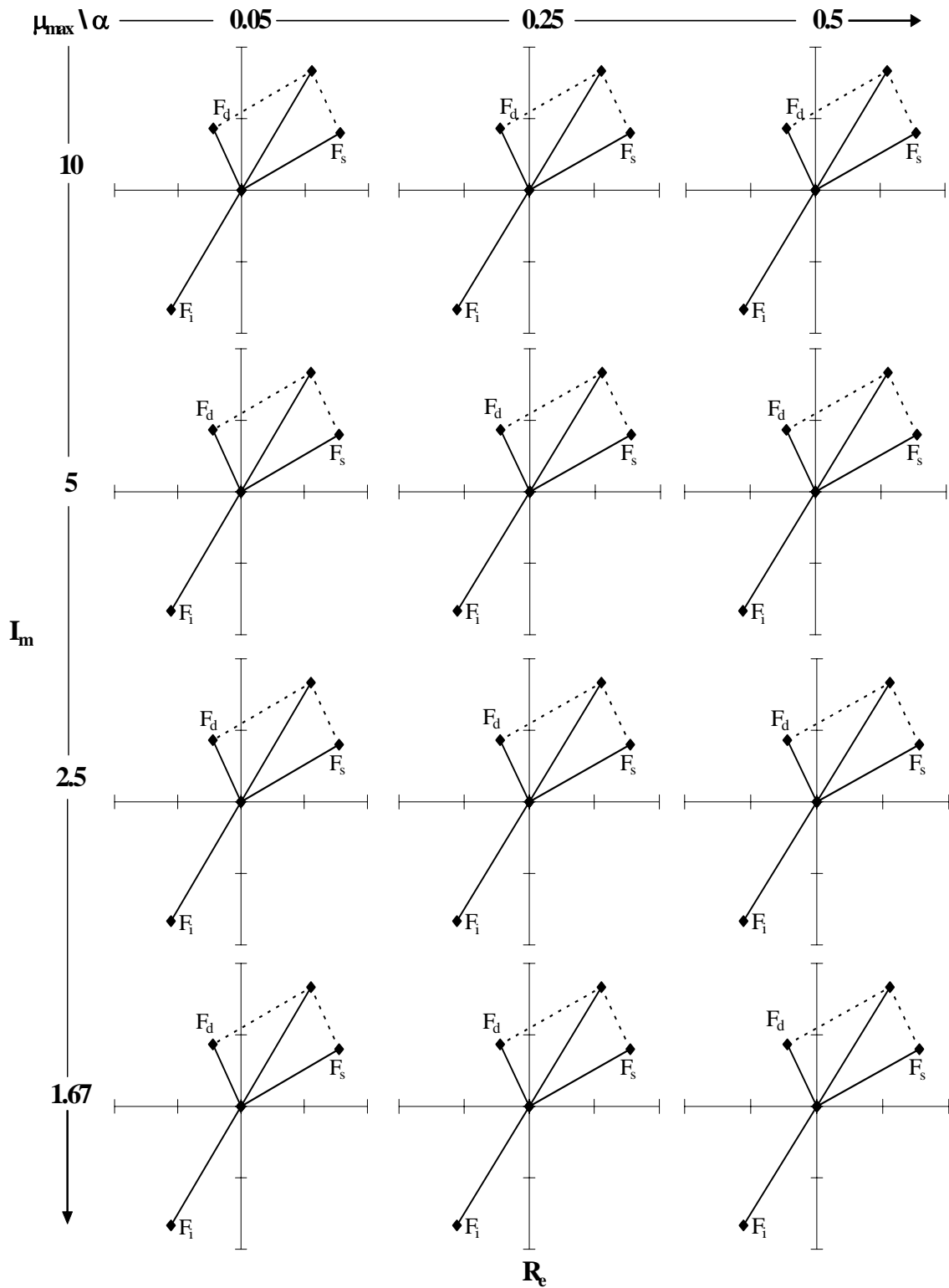


Figure 6.56. Complex Plane Representation of Inertial Force, F_i , Viscous Damper Force, F_d , and Hysteretic Force, F_s , for $T = 0.50$ s, $\eta = 1.0$, and 30% of Viscous Damping

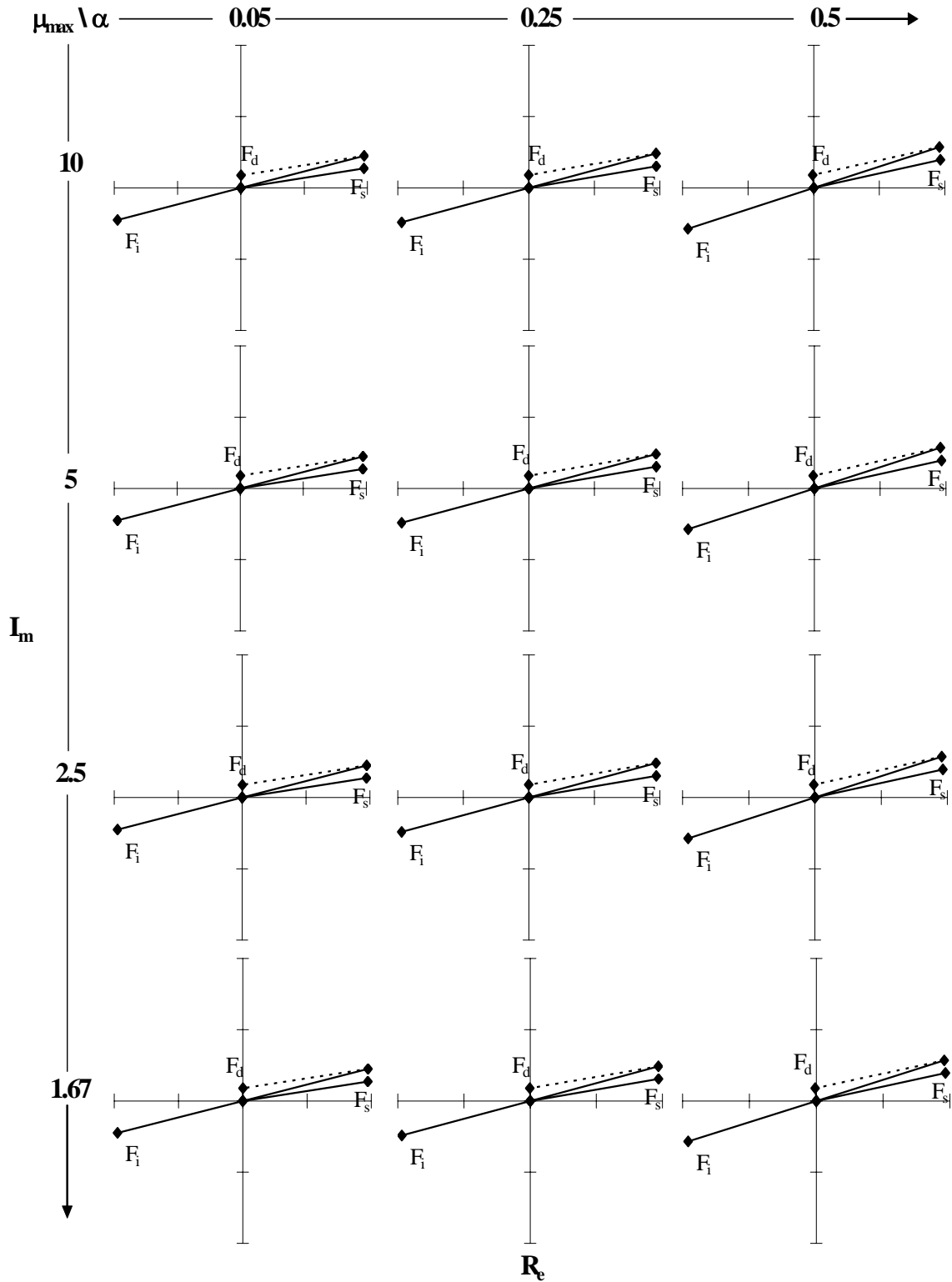


Figure 6.57. Complex Plane Representation of Inertial Force, F_i , Viscous Damper Force, F_d , and Hysteretic Force, F_s , for $T = 1.50$ s, $\eta = 0.2$, and 5% of Viscous Damping

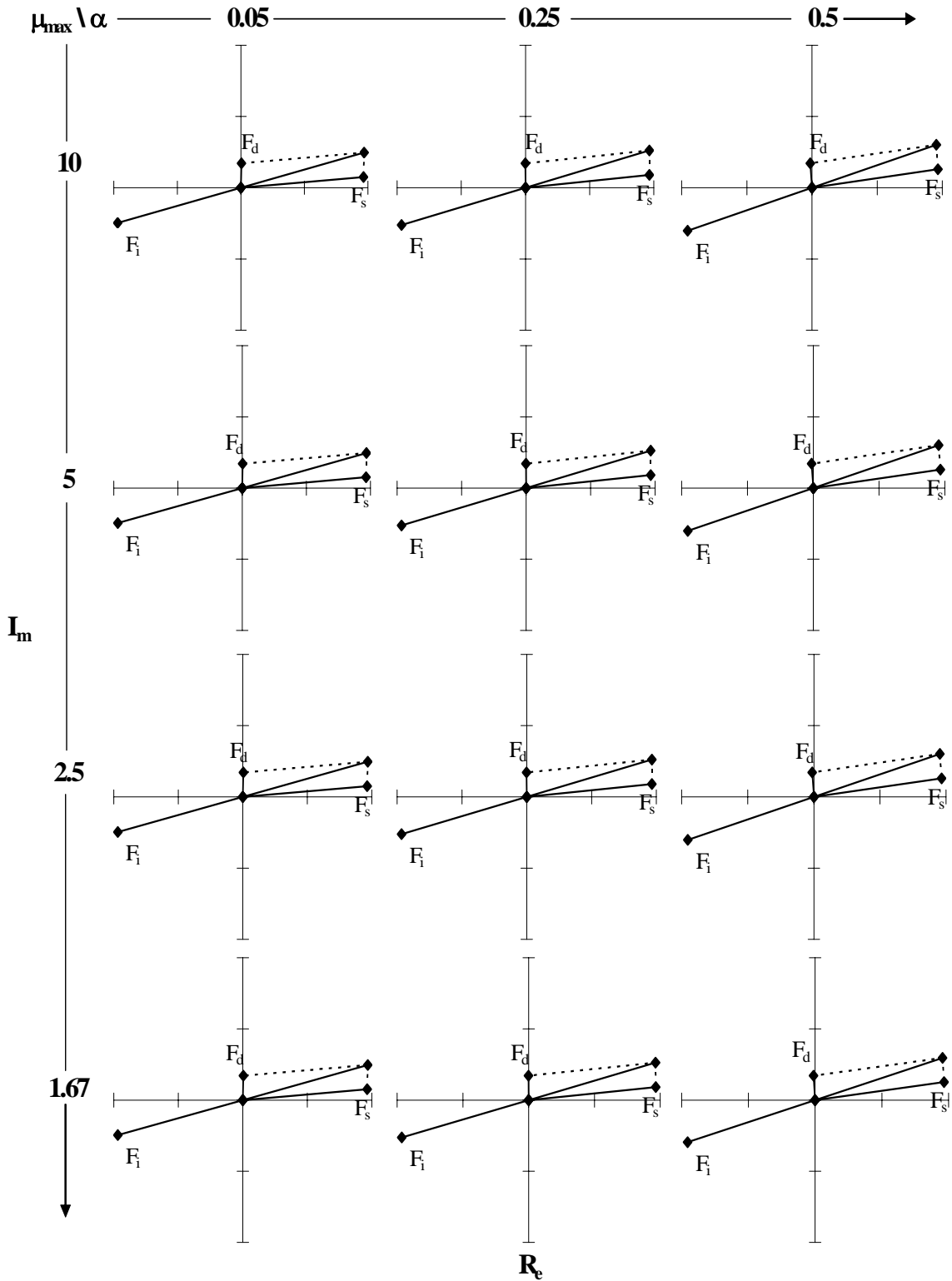


Figure 6.58. Complex Plane Representation of Inertial Force, F_i , Viscous Damper Force, F_d , and Hysteretic Force, F_s , for $T = 1.50$ s, $\eta = 0.2$, and 10% of Viscous Damping

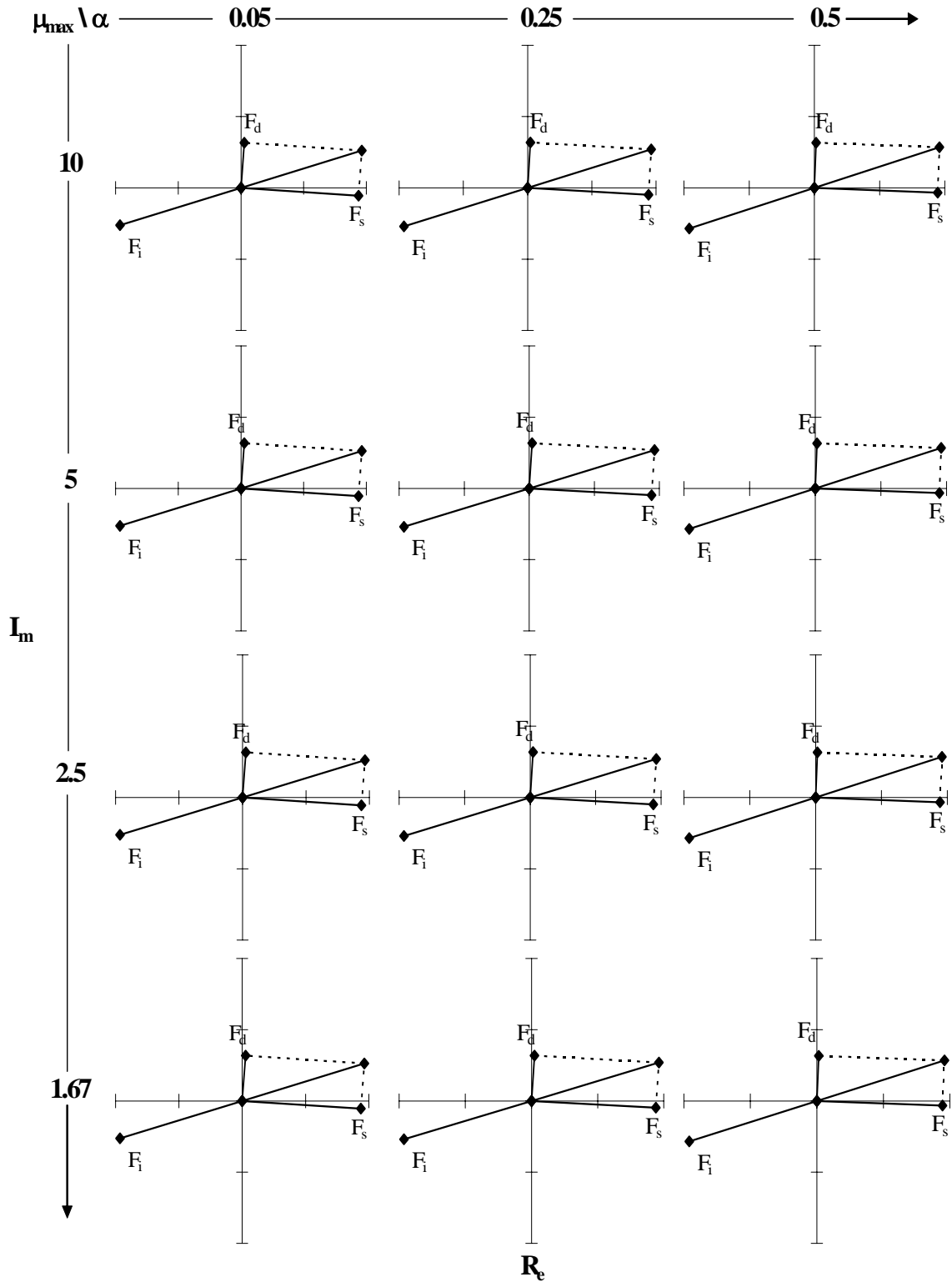


Figure 6.59. Complex Plane Representation of Inertial Force, F_i , Viscous Damper Force, F_d , and Hysteretic Force, F_s , for $T = 1.50$ s, $\eta = 0.2$, and 20% of Viscous Damping

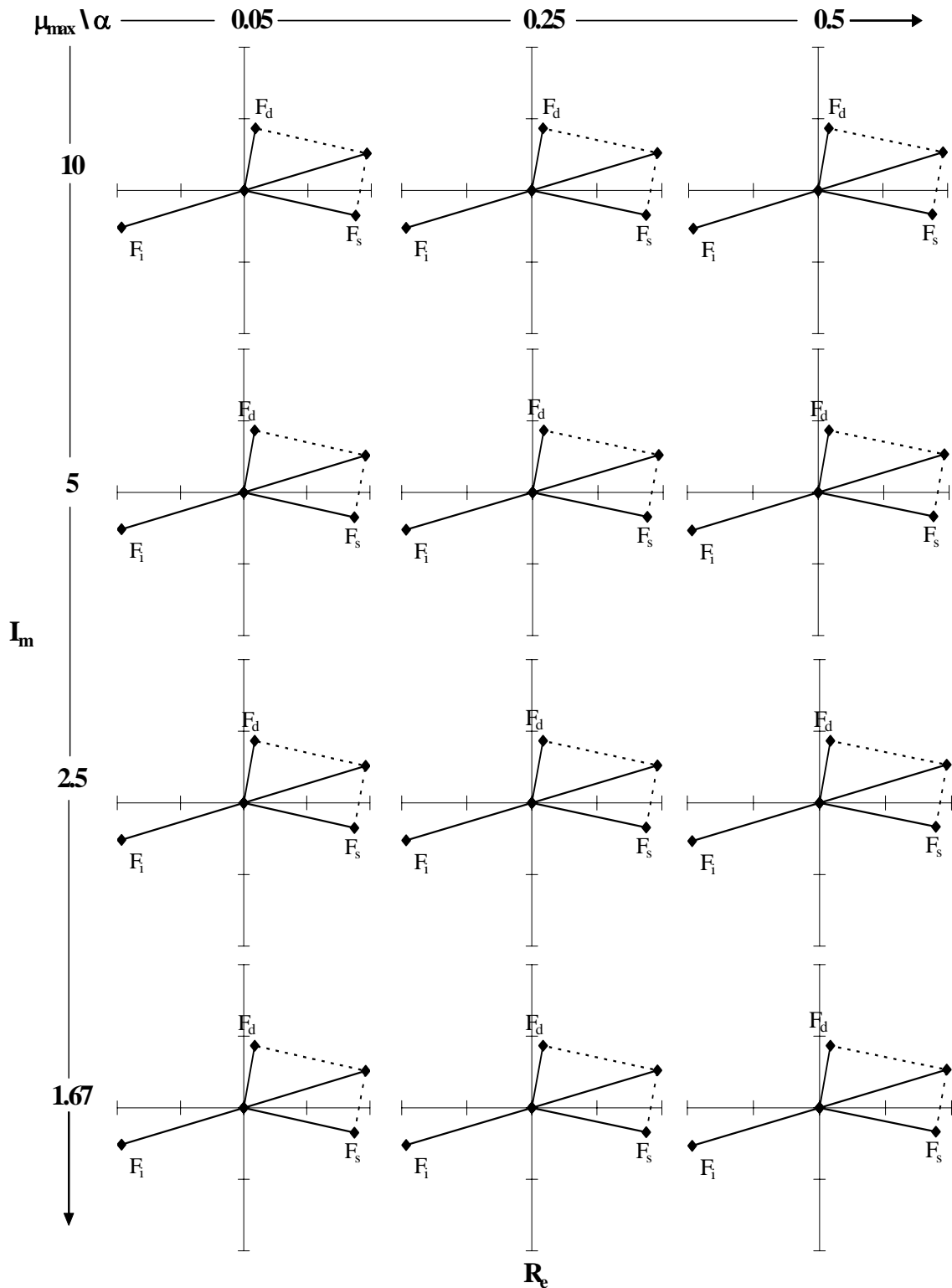


Figure 6.60. Complex Plane Representation of Inertial Force, F_i , Viscous Damper Force, F_d , and Hysteretic Force, F_s , for $T = 1.50$ s, $\eta = 0.2$, and 30% of Viscous Damping

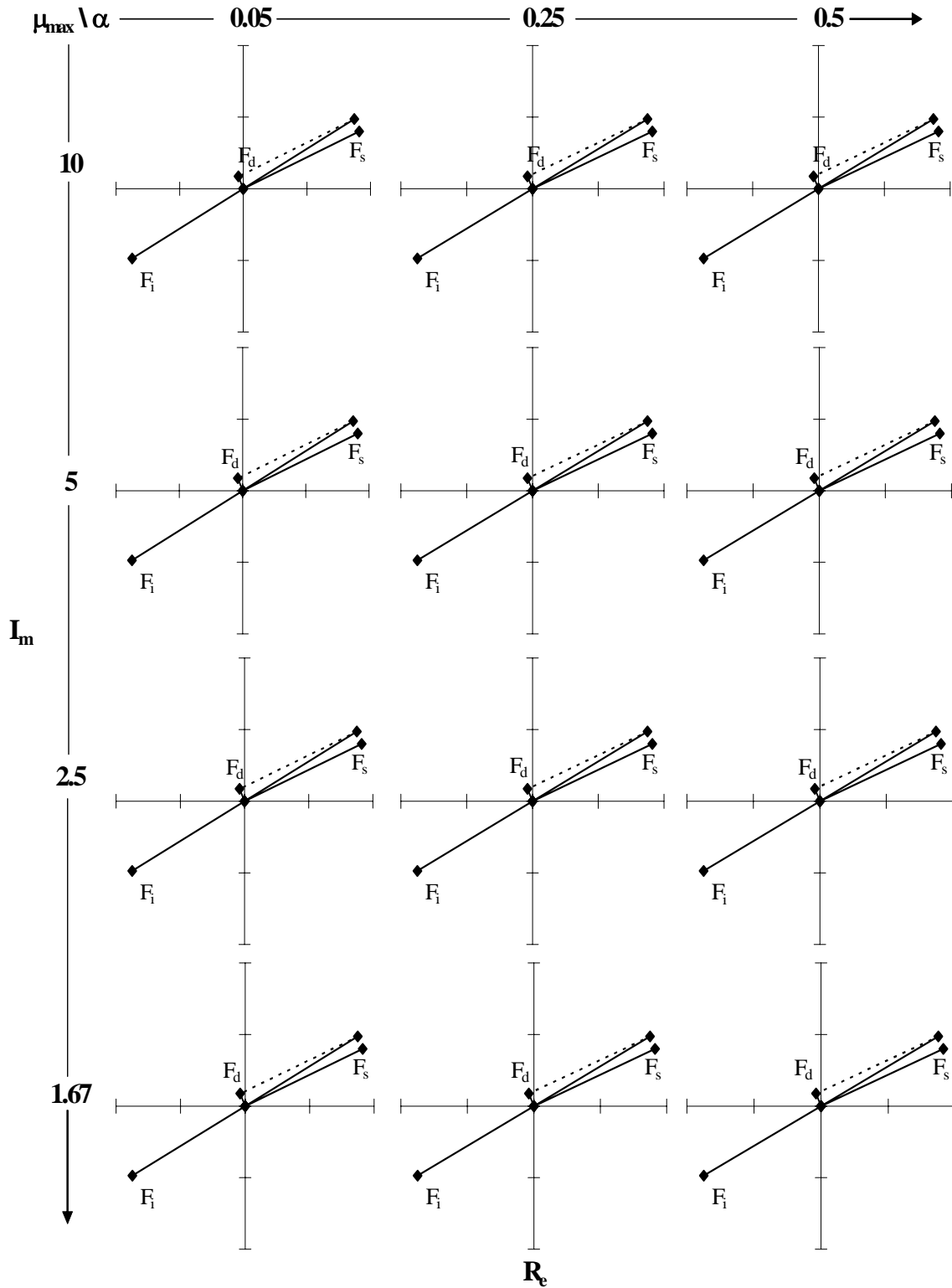


Figure 6.61. Complex Plane Representation of Inertial Force, F_i , Viscous Damper Force, F_d , and Hysteretic Force, F_s , for $T = 1.50$ s, $\eta = 1.0$, and 5% of Viscous Damping

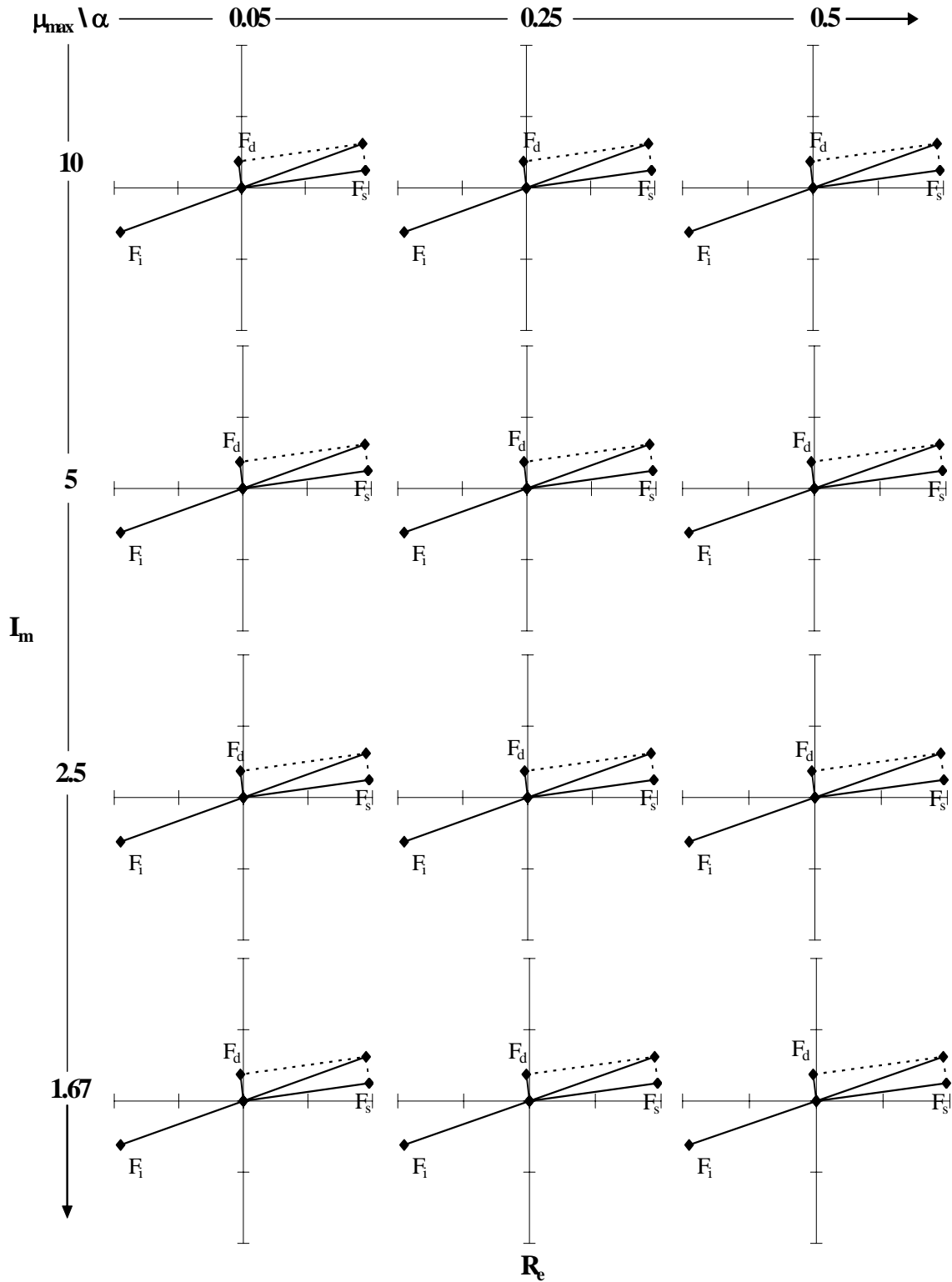


Figure 6.62. Complex Plane Representation of Inertial Force, F_i , Viscous Damper Force, F_d , and Hysteretic Force, F_s , for $T = 1.50$ s, $\eta = 1.0$, and 10% of Viscous Damping

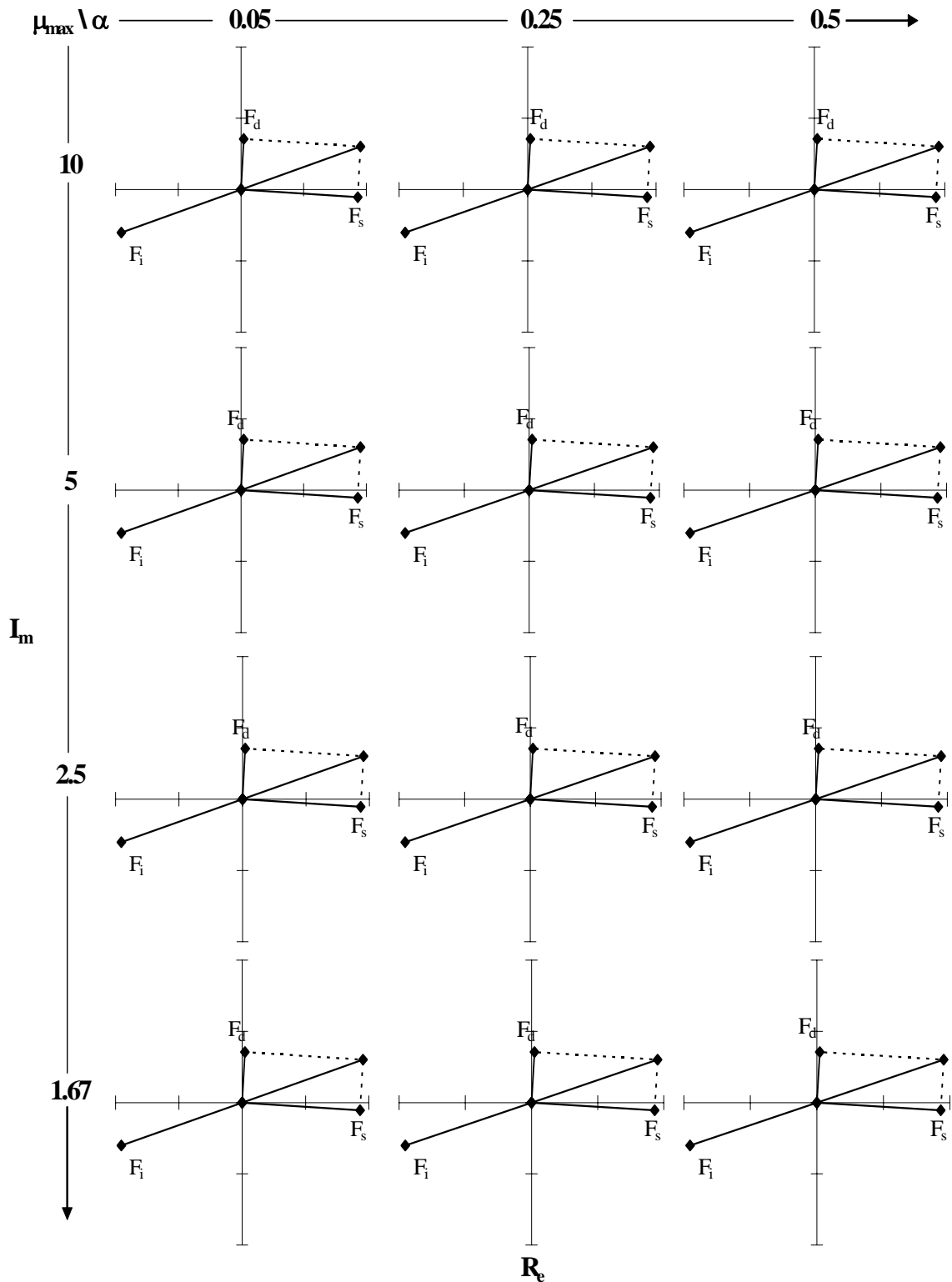


Figure 6.63. Complex Plane Representation of Inertial Force, F_i , Viscous Damper Force, F_d , and Hysteretic Force, F_s , for $T = 1.50$ s, $\eta = 1.0$, and 20% of Viscous Damping

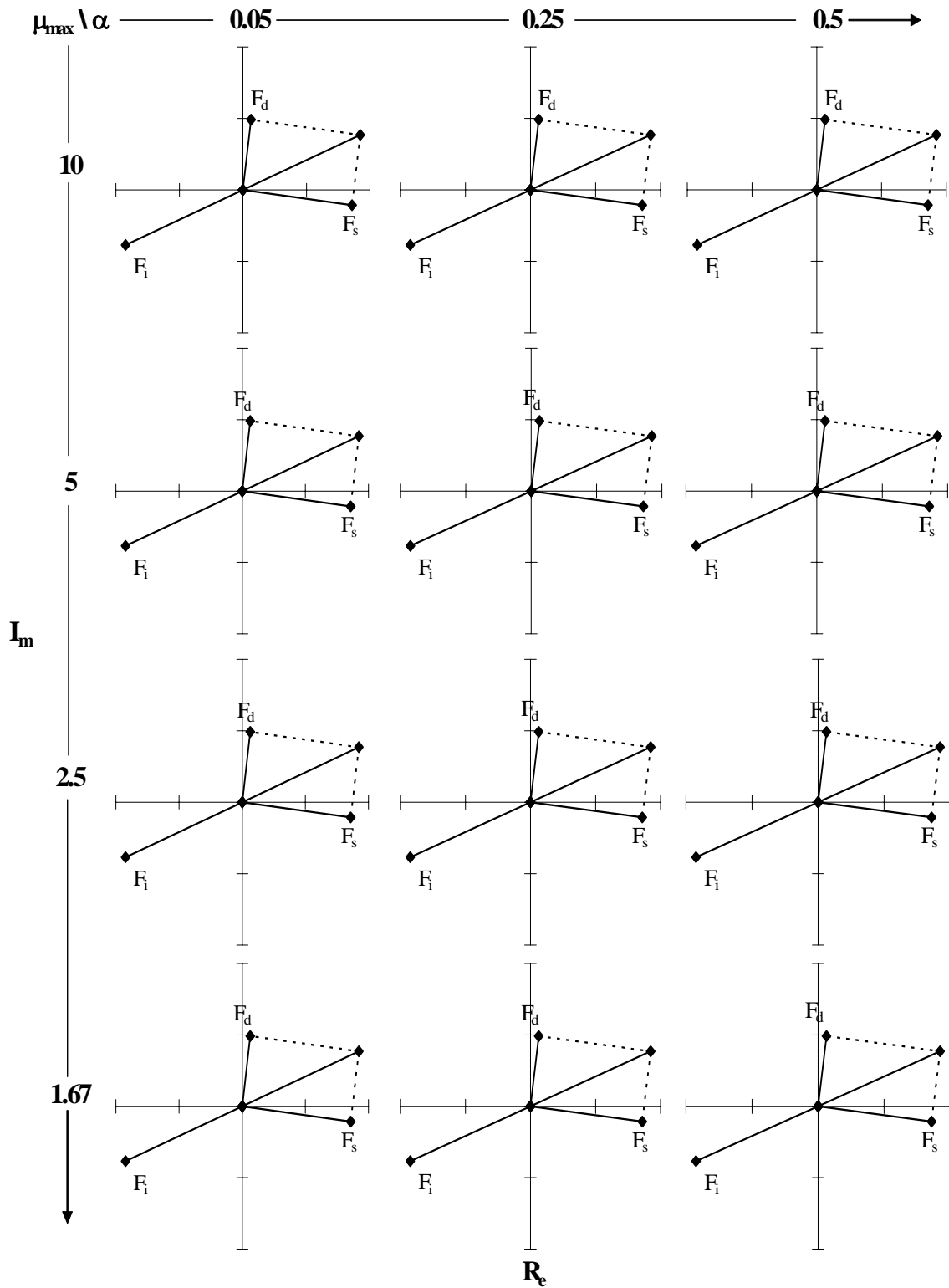


Figure 6.64. Complex Plane Representation of Inertial Force, F_i , Viscous Damper Force, F_d , and Hysteretic Force, F_s , for $T = 1.50$ s, $\eta = 1.0$, and 30% of Viscous Damping

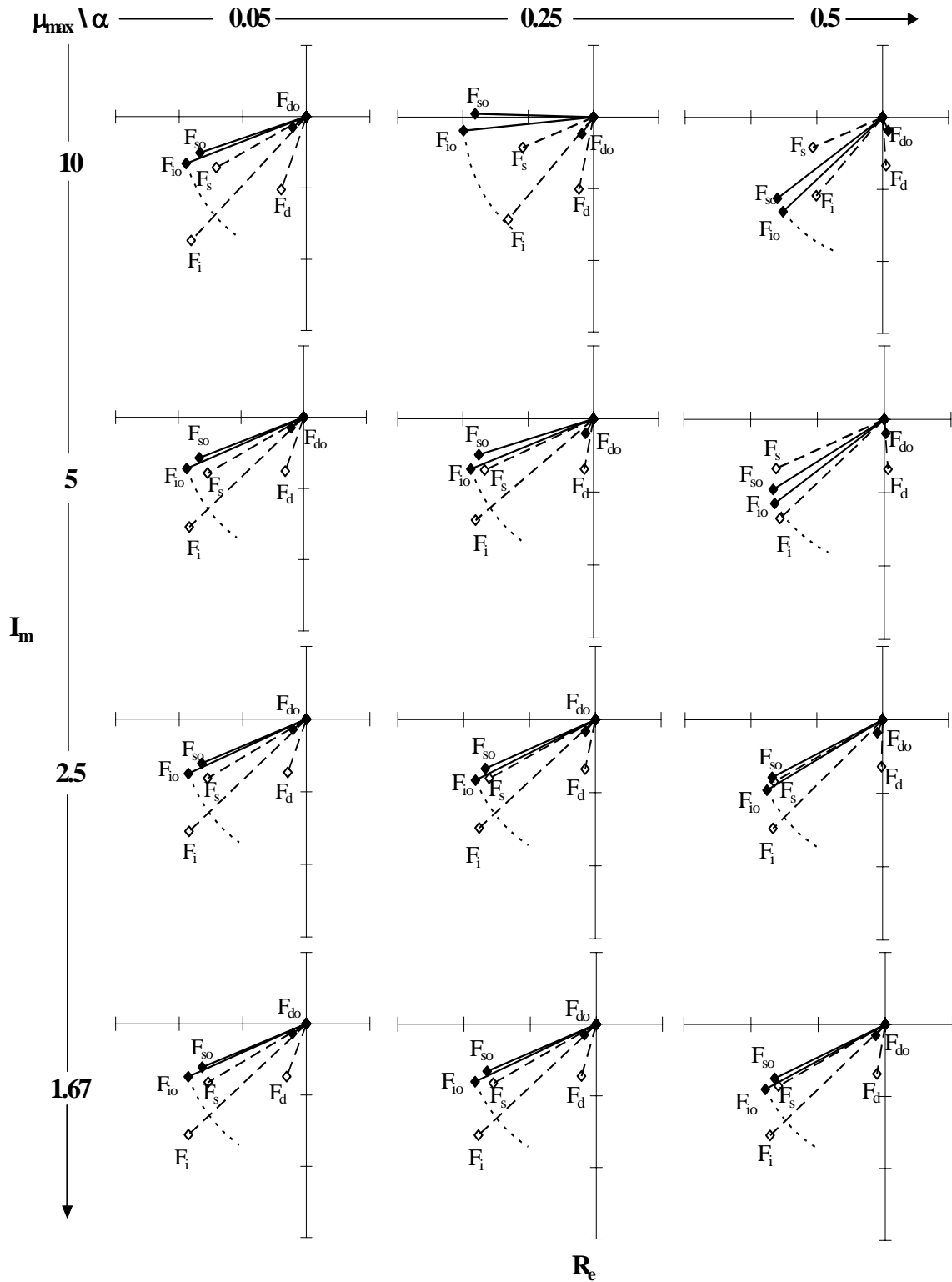


Figure 6.65. Increase in the Inertial Force between a System with 5% and a System with 30% of Viscous Damping, for $T = 0.25$ s and $\eta = 0.2$

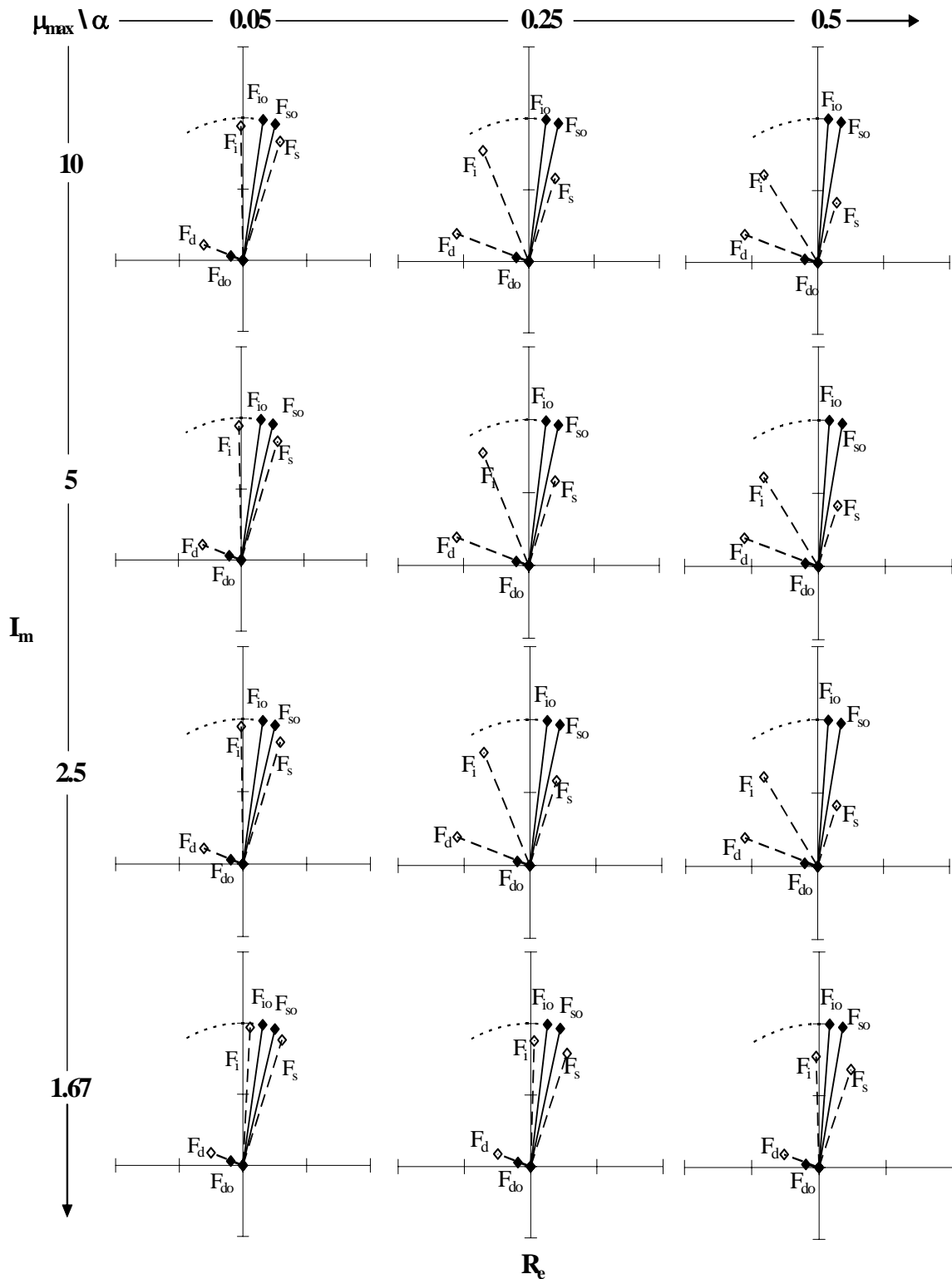


Figure 6.66. Increase in the Inertial Force between a System with 5% and a System with 30% of Viscous Damping, for $T = 0.25$ s and $\eta = 1.0$

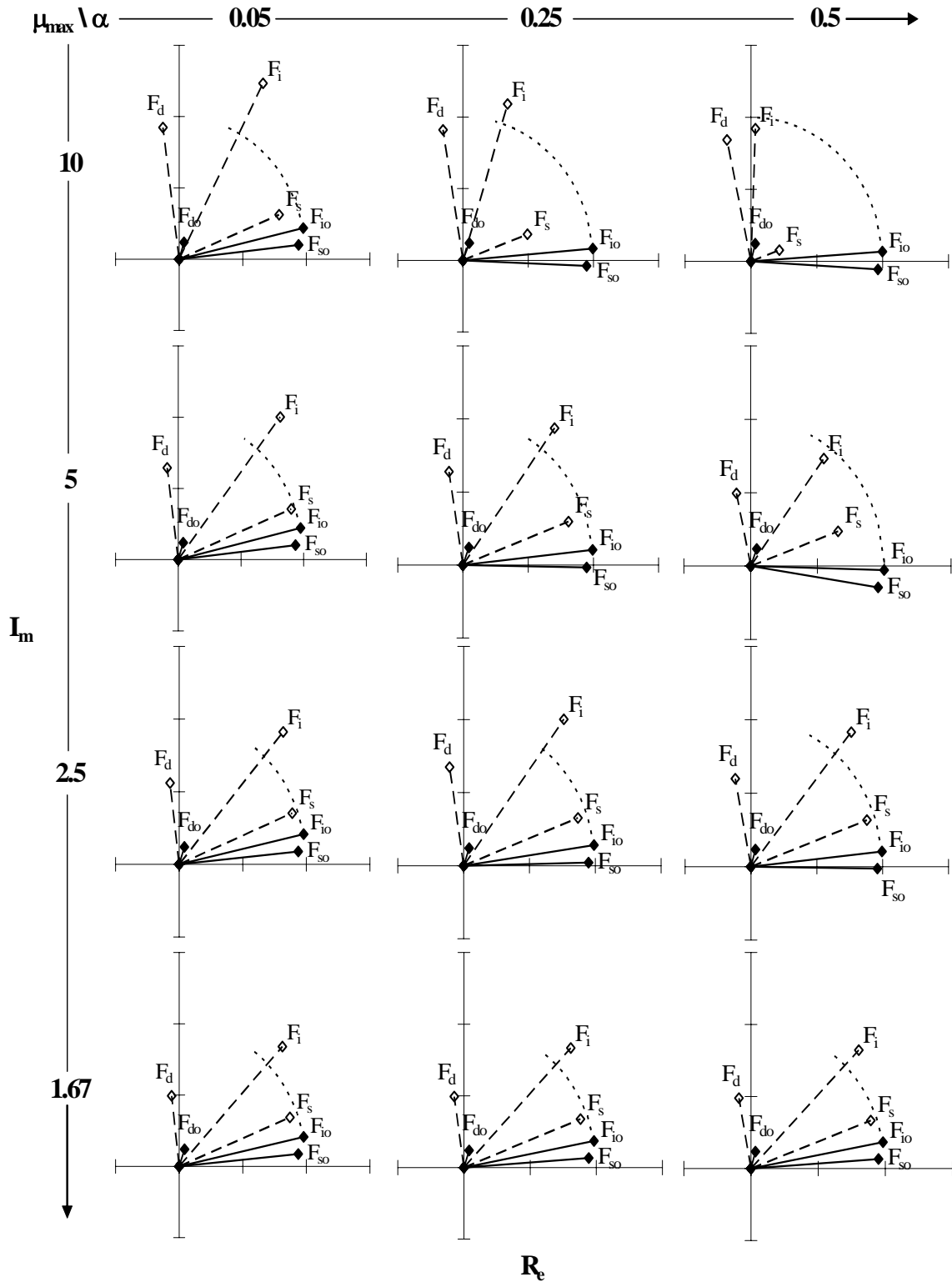


Figure 6.67. Increase in the Inertial Force between a System with 5% and a System with 30% of Viscous Damping, for $T = 0.50$ s and $\eta = 0.2$

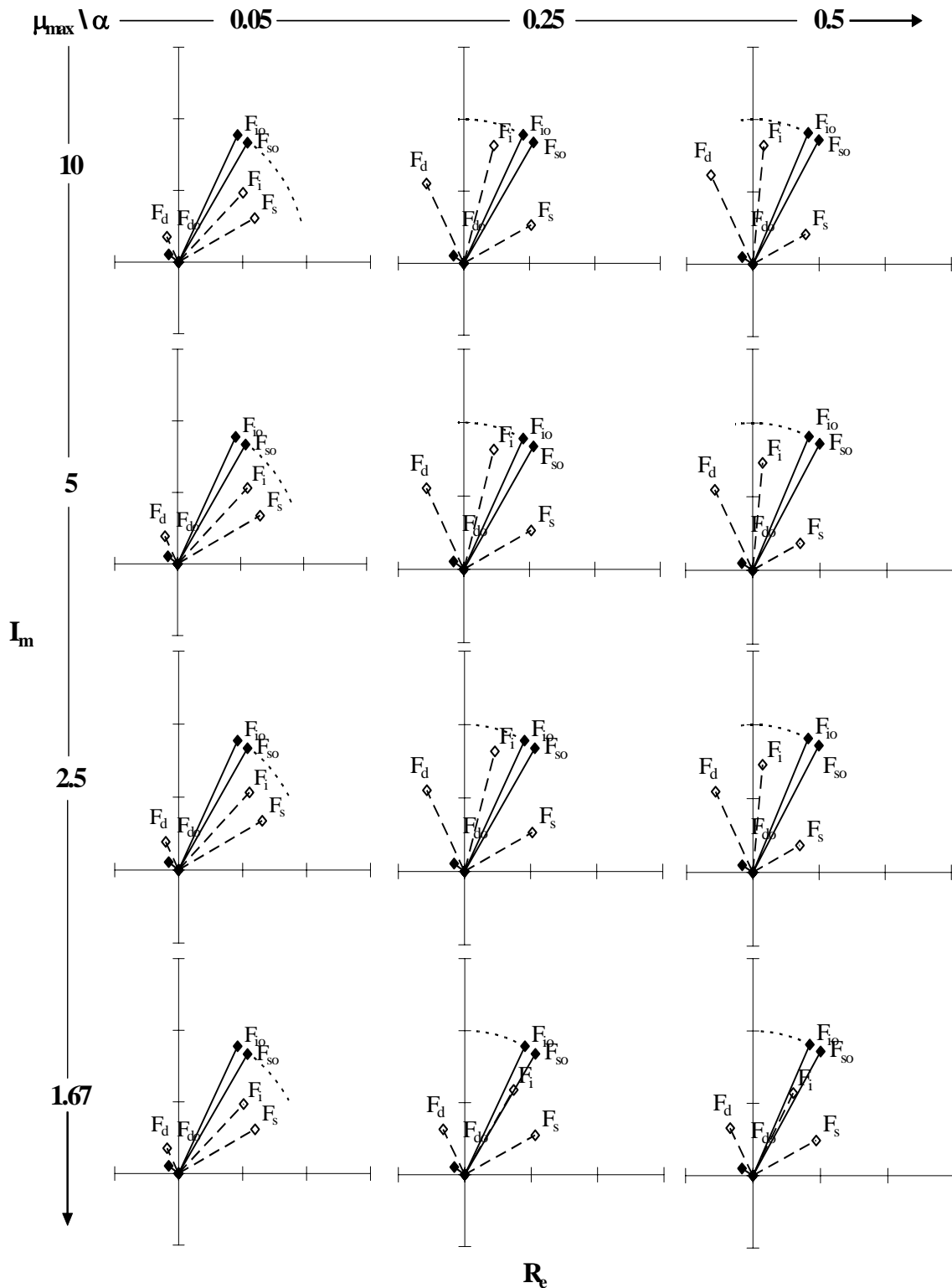


Figure 6.68. Increase in the Inertial Force between a System with 5% and a System with 30% of Viscous Damping, for $T = 0.50$ s and $\eta = 1.0$

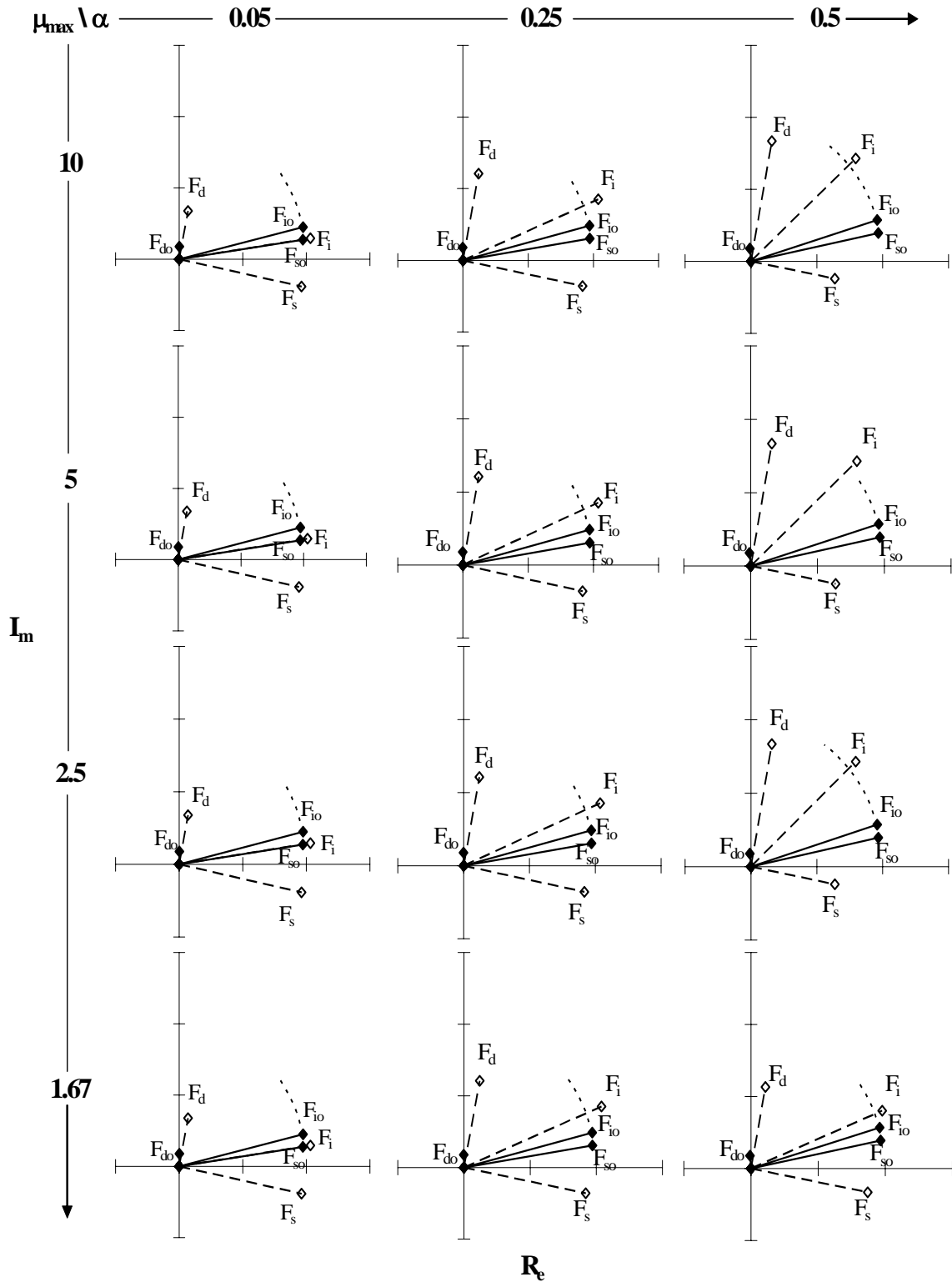


Figure 6.69. Increase in the Inertial Force between a System with 5% and a System with 30% of Viscous Damping, for $T = 1.50$ s and $\eta = 0.2$

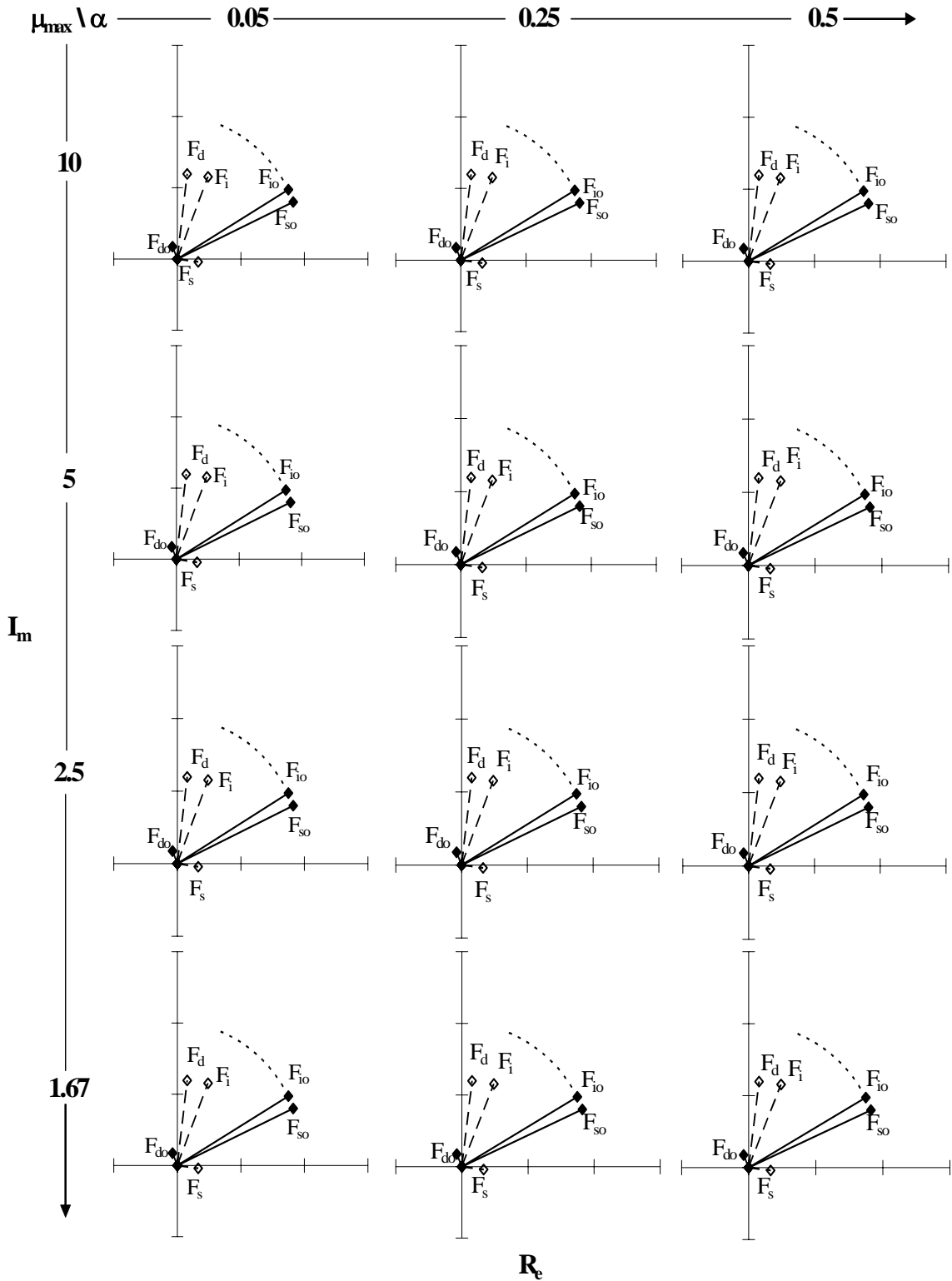


Figure 6.70. Increase in the Inertial Force between a System with 5% and a System with 30% of Viscous Damping, for $T = 1.50$ s and $\eta = 1.0$

6.7. Observations

Seismic response of hybrid systems having hysteretic and viscous dampers has been studied in this section through parametric analyses. It was found that increases in viscous damping reduce the effectiveness of hysteretic dampers, since the amplitude of motion (and thus ductility demand) is reduced. In some cases, when the amplitude of motion decreases to the point where the system behave elastically, the hysteretic dampers only work to provide additional stiffness to the system, which may be achieved by other conventional methods (e.g., steel braces as apposed to special ductile devices).

Although viscous dampers are known to decrease both displacements and acceleration demands in structures with elastic behavior, for structural fuse systems where hysteretic dampers are designed to behave inelastically (i.e., $\Delta_{ya} \leq u < \Delta_{yf}$), the floor accelerations are likely to increase if viscous dampers are added in parallel to hysteretic dampers, especially for systems with small stiffness ratio (i.e., $\alpha < 0.25$). Adding such viscous dampers in parallel is therefore not only ineffective but detrimental to the seismic performance of acceleration sensitive equipment and nonstructural components. This observation would also be true for buildings that have been retrofitted with viscous dampers and whose original frame still behaves inelastically under major earthquakes. Argand diagrams in the frequency domain is successfully used to explain these observations.

SECTION 7

DESIGN OF MULTI DEGREE OF FREEDOM SYSTEMS WITH METALLIC STRUCTURAL FUSES

7.1. Introduction

In Sections 3 and 4, the structural fuse concept was introduced as PED devices to seismically design and retrofit SDOF systems. Based on the results previously obtained, this section focuses on the implementation of the structural fuse concept in multi-degree of freedom (MDOF) systems. However, some modification are made to the procedure listed in Section 4, in order to apply the concept to multi-story buildings using BRB, T-ADAS, and SP as metallic fuses.

Some examples of application are presented using the MCEER Demonstration Hospital, described by Yang et al. (2002), as the system to be either designed or retrofitted with metallic fuses. Figure 7.1 shows one of the transverse moment-resisting frames of the MCEER Demonstration Hospital, which is a four-story building modeled in this study considering the masses lumped at floor levels. It may be noted that, for the purpose of this study, the damping system (i.e., metallic dampers and braces) is considered installed only in the middle panel of the frame, in a chevron configuration (shown as dashed lines in Figure 7.1).

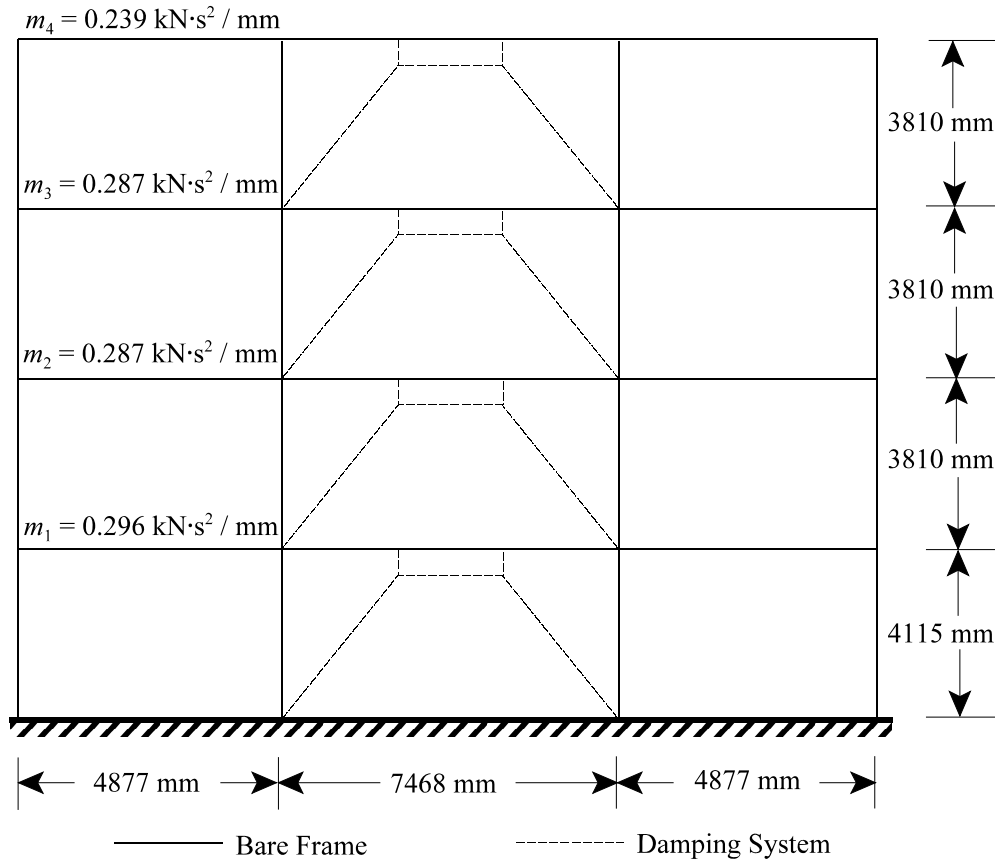


Figure 7.1. Elevation of MCEER Demonstration Hospital Transverse Frame (Adapted from Yang et al., 2002)

7.2. Design for a Specified Set of Parameters

A general procedure to design SDOF systems with metallic structural fuses was presented in Section 4. In this section, two modifications are introduced to the procedure, to make it applicable to MDOF systems: modification of the elastic period limit equation, and introduction of assumed mode shapes to establish the required story strength across the building height.

7.2.1. Elastic limit period for MDOF Systems

In Step 2 of the procedure listed in Section 4.3, the elastic period limit, T_L , was determined using (3.30), which in the case of MDOF systems should be modified as follows:

$$T_L = \frac{4\pi^2 \Delta_{ar}}{\Gamma_1 \phi_{r1} S_{DI}} \quad (7.1)$$

where Δ_{ar} is the allowable displacement of the roof, taken as a percentage of the building height (usually between 0.5% and 2%), ϕ_{r1} is the first mode component of the roof displacement, and Γ_1 is the modal participation factor of the first mode, calculated as:

$$\Gamma_1 = \frac{\phi_1^T \mathbf{M} \tilde{\mathbf{1}}}{\phi_1^T \mathbf{M} \phi_1} \quad (7.2)$$

where \mathbf{M} is the known mass matrix, ϕ_1 is the vector corresponding to the first mode shape, and $\tilde{\mathbf{1}}$ is a vector of unit values, which represents a rigid body motion of the system due to horizontal ground excitation.

Note that, to determine the modal participation factor, Γ_1 , a mode shape, ϕ_1 , should be assumed. Many approaches have been proposed to select appropriate mode shapes, and obtain “reasonable” estimation of system dynamic characteristics (Clough and Penzien, 1993). In this study, a linear mode shape is assumed, where every “ j ” component of the vector is calculated by:

$$\phi_{1j} = \frac{h_j}{h_r} \quad (7.3)$$

where h_j and h_r are the height measured from the base of the corresponding floor, and the height of the roof, respectively. Recall that to implement the equivalent lateral force procedure, the International Building Code (IBC-2000) uses the following expression to determine the vertical distribution factor, C_{vx} , for the seismic forces:

$$C_{vx} = \frac{w_x h_x^k}{\sum_{i=1}^n w_i h_i^k} \quad (7.4)$$

where w_x and w_i are the floors gravity loads, and k is a period-dependent exponent to account for higher modes contribution. For expediency, (7.3) is used in this study since it showed to be sufficiently accurate to determine the system dynamic properties.

Figure 7.2a shows the mode shapes corresponding to all the cases studied in this section (36 in total). Furthermore, Figure 7.2b shows a comparison between (7.3) and (7.4) with the average of the actual mode shapes obtained from modal analysis. Note that Figure 7.2b shows good agreement between the linear assumption and the actual mode shape of the system, with a difference less than 5%.

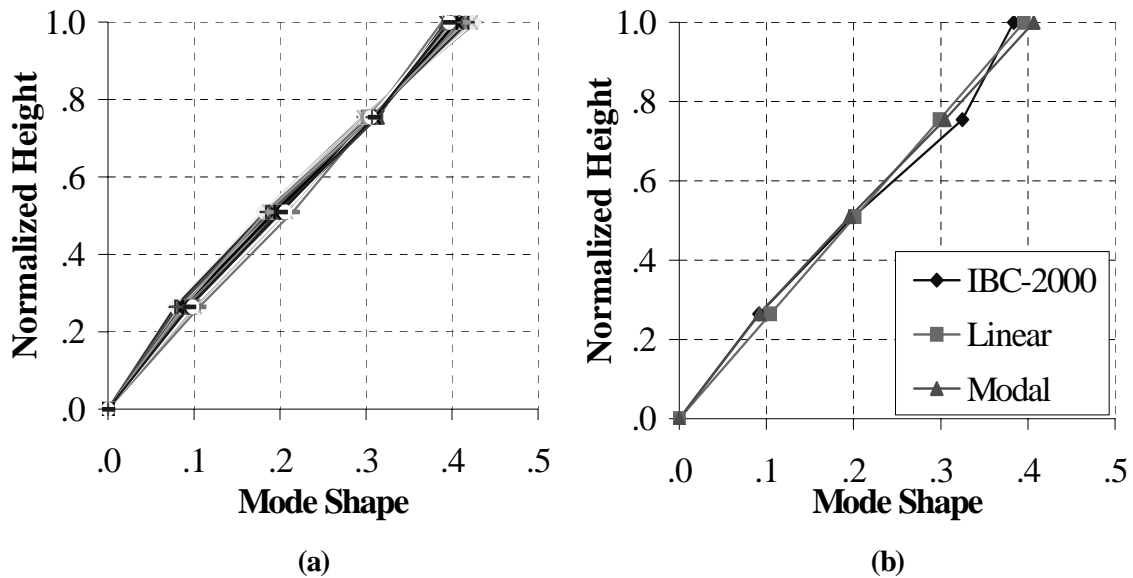


Figure 7.2. Mode Shapes: (a) All Studied Cases; (b) Comparison of Mode Shapes determined from different Methods

7.2.2. Story yield shear

Once the elastic limit period, T_L , has been determined, the procedure may be followed to calculate the required story yield shear, V_y , for a given set of target parameters (i.e., α , μ_{\max} , and η). In Fig 3.2, it was shown that, for SDOF systems, V_y can be expressed in terms of the required base shear capacity for the frame, V_{yf} , and the damping system, V_{yd} , respectively, as follows:

$$V_{yf} = \alpha \mu_{\max} V_y \quad (7.5)$$

and

$$V_{yd} = (1 - \alpha) V_y \quad (7.6)$$

Here, these specific shears are vertically distributed through the height of the building, using a vertical distribution function proportional to the assumed mode shape, ϕ_1 . Therefore, this makes it possible to design the frame and the metallic dampers for V_{yf} and V_{yd} , respectively. Further discussion on how to determine the shape of the lateral force distribution in the perspective of nonlinear response can be found in Reinhorn (1997), where general and simplified force distributions are presented. In the design procedure developed in this investigation, the approximation of the mode shape is based on the observations presented in the study by Reinhorn (1997).

7.2.3. Design Steps

The procedure listed below shows how satisfactory designs for new construction can be obtained for a MDOF system with given geometry, for given mass matrix and yield strength of beams and columns, and for given seismic conditions.

Step 1. Preliminary design the beams and columns neglecting the contribution of the structural fuse and using the portal frame method (i.e., assuming that inflection points are at the middle of members, and that exterior columns receive half of the frame story shear, V_{yf} , corresponding to interior columns).

- Step 2. Design the metallic dampers and braces for each story, using the vertically distributed story shear associated with the damping system, V_{yd} .
- Step 3. Determine the actual parameters (i.e., α , μ_{\max} , and η) for the designed system from a static pushover analysis, conducted using a load pattern proportional to ϕ_1 .
- Step 4. Solve the dynamic eigenvalue problem, and obtain the fundamental period of vibration of the structure, T .
- Step 5. Evaluate the response of the system either by performing time history analysis, or directly from Figures 3.8 and 3.9.
- Step 6. If the structural fuse concept is not satisfied, increase frame and damper stiffness and strength (i.e., greater K_f , V_{yf} , K_d , and V_{yd}) to improve the system seismic behavior, and repeat the procedure from Step 3, until a satisfactory response is achieved. For example, if the story drift limit is not satisfied, the system should be stiffened (i.e., greater K_f and K_d). On the other hand, if the frame undergoes inelastic deformations (i.e., $\mu_f > 1$), the system should be strengthened (i.e., greater V_{yf} and V_{yd}).

For retrofit existing structures, bare frame properties (i.e., K_f , V_{yf} , and Δ_{yf}) may be determined by performing a static pushover analysis of the existing system. Accordingly, the stiffness ratio, α , the required stiffness, K_1 , and the elastic period, T , may be calculated using (4.57), (4.58), and (4.59), respectively. Recall that restrictions listed in Section 4 for SDOF systems, apply again to the retrofit of MDOF buildings.

Subsequent sections present several examples of how the structural fuse concept can be applied to design and retrofit MDOF systems. Furthermore, two specific step-by-step examples are shown in Appendix C, to illustrate the process of implementing the structural fuse concept in MDOF systems.

7.3. New Buildings Design Examples

Figure 7.1 shows one of the four transverse moment-resisting frames of the MCEER Demonstration Hospital, which is used in this study as a model for the examples of application of the structural fuse concept to MDOF systems. The mass matrix for this frame (adapted from Yang et al., 2000) is equal to:

$$\mathbf{M} = \begin{bmatrix} 0.296 & 0 & 0 & 0 \\ 0 & 0.287 & 0 & 0 \\ 0 & 0 & 0.287 & 0 \\ 0 & 0 & 0 & 0.239 \end{bmatrix} \cdot \frac{kN \cdot s^2}{mm}$$

Using (7.3), the corresponding mode shape vector is:

$$\boldsymbol{\phi}_1^T = [0.26 \quad 0.51 \quad 0.75 \quad 1.00]$$

The elastic period limit, T_L , and the modal participation factor, Γ_1 , are obtained from (7.1) and (7.2), respectively. In this particular case, $T_L = 1.58$ s, and $\Gamma_1 = 1.37$, which correspond to an allowable story drift of 2% (i.e., $\Delta_{ar} = 311$ mm).

Actual designs for new construction were first conducted using BRB, T-ADAS, and SP as metallic fuses, following the procedure listed in Section 4.3, modified for MDOF systems as described in Section 7.2. A total of 12 designs were developed for every metallic fuse system studied in this section to match as closely as possible the target parameters α , μ_{max} , and η . Note that target η values are taken from Table 4.1 for a given set of α , μ_{max} and T_L .

Tables 7.1, 7.2, and 7.3 list the properties of the resulting designs conducted for MDOF systems having BRB, T-ADAS, and SP devices acting as metallic fuses, respectively. It may be noted that frame and metallic fuses cross-sectional properties vary in the same way as in SDOF systems. This is because frame base shear capacity is proportional to both α and μ_{max} values, while damping system base shear capacity is inversely

proportional to both α and μ_{\max} values. In the case of BRB's (Table 7.1), it may be seen how the area of the braces decreases with increases in α and μ_{\max} values. For example, the cross-sectional properties of BRB's in the first story decrease from $191 \times 51 \text{ mm} = 9741 \text{ mm}^2$ (for $\alpha = 0.05$ and $\mu_{\max} = 1.67$) to $102 \times 51 \text{ mm} = 5202 \text{ mm}^2$ (for $\alpha = 0.25$ and $\mu_{\max} = 1.67$), and also decrease to $127 \times 13 \text{ mm} = 1651 \text{ mm}^2$ (for $\alpha = 0.05$ and $\mu_{\max} = 10$).

Table 7.1. Design of MDOF Systems with BRB

Story	$\alpha = 0.05$				$\alpha = 0.25$				$\alpha = 0.50$			
	Beam	Ext. Col.	Int. Col.	BRB (mm)	Beam	Ext. Col.	Int. Col.	BRB (mm)	Beam	Ext. Col.	Int. Col.	BRB (mm)
(1)	(2)	(3)	(4)	(5)	(6)	(7)	(8)	(9)	(10)	(11)	(12)	(13)
$\mu_{max} = 10$												
4	W6x12	W10x22	W12x26	44x13	W12x22	W14x34	W14x68	38x13	W12x40	W14x68	W14x120	25x13
3	W12x14	W10x22	W12x26	83x13	W16x45	W14x34	W14x68	70x13	W18x76	W14x68	W14x120	44x13
2	W12x22	W10x22	W12x35	108x13	W21x57	W14x61	W14x99	89x13	W24x94	W14x99	W14x193	57x13
1	W14x22	W10x22	W12x35	127x13	W21x68	W14x61	W14x99	102x13	W30x99	W14x99	W14x193	70x13
$\mu_{max} = 5$												
4	W6x12	W10x22	W12x26	57x19	W12x22	W14x34	W14x68	51x19	W12x40	W14x68	W14x120	32x19
3	W12x14	W10x22	W12x26	114x19	W16x45	W14x34	W14x68	89x19	W18x76	W14x68	W14x120	57x19
2	W12x22	W10x22	W12x40	146x19	W21x57	W14x61	W14x99	114x19	W24x94	W14x99	W14x193	76x19
1	W14x22	W10x22	W12x40	171x19	W21x68	W14x61	W14x99	140x19	W30x99	W14x99	W14x193	89x19
$\mu_{max} = 2.5$												
4	W6x12	W10x22	W12x26	57x38	W12x22	W14x34	W14x68	51x38	W12x40	W14x68	W14x120	32x38
3	W12x14	W10x22	W12x26	114x38	W16x45	W14x34	W14x68	89x38	W18x76	W14x68	W14x120	57x38
2	W12x22	W10x22	W12x65	146x38	W21x57	W14x61	W14x99	114x38	W24x94	W14x99	W14x193	76x38
1	W14x22	W10x22	W12x65	171x38	W21x68	W14x61	W14x99	140x38	W30x99	W14x99	W14x193	89x38
$\mu_{max} = 1.67$												
4	W6x12	W10x22	W12x35	70x51	W12x22	W14x34	W14x68	51x51	W12x40	W14x68	W14x120	38x51
3	W12x14	W10x22	W12x35	127x51	W16x45	W14x34	W14x68	102x51	W18x76	W14x68	W14x120	70x51
2	W12x22	W10x22	W12x87	165x51	W21x57	W14x61	W14x99	127x51	W24x94	W14x99	W14x193	89x51
1	W14x22	W10x22	W12x87	191x51	W21x68	W14x61	W14x99	152x51	W30x99	W14x99	W14x193	102x51

Table 7.2. Design of MDOF Systems with T-ADAS

$\alpha = 0.05$			$\alpha = 0.25$			$\alpha = 0.50$						
St.	Beam	Ext. Col. (3)	Int. Col. (4)	TADAS (mm) (5)	Beam	Ext. Col. (7)	Int. Col. (8)	TADAS (mm) (9)	Beam	Ext. Col. (11)	Int. Col. (12)	TADAS (mm) (13)
(1)	(2)	(3)	(4)	(5)	(6)	(7)	(8)	(9)	(10)	(11)	(12)	(13)
$\mu_{\max} = 10$												
4	W6x12	W10x22	W12x26	3 254x381x38	W12x22	W14x34	W14x68	3 254x381x38	W12x40	W14x68	W14x120	2 254x381x38
3	W12x14	W10x22	W12x26	6 254x381x38	W16x45	W14x34	W14x68	5 254x381x38	W18x76	W14x68	W14x120	3 254x381x38
2	W12x22	W10x22	W12x35	8 254x381x38	W21x57	W14x61	W14x99	6 254x381x38	W24x94	W14x99	W14x193	4 254x381x38
1	W14x22	W10x22	W12x35	9 254x381x38	W21x68	W14x61	W14x99	7 254x381x38	W30x99	W14x99	W14x193	5 254x381x38
$\mu_{\max} = 5$												
4	W12x14	W10x22	W12x26	7 254x381x38	W12x22	W14x34	W14x68	5 254x381x38	W12x40	W14x68	W14x120	4 254x381x38
3	W12x22	W10x22	W12x26	12 254x381x38	W16x45	W14x34	W14x68	10 254x381x38	W18x76	W14x68	W14x120	7 254x381x38
2	W14x22	W10x22	W12x40	16 254x381x38	W21x57	W14x61	W14x99	13 254x381x38	W24x94	W14x99	W14x193	9 254x381x38
1	W14x26	W10x22	W12x40	18 254x381x38	W21x68	W14x61	W14x99	14 254x381x38	W30x99	W14x99	W14x193	10 254x381x38
$\mu_{\max} = 2.5$												
4	W12x22	W14x22	W12x40	9 254x381x38	W12x22	W14x34	W14x68	7 254x381x38	W12x40	W14x68	W14x120	5 254x381x38
3	W16x31	W14x22	W12x40	17 254x381x38	W16x45	W14x34	W14x68	14 254x381x38	W18x76	W14x68	W14x120	9 254x381x38
2	W18x35	W14x26	W12x65	23 254x381x38	W21x57	W14x61	W14x99	18 254x381x38	W24x94	W14x99	W14x193	12 254x381x38
1	W18x40	W14x26	W12x65	26 254x381x38	W21x68	W14x61	W14x99	21 254x381x38	W30x99	W14x99	W14x193	14 254x381x38
$\mu_{\max} = 1.67$												
4	W14x26	W14x26	W12x58	14 254x381x38	W12x22	W14x34	W14x68	11 254x381x38	W12x40	W14x68	W14x120	7 254x381x38
3	W18x40	W14x26	W12x58	26 254x381x38	W16x45	W14x34	W14x68	21 254x381x38	W18x76	W14x68	W14x120	14 254x381x38
2	W18x50	W14x38	W12x87	34 254x381x38	W21x57	W14x61	W14x99	27 254x381x38	W24x94	W14x99	W14x193	18 254x381x38
1	W21x50	W14x38	W12x87	39 254x381x38	W21x68	W14x61	W14x99	31 254x381x38	W30x99	W14x99	W14x193	21 254x381x38

Table 7.3. Design of MDOF Systems with SP

Story	$\alpha = 0.05$				$\alpha = 0.25$				$\alpha = 0.50$			
	Beam	Ext. Col.	Int. Col.	SP (mm)	Beam	Ext. Col.	Int. Col.	SP (mm)	Beam	Ext. Col.	Int. Col.	SP (mm)
(1)	(2)	(3)	(4)	(5)	(6)	(7)	(8)	(9)	(10)	(11)	(12)	(13)
$\mu_{max} = 10$												
4	W6x12	W10x22	W12x26	254x254	W12x22	W14x34	W14x68	254x254	W12x40	W14x68	W14x120	203x203
3	W12x14	W10x22	W12x26	381x381	W16x45	W14x34	W14x68	381x381	W18x76	W14x68	W14x120	254x254
2	W12x22	W10x22	W12x35	381x381	W21x57	W14x61	W14x99	381x381	W24x94	W14x99	W14x193	305x305
1	W14x22	W10x22	W12x35	381x381	W21x68	W14x61	W14x99	381x381	W30x99	W14x99	W14x193	381x381
$\mu_{max} = 5$												
4	W12x14	W10x22	W12x26	381x381	W12x22	W14x34	W14x68	381x381	W12x40	W14x68	W14x120	305x305
3	W12x22	W10x22	W12x26	381x381	W16x45	W14x34	W14x68	381x381	W18x76	W14x68	W14x120	381x381
2	W14x22	W10x22	W12x40	381x381	W21x57	W14x61	W14x99	381x381	W24x94	W14x99	W14x193	381x381
1	W14x26	W10x22	W12x40	381x381	W21x68	W14x61	W14x99	381x381	W30x99	W14x99	W14x193	381x381
$\mu_{max} = 2.5$												
4	W12x22	W14x22	W12x40	381x381	W12x22	W14x34	W14x68	381x381	W12x40	W14x68	W14x120	381x381
3	W16x31	W14x22	W12x40	381x381	W16x45	W14x34	W14x68	381x381	W18x76	W14x68	W14x120	381x381
2	W16x40	W14x26	W12x65	457x381	W21x57	W14x61	W14x99	457x381	W24x94	W14x99	W14x193	457x381
1	W18x40	W14x26	W12x65	457x381	W21x68	W14x61	W14x99	457x381	W30x99	W14x99	W14x193	457x381
$\mu_{max} = 1.67$												
4	W16x26	W14x26	W12x58	381x381	W12x22	W14x34	W14x68	381x381	W12x40	W14x68	W14x120	381x381
3	W18x40	W14x26	W12x58	508x381	W16x45	W14x34	W14x68	381x381	W18x76	W14x68	W14x120	381x381
2	W18x50	W14x38	W12x87	610x381	W21x57	W14x61	W14x99	508x381	W24x94	W14x99	W14x193	381x381
1	W24x55	W14x38	W12x87	660x381	W21x68	W14x61	W14x99	559x381	W30x99	W14x99	W14x193	381x381

Pushover analysis was conducted for each of the resulting design, and corresponding pushover curves for each MDOF system are shown in Figures 7.3 to 7.5, which show good correlation between target and actual results. This indicates that pushover curves depicted in Figure 3.3, can yet be used to adequately design MDOF structural fuse systems. However, although the yield point and maximum strength are often (not always) well predicted in MDOF, the actual pushover curve is not perfectly tri-linear because all structural fuses do not yield simultaneously. Some of these differences between target and actual parameters are shown in Figures 7.3 to 7.5. For example, one of the cases with a large discrepancy is for $\alpha = 0.05$ and $\mu_{\max} = 1.67$ in Figure 7.5. This is due to the difficulty in design of matching the target α and μ_{\max} in those cases, as explained below.

Actual parameters and seismic response of the designed systems are presented in Tables 7.4 to 7.9, tabulated with respect to the target parameters. Note that η is generally closely matched in all studied cases. The reason for this, is that the frame and damping system elements are directly designed to match the required yield base shear, V_y . However, it may be seen that other target parameters like α and μ_{\max} are more difficult to meet. Furthermore, seismic response parameters (i.e., μ_f , μ , R , R_{μ} , Ω_o , W_f , and ρ) are also shown in Tables 7.4 to 7.9. These results indicate that the observations made in Section 4 for these parameters in SDOF cases, apply as well to MDOF systems.

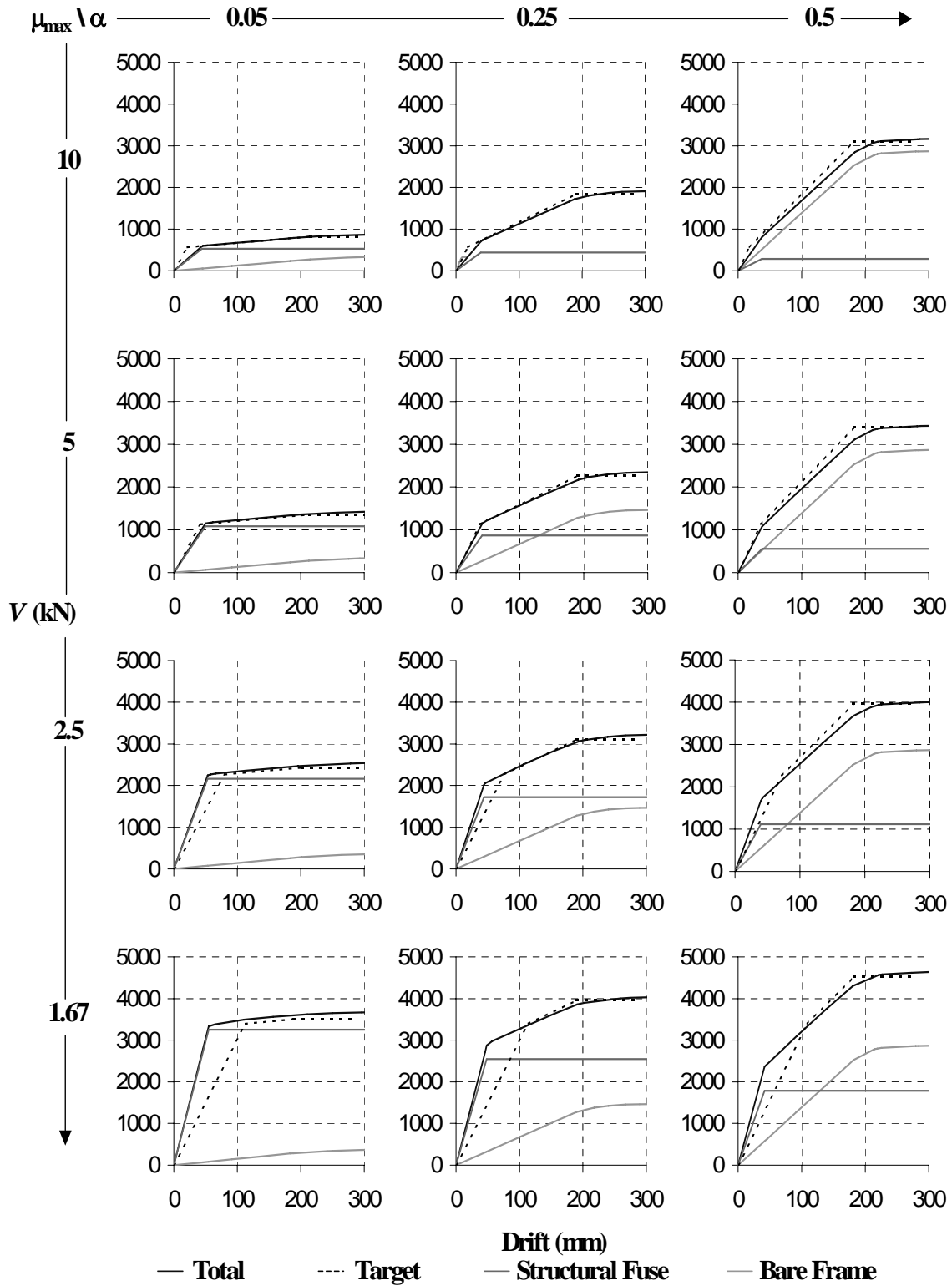


Figure 7.3. Pushover Curves of MODF Systems Designed with BRB

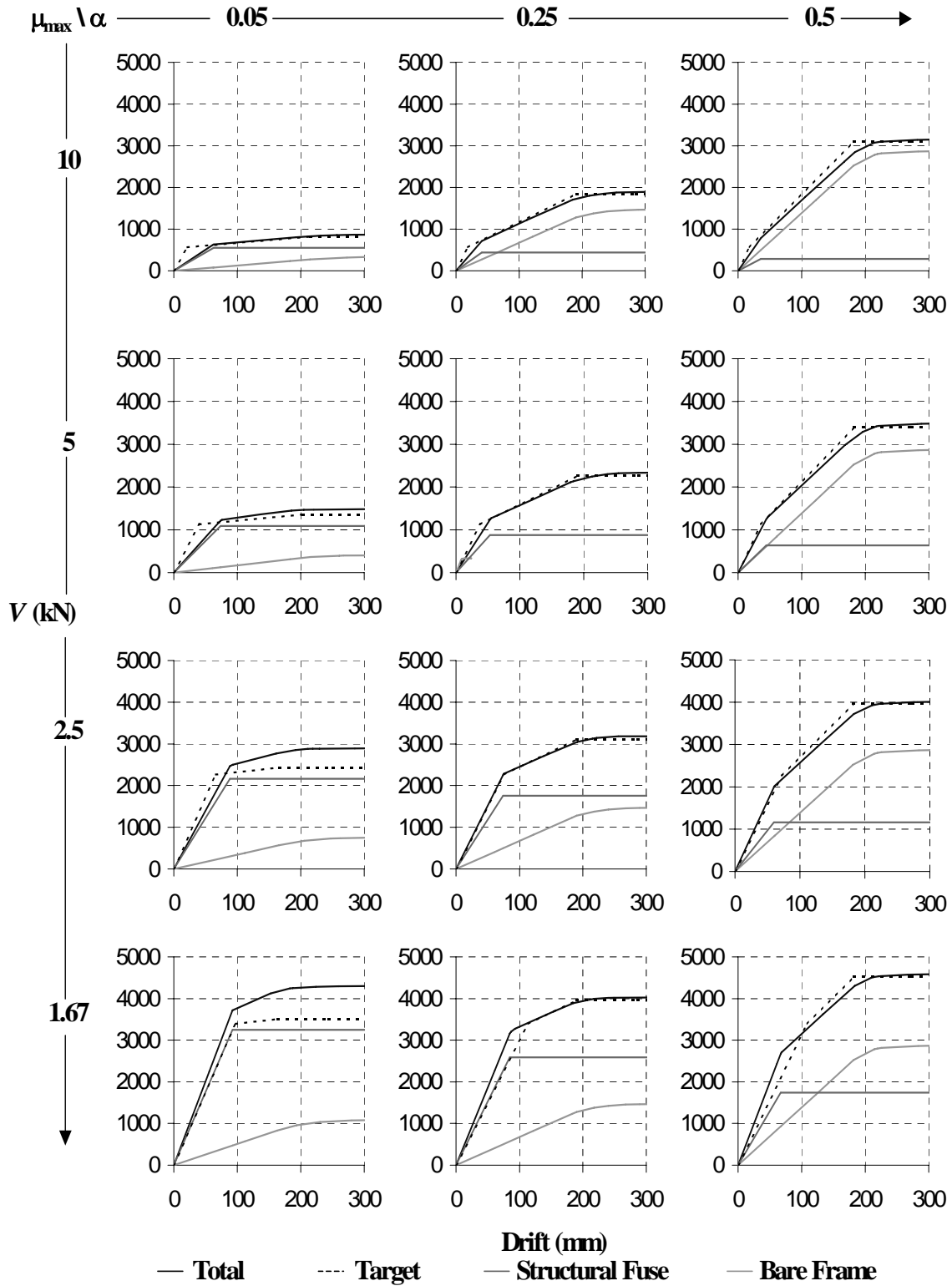


Figure 7.4. Pushover Curves of MODF Systems Designed with T-ADAS

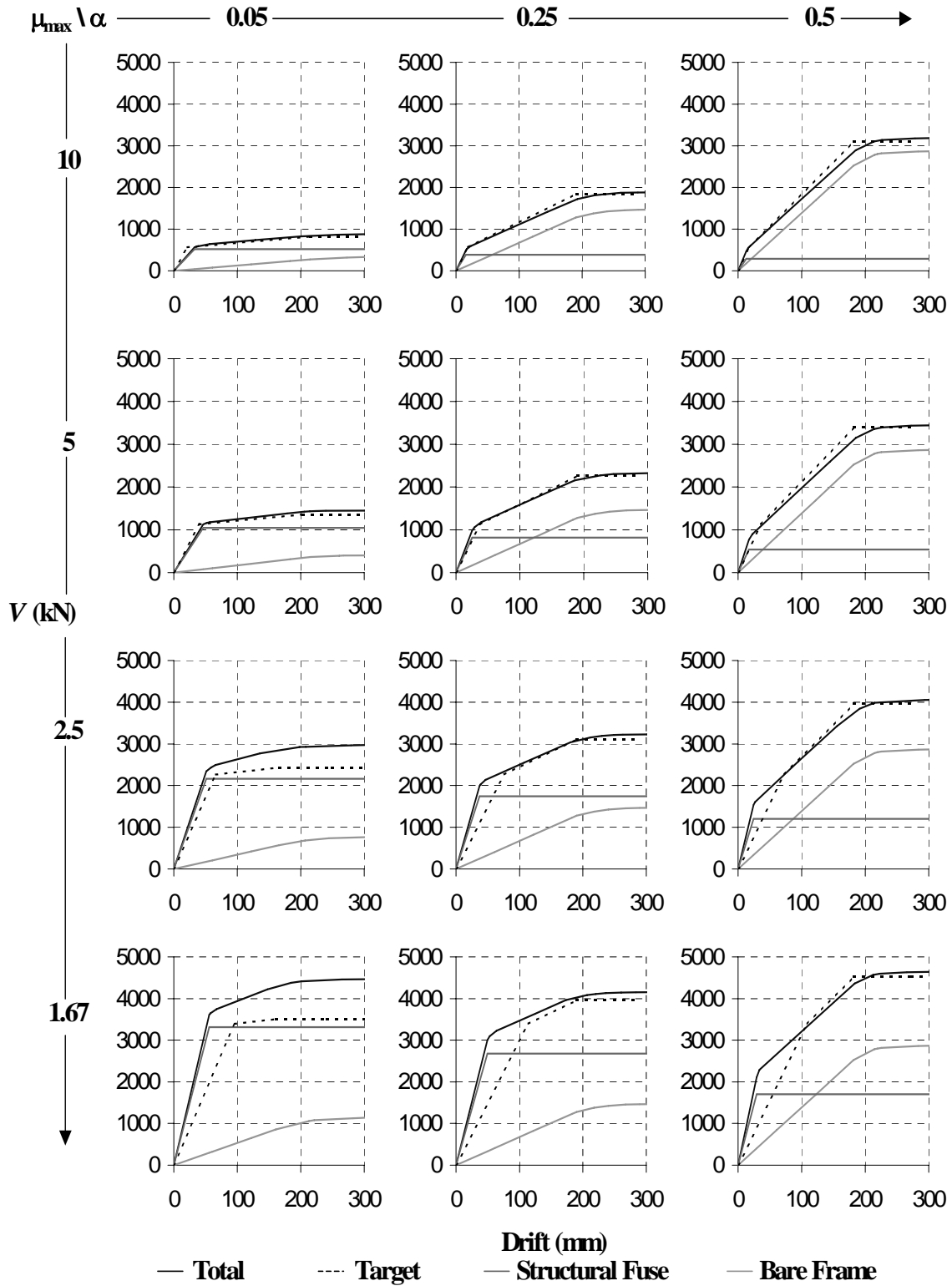


Figure 7.5. Pushover Curves of MODF Systems Designed with SP

Table 7.4. Design Parameters of MDOF Systems with BRB

$\alpha = 0.05$										$\alpha = 0.25$										$\alpha = 0.50$									
α	μ_{max}	η	T (s)	μ_f	μ	α	μ_{max}	η	T (s)	μ_f	μ	α	μ_{max}	η	T (s)	μ_f	μ	α	μ_{max}	η	T (s)	μ_f	μ						
(1)	(2)	(3)	(4)	(5)	(6)	(7)	(8)	(9)	(10)	(11)	(12)	(13)	(14)	(15)	(16)	(17)	(18)												
$\mu_{max} = 10$										$T_L = 1.58$ s																			
0.096	4.844	0.10	1.402	0.700	3.393	0.372	4.869	0.12	1.218	0.780	3.797	0.643	4.888	0.14	1.112	1.011	4.942												
$\mu_{max} = 5$										$T_L = 1.58$ s																			
0.056	4.254	0.20	1.057	0.613	2.609	0.240	4.689	0.20	0.975	0.678	3.180	0.487	4.805	0.19	0.969	0.741	3.560												
$\mu_{max} = 2.5$										$T_L = 1.58$ s																			
0.034	3.779	0.40	0.778	0.532	2.011	0.147	4.316	0.36	0.759	0.487	2.103	0.329	4.593	0.30	0.797	0.537	2.466												
$\mu_{max} = 1.67$										$T_L = 1.58$ s																			
0.025	3.446	0.59	0.647	0.486	1.676	0.113	3.934	0.51	0.661	0.446	1.753	0.244	4.376	0.42	0.687	0.515	2.254												

Table 7.5. Seismic Response of MDOF Systems with BRB

$\alpha = 0.05$										$\alpha = 0.25$										$\alpha = 0.50$									
Δ_r (mm)	R	R μ	Ω_0	W_t (kN)	ρ (%)	Δ_r (mm)	R	R μ	Ω_0	W_t (kN)	ρ (%)	Δ_r (mm)	R	R μ	Ω_0	W_t (kN)	ρ (%)												
(1)	(2)	(3)	(4)	(5)	(6)	(7)	(8)	(9)	(10)	(11)	(12)	(13)	(14)	(15)	(16)	(17)	(18)												
$\mu_{max} = 10$										$T_L = 1.58$ s																			
150	7.628	5.570	1.369	44.71	8.6%	148	7.346	3.009	2.441	107.38	2.9%	184	7.067	2.020	3.498	182.42	1.1%												
$\mu_{max} = 5$										$T_L = 1.58$ s																			
130	5.189	4.384	1.184	49.48	15.7%	129	5.687	3.018	1.885	110.48	5.7%	135	6.040	2.118	2.852	184.37	2.2%												
$\mu_{max} = 2.5$										$T_L = 1.58$ s																			
107	3.619	3.309	1.094	61.41	25.3%	93	4.118	2.769	1.487	116.73	10.7%	98	4.743	2.174	2.182	188.40	4.3%												
$\mu_{max} = 1.67$										$T_L = 1.58$ s																			
92	2.923	2.755	1.061	75.52	31.0%	85	3.322	2.494	1.332	122.51	14.9%	94	3.885	2.131	1.823	192.97	6.5%												

Table 7.6. Design Parameters of MDOF Systems with T-ADAS

$\alpha = 0.05$						$\alpha = 0.25$						$\alpha = 0.50$					
α	μ_{max}	η	T (s)	μ_f	μ	α	μ_{max}	η	T (s)	μ_f	μ	α	μ_{max}	η	T (s)	μ_f	μ
(1)	(2)	(3)	(4)	(5)	(6)	(7)	(8)	(9)	(10)	(11)	(12)	(13)	(14)	(15)	(16)	(17)	(18)
$\mu_{max} = 10$						$T_L = 1.58$ s											
0.127	3.426	0.11	1.596	0.731	2.506	0.385	4.642	0.13	1.247	0.779	3.614	0.636	5.071	0.14	1.110	0.997	5.058
$\mu_{max} = 5$						$T_L = 1.58$ s											
0.103	2.748	0.22	1.268	0.610	1.678	0.288	3.592	0.22	1.068	0.737	2.647	0.490	4.119	0.22	0.977	0.733	3.018
$\mu_{max} = 2.5$						$T_L = 1.58$ s											
0.123	1.877	0.44	0.973	0.746	1.400	0.221	2.565	0.40	0.931	0.620	1.591	0.416	3.042	0.35	0.896	0.637	1.937
$\mu_{max} = 1.67$						$T_L = 1.58$ s											
0.127	1.757	0.66	0.812	0.702	1.234	0.180	2.244	0.56	0.839	0.632	1.419	0.348	2.717	0.47	0.817	0.621	1.686

Table 7.7. Seismic Response of MDOF Systems with T-ADAS

$\alpha = 0.05$										$\alpha = 0.25$										$\alpha = 0.50$									
Δ_r (mm)	R	Rμ	Ω_0	W_t (kN)	ρ (%)	Δ_r (mm)	R	Rμ	Ω_0	W_t (kN)	ρ (%)	Δ_r (mm)	R	Rμ	Ω_0	W_t (kN)	ρ (%)												
(1)	(2)	(3)	(4)	(5)	(6)	(7)	(8)	(9)	(10)	(11)	(12)	(13)	(14)	(15)	(16)	(17)	(18)												
$\mu_{max} = 10$										$T_L = 1.58$ s																			
157	6.256	4.783	1.308	53.27	23.3%	148	7.077	2.944	2.404	115.62	9.9%	181	7.274	2.026	3.591	188.88	4.5%												
$\mu_{max} = 5$										$T_L = 1.58$ s																			
123	4.087	3.464	1.180	65.03	30.4%	140	4.778	2.735	1.747	120.33	13.4%	133	5.172	2.045	2.529	193.93	7.0%												
$\mu_{max} = 2.5$										$T_L = 1.58$ s																			
124	2.627	2.372	1.107	98.07	33.6%	118	3.002	2.231	1.346	130.94	20.4%	116	3.532	1.910	1.849	200.64	10.1%												
$\mu_{max} = 1.67$										$T_L = 1.58$ s																			
114	2.091	1.908	1.096	132.44	34.5%	120	2.381	1.944	1.224	139.78	25.4%	113	2.895	1.812	1.597	206.39	12.6%												

Table 7.8. Design Parameters of MDOF Systems with SP

$\alpha = 0.05$						$\alpha = 0.25$						$\alpha = 0.50$					
α	μ_{\max}	η	T (s)	μ_f	μ	α	μ_{\max}	η	T (s)	μ_f	μ	α	μ_{\max}	η	T (s)	μ_f	μ
(1)	(2)	(3)	(4)	(5)	(6)	(7)	(8)	(9)	(10)	(11)	(12)	(13)	(14)	(15)	(16)	(17)	(18)
$\mu_{\max} = 10$						$T_L = 1.58$ s											
0.074	6.579	0.10	1.224	0.539	3.547	0.211	12.322	0.09	0.932	0.701	8.639	0.375	14.310	0.08	0.859	0.798	11.419
$\mu_{\max} = 5$						$T_L = 1.58$ s											
0.070	4.363	0.20	1.047	0.575	2.509	0.173	7.506	0.17	0.834	0.535	4.019	0.303	10.801	0.14	0.775	0.579	6.251
$\mu_{\max} = 2.5$						$T_L = 1.58$ s											
0.075	3.244	0.41	0.762	0.542	1.759	0.125	5.146	0.35	0.703	0.442	2.276	0.218	7.511	0.27	0.655	0.443	3.325
$\mu_{\max} = 1.67$						$T_L = 1.58$ s											
0.083	2.869	0.64	0.638	0.508	1.457	0.111	3.845	0.53	0.657	0.401	1.540	0.192	6.234	0.37	0.614	0.427	2.663

Table 7.9. Seismic Response of MDOF Systems with SP

$\alpha = 0.05$											$\alpha = 0.25$											$\alpha = 0.50$										
Δ_r (mm)	R	Rμ	Ω_0	W_t (kN)	ρ (%)	Δ_r (mm)	R	Rμ	Ω_0	W_t (kN)	ρ (%)	Δ_r (mm)	R	Rμ	Ω_0	W_t (kN)	ρ (%)															
(1)	(2)	(3)	(4)	(5)	(6)	(7)	(8)	(9)	(10)	(11)	(12)	(13)	(14)	(15)	(16)	(17)	(18)															
$\mu_{\max} = 10$											$T_L = 1.58$ s																					
116	9.140	6.468	1.413	50.82	19.6%	133	13.789	4.064	3.393	113.20	7.9%	145	15.634	2.609	5.993	187.97	4.1%															
$\mu_{\max} = 5$											$T_L = 1.58$ s																					
116	5.348	4.328	1.235	58.88	23.2%	102	7.659	3.609	2.122	115.99	10.1%	105	10.559	2.661	3.968	190.44	5.3%															
$\mu_{\max} = 2.5$											$T_L = 1.58$ s																					
90	3.534	3.027	1.168	91.55	27.5%	84	4.504	2.969	1.517	124.49	16.3%	80	6.265	2.587	2.421	197.44	8.7%															
$\mu_{\max} = 1.67$											$T_L = 1.58$ s																					
81	2.738	2.372	1.155	120.25	26.9%	76	3.195	2.430	1.315	129.28	19.4%	78	4.874	2.432	2.004	200.73	10.2%															

Hysteresis loops of story shear versus drift are shown for all the systems in Figures 7.6 to 7.17. Note that the hysteresis loops in all cases are consistent with the schematic pushover curves depicted in Figure 3.3. The bilinear character of the loops indicates that the elastic behavior of the frame structure to be protected by the structural fuses is not exceeded (i.e., plastic plateau is not reached), which is also indicated by the tabulated results for μ_p . These figures also show that MDOF systems with BRB, T-ADAS, and SP devices have similar behavior, which was a desirable outcome since they all have been designed under the same target parameters (i.e., none of the studied systems can be considered better than the others based on hysteretic response only).

Finally, energy dissipated throughout the action of hysteretic and inherent viscous damping is presented in Figures 7.18 to 7.20. It may be seen that metallic dampers are more effective in terms of energy dissipation, for systems designed with large values of μ_{max} (i.e., large capacity to undergo inelastic deformations without exceeding the elastic behavior of the frames' beams and columns).

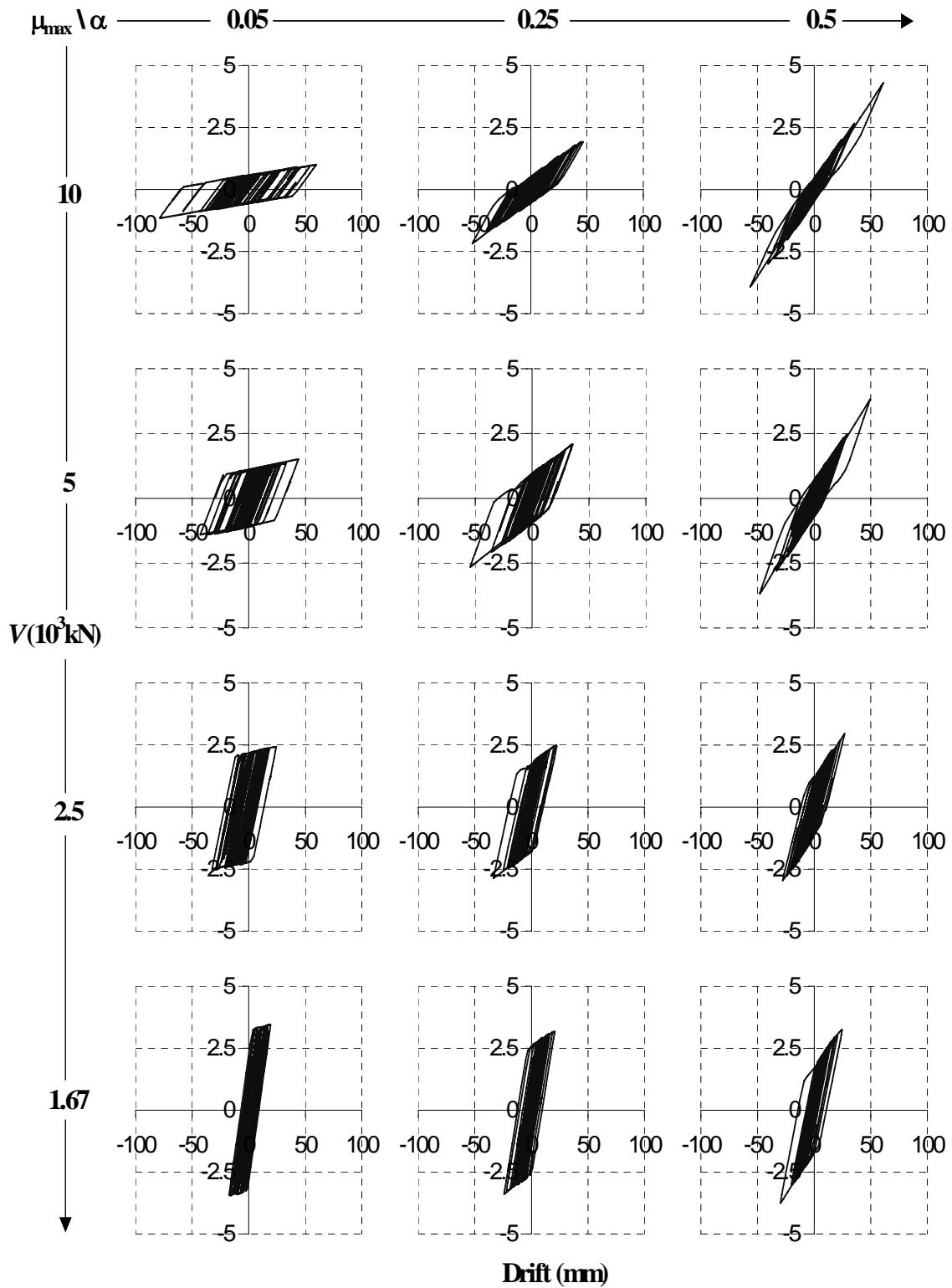


Figure 7.6. First Story Shear vs Drift of MDOF Systems Designed with BRB

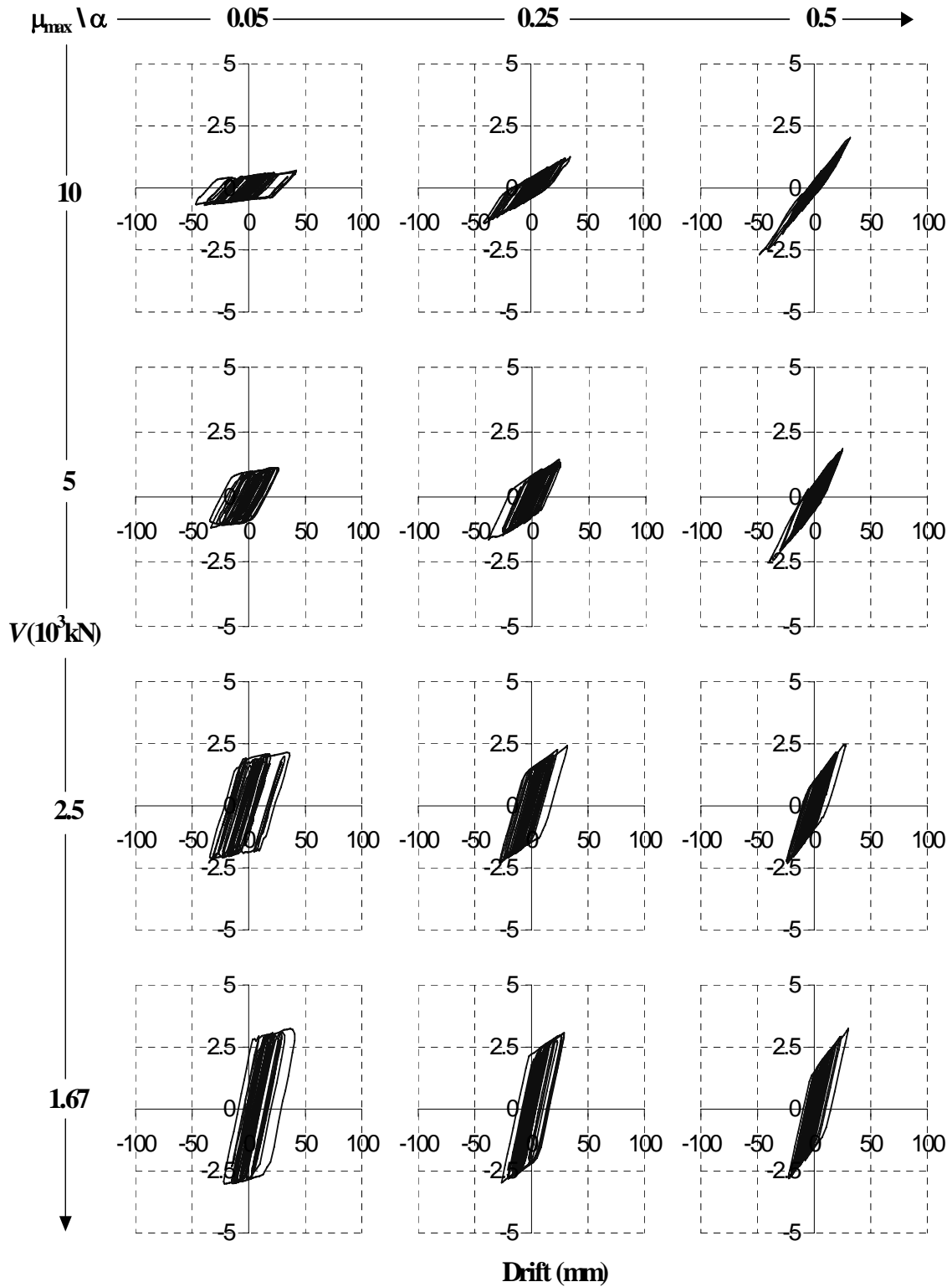


Figure 7.7. Second Story Shear vs Drift of MDOF Systems Designed with BRB

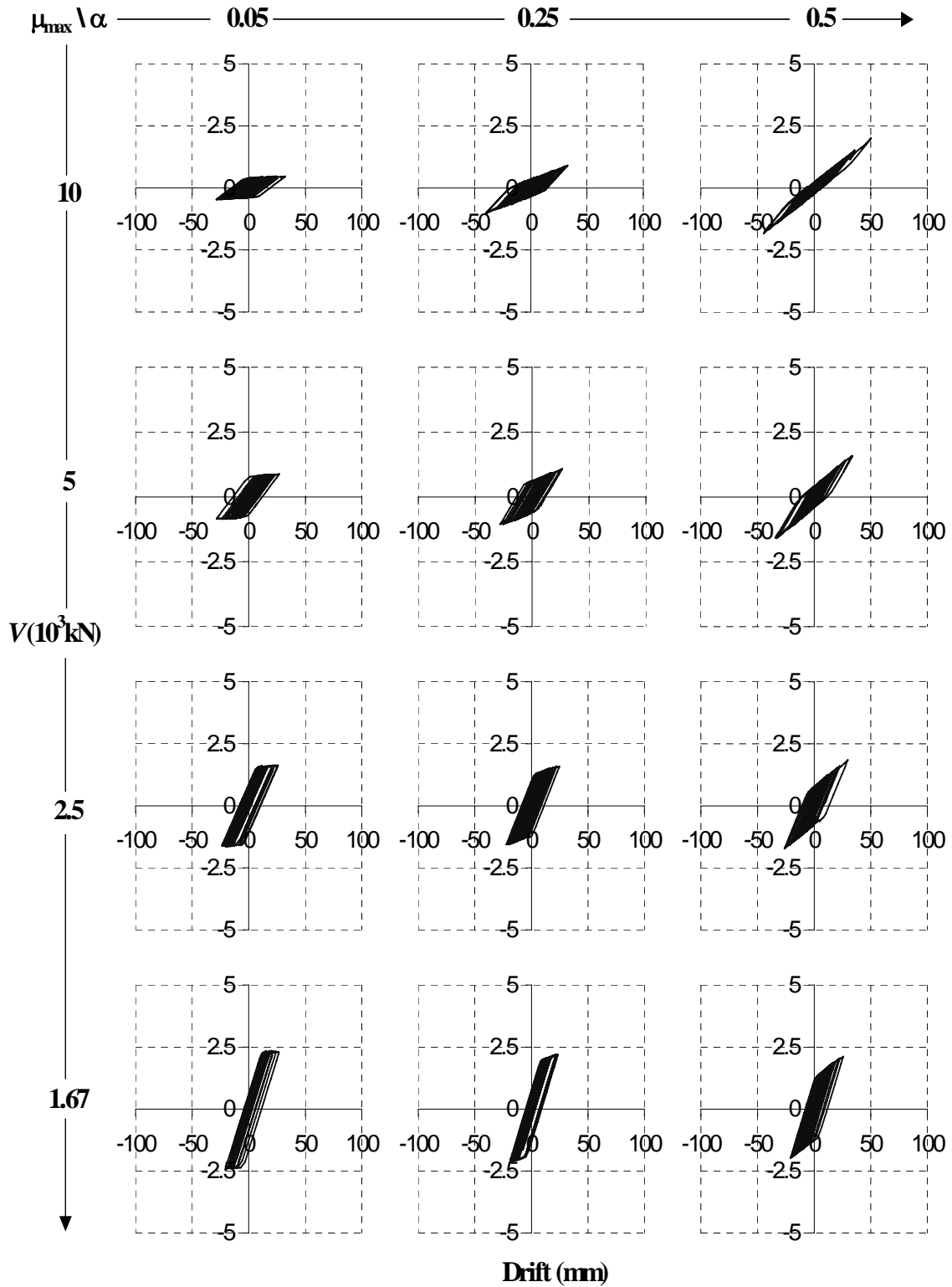


Figure 7.8. Third Story Shear vs Drift of MDOF Systems Designed with BRB

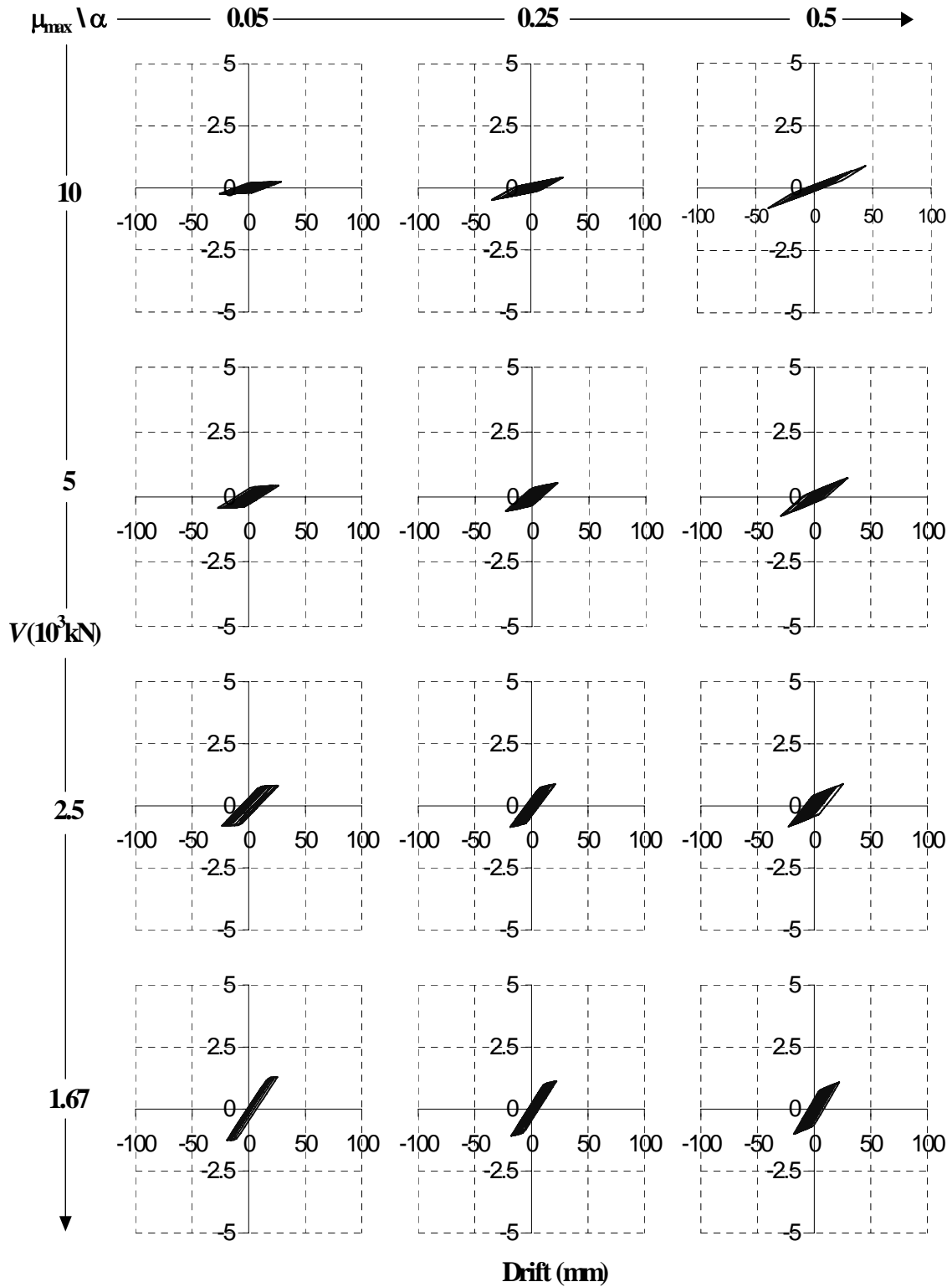


Figure 7.9. Fourth Story Shear vs Drift of MDOF Systems Designed with BRB

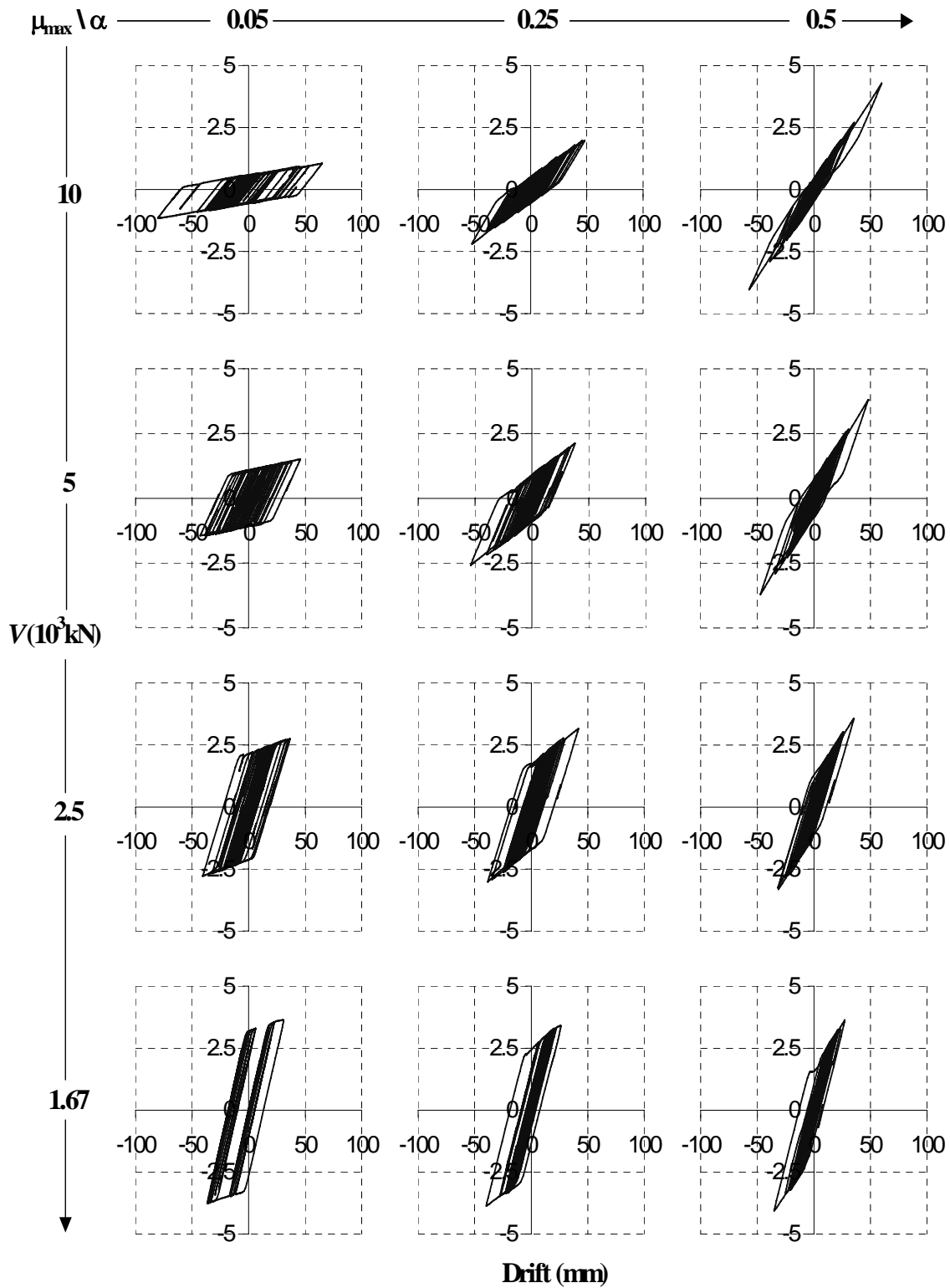


Figure 7.10. First Story Shear vs Drift of MDOF Systems Designed with T-ADAS

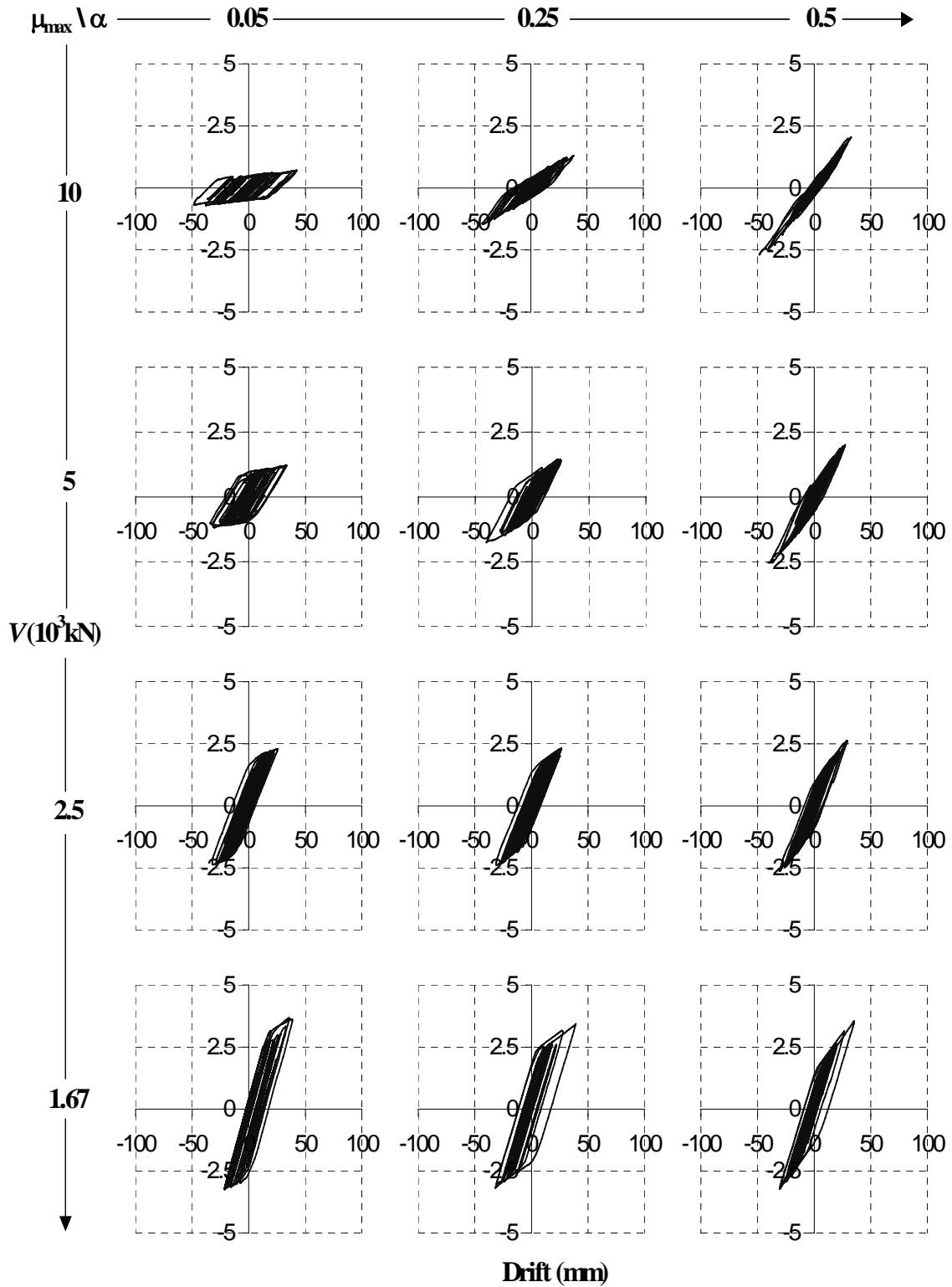


Figure 7.11. Second Story Shear vs Drift of MDOF Systems Designed with T-ADAS

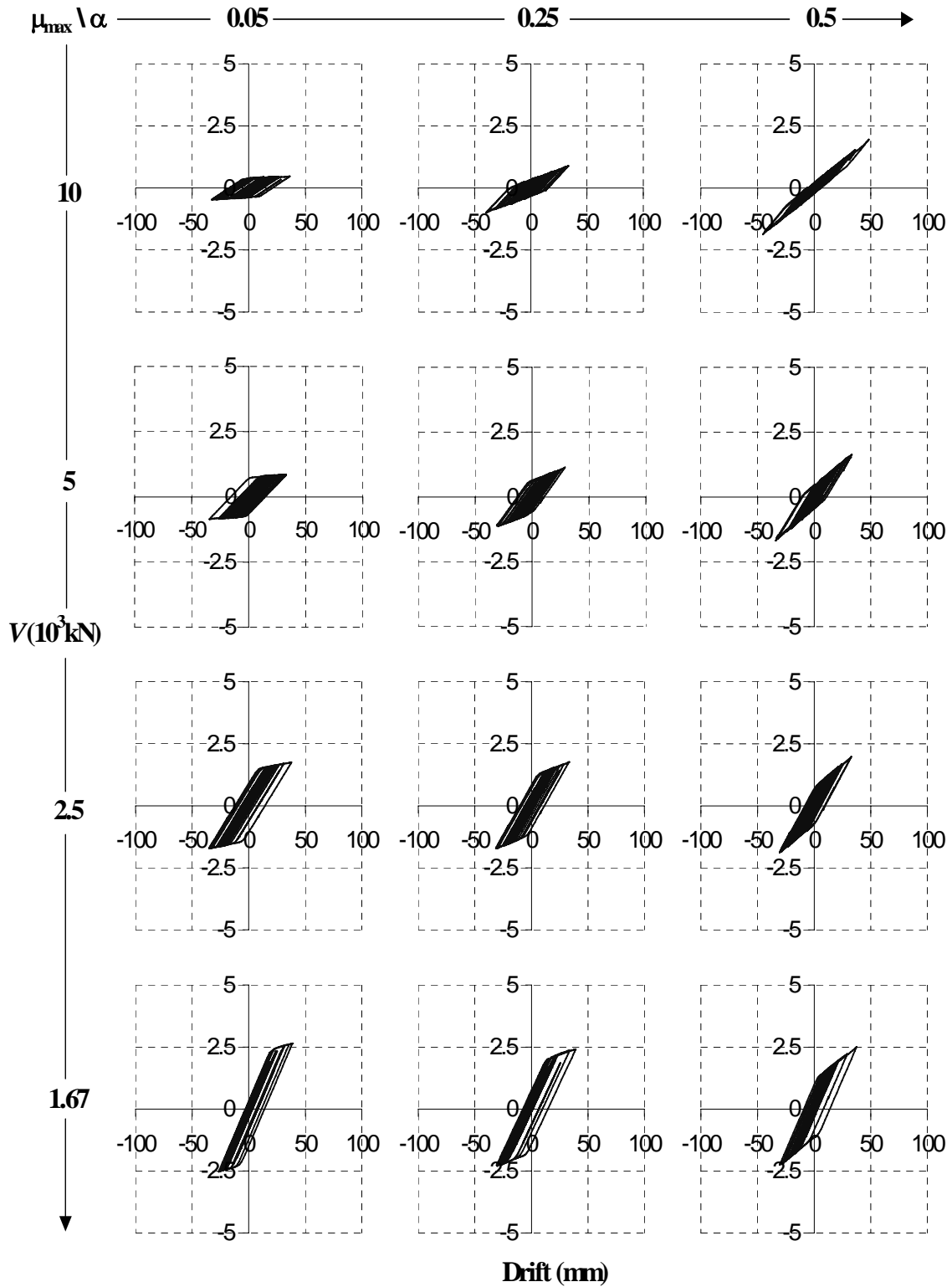


Figure 7.12. Third Story Shear vs Drift of MDOF Systems Designed with T-ADAS

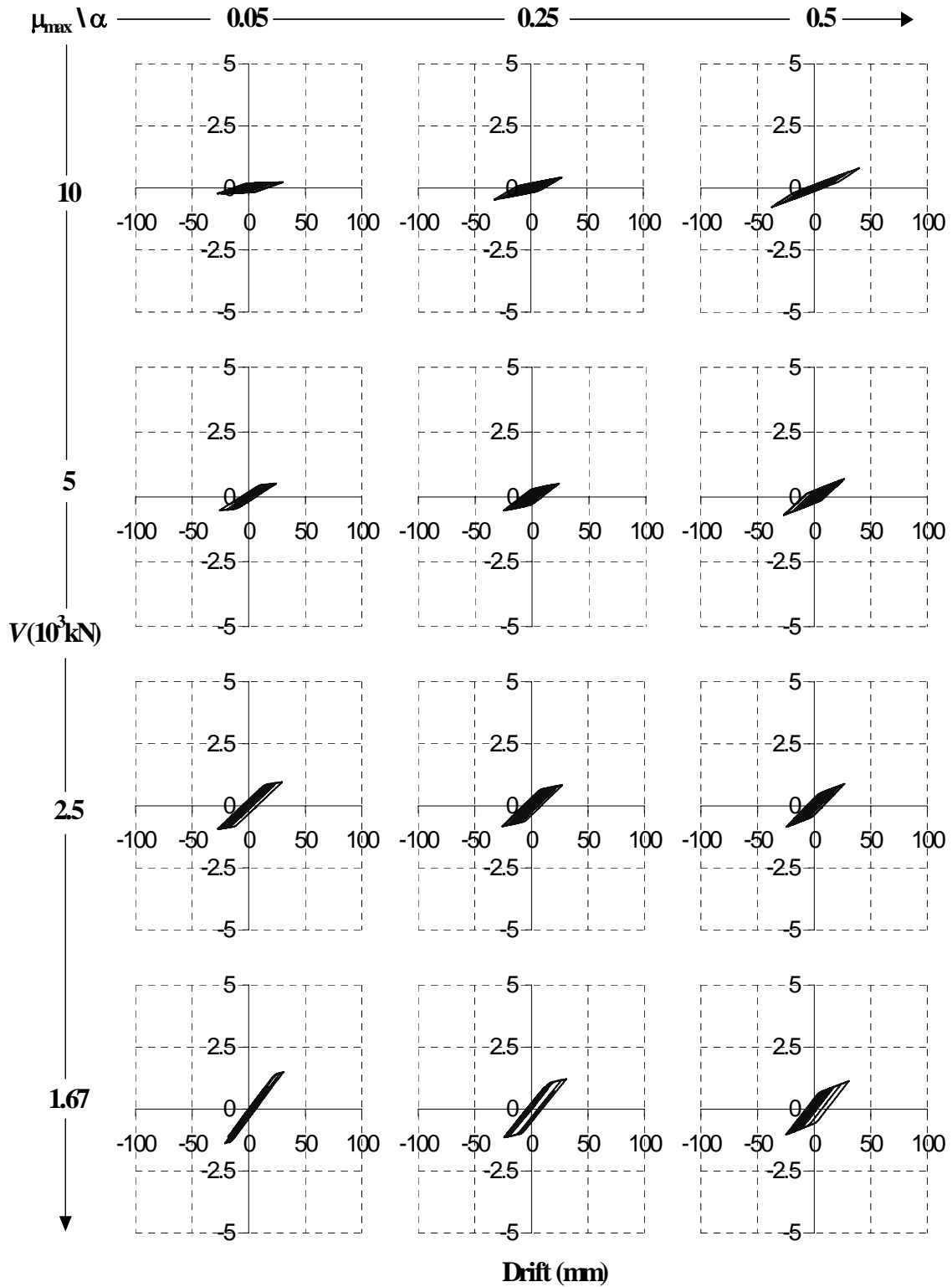


Figure 7.13. Fourth Story Shear vs Drift of MDOF Systems Designed with T-ADAS

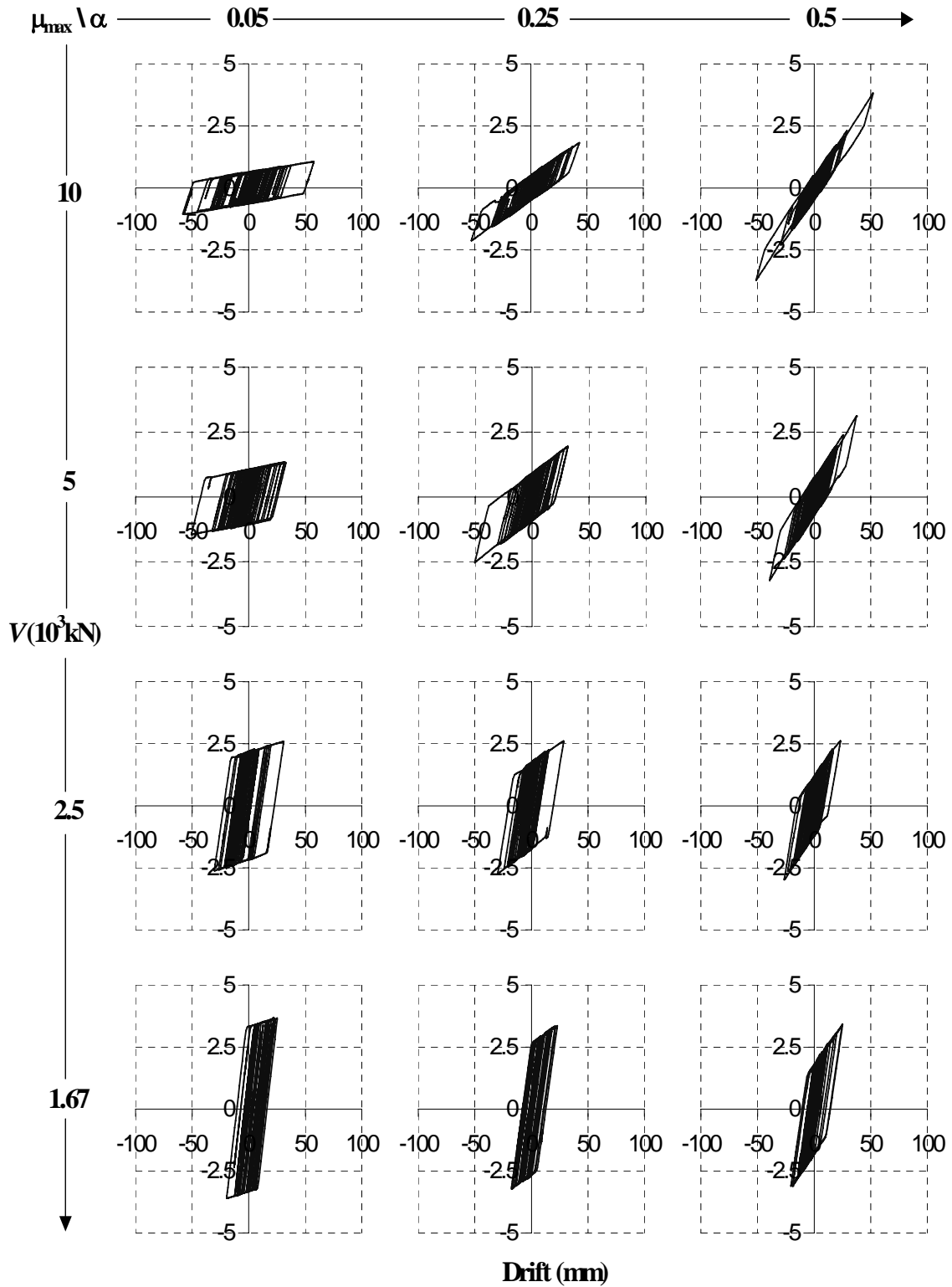


Figure 7.14. First Story Shear vs Drift of MDOF Systems Designed with SP

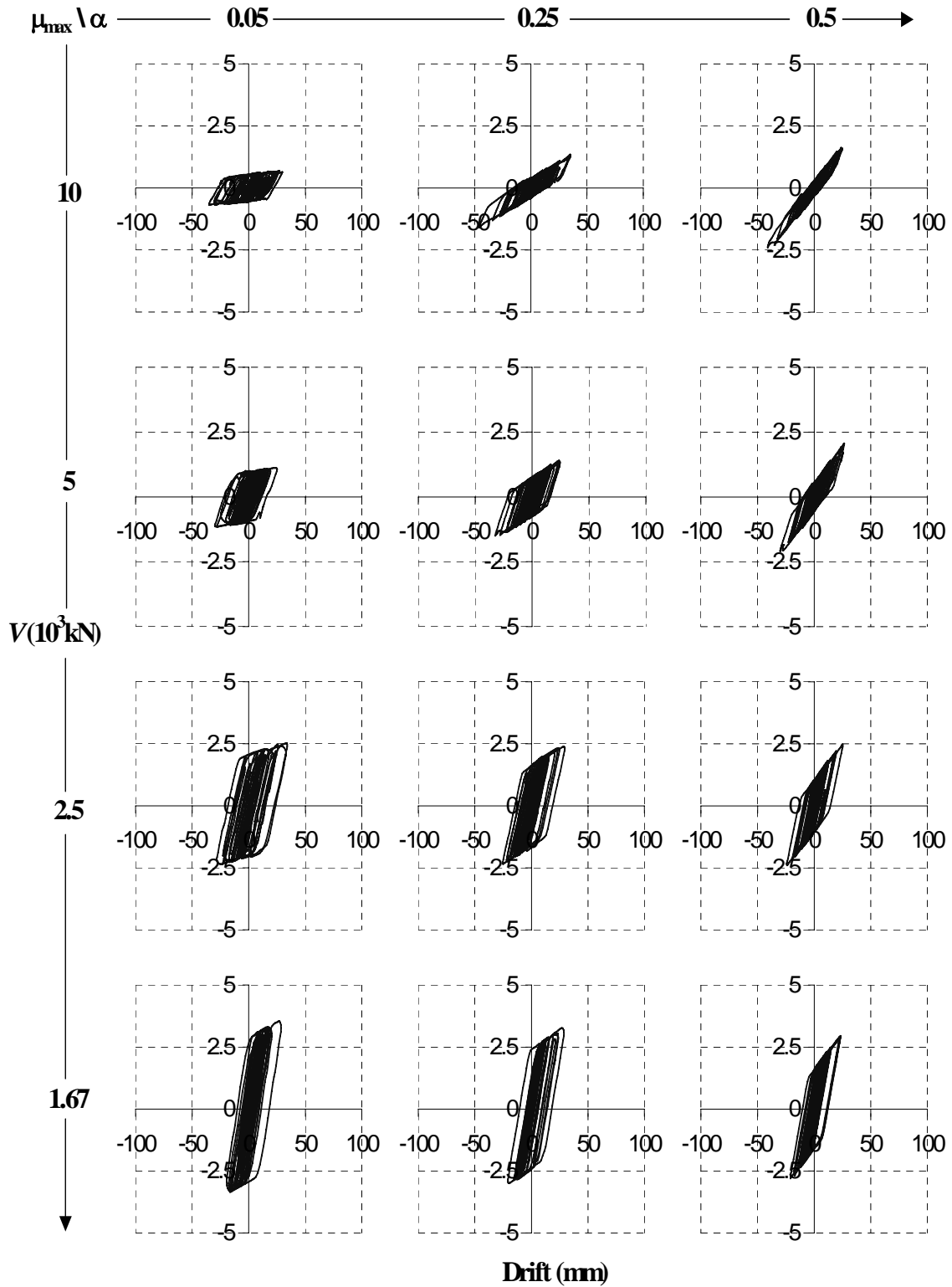


Figure 7.15. Second Story Shear vs Drift of MDOF Systems Designed with SP

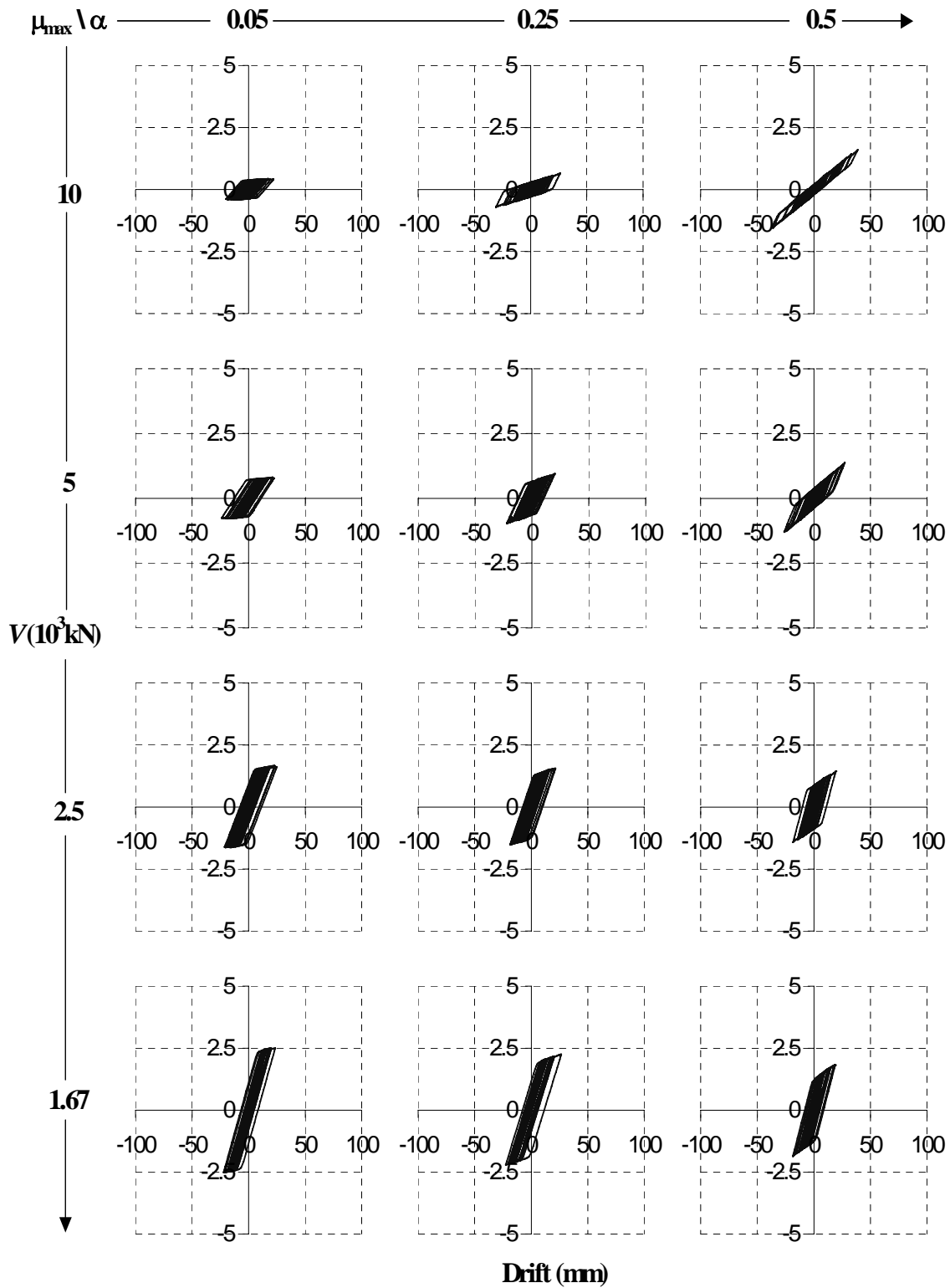


Figure 7.16. Third Story Shear vs Drift of MDOF Systems Designed with SP

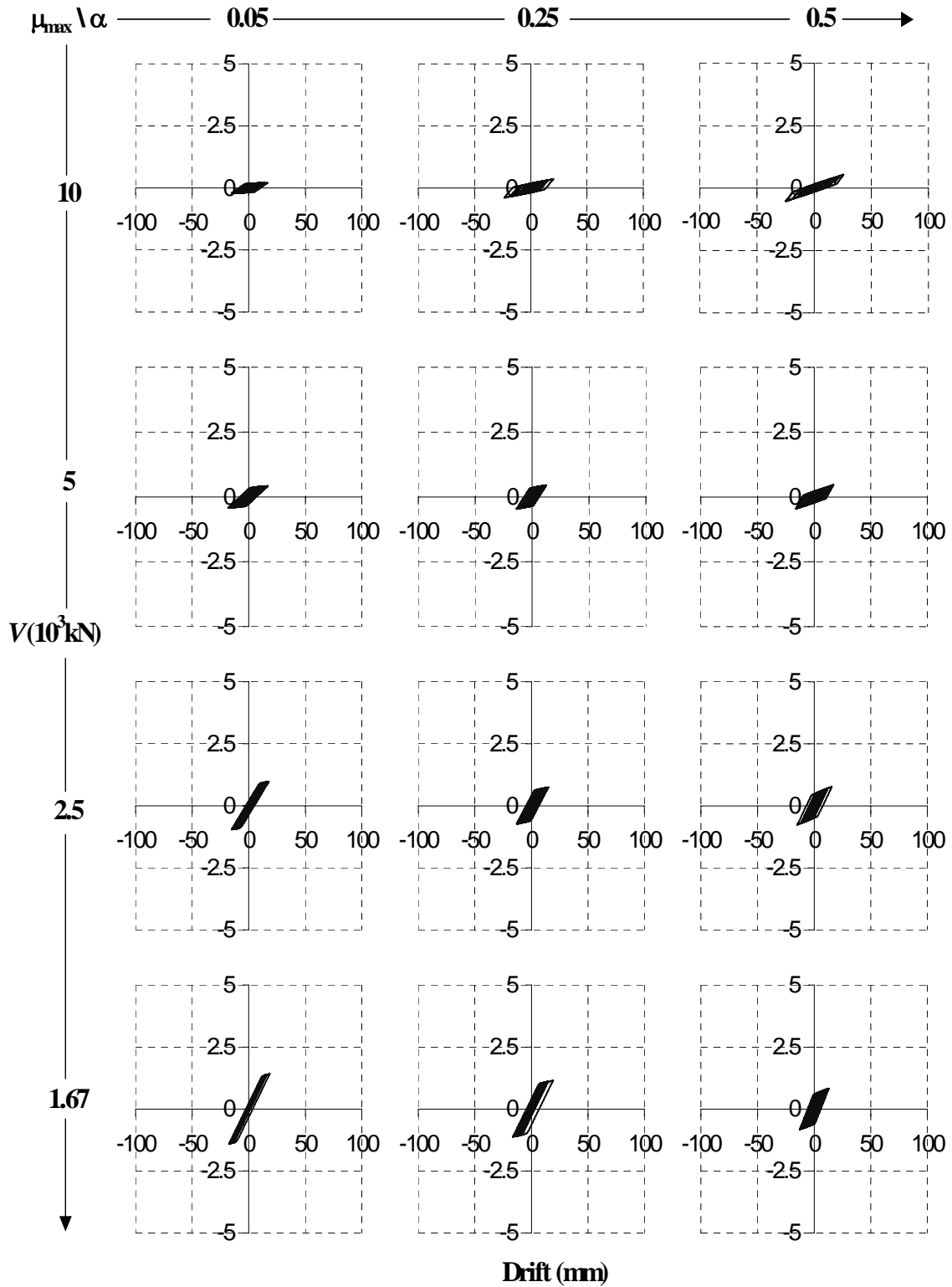


Figure 7.17. Fourth Story Shear vs Drift of MDOF Systems Designed with SP

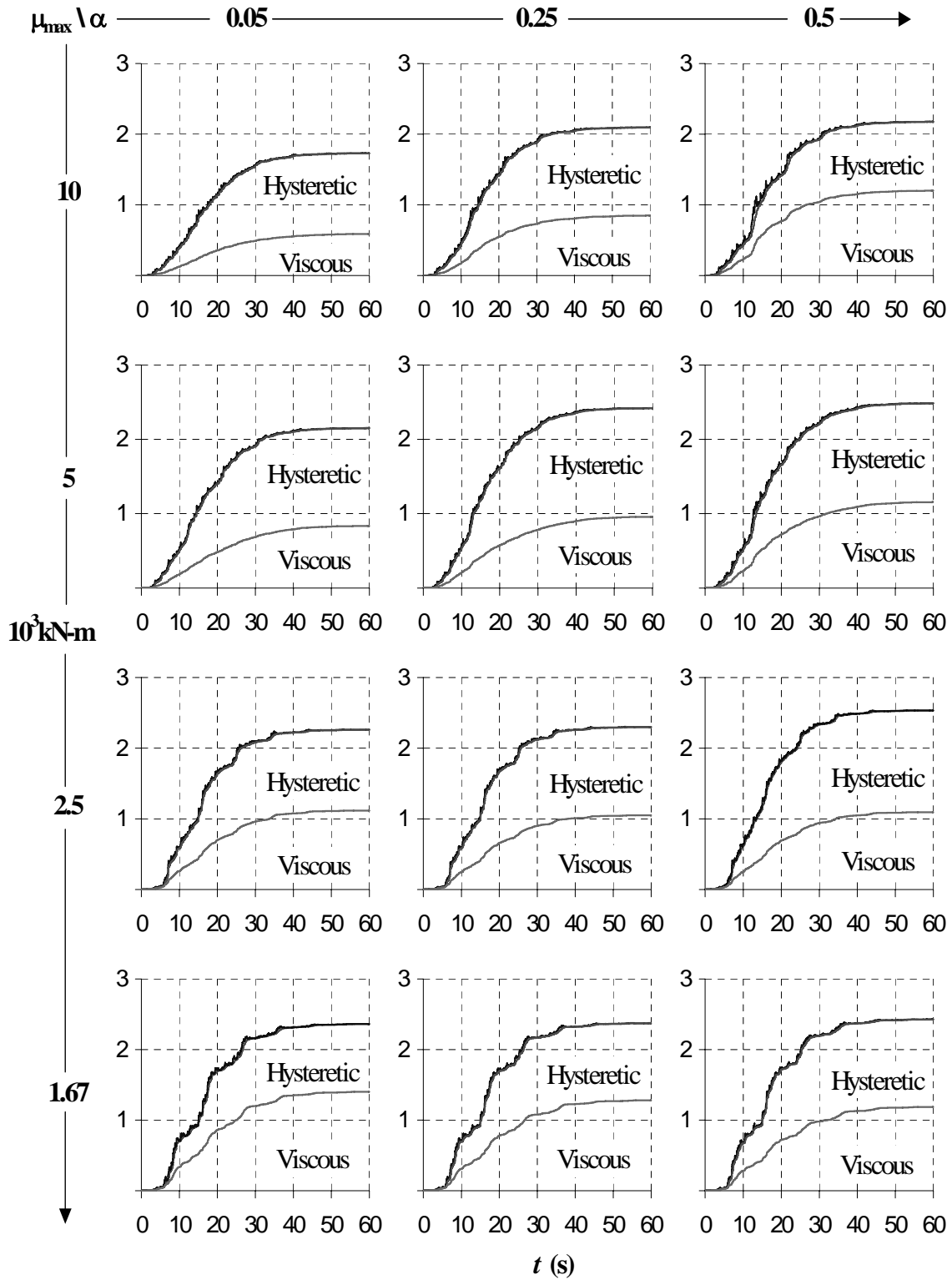


Figure 7.18. Energy of MDOF Systems Designed with BRB

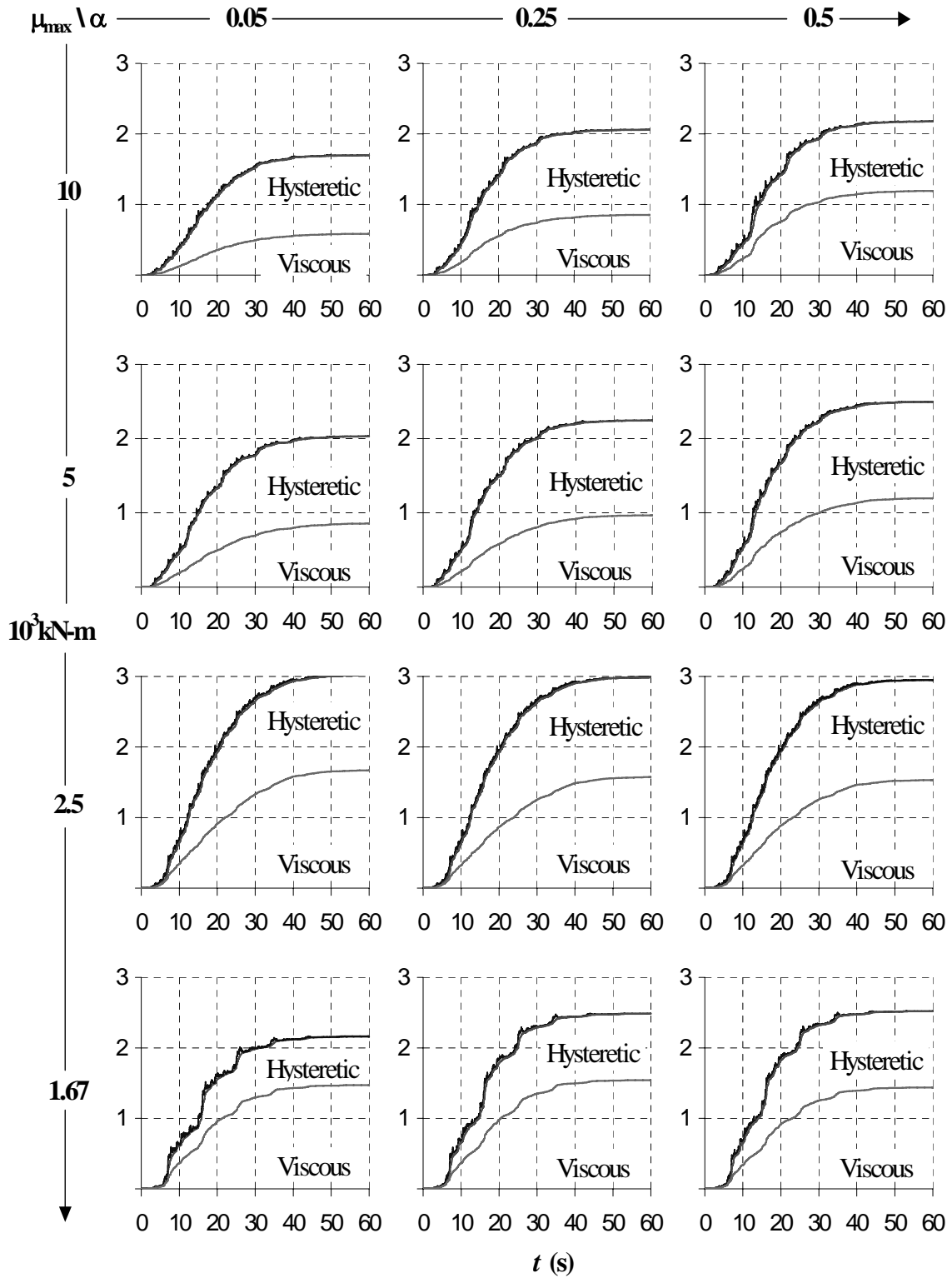


Figure 7.19. Energy of MDOF Systems Designed with T-ADAS

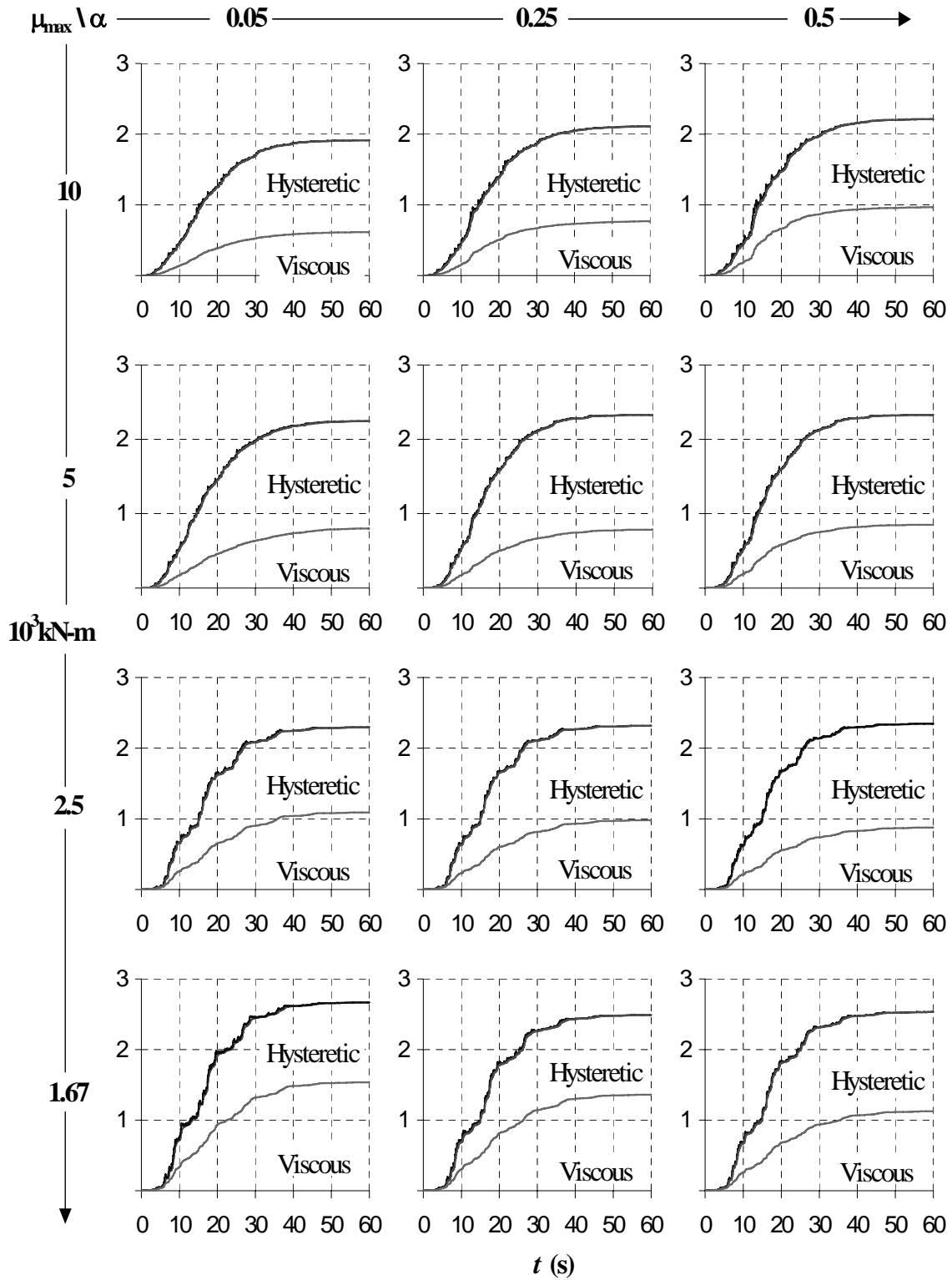


Figure 7.20. Energy of MDOF Systems Designed with SP

7.4. Retrofit Design Examples

Based on the geometry of the MCEER Demonstration Hospital, a bare frame has been arbitrarily selected to be retrofitted using BRB, T-ADAS, and SP devices in order to satisfy the structural fuse concept. The “existing” frame properties are presented in Table 7.10, along with the metallic dampers properties used in the retrofit process. For illustration purposes, the mass matrix and the mode shape used in the design examples for new construction are again used in this section.

Time history analysis performed for the bare frame indicates that the system maximum story drift is 2.5%, which is greater than the allowable story drift of 2% used in this study. Furthermore, the frame is subjected to a ductility demand of about 2, which implies some damage to the main structure due to inelastic rotations in plastic hinges (or fracture of pre-Northridge beam-to-column welded connections), during an earthquake compatible to the design spectrum. Using BRB, T-ADAS, and SP devices as metallic fuse systems, the existing frame is retrofitted in subsequent examples to improve its seismic performance, and also to satisfy the structural fuse concept.

Properties of the existing frame are: $V_{yf} = 1067$ kN, $\Delta_{yf} = 155$ mm (roof displacement), and $K_f = 6.88$ kN/mm (total base shear divided by roof displacement), and considered constant for all retrofits considered in this parametric study. The elastic limit period, T_L , is determined as the smallest value between (4.59) and (7.1) (i.e., $T_L = 1.09$ s for a story drift limit of 2%). Note that from Table 4.1, many sets of η and μ_{\max} values can be selected to provide a response in the region of admissible solutions, for a given elastic period limit (i.e., 1.09 s in this case). As described in Section 4.3, for this elastic period limit (i.e., 1.09 s), it is preferable to select $\eta \leq 0.2$ and $\mu_{\max} \geq 5$. Here, many different combinations are considered for proof of concept purposes.

Results of the retrofit examples are presented in Tables 7.10 to 7.12. Pushover curves of the retrofitted systems are presented in Figure 7.21, where generally good agreement

between target and actual response may be seen. Hysteresis loops and energy dissipation plots are also presented in Figures 7.22 to 7.26.

The tabulated results and illustrations indicate that all the observations previously made for the design examples (see Section 7.3.1) for new construction, apply again to the retrofitting cases.

Table 7.10. MDOF Systems Retrofitted with Structural Fuses

Story	Existing Frame			B R B		T - A D A S			S P	
	Beam	Ext. Col.	Int. Col.	Plate (mm)	Plate (mm)	Braces (HSS)	Plate (mm)	Braces (HSS)	Plate (mm)	Braces (HSS)
(1)	(2)	(3)	(4)	(5)	(6)	(7)	(8)	(9)	(8)	(9)
$\mu_{max} = 10$										
4	W18X40	W14x48	W14x53	25x13	8	254x381x19	203x203	4x4x3/16	4x4x3/16	4x4x3/16
3	W21X44	W14x48	W14x53	51x13	15	254x381x19	254x254	4.5x4.5x1/4	4.5x4.5x1/4	4.5x4.5x1/4
2	W21X50	W14x53	W14x82	70x13	20	254x381x19	305x305	5x5x1/4	5x5x1/4	5x5x1/4
1	W24X55	W14x53	W14x82	76x13	22	254x381x19	305x305	5x5x5/16	5x5x5/16	5x5x5/16
$\mu_{max} = 5$										
4	W18X40	W14x48	W14x53	38x19	9	254x381x25	254x254	5x5x3/16	5x5x3/16	5x5x3/16
3	W21X44	W14x48	W14x53	70x19	17	254x381x25	305x305	6x6x1/4	6x6x1/4	6x6x1/4
2	W21X50	W14x53	W14x82	89x19	22	254x381x25	381x381	6x6x5/16	6x6x5/16	6x6x5/16
1	W24X55	W14x53	W14x82	102x19	25	254x381x25	381x381	6x6x3/8	6x6x3/8	6x6x3/8
$\mu_{max} = 2.5$										
4	W18X40	W14x48	W14x53	51x25	11	254x381x32	254x254	5x5x3/8	5x5x3/8	5x5x3/8
3	W21X44	W14x48	W14x53	102x25	21	254x381x32	305x305	7x7x5/16	7x7x5/16	7x7x5/16
2	W21X50	W14x53	W14x82	133x25	28	254x381x32	381x381	7x7x1/2	7x7x1/2	7x7x1/2
1	W24X55	W14x53	W14x82	159x25	32	254x381x32	381x381	8x8x3/8	8x8x3/8	8x8x1/2
$\mu_{max} = 1.67$										
4	W18X40	W14x48	W14x53	64x32	12	254x381x38	305x305	7x7x1/4	7x7x1/4	7x7x1/4
3	W21X44	W14x48	W14x53	121x32	22	254x381x38	381x381	7x7x1/2	7x7x1/2	7x7x1/2
2	W21X50	W14x53	W14x82	159x32	29	254x381x38	508x381	8x8x1/2	8x8x1/2	8x8x1/2
1	W24X55	W14x53	W14x82	191x32	33	254x381x38	508x381	8x8x5/8	8x8x5/8	8x8x5/8

Table 7.11. Design Parameters of MDOF Systems Retrofitted with Structural Fuses

BRB						T-A D A S						SP					
α	μ_{max}	η	T (s)	μ_f	μ	α	μ_{max}	η	T (s)	μ_f	μ	α	μ_{max}	η	T (s)	μ_f	μ
(1)	(2)	(3)	(4)	(5)	(6)	(7)	(8)	(9)	(10)	(11)	(12)	(13)	(14)	(15)	(16)	(17)	(18)
$\mu_{max} = 10$ $\eta = 0.10$ $T_f = 1.09$ s																	
0.447	3.020	0.14	1.338	0.945	2.853	0.543	1.867	0.19	1.484	1.127	2.105	0.209	9.098	0.10	0.918	0.796	7.245
$\mu_{max} = 5$ $\eta = 0.20$ $T_f = 1.09$ s																	
0.293	2.921	0.22	1.082	0.893	2.610	0.357	2.060	0.26	1.198	1.000	2.060	0.166	5.570	0.20	0.812	0.638	3.552
$\mu_{max} = 2.5$ $\eta = 0.40$ $T_f = 1.09$ s																	
0.186	2.606	0.39	0.849	0.710	1.851	0.226	1.989	0.42	0.948	0.826	1.643	0.174	2.817	0.39	0.687	0.564	1.590
$\mu_{max} = 1.67$ $\eta = 0.60$ $T_f = 1.09$ s																	
0.140	2.427	0.53	0.733	0.666	1.616	0.169	1.903	0.59	0.814	0.781	1.486	0.108	3.473	0.50	0.645	0.499	1.732

Table 7.12. Seismic Response of MDOF Systems Retrofitted with Structural Fuses

BRB						T-A D A S						SP					
Δ_r (mm)	R	R μ	Ω_0	W_f (kN)	ρ (%)	Δ_r (mm)	R	R μ	Ω_0	W_f (kN)	ρ (%)	Δ_r (mm)	R	R μ	Ω_0	W_f (kN)	ρ (%)
(1)	(2)	(3)	(4)	(5)	(6)	(7)	(8)	(9)	(10)	(11)	(12)	(13)	(14)	(15)	(16)	(17)	(18)
$\mu_{max} = 10$ $\eta = 0.10$ $T_f = 1.09$ s																	
146	5.964	3.135	1.903	101.37	2.3%	175	4.043	2.748	1.471	112.33	11.9%	123	12.244	4.548	2.692	108.20	8.5%
$\mu_{max} = 5$ $\eta = 0.20$ $T_f = 1.09$ s																	
138	4.684	2.996	1.564	103.75	4.6%	155	3.633	2.635	1.379	118.20	16.2%	99	6.759	3.838	1.761	112.18	11.7%
$\mu_{max} = 2.5$ $\eta = 0.40$ $T_f = 1.09$ s																	
110	3.372	2.597	1.298	108.43	8.7%	128	2.810	2.296	1.224	129.32	23.4%	87	4.220	3.207	1.316	120.10	17.6%
$\mu_{max} = 1.67$ $\eta = 0.60$ $T_f = 1.09$ s																	
103	2.872	2.394	1.200	113.13	12.5%	121	2.339	2.029	1.153	138.55	28.5%	77	3.454	2.724	1.268	127.32	22.2%

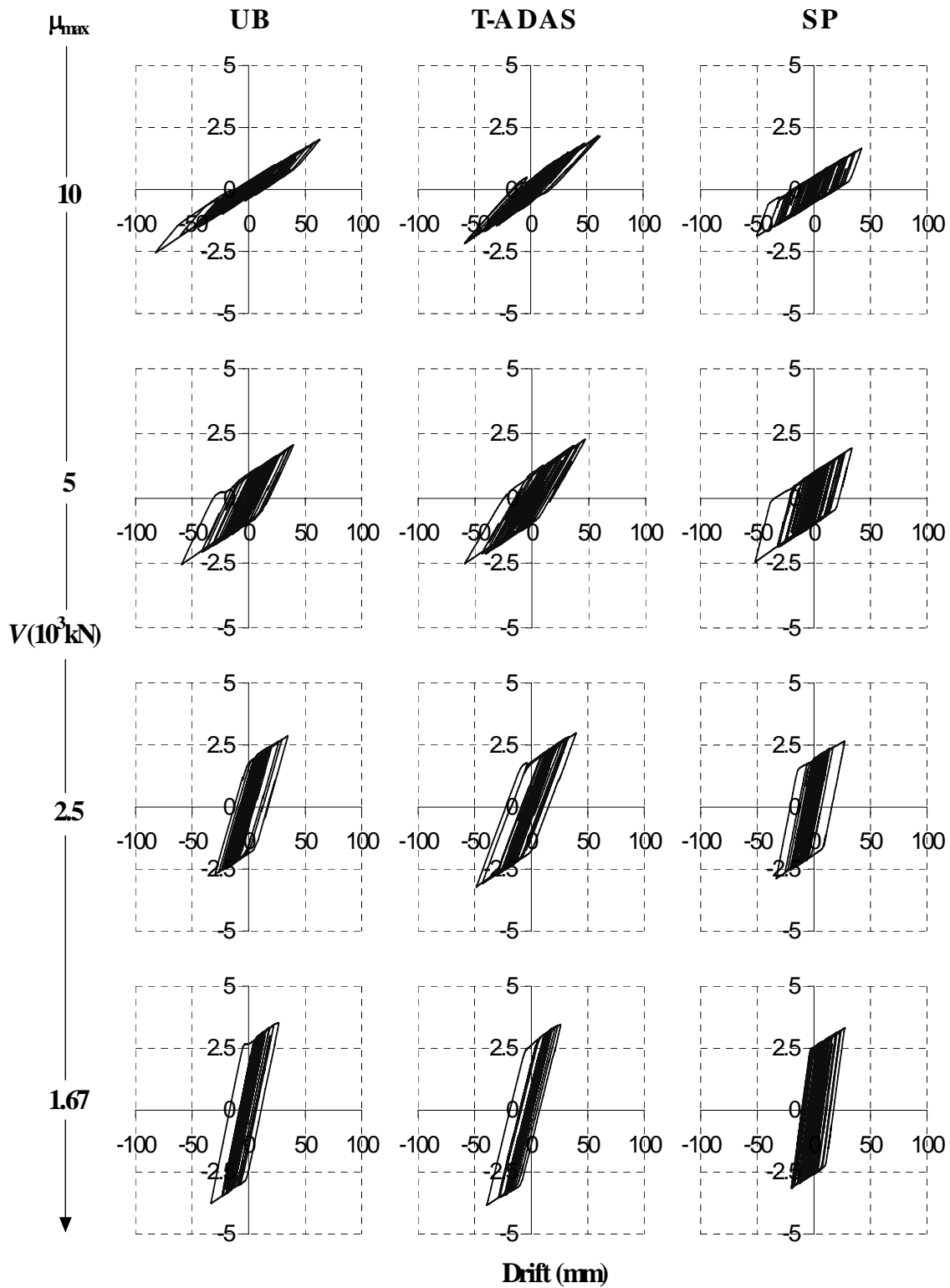


Figure 7.22. First Story Shear vs Drift of MDOF Systems Retrofitted with Structural Fuses

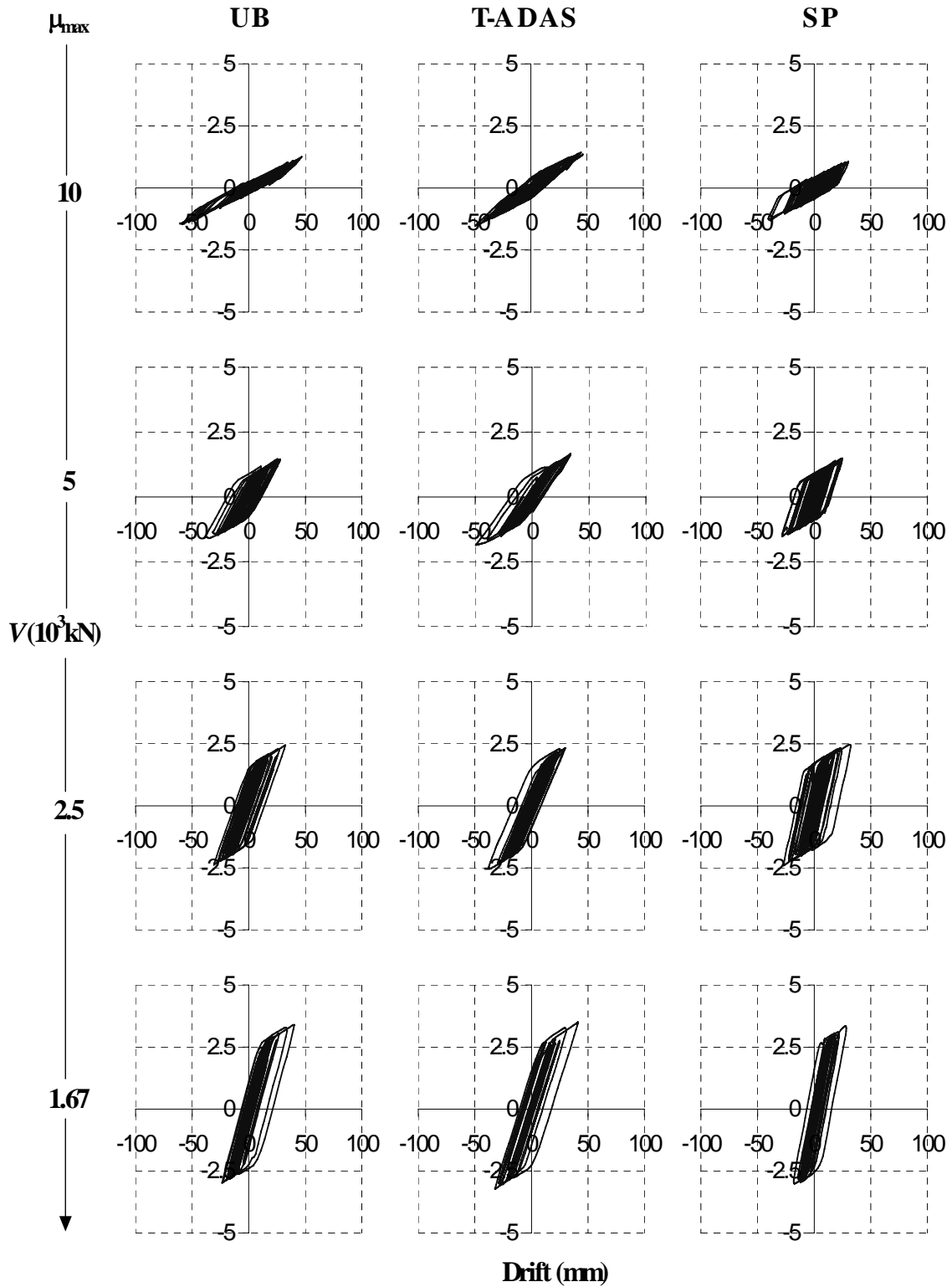


Figure 7.23. Second Story Shear vs Drift of MDOF Systems Retrofitted with Structural Fuses

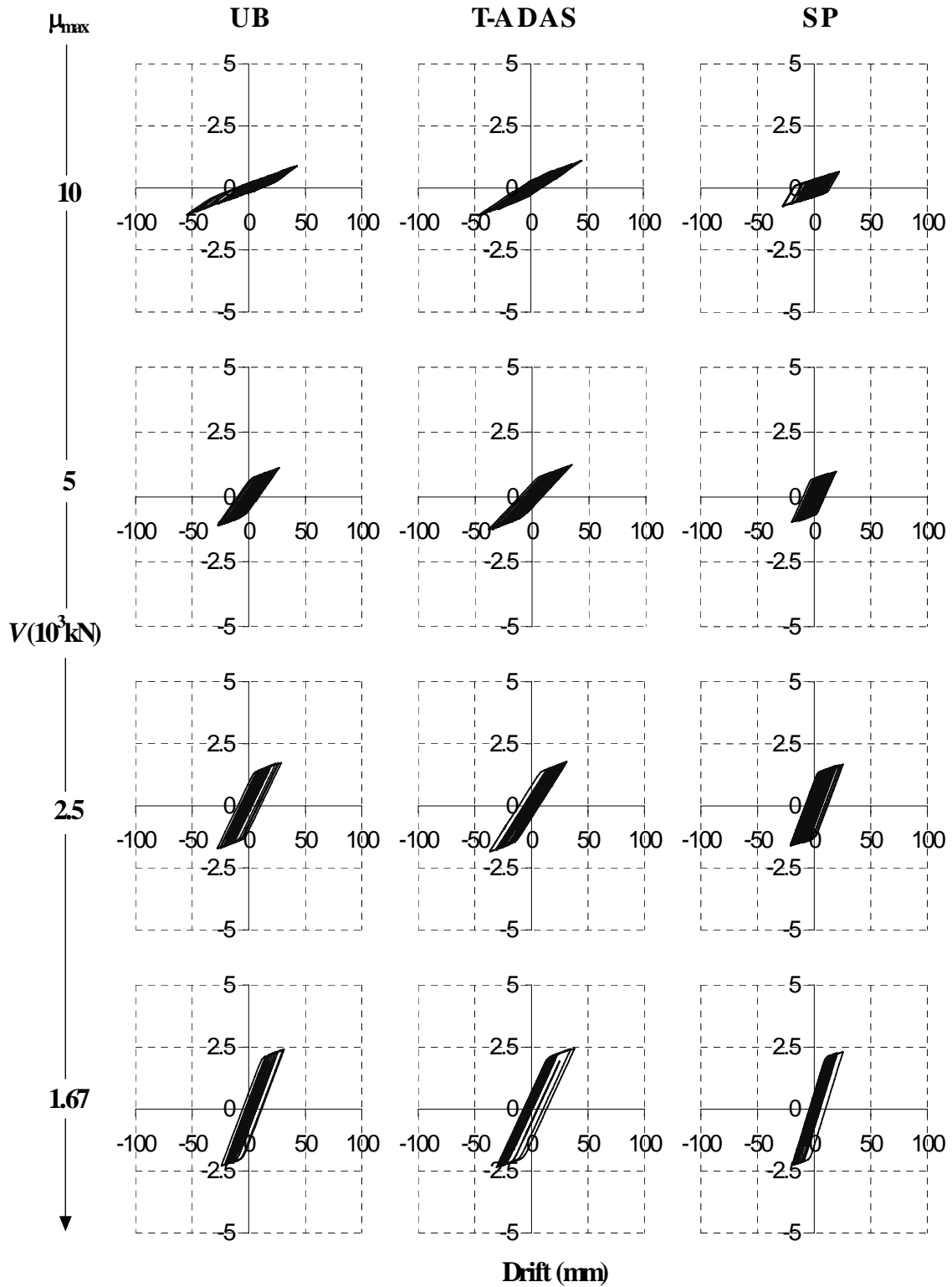


Figure 7.24. Third Story Shear vs Drift of MDOF Systems Retrofitted with Structural Fuses

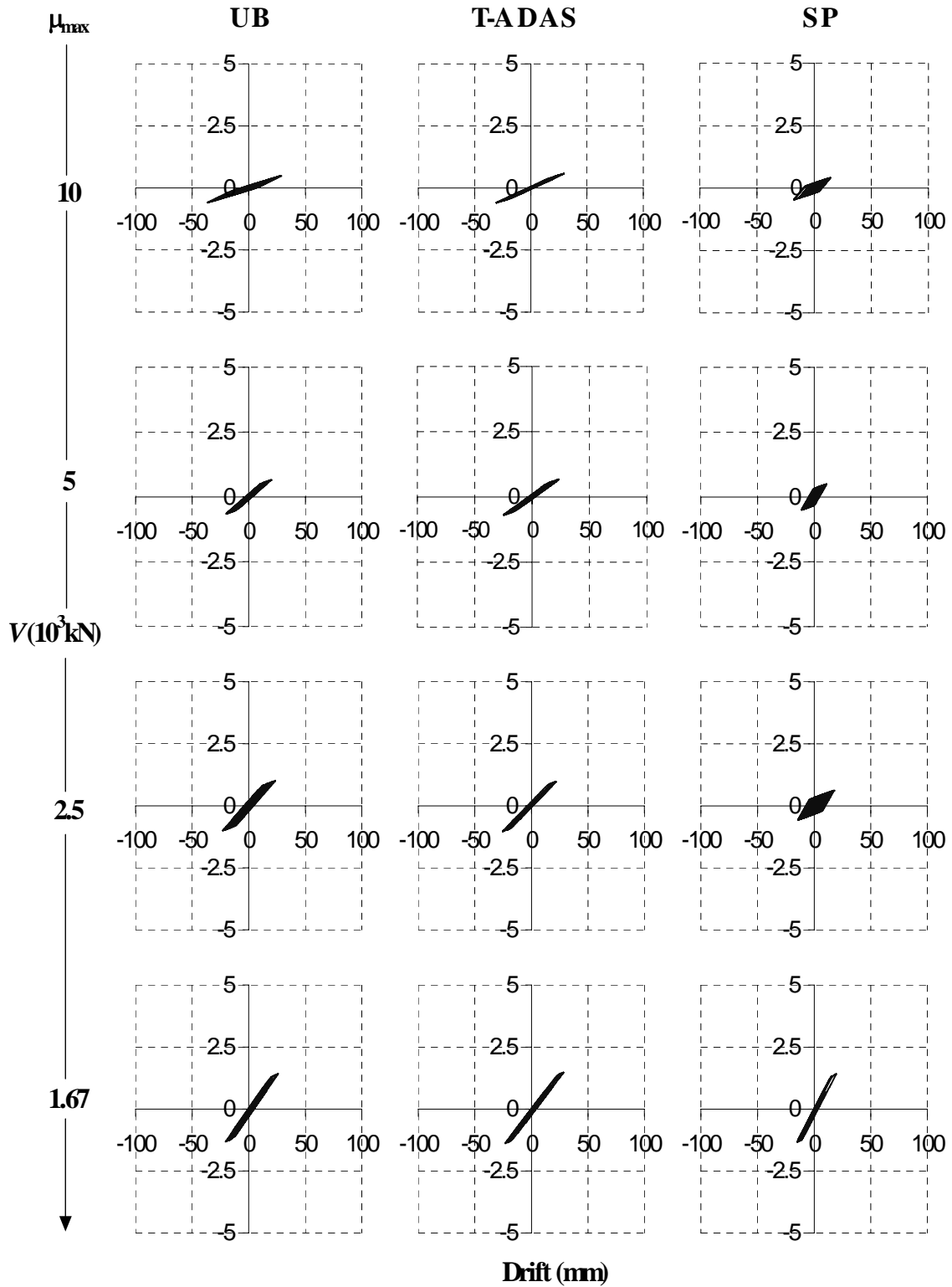


Figure 7.25. Fourth Story Shear vs Drift of MDOF Systems Retrofitted with Structural Fuses

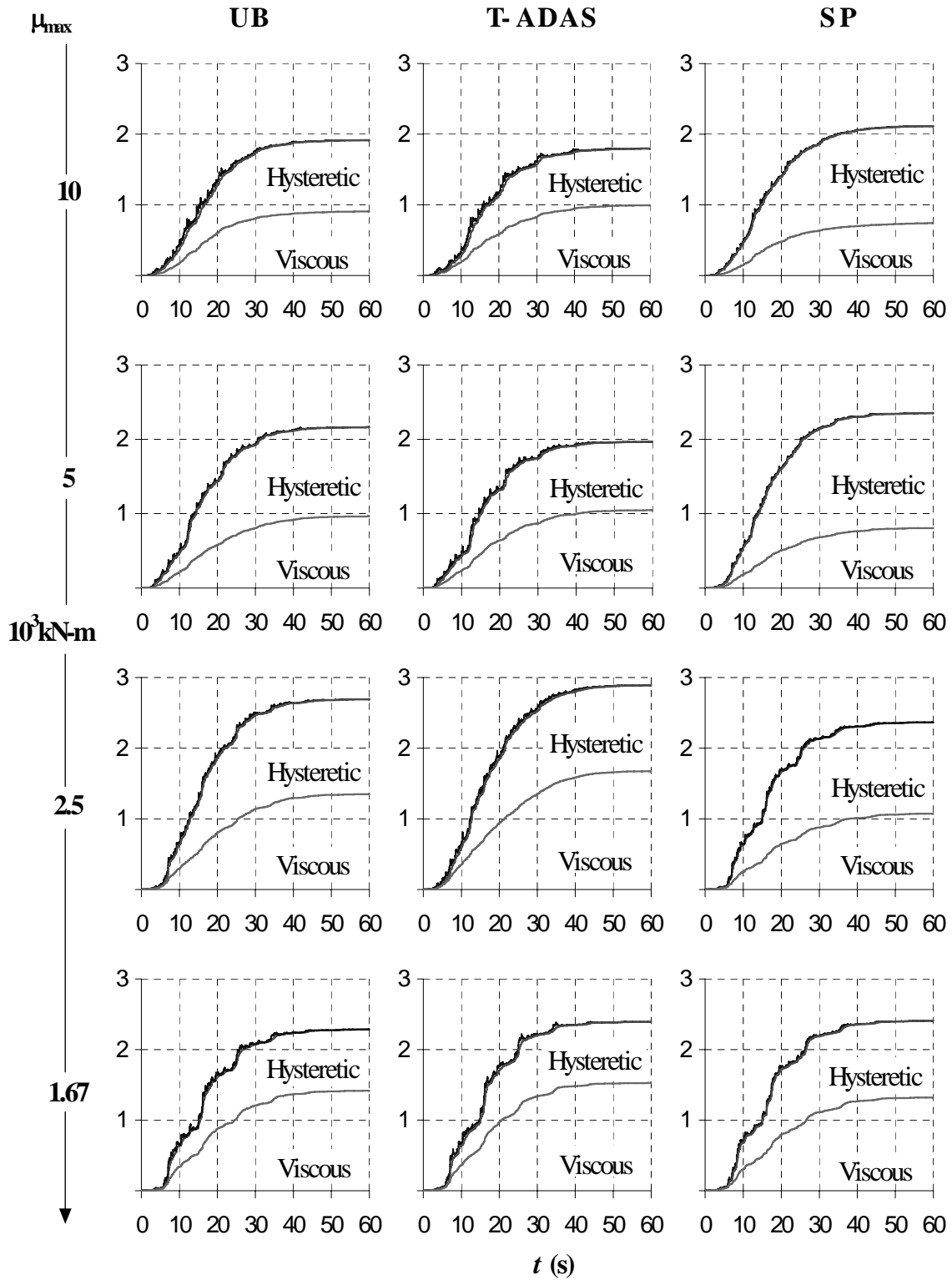


Figure 7.26. Energy of MDOF Systems Retrofitted with Structural Fuses

7.5. Observations

Examples of new construction designs and retrofit of existing structures using BRB, T-ADAS, and SP systems have been presented for the same set of α , μ_{\max} , and η values, consistently considered throughout this study. The designs obtained from this parametric study indicate that the modifications to the general procedure listed in Section 4, and introduced in this section to expand the application of the structural fuse concept from SDOF to MDOF systems, give satisfactory systems that perform as intended.

SECTION 8

CONCLUSIONS

The structural fuse concept has been studied in this report, using metallic dampers as passive energy dissipation devices designed to enhance the resilience of new and existing structures, by reducing seismically induced structural damage. In the perspective of resilience as the ability of a system to recover from damage (Bruneau et al., 2003), metallic dampers have been defined to be structural fuses when the system is designed such that all seismic damage is concentrated on easy-to-replace devices, allowing the primary structure to remain elastic. Self-recentering capabilities of the structure (i.e., elastic behavior of beams and columns), and replaceability of the metallic dampers (hence the “fuse” analogy) are the main features that define the structural fuse concept used here. Structural fuses are, therefore, an alternative to improve the resilience of structures by increasing the seismic capacity of a system and reducing the time to recovery after a major earthquake.

Through a parametric study the structural fuse concept has been investigated, considering the behavior of nonlinear SDOF systems subjected to seismic ground motions. Results were presented in dimensionless charts showing as shaded areas the range of admissible solutions that satisfy the structural fuse concept. From the results of the parametric analysis, it was noted that systems having large ductility capacity (i.e., $\mu_{\max} \geq 5$) offer a broader choice of acceptable designs over a greater range of the strength-ratio, η .

Based on the results obtained from dimensionless charts, a general design procedure is proposed to design SDOF systems using BRB, T-ADAS, or SP devices as examples of metallic structural fuses. A similar procedure was proposed also to retrofit an existing

structure, by introducing some modifications to the basic procedure to account for the fact that, in addition to other constraints, the bare frame properties of the existing structure are fixed in that case. The alternative of modifying the system original properties (e.g., by reinforcing or weakening beams and columns as part of the retrofit concept) was considered out of the scope of this study. Examples of the procedure were presented for new construction designs, and retrofitting of existing structures. From these examples, it was noted that systems having small stiffness ratio and large ductility capacity (i.e., $0.25 \leq \alpha < 0.50$ and $\mu_{\max} \geq 5$) exhibited the best seismic performance. Furthermore, it is important to emphasize that the design procedure presented in this study was developed to satisfy the structural fuse concept for earthquakes that do not exceed the level of design specifications. However, it is recommended to use target design spectra at maximum credible earthquake level (e.g., 2% of probability of being exceeded in 50 years) to reduce the probability of exceeding the design level, due to the high variability of earthquake records.

Floor demands of SDOF systems designed or retrofitted with metallic structural fuses were studied to analyze how they affect the seismic behavior of nonstructural components. Floor velocity and acceleration were obtained from a parametric analysis, and comparisons were made between the floor response of bare frames and the floor response of systems with metallic fuses. It was found that, in most of the cases, floor acceleration increases when metallic fuses are introduced to the system. Based on the velocity and acceleration spectra developed from the floor time history response, it was found that a critical period, T_c , can be used to identify when using metallic fuses can increase or decrease the dynamic acceleration and velocity response of nonstructural components. In this analysis, T_c is defined as the period where the floor acceleration spectra corresponding to the bare frame and the structural fuse system both intersect.

With the objective of reducing floor accelerations, the use of viscous dampers acting in parallel with metallic dampers was investigated. Parametric analyses were conducted and hysteretic damping and spectral acceleration results were presented for short,

intermediate, and long period structures. Although in structures with elastic behavior, displacements and acceleration demands both decrease when viscous dampers are added, in systems having hysteretic dampers designed to behave inelastically it was found that the floor accelerations are likely to increase if viscous dampers are added in parallel to hysteretic dampers, especially for systems with small stiffness ratio (i.e., $\alpha < 0.25$). It was also noted that increases in viscous damping reduce the effectiveness of hysteretic dampers, since the amplitude of motion (and thus ductility demand) is reduced. Therefore, adding viscous dampers to these systems seems to be not only ineffective in reducing floor accelerations, but also detrimental in most of the cases.

The structural fuse concept was also expanded from SDOF to MDOF systems by introducing some modification to the presented design / retrofit procedure. Examples were presented using the MCEER Demonstration Hospital as a system model to be either designed or retrofitted with metallic fuses in MDOF systems. Results indicate that the application of the structural fuse concept in MDOF buildings can give satisfactory system performance (as in SDOF cases).

Further research is needed to experimentally validate the structural fuse concept in actual or scaled structures.

SECTION 9

REFERENCES

Aiken, I., Clark, P., Trajirian, F., Kasai, K., Kimura, I., and Ko, E. (1999). “Unbonded Braces in the United States - Design Studies, Large-Scale Testing and the First Building Application.” *Proceedings of the International Post-SMiRT Conference Seminar*, Korea Earthquake Engineering Research Center, Volume I, pp. 317-337.

Amick, H., Bayat, A., and Kemeny, Z. (1998). “Seismic Isolation of Semiconductor Production Facilities.” *Proceedings of Seminar on Seismic Design, Retrofit, and Performance of Nonstructural Components*, ATC-29-1, Applied Technology Council, pp. 297-312.

Aristizabal-Ochoa, J. D. (1986). “Disposable Knee Bracing: Improvement in Seismic Design of Steel Frames.” *Journal of Structural Engineering*, Volume 112, No. 17, ASCE, pp. 1544-1552.

Basha, H. S., and Goel, S. C. (1996). “Ductile Truss Moment Frames.” *Los Angeles Tall Buildings Structural Design Council*, Annual Meeting: Modern Analysis Techniques in Practice, Los Angeles, California.

Bruneau, M., Chang, S.E., Eguchi, R.T., Lee, G.C., O’Rourke, T.D., Reinhorn, A.M., Shinozuka, M., Tierney, K., Wallace, W.A., and von Winterfeldt, D. (2003). “A Framework to Quantitatively Assess and Enhance the Seismic Resilience of Communities.” *Earthquake Spectra*, Earthquake Engineering Research Institute, Volume 19, No. 4, pp. 733-752.

Carter, C. J., and Iwankiw, N. R. (1998). "Improved Ductility in Seismic Steel Moment Frames with Dogbone Connections." *Second World Conference on Steel in Construction*, Elsevier Science Ltd., Paper No. 253.

Chopra, A.K. (2001). "Dynamics of Structures." Second Edition. Prentice Hall, Upper Saddle River, New Jersey.

Clough, R.W., and Penzien, J. (1993). "Dynamics of Structures." Second Edition. McGraw Hill, New York.

Chen, Y.Q., and Soong, T.T. (1989). "Seismic Behavior and Response Sensitivity of Secondary Structural Systems." *Report No. NCEER-89-0030*, National Center for Earthquake Engineering Research, University at Buffalo, State University of New York, Buffalo, NY.

Christopoulos, C., Filiatrault, A., and Folz, B. (2002). "Seismic Response of Self-Centring Hysteretic SDOF Systems." *Earthquake Engineering and Structural Dynamics*, John Wiley and Sons, Ltd., Volume 31, No. 5, pp. 1131-1150.

Computers and Structures Inc. (2000). "Structural Analysis Program, SAP-2000NL Version 7.40: Integrated Finite Element Analysis and Design of Structures." *Computers and Structures Inc.*, Berkeley, California.

Connor, J.J., Wada, A., Iwata, M., and Huang, Y.H. (1997). "Damage-Controlled Structures. I: Preliminary Design Methodology for Seismically Active Regions." *Journal of Structural Engineering*, Volume 123, No. 4, ASCE, pp. 423-431.

Constantinou, M.C., and Symans, M.D. (1992). "Experimental and Analytical Investigation of Seismic Response of Structures with Supplemental Fluid Viscous

Dampers.” *Report No. NCEER-92-0032*, National Center for Earthquake Engineering Research, University at Buffalo, State University of New York, Buffalo, NY.

Cooley, J.W., and Tukey, J.W. (1965). “An Algorithm for Machine Calculation of Complex Fourier Series.” *Mathematics of Computation*, American Mathematical Society, Volume 9, No. 90, pp. 297-301.

Dargush, G., and Soong, T.T. (1995). “Behavior of Metallic Plate Dampers in Seismic Passive Energy Dissipation Systems.” *Earthquake Spectra*, Earthquake Engineering Research Institute, Volume 11, No. 4, pp. 545-568.

Federal Emergency Management Agency (1997). “NEHRP Guidelines for the Seismic Rehabilitation of Building.” *Reports No. FEMA 273 and FEMA 274*, Washington, D.C.

Federal Emergency Management Agency (2000). “Prestandard and Commentary for the Seismic Rehabilitation of Buildings.” *Report No. FEMA 356*, Washington, D.C.

Federal Emergency Management Agency (2001). “NEHRP Recommended Provisions for Seismic Regulations for New Buildings and other Structures.” *Reports No. FEMA 368 and FEMA 369*, Washington, D.C.

Federal Emergency Management Agency (2003). “NEHRP Recommended Provisions for Seismic Regulations for New Buildings and other Structures.” *Report No. FEMA 450*, Washington, D.C.

Filiatrault, A., and Cherry, S. (1989). “Parameters Influencing the Design of Friction Damped Structures.” *Canadian Journal of Civil Engineering*, Volume 16, No. 5, pp. 753-766.

Filiatrault, A., and Cherry, S. (1990). "Seismic Design Spectra for Friction-Damped Structures." *Journal of Structural Engineering*, Volume 116, No. 5, ASCE, pp. 1334-1355.

Filiatrault, A., Christopoulos, C., and Stearns, C. (2002). "Guidelines, Specifications, and Seismic Performance Characterization of Nonstructural Building Components and Equipment." *Report No. PEER-2002/05*, Pacific Earthquake Engineering Research Center, University of California, Berkeley.

Fintel, M., and Ghosh, S.K. (1981). "The Structural Fuse: an Inelastic Approach to Seismic Design of Buildings." *Civil Engineering*. Volume 51, No. 1, ASCE, pp. 48-51.

FitzGerald, T.F., Anagnos, T., Goodson, M., and Zsutty, T. (1989). "Slotted Bolted Connections in Aseismic Design for Concentrically Braced Connections." *Earthquake Spectra*, Earthquake Engineering Research Institute, Volume 5, No. 2, pp. 383-391.

Fu, Y., and Cherry, S. (2000). "Design of Friction Damped Structures using Lateral force Procedure." *Earthquake Engineering and Structural Dynamics*, John Wiley and Sons, Ltd., Volume 29, No. 7, pp. 989-1010.

Grigoriu, M., Ibrahim, Y., and Soong, T.T. (1990). "Seismic Performance of Primary-Secondary Systems." *Proceedings of Seminar and Workshop on Seismic Design and Performance of Equipment and Nonstructural Elements in Buildings and Industrial Structures*, ATC-29, Applied Technology Council, pp. 253-264.

Grigoriu, M., and Waisman, F. (1998). "Seismic Reliability and Performance of Nonstructural Components." *Proceedings of Seminar on Seismic Design, Retrofit, and Performance of Nonstructural Components*, ATC-29-1, Applied Technology Council, pp. 337-348.

Hanson, R.D., and Soong, T.T. (2001). "Seismic Design with Supplemental Energy Dissipation Devices." *Monograph No. MNO-8*, Earthquake Engineering Research Institute, Oakland, California.

Huang, Y.H., Wada, A., Iwata, M., Mahin, S.A., and Connor, J.J. (2002). "Design of Damage-controlled Structures." *Innovative Approaches to Earthquake Engineering*, WIT Press, pp. 85-118.

Ibrahim, Y., Grigoriu, M., and Soong, T.T. (1989). "Random Vibration and Reliability Analysis of Primary-Secondary Structural Systems." *Report No. NCEER-89-0031*, National Center for Earthquake Engineering Research, University at Buffalo, State University of New York, Buffalo, NY.

International Code Council (2000). "International Building Code." *IBC-2000*, Virginia, USA.

Iwata, M., Kato, T., and Wada, A. (2000). "Buckling-Restrained Braces as Hysteretic Dampers." *Behavior of Steel Structures in Seismic Areas*, STESSA, pp. 33-38.

Lagorio, H.J. (1990). "Earthquakes, and Architect's Guide to Nonstructural Seismic Hazards." John Wiley & Sons Inc., New York.

Lai, M.L., and Soong, T.T. (1990). "Optimum Design of Secondary Structural Systems." *Proceedings of Seminar and Workshop on Seismic Design and Performance of Equipment and Nonstructural Elements in Buildings and Industrial Structures*, ATC-29, Applied Technology Council, pp. 229-239.

Li, C., and Reinhorn, A.M.(1995). "Experimental and Analytical Investigation of Seismic Retrofit of Structures with Supplemental Damping: Part II - Friction Devices."

Report No. NCEER-95-0009, National Center for Earthquake Engineering Research, University at Buffalo, State University of New York, Buffalo, NY.

Mahin, S.A., and Lin, J. (1983). “Construction of Inelastic Response Spectra for Single-Degree-of-Freedom Systems.” *Report No. UCB-83/17*, Earthquake Engineering Research Center, University of California, Berkeley.

Manolis, G.D., and Juhn, G. (1988). “Substructuring Techniques in the Time Domain for Primary-Secondary Structural Systems.” *Report No. NCEER-88-0003*, National Center for Earthquake Engineering Research, University at Buffalo, State University of New York, Buffalo, NY.

Miyama, T., Tanaka, K., Meng, L., Kato, Y., Hirasawa, M., and Sasaki, M. (1996). “Study on the Highly Damped Building with Low-Yield-Point Steel Shear Panel.” *Proceedings of Eleventh World Conference on Earthquake Engineering*, Paper No. 416, Elsevier Science, Ltd.

Nakashima, M. (1995a). “Strain-Hardening Behavior of Shear Panels Made of Low-Yield Steel. I: Test.” *Journal of Structural Engineering*, Volume 121, No. 12, ASCE, pp. 1742-1749.

Nakashima, M., Akazawa, T., and Tsuji, B. (1995b). “Strain-Hardening Behavior of Shear Panels Made of Low-Yield Steel. II: Model.” *Journal of Structural Engineering*, Volume 121, No. 12, ASCE, pp. 1750-1757.

Nims, D.K., Richter, P.J., and Bachman, R.E. (1993). “The Use of the Energy Dissipating Restraint for Seismic Hazard Mitigation.” *Earthquake Spectra*, Earthquake Engineering Research Institute, Volume 9, No. 3, pp. 467-489.

Pall, A.S., and Marsh, C., and Fazio, P. (1980). "Friction Joints for Seismic Control of Large Panel Structures." *Journal of Prestressed Concrete Institute*, Volume 25, No. 6, pp. 38-61.

Pall, A.S., and Marsh, C. (1982). "Response of Friction Damped Braced Frames." *Journal of the Structural Division*, Volume 108, No. ST6, pp. 1313-1323, ASCE.

Papageorgiou, A., Halldorsson, B., and Dong, G. (1999). "Target Acceleration Spectra Compatible Time Histories." TARSC THS - User's Manual, Version 1.0, *Engineering Seismology Laboratory*, University at Buffalo, State University of New York, Buffalo, NY. (<http://civil.eng.buffalo.edu/EngSeisLab/>).

Ramirez, O.M., Constantinou, M.C., Kircher, C.A., Whittaker, A.S., Johnson M.W., Gomez, J.D., and Chrysostomou, C.Z. (2001). "Development and Evaluation of Simplified Procedures for Analysis and Design of Buildings with Passive Energy Dissipation Systems." *Report No. MCEER-00-0010, Revision 1*, Multidisciplinary Center for Earthquake Engineering Research, University at Buffalo, State University of New York, Buffalo, NY.

Reinhorn, A.M., Li, C., and Constantinou, M.C. (1995). "Experimental and Analytical Investigation of Seismic Retrofit of Structures with Supplemental Damping: Part I - Fluid Viscous Damping." *Report No. NCEER-95-0001*, National Center for Earthquake Engineering Research, University at Buffalo, State University of New York, Buffalo, NY.

Reinhorn, A.M., and Li, C. (1995). "Experimental and Analytical Investigation of Seismic Retrofit of Structures with Supplemental Damping: Part III - Viscous Damping Walls." *Report No. NCEER-95-0013*, National Center for Earthquake Engineering Research, University at Buffalo, State University of New York, Buffalo, NY.

Reinhorn, A.M. (1997). "Inelastic Analysis Techniques in Seismic Evaluations." *Seismic Design Methodologies for the Next Generation of Codes*. Bled, Slovenia, pp. 277-287.

Rezai, M., Prion, H.G.L., Tremblay, R., Bouatay, N., and Timler, P. (2000). "Seismic Performance of Brace Fuse Elements for Concentrically Steel Braced Frames." *Behavior of Steel Structures in Seismic Areas*, STESSA, pp. 39-46.

Roeder, C., and Popov, E. (1977). "Inelastic Behavior of Eccentrically Braced Steel Frames under Cyclic Loadings." *Report No. UCB-77/17*, Earthquake Engineering Research Center, University of California, Berkeley.

Sabelli, R., Mahin, S., and Chang, C. (2003). "Seismic Demands on Steel Braced Buildings with Buckling-Restrained Braces." *Engineering Structures*, Elsevier Science Ltd., Volume 25, No. 5, pp. 655-666.

Saeki, E., Iwamatu, K., and Wada, A. (1996). "Analytical Study by Finite Element Method and Comparison with Experiment Results concerning Buckling-Restrained Unbonded Braces." *Journal of Structural and Construction Engineering*, Volume 484, Architectural Institute of Japan, Tokyo, Japan, pp. 111-120.

Shimizu, K., Hashimoto, J., Kawai, H., and Wada, A. (1998). "Application of Damage Control Structure using Energy Absorption Panel." Paper No. T105-2, *Structural Engineering World Wide 1998*, Elsevier Science, Ltd.

Singh, M.P., Moreschi, L., and Suarez, L. (1998). "Simplified Methods for Calculating Seismic Forces for Nonstructural Components." *Proceedings of Seminar on Seismic Design, Retrofit, and Performance of Nonstructural Components*, ATC-29-1, Applied Technology Council, pp. 43-56.

- Soong, T.T., and Dargush, G.F. (1997). "Passive Energy Dissipation Systems in Structural Engineering." John Wiley & Sons Ltd., New York.
- Soong, T.T., and Spencer, B.F. (2002). "Supplemental Energy Dissipation: State-of-the-art and State-of-the-practice." *Engineering Structures*, Elsevier Science Ltd., Volume 24, No. 3, pp. 243-259.
- Sugiyama, S. (1998). "Application of Hysteresis Steel Dampers to Tall Building." Paper No. T190-5, *Structural Engineering World Wide 1998*, Elsevier Science, Ltd.
- Tanaka, K., Torii, T., Sasaki, Y., Miyama, T., Kawai, H., Iwata, M., and Wada, A. (1998). "Practical Application of Damage Tolerant Structures with Seismic Control Panel using Low-Yield-Point-Steel to a High-Rise Steel Building." Paper No. T190-4, *Structural Engineering World Wide 1998*, Elsevier Science, Ltd.
- Tena-Colunga, A. (1997). "Mathematica Modelling of the ADAS Energy Dissipation Device." *Engineering Structures*, Elsevier Science, Ltd., Volumen 19, No. 10, pp. 811-820.
- Tokas, C. (2005). Personal Communication. Manager, California Hospital Seismic Retrofit Program, State of California Office of Statewide Health Planning and Development (OSHPD).
- Tsai, K.C., Chen, H.W., Hong, C.P., and Su, Y.F. (1993). "Design of Steel Triangular Plate Energy Absorbers for Seismic-Resistant Construction." *Earthquake Spectra*, Earthquake Engineering Research Institute, Volume 9, No. 3, pp. 505-528.
- Wada, A., Connor, J.J., Kawai, H., Iwata, M., and Watanabe, A. (1992). "Damage Tolerant Structures." *Proceedings of: Fifth U.S.-Japan Workshop on the Improvement of*

Structural Design and Construction Practices, ATC-15-4, Applied Technology Council, pp. 27-39.

Wada, A., and Huang, Y.H. (1995). "Preliminary Seismic Design of Damage Tolerant Tall Building Structures." *Proceedings of Symposium on a New Direction in Seismic Design*, Architectural Institute of Japan, Tokyo, Japan, pp. 77-93.

Wada, A., and Huang, Y.H. (1999). "Damage-controlled Structures in Japan." *U.S.-Japan Workshop on Performance-Based Earthquake Engineering Methodology for Reinforced Concrete Building Structures*, PEER Report 1999, Volume 10, pp. 279-289.

Wada, A., Huang, Y.H., and Iwata, M. (2000). "Passive Damping Technology for Buildings in Japan." *Progress in Structural Engineering and Materials*, John Wiley & Sons, Ltd., Volume 2, No. 3, pp. 335-350.

Watanabe, A., Hitomi, Y., Saeki, E., Wada, A., and Fujimoto, M. (1988). "Properties of Brace Encased in Buckling Restraining Concrete and Steel Tube." *Proceedings of Ninth World Conference on Earthquake Engineering*, Tokyo-Kyoto, Japan, No. 6-7-4, Volume 4, pp. 719-724.

Whittaker, A., Bertero, V.V., Alonso, L.J., and Thompson, C.L. (1989). "Earthquake Simulator Testing of Steel Plate Added Damping and Stiffness Elements." *Report No. UCB/EERC-89/02*, Earthquake Engineering Research Center, University of California, Berkeley, California.

Yang, T.Y., and Whittaker, A. (2002). "MCEER Demonstration Hospital - Mathematical Model and Preliminary Results." Technical Report, Multidisciplinary Center for Earthquake Engineering Research, University at Buffalo, State University of New York, Buffalo, NY.

APPENDIX A

EXAMPLES OF DESIGN AND RETROFIT OF SDOF SYSTEMS WITH BUCKLING-RESTRAINED BRACES

Example A-1: Design to Satisfy the Structural Fuse Concept of One Bay One Story Frame with Buckling-Restrained Braces

Frame Dimensions:

High: $H := 12.5\text{-ft}$ Width: $L := 16\text{-ft}$

Mass: $m := 2 \cdot \frac{\text{kip} \cdot \text{sec}^2}{\text{in}}$ Corresponds to 8" of concrete slab on steel deck, and 80 psf of additional dead load on a tributary area of 100' x 43'

Material Properties:

$F_{yf} := 50\text{-ksi}$ $E := 29000\text{-ksi}$ $G := 11200\text{-ksi}$

Site: Sherman Oaks, California (Lat.=34.154, Long.=-118.465), Site Class B

$S_s := 1.95\text{-g}$ $S_1 := 0.87\text{-g}$ $F_a := 1$ $F_v := 1$

$S_{MS} = 1.95\text{ g}$ $S_{M1} = 0.87\text{ g}$

$S_{DS} = 1.3\text{ g}$ $S_{D1} = 0.58\text{ g}$

Peak Ground Acceleration: $\ddot{u}_{g\max} := 0.4 \cdot S_{DS}$ $\ddot{u}_{g\max} = 0.52\text{ g}$

Step 1: Allowable Story Drift: $\Delta_a := 0.02 \cdot H$ $\Delta_a = 3\text{ in}$

Elastic Spectral Displacement: $S_d := \Delta_a$ $S_d = 3\text{ in}$

Step 2: Elastic Period Limit: $T_L := \max \left[\left(\frac{4 \cdot \pi}{S_{D1}} \right)^2 \cdot \frac{S_d}{1\text{ sec}}, 2 \cdot \pi \cdot \sqrt{\frac{S_d}{S_{DS}}} \right]$ $T_L = 0.53\text{ sec}$

Elastic Spectral Acceleration: $S_a := \min \left(\frac{S_{D1}}{T_L} \cdot 1\text{ sec}, S_{DS} \right)$ $S_a = 1.097\text{ g}$

Elastic Base Shear: $V_e := m \cdot S_a$ $V_e = 846.79\text{ kip}$

Step 3: Design Parameters (Table 1):

Target Design Parameters: $\alpha := 0.25$ $\mu_{\max} := 5$ $\eta := 0.4$

$\Omega_o := \alpha \cdot (\mu_{\max} - 1) + 1$ $\Omega_o = 2$

Step 4: Yield Shear: $V_y := \eta \cdot m \cdot \ddot{u}_{g\max}$ $V_y = 160.61\text{ kip}$

Shear Capacity: $V_p := \Omega_o \cdot V_y$ $V_p = 321.23\text{ kip}$

Step 5:	Required Stiffness:	$K_1 := \frac{4 \cdot \pi^2}{T_L^2} \cdot m$	$K_1 = 282.26 \frac{\text{kip}}{\text{in}}$
	Frame Stiffness:	$K_f := \alpha \cdot K_1$	$K_f = 70.57 \frac{\text{kip}}{\text{in}}$
	Structural Fuse Stiffness:	$K_a := (1 - \alpha) \cdot K_1$	$K_a = 211.7 \frac{\text{kip}}{\text{in}}$
Step 6:	SF Yield Displacement:	$\Delta_{ya} := \frac{V_y}{K_1}$	$\Delta_{ya} = 0.57 \text{ in}$
	BF Yield Displacement:	$\Delta_{yf} := \mu_{\max} \cdot \Delta_{ya}$	$\Delta_{yf} = 2.85 \text{ in}$
Step 7:	BF Shear Capacity:	$V_{yf} := K_f \cdot \Delta_{yf}$	$V_{yf} = 200.77 \text{ kip}$
	SF Shear Capacity:	$V_{ya} := K_a \cdot \Delta_{ya}$	$V_{ya} = 120.46 \text{ kip}$
Step 8:	Required Beam Plastic Modulus:	$Z_B := \frac{V_{yf} \cdot H}{2F_{yf}}$	$Z_B = 301.15 \text{ in}^3$
	Select Beam: W12x190	$Z_B := 311 \cdot \text{in}^3$	$I_B := 1890 \cdot \text{in}^4$
	Required Column Moment of inertia:	$I_C := \frac{2}{\left(\frac{12E}{H^3 \cdot K_f} - \frac{L}{I_B \cdot H} \right)}$	$I_C = 2551.18 \text{ in}^4$
	Select Column: W14x211	$Z_C := 390 \cdot \text{in}^3$	$I_C := 2660 \cdot \text{in}^4$
	Required Braces Area:	$A_b := \frac{K_a \cdot L}{4 \cdot E \cdot (\cos(\theta))^3}$	$A_b = 2.237 \text{ in}^2$
	Select Braces Area (Plate):	$A_b := 2.25 \cdot 1.0 \cdot \text{in}^2$	$A_b = 2.25 \text{ in}^2$
	Required Steel Yield Strength for the Braces:	$F_{yd} := \frac{V_{ya}}{2 \cdot A_b \cdot \cos(\theta)}$	$F_{yd} = 49.66 \text{ ksi}$
	Select Steel Yield Strength for the Braces:		$F_{yd} := 50 \cdot \text{ksi}$
Step 9:	Frame Properties:	$K_f := \frac{12E \cdot I_C}{H^3} \cdot \frac{1}{2 + \frac{I_C}{I_B} \cdot \frac{L}{H}}$	$K_f = 72.15 \frac{\text{kip}}{\text{in}}$
		$V_{yf} := \frac{2F_{yf} \cdot Z_B}{H}$	$V_{yf} = 207.33 \text{ kip}$
		$\Delta_{yf} := \frac{V_{yf}}{K_f}$	$\Delta_{yf} = 2.87 \text{ in}$

UB Properties:

$$K_a := \frac{4 \cdot A_b \cdot E}{L} \cdot (\cos(\theta))^3 \quad K_a = 212.93 \frac{\text{kip}}{\text{in}}$$

$$V_{ya} := 2 \cdot F_{yd} \cdot A_b \cdot \cos(\theta) \quad V_{ya} = 121.29 \text{ kip}$$

$$\Delta_{ya} := \frac{V_{ya}}{K_a} \quad \Delta_{ya} = 0.57 \text{ in}$$

New Parameters:

$$\alpha := \frac{1}{1 + \frac{K_a}{K_f}} \quad \alpha = 0.25$$

$$\mu_{\max} := \frac{\Delta_{yf}}{\Delta_{ya}} \quad \mu_{\max} = 5.04$$

$$\eta := \frac{V_y}{m \cdot \ddot{u}_{g\max}} \quad \eta = 0.4$$

$$T := 2 \cdot \pi \cdot \sqrt{\frac{m}{K_1}} \quad T = 0.53 \text{ sec}$$

Step 10: Time History Analysis Results:

$$\text{Frame Ductility:} \quad \mu_f := 0.86$$

$$\text{Global Ductility:} \quad \mu := \mu_{\max} \cdot \mu_f \quad \mu = 4.34$$

Approximate Results:

$$\text{Frame Ductility:} \quad \mu_f := \frac{0.8239}{\mu_{\max}} \cdot \eta^A \cdot \left(\frac{T}{1 \text{ sec}}\right)^{B \cdot \eta^C} \quad \mu_f = 0.73$$

$$\text{Global Ductility:} \quad \mu := \mu_{\max} \cdot \mu_f \quad \mu = 3.68$$

Step 11: Design Parameters:

$$V_y := K_f \cdot \Delta_{ya} + V_{ya} \quad V_y = 162.38 \text{ kip}$$

$$K_1 := K_f + K_a \quad K_1 = 285.08 \frac{\text{kip}}{\text{in}}$$

$$S_a := \min\left(\frac{S_{D1}}{T} \cdot 1 \text{ sec}, S_{D5}\right) \quad S_a = 1.1021 \text{ g}$$

$$V_e := m \cdot S_a \quad V_e = 851 \text{ kip}$$

$$V_p := V_{yf} + V_{ya} \quad V_p = 328.62 \text{ kip}$$

$$R := \frac{V_e}{V_y} \quad R = 5.24$$

$$\Omega_o := \frac{V_p}{V_y} \quad \Omega_o = 2.02$$

$$R_\mu := \frac{R}{\Omega_o} \quad R_\mu = 2.59$$

Example A-2: Design to Satisfy the Structural Fuse Concept of One Bay One Story Frame with Buckling-restrained Braces

Frame Dimensions:

High: $H := 12.5\text{-ft}$ Width: $L := 16\text{-ft}$

Mass: $m := 2 \cdot \frac{\text{kip} \cdot \text{sec}^2}{\text{in}}$ Corresponds to 8" of concrete slab on steel deck, and 80 psf of additional dead load on a tributary area of 100' x 43'

Material Properties:

$F_{yf} := 50\text{-ksi}$ $E := 29000\text{-ksi}$ $G := 11200\text{-ksi}$

Site: Sherman Oaks, California (Lat.=34.154, Long.=-118.465), Site Class B

$S_s := 1.95\text{-g}$ $S_1 := 0.87\text{-g}$ $F_a := 1$ $F_v := 1$

$S_{MS} = 1.95\text{ g}$ $S_{M1} = 0.87\text{ g}$

$S_{DS} = 1.3\text{ g}$ $S_{D1} = 0.58\text{ g}$

Peak Ground Acceleration: $\ddot{u}_{gmax} := 0.4 \cdot S_{DS}$ $\ddot{u}_{gmax} = 0.52\text{ g}$

Step 1: Allowable Story Drift: $\Delta_a := 0.02 \cdot H$ $\Delta_a = 3\text{ in}$

Elastic Spectral Displacement: $S_d := \Delta_a$ $S_d = 3\text{ in}$

Step 2: Elastic Period Limit: $T_L := \max \left[\left(\frac{4 \cdot \pi}{S_{D1}} \right)^2 \cdot \frac{S_d}{1\text{ sec}}, 2 \cdot \pi \cdot \sqrt{\frac{S_d}{S_{DS}}} \right]$ $T_L = 0.53\text{ sec}$

Elastic Spectral Acceleration: $S_a := \min \left(\frac{S_{D1}}{T_L} \cdot 1\text{ sec}, S_{DS} \right)$ $S_a = 1.097\text{ g}$

Elastic Base Shear: $V_e := m \cdot S_a$ $V_e = 846.79\text{ kip}$

Step 3: Design Parameters (Table 1):

Target Design Parameters: $\alpha := 0.25$ $\mu_{max} = 1.67$ $\eta := 1.0$

$\Omega_o := \alpha \cdot (\mu_{max} - 1) + 1$ $\Omega_o = 1.17$

Step 4: Yield Shear: $V_y := \eta \cdot m \cdot \ddot{u}_{gmax}$ $V_y = 401.53\text{ kip}$

Shear Capacity: $V_p := \Omega_o \cdot V_y$ $V_p = 468.45\text{ kip}$

Step 5: Required Stiffness:	$K_1 := \frac{4 \cdot \pi^2}{T_L^2} \cdot m$	$K_1 = 282.26 \frac{\text{kip}}{\text{in}}$
Frame Stiffness:	$K_f := \alpha \cdot K_1$	$K_f = 70.57 \frac{\text{kip}}{\text{in}}$
Structural Fuse Stiffness:	$K_a := (1 - \alpha) \cdot K_1$	$K_a = 211.7 \frac{\text{kip}}{\text{in}}$
Step 6: SF Yield Displacement:	$\Delta_{ya} := \frac{V_y}{K_1}$	$\Delta_{ya} = 1.42 \text{ in}$
BF Yield Displacement:	$\Delta_{yf} := \mu_{\max} \cdot \Delta_{ya}$	$\Delta_{yf} = 2.37 \text{ in}$
Step 7: BF Shear Capacity:	$V_{yf} := K_f \cdot \Delta_{yf}$	$V_{yf} = 167.3 \text{ kip}$
SF Shear Capacity:	$V_{ya} := K_a \cdot \Delta_{ya}$	$V_{ya} = 301.15 \text{ kip}$
Step 8: Required Beam Plastic Modulus:	$Z_B := \frac{V_{yf} \cdot H}{2F_{yf}}$	$Z_B = 250.96 \text{ in}^3$
Select Beam: W24x94	$Z_B := 254 \cdot \text{in}^3$	$I_B := 2700 \cdot \text{in}^4$
Required Column Moment of inertia:	$I_C := \frac{2}{\left(\frac{12E}{H^3 \cdot K_f} - \frac{L}{I_B \cdot H} \right)}$	$I_C = 2026.09 \text{ in}^4$
Select Column: W14x176	$Z_C := 320 \cdot \text{in}^3$	$I_C := 2140 \cdot \text{in}^4$
Required Braces Area:	$A_b := \frac{K_a \cdot L}{4 \cdot E \cdot (\cos(\theta))^3}$	$A_b = 2.237 \text{ in}^2$
Select Braces Area (Plate):	$A_b := 2.25 \cdot 1.0 \cdot \text{in}^2$	$A_b = 2.25 \text{ in}^2$
Required Steel Yield Strength for the Braces:	$F_{yd} := \frac{V_{ya}}{2 \cdot A_b \cdot \cos(\theta)}$	$F_{yd} = 124.15 \text{ ksi}$
Select Steel Yield Strength for the Braces:		$F_{yd} := 70 \cdot \text{ksi}$
Step 9: Frame Properties:	$K_f := \frac{12E \cdot I_C}{H^3} \cdot \frac{1}{2 + \frac{I_C}{I_B} \cdot \frac{L}{H}}$	$K_f = 73.2 \frac{\text{kip}}{\text{in}}$
	$V_{yf} := \frac{2F_{yf} \cdot Z_B}{H}$	$V_{yf} = 169.33 \text{ kip}$
	$\Delta_{yf} := \frac{V_{yf}}{K_f}$	$\Delta_{yf} = 2.31 \text{ in}$

UB Properties:

$$K_a := \frac{4 \cdot A_b \cdot E}{L} \cdot (\cos(\theta))^3 \quad K_a = 212.93 \frac{\text{kip}}{\text{in}}$$

$$V_{ya} := 2 \cdot F_{yd} \cdot A_b \cdot \cos(\theta) \quad V_{ya} = 169.8 \text{ kip}$$

$$\Delta_{ya} := \frac{V_{ya}}{K_a} \quad \Delta_{ya} = 0.8 \text{ in}$$

New Parameters:

$$\alpha := \frac{1}{1 + \frac{K_a}{K_f}} \quad \alpha = 0.26$$

$$\mu_{\max} := \frac{\Delta_{yf}}{\Delta_{ya}} \quad \mu_{\max} = 2.9$$

$$\eta := \frac{V_y}{m \cdot \ddot{u}_{g\max}} \quad \eta = 0.68$$

$$T := 2 \cdot \pi \cdot \sqrt{\frac{m}{K_1}} \quad T = 0.53 \text{ sec}$$

Step 10: Time History Analysis Results:

$$\text{Frame Ductility:} \quad \mu_f := 1.07$$

$$\text{Global Ductility:} \quad \mu := \mu_{\max} \cdot \mu_f \quad \mu = 3.1$$

Approximate Results:

$$\text{Frame Ductility:} \quad \mu_f := \frac{0.8239}{\mu_{\max}} \cdot \eta^A \cdot \left(\frac{T}{1 \text{ sec}}\right)^{B \cdot \eta^C} \quad \mu_f = 0.8$$

$$\text{Global Ductility:} \quad \mu := \mu_{\max} \cdot \mu_f \quad \mu = 2.31$$

Step 11: Design Parameters:

$$V_y := K_f \cdot \Delta_{ya} + V_{ya} \quad V_y = 228.17 \text{ kip}$$

$$K_1 := K_f + K_a \quad K_1 = 283.5 \frac{\text{kip}}{\text{in}}$$

$$S_a := \min\left(\frac{S_{D1}}{T} \cdot 1 \text{ sec}, S_{D5}\right) \quad S_a = 1.1041 \text{ g}$$

$$V_e := m \cdot S_a \quad V_e = 852.57 \text{ kip}$$

$$V_p := V_{yf} + V_{ya} \quad V_p = 339.14 \text{ kip}$$

$$R := \frac{V_e}{V_y} \quad R = 3.74$$

$$\Omega_o := \frac{V_p}{V_y} \quad \Omega_o = 1.49$$

$$R_\mu := \frac{R}{\Omega_o} \quad R_\mu = 2.51$$

Try to adjust μ_{\max} and η by changing frame and damper properties:

Step 8: Required Beam Plastic Modulus: $Z_B := \frac{V_{yf} \cdot H}{2F_{yf}}$ $Z_B = 247.14 \text{ in}^3$

Select Beam: W21x68 $Z_B := 160 \cdot \text{in}^3$ $I_B := 1480 \cdot \text{in}^4$

Required Column Moment of inertia: $I_C := \frac{2}{\left(\frac{12E}{H^3 \cdot K_f} - \frac{L}{I_B \cdot H} \right)}$ $I_C = 3353.83 \text{ in}^4$

Select Column: W12x279 $Z_C := 481 \cdot \text{in}^3$ $I_C := 3110 \cdot \text{in}^4$

Required Braces Area: $A_b := \frac{K_a \cdot L}{4 \cdot E \cdot (\cos(\theta))^3}$ $A_b = 2.247 \text{ in}^2$

Select Braces Area (Plate): $A_b := 3.75 \cdot 1.0 \cdot \text{in}^2$ $A_b = 3.75 \text{ in}^2$

Required Steel Yield Strength for the Braces: $F_{yd} := \frac{V_{ya}}{2 \cdot A_b \cdot \cos(\theta)}$ $F_{yd} = 42.33 \text{ ksi}$

Select Steel Yield Strength for the Braces: $F_{yd} := 70 \cdot \text{ksi}$

Step 9: Frame Properties: $K_f := \frac{12E \cdot I_C}{H^3} \cdot \frac{1}{2 + \frac{I_C}{I_B} \cdot \frac{L}{H}}$ $K_f = 68.38 \frac{\text{kip}}{\text{in}}$

$V_{yf} := \frac{2F_{yf} \cdot Z_B}{H}$ $V_{yf} = 106.67 \text{ kip}$

$\Delta_{yf} := \frac{V_{yf}}{K_f}$ $\Delta_{yf} = 1.56 \text{ in}$

UB Properties: $K_a := \frac{4 \cdot A_b \cdot E}{L} \cdot (\cos(\theta))^3$ $K_a = 354.88 \frac{\text{kip}}{\text{in}}$

$V_{ya} := 2 \cdot F_{yd} \cdot A_b \cdot \cos(\theta)$ $V_{ya} = 283 \text{ kip}$

$\Delta_{ya} := \frac{V_{ya}}{K_a}$ $\Delta_{ya} = 0.8 \text{ in}$

New Parameters:

$$\alpha := \frac{1}{1 + \frac{K_a}{K_f}} \quad \alpha = 0.16$$

$$\mu_{\max} := \frac{\Delta_{yf}}{\Delta_{ya}} \quad \mu_{\max} = 1.96$$

$$\eta := \frac{V_y}{m \cdot \ddot{u}_{g\max}} \quad \eta = 0.84$$

$$T := 2 \cdot \pi \cdot \sqrt{\frac{m}{K_1}} \quad T = 0.43 \text{ sec}$$

Step 10: Time History Analysis Results:

Frame Ductility: $\mu_f := 1.00$

Global Ductility: $\mu := \mu_{\max} \cdot \mu_f \quad \mu = 1.96$

Approximate Results:

Frame Ductility: $\mu_f := \frac{0.8239}{\mu_{\max}} \cdot \eta^A \cdot \left(\frac{T}{1 \text{ sec}}\right)^{B \cdot \eta^C} \quad \mu_f = 1.07$

Global Ductility: $\mu := \mu_{\max} \cdot \mu_f \quad \mu = 2.09$

Step 11: Design Parameters:

$V_y := K_f \cdot \Delta_{ya} + V_{ya} \quad V_y = 337.53 \text{ kip}$

$K_1 := K_f + K_a \quad K_1 = 423.26 \frac{\text{kip}}{\text{in}}$

$S_a := \min\left(\frac{S_{D1}}{T} \cdot 1 \text{ sec}, S_{D5}\right) \quad S_a = 1.3 \text{ g}$

$V_e := m \cdot S_a \quad V_e = 1003.83 \text{ kip}$

$V_p := V_{yf} + V_{ya} \quad V_p = 389.67 \text{ kip}$

$R := \frac{V_e}{V_y} \quad R = 2.97$

$\Omega_o := \frac{V_p}{V_y} \quad \Omega_o = 1.15$

$R_\mu := \frac{R}{\Omega_o} \quad R_\mu = 2.58$

APPENDIX B

MATHEMATICAL DERIVATION OF EQUATIONS 6.3 AND 6.4

The energy dissipated per cycle by a bilinear structural frame, E_{hf} , may be determined from Ramirez et al. (2000) by calculating the area within the hysteresis loop at the maximum displacement (see Figure B.1a), which is equal to:

$$\frac{1}{2}E_{hf} = 2mAD - A_1 - A_2 - A_3 \quad (\text{B.1})$$

where A and D are the maximum acceleration and displacement of the system, respectively, and A_1 , A_2 , and A_3 are the shaded areas in Figure B.1a that need to be subtracted from $2mAD$ to obtain the area of half of the hysteresis loop. Substituting the geometric values of A_1 , A_2 , and A_3 , (B.1) can be written as:

$$\begin{aligned} \frac{1}{2}E_{hf} = 2mAD - \left(\frac{1}{2}\right) \frac{m(A - A_y)D^2}{(D - D_y)} - \left(\frac{1}{2}\right) \left[\frac{m(A - A_y)D}{(D - D_y)} + 2m(A - A_y) \right] (D - 2D_y) - \\ - \left(\frac{1}{2}\right) [2m(A - A_y) + 2mA](2D_y) \end{aligned} \quad (\text{B.2})$$

where A_y and D_y are the acceleration and displacement corresponding to the yield point of the structural frame, respectively (see Figure B.1a). Note that (B.2) can be further simplified as:

$$E_{hf} = 4m(A_y D - AD_y) \quad (\text{B.3})$$

To account for the effects of stiffness degradation, Ramirez et al. (2000) multiply the area of the hysteresis loop by a reduction factor (a.k.a. quality factor), q_h , which is equal to 1.0 for a non-degrading bilinear system. Introducing the quality factor, q_h , (B.3) can be finally written as:

$$E_{hf} = 4mq_h(A_y D - AD_y) \quad (\text{B.4})$$

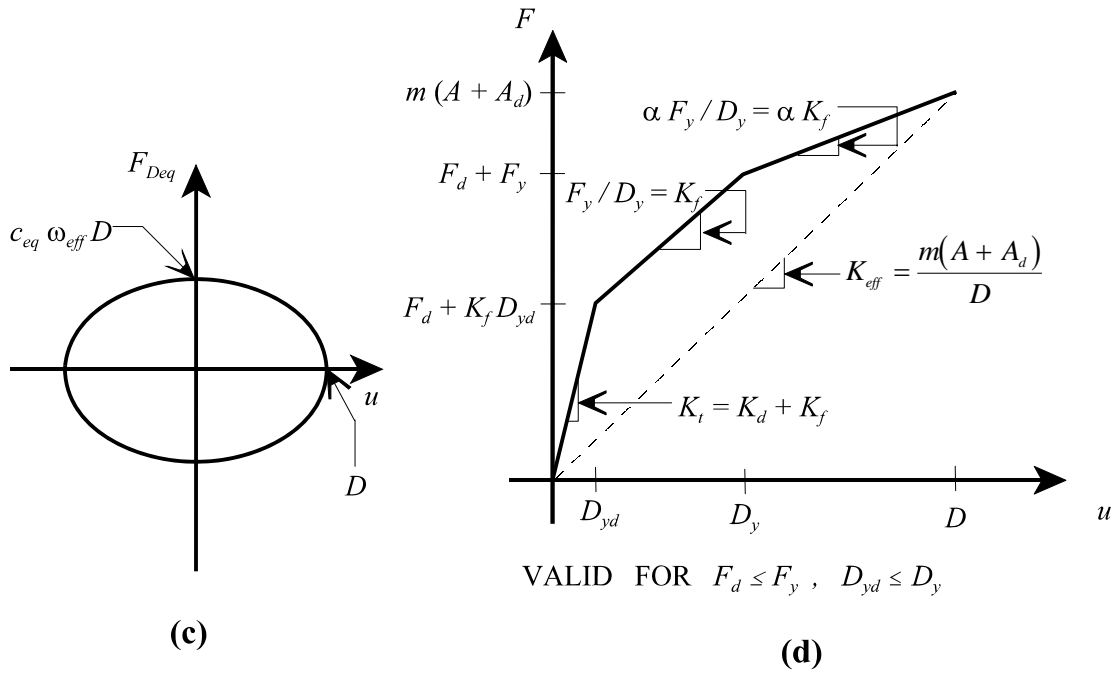
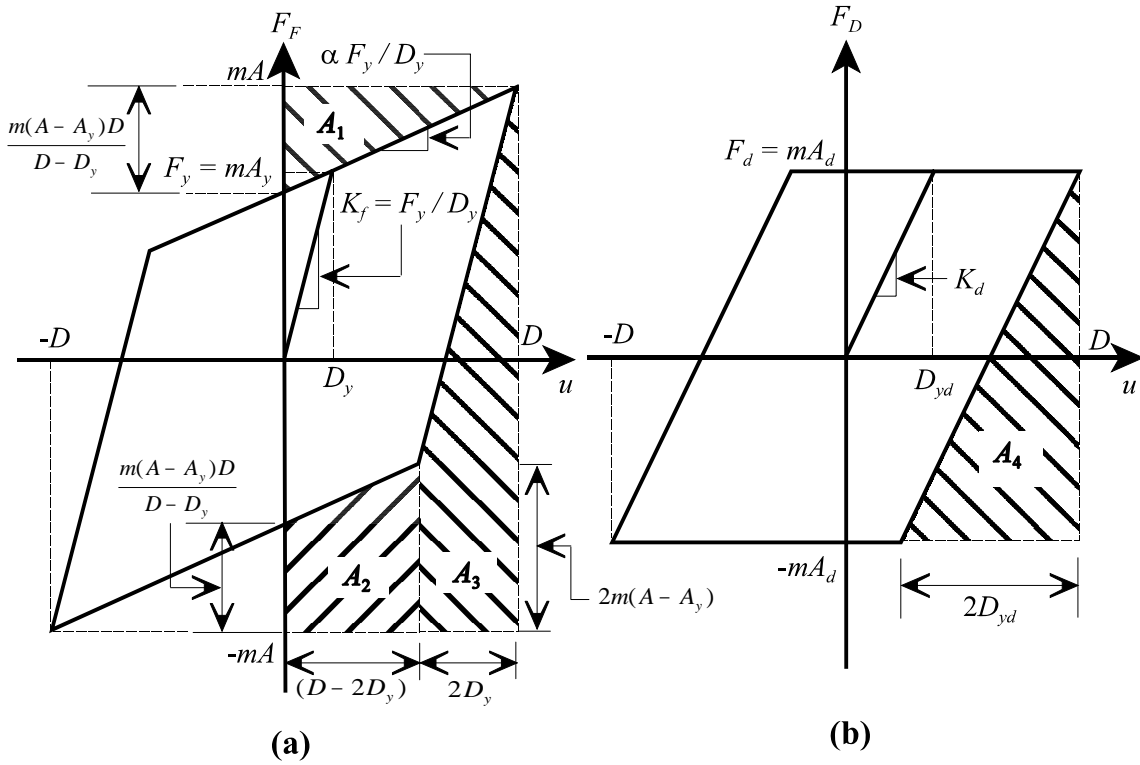


Figure B.1. Behavior of Bilinear Hysteretic System; a) Structural Frame, b) Yielding Damping Devices, c) Equivalent Viscous Damping Device, d) Total System (Adapted from Ramirez et al., 2000)

Likewise, the energy dissipated per cycle by a metallic damper, E_{hd} , may be determined as the area within the hysteresis loop of a yielding damping devices (as shown in Figure B.1b), which is equal to:

$$\frac{1}{2}E_{hd} = 2mA_dD - A_4 \quad (\text{B.5})$$

where A_d is the acceleration corresponding to the yield point of the metallic damper, and A_4 is the shaded area in Figure B.1b that need to be subtracted from $2mA_dD$ to obtain the area of half of the hysteresis loop. Substituting the geometric value of A_4 , (B.5) can be written as:

$$\frac{1}{2}E_{hd} = 2mA_dD - \left(\frac{1}{2}\right)(2mA_d)(2D_{yd}) \quad (\text{B.6})$$

where D_{yd} is the displacement corresponding to the yield point of the metallic damper. Note that (B.6) can be further simplified as:

$$E_{hd} = 4mA_d(D - D_{yd}) \quad (\text{B.7})$$

The total energy dissipated hysteretically, E_h , can be calculated by adding (B.4) and (B.7), which gives:

$$E_h = 4m[q_h(A_yD - AD_y) + A_d(D - D_{yd})] \quad (\text{B.8})$$

Furthermore, the total hysteretic energy can be transformed to an equivalent viscous energy, E_v , by equating E_h to the area within the ellipse of a viscous damper (as shown in Figure B.1c), which is equal to:

$$E_v = \pi c_{eq} \omega_{eff} D^2 \quad (\text{B.9})$$

where c_{eq} is the equivalent viscous damping coefficient, and ω_{eff} is the effective frequency of the system. Knowing that $c_{eq} = 2m\omega_{eff}\xi_h$, (B.9) can be written as:

$$E_v = 2\pi\xi_h m\omega_{eff}^2 D^2 \quad (\text{B.10})$$

where ξ_h is equivalent damping ratio corresponding to a hysteretic system (i.e., hysteretic

damping). Note that $m \omega_{eff}^2$ is equal to the effective stiffness, K_{eff} , which can be calculated from Figure B.1d as the secant stiffness of the total system at the maximum displacement, defined as:

$$K_{eff} = m \omega_{eff}^2 = \frac{m(A + A_d)}{D} \quad (B.11)$$

Substituting (B.11) into (B.10) gives:

$$E_v = 2m \xi_h \pi (A + A_d) D \quad (B.12)$$

Equating (B.8) and (B.12), and solving for ξ_h gives:

$$\xi_h = \frac{2q_h (A_y D - A D_y) + 2A_d (D - D_{yd})}{\pi (A + A_d) D} \quad (B.13)$$

which the expression used by Ramirez et al. (2000) to determine the equivalent damping ratio of a hysteretic system.

Knowing that $A / A_y = 1$ for an elasto-plastic structural frame, (B.13) may be written as:

$$\xi_h = \frac{2q_h \left(1 - \frac{D_y}{D}\right) + 2 \left(\frac{A_d}{A_y}\right) \left(1 - \frac{D_{yd}}{D}\right)}{\pi \left(1 + \frac{A_d}{A_y}\right)} \quad (B.14)$$

It may be noted that (B.14) may be expressed in terms of the ductility of the metallic damper and the ductility of the bare frame, μ_d and μ_f , respectively (i.e., $\mu_d = D / D_{yd}$, and $\mu_f = D / D_y$), which gives:

$$\xi_h = \frac{2q_h \left(1 - \frac{1}{\mu_f}\right) + 2 \left(\frac{A_d}{A_y}\right) \left(1 - \frac{1}{\mu_d}\right)}{\pi \left(1 + \frac{A_d}{A_y}\right)} \quad (B.15)$$

Note that the ductility of the metallic damper, μ_d is equal to the global ductility, μ , in this study (i.e., $\mu_d = \mu$). According to Figure 3.2, A_d and A_y can be defined, respectively, as:

$$A_d = \frac{V_{yd}}{m} \quad (\text{B.16})$$

$$A_y = \frac{V_{yf}}{m} \quad (\text{B.17})$$

Substituting $\mu_d = \mu$, and (B.16) and (B.17) into (B.15), gives (6.3) used in this study:

$$\xi_h = \left(\frac{2q_h}{\pi} \right) \left[\frac{\left(1 - \frac{1}{\mu_f} \right) + \left(\frac{V_{yd}}{V_{yf}} \right) \left(1 - \frac{1}{\mu} \right)}{1 + \left(\frac{V_{yd}}{V_{yf}} \right)} \right] \quad (\text{B.18})$$

where V_{yd} and V_{yf} are the yield capacity of the metallic damper and the bare frame, respectively, which may be determined from Figure 3.2 as:

$$V_{yd} = V_y (1 - \alpha) \quad (\text{B.19})$$

$$V_{yf} = V_y \alpha \mu_{\max} \quad (\text{B.20})$$

Finally, substituting $q_h = 1.0$, and (B.19) and (B.20) into (B.18), gives (6.4) used in this study:

$$\xi_h = \left(\frac{2}{\pi} \right) \left[\frac{\left(1 - \frac{1}{\mu_f} \right) + \frac{(1 - \alpha)}{\alpha \mu_{\max}} \left(1 - \frac{1}{\mu} \right)}{1 + \frac{(1 - \alpha)}{\alpha \mu_{\max}}} \right] \quad (\text{B.21})$$

APPENDIX C

EXAMPLES OF DESIGN AND RETROFIT OF MDOF SYSTEMS WITH BUCKLING-RESTRAINED BRACES

Example C-1: Design to Satisfy the Structural Fuse Concept of MDOF System with Buckling-restrained Braces

Frame Properties:

Building High: $H := 15545 \cdot \text{mm}$ Panel Width: $L := 7468 \cdot \text{mm}$

Mass Matrix: $M := \begin{pmatrix} 0.296 & 0 & 0 & 0 \\ 0 & 0.287 & 0 & 0 \\ 0 & 0 & 0.287 & 0 \\ 0 & 0 & 0 & 0.239 \end{pmatrix}$ Total Mass: $m_t := 1.109 \cdot \frac{\text{kN} \cdot \text{sec}^2}{\text{mm}}$

Assumed Mode Shape: $\phi_1 := \begin{pmatrix} 0.26 \\ 0.51 \\ 0.75 \\ 1.00 \end{pmatrix}$ $r := \begin{pmatrix} 1 \\ 1 \end{pmatrix}$

Modal Participation Factor: $\Gamma_1 := \frac{|\phi_1^T \cdot M \cdot r|}{|(\phi_1^T \cdot M) \cdot \phi_1|}$ $\Gamma_1 = 1.37$

Story high: $h_1 := 4115 \text{mm}$ $h_2 := 3810 \text{mm}$ $h_3 := 3810 \text{mm}$ $h_4 := 3810 \text{mm}$

Bay Length: $L_1 := 4877 \text{mm}$ $L_2 := 7468 \text{mm}$ $L_3 := 4877 \text{mm}$

Material Properties:

$F_{yf} := 345 \cdot \text{MPa}$ $E := 200000 \cdot \text{MPa}$ $G := 77240 \cdot \text{MPa}$ $F_{yd} := 248 \cdot \text{MPa}$

Site: Sherman Oaks, California (Lat.=34.154, Long.=-118.465), Site Class B

$S_s := 1.95 \cdot g$ $S_1 := 0.87 \cdot g$ $F_a := 1$ $F_v := 1$

$S_{MS} = 1.95 \cdot g$ $S_{M1} = 0.87 \cdot g$

$S_{DS} = 1.3 \cdot g$ $S_{D1} = 0.58 \cdot g$

Peak Ground Acceleration: $\ddot{u}_{g\max} := 0.4 \cdot S_{DS}$ $\ddot{u}_{g\max} = 0.52 \cdot g$

Step 1: Allowable Roof Displacement: $\Delta_a := 0.02 \cdot H$ $\Delta_a = 311 \text{mm}$

Elastic Spectral Displacement: $S_d := \Delta_a$ $S_d = 311 \text{mm}$

Step 2: Elastic Period Limit: $T_L := \frac{4 \cdot \pi^2}{\Gamma_1 \cdot S_{D1}} \cdot \frac{S_d}{1 \text{sec}}$ $T_L = 1.58 \text{sec}$

Elastic Spectral Acceleration: $S_a := \min\left(\frac{S_{D1}}{T_L} \cdot 1 \text{sec}, S_{DS}\right)$ $S_a = 0.368 \cdot g$

Elastic Base Shear: $V_e := m_t \cdot S_a$ $V_e = 4001 \text{ kN}$

Step 3: Design Parameters (Table 1):

Target Design Parameters: $\alpha := 0.25$ $\mu_{\max} := 5$ $\eta := 0.2$
 $\Omega_o := \alpha \cdot (\mu_{\max} - 1) + 1$ $\Omega_o = 2$

Step 4: Yield Shear: $V_y := \eta \cdot m_t \cdot \ddot{u}_{g\max}$ $V_y = 1131 \text{ kN}$

Shear Capacity: $V_p := \Omega_o \cdot V_y$ $V_p = 2262 \text{ kN}$

Step 5: Required Stiffness: $K_1 := \frac{4 \cdot \pi^2}{T_L^2} \cdot m_t$ $K_1 = 17.61 \frac{\text{kN}}{\text{mm}}$

Frame Stiffness: $K_f := \alpha \cdot K_1$ $K_f = 4.4 \frac{\text{kN}}{\text{mm}}$

Structural Fuse Stiffness: $K_a := (1 - \alpha) \cdot K_1$ $K_a = 13.21 \frac{\text{kN}}{\text{mm}}$

Step 6: SF Yield Displacement: $\Delta_{ya} := \frac{V_y}{K_1}$ $\Delta_{ya} = 64 \text{ mm}$

BF Yield Displacement: $\Delta_{yf} := \mu_{\max} \cdot \Delta_{ya}$ $\Delta_{yf} = 321 \text{ mm}$

Step 7: BF Shear Capacity: $V_{yf} := V_y \cdot \alpha \cdot \mu_{\max}$ $V_{yf} = 1414 \text{ kN}$

SF Shear Capacity: $V_{ya} := V_y \cdot (1 - \alpha)$ $V_{ya} = 848 \text{ kN}$

Step 8: Vertical Distribution of BF and SF Base Shear:

$F_{f1} := \Phi_1 \cdot V_{yf}$ $F_{f1} = \begin{pmatrix} 146 \\ 286 \\ 421 \\ 561 \end{pmatrix} \text{ kN}$

$F_{a1} := \Phi_1 \cdot V_{ya}$ $F_{a1} = \begin{pmatrix} 88 \\ 172 \\ 252 \\ 337 \end{pmatrix} \text{ kN}$

BF Story Shear: $V_{yf1} = 1414 \text{ kN}$ $V_{yf2} = 1268 \text{ kN}$

$V_{yf3} = 982 \text{ kN}$ $V_{yf4} = 561 \text{ kN}$

SF Story Shear: $V_{ya1} = 848 \text{ kN}$ $V_{ya2} = 761 \text{ kN}$
 $V_{ya3} = 589 \text{ kN}$ $V_{ya4} = 337 \text{ kN}$

Beams Moments: $M_{B1} := (V_{yf2} \cdot h_2 + V_{yf1} \cdot h_1) \cdot \frac{1}{12}$ $M_{B1} = 887 \text{ kN}\cdot\text{m}$
 $M_{B2} := (V_{yf3} \cdot h_3 + V_{yf2} \cdot h_2) \cdot \frac{1}{12}$ $M_{B2} = 714 \text{ kN}\cdot\text{m}$
 $M_{B3} := (V_{yf4} \cdot h_4 + V_{yf3} \cdot h_3) \cdot \frac{1}{12}$ $M_{B3} = 490 \text{ kN}\cdot\text{m}$
 $M_{B4} := V_{yf4} \cdot h_4 \cdot \frac{1}{12}$ $M_{B4} = 178 \text{ kN}\cdot\text{m}$

Required Beams Plastic Modulus: $Z_{B1} := \frac{M_{B1}}{F_{yf}}$ $Z_{B1} = 2572168 \text{ mm}^3$
 $Z_{B2} := \frac{M_{B2}}{F_{yf}}$ $Z_{B2} = 2070444 \text{ mm}^3$
 $Z_{B3} := \frac{M_{B3}}{F_{yf}}$ $Z_{B3} = 1419880 \text{ mm}^3$
 $Z_{B4} := \frac{M_{B4}}{F_{yf}}$ $Z_{B4} = 516320 \text{ mm}^3$

Exterior Columns Moments: $M_{EC1} := V_{yf1} \cdot h_1 \cdot \frac{1}{12}$ $M_{EC1} = 485 \text{ kN}\cdot\text{m}$
 $M_{EC2} := V_{yf2} \cdot h_2 \cdot \frac{1}{12}$ $M_{EC2} = 403 \text{ kN}\cdot\text{m}$
 $M_{EC3} := V_{yf3} \cdot h_3 \cdot \frac{1}{12}$ $M_{EC3} = 312 \text{ kN}\cdot\text{m}$
 $M_{EC4} := V_{yf4} \cdot h_4 \cdot \frac{1}{12}$ $M_{EC4} = 178 \text{ kN}\cdot\text{m}$

Required Exterior Columns Plastic Modulus: $Z_{EC1} := \frac{M_{EC1}}{F_{yf}}$ $Z_{EC1} = 1405285 \text{ mm}^3$
 $Z_{EC2} := \frac{M_{EC2}}{F_{yf}}$ $Z_{EC2} = 1166883 \text{ mm}^3$
 $Z_{EC3} := \frac{M_{EC3}}{F_{yf}}$ $Z_{EC3} = 903560 \text{ mm}^3$
 $Z_{EC4} := \frac{M_{EC4}}{F_{yf}}$ $Z_{EC4} = 516320 \text{ mm}^3$

Interior Columns Moments:

$$M_{IC1} := V_{yf1} \cdot h_1 \cdot \frac{1}{6} \quad M_{IC1} = 970 \text{ kN}\cdot\text{m}$$

$$M_{IC2} := V_{yf2} \cdot h_2 \cdot \frac{1}{6} \quad M_{IC2} = 805 \text{ kN}\cdot\text{m}$$

$$M_{IC3} := V_{yf3} \cdot h_3 \cdot \frac{1}{6} \quad M_{IC3} = 623 \text{ kN}\cdot\text{m}$$

$$M_{IC4} := V_{yf4} \cdot h_4 \cdot \frac{1}{6} \quad M_{IC4} = 356 \text{ kN}\cdot\text{m}$$

Required Exterior Columns Plastic Modulus:

$$Z_{IC1} := \frac{M_{IC1}}{F_{yf}} \quad Z_{IC1} = 2810570 \text{ mm}^3$$

$$Z_{IC2} := \frac{M_{IC2}}{F_{yf}} \quad Z_{IC2} = 2333767 \text{ mm}^3$$

$$Z_{IC3} := \frac{M_{IC3}}{F_{yf}} \quad Z_{IC3} = 1807120 \text{ mm}^3$$

$$Z_{IC4} := \frac{M_{IC4}}{F_{yf}} \quad Z_{IC4} = 1032640 \text{ mm}^3$$

Select Beams:

First Floor:	W21x68	$Z_{b1} = 2621930 \text{ mm}^3$
Second Floor:	W21x57	$Z_{b2} = 2113931 \text{ mm}^3$
Third Floor:	W16x45	$Z_{b3} = 1348655 \text{ mm}^3$
Fourth Floor:	W12x22	$Z_{b4} = 480141 \text{ mm}^3$

Select Exterior Columns

First and Second Story:	W14x61	$Z_{ec12} = 1671481 \text{ mm}^3$
Third and Fourth Floor:	W14x34	$Z_{ec34} = 894734 \text{ mm}^3$

Select Interior Columns

First and Second Story:	W14x99	$Z_{ic12} = 2834962 \text{ mm}^3$
Third and Fourth Floor:	W14x68	$Z_{ic34} = 1884512 \text{ mm}^3$

Required Unbonded Braces Area:

First Story:	$A_{br1} := \frac{V_{ya1}}{2 \cdot F_{yd} \cdot \cos(\theta_1)}$	$A_{br1} = 2545 \text{ mm}^2$
Second Story:	$A_{br2} := \frac{V_{ya2}}{2 \cdot F_{yd} \cdot \cos(\theta_2)}$	$A_{br2} = 2191 \text{ mm}^2$
Third Story:	$A_{br3} := \frac{V_{ya3}}{2 \cdot F_{yd} \cdot \cos(\theta_3)}$	$A_{br3} = 1697 \text{ mm}^2$

$$\text{Fourth Story: } A_{br4} := \frac{V_{ya4}}{2 \cdot F_{yd} \cdot \cos(\theta_4)} \quad A_{br4} = 970 \text{ mm}^2$$

Select Unbonded Braces Properties:

$$\text{First Story: } b_1 := 144 \text{ mm} \quad t_1 := 19 \text{ mm} \quad A_{b1} := b_1 \cdot t_1 \rightarrow 2736 \cdot \text{mm}^2$$

$$\text{Second Story: } b_2 := 114 \text{ mm} \quad t_2 := 19 \text{ mm} \quad A_{b2} := b_2 \cdot t_2 \rightarrow 2166 \cdot \text{mm}^2$$

$$\text{Third Story: } b_3 := 89 \text{ mm} \quad t_3 := 19 \text{ mm} \quad A_{b3} := b_3 \cdot t_3 \rightarrow 1691 \cdot \text{mm}^2$$

$$\text{Fourth Story: } b_4 := 51 \text{ mm} \quad t_4 := 19 \text{ mm} \quad A_{b4} := b_4 \cdot t_4 \rightarrow 969 \cdot \text{mm}^2$$

Step 9: Pushover Analysis:

$$\text{Frame Properties: } K_f = 6.73 \frac{\text{kN}}{\text{mm}} \quad V_{yf} = 1279 \text{ kN} \quad \Delta_{yf} = 190 \text{ mm}$$

$$\text{UB Properties: } K_a = 21.33 \frac{\text{kN}}{\text{mm}} \quad V_{ya} = 865 \text{ kN} \quad \Delta_{ya} = 41 \text{ mm}$$

$$\text{Total Stiffness: } K_1 := K_f + K_a \quad K_1 = 28.06 \frac{\text{kN}}{\text{mm}}$$

$$\text{Total Yield Shear: } V_y := K_f \cdot \Delta_{ya} + V_{ya} \quad V_y = 1137 \text{ kN}$$

$$\text{New Parameters: } \alpha := \frac{1}{1 + \frac{K_a}{K_f}} \quad \alpha = 0.24$$

$$\mu_{\max} := \frac{\Delta_{yf}}{\Delta_{ya}} \quad \mu_{\max} = 4.69$$

$$\eta := \frac{V_y}{m_t \cdot \ddot{u}_{g\max}} \quad \eta = 0.2$$

$$\text{Period from Dynamic Analysis: } T := 0.975 \text{ sec}$$

Step 10: Time History Analysis Results:

$$\text{Frame Ductility: } \mu_f := 0.678$$

$$\text{Global Ductility: } \mu := \mu_{\max} \cdot \mu_f \quad \mu = 3.18$$

Approximate Results:

$$\text{Frame Ductility: } \mu_f := \frac{0.8239}{\mu_{\max}} \cdot \eta^A \cdot \left(\frac{T}{1 \text{ sec}} \right)^{B \cdot \eta^C} \quad \mu_f = 1.04$$

Global Ductility: $\mu := \mu_{\max} \cdot \mu_f$ $\mu = 4.89$

Step 11: Design Parameters:

$$S_a := \min \left(\frac{S_{D1}}{T} \cdot 1 \text{ sec}, S_{DS} \right) \quad S_a = 0.5949 \text{ g}$$

$$V_e := m_t \cdot S_a \quad V_e = 6470 \text{ kN}$$

$$V_p := V_{yf} + V_{ya} \quad V_p = 2144 \text{ kN}$$

$$R := \frac{V_e}{V_y} \quad R = 5.688$$

$$\Omega_o := \frac{V_p}{V_y} \quad \Omega_o = 1.885$$

$$R_\mu := \frac{R}{\Omega_o} \quad R_\mu = 3.018$$

Example C-2: Retrofit of a MDOF System to Satisfy the Structural Fuse Concept with Buckling-Restrained Braces

Frame Properties:

Building High: $H := 15545 \cdot \text{mm}$ Panel Width: $L := 7468 \cdot \text{mm}$

Mass Matrix: $M := \begin{pmatrix} 0.296 & 0 & 0 & 0 \\ 0 & 0.287 & 0 & 0 \\ 0 & 0 & 0.287 & 0 \\ 0 & 0 & 0 & 0.239 \end{pmatrix}$ Total Mass: $m_t := 1.109 \cdot \frac{\text{kN} \cdot \text{sec}^2}{\text{mm}}$

Assumed Mode Shape: $\phi_1 := \begin{pmatrix} 0.26 \\ 0.51 \\ 0.75 \\ 1.00 \end{pmatrix}$ $r := \begin{pmatrix} 1 \\ 1 \end{pmatrix}$

Modal Participation Factor: $\Gamma_1 := \frac{|\phi_1^T \cdot M \cdot r|}{|(\phi_1^T \cdot M) \cdot \phi_1|}$ $\Gamma_1 = 1.37$

Story high: $h_1 := 4115 \text{mm}$ $h_2 := 3810 \text{mm}$ $h_3 := 3810 \text{mm}$ $h_4 := 3810 \text{mm}$

Bay Length: $L_1 := 4877 \text{mm}$ $L_2 := 7468 \text{mm}$ $L_3 := 4877 \text{mm}$

Material Properties:

$F_{yf} := 345 \cdot \text{MPa}$ $E := 200000 \cdot \text{MPa}$ $G := 77240 \cdot \text{MPa}$ $F_{yd} := 345 \cdot \text{MPa}$

Site: Sherman Oaks, California (Lat.=34.154, Long.=-118.465), Site Class B

$S_s := 1.95 \cdot g$ $S_1 := 0.87 \cdot g$ $F_a := 1$ $F_v := 1$

$S_{MS} = 1.95 \cdot g$ $S_{M1} = 0.87 \cdot g$

$S_{DS} = 1.3 \cdot g$ $S_{D1} = 0.58 \cdot g$

Peak Ground Acceleration: $\ddot{u}_{g\max} := 0.4 \cdot S_{DS}$ $\ddot{u}_{g\max} = 0.52 \cdot g$

Existing Frame Properties:

Existing Beams:

First Floor: W24x55 $Z_{b1} = 2195867 \text{mm}^3$

Second Floor: W21x50 $Z_{b2} = 1802577 \text{mm}^3$

Third Floor: W21x44 $Z_{b3} = 1563326 \text{mm}^3$

Fourth Floor: W18x40 $Z_{b4} = 1284746 \text{mm}^3$

Existing Exterior Columns

First and Second Story: W14x53 $Z_{ec12} = 1427313 \text{ mm}^3$

Third and Fourth Floor: W14x48 $Z_{ec34} = 1284746 \text{ mm}^3$

Existing Interior Columns

First and Second Story: W14x82 $Z_{ic12} = 2277802 \text{ mm}^3$

Third and Fourth Floor: W14x53 $Z_{ic34} = 1427313 \text{ mm}^3$

Pushover Analysis: $K_f = 6.88 \frac{\text{kN}}{\text{mm}}$ $V_{yf} = 1067 \text{ kN}$ $\Delta_{yf} = 155 \text{ mm}$

Step 1: Allowable Roof Displacement: $\Delta_a := 0.02 \cdot H$ $\Delta_a = 311 \text{ mm}$

Elastic Spectral Displacement: $S_d := \Delta_a$ $S_d = 311 \text{ mm}$

Step 2: Elastic Period Limit: $T_L := \frac{4 \cdot \pi^2}{\Gamma_1 \cdot S_{D1}} \cdot \frac{S_d}{1 \text{ sec}}$ $T_L = 1.58 \text{ sec}$

Elastic Spectral Acceleration: $S_a := \min\left(\frac{S_{D1}}{T_L} \cdot 1 \text{ sec}, S_{DS}\right)$ $S_a = 0.368 \text{ g}$

Elastic Base Shear: $V_e := m_t \cdot S_a$ $V_e = 4001 \text{ kN}$

Step 3: Design Parameters (Table 1):

Target Design Parameters: $\mu_{\max} := 5$ $\eta := 0.2$

$\alpha := \min\left(\frac{V_{yf}}{\eta \cdot \mu_{\max} \cdot m_t \cdot \ddot{u}_{g\max}}, \frac{T_L^2 \cdot K_f}{4 \cdot \pi^2 \cdot m_t}\right)$ $\alpha = 0.19$

$\Omega_o := \alpha \cdot (\mu_{\max} - 1) + 1$ $\Omega_o = 1.75$

Step 4: Yield Shear: $V_y := \eta \cdot m_t \cdot \ddot{u}_{g\max}$ $V_y = 1131 \text{ kN}$

Shear Capacity: $V_p := \Omega_o \cdot V_y$ $V_p = 1985 \text{ kN}$

Step 5: Required Stiffness: $K_I := \max\left(\frac{\eta \cdot m_t \cdot \ddot{u}_{g\max} \cdot \mu_{\max}}{\Delta_{yf}}, \frac{4 \cdot \pi^2}{T_L^2} \cdot m_t\right)$ $K_I = 36.49 \frac{\text{kN}}{\text{mm}}$

Required Period: $T := \min\left(2 \cdot \pi \cdot \sqrt{\frac{\Delta_{yf}}{\eta \cdot \mu_{\max} \cdot \ddot{u}_{g\max}}}, T_L\right)$ $T = 1.095 \text{ sec}$

Structural Fuse Stiffness: $K_a := (1 - \alpha) \cdot K_1$ $K_a = 29.6 \frac{\text{kN}}{\text{mm}}$

Step 6: SF Yield Displacement: $\Delta_{ya} := \frac{V_y}{K_1}$ $\Delta_{ya} = 31 \text{ mm}$

Step 7: SF Shear Capacity: $V_{ya} := V_y \cdot (1 - \alpha)$ $V_{ya} = 918 \text{ kN}$

Step 8: Vertical Distribution of SF Base Shear:

$$F_{a1} := \Phi_1 \cdot V_{ya} \quad F_{a1} = \begin{pmatrix} 95 \\ 186 \\ 273 \\ 364 \end{pmatrix} \text{ kN}$$

SF Story Shear: $V_{ya1} = 918 \text{ kN}$ $V_{ya2} = 823 \text{ kN}$
 $V_{ya3} = 637 \text{ kN}$ $V_{ya4} = 364 \text{ kN}$

Required Unbonded Braces Area:

First Story: $A_{br1} := \frac{V_{ya1}}{2 \cdot F_{yd} \cdot \cos(\theta_1)}$ $A_{br1} = 1979 \text{ mm}^2$

Second Story: $A_{br2} := \frac{V_{ya2}}{2 \cdot F_{yd} \cdot \cos(\theta_2)}$ $A_{br2} = 1704 \text{ mm}^2$

Third Story: $A_{br3} := \frac{V_{ya3}}{2 \cdot F_{yd} \cdot \cos(\theta_3)}$ $A_{br3} = 1320 \text{ mm}^2$

Fourth Story: $A_{br4} := \frac{V_{ya4}}{2 \cdot F_{yd} \cdot \cos(\theta_4)}$ $A_{br4} = 754 \text{ mm}^2$

Select Unbonded Braces Properties:

First Story: $b_1 := 102 \text{ mm}$ $t_1 := 19 \text{ mm}$ $A_{b1} := b_1 \cdot t_1 \rightarrow 1938 \cdot \text{mm}^2$

Second Story: $b_2 := 89 \text{ mm}$ $t_2 := 19 \text{ mm}$ $A_{b2} := b_2 \cdot t_2 \rightarrow 1691 \cdot \text{mm}^2$

Third Story: $b_3 := 70 \text{ mm}$ $t_3 := 19 \text{ mm}$ $A_{b3} := b_3 \cdot t_3 \rightarrow 1330 \cdot \text{mm}^2$

Fourth Story: $b_4 := 38 \text{ mm}$ $t_4 := 19 \text{ mm}$ $A_{b4} := b_4 \cdot t_4 \rightarrow 722 \cdot \text{mm}^2$

Step 9: UB Properties: $K_a = 16.58 \frac{\text{kN}}{\text{mm}}$ $V_{ya} = 880 \text{ kN}$ $\Delta_{ya} = 53 \text{ mm}$

Total Stiffness: $K_1 := K_f + K_a$ $K_1 = 23.46 \frac{\text{kN}}{\text{mm}}$

Total Yield Shear: $V_y := K_f \cdot \Delta_{ya} + V_{ya}$ $V_y = 1245 \text{ kN}$

New Parameters:

$$\alpha := \frac{1}{1 + \frac{K_a}{K_f}} \quad \alpha = 0.29$$

$$\mu_{\max} := \frac{\Delta_{yf}}{\Delta_{ya}} \quad \mu_{\max} = 2.92$$

$$\eta := \frac{V_y}{m_t \cdot \ddot{u}_{g\max}} \quad \eta = 0.22$$

Period from Dynamic Analysis: $T := 1.0819\text{sec}$

Step 10: Time History Analysis Results:

Frame Ductility: $\mu_f := .893$

Global Ductility: $\mu := \mu_{\max} \cdot \mu_f \quad \mu = 2.61$

Approximate Results:

Frame Ductility: $\mu_f := \frac{0.8239}{\mu_{\max}} \cdot \eta^A \cdot \left(\frac{T}{1\text{sec}}\right)^{B \cdot \eta^C} \quad \mu_f = 1.397$

Global Ductility: $\mu := \mu_{\max} \cdot \mu_f \quad \mu = 4.08$

Step 11: Design Parameters:

$$S_a := \min \left(\frac{S_{D1}}{T} \cdot 1\text{sec}, S_{DS} \right) \quad S_a = 0.5361 \text{ g}$$

$$V_e := m_t \cdot S_a \quad V_e = 5830 \text{ kN}$$

$$V_p := V_{yf} + V_{ya} \quad V_p = 1947 \text{ kN}$$

$$R := \frac{V_e}{V_y} \quad R = 4.684$$

$$\Omega_o := \frac{V_p}{V_y} \quad \Omega_o = 1.564$$

$$R_\mu := \frac{R}{\Omega_o} \quad R_\mu = 2.995$$

Multidisciplinary Center for Earthquake Engineering Research List of Technical Reports

The Multidisciplinary Center for Earthquake Engineering Research (MCEER) publishes technical reports on a variety of subjects related to earthquake engineering written by authors funded through MCEER. These reports are available from both MCEER Publications and the National Technical Information Service (NTIS). Requests for reports should be directed to MCEER Publications, Multidisciplinary Center for Earthquake Engineering Research, State University of New York at Buffalo, Red Jacket Quadrangle, Buffalo, New York 14261. Reports can also be requested through NTIS, 5285 Port Royal Road, Springfield, Virginia 22161. NTIS accession numbers are shown in parenthesis, if available.

- NCEER-87-0001 "First-Year Program in Research, Education and Technology Transfer," 3/5/87, (PB88-134275, A04, MF-A01).
- NCEER-87-0002 "Experimental Evaluation of Instantaneous Optimal Algorithms for Structural Control," by R.C. Lin, T.T. Soong and A.M. Reinhorn, 4/20/87, (PB88-134341, A04, MF-A01).
- NCEER-87-0003 "Experimentation Using the Earthquake Simulation Facilities at University at Buffalo," by A.M. Reinhorn and R.L. Ketter, to be published.
- NCEER-87-0004 "The System Characteristics and Performance of a Shaking Table," by J.S. Hwang, K.C. Chang and G.C. Lee, 6/1/87, (PB88-134259, A03, MF-A01). This report is available only through NTIS (see address given above).
- NCEER-87-0005 "A Finite Element Formulation for Nonlinear Viscoplastic Material Using a Q Model," by O. Gyebe and G. Dasgupta, 11/2/87, (PB88-213764, A08, MF-A01).
- NCEER-87-0006 "Symbolic Manipulation Program (SMP) - Algebraic Codes for Two and Three Dimensional Finite Element Formulations," by X. Lee and G. Dasgupta, 11/9/87, (PB88-218522, A05, MF-A01).
- NCEER-87-0007 "Instantaneous Optimal Control Laws for Tall Buildings Under Seismic Excitations," by J.N. Yang, A. Akbarpour and P. Ghaemmaghami, 6/10/87, (PB88-134333, A06, MF-A01). This report is only available through NTIS (see address given above).
- NCEER-87-0008 "IDARC: Inelastic Damage Analysis of Reinforced Concrete Frame - Shear-Wall Structures," by Y.J. Park, A.M. Reinhorn and S.K. Kunnath, 7/20/87, (PB88-134325, A09, MF-A01). This report is only available through NTIS (see address given above).
- NCEER-87-0009 "Liquefaction Potential for New York State: A Preliminary Report on Sites in Manhattan and Buffalo," by M. Budhu, V. Vijayakumar, R.F. Giese and L. Baumgras, 8/31/87, (PB88-163704, A03, MF-A01). This report is available only through NTIS (see address given above).
- NCEER-87-0010 "Vertical and Torsional Vibration of Foundations in Inhomogeneous Media," by A.S. Veletsos and K.W. Dotson, 6/1/87, (PB88-134291, A03, MF-A01). This report is only available through NTIS (see address given above).
- NCEER-87-0011 "Seismic Probabilistic Risk Assessment and Seismic Margins Studies for Nuclear Power Plants," by Howard H.M. Hwang, 6/15/87, (PB88-134267, A03, MF-A01). This report is only available through NTIS (see address given above).
- NCEER-87-0012 "Parametric Studies of Frequency Response of Secondary Systems Under Ground-Acceleration Excitations," by Y. Yong and Y.K. Lin, 6/10/87, (PB88-134309, A03, MF-A01). This report is only available through NTIS (see address given above).
- NCEER-87-0013 "Frequency Response of Secondary Systems Under Seismic Excitation," by J.A. HoLung, J. Cai and Y.K. Lin, 7/31/87, (PB88-134317, A05, MF-A01). This report is only available through NTIS (see address given above).
- NCEER-87-0014 "Modelling Earthquake Ground Motions in Seismically Active Regions Using Parametric Time Series Methods," by G.W. Ellis and A.S. Cakmak, 8/25/87, (PB88-134283, A08, MF-A01). This report is only available through NTIS (see address given above).

- NCEER-87-0015 "Detection and Assessment of Seismic Structural Damage," by E. DiPasquale and A.S. Cakmak, 8/25/87, (PB88-163712, A05, MF-A01). This report is only available through NTIS (see address given above).
- NCEER-87-0016 "Pipeline Experiment at Parkfield, California," by J. Isenberg and E. Richardson, 9/15/87, (PB88-163720, A03, MF-A01). This report is available only through NTIS (see address given above).
- NCEER-87-0017 "Digital Simulation of Seismic Ground Motion," by M. Shinozuka, G. Deodatis and T. Harada, 8/31/87, (PB88-155197, A04, MF-A01). This report is available only through NTIS (see address given above).
- NCEER-87-0018 "Practical Considerations for Structural Control: System Uncertainty, System Time Delay and Truncation of Small Control Forces," J.N. Yang and A. Akbarpour, 8/10/87, (PB88-163738, A08, MF-A01). This report is only available through NTIS (see address given above).
- NCEER-87-0019 "Modal Analysis of Nonclassically Damped Structural Systems Using Canonical Transformation," by J.N. Yang, S. Sarkani and F.X. Long, 9/27/87, (PB88-187851, A04, MF-A01).
- NCEER-87-0020 "A Nonstationary Solution in Random Vibration Theory," by J.R. Red-Horse and P.D. Spanos, 11/3/87, (PB88-163746, A03, MF-A01).
- NCEER-87-0021 "Horizontal Impedances for Radially Inhomogeneous Viscoelastic Soil Layers," by A.S. Veletsos and K.W. Dotson, 10/15/87, (PB88-150859, A04, MF-A01).
- NCEER-87-0022 "Seismic Damage Assessment of Reinforced Concrete Members," by Y.S. Chung, C. Meyer and M. Shinozuka, 10/9/87, (PB88-150867, A05, MF-A01). This report is available only through NTIS (see address given above).
- NCEER-87-0023 "Active Structural Control in Civil Engineering," by T.T. Soong, 11/11/87, (PB88-187778, A03, MF-A01).
- NCEER-87-0024 "Vertical and Torsional Impedances for Radially Inhomogeneous Viscoelastic Soil Layers," by K.W. Dotson and A.S. Veletsos, 12/87, (PB88-187786, A03, MF-A01).
- NCEER-87-0025 "Proceedings from the Symposium on Seismic Hazards, Ground Motions, Soil-Liquefaction and Engineering Practice in Eastern North America," October 20-22, 1987, edited by K.H. Jacob, 12/87, (PB88-188115, A23, MF-A01). This report is available only through NTIS (see address given above).
- NCEER-87-0026 "Report on the Whittier-Narrows, California, Earthquake of October 1, 1987," by J. Pantelic and A. Reinhorn, 11/87, (PB88-187752, A03, MF-A01). This report is available only through NTIS (see address given above).
- NCEER-87-0027 "Design of a Modular Program for Transient Nonlinear Analysis of Large 3-D Building Structures," by S. Srivastav and J.F. Abel, 12/30/87, (PB88-187950, A05, MF-A01). This report is only available through NTIS (see address given above).
- NCEER-87-0028 "Second-Year Program in Research, Education and Technology Transfer," 3/8/88, (PB88-219480, A04, MF-A01).
- NCEER-88-0001 "Workshop on Seismic Computer Analysis and Design of Buildings With Interactive Graphics," by W. McGuire, J.F. Abel and C.H. Conley, 1/18/88, (PB88-187760, A03, MF-A01). This report is only available through NTIS (see address given above).
- NCEER-88-0002 "Optimal Control of Nonlinear Flexible Structures," by J.N. Yang, F.X. Long and D. Wong, 1/22/88, (PB88-213772, A06, MF-A01).
- NCEER-88-0003 "Substructuring Techniques in the Time Domain for Primary-Secondary Structural Systems," by G.D. Manolis and G. Juhn, 2/10/88, (PB88-213780, A04, MF-A01).
- NCEER-88-0004 "Iterative Seismic Analysis of Primary-Secondary Systems," by A. Singhal, L.D. Lutes and P.D. Spanos, 2/23/88, (PB88-213798, A04, MF-A01).

- NCEER-88-0005 "Stochastic Finite Element Expansion for Random Media," by P.D. Spanos and R. Ghanem, 3/14/88, (PB88-213806, A03, MF-A01).
- NCEER-88-0006 "Combining Structural Optimization and Structural Control," by F.Y. Cheng and C.P. Pantelides, 1/10/88, (PB88-213814, A05, MF-A01).
- NCEER-88-0007 "Seismic Performance Assessment of Code-Designed Structures," by H.H-M. Hwang, J-W. Jaw and H-J. Shau, 3/20/88, (PB88-219423, A04, MF-A01). This report is only available through NTIS (see address given above).
- NCEER-88-0008 "Reliability Analysis of Code-Designed Structures Under Natural Hazards," by H.H-M. Hwang, H. Ushiba and M. Shinozuka, 2/29/88, (PB88-229471, A07, MF-A01). This report is only available through NTIS (see address given above).
- NCEER-88-0009 "Seismic Fragility Analysis of Shear Wall Structures," by J-W Jaw and H.H-M. Hwang, 4/30/88, (PB89-102867, A04, MF-A01).
- NCEER-88-0010 "Base Isolation of a Multi-Story Building Under a Harmonic Ground Motion - A Comparison of Performances of Various Systems," by F-G Fan, G. Ahmadi and I.G. Tadjbakhsh, 5/18/88, (PB89-122238, A06, MF-A01). This report is only available through NTIS (see address given above).
- NCEER-88-0011 "Seismic Floor Response Spectra for a Combined System by Green's Functions," by F.M. Lavelle, L.A. Bergman and P.D. Spanos, 5/1/88, (PB89-102875, A03, MF-A01).
- NCEER-88-0012 "A New Solution Technique for Randomly Excited Hysteretic Structures," by G.Q. Cai and Y.K. Lin, 5/16/88, (PB89-102883, A03, MF-A01).
- NCEER-88-0013 "A Study of Radiation Damping and Soil-Structure Interaction Effects in the Centrifuge," by K. Weissman, supervised by J.H. Prevost, 5/24/88, (PB89-144703, A06, MF-A01).
- NCEER-88-0014 "Parameter Identification and Implementation of a Kinematic Plasticity Model for Frictional Soils," by J.H. Prevost and D.V. Griffiths, to be published.
- NCEER-88-0015 "Two- and Three- Dimensional Dynamic Finite Element Analyses of the Long Valley Dam," by D.V. Griffiths and J.H. Prevost, 6/17/88, (PB89-144711, A04, MF-A01).
- NCEER-88-0016 "Damage Assessment of Reinforced Concrete Structures in Eastern United States," by A.M. Reinhorn, M.J. Seidel, S.K. Kunnath and Y.J. Park, 6/15/88, (PB89-122220, A04, MF-A01). This report is only available through NTIS (see address given above).
- NCEER-88-0017 "Dynamic Compliance of Vertically Loaded Strip Foundations in Multilayered Viscoelastic Soils," by S. Ahmad and A.S.M. Israil, 6/17/88, (PB89-102891, A04, MF-A01).
- NCEER-88-0018 "An Experimental Study of Seismic Structural Response With Added Viscoelastic Dampers," by R.C. Lin, Z. Liang, T.T. Soong and R.H. Zhang, 6/30/88, (PB89-122212, A05, MF-A01). This report is available only through NTIS (see address given above).
- NCEER-88-0019 "Experimental Investigation of Primary - Secondary System Interaction," by G.D. Manolis, G. Juhn and A.M. Reinhorn, 5/27/88, (PB89-122204, A04, MF-A01).
- NCEER-88-0020 "A Response Spectrum Approach For Analysis of Nonclassically Damped Structures," by J.N. Yang, S. Sarkani and F.X. Long, 4/22/88, (PB89-102909, A04, MF-A01).
- NCEER-88-0021 "Seismic Interaction of Structures and Soils: Stochastic Approach," by A.S. Veletsos and A.M. Prasad, 7/21/88, (PB89-122196, A04, MF-A01). This report is only available through NTIS (see address given above).
- NCEER-88-0022 "Identification of the Serviceability Limit State and Detection of Seismic Structural Damage," by E. DiPasquale and A.S. Cakmak, 6/15/88, (PB89-122188, A05, MF-A01). This report is available only through NTIS (see address given above).

- NCEER-88-0023 "Multi-Hazard Risk Analysis: Case of a Simple Offshore Structure," by B.K. Bhartia and E.H. Vanmarcke, 7/21/88, (PB89-145213, A05, MF-A01).
- NCEER-88-0024 "Automated Seismic Design of Reinforced Concrete Buildings," by Y.S. Chung, C. Meyer and M. Shinozuka, 7/5/88, (PB89-122170, A06, MF-A01). This report is available only through NTIS (see address given above).
- NCEER-88-0025 "Experimental Study of Active Control of MDOF Structures Under Seismic Excitations," by L.L. Chung, R.C. Lin, T.T. Soong and A.M. Reinhorn, 7/10/88, (PB89-122600, A04, MF-A01).
- NCEER-88-0026 "Earthquake Simulation Tests of a Low-Rise Metal Structure," by J.S. Hwang, K.C. Chang, G.C. Lee and R.L. Ketter, 8/1/88, (PB89-102917, A04, MF-A01).
- NCEER-88-0027 "Systems Study of Urban Response and Reconstruction Due to Catastrophic Earthquakes," by F. Kozin and H.K. Zhou, 9/22/88, (PB90-162348, A04, MF-A01).
- NCEER-88-0028 "Seismic Fragility Analysis of Plane Frame Structures," by H.H-M. Hwang and Y.K. Low, 7/31/88, (PB89-131445, A06, MF-A01).
- NCEER-88-0029 "Response Analysis of Stochastic Structures," by A. Kardara, C. Bucher and M. Shinozuka, 9/22/88, (PB89-174429, A04, MF-A01).
- NCEER-88-0030 "Nonnormal Accelerations Due to Yielding in a Primary Structure," by D.C.K. Chen and L.D. Lutes, 9/19/88, (PB89-131437, A04, MF-A01).
- NCEER-88-0031 "Design Approaches for Soil-Structure Interaction," by A.S. Veletsos, A.M. Prasad and Y. Tang, 12/30/88, (PB89-174437, A03, MF-A01). This report is available only through NTIS (see address given above).
- NCEER-88-0032 "A Re-evaluation of Design Spectra for Seismic Damage Control," by C.J. Turkstra and A.G. Tallin, 11/7/88, (PB89-145221, A05, MF-A01).
- NCEER-88-0033 "The Behavior and Design of Noncontact Lap Splices Subjected to Repeated Inelastic Tensile Loading," by V.E. Sagan, P. Gergely and R.N. White, 12/8/88, (PB89-163737, A08, MF-A01).
- NCEER-88-0034 "Seismic Response of Pile Foundations," by S.M. Mamoon, P.K. Banerjee and S. Ahmad, 11/1/88, (PB89-145239, A04, MF-A01).
- NCEER-88-0035 "Modeling of R/C Building Structures With Flexible Floor Diaphragms (IDARC2)," by A.M. Reinhorn, S.K. Kunnath and N. Panahshahi, 9/7/88, (PB89-207153, A07, MF-A01).
- NCEER-88-0036 "Solution of the Dam-Reservoir Interaction Problem Using a Combination of FEM, BEM with Particular Integrals, Modal Analysis, and Substructuring," by C-S. Tsai, G.C. Lee and R.L. Ketter, 12/31/88, (PB89-207146, A04, MF-A01).
- NCEER-88-0037 "Optimal Placement of Actuators for Structural Control," by F.Y. Cheng and C.P. Pantelides, 8/15/88, (PB89-162846, A05, MF-A01).
- NCEER-88-0038 "Teflon Bearings in Aseismic Base Isolation: Experimental Studies and Mathematical Modeling," by A. Mokha, M.C. Constantinou and A.M. Reinhorn, 12/5/88, (PB89-218457, A10, MF-A01). This report is available only through NTIS (see address given above).
- NCEER-88-0039 "Seismic Behavior of Flat Slab High-Rise Buildings in the New York City Area," by P. Weidlinger and M. Ettouney, 10/15/88, (PB90-145681, A04, MF-A01).
- NCEER-88-0040 "Evaluation of the Earthquake Resistance of Existing Buildings in New York City," by P. Weidlinger and M. Ettouney, 10/15/88, to be published.
- NCEER-88-0041 "Small-Scale Modeling Techniques for Reinforced Concrete Structures Subjected to Seismic Loads," by W. Kim, A. El-Attar and R.N. White, 11/22/88, (PB89-189625, A05, MF-A01).

- NCEER-88-0042 "Modeling Strong Ground Motion from Multiple Event Earthquakes," by G.W. Ellis and A.S. Cakmak, 10/15/88, (PB89-174445, A03, MF-A01).
- NCEER-88-0043 "Nonstationary Models of Seismic Ground Acceleration," by M. Grigoriu, S.E. Ruiz and E. Rosenblueth, 7/15/88, (PB89-189617, A04, MF-A01).
- NCEER-88-0044 "SARCF User's Guide: Seismic Analysis of Reinforced Concrete Frames," by Y.S. Chung, C. Meyer and M. Shinozuka, 11/9/88, (PB89-174452, A08, MF-A01).
- NCEER-88-0045 "First Expert Panel Meeting on Disaster Research and Planning," edited by J. Pantelic and J. Stoyke, 9/15/88, (PB89-174460, A05, MF-A01).
- NCEER-88-0046 "Preliminary Studies of the Effect of Degrading Infill Walls on the Nonlinear Seismic Response of Steel Frames," by C.Z. Chrysostomou, P. Gergely and J.F. Abel, 12/19/88, (PB89-208383, A05, MF-A01).
- NCEER-88-0047 "Reinforced Concrete Frame Component Testing Facility - Design, Construction, Instrumentation and Operation," by S.P. Pessiki, C. Conley, T. Bond, P. Gergely and R.N. White, 12/16/88, (PB89-174478, A04, MF-A01).
- NCEER-89-0001 "Effects of Protective Cushion and Soil Compliancy on the Response of Equipment Within a Seismically Excited Building," by J.A. HoLung, 2/16/89, (PB89-207179, A04, MF-A01).
- NCEER-89-0002 "Statistical Evaluation of Response Modification Factors for Reinforced Concrete Structures," by H.H-M. Hwang and J-W. Jaw, 2/17/89, (PB89-207187, A05, MF-A01).
- NCEER-89-0003 "Hysteretic Columns Under Random Excitation," by G-Q. Cai and Y.K. Lin, 1/9/89, (PB89-196513, A03, MF-A01).
- NCEER-89-0004 "Experimental Study of 'Elephant Foot Bulge' Instability of Thin-Walled Metal Tanks," by Z-H. Jia and R.L. Ketter, 2/22/89, (PB89-207195, A03, MF-A01).
- NCEER-89-0005 "Experiment on Performance of Buried Pipelines Across San Andreas Fault," by J. Isenberg, E. Richardson and T.D. O'Rourke, 3/10/89, (PB89-218440, A04, MF-A01). This report is available only through NTIS (see address given above).
- NCEER-89-0006 "A Knowledge-Based Approach to Structural Design of Earthquake-Resistant Buildings," by M. Subramani, P. Gergely, C.H. Conley, J.F. Abel and A.H. Zaghaw, 1/15/89, (PB89-218465, A06, MF-A01).
- NCEER-89-0007 "Liquefaction Hazards and Their Effects on Buried Pipelines," by T.D. O'Rourke and P.A. Lane, 2/1/89, (PB89-218481, A09, MF-A01).
- NCEER-89-0008 "Fundamentals of System Identification in Structural Dynamics," by H. Imai, C-B. Yun, O. Maruyama and M. Shinozuka, 1/26/89, (PB89-207211, A04, MF-A01).
- NCEER-89-0009 "Effects of the 1985 Michoacan Earthquake on Water Systems and Other Buried Lifelines in Mexico," by A.G. Ayala and M.J. O'Rourke, 3/8/89, (PB89-207229, A06, MF-A01).
- NCEER-89-R010 "NCEER Bibliography of Earthquake Education Materials," by K.E.K. Ross, Second Revision, 9/1/89, (PB90-125352, A05, MF-A01). This report is replaced by NCEER-92-0018.
- NCEER-89-0011 "Inelastic Three-Dimensional Response Analysis of Reinforced Concrete Building Structures (IDARC-3D), Part I - Modeling," by S.K. Kunnath and A.M. Reinhorn, 4/17/89, (PB90-114612, A07, MF-A01). This report is available only through NTIS (see address given above).
- NCEER-89-0012 "Recommended Modifications to ATC-14," by C.D. Poland and J.O. Malley, 4/12/89, (PB90-108648, A15, MF-A01).
- NCEER-89-0013 "Repair and Strengthening of Beam-to-Column Connections Subjected to Earthquake Loading," by M. Corazao and A.J. Durrani, 2/28/89, (PB90-109885, A06, MF-A01).

- NCEER-89-0014 "Program EXKAL2 for Identification of Structural Dynamic Systems," by O. Maruyama, C-B. Yun, M. Hoshiya and M. Shinozuka, 5/19/89, (PB90-109877, A09, MF-A01).
- NCEER-89-0015 "Response of Frames With Bolted Semi-Rigid Connections, Part I - Experimental Study and Analytical Predictions," by P.J. DiCorso, A.M. Reinhorn, J.R. Dickerson, J.B. Radzinski and W.L. Harper, 6/1/89, to be published.
- NCEER-89-0016 "ARMA Monte Carlo Simulation in Probabilistic Structural Analysis," by P.D. Spanos and M.P. Mignolet, 7/10/89, (PB90-109893, A03, MF-A01).
- NCEER-89-P017 "Preliminary Proceedings from the Conference on Disaster Preparedness - The Place of Earthquake Education in Our Schools," Edited by K.E.K. Ross, 6/23/89, (PB90-108606, A03, MF-A01).
- NCEER-89-0017 "Proceedings from the Conference on Disaster Preparedness - The Place of Earthquake Education in Our Schools," Edited by K.E.K. Ross, 12/31/89, (PB90-207895, A012, MF-A02). This report is available only through NTIS (see address given above).
- NCEER-89-0018 "Multidimensional Models of Hysteretic Material Behavior for Vibration Analysis of Shape Memory Energy Absorbing Devices, by E.J. Graesser and F.A. Cozzarelli, 6/7/89, (PB90-164146, A04, MF-A01).
- NCEER-89-0019 "Nonlinear Dynamic Analysis of Three-Dimensional Base Isolated Structures (3D-BASIS)," by S. Nagarajaiah, A.M. Reinhorn and M.C. Constantinou, 8/3/89, (PB90-161936, A06, MF-A01). This report has been replaced by NCEER-93-0011.
- NCEER-89-0020 "Structural Control Considering Time-Rate of Control Forces and Control Rate Constraints," by F.Y. Cheng and C.P. Pantelides, 8/3/89, (PB90-120445, A04, MF-A01).
- NCEER-89-0021 "Subsurface Conditions of Memphis and Shelby County," by K.W. Ng, T-S. Chang and H-H.M. Hwang, 7/26/89, (PB90-120437, A03, MF-A01).
- NCEER-89-0022 "Seismic Wave Propagation Effects on Straight Jointed Buried Pipelines," by K. Elhadi and M.J. O'Rourke, 8/24/89, (PB90-162322, A10, MF-A02).
- NCEER-89-0023 "Workshop on Serviceability Analysis of Water Delivery Systems," edited by M. Grigoriu, 3/6/89, (PB90-127424, A03, MF-A01).
- NCEER-89-0024 "Shaking Table Study of a 1/5 Scale Steel Frame Composed of Tapered Members," by K.C. Chang, J.S. Hwang and G.C. Lee, 9/18/89, (PB90-160169, A04, MF-A01).
- NCEER-89-0025 "DYNA1D: A Computer Program for Nonlinear Seismic Site Response Analysis - Technical Documentation," by Jean H. Prevost, 9/14/89, (PB90-161944, A07, MF-A01). This report is available only through NTIS (see address given above).
- NCEER-89-0026 "1:4 Scale Model Studies of Active Tendon Systems and Active Mass Dampers for Aseismic Protection," by A.M. Reinhorn, T.T. Soong, R.C. Lin, Y.P. Yang, Y. Fukao, H. Abe and M. Nakai, 9/15/89, (PB90-173246, A10, MF-A02). This report is available only through NTIS (see address given above).
- NCEER-89-0027 "Scattering of Waves by Inclusions in a Nonhomogeneous Elastic Half Space Solved by Boundary Element Methods," by P.K. Hadley, A. Askar and A.S. Cakmak, 6/15/89, (PB90-145699, A07, MF-A01).
- NCEER-89-0028 "Statistical Evaluation of Deflection Amplification Factors for Reinforced Concrete Structures," by H.H.M. Hwang, J-W. Jaw and A.L. Ch'ng, 8/31/89, (PB90-164633, A05, MF-A01).
- NCEER-89-0029 "Bedrock Accelerations in Memphis Area Due to Large New Madrid Earthquakes," by H.H.M. Hwang, C.H.S. Chen and G. Yu, 11/7/89, (PB90-162330, A04, MF-A01).
- NCEER-89-0030 "Seismic Behavior and Response Sensitivity of Secondary Structural Systems," by Y.Q. Chen and T.T. Soong, 10/23/89, (PB90-164658, A08, MF-A01).
- NCEER-89-0031 "Random Vibration and Reliability Analysis of Primary-Secondary Structural Systems," by Y. Ibrahim, M. Grigoriu and T.T. Soong, 11/10/89, (PB90-161951, A04, MF-A01).

- NCEER-89-0032 "Proceedings from the Second U.S. - Japan Workshop on Liquefaction, Large Ground Deformation and Their Effects on Lifelines, September 26-29, 1989," Edited by T.D. O'Rourke and M. Hamada, 12/1/89, (PB90-209388, A22, MF-A03).
- NCEER-89-0033 "Deterministic Model for Seismic Damage Evaluation of Reinforced Concrete Structures," by J.M. Bracci, A.M. Reinhorn, J.B. Mander and S.K. Kunnath, 9/27/89, (PB91-108803, A06, MF-A01).
- NCEER-89-0034 "On the Relation Between Local and Global Damage Indices," by E. DiPasquale and A.S. Cakmak, 8/15/89, (PB90-173865, A05, MF-A01).
- NCEER-89-0035 "Cyclic Undrained Behavior of Nonplastic and Low Plasticity Silts," by A.J. Walker and H.E. Stewart, 7/26/89, (PB90-183518, A10, MF-A01).
- NCEER-89-0036 "Liquefaction Potential of Surficial Deposits in the City of Buffalo, New York," by M. Budhu, R. Giese and L. Baumgrass, 1/17/89, (PB90-208455, A04, MF-A01).
- NCEER-89-0037 "A Deterministic Assessment of Effects of Ground Motion Incoherence," by A.S. Veletsos and Y. Tang, 7/15/89, (PB90-164294, A03, MF-A01).
- NCEER-89-0038 "Workshop on Ground Motion Parameters for Seismic Hazard Mapping," July 17-18, 1989, edited by R.V. Whitman, 12/1/89, (PB90-173923, A04, MF-A01).
- NCEER-89-0039 "Seismic Effects on Elevated Transit Lines of the New York City Transit Authority," by C.J. Costantino, C.A. Miller and E. Heymsfield, 12/26/89, (PB90-207887, A06, MF-A01).
- NCEER-89-0040 "Centrifugal Modeling of Dynamic Soil-Structure Interaction," by K. Weissman, Supervised by J.H. Prevost, 5/10/89, (PB90-207879, A07, MF-A01).
- NCEER-89-0041 "Linearized Identification of Buildings With Cores for Seismic Vulnerability Assessment," by I-K. Ho and A.E. Aktan, 11/1/89, (PB90-251943, A07, MF-A01).
- NCEER-90-0001 "Geotechnical and Lifeline Aspects of the October 17, 1989 Loma Prieta Earthquake in San Francisco," by T.D. O'Rourke, H.E. Stewart, F.T. Blackburn and T.S. Dickerman, 1/90, (PB90-208596, A05, MF-A01).
- NCEER-90-0002 "Nonnormal Secondary Response Due to Yielding in a Primary Structure," by D.C.K. Chen and L.D. Lutes, 2/28/90, (PB90-251976, A07, MF-A01).
- NCEER-90-0003 "Earthquake Education Materials for Grades K-12," by K.E.K. Ross, 4/16/90, (PB91-251984, A05, MF-A05). This report has been replaced by NCEER-92-0018.
- NCEER-90-0004 "Catalog of Strong Motion Stations in Eastern North America," by R.W. Busby, 4/3/90, (PB90-251984, A05, MF-A01).
- NCEER-90-0005 "NCEER Strong-Motion Data Base: A User Manual for the GeoBase Release (Version 1.0 for the Sun3)," by P. Friberg and K. Jacob, 3/31/90 (PB90-258062, A04, MF-A01).
- NCEER-90-0006 "Seismic Hazard Along a Crude Oil Pipeline in the Event of an 1811-1812 Type New Madrid Earthquake," by H.H.M. Hwang and C-H.S. Chen, 4/16/90, (PB90-258054, A04, MF-A01).
- NCEER-90-0007 "Site-Specific Response Spectra for Memphis Sheahan Pumping Station," by H.H.M. Hwang and C.S. Lee, 5/15/90, (PB91-108811, A05, MF-A01).
- NCEER-90-0008 "Pilot Study on Seismic Vulnerability of Crude Oil Transmission Systems," by T. Ariman, R. Dobry, M. Grigoriu, F. Kozin, M. O'Rourke, T. O'Rourke and M. Shinozuka, 5/25/90, (PB91-108837, A06, MF-A01).
- NCEER-90-0009 "A Program to Generate Site Dependent Time Histories: EQGEN," by G.W. Ellis, M. Srinivasan and A.S. Cakmak, 1/30/90, (PB91-108829, A04, MF-A01).
- NCEER-90-0010 "Active Isolation for Seismic Protection of Operating Rooms," by M.E. Talbott, Supervised by M. Shinozuka, 6/8/9, (PB91-110205, A05, MF-A01).

- NCEER-90-0011 "Program LINEARID for Identification of Linear Structural Dynamic Systems," by C-B. Yun and M. Shinozuka, 6/25/90, (PB91-110312, A08, MF-A01).
- NCEER-90-0012 "Two-Dimensional Two-Phase Elasto-Plastic Seismic Response of Earth Dams," by A.N. Yiagos, Supervised by J.H. Prevost, 6/20/90, (PB91-110197, A13, MF-A02).
- NCEER-90-0013 "Secondary Systems in Base-Isolated Structures: Experimental Investigation, Stochastic Response and Stochastic Sensitivity," by G.D. Manolis, G. Juhn, M.C. Constantinou and A.M. Reinhorn, 7/1/90, (PB91-110320, A08, MF-A01).
- NCEER-90-0014 "Seismic Behavior of Lightly-Reinforced Concrete Column and Beam-Column Joint Details," by S.P. Pessiki, C.H. Conley, P. Gergely and R.N. White, 8/22/90, (PB91-108795, A11, MF-A02).
- NCEER-90-0015 "Two Hybrid Control Systems for Building Structures Under Strong Earthquakes," by J.N. Yang and A. Danielians, 6/29/90, (PB91-125393, A04, MF-A01).
- NCEER-90-0016 "Instantaneous Optimal Control with Acceleration and Velocity Feedback," by J.N. Yang and Z. Li, 6/29/90, (PB91-125401, A03, MF-A01).
- NCEER-90-0017 "Reconnaissance Report on the Northern Iran Earthquake of June 21, 1990," by M. Mehrain, 10/4/90, (PB91-125377, A03, MF-A01).
- NCEER-90-0018 "Evaluation of Liquefaction Potential in Memphis and Shelby County," by T.S. Chang, P.S. Tang, C.S. Lee and H. Hwang, 8/10/90, (PB91-125427, A09, MF-A01).
- NCEER-90-0019 "Experimental and Analytical Study of a Combined Sliding Disc Bearing and Helical Steel Spring Isolation System," by M.C. Constantinou, A.S. Mokha and A.M. Reinhorn, 10/4/90, (PB91-125385, A06, MF-A01). This report is available only through NTIS (see address given above).
- NCEER-90-0020 "Experimental Study and Analytical Prediction of Earthquake Response of a Sliding Isolation System with a Spherical Surface," by A.S. Mokha, M.C. Constantinou and A.M. Reinhorn, 10/11/90, (PB91-125419, A05, MF-A01).
- NCEER-90-0021 "Dynamic Interaction Factors for Floating Pile Groups," by G. Gazetas, K. Fan, A. Kaynia and E. Kausel, 9/10/90, (PB91-170381, A05, MF-A01).
- NCEER-90-0022 "Evaluation of Seismic Damage Indices for Reinforced Concrete Structures," by S. Rodriguez-Gomez and A.S. Cakmak, 9/30/90, PB91-171322, A06, MF-A01).
- NCEER-90-0023 "Study of Site Response at a Selected Memphis Site," by H. Desai, S. Ahmad, E.S. Gazetas and M.R. Oh, 10/11/90, (PB91-196857, A03, MF-A01).
- NCEER-90-0024 "A User's Guide to Strongmo: Version 1.0 of NCEER's Strong-Motion Data Access Tool for PCs and Terminals," by P.A. Friberg and C.A.T. Susch, 11/15/90, (PB91-171272, A03, MF-A01).
- NCEER-90-0025 "A Three-Dimensional Analytical Study of Spatial Variability of Seismic Ground Motions," by L-L. Hong and A.H.-S. Ang, 10/30/90, (PB91-170399, A09, MF-A01).
- NCEER-90-0026 "MUMOID User's Guide - A Program for the Identification of Modal Parameters," by S. Rodriguez-Gomez and E. DiPasquale, 9/30/90, (PB91-171298, A04, MF-A01).
- NCEER-90-0027 "SARCF-II User's Guide - Seismic Analysis of Reinforced Concrete Frames," by S. Rodriguez-Gomez, Y.S. Chung and C. Meyer, 9/30/90, (PB91-171280, A05, MF-A01).
- NCEER-90-0028 "Viscous Dampers: Testing, Modeling and Application in Vibration and Seismic Isolation," by N. Makris and M.C. Constantinou, 12/20/90 (PB91-190561, A06, MF-A01).
- NCEER-90-0029 "Soil Effects on Earthquake Ground Motions in the Memphis Area," by H. Hwang, C.S. Lee, K.W. Ng and T.S. Chang, 8/2/90, (PB91-190751, A05, MF-A01).

- NCEER-91-0001 "Proceedings from the Third Japan-U.S. Workshop on Earthquake Resistant Design of Lifeline Facilities and Countermeasures for Soil Liquefaction, December 17-19, 1990," edited by T.D. O'Rourke and M. Hamada, 2/1/91, (PB91-179259, A99, MF-A04).
- NCEER-91-0002 "Physical Space Solutions of Non-Proportionally Damped Systems," by M. Tong, Z. Liang and G.C. Lee, 1/15/91, (PB91-179242, A04, MF-A01).
- NCEER-91-0003 "Seismic Response of Single Piles and Pile Groups," by K. Fan and G. Gazetas, 1/10/91, (PB92-174994, A04, MF-A01).
- NCEER-91-0004 "Damping of Structures: Part 1 - Theory of Complex Damping," by Z. Liang and G. Lee, 10/10/91, (PB92-197235, A12, MF-A03).
- NCEER-91-0005 "3D-BASIS - Nonlinear Dynamic Analysis of Three Dimensional Base Isolated Structures: Part II," by S. Nagarajaiah, A.M. Reinhorn and M.C. Constantinou, 2/28/91, (PB91-190553, A07, MF-A01). This report has been replaced by NCEER-93-0011.
- NCEER-91-0006 "A Multidimensional Hysteretic Model for Plasticity Deforming Metals in Energy Absorbing Devices," by E.J. Graesser and F.A. Cozzarelli, 4/9/91, (PB92-108364, A04, MF-A01).
- NCEER-91-0007 "A Framework for Customizable Knowledge-Based Expert Systems with an Application to a KBES for Evaluating the Seismic Resistance of Existing Buildings," by E.G. Ibarra-Anaya and S.J. Fenves, 4/9/91, (PB91-210930, A08, MF-A01).
- NCEER-91-0008 "Nonlinear Analysis of Steel Frames with Semi-Rigid Connections Using the Capacity Spectrum Method," by G.G. Deierlein, S-H. Hsieh, Y-J. Shen and J.F. Abel, 7/2/91, (PB92-113828, A05, MF-A01).
- NCEER-91-0009 "Earthquake Education Materials for Grades K-12," by K.E.K. Ross, 4/30/91, (PB91-212142, A06, MF-A01). This report has been replaced by NCEER-92-0018.
- NCEER-91-0010 "Phase Wave Velocities and Displacement Phase Differences in a Harmonically Oscillating Pile," by N. Makris and G. Gazetas, 7/8/91, (PB92-108356, A04, MF-A01).
- NCEER-91-0011 "Dynamic Characteristics of a Full-Size Five-Story Steel Structure and a 2/5 Scale Model," by K.C. Chang, G.C. Yao, G.C. Lee, D.S. Hao and Y.C. Yeh, 7/2/91, (PB93-116648, A06, MF-A02).
- NCEER-91-0012 "Seismic Response of a 2/5 Scale Steel Structure with Added Viscoelastic Dampers," by K.C. Chang, T.T. Soong, S-T. Oh and M.L. Lai, 5/17/91, (PB92-110816, A05, MF-A01).
- NCEER-91-0013 "Earthquake Response of Retaining Walls; Full-Scale Testing and Computational Modeling," by S. Alampalli and A-W.M. Elgamal, 6/20/91, to be published.
- NCEER-91-0014 "3D-BASIS-M: Nonlinear Dynamic Analysis of Multiple Building Base Isolated Structures," by P.C. Tsopelas, S. Nagarajaiah, M.C. Constantinou and A.M. Reinhorn, 5/28/91, (PB92-113885, A09, MF-A02).
- NCEER-91-0015 "Evaluation of SEAOC Design Requirements for Sliding Isolated Structures," by D. Theodossiou and M.C. Constantinou, 6/10/91, (PB92-114602, A11, MF-A03).
- NCEER-91-0016 "Closed-Loop Modal Testing of a 27-Story Reinforced Concrete Flat Plate-Core Building," by H.R. Somaprasad, T. Toksoy, H. Yoshiyuki and A.E. Aktan, 7/15/91, (PB92-129980, A07, MF-A02).
- NCEER-91-0017 "Shake Table Test of a 1/6 Scale Two-Story Lightly Reinforced Concrete Building," by A.G. El-Attar, R.N. White and P. Gergely, 2/28/91, (PB92-222447, A06, MF-A02).
- NCEER-91-0018 "Shake Table Test of a 1/8 Scale Three-Story Lightly Reinforced Concrete Building," by A.G. El-Attar, R.N. White and P. Gergely, 2/28/91, (PB93-116630, A08, MF-A02).
- NCEER-91-0019 "Transfer Functions for Rigid Rectangular Foundations," by A.S. Veletsos, A.M. Prasad and W.H. Wu, 7/31/91, to be published.

- NCEER-91-0020 "Hybrid Control of Seismic-Excited Nonlinear and Inelastic Structural Systems," by J.N. Yang, Z. Li and A. Daniellians, 8/1/91, (PB92-143171, A06, MF-A02).
- NCEER-91-0021 "The NCEER-91 Earthquake Catalog: Improved Intensity-Based Magnitudes and Recurrence Relations for U.S. Earthquakes East of New Madrid," by L. Seeber and J.G. Armbruster, 8/28/91, (PB92-176742, A06, MF-A02).
- NCEER-91-0022 "Proceedings from the Implementation of Earthquake Planning and Education in Schools: The Need for Change - The Roles of the Changemakers," by K.E.K. Ross and F. Winslow, 7/23/91, (PB92-129998, A12, MF-A03).
- NCEER-91-0023 "A Study of Reliability-Based Criteria for Seismic Design of Reinforced Concrete Frame Buildings," by H.H.M. Hwang and H-M. Hsu, 8/10/91, (PB92-140235, A09, MF-A02).
- NCEER-91-0024 "Experimental Verification of a Number of Structural System Identification Algorithms," by R.G. Ghanem, H. Gavin and M. Shinozuka, 9/18/91, (PB92-176577, A18, MF-A04).
- NCEER-91-0025 "Probabilistic Evaluation of Liquefaction Potential," by H.H.M. Hwang and C.S. Lee," 11/25/91, (PB92-143429, A05, MF-A01).
- NCEER-91-0026 "Instantaneous Optimal Control for Linear, Nonlinear and Hysteretic Structures - Stable Controllers," by J.N. Yang and Z. Li, 11/15/91, (PB92-163807, A04, MF-A01).
- NCEER-91-0027 "Experimental and Theoretical Study of a Sliding Isolation System for Bridges," by M.C. Constantinou, A. Kartoum, A.M. Reinhorn and P. Bradford, 11/15/91, (PB92-176973, A10, MF-A03).
- NCEER-92-0001 "Case Studies of Liquefaction and Lifeline Performance During Past Earthquakes, Volume 1: Japanese Case Studies," Edited by M. Hamada and T. O'Rourke, 2/17/92, (PB92-197243, A18, MF-A04).
- NCEER-92-0002 "Case Studies of Liquefaction and Lifeline Performance During Past Earthquakes, Volume 2: United States Case Studies," Edited by T. O'Rourke and M. Hamada, 2/17/92, (PB92-197250, A20, MF-A04).
- NCEER-92-0003 "Issues in Earthquake Education," Edited by K. Ross, 2/3/92, (PB92-222389, A07, MF-A02).
- NCEER-92-0004 "Proceedings from the First U.S. - Japan Workshop on Earthquake Protective Systems for Bridges," Edited by I.G. Buckle, 2/4/92, (PB94-142239, A99, MF-A06).
- NCEER-92-0005 "Seismic Ground Motion from a Haskell-Type Source in a Multiple-Layered Half-Space," A.P. Theoharis, G. Deodatis and M. Shinozuka, 1/2/92, to be published.
- NCEER-92-0006 "Proceedings from the Site Effects Workshop," Edited by R. Whitman, 2/29/92, (PB92-197201, A04, MF-A01).
- NCEER-92-0007 "Engineering Evaluation of Permanent Ground Deformations Due to Seismically-Induced Liquefaction," by M.H. Baziar, R. Dobry and A-W.M. Elgarnal, 3/24/92, (PB92-222421, A13, MF-A03).
- NCEER-92-0008 "A Procedure for the Seismic Evaluation of Buildings in the Central and Eastern United States," by C.D. Poland and J.O. Malley, 4/2/92, (PB92-222439, A20, MF-A04).
- NCEER-92-0009 "Experimental and Analytical Study of a Hybrid Isolation System Using Friction Controllable Sliding Bearings," by M.Q. Feng, S. Fujii and M. Shinozuka, 5/15/92, (PB93-150282, A06, MF-A02).
- NCEER-92-0010 "Seismic Resistance of Slab-Column Connections in Existing Non-Ductile Flat-Plate Buildings," by A.J. Durrani and Y. Du, 5/18/92, (PB93-116812, A06, MF-A02).
- NCEER-92-0011 "The Hysteretic and Dynamic Behavior of Brick Masonry Walls Upgraded by Ferrocement Coatings Under Cyclic Loading and Strong Simulated Ground Motion," by H. Lee and S.P. Prawl, 5/11/92, to be published.
- NCEER-92-0012 "Study of Wire Rope Systems for Seismic Protection of Equipment in Buildings," by G.F. Demetriades, M.C. Constantinou and A.M. Reinhorn, 5/20/92, (PB93-116655, A08, MF-A02).

- NCEER-92-0013 "Shape Memory Structural Dampers: Material Properties, Design and Seismic Testing," by P.R. Witting and F.A. Cozzarelli, 5/26/92, (PB93-116663, A05, MF-A01).
- NCEER-92-0014 "Longitudinal Permanent Ground Deformation Effects on Buried Continuous Pipelines," by M.J. O'Rourke, and C. Nordberg, 6/15/92, (PB93-116671, A08, MF-A02).
- NCEER-92-0015 "A Simulation Method for Stationary Gaussian Random Functions Based on the Sampling Theorem," by M. Grigoriu and S. Balopoulou, 6/11/92, (PB93-127496, A05, MF-A01).
- NCEER-92-0016 "Gravity-Load-Designed Reinforced Concrete Buildings: Seismic Evaluation of Existing Construction and Detailing Strategies for Improved Seismic Resistance," by G.W. Hoffmann, S.K. Kunnath, A.M. Reinhorn and J.B. Mander, 7/15/92, (PB94-142007, A08, MF-A02).
- NCEER-92-0017 "Observations on Water System and Pipeline Performance in the Limón Area of Costa Rica Due to the April 22, 1991 Earthquake," by M. O'Rourke and D. Ballantyne, 6/30/92, (PB93-126811, A06, MF-A02).
- NCEER-92-0018 "Fourth Edition of Earthquake Education Materials for Grades K-12," Edited by K.E.K. Ross, 8/10/92, (PB93-114023, A07, MF-A02).
- NCEER-92-0019 "Proceedings from the Fourth Japan-U.S. Workshop on Earthquake Resistant Design of Lifeline Facilities and Countermeasures for Soil Liquefaction," Edited by M. Hamada and T.D. O'Rourke, 8/12/92, (PB93-163939, A99, MF-E11).
- NCEER-92-0020 "Active Bracing System: A Full Scale Implementation of Active Control," by A.M. Reinhorn, T.T. Soong, R.C. Lin, M.A. Riley, Y.P. Wang, S. Aizawa and M. Higashino, 8/14/92, (PB93-127512, A06, MF-A02).
- NCEER-92-0021 "Empirical Analysis of Horizontal Ground Displacement Generated by Liquefaction-Induced Lateral Spreads," by S.F. Bartlett and T.L. Youd, 8/17/92, (PB93-188241, A06, MF-A02).
- NCEER-92-0022 "IDARC Version 3.0: Inelastic Damage Analysis of Reinforced Concrete Structures," by S.K. Kunnath, A.M. Reinhorn and R.F. Lobo, 8/31/92, (PB93-227502, A07, MF-A02).
- NCEER-92-0023 "A Semi-Empirical Analysis of Strong-Motion Peaks in Terms of Seismic Source, Propagation Path and Local Site Conditions, by M. Kamiyama, M.J. O'Rourke and R. Flores-Berrones, 9/9/92, (PB93-150266, A08, MF-A02).
- NCEER-92-0024 "Seismic Behavior of Reinforced Concrete Frame Structures with Nonductile Details, Part I: Summary of Experimental Findings of Full Scale Beam-Column Joint Tests," by A. Beres, R.N. White and P. Gergely, 9/30/92, (PB93-227783, A05, MF-A01).
- NCEER-92-0025 "Experimental Results of Repaired and Retrofitted Beam-Column Joint Tests in Lightly Reinforced Concrete Frame Buildings," by A. Beres, S. El-Borgi, R.N. White and P. Gergely, 10/29/92, (PB93-227791, A05, MF-A01).
- NCEER-92-0026 "A Generalization of Optimal Control Theory: Linear and Nonlinear Structures," by J.N. Yang, Z. Li and S. Vongchavalitkul, 11/2/92, (PB93-188621, A05, MF-A01).
- NCEER-92-0027 "Seismic Resistance of Reinforced Concrete Frame Structures Designed Only for Gravity Loads: Part I - Design and Properties of a One-Third Scale Model Structure," by J.M. Bracci, A.M. Reinhorn and J.B. Mander, 12/1/92, (PB94-104502, A08, MF-A02).
- NCEER-92-0028 "Seismic Resistance of Reinforced Concrete Frame Structures Designed Only for Gravity Loads: Part II - Experimental Performance of Subassemblages," by L.E. Aycaardi, J.B. Mander and A.M. Reinhorn, 12/1/92, (PB94-104510, A08, MF-A02).
- NCEER-92-0029 "Seismic Resistance of Reinforced Concrete Frame Structures Designed Only for Gravity Loads: Part III - Experimental Performance and Analytical Study of a Structural Model," by J.M. Bracci, A.M. Reinhorn and J.B. Mander, 12/1/92, (PB93-227528, A09, MF-A01).

- NCEER-92-0030 "Evaluation of Seismic Retrofit of Reinforced Concrete Frame Structures: Part I - Experimental Performance of Retrofitted Subassemblages," by D. Choudhuri, J.B. Mander and A.M. Reinhorn, 12/8/92, (PB93-198307, A07, MF-A02).
- NCEER-92-0031 "Evaluation of Seismic Retrofit of Reinforced Concrete Frame Structures: Part II - Experimental Performance and Analytical Study of a Retrofitted Structural Model," by J.M. Bracci, A.M. Reinhorn and J.B. Mander, 12/8/92, (PB93-198315, A09, MF-A03).
- NCEER-92-0032 "Experimental and Analytical Investigation of Seismic Response of Structures with Supplemental Fluid Viscous Dampers," by M.C. Constantinou and M.D. Symans, 12/21/92, (PB93-191435, A10, MF-A03). This report is available only through NTIS (see address given above).
- NCEER-92-0033 "Reconnaissance Report on the Cairo, Egypt Earthquake of October 12, 1992," by M. Khater, 12/23/92, (PB93-188621, A03, MF-A01).
- NCEER-92-0034 "Low-Level Dynamic Characteristics of Four Tall Flat-Plate Buildings in New York City," by H. Gavin, S. Yuan, J. Grossman, E. Pekelis and K. Jacob, 12/28/92, (PB93-188217, A07, MF-A02).
- NCEER-93-0001 "An Experimental Study on the Seismic Performance of Brick-Infilled Steel Frames With and Without Retrofit," by J.B. Mander, B. Nair, K. Wojtkowski and J. Ma, 1/29/93, (PB93-227510, A07, MF-A02).
- NCEER-93-0002 "Social Accounting for Disaster Preparedness and Recovery Planning," by S. Cole, E. Pantoja and V. Razak, 2/22/93, (PB94-142114, A12, MF-A03).
- NCEER-93-0003 "Assessment of 1991 NEHRP Provisions for Nonstructural Components and Recommended Revisions," by T.T. Soong, G. Chen, Z. Wu, R-H. Zhang and M. Grigoriu, 3/1/93, (PB93-188639, A06, MF-A02).
- NCEER-93-0004 "Evaluation of Static and Response Spectrum Analysis Procedures of SEAOC/UBC for Seismic Isolated Structures," by C.W. Winters and M.C. Constantinou, 3/23/93, (PB93-198299, A10, MF-A03).
- NCEER-93-0005 "Earthquakes in the Northeast - Are We Ignoring the Hazard? A Workshop on Earthquake Science and Safety for Educators," edited by K.E.K. Ross, 4/2/93, (PB94-103066, A09, MF-A02).
- NCEER-93-0006 "Inelastic Response of Reinforced Concrete Structures with Viscoelastic Braces," by R.F. Lobo, J.M. Bracci, K.L. Shen, A.M. Reinhorn and T.T. Soong, 4/5/93, (PB93-227486, A05, MF-A02).
- NCEER-93-0007 "Seismic Testing of Installation Methods for Computers and Data Processing Equipment," by K. Kosar, T.T. Soong, K.L. Shen, J.A. HoLung and Y.K. Lin, 4/12/93, (PB93-198299, A07, MF-A02).
- NCEER-93-0008 "Retrofit of Reinforced Concrete Frames Using Added Dampers," by A. Reinhorn, M. Constantinou and C. Li, to be published.
- NCEER-93-0009 "Seismic Behavior and Design Guidelines for Steel Frame Structures with Added Viscoelastic Dampers," by K.C. Chang, M.L. Lai, T.T. Soong, D.S. Hao and Y.C. Yeh, 5/1/93, (PB94-141959, A07, MF-A02).
- NCEER-93-0010 "Seismic Performance of Shear-Critical Reinforced Concrete Bridge Piers," by J.B. Mander, S.M. Waheed, M.T.A. Chaudhary and S.S. Chen, 5/12/93, (PB93-227494, A08, MF-A02).
- NCEER-93-0011 "3D-BASIS-TABS: Computer Program for Nonlinear Dynamic Analysis of Three Dimensional Base Isolated Structures," by S. Nagarajaiah, C. Li, A.M. Reinhorn and M.C. Constantinou, 8/2/93, (PB94-141819, A09, MF-A02).
- NCEER-93-0012 "Effects of Hydrocarbon Spills from an Oil Pipeline Break on Ground Water," by O.J. Helweg and H.H.M. Hwang, 8/3/93, (PB94-141942, A06, MF-A02).
- NCEER-93-0013 "Simplified Procedures for Seismic Design of Nonstructural Components and Assessment of Current Code Provisions," by M.P. Singh, L.E. Suarez, E.E. Matheu and G.O. Maldonado, 8/4/93, (PB94-141827, A09, MF-A02).
- NCEER-93-0014 "An Energy Approach to Seismic Analysis and Design of Secondary Systems," by G. Chen and T.T. Soong, 8/6/93, (PB94-142767, A11, MF-A03).

- NCEER-93-0015 "Proceedings from School Sites: Becoming Prepared for Earthquakes - Commemorating the Third Anniversary of the Loma Prieta Earthquake," Edited by F.E. Winslow and K.E.K. Ross, 8/16/93, (PB94-154275, A16, MF-A02).
- NCEER-93-0016 "Reconnaissance Report of Damage to Historic Monuments in Cairo, Egypt Following the October 12, 1992 Dahshur Earthquake," by D. Sykora, D. Look, G. Croci, E. Karaesmen and E. Karaesmen, 8/19/93, (PB94-142221, A08, MF-A02).
- NCEER-93-0017 "The Island of Guam Earthquake of August 8, 1993," by S.W. Swan and S.K. Harris, 9/30/93, (PB94-141843, A04, MF-A01).
- NCEER-93-0018 "Engineering Aspects of the October 12, 1992 Egyptian Earthquake," by A.W. Elgamal, M. Amer, K. Adalier and A. Abul-Fadl, 10/7/93, (PB94-141983, A05, MF-A01).
- NCEER-93-0019 "Development of an Earthquake Motion Simulator and its Application in Dynamic Centrifuge Testing," by I. Krstelj, Supervised by J.H. Prevost, 10/23/93, (PB94-181773, A-10, MF-A03).
- NCEER-93-0020 "NCEER-Taisei Corporation Research Program on Sliding Seismic Isolation Systems for Bridges: Experimental and Analytical Study of a Friction Pendulum System (FPS)," by M.C. Constantinou, P. Tsopelas, Y-S. Kim and S. Okamoto, 11/1/93, (PB94-142775, A08, MF-A02).
- NCEER-93-0021 "Finite Element Modeling of Elastomeric Seismic Isolation Bearings," by L.J. Billings, Supervised by R. Shepherd, 11/8/93, to be published.
- NCEER-93-0022 "Seismic Vulnerability of Equipment in Critical Facilities: Life-Safety and Operational Consequences," by K. Porter, G.S. Johnson, M.M. Zadeh, C. Scawthorn and S. Eder, 11/24/93, (PB94-181765, A16, MF-A03).
- NCEER-93-0023 "Hokkaido Nansei-oki, Japan Earthquake of July 12, 1993, by P.I. Yanev and C.R. Scawthorn, 12/23/93, (PB94-181500, A07, MF-A01).
- NCEER-94-0001 "An Evaluation of Seismic Serviceability of Water Supply Networks with Application to the San Francisco Auxiliary Water Supply System," by I. Markov, Supervised by M. Grigoriu and T. O'Rourke, 1/21/94, (PB94-204013, A07, MF-A02).
- NCEER-94-0002 "NCEER-Taisei Corporation Research Program on Sliding Seismic Isolation Systems for Bridges: Experimental and Analytical Study of Systems Consisting of Sliding Bearings, Rubber Restoring Force Devices and Fluid Dampers," Volumes I and II, by P. Tsopelas, S. Okamoto, M.C. Constantinou, D. Ozaki and S. Fujii, 2/4/94, (PB94-181740, A09, MF-A02 and PB94-181757, A12, MF-A03).
- NCEER-94-0003 "A Markov Model for Local and Global Damage Indices in Seismic Analysis," by S. Rahman and M. Grigoriu, 2/18/94, (PB94-206000, A12, MF-A03).
- NCEER-94-0004 "Proceedings from the NCEER Workshop on Seismic Response of Masonry Infills," edited by D.P. Abrams, 3/1/94, (PB94-180783, A07, MF-A02).
- NCEER-94-0005 "The Northridge, California Earthquake of January 17, 1994: General Reconnaissance Report," edited by J.D. Goltz, 3/11/94, (PB94-193943, A10, MF-A03).
- NCEER-94-0006 "Seismic Energy Based Fatigue Damage Analysis of Bridge Columns: Part I - Evaluation of Seismic Capacity," by G.A. Chang and J.B. Mander, 3/14/94, (PB94-219185, A11, MF-A03).
- NCEER-94-0007 "Seismic Isolation of Multi-Story Frame Structures Using Spherical Sliding Isolation Systems," by T.M. Al-Hussaini, V.A. Zayas and M.C. Constantinou, 3/17/94, (PB94-193745, A09, MF-A02).
- NCEER-94-0008 "The Northridge, California Earthquake of January 17, 1994: Performance of Highway Bridges," edited by I.G. Buckle, 3/24/94, (PB94-193851, A06, MF-A02).
- NCEER-94-0009 "Proceedings of the Third U.S.-Japan Workshop on Earthquake Protective Systems for Bridges," edited by I.G. Buckle and I. Friedland, 3/31/94, (PB94-195815, A99, MF-A06).

- NCEER-94-0010 "3D-BASIS-ME: Computer Program for Nonlinear Dynamic Analysis of Seismically Isolated Single and Multiple Structures and Liquid Storage Tanks," by P.C. Tsopelas, M.C. Constantinou and A.M. Reinhorn, 4/12/94, (PB94-204922, A09, MF-A02).
- NCEER-94-0011 "The Northridge, California Earthquake of January 17, 1994: Performance of Gas Transmission Pipelines," by T.D. O'Rourke and M.C. Palmer, 5/16/94, (PB94-204989, A05, MF-A01).
- NCEER-94-0012 "Feasibility Study of Replacement Procedures and Earthquake Performance Related to Gas Transmission Pipelines," by T.D. O'Rourke and M.C. Palmer, 5/25/94, (PB94-206638, A09, MF-A02).
- NCEER-94-0013 "Seismic Energy Based Fatigue Damage Analysis of Bridge Columns: Part II - Evaluation of Seismic Demand," by G.A. Chang and J.B. Mander, 6/1/94, (PB95-18106, A08, MF-A02).
- NCEER-94-0014 "NCEER-Taisei Corporation Research Program on Sliding Seismic Isolation Systems for Bridges: Experimental and Analytical Study of a System Consisting of Sliding Bearings and Fluid Restoring Force/Damping Devices," by P. Tsopelas and M.C. Constantinou, 6/13/94, (PB94-219144, A10, MF-A03).
- NCEER-94-0015 "Generation of Hazard-Consistent Fragility Curves for Seismic Loss Estimation Studies," by H. Hwang and J-R. Huo, 6/14/94, (PB95-181996, A09, MF-A02).
- NCEER-94-0016 "Seismic Study of Building Frames with Added Energy-Absorbing Devices," by W.S. Pong, C.S. Tsai and G.C. Lee, 6/20/94, (PB94-219136, A10, A03).
- NCEER-94-0017 "Sliding Mode Control for Seismic-Excited Linear and Nonlinear Civil Engineering Structures," by J. Yang, J. Wu, A. Agrawal and Z. Li, 6/21/94, (PB95-138483, A06, MF-A02).
- NCEER-94-0018 "3D-BASIS-TABS Version 2.0: Computer Program for Nonlinear Dynamic Analysis of Three Dimensional Base Isolated Structures," by A.M. Reinhorn, S. Nagarajaiah, M.C. Constantinou, P. Tsopelas and R. Li, 6/22/94, (PB95-182176, A08, MF-A02).
- NCEER-94-0019 "Proceedings of the International Workshop on Civil Infrastructure Systems: Application of Intelligent Systems and Advanced Materials on Bridge Systems," Edited by G.C. Lee and K.C. Chang, 7/18/94, (PB95-252474, A20, MF-A04).
- NCEER-94-0020 "Study of Seismic Isolation Systems for Computer Floors," by V. Lambrou and M.C. Constantinou, 7/19/94, (PB95-138533, A10, MF-A03).
- NCEER-94-0021 "Proceedings of the U.S.-Italian Workshop on Guidelines for Seismic Evaluation and Rehabilitation of Unreinforced Masonry Buildings," Edited by D.P. Abrams and G.M. Calvi, 7/20/94, (PB95-138749, A13, MF-A03).
- NCEER-94-0022 "NCEER-Taisei Corporation Research Program on Sliding Seismic Isolation Systems for Bridges: Experimental and Analytical Study of a System Consisting of Lubricated PTFE Sliding Bearings and Mild Steel Dampers," by P. Tsopelas and M.C. Constantinou, 7/22/94, (PB95-182184, A08, MF-A02).
- NCEER-94-0023 "Development of Reliability-Based Design Criteria for Buildings Under Seismic Load," by Y.K. Wen, H. Hwang and M. Shinozuka, 8/1/94, (PB95-211934, A08, MF-A02).
- NCEER-94-0024 "Experimental Verification of Acceleration Feedback Control Strategies for an Active Tendon System," by S.J. Dyke, B.F. Spencer, Jr., P. Quast, M.K. Sain, D.C. Kaspari, Jr. and T.T. Soong, 8/29/94, (PB95-212320, A05, MF-A01).
- NCEER-94-0025 "Seismic Retrofitting Manual for Highway Bridges," Edited by I.G. Buckle and I.F. Friedland, published by the Federal Highway Administration (PB95-212676, A15, MF-A03).
- NCEER-94-0026 "Proceedings from the Fifth U.S.-Japan Workshop on Earthquake Resistant Design of Lifeline Facilities and Countermeasures Against Soil Liquefaction," Edited by T.D. O'Rourke and M. Hamada, 11/7/94, (PB95-220802, A99, MF-E08).

- NCEER-95-0001 “Experimental and Analytical Investigation of Seismic Retrofit of Structures with Supplemental Damping: Part I - Fluid Viscous Damping Devices,” by A.M. Reinhorn, C. Li and M.C. Constantinou, 1/3/95, (PB95-266599, A09, MF-A02).
- NCEER-95-0002 “Experimental and Analytical Study of Low-Cycle Fatigue Behavior of Semi-Rigid Top-And-Seat Angle Connections,” by G. Pekcan, J.B. Mander and S.S. Chen, 1/5/95, (PB95-220042, A07, MF-A02).
- NCEER-95-0003 “NCEER-ATC Joint Study on Fragility of Buildings,” by T. Anagnos, C. Rojahn and A.S. Kiremidjian, 1/20/95, (PB95-220026, A06, MF-A02).
- NCEER-95-0004 “Nonlinear Control Algorithms for Peak Response Reduction,” by Z. Wu, T.T. Soong, V. Gattulli and R.C. Lin, 2/16/95, (PB95-220349, A05, MF-A01).
- NCEER-95-0005 “Pipeline Replacement Feasibility Study: A Methodology for Minimizing Seismic and Corrosion Risks to Underground Natural Gas Pipelines,” by R.T. Eguchi, H.A. Seligson and D.G. Honegger, 3/2/95, (PB95-252326, A06, MF-A02).
- NCEER-95-0006 “Evaluation of Seismic Performance of an 11-Story Frame Building During the 1994 Northridge Earthquake,” by F. Naeim, R. DiSulio, K. Benuska, A. Reinhorn and C. Li, to be published.
- NCEER-95-0007 “Prioritization of Bridges for Seismic Retrofitting,” by N. Basöz and A.S. Kiremidjian, 4/24/95, (PB95-252300, A08, MF-A02).
- NCEER-95-0008 “Method for Developing Motion Damage Relationships for Reinforced Concrete Frames,” by A. Singhal and A.S. Kiremidjian, 5/11/95, (PB95-266607, A06, MF-A02).
- NCEER-95-0009 “Experimental and Analytical Investigation of Seismic Retrofit of Structures with Supplemental Damping: Part II - Friction Devices,” by C. Li and A.M. Reinhorn, 7/6/95, (PB96-128087, A11, MF-A03).
- NCEER-95-0010 “Experimental Performance and Analytical Study of a Non-Ductile Reinforced Concrete Frame Structure Retrofitted with Elastomeric Spring Dampers,” by G. Pekcan, J.B. Mander and S.S. Chen, 7/14/95, (PB96-137161, A08, MF-A02).
- NCEER-95-0011 “Development and Experimental Study of Semi-Active Fluid Damping Devices for Seismic Protection of Structures,” by M.D. Symans and M.C. Constantinou, 8/3/95, (PB96-136940, A23, MF-A04).
- NCEER-95-0012 “Real-Time Structural Parameter Modification (RSPM): Development of Innervated Structures,” by Z. Liang, M. Tong and G.C. Lee, 4/11/95, (PB96-137153, A06, MF-A01).
- NCEER-95-0013 “Experimental and Analytical Investigation of Seismic Retrofit of Structures with Supplemental Damping: Part III - Viscous Damping Walls,” by A.M. Reinhorn and C. Li, 10/1/95, (PB96-176409, A11, MF-A03).
- NCEER-95-0014 “Seismic Fragility Analysis of Equipment and Structures in a Memphis Electric Substation,” by J-R. Huo and H.H.M. Hwang, 8/10/95, (PB96-128087, A09, MF-A02).
- NCEER-95-0015 “The Hanshin-Awaji Earthquake of January 17, 1995: Performance of Lifelines,” Edited by M. Shinozuka, 11/3/95, (PB96-176383, A15, MF-A03).
- NCEER-95-0016 “Highway Culvert Performance During Earthquakes,” by T.L. Youd and C.J. Beckman, available as NCEER-96-0015.
- NCEER-95-0017 “The Hanshin-Awaji Earthquake of January 17, 1995: Performance of Highway Bridges,” Edited by I.G. Buckle, 12/1/95, to be published.
- NCEER-95-0018 “Modeling of Masonry Infill Panels for Structural Analysis,” by A.M. Reinhorn, A. Madan, R.E. Valles, Y. Reichmann and J.B. Mander, 12/8/95, (PB97-110886, MF-A01, A06).
- NCEER-95-0019 “Optimal Polynomial Control for Linear and Nonlinear Structures,” by A.K. Agrawal and J.N. Yang, 12/11/95, (PB96-168737, A07, MF-A02).

- NCEER-95-0020 "Retrofit of Non-Ductile Reinforced Concrete Frames Using Friction Dampers," by R.S. Rao, P. Gergely and R.N. White, 12/22/95, (PB97-133508, A10, MF-A02).
- NCEER-95-0021 "Parametric Results for Seismic Response of Pile-Supported Bridge Bents," by G. Mylonakis, A. Nikolaou and G. Gazetas, 12/22/95, (PB97-100242, A12, MF-A03).
- NCEER-95-0022 "Kinematic Bending Moments in Seismically Stressed Piles," by A. Nikolaou, G. Mylonakis and G. Gazetas, 12/23/95, (PB97-113914, MF-A03, A13).
- NCEER-96-0001 "Dynamic Response of Unreinforced Masonry Buildings with Flexible Diaphragms," by A.C. Costley and D.P. Abrams, 10/10/96, (PB97-133573, MF-A03, A15).
- NCEER-96-0002 "State of the Art Review: Foundations and Retaining Structures," by I. Po Lam, to be published.
- NCEER-96-0003 "Ductility of Rectangular Reinforced Concrete Bridge Columns with Moderate Confinement," by N. Wehbe, M. Saiidi, D. Sanders and B. Douglas, 11/7/96, (PB97-133557, A06, MF-A02).
- NCEER-96-0004 "Proceedings of the Long-Span Bridge Seismic Research Workshop," edited by I.G. Buckle and I.M. Friedland, to be published.
- NCEER-96-0005 "Establish Representative Pier Types for Comprehensive Study: Eastern United States," by J. Kulicki and Z. Prucz, 5/28/96, (PB98-119217, A07, MF-A02).
- NCEER-96-0006 "Establish Representative Pier Types for Comprehensive Study: Western United States," by R. Imbsen, R.A. Schamber and T.A. Osterkamp, 5/28/96, (PB98-118607, A07, MF-A02).
- NCEER-96-0007 "Nonlinear Control Techniques for Dynamical Systems with Uncertain Parameters," by R.G. Ghanem and M.I. Bujakov, 5/27/96, (PB97-100259, A17, MF-A03).
- NCEER-96-0008 "Seismic Evaluation of a 30-Year Old Non-Ductile Highway Bridge Pier and Its Retrofit," by J.B. Mander, B. Mahmoodzadegan, S. Bhadra and S.S. Chen, 5/31/96, (PB97-110902, MF-A03, A10).
- NCEER-96-0009 "Seismic Performance of a Model Reinforced Concrete Bridge Pier Before and After Retrofit," by J.B. Mander, J.H. Kim and C.A. Ligozio, 5/31/96, (PB97-110910, MF-A02, A10).
- NCEER-96-0010 "IDARC2D Version 4.0: A Computer Program for the Inelastic Damage Analysis of Buildings," by R.E. Valles, A.M. Reinhorn, S.K. Kunnath, C. Li and A. Madan, 6/3/96, (PB97-100234, A17, MF-A03).
- NCEER-96-0011 "Estimation of the Economic Impact of Multiple Lifeline Disruption: Memphis Light, Gas and Water Division Case Study," by S.E. Chang, H.A. Seligson and R.T. Eguchi, 8/16/96, (PB97-133490, A11, MF-A03).
- NCEER-96-0012 "Proceedings from the Sixth Japan-U.S. Workshop on Earthquake Resistant Design of Lifeline Facilities and Countermeasures Against Soil Liquefaction, Edited by M. Hamada and T. O'Rourke, 9/11/96, (PB97-133581, A99, MF-A06).
- NCEER-96-0013 "Chemical Hazards, Mitigation and Preparedness in Areas of High Seismic Risk: A Methodology for Estimating the Risk of Post-Earthquake Hazardous Materials Release," by H.A. Seligson, R.T. Eguchi, K.J. Tierney and K. Richmond, 11/7/96, (PB97-133565, MF-A02, A08).
- NCEER-96-0014 "Response of Steel Bridge Bearings to Reversed Cyclic Loading," by J.B. Mander, D-K. Kim, S.S. Chen and G.J. Premus, 11/13/96, (PB97-140735, A12, MF-A03).
- NCEER-96-0015 "Highway Culvert Performance During Past Earthquakes," by T.L. Youd and C.J. Beckman, 11/25/96, (PB97-133532, A06, MF-A01).
- NCEER-97-0001 "Evaluation, Prevention and Mitigation of Pounding Effects in Building Structures," by R.E. Valles and A.M. Reinhorn, 2/20/97, (PB97-159552, A14, MF-A03).
- NCEER-97-0002 "Seismic Design Criteria for Bridges and Other Highway Structures," by C. Rojahn, R. Mayes, D.G. Anderson, J. Clark, J.H. Hom, R.V. Nutt and M.J. O'Rourke, 4/30/97, (PB97-194658, A06, MF-A03).

- NCEER-97-0003 "Proceedings of the U.S.-Italian Workshop on Seismic Evaluation and Retrofit," Edited by D.P. Abrams and G.M. Calvi, 3/19/97, (PB97-194666, A13, MF-A03).
- NCEER-97-0004 "Investigation of Seismic Response of Buildings with Linear and Nonlinear Fluid Viscous Dampers," by A.A. Seleemah and M.C. Constantinou, 5/21/97, (PB98-109002, A15, MF-A03).
- NCEER-97-0005 "Proceedings of the Workshop on Earthquake Engineering Frontiers in Transportation Facilities," edited by G.C. Lee and I.M. Friedland, 8/29/97, (PB98-128911, A25, MR-A04).
- NCEER-97-0006 "Cumulative Seismic Damage of Reinforced Concrete Bridge Piers," by S.K. Kunnath, A. El-Bahy, A. Taylor and W. Stone, 9/2/97, (PB98-108814, A11, MF-A03).
- NCEER-97-0007 "Structural Details to Accommodate Seismic Movements of Highway Bridges and Retaining Walls," by R.A. Imbsen, R.A. Schamber, E. Thorkildsen, A. Kartoum, B.T. Martin, T.N. Rosser and J.M. Kulicki, 9/3/97, (PB98-108996, A09, MF-A02).
- NCEER-97-0008 "A Method for Earthquake Motion-Damage Relationships with Application to Reinforced Concrete Frames," by A. Singhal and A.S. Kiremidjian, 9/10/97, (PB98-108988, A13, MF-A03).
- NCEER-97-0009 "Seismic Analysis and Design of Bridge Abutments Considering Sliding and Rotation," by K. Fishman and R. Richards, Jr., 9/15/97, (PB98-108897, A06, MF-A02).
- NCEER-97-0010 "Proceedings of the FHWA/NCEER Workshop on the National Representation of Seismic Ground Motion for New and Existing Highway Facilities," edited by I.M. Friedland, M.S. Power and R.L. Mayes, 9/22/97, (PB98-128903, A21, MF-A04).
- NCEER-97-0011 "Seismic Analysis for Design or Retrofit of Gravity Bridge Abutments," by K.L. Fishman, R. Richards, Jr. and R.C. Divito, 10/2/97, (PB98-128937, A08, MF-A02).
- NCEER-97-0012 "Evaluation of Simplified Methods of Analysis for Yielding Structures," by P. Tsopelas, M.C. Constantinou, C.A. Kircher and A.S. Whittaker, 10/31/97, (PB98-128929, A10, MF-A03).
- NCEER-97-0013 "Seismic Design of Bridge Columns Based on Control and Repairability of Damage," by C-T. Cheng and J.B. Mander, 12/8/97, (PB98-144249, A11, MF-A03).
- NCEER-97-0014 "Seismic Resistance of Bridge Piers Based on Damage Avoidance Design," by J.B. Mander and C-T. Cheng, 12/10/97, (PB98-144223, A09, MF-A02).
- NCEER-97-0015 "Seismic Response of Nominally Symmetric Systems with Strength Uncertainty," by S. Balopoulou and M. Grigoriu, 12/23/97, (PB98-153422, A11, MF-A03).
- NCEER-97-0016 "Evaluation of Seismic Retrofit Methods for Reinforced Concrete Bridge Columns," by T.J. Wipf, F.W. Klaiber and F.M. Russo, 12/28/97, (PB98-144215, A12, MF-A03).
- NCEER-97-0017 "Seismic Fragility of Existing Conventional Reinforced Concrete Highway Bridges," by C.L. Mullen and A.S. Cakmak, 12/30/97, (PB98-153406, A08, MF-A02).
- NCEER-97-0018 "Loss Assessment of Memphis Buildings," edited by D.P. Abrams and M. Shinozuka, 12/31/97, (PB98-144231, A13, MF-A03).
- NCEER-97-0019 "Seismic Evaluation of Frames with Infill Walls Using Quasi-static Experiments," by K.M. Mosalam, R.N. White and P. Gergely, 12/31/97, (PB98-153455, A07, MF-A02).
- NCEER-97-0020 "Seismic Evaluation of Frames with Infill Walls Using Pseudo-dynamic Experiments," by K.M. Mosalam, R.N. White and P. Gergely, 12/31/97, (PB98-153430, A07, MF-A02).
- NCEER-97-0021 "Computational Strategies for Frames with Infill Walls: Discrete and Smeared Crack Analyses and Seismic Fragility," by K.M. Mosalam, R.N. White and P. Gergely, 12/31/97, (PB98-153414, A10, MF-A02).

- NCEER-97-0022 "Proceedings of the NCEER Workshop on Evaluation of Liquefaction Resistance of Soils," edited by T.L. Youd and I.M. Idriss, 12/31/97, (PB98-155617, A15, MF-A03).
- MCEER-98-0001 "Extraction of Nonlinear Hysteretic Properties of Seismically Isolated Bridges from Quick-Release Field Tests," by Q. Chen, B.M. Douglas, E.M. Maragakis and I.G. Buckle, 5/26/98, (PB99-118838, A06, MF-A01).
- MCEER-98-0002 "Methodologies for Evaluating the Importance of Highway Bridges," by A. Thomas, S. Eshenaur and J. Kulicki, 5/29/98, (PB99-118846, A10, MF-A02).
- MCEER-98-0003 "Capacity Design of Bridge Piers and the Analysis of Overstrength," by J.B. Mander, A. Dutta and P. Goel, 6/1/98, (PB99-118853, A09, MF-A02).
- MCEER-98-0004 "Evaluation of Bridge Damage Data from the Loma Prieta and Northridge, California Earthquakes," by N. Basoz and A. Kiremidjian, 6/2/98, (PB99-118861, A15, MF-A03).
- MCEER-98-0005 "Screening Guide for Rapid Assessment of Liquefaction Hazard at Highway Bridge Sites," by T. L. Youd, 6/16/98, (PB99-118879, A06, not available on microfiche).
- MCEER-98-0006 "Structural Steel and Steel/Concrete Interface Details for Bridges," by P. Ritchie, N. Kaulh and J. Kulicki, 7/13/98, (PB99-118945, A06, MF-A01).
- MCEER-98-0007 "Capacity Design and Fatigue Analysis of Confined Concrete Columns," by A. Dutta and J.B. Mander, 7/14/98, (PB99-118960, A14, MF-A03).
- MCEER-98-0008 "Proceedings of the Workshop on Performance Criteria for Telecommunication Services Under Earthquake Conditions," edited by A.J. Schiff, 7/15/98, (PB99-118952, A08, MF-A02).
- MCEER-98-0009 "Fatigue Analysis of Unconfined Concrete Columns," by J.B. Mander, A. Dutta and J.H. Kim, 9/12/98, (PB99-123655, A10, MF-A02).
- MCEER-98-0010 "Centrifuge Modeling of Cyclic Lateral Response of Pile-Cap Systems and Seat-Type Abutments in Dry Sands," by A.D. Gadre and R. Dobry, 10/2/98, (PB99-123606, A13, MF-A03).
- MCEER-98-0011 "IDARC-BRIDGE: A Computational Platform for Seismic Damage Assessment of Bridge Structures," by A.M. Reinhorn, V. Simeonov, G. Mylonakis and Y. Reichman, 10/2/98, (PB99-162919, A15, MF-A03).
- MCEER-98-0012 "Experimental Investigation of the Dynamic Response of Two Bridges Before and After Retrofitting with Elastomeric Bearings," by D.A. Wendichansky, S.S. Chen and J.B. Mander, 10/2/98, (PB99-162927, A15, MF-A03).
- MCEER-98-0013 "Design Procedures for Hinge Restrainers and Hinge Sear Width for Multiple-Frame Bridges," by R. Des Roches and G.L. Fenves, 11/3/98, (PB99-140477, A13, MF-A03).
- MCEER-98-0014 "Response Modification Factors for Seismically Isolated Bridges," by M.C. Constantinou and J.K. Quarshie, 11/3/98, (PB99-140485, A14, MF-A03).
- MCEER-98-0015 "Proceedings of the U.S.-Italy Workshop on Seismic Protective Systems for Bridges," edited by I.M. Friedland and M.C. Constantinou, 11/3/98, (PB2000-101711, A22, MF-A04).
- MCEER-98-0016 "Appropriate Seismic Reliability for Critical Equipment Systems: Recommendations Based on Regional Analysis of Financial and Life Loss," by K. Porter, C. Scawthorn, C. Taylor and N. Blais, 11/10/98, (PB99-157265, A08, MF-A02).
- MCEER-98-0017 "Proceedings of the U.S. Japan Joint Seminar on Civil Infrastructure Systems Research," edited by M. Shinozuka and A. Rose, 11/12/98, (PB99-156713, A16, MF-A03).
- MCEER-98-0018 "Modeling of Pile Footings and Drilled Shafts for Seismic Design," by I. PoLam, M. Kapuskar and D. Chaudhuri, 12/21/98, (PB99-157257, A09, MF-A02).

- MCEER-99-0001 "Seismic Evaluation of a Masonry Infilled Reinforced Concrete Frame by Pseudodynamic Testing," by S.G. Buonopane and R.N. White, 2/16/99, (PB99-162851, A09, MF-A02).
- MCEER-99-0002 "Response History Analysis of Structures with Seismic Isolation and Energy Dissipation Systems: Verification Examples for Program SAP2000," by J. Scheller and M.C. Constantinou, 2/22/99, (PB99-162869, A08, MF-A02).
- MCEER-99-0003 "Experimental Study on the Seismic Design and Retrofit of Bridge Columns Including Axial Load Effects," by A. Dutta, T. Kokorina and J.B. Mander, 2/22/99, (PB99-162877, A09, MF-A02).
- MCEER-99-0004 "Experimental Study of Bridge Elastomeric and Other Isolation and Energy Dissipation Systems with Emphasis on Uplift Prevention and High Velocity Near-source Seismic Excitation," by A. Kasalanati and M. C. Constantinou, 2/26/99, (PB99-162885, A12, MF-A03).
- MCEER-99-0005 "Truss Modeling of Reinforced Concrete Shear-flexure Behavior," by J.H. Kim and J.B. Mander, 3/8/99, (PB99-163693, A12, MF-A03).
- MCEER-99-0006 "Experimental Investigation and Computational Modeling of Seismic Response of a 1:4 Scale Model Steel Structure with a Load Balancing Supplemental Damping System," by G. Pekcan, J.B. Mander and S.S. Chen, 4/2/99, (PB99-162893, A11, MF-A03).
- MCEER-99-0007 "Effect of Vertical Ground Motions on the Structural Response of Highway Bridges," by M.R. Button, C.J. Cronin and R.L. Mayes, 4/10/99, (PB2000-101411, A10, MF-A03).
- MCEER-99-0008 "Seismic Reliability Assessment of Critical Facilities: A Handbook, Supporting Documentation, and Model Code Provisions," by G.S. Johnson, R.E. Sheppard, M.D. Quilici, S.J. Eder and C.R. Scawthorn, 4/12/99, (PB2000-101701, A18, MF-A04).
- MCEER-99-0009 "Impact Assessment of Selected MCEER Highway Project Research on the Seismic Design of Highway Structures," by C. Rojahn, R. Mayes, D.G. Anderson, J.H. Clark, D'Appolonia Engineering, S. Gloyd and R.V. Nutt, 4/14/99, (PB99-162901, A10, MF-A02).
- MCEER-99-0010 "Site Factors and Site Categories in Seismic Codes," by R. Dobry, R. Ramos and M.S. Power, 7/19/99, (PB2000-101705, A08, MF-A02).
- MCEER-99-0011 "Restrainer Design Procedures for Multi-Span Simply-Supported Bridges," by M.J. Randall, M. Saiidi, E. Maragakis and T. Isakovic, 7/20/99, (PB2000-101702, A10, MF-A02).
- MCEER-99-0012 "Property Modification Factors for Seismic Isolation Bearings," by M.C. Constantinou, P. Tsopelas, A. Kasalanati and E. Wolff, 7/20/99, (PB2000-103387, A11, MF-A03).
- MCEER-99-0013 "Critical Seismic Issues for Existing Steel Bridges," by P. Ritchie, N. Kauh and J. Kulicki, 7/20/99, (PB2000-101697, A09, MF-A02).
- MCEER-99-0014 "Nonstructural Damage Database," by A. Kao, T.T. Soong and A. Vender, 7/24/99, (PB2000-101407, A06, MF-A01).
- MCEER-99-0015 "Guide to Remedial Measures for Liquefaction Mitigation at Existing Highway Bridge Sites," by H.G. Cooke and J. K. Mitchell, 7/26/99, (PB2000-101703, A11, MF-A03).
- MCEER-99-0016 "Proceedings of the MCEER Workshop on Ground Motion Methodologies for the Eastern United States," edited by N. Abrahamson and A. Becker, 8/11/99, (PB2000-103385, A07, MF-A02).
- MCEER-99-0017 "Quindío, Colombia Earthquake of January 25, 1999: Reconnaissance Report," by A.P. Asfura and P.J. Flores, 10/4/99, (PB2000-106893, A06, MF-A01).
- MCEER-99-0018 "Hysteretic Models for Cyclic Behavior of Deteriorating Inelastic Structures," by M.V. Sivaselvan and A.M. Reinhorn, 11/5/99, (PB2000-103386, A08, MF-A02).

- MCEER-99-0019 "Proceedings of the 7th U.S.- Japan Workshop on Earthquake Resistant Design of Lifeline Facilities and Countermeasures Against Soil Liquefaction," edited by T.D. O'Rourke, J.P. Bardet and M. Hamada, 11/19/99, (PB2000-103354, A99, MF-A06).
- MCEER-99-0020 "Development of Measurement Capability for Micro-Vibration Evaluations with Application to Chip Fabrication Facilities," by G.C. Lee, Z. Liang, J.W. Song, J.D. Shen and W.C. Liu, 12/1/99, (PB2000-105993, A08, MF-A02).
- MCEER-99-0021 "Design and Retrofit Methodology for Building Structures with Supplemental Energy Dissipating Systems," by G. Pekcan, J.B. Mander and S.S. Chen, 12/31/99, (PB2000-105994, A11, MF-A03).
- MCEER-00-0001 "The Marmara, Turkey Earthquake of August 17, 1999: Reconnaissance Report," edited by C. Scawthorn; with major contributions by M. Bruneau, R. Eguchi, T. Holzer, G. Johnson, J. Mander, J. Mitchell, W. Mitchell, A. Papageorgiou, C. Scaethorn, and G. Webb, 3/23/00, (PB2000-106200, A11, MF-A03).
- MCEER-00-0002 "Proceedings of the MCEER Workshop for Seismic Hazard Mitigation of Health Care Facilities," edited by G.C. Lee, M. Ettouney, M. Grigoriu, J. Hauer and J. Nigg, 3/29/00, (PB2000-106892, A08, MF-A02).
- MCEER-00-0003 "The Chi-Chi, Taiwan Earthquake of September 21, 1999: Reconnaissance Report," edited by G.C. Lee and C.H. Loh, with major contributions by G.C. Lee, M. Bruneau, I.G. Buckle, S.E. Chang, P.J. Flores, T.D. O'Rourke, M. Shinozuka, T.T. Soong, C-H. Loh, K-C. Chang, Z-J. Chen, J-S. Hwang, M-L. Lin, G-Y. Liu, K-C. Tsai, G.C. Yao and C-L. Yen, 4/30/00, (PB2001-100980, A10, MF-A02).
- MCEER-00-0004 "Seismic Retrofit of End-Sway Frames of Steel Deck-Truss Bridges with a Supplemental Tendon System: Experimental and Analytical Investigation," by G. Pekcan, J.B. Mander and S.S. Chen, 7/1/00, (PB2001-100982, A10, MF-A02).
- MCEER-00-0005 "Sliding Fragility of Unrestrained Equipment in Critical Facilities," by W.H. Chong and T.T. Soong, 7/5/00, (PB2001-100983, A08, MF-A02).
- MCEER-00-0006 "Seismic Response of Reinforced Concrete Bridge Pier Walls in the Weak Direction," by N. Abo-Shadi, M. Saiidi and D. Sanders, 7/17/00, (PB2001-100981, A17, MF-A03).
- MCEER-00-0007 "Low-Cycle Fatigue Behavior of Longitudinal Reinforcement in Reinforced Concrete Bridge Columns," by J. Brown and S.K. Kunnath, 7/23/00, (PB2001-104392, A08, MF-A02).
- MCEER-00-0008 "Soil Structure Interaction of Bridges for Seismic Analysis," I. PoLam and H. Law, 9/25/00, (PB2001-105397, A08, MF-A02).
- MCEER-00-0009 "Proceedings of the First MCEER Workshop on Mitigation of Earthquake Disaster by Advanced Technologies (MEDAT-1), edited by M. Shinozuka, D.J. Inman and T.D. O'Rourke, 11/10/00, (PB2001-105399, A14, MF-A03).
- MCEER-00-0010 "Development and Evaluation of Simplified Procedures for Analysis and Design of Buildings with Passive Energy Dissipation Systems," by O.M. Ramirez, M.C. Constantinou, C.A. Kircher, A.S. Whittaker, M.W. Johnson, J.D. Gomez and C. Chrysostomou, 11/16/01, (PB2001-105523, A23, MF-A04).
- MCEER-00-0011 "Dynamic Soil-Foundation-Structure Interaction Analyses of Large Caissons," by C-Y. Chang, C-M. Mok, Z-L. Wang, R. Settgast, F. Waggoner, M.A. Ketchum, H.M. Gonnermann and C-C. Chin, 12/30/00, (PB2001-104373, A07, MF-A02).
- MCEER-00-0012 "Experimental Evaluation of Seismic Performance of Bridge Restrainers," by A.G. Vlassis, E.M. Maragakis and M. Saiid Saiidi, 12/30/00, (PB2001-104354, A09, MF-A02).
- MCEER-00-0013 "Effect of Spatial Variation of Ground Motion on Highway Structures," by M. Shinozuka, V. Saxena and G. Deodatis, 12/31/00, (PB2001-108755, A13, MF-A03).
- MCEER-00-0014 "A Risk-Based Methodology for Assessing the Seismic Performance of Highway Systems," by S.D. Werner, C.E. Taylor, J.E. Moore, II, J.S. Walton and S. Cho, 12/31/00, (PB2001-108756, A14, MF-A03).

- MCEER-01-0001 "Experimental Investigation of P-Delta Effects to Collapse During Earthquakes," by D. Vian and M. Bruneau, 6/25/01, (PB2002-100534, A17, MF-A03).
- MCEER-01-0002 "Proceedings of the Second MCEER Workshop on Mitigation of Earthquake Disaster by Advanced Technologies (MEDAT-2)," edited by M. Bruneau and D.J. Inman, 7/23/01, (PB2002-100434, A16, MF-A03).
- MCEER-01-0003 "Sensitivity Analysis of Dynamic Systems Subjected to Seismic Loads," by C. Roth and M. Grigoriu, 9/18/01, (PB2003-100884, A12, MF-A03).
- MCEER-01-0004 "Overcoming Obstacles to Implementing Earthquake Hazard Mitigation Policies: Stage 1 Report," by D.J. Alesch and W.J. Petak, 12/17/01, (PB2002-107949, A07, MF-A02).
- MCEER-01-0005 "Updating Real-Time Earthquake Loss Estimates: Methods, Problems and Insights," by C.E. Taylor, S.E. Chang and R.T. Eguchi, 12/17/01, (PB2002-107948, A05, MF-A01).
- MCEER-01-0006 "Experimental Investigation and Retrofit of Steel Pile Foundations and Pile Bents Under Cyclic Lateral Loadings," by A. Shama, J. Mander, B. Blabac and S. Chen, 12/31/01, (PB2002-107950, A13, MF-A03).
- MCEER-02-0001 "Assessment of Performance of Bolu Viaduct in the 1999 Duzce Earthquake in Turkey" by P.C. Roussis, M.C. Constantinou, M. Erdik, E. Durukal and M. Dicleli, 5/8/02, (PB2003-100883, A08, MF-A02).
- MCEER-02-0002 "Seismic Behavior of Rail Counterweight Systems of Elevators in Buildings," by M.P. Singh, Rildova and L.E. Suarez, 5/27/02. (PB2003-100882, A11, MF-A03).
- MCEER-02-0003 "Development of Analysis and Design Procedures for Spread Footings," by G. Mylonakis, G. Gazetas, S. Nikolaou and A. Chauncey, 10/02/02, (PB2004-101636, A13, MF-A03, CD-A13).
- MCEER-02-0004 "Bare-Earth Algorithms for Use with SAR and LIDAR Digital Elevation Models," by C.K. Huyck, R.T. Eguchi and B. Houshmand, 10/16/02, (PB2004-101637, A07, CD-A07).
- MCEER-02-0005 "Review of Energy Dissipation of Compression Members in Concentrically Braced Frames," by K.Lee and M. Bruneau, 10/18/02, (PB2004-101638, A10, CD-A10).
- MCEER-03-0001 "Experimental Investigation of Light-Gauge Steel Plate Shear Walls for the Seismic Retrofit of Buildings" by J. Berman and M. Bruneau, 5/2/03, (PB2004-101622, A10, MF-A03, CD-A10).
- MCEER-03-0002 "Statistical Analysis of Fragility Curves," by M. Shinozuka, M.Q. Feng, H. Kim, T. Uzawa and T. Ueda, 6/16/03, (PB2004-101849, A09, CD-A09).
- MCEER-03-0003 "Proceedings of the Eighth U.S.-Japan Workshop on Earthquake Resistant Design of Lifeline Facilities and Countermeasures Against Liquefaction," edited by M. Hamada, J.P. Bardet and T.D. O'Rourke, 6/30/03, (PB2004-104386, A99, CD-A99).
- MCEER-03-0004 "Proceedings of the PRC-US Workshop on Seismic Analysis and Design of Special Bridges," edited by L.C. Fan and G.C. Lee, 7/15/03, (PB2004-104387, A14, CD-A14).
- MCEER-03-0005 "Urban Disaster Recovery: A Framework and Simulation Model," by S.B. Miles and S.E. Chang, 7/25/03, (PB2004-104388, A07, CD-A07).
- MCEER-03-0006 "Behavior of Underground Piping Joints Due to Static and Dynamic Loading," by R.D. Meis, M. Maragakis and R. Siddharthan, 11/17/03, (PB2005-102194, A13, MF-A03, CD-A00).
- MCEER-03-0007 "Seismic Vulnerability of Timber Bridges and Timber Substructures," by A.A. Shama, J.B. Mander, I.M. Friedland and D.R. Allicock, 12/15/03.
- MCEER-04-0001 "Experimental Study of Seismic Isolation Systems with Emphasis on Secondary System Response and Verification of Accuracy of Dynamic Response History Analysis Methods," by E. Wolff and M. Constantinou, 1/16/04 (PB2005-102195, A99, MF-E08, CD-A00).

- MCEER-04-0002 “Tension, Compression and Cyclic Testing of Engineered Cementitious Composite Materials,” by K. Kesner and S.L. Billington, 3/1/04, (PB2005-102196, A08, CD-A08).
- MCEER-04-0003 “Cyclic Testing of Braces Laterally Restrained by Steel Studs to Enhance Performance During Earthquakes,” by O.C. Celik, J.W. Berman and M. Bruneau, 3/16/04, (PB2005-102197, A13, MF-A03, CD-A00).
- MCEER-04-0004 “Methodologies for Post Earthquake Building Damage Detection Using SAR and Optical Remote Sensing: Application to the August 17, 1999 Marmara, Turkey Earthquake,” by C.K. Huyck, B.J. Adams, S. Cho, R.T. Eguchi, B. Mansouri and B. Houshmand, 6/15/04, (PB2005-104888, A10, CD-A00).
- MCEER-04-0005 “Nonlinear Structural Analysis Towards Collapse Simulation: A Dynamical Systems Approach,” by M.V. Sivaselvan and A.M. Reinhorn, 6/16/04, (PB2005-104889, A11, MF-A03, CD-A00).
- MCEER-04-0006 “Proceedings of the Second PRC-US Workshop on Seismic Analysis and Design of Special Bridges,” edited by G.C. Lee and L.C. Fan, 6/25/04, (PB2005-104890, A16, CD-A00).
- MCEER-04-0007 “Seismic Vulnerability Evaluation of Axially Loaded Steel Built-up Laced Members,” by K. Lee and M. Bruneau, 6/30/04, (PB2005-104891, A16, CD-A00).
- MCEER-04-0008 “Evaluation of Accuracy of Simplified Methods of Analysis and Design of Buildings with Damping Systems for Near-Fault and for Soft-Soil Seismic Motions,” by E.A. Pavlou and M.C. Constantinou, 8/16/04, (PB2005-104892, A08, MF-A02, CD-A00).
- MCEER-04-0009 “Assessment of Geotechnical Issues in Acute Care Facilities in California,” by M. Lew, T.D. O’Rourke, R. Dobry and M. Koch, 9/15/04, (PB2005-104893, A08, CD-A00).
- MCEER-04-0010 “Scissor-Jack-Damper Energy Dissipation System,” by A.N. Sigaher-Boyle and M.C. Constantinou, 12/1/04 (PB2005-108221).
- MCEER-04-0011 “Seismic Retrofit of Bridge Steel Truss Piers Using a Controlled Rocking Approach,” by M. Pollino and M. Bruneau, 12/20/04.
- MCEER-05-0001 “Experimental and Analytical Studies of Structures Seismically Isolated with an Uplift-Restraint Isolation System,” by P.C. Roussis and M.C. Constantinou, 1/10/05 (PB2005-108222).
- MCEER-05-0002 “A Versatile Experimentation Model for Study of Structures Near Collapse Applied to Seismic Evaluation of Irregular Structures,” by D. Kusumastuti, A.M. Reinhorn and A. Rutenberg, 3/31/05 (PB2006-101523).
- MCEER-05-0003 “Proceedings of the Third PRC-US Workshop on Seismic Analysis and Design of Special Bridges,” edited by L.C. Fan and G.C. Lee, 4/20/05.
- MCEER-05-0004 “Approaches for the Seismic Retrofit of Braced Steel Bridge Piers and Proof-of-Concept Testing of an Eccentrically Braced Frame with Tubular Link,” by J.W. Berman and M. Bruneau, 4/21/05 (PB2006-101524).
- MCEER-05-0005 “Simulation of Strong Ground Motions for Seismic Fragility Evaluation of Nonstructural Components in Hospitals,” by A. Wanitkorkul and A. Filiatrault, 5/26/05.
- MCEER-05-0006 “Seismic Safety in California Hospitals: Assessing an Attempt to Accelerate the Replacement or Seismic Retrofit of Older Hospital Facilities,” by D.J. Alesch, L.A. Arendt and W.J. Petak, 6/6/05.
- MCEER-05-0007 “Development of Seismic Strengthening and Retrofit Strategies for Critical Facilities Using Engineered Cementitious Composite Materials,” by K. Kesner and S.L. Billington, 8/29/05.
- MCEER-05-0008 “Experimental and Analytical Studies of Base Isolation Systems for Seismic Protection of Power Transformers,” by N. Murota, M.Q. Feng and G-Y. Liu, 9/30/05.
- MCEER-05-0009 “3D-BASIS-ME-MB: Computer Program for Nonlinear Dynamic Analysis of Seismically Isolated Structures,” by P.C. Tsopelas, P.C. Roussis, M.C. Constantinou, R. Buchanan and A.M. Reinhorn, 10/3/05.

- MCEER-05-0010 “Steel Plate Shear Walls for Seismic Design and Retrofit of Building Structures,” by D. Vian and M. Bruneau, 12/15/05.
- MCEER-05-0011 “The Performance-Based Design Paradigm,” by M.J. Astrella and A. Whittaker, 12/15/05.
- MCEER-06-0001 “Seismic Fragility of Suspended Ceiling Systems,” H. Badillo-Almaraz, A.S. Whittaker, A.M. Reinhorn and G.P. Cimellaro, 2/4/06.
- MCEER-06-0002 “Multi-Dimensional Fragility of Structures,” by G.P. Cimellaro, A.M. Reinhorn and M. Bruneau, 3/1/06.
- MCEER-06-0003 “Built-Up Shear Links as Energy Dissipators for Seismic Protection of Bridges,” by P. Dusicka, A.M. Itani and I.G. Buckle, 3/15/06.
- MCEER-06-0004 “Analytical Investigation of the Structural Fuse Concept,” by R.E. Vargas and M. Bruneau, 3/16/06.



MULTIDISCIPLINARY CENTER FOR EARTHQUAKE ENGINEERING RESEARCH

A National Center of Excellence in Advanced Technology Applications

University at Buffalo, State University of New York

Red Jacket Quadrangle ■ Buffalo, New York 14261

Phone: (716) 645-3391 ■ Fax: (716) 645-3399

E-mail: mceer@mceermail.buffalo.edu ■ WWW Site <http://mceer.buffalo.edu>



University at Buffalo *The State University of New York*

ISSN 1520-295X